

This Page Is Inserted by IFW Operations
and is not a part of the Official Record

BEST AVAILABLE IMAGES

Defective images within this document are accurate representations of the original documents submitted by the applicant.

Defects in the images may include (but are not limited to):

- BLACK BORDERS
- TEXT CUT OFF AT TOP, BOTTOM OR SIDES
- FADED TEXT
- ILLEGIBLE TEXT
- SKEWED/SLANTED IMAGES
- COLORED PHOTOS
- BLACK OR VERY BLACK AND WHITE DARK PHOTOS
- GRAY SCALE DOCUMENTS

IMAGES ARE BEST AVAILABLE COPY.

As rescanning documents *will not* correct images,
please do not report the images to the
Image Problem Mailbox.

THIS PAGE BLANK (USPTO)

DECLARATION OF DR. RANDELL L. MILLS

I, Randell L. Mills, declare and state as follows:

1. I am the founder and CEO of BlackLight Power, Inc., located at 493 Old Trenton Road, Cranbury, New Jersey 08512.
2. I majored in chemistry and received my bachelor of arts degree, *summa cum laude* and Phi Beta Kappa, from Franklin & Marshall College in 1982. I received a medical degree from Harvard Medical School in 1986. While attending Harvard Medical School, I concurrently spent a year taking courses in advanced electrical engineering at the Massachusetts Institute of Technology. I have also had significant academic training in biology, chemistry, mathematics and physics.
3. I began my research in the field of energy technology over ten years ago. I have authored, co-authored or collaborated on numerous publications, reports and presentations at scientific meetings in the field of energy technology and novel hydrogen chemistry, as shown in the attachment hereto.
4. I am fully qualified to conduct the research that led to the discovery and development of BlackLight's lower-energy hydrogen technology.
5. I personally conducted and/or supervised the experimental data disclosed in the articles submitted to the U.S. Patent and Trademark Office ("PTO"), which are described in the following Paragraph Nos. 6 through 27. The coauthors, if any, assisted me in preparing the data.
6. H. Conrads, R. Mills, Th. Wrubel, "Emission in the Deep Vacuum Ultraviolet from an Incandescently Driven Plasma in a Potassium Carbonate Cell", Plasma Sources Science and Technology, submitted. Electromagnetic radiation in both the visible and vacuum ultraviolet (VUV) spectral ranges was emitted from an incandescently driven plasma in a potassium carbonate cell after the potassium carbonate coated on a titanium mesh was heated to

THIS PAGE BLANK (USPTO)

above 750°C in a hydrogen atmosphere. The pressure was between 0.1 and 1 mbar, and the hydrogen was dissociated by a hot tungsten wire. Bright visible light filled the annulus between the coaxial tungsten heater and the titanium mesh. This grid was at a floating potential. The emission of the H_α and H_β transitions as well as the L_α and L_β transitions were recorded and analyzed. In the latter spectral range, the spectra showed rotational-vibrational transitions of molecular hydrogen which belong to the Werner-band-system of molecular hydrogen. The plasma generated in the incandescently driven cell had phenomenological similarities to that of low pressure electrical driven discharges such as striations of the plasma or the appearance of unipolar arcs ending on metal surfaces. However, the plasma seemed to be far from thermal equilibrium and dependent on the chemistry of atomic hydrogen with potassium. Details of the chemistry powering a novel VUV-light source could not be revealed within the frame of this contribution.

7. R. L. Mills, P. Ray, "Stationary Inverted Lyman Population Formed from Incandescently Heated Hydrogen Gas with Certain Catalysts", Chem. Phys. Letts., submitted. Rb^+ to Rb^{2+} and $2K^+$ to $K + K^{2+}$ each provide a reaction with a net enthalpy equal to the potential energy of atomic hydrogen. The presence of these gaseous ions with thermally dissociated hydrogen formed a plasma having strong VUV emission with a stationary inverted Lyman population. We propose an energetic catalytic reaction involving a resonance energy transfer between hydrogen atoms and Rb^+ or $2K^+$ to form a very stable novel hydride ion. Its predicted binding energy of 3.0468 eV was observed at 4070.0 Å with its predicted bound-free hyperfine structure lines $E_{HF} = j^2 3.0056 \times 10^{-5} + 3.0575$ eV (j is an integer) that matched for $j = 1$ to $j = 37$ to within a 1 part per 10^5 . This catalytic reaction may pump a cw HI laser.

8. R. L. Mills, B. Dhandapani, J. He, "Synthesis and Characterization of a Highly Stable Amorphous Silicon Hydride", Int. J. Hydrogen Energy, submitted. A novel highly stable surface coating $SiH(1/p)$ which comprised high binding energy hydride ions was synthesized by microwave plasma reaction of mixture of silane, hydrogen, and helium wherein it is proposed that He^+ served as a catalyst with atomic hydrogen to form the highly stable hydride ions. Novel silicon hydride was identified by time of flight secondary ion mass spectroscopy and X-

THIS PAGE BLANK (USPTO)

ray photoelectron spectroscopy. The ToF-SIMS identified the coatings as hydride by the large SiH^+ peak in the positive spectrum and the dominant H^- in the negative spectrum. XPS identified the H content of the SiH coatings as hydride ions, $H^-(1/4)$, $H^-(1/9)$, and $H^-(1/11)$ corresponding to peaks at 11, 43, and 55 eV, respectively. The silicon hydride surface was remarkably stable to air as shown by XPS. The highly stable amorphous silicon hydride coating may advance the production of integrated circuits and microdevices by resisting the oxygen passivation of the surface and possibly altering the dielectric constant and band gap to increase device performance.

9. R. L. Mills, A. Voigt, B. Dhandapani, J. He, "Synthesis and Characterization of Lithium Chloro Hydride", Int. J. Hydrogen Energy, submitted. A novel inorganic hydride compound lithium chloro hydride, LiHCl , which comprises a high binding energy hydride ion was synthesized by reaction of atomic hydrogen with potassium metal and lithium chloride. Lithium chloro hydride was identified by time of flight secondary ion mass spectroscopy, X-ray photoelectron spectroscopy, ^1H nuclear magnetic resonance spectroscopy, and powder X-ray diffraction. Hydride ions with increased binding energies may form many novel compounds with broad applications such as the oxidant of a high voltage battery.

10. R. L. Mills, P. Ray, "Substantial Changes in the Characteristics of a Microwave Plasma Due to Combining Argon and Hydrogen", New Journal of Physics, submitted. Upon the addition of 5% argon to a hydrogen plasma, the Lyman α emission was observed to increase by about an order of magnitude; whereas, xenon control had no effect. With a microwave input power of 40 W, the gas temperature of an argon plasma increased from 400°C to over 750°C with the addition of 3% flowing hydrogen; whereas, the 400°C temperature of a xenon plasma run under identical conditions was essentially unchanged with the addition of hydrogen. The average hydrogen atom temperature of the argon-hydrogen plasma was measured to be 110-130 eV versus ≈ 3 eV for pure hydrogen or xenon-hydrogen. Stark broadening or acceleration of charged species due to high fields (e. g. over 10 kV/cm) can not be invoked to explain the results with argon since no high field was observationally present. The electron temperature T_e for the argon-hydrogen and xenon-hydrogen plasmas was $11,600 \pm 5\% K$ and $6500 \pm 5\% K$,

THIS PAGE BLANK

respectively, compared to $4800 \pm 5\% K$ and $4980 \pm 5\% K$ for argon and xenon alone, respectively. The observation of higher temperatures corresponding to three possibly independent plasma parameters for only argon with hydrogen may be explained by the release of energy from atomic hydrogen by a resonant nonradiative energy transfer mechanism.

11. R. L. Mills, P. Ray, " High Resolution Spectroscopic Observation of the Bound-Free Hyperfine Levels of a Novel Hydride Ion Corresponding to a Fractional Rydberg State of Atomic Hydrogen", Int. J. Hydrogen Energy, in press. From a solution of a Schrödinger-type wave equation with a nonradiative boundary condition based on Maxwell's equations, Mills solves the hydrogen atom, the hydride ion, and predicts corresponding species having fractional principal quantum numbers. Atomic hydrogen may undergo a catalytic reaction with certain atomized elements and ions which singly or multiply ionize at integer multiples of the potential energy of atomic hydrogen, $m \cdot 27.2 \text{ eV}$ wherein m is an integer. The reaction involves a nonradiative energy transfer to form a hydrogen atom $H(1/p)$ that is lower in energy than unreacted atomic hydrogen that corresponds to a fractional principal quantum number ($n = \frac{1}{p} = \frac{1}{\text{integer}}$ replaces the well known parameter $n = \text{integer}$ in the Rydberg equation for hydrogen excited states). The ionization of Rb^+ and an electron transfer between two K^+ ions (K^+ / K^+) provide a reaction with a net enthalpy of 27.2 eV which serve as catalysts of atomic hydrogen to form $H(1/2)$. Intense extreme ultraviolet (EUV) emission was observed from incandescently heated atomic hydrogen and each of atomized potassium and rubidium ions that generated a plasma called a resonance transfer or rt-plasma at low temperatures (e.g. $\approx 10^3 \text{ K}$) and an extraordinary low field strength of about $1-2 \text{ V/cm}$. For further characterization, the width of the 6562 \AA Balmer α line was recorded. Significant line broadening of 17 and 9 eV was observed from a rt-plasma of hydrogen with K^+ / K^+ and Rb^+ respectively. These results could not be explained by Stark or thermal broadening or electric field acceleration of charged species since the measured field of the incandescent heater was extremely weak, 1 V/cm , corresponding to a broadening of much less than 1 eV . Rather the source of the excessive line broadening is consistent with that of the observed EUV emission, an energetic reaction caused by a resonance energy transfer between hydrogen atoms and K^+ / K^+ or Rb^+ . The catalyst

THIS PAGE BLANK (USPTO)

product $H(1/2)$ was predicted to be a highly reactive intermediate which further reacts to form a novel hydride ion $H^-(1/2)$. This hydride ion with a predicted binding energy of 3.0468 eV was observed by high resolution visible spectroscopy as a broad peak at 4070.0 \AA with a FWHM of 1.4 \AA . From the electron g factor, bound-free hyperfine structure lines of $H^-(1/2)$ were predicted with energies E_{HF} given by $E_{HF} = j^2 3.0056 \times 10^{-5} + 3.0575\text{ eV}$ (j is an integer) as an inverse Rydberg-type series that converges at increasing wavelengths and terminates at 3.0575 eV —the hydride spin-pairing energy plus the binding energy. The high resolution visible plasma emission spectra in the region of 4000 \AA to 4060 \AA matched the predicted emission lines for $j = 1$ to $j = 37$ to 1 part in 10^5 ,

12. R. L. Mills, E. Dayalan, "Novel Alkali and Alkaline Earth Hydrides for High Voltage and High Energy Density Batteries", Proceedings of the 17th Annual Battery Conference on Applications and Advances, California State University, Long Beach, CA, (January 15-18, 2002), in press. BLACKLIGHT POWER, Inc. (BLP) of Cranbury, New Jersey, is developing a revolutionary technology based on novel hydrogen chemistry. More explicitly, energy is catalytically released as the electrons of atomic hydrogen are induced to undergo transitions to lower energy levels corresponding to fractional quantum numbers with the production of plasma, light, and novel hydrogen compounds [1-35]. The Company uses a chemically generated or assisted plasma to form atomic hydrogen and a catalyst which react through a nonradiative energy transfer to form lower-energy hydrogen atoms called hydrinos. Since hydrinos have energy levels much lower than uncatalyzed hydrogen atoms, the energy release is intermediate between chemical and nuclear energies. The net enthalpy released may be over several hundred times that of combustion. Thus, the catalysis of atomic hydrogen represents a new source of energy with H_2O as the source of hydrogen fuel obtained by diverting a fraction of the output energy of the process to split water into its elemental constituents. Moreover, rather than air pollutants or radioactive waste, the products are novel compounds having hydride ions with increased binding energies that may be the basis of a high voltage battery. Such a high voltage battery would have the advantages of much greater power and much higher energy density where the limitations of battery chemistry attributed to the binding energy of the anion of the oxidant

THIS PAGE BLANK (USPTO)

are addressed. The concept of our novel hydride battery and some preliminary results will be discussed during the presentation.

13. R. Mayo, R. Mills, M. Nansteel, "On the Potential of Direct and MHD Conversion of Power from a Novel Plasma Source to Electricity for Microdistributed Power Applications", IEEE Transactions on Plasma Science, submitted. The generation of electricity using direct electrostatic and magnetohydrodynamic (MHD) conversion of the plasma particle energy of small to mid-size chemically assisted microwave or glow discharge plasmas (CA-plasma) power sources in the range of a few hundred Watts to several 10's of kW for microdistributed commercial applications (e.g. household, automotive, light industry, and space based power) is studied for the first time. In the determination of the effect of plasma parameters on conversion efficiency, careful attention is paid to the unique plasma conditions of low pressure, low ionization fraction, and nonthermal ion energies that are much greater than that of the thermal ions of traditional MHD but much lower than those of a fully ionized plasma typically generated for fusion experiments. The density of plasma ions and neutrals and their cross sections for processes such as charge exchange were also considered. The most important parameters were found to be charged particle density and energy, as well as the large inventory of neutral gas atoms and molecules. Momentum and charge exchange of plasma ions with the large background fraction of neutrals represents a limitation to conversion efficiency. Two conversion technologies were examined in some detail. We considered the possibility of converting a CA-plasma using adaptations of a member of the broad category of electromagnetic direct converters previously developed for recovery and conversion of the high energy particles lost from tandem mirror and magnetically confined plasmas, and an MHD converter previously developed for conversion of high pressure combustion gases to electricity. While it was found that both conversion techniques performed well under ideal conditions for conversion of plasma to electricity showing conversion efficiencies of ~70% are possible, the tight coupling of plasma cell and converter, size limitations, particle energy, and the substantial inventory of relatively low energy neutrals eliminate direct electrostatic converters as practical converters under these conditions. However, MHD conversion of CA-plasmas appears feasible at ~50% efficiency with a simple compact design.

THIS PAGE BLANK (USPTO)

14. R. Mills, P. Ray, J. Dong, M. Nansteel, W. Good, P. Jansson, B. Dhandapani, J. He, "Excessive Balmer α Line Broadening, Power Balance, and Novel Hydride Ion Product of Plasma Formed from Incandescently Heated Hydrogen Gas with Certain Catalysts", Int. J. Hydrogen Energy, submitted. Typically the emission of vacuum ultraviolet light from hydrogen gas is achieved using discharges at high voltage, synchrotron devices, high power inductively coupled plasma generators, or a plasma is created and heated to extreme temperatures by RF coupling (e.g. $> 10^6 K$) with confinement provided by a toroidal magnetic field. Observation of intense extreme ultraviolet (EUV) emission at low temperatures (e.g. $\approx 10^3 K$) from atomic hydrogen generated at a tungsten filament that heated a titanium dissociator and certain gaseous atoms or ions vaporized by filament heating has been reported previously [R. Mills, J. Dong, Y. Lu, "Observation of Extreme Ultraviolet Hydrogen Emission from Incandescently Heated Hydrogen Gas with Certain Catalysts", Int. J. Hydrogen Energy, Vol. 25, (2000), pp. 919-943]. Each of the ionization of potassium, cesium, strontium, and Rb^+ and an electron transfer between two K^+ ions (K^+ / K^+) provide a reaction with a net enthalpy of an integer multiple of the potential energy of atomic hydrogen. The presence of each of the corresponding reactants formed the low applied temperature, extremely low voltage plasma called a resonance transfer or rt-plasma having strong EUV emission. Similarly, the ionization energy of Ar^+ is 27.63 eV, and the emission intensity of the plasma generated by atomic strontium increased significantly with the introduction of argon gas only when Ar^+ emission was observed [R. Mills, "Spectroscopic Identification of a Novel Catalytic Reaction of Atomic Hydrogen and the Hydride Ion Product", Int. J. Hydrogen Energy, Vol. 26, No. 10, (2001), pp. 1041-1058.]. In contrast, the chemically similar atoms, sodium, magnesium and barium, do not ionize at integer multiples of the potential energy of atomic hydrogen did not form a plasma and caused no emission. For further characterization, we recorded the width of the 656.2 nm Balmer α line on light emitted from rt-plasmas. Significant line broadening of 17, 9, 11, 14, and 24 eV was observed from a rt-plasma of hydrogen with K^+ / K^+ , Rb^+ , cesium, strontium, and strontium with Ar^+ , respectively. These results could not be explained by Stark or thermal broadening or electric field acceleration of charged species since the measured field of the incandescent heater was extremely weak, 1 V/cm, corresponding to a broadening of much less than 1 eV. Rather the

THIS PAGE BLANK (USPTO)

source of the excessive line broadening is consistent with that of the observed EUV emission, an energetic reaction caused by a resonance energy transfer between hydrogen atoms and K^+ / K^+ , Rb^+ , cesium, strontium, or Ar^+ . Since line broadening is a measure of temperature, the excess power was measured calorimetrically on rt-plasmas formed by K^+ / K^+ and Ar^+ as catalysts. The product hydride ion with each of K^+ / K^+ , Rb^+ , Cs , and Ar^+ as the catalyst was predicted to have a binding energy of 3.05 eV and was observed by high resolution visible spectroscopy at 407 nm.

15. R. Mills, E. Dayalan, P. Ray, B. Dhandapani, J. He, "Highly Stable Novel Inorganic Hydrides from Aqueous Electrolysis and Plasma Electrolysis", Japanese Journal of Applied Physics, submitted. Based on a solution of a Schrödinger-type wave equation with a nonradiative boundary condition from Maxwell's equations, atomic hydrogen is predicted to undergo a catalytic reaction with reactants which provide a net enthalpy of reaction of integer multiples of the potential energy of atomic hydrogen, 27.2 eV. The reaction involves a nonradiative energy transfer to form a hydrogen atom that is lower in energy than unreacted atomic hydrogen with the release of energy. Each of the ionization of potassium, cesium, and Rb^+ and an electron transfer between two K^+ ions (K^+ / K^+) provide a reaction with a net enthalpy of an integer multiple of the potential energy of atomic hydrogen. For each of K^+ / K^+ , Rb^+ , and cesium, the net enthalpy of reaction of the catalyst is about 27.2 eV, and the lower-energy hydrogen atom catalysis product is predicted to be a highly reactive intermediate which further reacts to form a novel hydride ion $H^- (1/2)$. This ion formed by plasma electrolysis of a K_2CO_3 , Rb_2CO_3 , or Cs_2CO_3 electrolyte was observed by high resolution visible spectroscopy at 407.0 nm corresponding to its predicted binding energy of 3.05 eV. Whereas, no peak was observed during plasma electrolysis with the control Na_2CO_3 electrolyte. Furthermore, novel inorganic hydride compounds $KHKHCO_3$ and KH were isolated following the electrolysis of a K_2CO_3 electrolyte. The compounds which comprised high binding energy hydride ions were stable in water, and KH was stable at elevated temperature (600 °C). Inorganic hydride clusters $K[KHKHCO_3]$ were identified by positive ToF-SIMS of $KHKHCO_3$. The negative ToF-SIMS was dominated by hydride ion. The positive and negative ToF-SIMS of KH showed

THIS PAGE BLANK

essentially K^+ and H^- only, respectively. Moreover, the existence of novel hydride ions was determined using X-ray photoelectron spectroscopy, and proton nuclear magnetic resonance spectroscopy. Hydride ions with increased binding energies may be the basis of a high voltage battery for electric vehicles.

16. R. L. Mills, P. Ray, B. Dhandapani, J. He, "Comparison of Excessive Balmer α Line Broadening of Glow Discharge and Microwave Hydrogen Plasmas with Certain Catalysts", Chem. Phys., submitted. The width of the 656.2 nm Balmer α line emitted from microwave and glow discharge plasmas of hydrogen alone, strontium or magnesium with hydrogen, or helium, neon, argon, or xenon with 10% hydrogen was recorded with a high resolution visible spectrometer. It was found that the strontium-hydrogen microwave plasma showed a broadening similar to that observed in the glow discharge cell of 27 - 33 eV; whereas, in both sources, no broadening was observed for magnesium-hydrogen. With noble-gas hydrogen mixtures, the trend of broadening with the particular noble gas was the same for both sources, but the magnitude of broadening was dramatically different. The microwave helium-hydrogen and argon-hydrogen plasmas showed extraordinary broadening corresponding to an average hydrogen atom temperature of 110 - 130 eV and 180 - 210 eV, respectively. The corresponding results from the glow discharge plasmas were 30 - 35 eV and 33 - 38 eV, respectively. Whereas, plasmas of pure hydrogen, neon-hydrogen, krypton-hydrogen, and xenon-hydrogen maintained in either source showed no excessive broadening corresponding to an average hydrogen atom temperature of ≈ 4 eV. In the case of the helium-hydrogen mixture and argon-hydrogen mixture microwave plasmas, the electron temperature T_e was measured from the ratio of the intensity of the He 501.6 nm line to that of the He 492.2 line and the ratio of the intensity of the Ar 104.8 nm line to that of the Ar 420.06 nm line, respectively. Similarly, the average electron temperature for helium-hydrogen and argon-hydrogen plasmas were high, 28,000 K and 11,600 K, respectively; whereas, the corresponding temperatures of helium and argon alone were only 6800 K and 4800 K, respectively. Stark broadening or acceleration of charged species due to high fields (e. g. over 10 kV/cm) can not be invoked to explain the microwave results since no high field was observationally present. Rather, the results may be explained by a resonant

THIS PAGE BLANK (USPS)

energy transfer between atomic hydrogen and atomic strontium, Ar^+ , or He^+ which ionize at an integer multiple of the potential energy of atomic hydrogen.

17. R. L. Mills, P. Ray, B. Dhandapani, J. He, "Spectroscopic Identification of Fractional Rydberg States of Atomic Hydrogen", J. of Phys. Chem. (letter), submitted. Extreme ultraviolet (EUV) spectroscopy was recorded on microwave discharges of helium with 2% hydrogen. Novel emission lines were observed with energies of $q \cdot 13.6\text{ eV}$ where $q = 1, 2, 3, 4, 6, 7, 8, 9, 11, 12$ or these lines inelastically scattered by helium atoms wherein 21.2 eV was absorbed in the excitation of $He(1s^2)$ to $He(1s^1 2p^1)$. These lines can be explained as fractional Rydberg states of atomic hydrogen. Novel emission lines were also observed at 44.2 nm and 40.5 nm with energies of $q \cdot 13.6 + \left(\frac{1}{n_f^2} - \frac{1}{n_i^2} \right) \times 13.6\text{ eV}$ where $q = 2$ and $n_f = 2, 4$ $n_i = \infty$ that corresponded to multipole coupling to give two photon emission from a continuum excited state atom and an atom undergoing a fractional Rydberg state transition. Such transitions would be extremely energetic; so, the width of the 656.2 nm Balmer α line emitted from the plasmas was measured, and the electron temperature T_e was measured from the ratio of the intensity of the He 501.6 nm line to that of the He 492.2 nm line. Significant line broadening corresponding to an average hydrogen atom temperature of $180 - 210\text{ eV}$ was observed for helium-hydrogen microwave plasmas; whereas, pure hydrogen showed no excessive broadening corresponding to an average hydrogen atom temperature of $\approx 3\text{ eV}$. Similarly, the average electron temperature for helium-hydrogen plasma was $28,000\text{ K}$; whereas, the corresponding temperature of helium alone was only 6800 K .

18. R. L. Mills, P. Ray, B. Dhandapani, M. Nansteel, X. Chen, J. He, "New Power Source from Fractional Rydberg States of Atomic Hydrogen", Chem. Phys. Letts., submitted. Extreme ultraviolet spectroscopy was recorded on microwave discharges of helium with 2% hydrogen. Novel emission lines were observed with energies of $q \cdot 13.6\text{ eV}$ where $q = 1, 2, 3, 4, 6, 7, 8, 9, 11$ or these lines inelastically scattered by helium atoms wherein 21.2 eV was absorbed in the excitation of $He(1s^2)$ to $He(1s^1 2p^1)$. The average hydrogen atom temperature was $180 - 210\text{ eV}$ versus $\approx 3\text{ eV}$ for pure hydrogen. Similarly, T_e for helium-hydrogen was $28,000\text{ K}$.

THIS PAGE BLANK (USPTO)

compared to 6800 K for pure helium. With a microwave input power of 40 W, the thermal output power was measured to be at least 400 W corresponding to a power density of 40 MW/m³ and an energy balance of at least -5×10^5 kJ/mole H₂ compared to the enthalpy of combustion of hydrogen of -241.8 kJ/mole H₂.

19. R. L. Mills, P. Ray, B. Dhandapani, M. Nansteel, X. Chen, J. He, "New Power Source from Fractional Rydberg States of Atomic Hydrogen that Surpasses Internal Combustion", Quantitative Spectroscopy and Energy Transfer, submitted. Extreme ultraviolet (EUV) spectroscopy was recorded on microwave discharges of helium with 2% hydrogen. Novel emission lines were observed with energies of $q \cdot 13.6\text{ eV}$ where $q = 1, 2, 3, 4, 6, 7, 8, 9, \text{ or } 11$ or these lines inelastically scattered by helium atoms wherein 21.2 eV was absorbed in the excitation of He (1s²) to He (1s¹2p¹). These lines can be explained as fractional Rydberg states of atomic hydrogen. Such transitions would be extremely energetic; so, the width of the 656.2 nm Balmer α line emitted from the plasmas was measured, and the electron temperature T_e was measured from the ratio of the intensity of the He 501.6 nm line to that of the He 492.2 line. Significant line broadening corresponding to an average hydrogen atom temperature of 33 - 38 eV was observed for helium-hydrogen glow discharge plasmas; whereas, pure hydrogen showed no excessive broadening corresponding to an average hydrogen atom temperature of $\approx 3\text{ eV}$. Similarly, the average electron temperature for helium-hydrogen microwave plasmas was 28,000 K; whereas, the corresponding temperature of helium alone was only 6800 K. Since a significant increase in ion and electron temperature was observed with helium-hydrogen discharge and microwave plasmas, respectively, and energetic hydrino lines were observed at short wavelengths in the corresponding microwave plasmas that required a very significant reaction rate due to low photon detection efficiency in this region, the power balance was measured on the helium-hydrogen microwave plasmas. With a microwave input power of 40 W, the thermal output power was measured to be $238 \pm 8\text{ W}$ corresponding to a reactor temperature rise from room temperature to 1240 °C within 60 seconds, a power density of 24 MW/m³, and an energy balance of at least -3×10^5 kJ/mole H₂ compared to the enthalpy of combustion of hydrogen of -241.8 kJ/mole H₂.

THIS PAGE BLANK (USPTO)

20. R. L. Mills, P. Ray, B. Dhandapani, M. Nansteel, X. Chen, J. He, "New Power Source from Fractional Quantum Energy Levels of Atomic Hydrogen that Surpasses Internal Combustion", Spectrochimica Acta, Part A, submitted. Extreme ultraviolet (EUV) spectroscopy was recorded on microwave discharges of helium with 2% hydrogen. Novel emission lines were observed with energies of $q \cdot 13.6 \text{ eV}$ where $q = 1, 2, 3, 4, 6, 7, 8, 9, \text{ or } 11$ or these lines inelastically scattered by helium atoms wherein 21.2 eV was absorbed in the excitation of $\text{He}(1s^2)$ to $\text{He}(1s^1 2p^1)$. These lines were identified as hydrogen transitions to electronic energy levels below the "ground" state corresponding to fractional quantum numbers. Significant line broadening corresponding to an average hydrogen atom temperature of $33 - 38 \text{ eV}$ was observed for helium-hydrogen discharge plasmas; whereas, pure hydrogen showed no excessive broadening corresponding to an average hydrogen atom temperature of $\approx 3 \text{ eV}$. Since a significant increase in ion temperature was observed with helium-hydrogen discharge plasmas, and energetic hydron lines were observed at short wavelengths in the corresponding microwave plasmas that required a very significant reaction rate due to low photon detection efficiency in this region, the power balance was measured on the helium-hydrogen microwave plasmas. With a microwave input power of 30 W , the thermal output power was measured to be at least 300 W corresponding to a reactor temperature rise from room temperature to $900 \text{ }^\circ\text{C}$ within 90 seconds, a power density of 30 MW/m^3 , and an energy balance of about $-4 \times 10^5 \text{ kJ/mole H}_2$ compared to the enthalpy of combustion of hydrogen of $-241.8 \text{ kJ/mole H}_2$.

21. R. L. Mills, P. Ray, "Spectroscopic Identification of a Novel Catalytic Reaction of Rubidium Ion with Atomic Hydrogen and the Hydride Ion Product", Int. J. Hydrogen Energy, in press. From a solution of a Schrödinger-type wave equation with a nonradiative boundary condition based on Maxwell's equations, Mills predicts that atomic hydrogen may undergo a catalytic reaction with certain atomized elements and ions which singly or multiply ionize at integer multiples of the potential energy of atomic hydrogen, 27.2 eV . The reaction involves a nonradiative energy transfer to form a hydrogen atom that is lower in energy than unreacted atomic hydrogen with the release of energy. One such atomic catalytic system involves Rb^+ from RbNO_3 . Since the second ionization energy of rubidium is 27.28 eV , the reaction Rb^+ to

THIS PAGE BLANK (USPTO)

Rb^{2+} has a net enthalpy of reaction of 27.28 eV . Intense extreme ultraviolet (EUV) emission was observed from incandescently heated atomic hydrogen and the atomized Rb^+ catalyst that generated an anomalous plasma at low temperatures (e.g. $\approx 10^3\text{ K}$) and an extraordinary low field strength of about $1\text{-}2\text{ V/cm}$. No emission was observed with Rb^+ or hydrogen alone or when $NaNO_3$ replaced $RbNO_3$ with hydrogen. Emission was observed from Rb^{2+} that confirmed the resonant nonradiative energy transfer of 27.2 eV from atomic hydrogen to atomic Rb^+ . The catalysis product, a lower-energy hydrogen atom, was predicted to be a highly reactive intermediate which further reacts to form a novel hydride ion. The predicted hydride ion of hydrogen catalysis by Rb^+ is the hydride ion $H^-(1/2)$. This ion was observed spectroscopically at 407 nm corresponding to its predicted binding energy of 3.05 eV .

22. R. Mills, J. Dong, W. Good, P. Ray, J. He, B. Dhandapani, "Measurement of Energy Balances of Noble Gas-Hydrogen Discharge Plasmas Using Calvet Calorimetry", Int. J. Hydrogen Energy, in press. From a solution of a Schrödinger-type wave equation with a nonradiative boundary condition based on Maxwell's equations, Mills predicts that atomic hydrogen may undergo a catalytic reaction with certain gaseous ions such as Ar^+ which ionize at integer multiples of the potential energy of atomic hydrogen, 27.2 eV . The reaction involves a nonradiative energy transfer to form a hydrogen atom that is lower in energy than unreacted atomic hydrogen with the release of energy. Upon the addition of 5% argon catalyst to a hydrogen plasma, the Lyman α emission was observed to increase by about an order of magnitude which indicated an increase in the plasma temperature; whereas, krypton control had no effect. Thus, the energy balances of argon-hydrogen glow discharge plasmas were measured using Calvet calorimetry. The steady state Calvet voltage significantly increased upon the addition of 3% hydrogen, and the output signal was integrated until the signal returned to baseline. An energy balance of over $-151,000\text{ kJ/mole }H_2$ was measured compared to the enthalpy of combustion of hydrogen of $-241.8\text{ kJ/mole }H_2$. Whereas, under identical conditions no change in the Calvet voltage was observed when hydrogen was added to a plasma of krypton which does not provide a reaction with a net enthalpy of a multiple of the potential energy of atomic hydrogen under these conditions.

THIS PAGE BLANK (USPS).

23. R. L. Mills, A. Voigt, P. Ray, M. Nansteel, B. Dhandapani, "Measurement of Hydrogen Balmer α Line Broadening and Thermal Power Balances of Noble Gas-Hydrogen Discharge Plasmas", Int. J. Hydrogen Energy, in press. Line broadening of the hydrogen Balmer lines provides a sensitive measure of the number and energy of excited hydrogen atoms in a glow discharge plasma. The width of the 656.5 nm Balmer α line emitted from gas discharge plasmas having atomized hydrogen from pure hydrogen alone, hydrogen with magnesium or strontium, a mixture of 10% hydrogen and helium, argon, krypton, or xenon, and a mixture of 10% hydrogen and helium or argon with strontium was measured with a high resolution ($\pm 0.025 \text{ nm}$) visible spectrometer. It was found that strontium-hydrogen, helium-hydrogen, argon-hydrogen, strontium-helium-hydrogen, and strontium-argon-hydrogen plasmas showed significant broadening corresponding to an average hydrogen atom temperature of $25\text{--}45 \text{ eV}$; whereas, pure hydrogen, krypton-hydrogen, xenon-hydrogen, and magnesium-hydrogen showed no excessive broadening corresponding to an average hydrogen atom temperature of $\approx 3 \text{ eV}$. Since line broadening is a measure of the plasma temperature, and a significant difference was observed between these noble gases, the power balances of gas discharge plasmas having atomized hydrogen from 1.) pure krypton alone, 2.) a mixture of hydrogen with argon or krypton and 3.) a mixture of hydrogen and helium or argon with vaporized strontium were measured. The power emitted for power supplied to the glow discharge increased by 35-83 W depending on the presence of helium or argon and less than 1% partial pressure of strontium metal in noble gas-hydrogen mixtures. Whereas, the chemically similar noble gas krypton alone or with hydrogen had no effect on the power balance. Catalyst atoms or ions which ionize at integer multiples of the potential energy of atomic hydrogen (Sr^+ , He^+ , or Ar^+) caused an increase in power; whereas, no excess power was observed in the case of krypton which does not provide a reaction with a net enthalpy of a multiple of the potential energy of atomic hydrogen under these conditions. For a power input to the glow discharge of 110 W, the excess output power of mixtures of strontium with argon-hydrogen (95/5%), strontium with hydrogen, strontium with helium-hydrogen (95/5%), and argon-hydrogen (95/5%) was 75, 58, 50, and 28 W, respectively, based a comparison of the temperature rise of the cell with krypton-hydrogen mixture (95/5%) and krypton alone. The input power was varied to find conditions that resulted in the optimal output for the strontium-hydrogen plasma. At 136 W input, the excess power

THIS PAGE BLANK (USPTO)

significantly increased to 184 W. These studies provide a useful comparison of catalysts for the optimization of the catalytic reaction of atomic hydrogen which represents an important new power source.

24. R. Mills, P. Ray, "Vibrational Spectral Emission of Fractional-Principal-Quantum-Energy-Level Hydrogen Molecular Ion", Int. J. Hydrogen Energy, in press. From a solution of a Schrödinger-type wave equation with a nonradiative boundary condition based on Maxwell's equations, Mills solves the hydrogen atom, the hydrogen molecular ion, the hydrogen molecule and predicts corresponding species having fractional principal quantum numbers. Atomic hydrogen may undergo a catalytic reaction with certain atomized elements and ions which singly or multiply ionize at integer multiples of the potential energy of atomic hydrogen, $m \cdot 27.2 \text{ eV}$ wherein m is an integer. The reaction involves a nonradiative energy transfer to form a hydrogen atom $H(1/p)$ that is lower in energy than unreacted atomic hydrogen that corresponds to a fractional principal quantum number ($n = \frac{1}{p} = \frac{1}{\text{integer}}$ replaces the well known parameter $n = \text{integer}$ in the Rydberg equation for hydrogen excited states). One such atomic catalytic system involves argon ions. The reaction Ar^+ to Ar^{2+} has a net enthalpy of reaction of 27.63 eV , which is equivalent to $m = 1$. Thus, it may serve as a catalyst to form $H(1/2)$. Also, the second ionization energy of helium is 54.4 eV ; thus, the ionization reaction of He^+ to He^{2+} has a net enthalpy of reaction of 54.4 eV which is equivalent to $2 \cdot 27.2 \text{ eV}$. The products of the catalysis reaction $H(1/3)$ may further serve as catalysts to form $H(1/4)$ and $H(1/2)$. $H(1/p)$ may react with a proton to form an excited state molecular ion $H_2^*(1/p)^+$ that has a bond energy and vibrational levels that are p^2 times those of the molecular ion comprising uncatalyzed atomic hydrogen where p is an integer. Thus, the excited state spectrum of $H_2^*[n = 1/4; n^* = 2]^+$ was predicted to comprise rotationally broadened vibrational transitions at 1.185 eV increments to the dissociation limit of $H_2[n = 1/4]^+$, $E_D = 42.88 \text{ eV}$ (28.92 nm). Extreme ultraviolet (EUV) spectroscopy was recorded on microwave discharges of argon or helium with 10% hydrogen in the range $10 - 65 \text{ nm}$. Novel emission lines assigned to vibrational transitions of $H_2^*[n = 1/4; n^* = 2]^+$ were observed in this range with energies of $\nu \cdot 1.185 \text{ eV}$, $\nu = 17$ to 38 that terminated at 28.9 nm . In addition, fractional molecular hydrogen rotational transitions were

THIS PAGE BLANK (USPTO)

assigned to previously unidentified lines in the Solar coronal spectrum that matched theoretical predictions to five figures.

25. R. Mills, P. Ray, "Spectral Emission of Fractional Quantum Energy Levels of Atomic Hydrogen from a Helium-Hydrogen Plasma and the Implications for Dark Matter", Int. J. Hydrogen Energy, Vol. 27, No. 3, (2002), pp. 301-322. From a solution of a Schrödinger-type wave equation with a nonradiative boundary condition based on Maxwell's equations, Mills predicts that atomic hydrogen may undergo a catalytic reaction with certain atomized elements and ions which singly or multiply ionize at integer multiples of the potential energy of atomic hydrogen, $m \cdot 27.2 \text{ eV}$ wherein m is an integer. The reaction involves a nonradiative energy transfer to form a hydrogen atom that is lower in energy than unreacted atomic hydrogen that corresponds to a fractional principal quantum number ($n = \frac{1}{p} = \frac{1}{\text{integer}}$ replaces the well known

parameter $n = \text{integer}$ in the Rydberg equation for hydrogen excited states). One such atomic catalytic system involves helium ions. The second ionization energy of helium is 54.4 eV ; thus, the ionization reaction of He^+ to He^{2+} has a net enthalpy of reaction of 54.4 eV which is equivalent to $2 \cdot 27.2 \text{ eV}$. Since the products of the catalysis reaction have binding energies of $m \cdot 27.2 \text{ eV}$, they may further serve as catalysts. Extreme ultraviolet (EUV) spectroscopy was recorded on microwave and glow discharges of helium with 2% hydrogen. Novel emission lines were observed with energies of $q \cdot 13.6 \text{ eV}$ where $q = 1, 2, 3, 4, 6, 7, 8, 9, \text{ or } 11$ or these lines inelastically scattered by helium atoms wherein 21.2 eV was absorbed in the excitation of $\text{He}(1s^2)$ to $\text{He}(1s^1 2p^1)$. These lines were identified as hydrogen transitions to electronic energy levels below the "ground" state corresponding to fractional quantum numbers. Furthermore, astrophysical data was reviewed and such transitions were found to match the spectral lines of the extreme ultraviolet background of interstellar space. They may resolve the paradox of the identity of dark matter and account for many celestial observations such as: diffuse H α emission is ubiquitous throughout the Galaxy and widespread sources of flux shortward of 912 \AA are required. Fractional hydrogen transitions were also assigned to unidentified lines in the Solar EUV spectrum which may resolve the solar neutrino problem, the mystery of the cause of sunspots and other solar activity, and why the Sun emits X-rays.

THIS PAGE BLANK (USPTO)

26. R. Mills, P. Ray, "Spectroscopic Identification of a Novel Catalytic Reaction of Potassium and Atomic Hydrogen and the Hydride Ion Product", Int. J. Hydrogen Energy, Vol. 27, No. 2, February, (2002), pp. 183-192. From a solution of a Schrödinger-type wave equation with a nonradiative boundary condition based on Maxwell's equations, Mills predicts that atomic hydrogen may undergo a catalytic reaction with certain atomized elements and ions which singly or multiply ionize at integer multiples of the potential energy of atomic hydrogen, 27.2 eV , $m \cdot 27.2\text{ eV}$ wherein m is an integer. The reaction involves a nonradiative energy transfer to form a hydrogen atom that is lower in energy than unreacted atomic hydrogen with the release of energy. One such atomic catalytic system involves potassium atoms. The first, second, and third ionization energies of potassium are 4.34066 eV , 31.63 eV , 45.806 eV , respectively. The triple ionization ($t = 3$) reaction of K to K^{3+} , then, has a net enthalpy of reaction of 81.7766 eV , which is equivalent to $3 \cdot 27.2\text{ eV}$. Intense extreme ultraviolet (EUV) emission was observed from incandescently heated atomic hydrogen and the atomized potassium catalyst that generated an anomalous plasma at low temperatures (e.g. $\approx 10^3\text{ K}$) and an extraordinary low field strength of about 1-2 V/cm. No emission was observed with potassium or hydrogen alone or when sodium replaced potassium with hydrogen. Emission was observed from K^{3+} that confirmed the resonant nonradiative energy transfer of $3 \cdot 27.2\text{ eV}$ from atomic hydrogen to atomic potassium. The catalysis product, a lower-energy hydrogen atom, was predicted to be a highly reactive intermediate which further reacts to form a novel hydride ion. The predicted hydride ion of hydrogen catalysis by atomic potassium is the hydride ion $H^- (1/4)$. This ion was observed spectroscopically at 110 nm corresponding to its predicted binding energy of 11.2 eV .

27. R. Mills, "BlackLight Power Technology-A New Clean Hydrogen Energy Source with the Potential for Direct Conversion to Electricity", Proceedings of the National Hydrogen Association, 12 th Annual U.S. Hydrogen Meeting and Exposition, *Hydrogen: The Common Thread*, The Washington Hilton and Towers, Washington DC, (March 6-8, 2001), pp. 671-697.

BlackLight Power, Inc. (the Company), a Delaware corporation based in its 53,000 sq. ft. headquarters in Cranbury, New Jersey, believes it has developed a new hydrogen chemical process that generates power, plasma (a hot ionized glowing gas), and a vast class of new

THIS PAGE BLANK (USPS) L

compositions of matter. Specifically, the Company has designed and tested a new proprietary energy-producing chemical process. The Company has developed high-power density, high-temperature, hydrogen gas cells that produce intense light, power orders of magnitude greater than that of the combustion of hydrogen at high temperatures, and power densities equal to those of many electric power plants. The Company is focusing on cells for generating light and plasma for lighting applications and direct conversion to electricity, respectively.

The cells generate energy through a chemical process (BlackLight Process) which the Company believes causes the electrons of hydrogen atoms to drop to lower orbits thus releasing energy in excess of the energy required to start the process. The lower-energy atomic hydrogen product of the BlackLight Process reacts with an electron to form a hydride ion which further reacts with elements other than hydrogen to form novel compounds called hydrino hydride compounds (HHCs) which are proprietary to the Company. The Company is developing the vast class of proprietary chemical compounds formed via the BlackLight Process. Its technology has far-reaching applications in many industries.

The power may be in the form of a plasma, a hot ionized glowing gas. The plasma may be converted directly to electricity with high efficiency, thus, avoiding a heat engine such as a turbine. The Company is working on direct plasma to electricity conversion. The device may be linearly scaleable from the size of hand held units to large units which could replace large turbines.

There are many advantages of the technology. The energy balance permits the use of electrolysis of water to split water into its elemental constituents of hydrogen and oxygen as the source of hydrogen fuel using a small fraction of the output electricity. Additionally, pollution produced by fossil and nuclear fuels should be eliminated since no green house gases, air pollutants, or hazardous wastes are produced. As no fossil fuels are required, the projected commercial operating costs are much less than that of any known competing energy source.

The Company's process may start with water as the hydrogen source and convert it to HHCs; whereas, fuel cells typically require a hydrocarbon fuel and an expensive reformer to convert hydrocarbons to hydrogen and carbon dioxide. The Company's plasma to electric conversion technology with no reformer, no fuel cost, creation of a valuable chemical by-product rather than pollutants or green house gases such as carbon dioxide, and significantly lower

THIS PAGE BLANK (USPTO)

Declaration of Dr. Randell L. Mills

Page 19 of 28

capital costs and operating and maintenance (O&M) costs are anticipated to result in household units that are competitive with central power and significantly superior to competing microdistributed power technologies such as fuel cells.

28. I declare further that all statements made herein of my own knowledge are true and that all statements made on information and belief are believed to be true; and further that these statements were made with the knowledge that willful false statements and the like so made are punishable by fine or imprisonment, or both, under Section 1001 of Title 18 of the United States Code and that such willful false statements may jeopardize the validity of the application or any patent issuing thereon.

By 

Dr. Randell L. Mills

Date: 1/21/02

THIS PAGE BLANK (USPTO)

Publications:

1. H. Conrads, R. Mills, Th. Wrubel, "Emission in the Deep Vacuum Ultraviolet from an Incandescently Driven Plasma in a Potassium Carbonate Cell", *Plasma Sources Science and Technology*, submitted.
2. R. L. Mills, P. Ray, "Stationary Inverted Lyman Population Formed from Incandescently Heated Hydrogen Gas with Certain Catalysts", *Chem. Phys. Letts.*, submitted.
3. R. L. Mills, B. Dhandapani, J. He, "Synthesis and Characterization of a Highly Stable Amorphous Silicon Hydride", *Int. J. Hydrogen Energy*, submitted.
4. R. L. Mills, A. Voigt, B. Dhandapani, J. He, "Synthesis and Characterization of Lithium Chloro Hydride", *Int. J. Hydrogen Energy*, submitted.
5. R. L. Mills, P. Ray, "Substantial Changes in the Characteristics of a Microwave Plasma Due to Combining Argon and Hydrogen", *New Journal of Physics*, submitted.
6. R. L. Mills, P. Ray, "High Resolution Spectroscopic Observation of the Bound-Free Hyperfine Levels of a Novel Hydride Ion Corresponding to a Fractional Rydberg State of Atomic Hydrogen", *Int. J. Hydrogen Energy*, in press.
7. R. L. Mills, E. Dayalan, "Novel Alkali and Alkaline Earth Hydrides for High Voltage and High Energy Density Batteries", *Proceedings of the 17th Annual Battery Conference on Applications and Advances*, California State University, Long Beach, CA, (January 15-18, 2002), in press.
8. R. Mayo, R. Mills, M. Nansteel, "On the Potential of Direct and MHD Conversion of Power from a Novel Plasma Source to Electricity for Microdistributed Power Applications", *IEEE Transactions on Plasma Science*, submitted.
9. R. Mills, P. Ray, J. Dong, M. Nansteel, W. Good, P. Jansson, B. Dhandapani, J. He, "Excessive Balmer α Line Broadening, Power Balance, and Novel Hydride Ion Product of Plasma Formed from Incandescently Heated Hydrogen Gas with Certain Catalysts", *Int. J. Hydrogen Energy*, submitted.
10. R. Mills, E. Dayalan, P. Ray, B. Dhandapani, J. He, "Highly Stable Novel Inorganic Hydrides from Aqueous Electrolysis and Plasma Electrolysis", *Japanese Journal of Applied Physics*, submitted.
11. R. L. Mills, P. Ray, B. Dhandapani, J. He, "Comparison of Excessive Balmer α Line Broadening of Glow Discharge and Microwave Hydrogen Plasmas with Certain Catalysts", *Chem. Phys.*, submitted.
12. R. L. Mills, P. Ray, B. Dhandapani, J. He, "Spectroscopic Identification of Fractional Rydberg States of Atomic Hydrogen", *J. of Phys. Chem. (letter)*, submitted.

THIS PAGE BLANK (USPTO)

13. R. L. Mills, P. Ray, B. Dhandapani, M. Nansteel, X. Chen, J. He, "New Power Source from Fractional Rydberg States of Atomic Hydrogen", Chem. Phys. Letts., submitted.
14. R. L. Mills, P. Ray, B. Dhandapani, M. Nansteel, X. Chen, J. He, "Spectroscopic Identification of Transitions of Fractional Rydberg States of Atomic Hydrogen", Quantitative Spectroscopy and Energy Transfer, submitted.
15. R. L. Mills, P. Ray, B. Dhandapani, M. Nansteel, X. Chen, J. He, "New Power Source from Fractional Quantum Energy Levels of Atomic Hydrogen that Surpasses Internal Combustion", Spectrochimica Acta, Part A, submitted.
16. R. L. Mills, P. Ray, "Spectroscopic Identification of a Novel Catalytic Reaction of Rubidium Ion with Atomic Hydrogen and the Hydride Ion Product", Int. J. Hydrogen Energy, in press.
17. R. Mills, J. Dong, W. Good, P. Ray, J. He, B. Dhandapani, "Measurement of Energy Balances of Noble Gas-Hydrogen Discharge Plasmas Using Calvet Calorimetry", Int. J. Hydrogen Energy, in press.
18. R. L. Mills, A. Voigt, P. Ray, M. Nansteel, B. Dhandapani, "Measurement of Hydrogen Balmer α Line Broadening and Thermal Power Balances of Noble Gas-Hydrogen Discharge Plasmas", Int. J. Hydrogen Energy, in press.
19. R. Mills, P. Ray, "Vibrational Spectral Emission of Fractional-Principal-Quantum-Energy-Level Hydrogen Molecular Ion", Int. J. Hydrogen Energy, in press.
20. R. Mills, P. Ray, "Spectral Emission of Fractional Quantum Energy Levels of Atomic Hydrogen from a Helium-Hydrogen Plasma and the Implications for Dark Matter", Int. J. Hydrogen Energy, Vol. 27, No. 3, pp. 301-322.
21. R. Mills, P. Ray, "Spectroscopic Identification of a Novel Catalytic Reaction of Potassium and Atomic Hydrogen and the Hydride Ion Product", Int. J. Hydrogen Energy, Vol. 27, No. 2, (2002), pp. 183-192.
22. R. Mills, "BlackLight Power Technology-A New Clean Hydrogen Energy Source with the Potential for Direct Conversion to Electricity", Proceedings of the National Hydrogen Association, 12 th Annual U.S. Hydrogen Meeting and Exposition, *Hydrogen: The Common Thread*, The Washington Hilton and Towers, Washington DC, (March 6-8, 2001), pp. 671-697.
23. R. Mills, W. Good, A. Voigt, Jinquan Dong, "Minimum Heat of Formation of Potassium Iodo Hydride", Int. J. Hydrogen Energy, Vol. 26, No. 11 (2001), pp. 1199-1208.
24. R. Mills, "Spectroscopic Identification of a Novel Catalytic Reaction of Atomic Hydrogen and the Hydride Ion Product", Int. J. Hydrogen Energy, Vol. 26, No. 10, (2001), pp. 1041-1058.
25. R. Mills, N. Greenig, S. Hicks, "Optically Measured Power Balances of Glow Discharges of Mixtures of Argon, Hydrogen, and Potassium, Rubidium, Cesium, or Strontium Vapor", Int. J. Hydrogen Energy, in press.

THIS PAGE BLANK (USPTO)

26. R. Mills, "The Grand Unified Theory of Classical Quantum Mechanics", Global Foundation, Inc. Orbis Scientiae entitled *The Role of Attractive and Repulsive Gravitational Forces in Cosmic Acceleration of Particles The Origin of the Cosmic Gamma Ray Bursts*, (29th Conference on High Energy Physics and Cosmology Since 1964) Dr. Behram N. Kursunoglu, Chairman, December 14-17, 2000, Lago Mar Resort, Fort Lauderdale, FL, Kluwer Academic/Plenum Publishers, New York, pp. 243-258.
27. R. Mills, "The Grand Unified Theory of Classical Quantum Mechanics", Int. J. Hydrogen Energy, in press.
28. R. Mills and M. Nansteel, P. Ray, "Argon-Hydrogen-Strontium Discharge Light Source", IEEE Transactions on Plasma Science, in press.
29. R. Mills, B. Dhandapani, M. Nansteel, J. He, A. "Voigt, Identification of Compounds Containing Novel Hydride Ions by Nuclear Magnetic Resonance Spectroscopy", Int. J. Hydrogen Energy, Vol. 26, No. 9 (2001), pp. 965-979.
30. R. Mills, "BlackLight Power Technology-A New Clean Energy Source with the Potential for Direct Conversion to Electricity", Global Foundation International Conference on "Global Warming and Energy Policy", Dr. Behram N. Kursunoglu, Chairman, Fort Lauderdale, FL, November 26-28, 2000, Kluwer Academic/Plenum Publishers, New York, pp. 1059-1096.
31. R. Mills, "The Nature of Free Electrons in Superfluid Helium--a Test of Quantum Mechanics and a Basis to Review its Foundations and Make a Comparison to Classical Theory", Int. J. Hydrogen Energy, Vol. 26, No. 10, (2001), pp. 1059-1096.
32. R. Mills, M. Nansteel, and Y. Lu, "Excessively Bright Hydrogen-Strontium Plasma Light Source Due to Energy Resonance of Strontium with Hydrogen", Plasma Chemistry and Plasma Processing, submitted.
33. R. Mills, J. Dong, Y. Lu, "Observation of Extreme Ultraviolet Hydrogen Emission from Incandescently Heated Hydrogen Gas with Certain Catalysts", Int. J. Hydrogen Energy, Vol. 25, (2000), pp. 919-943.
34. R. Mills, "Observation of Extreme Ultraviolet Emission from Hydrogen-KI Plasmas Produced by a Hollow Cathode Discharge", Int. J. Hydrogen Energy, Vol. 26, No. 6, (2001), pp. 579-592.
35. R. Mills, "Temporal Behavior of Light-Emission in the Visible Spectral Range from a Ti-K₂CO₃-H-Cell", Int. J. Hydrogen Energy, Vol. 26, No. 4, (2001), pp. 327-332.
36. R. Mills, T. Onuma, and Y. Lu, "Formation of a Hydrogen Plasma from an Incandescently Heated Hydrogen-Catalyst Gas Mixture with an Anomalous Afterglow Duration", Int. J. Hydrogen Energy, Vol. 26, No. 7, July, (2001), pp. 749-762.

THIS PAGE BLANK (USPTO)

37. R. Mills, M. Nansteel, and Y. Lu, "Observation of Extreme Ultraviolet Hydrogen Emission from Incandescently Heated Hydrogen Gas with Strontium that Produced an Anomalous Optically Measured Power Balance", Int. J. Hydrogen Energy, Vol. 26, No. 4, (2001), pp. 309-326.
38. R. Mills, *The Grand Unified Theory of Classical Quantum Mechanics*, September 2001 Edition, BlackLight Power, Inc., Cranbury, New Jersey, Distributed by Amazon.com.
39. R. Mills, B. Dhandapani, N. Greenig, J. He, "Synthesis and Characterization of Potassium Iodo Hydride", Int. J. of Hydrogen Energy, Vol. 25, No. 12 (2000), pp. 1185-1203.
40. R. Mills, "Novel Inorganic Hydride", Int. J. of Hydrogen Energy, Vol. 25, (2000), pp. 669-683.
41. R. Mills, B. Dhandapani, M. Nansteel, J. He, T. Shannon, A. Echezuria, "Synthesis and Characterization of Novel Hydride Compounds", Int. J. of Hydrogen Energy, Vol. 26, No. 4, (2001), pp. 339-367.
42. R. Mills, "Highly Stable Novel Inorganic Hydrides", Journal of New Materials for Electrochemical Systems, in press.
43. R. Mills, "Novel Hydrogen Compounds from a Potassium Carbonate Electrolytic Cell", Fusion Technology, Vol. 37, No. 2, March, (2000), pp. 157-182.
44. R. Mills, "The Hydrogen Atom Revisited", Int. J. of Hydrogen Energy, Vol. 25, No. 12 (2000), pp. 1171-1183.
45. Mills, R., Good, W., "Fractional Quantum Energy Levels of Hydrogen", Fusion Technology, Vol. 28, No. 4, November, (1995), pp. 1697-1719.
46. Mills, R., Good, W., Shaubach, R., "Dihydrido Molecule Identification", Fusion Technology, Vol. 25, 103 (1994).
47. R. Mills and S. Kneizys, Fusion Technol. Vol. 20, 65 (1991).
48. V. Noninski, Fusion Technol., Vol. 21, 163 (1992).
49. Niedra, J., Meyers, I., Fralick, G. C., and Baldwin, R., "Replication of the Apparent Excess Heat Effect in a Light Water-Potassium Carbonate-Nickel Electrolytic Cell, NASA Technical Memorandum 107167, February, (1996). pp. 1-20.; Niedra, J., Baldwin, R., Meyers, I., NASA Presentation of Light Water Electrolytic Tests, May 15, 1994.

Correspondence

1. R. Mills, Response to T. Ohta, Int J of Hydrogen Energy, Vol. 26, Issue 11, (2001), pp. 1225.
2. R. Mills, Response to I Shechtman, Int J of Hydrogen Energy, Vol. 26, Issue 11, (2001), pp. 1229–1231.
3. R. Mills, Response to A. K. Vijh, Int J of Hydrogen Energy, Vol. 26, Issue 11, (2001), pp. 1233.

THIS PAGE BLANK (USPTO)

Test Reports

Numerous test reports are available from BlackLight Power (e.g. Haldeman, C. W., Savoye, G. W., Iseler, G. W., Clark, H. R., MIT Lincoln Laboratories Excess Energy Cell Final report ACC Project 174 (3), April 25, 1995; Peterson, S., H., Evaluation of Heat Production from Light Water Electrolysis Cells of HydroCatalysis Power Corporation, Report from Westinghouse STC, 1310 Beulah Road, Pittsburgh, PA, February 25, 1994; Craw-Ivanco, M. T.; Tremblay, R. P.; Boniface, H. A.; Hilborn, J. W.; "Calorimetry for a Ni/K₂CO₃ Cell", Atomic Energy Canada Limited, Chemical Engineering Branch, Chalk River Laboratories, Chalk River, Ontario, June 1994; Nesterov, S. B., Kryukov, A. P., Moscow Power Engineering Institute Affidavit, February, 26, 1993; Jacox, M. G., Watts, G. R., "The Search for Excess Heat in the Mills Electrolytic Cell", Idaho National Engineering Laboratory, EG&G Idaho, Inc., Idaho Falls, Idaho, 83415, January 7, 1993; Gernert, N., Shaubach, R. M., Mills, R., Good, W., "Nascent Hydrogen: An Energy Source," Final Report prepared by Thermacore, Inc., for the Aero Propulsion and Power Directorate, Wright Laboratory, Air Force Material Command (ASC), Wright-Patterson Air Force Base, Contract Number F33615-93-C-2326, May, (1994); Phillips, J., Smith, J., Kurtz, S., "Report On Calorimetric Investigations Of Gas-Phase Catalyzed Hydrido Formation" Final report for Period October-December 1996", January 1, 1997, A Confidential Report submitted to BlackLight Power, Inc. provided by BlackLight Power, Inc., Great Valley Corporate Center, 41 Great Valley Parkway, Malvern, PA 19355; B. N. Popov, "Electrochemical Characterization of BlackLight Power, Inc. MH as Electrodes for Li-ion Batteries, Dept. of Chemical Engineering, University of South Carolina, February 6, 2000; Scores of Independent Tests of BlackLight Power's Novel Hydride Compounds from over 20 Independent Testing Laboratories.)

Upcoming Conference Presentations

1. R. L. Mills, J. Dong, J. He, B. Dhandapani, W. Good, A. Voigt, S. Hicks, M. Nansteel, E. Dayalan, P. Chandra, "Spectroscopic Identification of a Novel Catalytic Reaction of Hydrogen", Division of Inorganic Chemistry, Oral Presentation, 223rd ACS National Meeting, (April 7–11, 2002), Orlando, FL.
2. R. L. Mills, J. Dong, J. He, B. Dhandapani, W. Good, A. Voigt, S. Hicks, M. Nansteel, E. Dayalan, P. Chandra, "Novel Catalytic Reaction of Hydrogen as a Potential New Energy Source", Division of Inorganic Chemistry, Oral Presentation, 223rd ACS National Meeting, (April 7–11, 2002), Orlando, FL.

THIS PAGE BLANK (USPTO)

3. R. L. Mills, J. Dong, J. He, B. Dhandapani, W. Good, A. Voigt, S. Hicks, M. Nansteel, E. Dayalan, P. Chandra, "Novel Catalytic Reaction of Hydrogen as a Potential New Energy Source", Division of Industrial and Engineering Chemistry, Oral Presentation, 223rd ACS National Meeting, (April 7–11, 2002), Orlando, FL.
4. R. L. Mills, J. Dong, J. He, B. Dhandapani, W. Good, A. Voigt, S. Hicks, M. Nansteel, E. Dayalan, P. Chandra, "Novel Catalytic Reaction of Hydrogen as a Potential New Energy Source", Catalysis and Surface Science Secretariat, Oral Presentation, 223rd ACS National Meeting, (April 7–11, 2002), Orlando, FL.
5. R. L. Mills, J. Dong, J. He, B. Dhandapani, W. Good, A. Voigt, S. Hicks, M. Nansteel, E. Dayalan, P. Chandra, "Novel Catalytic Reaction of Hydrogen as a Potential New Energy Source", Division of Physical Chemistry, Poster Presentation, 223rd ACS National Meeting, (April 7–11, 2002), Orlando, FL.
6. R. L. Mills, J. Dong, J. He, B. Dhandapani, W. Good, A. Voigt, S. Hicks, M. Nansteel, E. Dayalan, P. Chandra, "Novel Catalytic Reaction of Hydrogen as a Potential New Energy Source", Division of Physical Chemistry, Sci-Mix Poster Presentation, 223rd ACS National Meeting, (April 7–11, 2002), Orlando, FL.
7. R. M. Mayo, R. L. Mills, M. Nansteel, "Direct Plasmadynamic Conversion of Plasma Thermal Power from a Novel Plasma Source to Electricity for Microdistributed Power Applications", 40th Power Sources Conference, (June 6–13, 2002), Cherry Hill, NJ.
8. R. L. Mills, E. Dayalan, "Novel Alkali and Alkaline Earth Hydrides for High Voltage and High Energy Density Batteries", Proceedings of the 17th Annual Battery Conference on Applications and Advances, California State University, Long Beach, CA, (January 15–18, 2002), in press.

Prior Conference Presentations

1. R. Mills, "Novel catalytic reaction of hydrogen as a potential new energy source", Division of Industrial and Engineering Chemistry; Session: Industrial Bio-Based Technology, 222nd American Chemical Society Fall National Meeting, (August 26–30, 2001), Chicago, IL.
2. R. Mills, "Spectroscopic identification of a novel catalytic reaction of hydrogen", Division of Inorganic Chemistry; Session: Catalysis, 222nd American Chemical Society Fall National Meeting, (August 26–30, 2001), Chicago, IL.
3. R. Mills, "Spectroscopic identification of a novel catalytic reaction of hydrogen", Division of Physical Chemistry; Session: Physical Chemistry Poster Session, 222nd American Chemical Society Fall National Meeting, (August 26–30, 2001), Chicago, IL.

THIS PAGE BLANK (USPTO)

4. P. Ray, R. Mills, "Spectroscopic identification of a novel catalytic reaction of hydrogen plasma", Session ET1: Lighting, American Physical Society Meeting, 54th Annual Gaseous Electronics Conference, October 9–12, 2001, Pennsylvania State University, State College, PA.
5. R. Mills, J. He, "Spectroscopic Identification of a Novel Catalytic Reaction of Atomic Hydrogen and the Hydride Ion Product", National Hydrogen Association, 12 th Annual U.S. Hydrogen Meeting and Exposition, *Hydrogen: The Common Thread*, The Washington Hilton and Towers, Washington DC, (March 6-8, 2001).
6. R. Mills, B. Dhandapani, M. Nansteel, N. Greenig, S. Hicks, J. Dong, "Optically Measured Power Balances of Anomalous Discharges of Mixtures of Argon, Hydrogen, and Potassium, Rubidium, Cesium, or Strontium Vapor", National Hydrogen Association, 12 th Annual U.S. Hydrogen Meeting and Exposition, *Hydrogen: The Common Thread*, The Washington Hilton and Towers, Washington DC, (March 6-8, 2001).
7. R. Mills, M. Nansteel, N. Greenig, S. Hicks, "BlackLight Power Technology-A New Clean Energy Source with the Potential for Direct Conversion to Electricity", National Hydrogen Association, 12 th Annual U.S. Hydrogen Meeting and Exposition, *Hydrogen: The Common Thread*, The Washington Hilton and Towers, Washington DC, (March 6-8, 2001).
8. R. Mills, B. Dhandapani, M. Nansteel, J. He, A. Voigt, "Identification of Compounds Containing Novel Hydride Ions by Nuclear Magnetic Resonance Spectroscopy", National Hydrogen Association, 12 th Annual U.S. Hydrogen Meeting and Exposition, *Hydrogen: The Common Thread*, The Washington Hilton and Towers, Washington DC, (March 6-8, 2001).
9. R. Mills, "BlackLight Power Technology-A New Clean Energy Source with the Potential for Direct Conversion to Electricity", *The 8 th Annual Emerald Groundhog Day Investment Forum*, February 1, 2001, Wyndham Franklin Plaza Hotel, Philadelphia, PA, Organized by Emerald Asset Management, Lancaster, PA.
10. R. Mills, "The Grand Unified Theory of Classical Quantum Mechanics", Global Foundation, Inc. Orbis Scientiae entitled *The Role of Attractive and Repulsive Gravitational Forces in Cosmic Acceleration of Particles The Origin of the Cosmic Gamma Ray Bursts*, (29th Conference on High Energy Physics and Cosmology Since 1964) Dr. Behram N. Kursunoglu, Chairman, December 14-17, 2000, Lago Mar Resort, Fort Lauderdale, FL.
11. R. Mills, "BlackLight Power Technology-A New Clean Energy Source with the Potential for Direct Conversion to Electricity", Global Foundation, Inc. conference entitled *Global Warming and Energy Policy*, Fort Lauderdale, FL, November 26-28, 2000.
12. R. Mills, B. Dhandapani, N. Greenig, J. He, J. Dong, Y. Lu, and H. Conrads, "Formation of an Energetic Plasma and Novel Hydrides from Incandescently Heated Hydrogen Gas with Certain

THIS PAGE BLANK (USPTO)

- Catalysts", August National ACS Meeting (220th ACS National Meeting, Washington, DC, (August 20-24, 2000)).
- 13. R. Mills, J. He, and B. Dhandapani, "Novel Alkali and Alkaline Earth Hydrides", August National ACS Meeting (220th ACS National Meeting, Washington, DC, (August 20-24, 2000)).
 - 14. R. Mills, B. Dhandapani, N. Greenig, J. He, J. Dong, Y. Lu, and H. Conrads, "Formation of an Energetic Plasma and Novel Hydrides from Incandescently Heated Hydrogen Gas with Certain Catalysts", June ACS Meeting (29th Northeast Regional Meeting, University of Connecticut, Storrs, CT, (June 18-21, 2000)).
 - 15. Mills, J. Dong, N. Greenig, and Y. Lu, "Observation of Extreme Ultraviolet Hydrogen Emission from Incandescently Heated Hydrogen Gas with Certain Catalysts", 219 th National ACS Meeting, San Francisco, California, (March 26-30, 2000).
 - 16. R. Mills, B. Dhandapani, N. Greenig, J. He, J. Dong, Y. Lu, and H. Conrads, "Formation of an Energetic Plasma and Novel Hydrides from Incandescently Heated Hydrogen Gas with Certain Catalysts", 219 th National ACS Meeting, San Francisco, California, (March 26-30, 2000).
 - 17. R. Mills, "Novel Hydride Compound", 219 th National ACS Meeting, San Francisco, California, (March 26-30, 2000).
 - 18. R. Mills, J. He, and B. Dhandapani, "Novel Alkali and Alkaline Earth Hydrides", 219 th National ACS Meeting, San Francisco, California, (March 26-30, 2000).
 - 19. R. Mills, J. Dong, N. Greenig, and Y. Lu, "Observation of Extreme Ultraviolet Hydrogen Emission from Incandescently Heated Hydrogen Gas with Certain Catalysts", National Hydrogen Association, 11 th Annual U.S. Hydrogen Meeting, Vienna, VA, (February 29-March 2, 2000).
 - 20. R. Mills, B. Dhandapani, N. Greenig, J. He, J. Dong, Y. Lu, and H. Conrads, "Formation of an Energetic Plasma and Novel Hydrides from Incandescently Heated Hydrogen Gas with Certain Catalysts", National Hydrogen Association, 11 th Annual U.S. Hydrogen Meeting, Vienna, VA, (February 29-March 2, 2000).
 - 21. R. Mills, "Novel Hydride Compound", National Hydrogen Association, 11 th Annual U.S. Hydrogen Meeting, Vienna, VA, (February 29-March 2, 2000).
 - 22. R. Mills, J. He, and B. Dhandapani, "Novel Alkali and Alkaline Earth Hydrides", National Hydrogen Association, 11 th Annual U.S. Hydrogen Meeting, Vienna, VA, (February 29-March 2, 2000).
 - 23. R. Mills, J. Dong, Y. Lu, J. Conrads, "Observation of Extreme Ultraviolet Hydrogen Emission from Incandescently Heated Hydrogen Gas with Certain Catalysts", 1999 Pacific Conference on Chemistry and Spectroscopy and the 35th ACS Western Regional Meeting, Ontario Convention Center, California, (October 6-8, 1999).

THIS PAGE BLANK (USPTO)

Declaration of Dr. Randell L. Mills

Page 28 of 28

24. R. Mills, "Novel Hydride Compound", 1999 Pacific Conference on Chemistry and Spectroscopy and the 35th ACS Western Regional Meeting, Ontario Convention Center, California, (October 6-8, 1999).
25. R. Mills, B. Dhandapani, N. Greenig, J. He, "Synthesis and Characterization of Potassium Iodo Hydride", 1999 Pacific Conference on Chemistry and Spectroscopy and the 35th ACS Western Regional Meeting, Ontario Convention Center, California, (October 6-8, 1999).
26. R. Mills, J. He, and B. Dhandapani, "Novel Hydrogen Compounds", 1999 Pacific Conference on Chemistry and Spectroscopy and the 35th ACS Western Regional Meeting, Ontario Convention Center, California, (October 6-8, 1999).
27. R. Mills, "Excess Heat Production by the Electrolysis of an Aqueous Potassium Carbonate Electrolyte", August 1991 meeting of the American Chemical Society, NY, NY.

Other publications:

A Novel Cancer Therapy Using a Mossbauer-Isotope Compound, Randell L. Mills, Carl W. Walter, Lata Venkataraman, Kevin Pang, John Farrell, Nature, 336,787, (1988).

On the Potentialities of Nuclear Gamma Resonance (Mossbauer Effect) Spectroscopy as a New, Low Dose Approach to Cancer Radiation Therapy, W.M. Reiff, R.L. Mills, J.J. Farrell, The Proceedings of the International Conference on the Applications of the Mossbauer Effect, ICAME 1989, Budapest, Hungary-Sept (Hyperfine Interactions 1990).

THIS PAGE BLANK (USPTO)

Attachment B

TABLE OF REFERENCES

1. H. Conrads, R. Mills, Th. Wrubel, "Emission in the Deep Vacuum Ultraviolet from an Incandescently Driven Plasma in a Potassium Carbonate Cell", *Plasma Sources Science and Technology*, submitted. [Copy provided in Attachment 70]
2. R. L. Mills, P. Ray, "Stationary Inverted Lyman Population Formed from Incandescently Heated Hydrogen Gas with Certain Catalysts", *Chem. Phys. Letts.*, submitted. [Copy provided in Attachment 71]
3. R. L. Mills, B. Dhandapani, J. He, "Synthesis and Characterization of a Highly Stable Amorphous Silicon Hydride", *Int. J. Hydrogen Energy*, submitted. [Copy provided in Attachment 72]
4. R. L. Mills, A. Voigt, B. Dhandapani, J. He, "Synthesis and Characterization of Lithium Chloro Hydride", *Int. J. Hydrogen Energy*, submitted. [Copy provided in Attachment 73]
5. R. L. Mills, P. Ray, "Substantial Changes in the Characteristics of a Microwave Plasma Due to Combining Argon and Hydrogen", *New Journal of Physics*, submitted. [Copy provided in Attachment 74]
6. [Purposely Omitted].
7. R. L. Mills, P. Ray, "High Resolution Spectroscopic Observation of the Bound-Free Hyperfine Levels of a Novel Hydride Ion Corresponding to a Fractional Rydberg State of Atomic Hydrogen", *Int. J. Hydrogen Energy*, in press. [Copy provided in Attachment 75]
8. R. L. Mills, E. Dayalan, "Novel Alkali and Alkaline Earth Hydrides for High Voltage and High Energy Density Batteries", *Proceedings of the 17th Annual Battery Conference on Applications and Advances*, California State University, Long Beach, CA, (January 15-18, 2002), in press. [Copy provided in Attachment 76]
9. R. Mayo, R. Mills, M. Nansteel, "On the Potential of Direct and MHD Conversion of Power from a Novel Plasma Source to Electricity for Microdistributed Power Applications", *IEEE Transactions on Plasma Science*, submitted. [Copy provided in Attachment 77]
10. R. Mills, P. Ray, J. Dong, M. Nansteel, W. Good, P. Jansson, B. Dhandapani, J. He, "Excessive Balmer α Line Broadening, Power Balance, and Novel Hydride Ion Product of Plasma Formed

THIS PAGE BLANK (USPTO)

- from Incandescently Heated Hydrogen Gas with Certain Catalysts", Int. J. Hydrogen Energy, submitted. [Copy provided in Attachment 78]
11. R. Mills, E. Dayalan, P. Ray, B. Dhandapani, J. He, "Highly Stable Novel Inorganic Hydrides from Aqueous Electrolysis and Plasma Electrolysis", Japanese Journal of Applied Physics, submitted. [Copy provided in Attachment 79]
12. R. L. Mills, P. Ray, B. Dhandapani, J. He, "Comparison of Excessive Balmer α Line Broadening of Glow Discharge and Microwave Hydrogen Plasmas with Certain Catalysts", Chem. Phys., submitted. [Copy provided in Attachment 80]
13. R. L. Mills, P. Ray, B. Dhandapani, J. He, "Spectroscopic Identification of Fractional Rydberg States of Atomic Hydrogen", J. of Phys. Chem. (letter), submitted. [Copy provided in Attachment 81]
14. R. L. Mills, P. Ray, B. Dhandapani, M. Nansteel, X. Chen, J. He, "New Power Source from Fractional Rydberg States of Atomic Hydrogen", Chem. Phys. Letts., submitted. [Copy provided in Attachment 82]
15. R. L. Mills, P. Ray, B. Dhandapani, M. Nansteel, X. Chen, J. He, "Spectroscopic Identification of Transitions of Fractional Rydberg States of Atomic Hydrogen", Quantitative Spectroscopy and Energy Transfer, submitted. [Copy provided in Attachment 83]
16. R. L. Mills, P. Ray, B. Dhandapani, M. Nansteel, X. Chen, J. He, "New Power Source from Fractional Quantum Energy Levels of Atomic Hydrogen that Surpasses Internal Combustion", Spectrochimica Acta, Part A, submitted. [Copy provided in Attachment 84]
17. R. L. Mills, P. Ray, "Spectroscopic Identification of a Novel Catalytic Reaction of Rubidium Ion with Atomic Hydrogen and the Hydride Ion Product", Int. J. Hydrogen Energy, in press. [Copy provided in Attachment 85]
18. R. Mills, J. Dong, W. Good, P. Ray, J. He, B. Dhandapani, "Measurement of Energy Balances of Noble Gas-Hydrogen Discharge Plasmas Using Calvet Calorimetry", Int. J. Hydrogen Energy, in press. [Copy provided in Attachment 86]
19. R. L. Mills, A. Voigt, P. Ray, M. Nansteel, B. Dhandapani, "Measurement of Hydrogen Balmer α Line Broadening and Thermal Power Balances of Noble Gas-Hydrogen Discharge Plasmas", Int. J. Hydrogen Energy, in press. [Copy provided in Attachment 87]

THIS PAGE BLANK (USPTO)

20. R. Mills, P. Ray, "Vibrational Spectral Emission of Fractional-Principal-Quantum-Energy-Level Hydrogen Molecular Ion", Int. J. Hydrogen Energy, in press. [Copy provided in Attachment 88]
21. R. Mills, P. Ray, "Spectral Emission of Fractional Quantum Energy Levels of Atomic Hydrogen from a Helium-Hydrogen Plasma and the Implications for Dark Matter", Int. J. Hydrogen Energy, Vol. 27, No. 3, (2002) pp. 301-322. [Copy provided in Attachment 89]
22. R. Mills, P. Ray, "Spectroscopic Identification of a Novel Catalytic Reaction of Potassium and Atomic Hydrogen and the Hydride Ion Product", Int. J. Hydrogen Energy, Vol. 27, No. 2, (2002), pp. 183-192. [Copy provided in Attachment 90]
23. R. Mills, "BlackLight Power Technology-A New Clean Hydrogen Energy Source with the Potential for Direct Conversion to Electricity", Proceedings of the National Hydrogen Association, 12 th Annual U.S. Hydrogen Meeting and Exposition, *Hydrogen: The Common Thread*, The Washington Hilton and Towers, Washington DC, (March 6-8, 2001), pp. 671-697. [Copy provided in Attachment 91]
24. R. Mills, W. Good, A. Voigt, Jinquan Dong, "Minimum Heat of Formation of Potassium Iodo Hydride", Int. J. Hydrogen Energy, Vol. 26, No. 11, (2001), pp. 1199-1208.
25. R. Mills, "Spectroscopic Identification of a Novel Catalytic Reaction of Atomic Hydrogen and the Hydride Ion Product", Int. J. Hydrogen Energy, Vol. 26, No. 10, (2001), pp. 1041-1058.
26. R. Mills, N. Greenig, S. Hicks, "Optically Measured Power Balances of Glow Discharges of Mixtures of Argon, Hydrogen, and Potassium, Rubidium, Cesium, or Strontium Vapor", Int. J. Hydrogen Energy, in press.
27. R. Mills, "The Grand Unified Theory of Classical Quantum Mechanics", Global Foundation, Inc. Orbis Scientiae entitled *The Role of Attractive and Repulsive Gravitational Forces in Cosmic Acceleration of Particles The Origin of the Cosmic Gamma Ray Bursts*, (29th Conference on High Energy Physics and Cosmology Since 1964) Dr. Behram N. Kursunoglu, Chairman, December 14-17, 2000, Lago Mar Resort, Fort Lauderdale, FL, Kluwer Academic/Plenum Publishers, New York, pp. 243-258. [Copy provided in Attachment 92]
28. R. Mills, "The Grand Unified Theory of Classical Quantum Mechanics", Int. J. Hydrogen Energy, in press. [Copy provided in Attachment 93]
29. R. Mills and M. Nansteel, P. Ray, "Argon-Hydrogen-Strontium Discharge Light Source", IEEE

THIS PAGE BLANK (USPTO)

Transactions on Plasma Science, in press.

30. R. Mills, B. Dhandapani, M. Nansteel, J. He, A. Voigt, "Identification of Compounds Containing Novel Hydride Ions by Nuclear Magnetic Resonance Spectroscopy", Int. J. Hydrogen Energy, Vol. 26, No. 9, (2001), pp. 965-979.
31. R. Mills, "BlackLight Power Technology-A New Clean Energy Source with the Potential for Direct Conversion to Electricity", Global Foundation International Conference on "Global Warming and Energy Policy", Dr. Behram N. Kursunoglu, Chairman, Fort Lauderdale, FL, November 26-28, 2000, Kluwer Academic/Plenum Publishers, New York, pp. 1059-1096. [Copy provided in Attachment 94]
32. R. Mills, "The Nature of Free Electrons in Superfluid Helium--a Test of Quantum Mechanics and a Basis to Review its Foundations and Make a Comparison to Classical Theory", Int. J. Hydrogen Energy, Vol. 26, No. 10, (2001), pp. 1059-1096. [Copy provided in Attachment 95]
33. R. Mills, M. Nansteel, and Y. Lu, "Excessively Bright Hydrogen-Strontium Plasma Light Source Due to Energy Resonance of Strontium with Hydrogen", Plasma Chemistry and Plasma Processing, submitted.
34. R. Mills, J. Dong, Y. Lu, "Observation of Extreme Ultraviolet Hydrogen Emission from Incandescently Heated Hydrogen Gas with Certain Catalysts", Int. J. Hydrogen Energy, Vol. 25, (2000), pp. 919-943.
35. R. Mills, "Observation of Extreme Ultraviolet Emission from Hydrogen-KI Plasmas Produced by a Hollow Cathode Discharge", Int. J. Hydrogen Energy, Vol. 26, No. 6, (2001), pp. 579-592.
36. R. Mills, "Temporal Behavior of Light-Emission in the Visible Spectral Range from a Ti-K₂CO₃-H-Cell", Int. J. Hydrogen Energy, Vol. 26, No. 4, (2001), pp. 327-332.
37. R. Mills, T. Onuma, and Y. Lu, "Formation of a Hydrogen Plasma from an Incandescently Heated Hydrogen-Catalyst Gas Mixture with an Anomalous Afterglow Duration", Int. J. Hydrogen Energy, Vol. 26, No. 7, (2001), pp. 749-762.
38. R. Mills, M. Nansteel, and Y. Lu, "Observation of Extreme Ultraviolet Hydrogen Emission from Incandescently Heated Hydrogen Gas with Strontium that Produced an Anomalous Optically Measured Power Balance", Int. J. Hydrogen Energy, Vol. 26, No. 4, (2001), pp. 309-326.
39. R. Mills, *The Grand Unified Theory of Classical Quantum Mechanics*, September 2001 Edition,

THIS PAGE BLANK (USPTO)

BlackLight Power, Inc., Cranbury, New Jersey, Distributed by Amazon.com. [Copy of book Attached]

40. R. Mills, B. Dhandapani, N. Greenig, J. He, "Synthesis and Characterization of Potassium Iodo Hydride", Int. J. of Hydrogen Energy, Vol. 25, No. 12, December, (2000), pp. 1185-1203.
41. R. Mills, "Novel Inorganic Hydride", Int. J. of Hydrogen Energy, Vol. 25, (2000), pp. 669-683.
42. R. Mills, B. Dhandapani, M. Nansteel, J. He, T. Shannon, A. Echezuria, "Synthesis and Characterization of Novel Hydride Compounds", Int. J. of Hydrogen Energy, Vol. 26, No. 4, (2001), pp. 339-367.
43. R. Mills, "Highly Stable Novel Inorganic Hydrides", Journal of New Materials for Electrochemical Systems, in press.
44. R. Mills, "Novel Hydrogen Compounds from a Potassium Carbonate Electrolytic Cell", Fusion Technology, Vol. 37, No. 2, March, (2000), pp. 157-182.
45. R. Mills, "The Hydrogen Atom Revisited", Int. J. of Hydrogen Energy, Vol. 25, No. 12, (2000), pp. 1171-1183. [Copy provided in Attachment 96]
46. R. Mills, W. Good, "Fractional Quantum Energy Levels of Hydrogen", Fusion Technology, Vol. 28, No. 4, November, (1995), pp. 1697-1719.
47. R. Mills, W. Good, R. Shaubach, "Dihydrido Molecule Identification", Fusion Technology, Vol. 25, 103 (1994).
48. R. Mills and S. Kneizys, Fusion Technol. Vol. 20, 65 (1991).
49. Haus, H. A., "On the radiation from point charges", American Journal of Physics, 54, (1986), pp. 1126-1129.
50. H. J. Maris, Journal of Low Temperature Physics, Vol. 120, (2000), p. 173.
51. C. A. Fuchs and A. Peres, "Quantum Theory Needs No "Interpretation", Physics Today, March (2000), p. 70.
52. F. Dyson, "Feynman's proof of Maxwell equations", Am. J. Phys., Vol. 58, (1990), pp. 209-211.
53. J. Horgan, "Quantum Philosophy", Scientific American, July, (1992), pp. 94-104.
54. M. M. Waldrop, Science, Vol. 242, December, 2, (1988), pp. 1248-1250.
55. S. Durr, T. Nonn, G. Rempe, Nature, September 3, (1998), Vol. 395, pp. 33-37.

THIS PAGE BLANK (USPTO)

56. R. L. Finney, D. R. Ostberg, R. G. Kuller, *Elementary Differential Equations*, Addison-Wesley Publishing Company, Reading Massachusetts., (1976), Chp. 7.
57. H. Margenau, G. M. Murphy, *The Mathematics of Chemistry and Physics*, D. Van Nostrand Company, Inc., New York, (1943), pp. 77-78.
58. Niedra, J., Meyers, I., Fralick, G. C., and Baldwin, R., "Replication of the Apparent Excess Heat Effect in a Light Water-Potassium Carbonate-Nickel Electrolytic Cell, NASA Technical Memorandum 107167, February, (1996). pp. 1-20.; Niedra, J., Baldwin, R., Meyers, I., NASA Presentation of Light Water Electrolytic Tests, May 15, 1994.
59. V. Noninski, *Fusion Technol.*, Vol. 21, 163 (1992).
60. F. Laloë, Do we really understand quantum mechanics? Strange correlations, paradoxes, and theorems, *Am. J. Phys.* 69 (6), June 2001, 655-701.
61. N. V. Sidgwick, *The Chemical Elements and Their Compounds*, Volume I, Oxford, Clarendon Press, (1950).
62. M. D. Lamb, *Luminescence Spectroscopy*, Academic Press, London, (1978).
63. L. I. Ponomarev, "Muon catalyzed fusion", *Contemporary Physics*, Vol. 31, No. 4, (1990), pp. 219-245.
64. J. Zmeskal, P. Kammel, A. Scrinzi, W. H. Breunlich, M. Cargnelli, J. Marton, N. Nagele, J. Werner, W. Bertl, and C. Petitjean, "Muon-catalyzed dd fusion between 25 and 150 K: experiment," *Phys. Rev. A*, Vol. 42, (1990), pp. 1165-1177.
65. D. A. McQuarrie, *Quantum Chemistry*, University Science Books, Mill Valley, CA, (1983).
66. A. Einstein, *Phys. Z.*, Vol. 18, (1917), 121.
67. A. L. Schawlow and C. H. Townes, *Phys. Rev.*, (112), (1958), pp. 1940-1949.
68. "The Interview Carver Meade", *The American Spectator*, September/October, (2001), www.gilder.com/AmericanSpectatorArticles/carver.htm.
69. S. Patz, *Cardiovasc Interven Radiol.*, (1986), 8:25, pp. 225-237.
70. T. A. Abbott, D. J. Griffiths, *Am. J. Phys.*, Vol. 153, No. 12, (1985), pp. 1203-1211.
71. L. C. Shi, J. A.; J. Daboul and J. H. D. Jensen, *Z. Physik*, Vol. 265, (1973), pp. 455-478.
72. P. Pearle, "Classical electron Models", *Electromagnetism: Paths to Research*, edited by D. Teplitz, Plenum, New York, Chp. 7 Pt 6, *Radiationless Motion*" (1982), pp. 237-240.

THIS PAGE BLANK (USPTO)

73. G. Goedecke, Phys. Rev., Vol. 135B, (1964), pp. 281-288.
74. J. D. Jackson, Classical Electrodynamics, Second Edition, John Wiley & Sons, New York, (1962), p. 111.
75. W. Kolos and L. Wolniewicz, J. Chem. Phys., Vol. 41, (1964), p. 3663; Vol. 49, (1968).
76. P. W. Atkins, Physical Chemistry, Second Edition, W. H. Freeman, San Francisco, (1982).
77. M. Karplus and R. N. Porter, *Atoms and Molecules an Introduction for Students of Physical Chemistry*, The Benjamin/Cummings Publishing Company, Menlo Park, California, (1970).
78. A. Beiser, *Concepts of Modern Physics*, Fourth Edition, McGraw-Hill Book Company, New York, (1978).
79. R. Mills, *The Grand Unified Theory of Classical Quantum Mechanics*, January 2000 Edition, BlackLight Power, Inc., Cranbury, New Jersey, Distributed by Amazon.com.
80. N. A. Bahcall, J. P. Ostriker, S. Perlmutter, P. J. Steinhardt, Science, May 28, 1999, Vol. 284, pp. 1481-1488.
81. See R. Mills, *The Grand Unified Theory of Classical Quantum Mechanics*, November 1995 Edition.
82. Jang-Jung Lee, Charles Evans & Associates Time-Of-Flight Secondary Ion Mass Spectroscopy (TOF-SIMS) Surface Analysis Report, CE&A Number 40150, March 18, 1994.
83. H. Wiesmann, Brookhaven National Laboratory, Department of Applied Science, Letter to Dr. Walter Polansky of the Department of Energy Regarding Excess Energy Verification at Brookhaven National Laboratory, October 16, 1991.
84. Keith Keefer, Ph.D., "Interim Report on BlackLight Power Technology: Its Apparent Scientific Basis, State of Development and Suitability for Commercialization by Liebert Corporation." [Copy provided in Attachment 97]
85. David R. Linde, *CRC Handbook of Chemistry and Physics*, 79 th Edition, CRC Press, Boca Raton, Florida, (1998-9), p. 10-175 to p. 10-177.

THIS PAGE BLANK (USPTO,

Affidavits, Publications and Reports

Dr. Randell L. Mills
BlackLight Power, Inc.

Part I of 2

1. R. Mills, W. Good, A. Voigt, Jinquan Dong, Minimum Heat of Formation of Potassium Iodo Hydride, Int. J. Hydrogen Energy, submitted.

It was previously reported [R. Mills, B. Dhandapani, N. Greenig, J. He, "Synthesis and Characterization of Potassium Iodo Hydride", Int. J. of Hydrogen Energy, Vol. 25, Issue 12, December, (2000), pp. 1185-1203.] that a novel inorganic hydride compound *KHI* which comprised a high binding energy hydride ion was synthesized by reaction of atomic hydrogen with potassium metal and potassium iodide. Potassium iodo hydride was identified by time of flight secondary ion mass spectroscopy, X-ray photoelectron spectroscopy, 1H and ^{39}K nuclear magnetic resonance spectroscopy, Fourier transform infrared spectroscopy, electrospray ionization time of flight mass spectroscopy, liquid chromatography/mass spectroscopy, thermal decomposition with analysis by gas chromatography, and mass spectroscopy, and elemental analysis. We report measurements of heats of formation of *KHI* by differential scanning calorimetry (DSC) on a very reliable commercial instrument, a Setaram HT 1000 DSC. With reactant *KI* present, potassium metal catalyst and atomic hydrogen were produced by decomposition of *KH* at an extremely slow rate under a helium atmosphere to increase the amount of atomic hydrogen by slowing the rate of molecular hydrogen formation. Since not all of the starting materials reacted, the observed minimum heats of formation were over -2000 kJ / mole H_2 , compared to the enthalpy of combustion of hydrogen of -241.8 kJ / mole H_2 .

2. R. Mills, "Spectroscopic Identification of a Novel Catalytic Reaction of Atomic Hydrogen and the Hydride Ion Product", Int. J. Hydrogen Energy, submitted.

From a solution of a Schrödinger-type wave equation with a nonradiative boundary condition based on Maxwell's equations, Mills predicts that atomic hydrogen may undergo a catalytic reaction with certain atomized elements such as cesium and strontium atoms or certain gaseous ions such as Ar^+ which singly or multiply ionize at integer multiples of the potential energy of atomic hydrogen, 27.2 eV. The reaction involves a nonradiative energy transfer to form a hydrogen atom that is lower in energy than unreacted atomic hydrogen with the release of energy. Intense extreme

THIS PAGE BLANK (USPTO)

ultraviolet (EUV) emission was observed from incandescently heated atomic hydrogen and the atomized catalysts that generated the plasma at low temperatures (e.g. $\approx 10^3 K$). No emission was observed with cesium, strontium, argon, hydrogen, or an argon-hydrogen mixture (97/3%) alone or when sodium, magnesium, or barium replaced strontium or cesium with hydrogen or with an argon-hydrogen mixture. The emission intensity of the plasma generated by the cesium or strontium catalyst increased significantly with the introduction of argon gas only when Ar^+ emission was observed. Ar^+ which served as a second catalyst was generated by the formation of a plasma with cesium or strontium catalyst. Emission was observed from a continuum state of Cs^{2+} and Ar^{2+} at $53.3 nm$ and $45.6 nm$, respectively. The single emission feature with the absence of the other corresponding Rydberg series of lines from these species confirmed the resonate nonradiative energy transfer of $27.2 eV$ from atomic hydrogen to atomic cesium or Ar^+ . The catalysis product, a lower-energy hydrogen atom, was predicted to be a highly reactive intermediate which further reacts to form a novel hydride ion. The predicted hydride ion of hydrogen catalysis by either cesium atom or Ar^+ catalyst is the hydride ion $H^{-}(1/2)$. This ion was observed spectroscopically at $407 nm$ corresponding to its predicted binding energy of $3.05 eV$.

3. R. Mills, N. Greenig, S. Hicks, "Optically Measured Power Balances of Anomalous Discharges of Mixtures of Argon, Hydrogen, and Potassium, Rubidium, Cesium, or Strontium Vapor", Int. J. Hydrogen Energy, submitted.

The power balances of gas cells having atomized hydrogen from pure hydrogen alone, an argon-hydrogen mixture alone, or pure hydrogen or an argon-hydrogen mixture with vaporized potassium, rubidium, cesium, strontium, sodium, or magnesium were measured by integrating the total light output corrected for spectrometer system response and energy over the visible range. The light emitted for power supplied to the glow discharge increased by over two orders of magnitude depending on the presence of less than 1% partial pressure of certain of the alkali or alkaline earth metals in hydrogen gas or argon-hydrogen gas mixtures. Whereas, other chemically similar metals had no effect on the plasma. The metal vapor enhancement of the emission was dramatically greater with an argon-hydrogen mixture versus pure hydrogen, and a 97 % argon and 3 % hydrogen mixture had greater emission than either gas alone. Only those atoms or ions which ionize at integer multiples of the potential energy of atomic hydrogen, potassium, cesium, Rb^+ , strontium, and Ar^+ caused an increase in emission; whereas, no anomalous behavior was observed in the case of $Mg(m)$ and $Na(m)$ which do not provide a reaction with a net

THIS PAGE BLANK (USPTO)

enthalpy of a multiple of the potential energy of atomic hydrogen. The light intensity versus power input of a mixture of these metals with hydrogen, argon, or argon-hydrogen gas was the same as that of the corresponding gas alone. At an input power to the glow discharge of 10 watts, the optically measured light output power of a mixture of strontium, cesium, potassium, and rubidium with 97 % argon and 3 % hydrogen was 750, 70, 25, 15, and $10 \mu\text{W/cm}^2$, respectively. Whereas, the optically measured light output power of sodium or magnesium with 97 % argon and 3 % hydrogen was about $5 \mu\text{W/cm}^2$, and the result for hydrogen or argon gas alone was $1.5 \mu\text{W/cm}^2$. A temperature dependence of some of the anomalous plasmas was determined corresponding to the partial pressure dependence of the metal. These studies provide useful parameters for the optimization of the catalytic reaction of atomic hydrogen.

4. R. Mills, "The Grand Unified Theory of Classical Quantum Mechanics", Global Foundation, Inc. Orbis Scientiae entitled The Role of Attractive and Repulsive Gravitational Forces in Cosmic Acceleration of Particles The Origin of the Cosmic Gamma Ray Bursts, (29th Conference on High Energy Physics and Cosmology Since 1964) Dr. Behram N. Kursunoglu, Chairman, December 14-17, 2000, Lago Mar Resort, Fort Lauderdale, FL, in press.

A theory of classical quantum mechanics (CQM), derived from first principles [1], successfully applies physical laws on all scales. The classical wave equation is solved with the constraint that a bound electron cannot radiate energy. The mathematical formulation for zero radiation based on Maxwell's equation's follows from a derivation by Haus [2]. The function that describes the motion of the electron must not possess spacetime Fourier components that are synchronous with waves traveling at the speed of light. CQM gives closed form solutions for the atom including the stability of the n=1 state and the instability of the excited states, the equation of the photon and electron in excited states, the equation of the free electron, and photon which predict the wave particle duality behavior of particles and light. The current and charge density functions of the electron may be directly physically interpreted. For example, spin angular momentum results from the motion of negatively charged mass moving systematically, and the equation for angular momentum, $r \times p$, can be applied directly to the wave function (a current density function) that describes the electron. The magnetic moment of a Bohr magneton, Stern Gerlach experiment, g factor, Lamb shift, resonant line width and shape, selection rules, correspondence principle, wave particle duality, excited states, reduced mass, rotational energies, and momenta, orbital and spin splitting, spin-orbital coupling, Knight shift, and spin-nuclear coupling

THIS PAGE BLANK (USPTO)

are derived in closed form equations based on Maxwell's equations. The calculations agree with experimental observations.

For or any kind of wave advancing with limiting velocity and capable of transmitting signals, the equation of front propagation is the same as the equation for the front of a light wave. By applying this condition to electromagnetic and gravitational fields at particle production, the Schwarzschild metric (SM) is derived from the classical wave equation which modifies general relativity to include conservation of spacetime in addition to momentum and matter/energy. The result gives a natural relationship between Maxwell's equations, special relativity, and general relativity. It gives gravitation from the atom to the cosmos. The universe is time harmonically oscillatory in matter energy and spacetime expansion and contraction with a minimum radius that is the gravitational radius. In closed form equations with fundamental constants only, CQM gives the deflection of light by stars, the precession of the perihelion of Mercury, the particle masses, the Hubble constant, the age of the universe, the observed acceleration of the expansion, the power of the universe, the power spectrum of the universe, the microwave background temperature, the uniformity of the microwave background radiation, the microkelvin spatial variation of the microwave background radiation, the observed violation of the GZK cutoff, the mass density, the large scale structure of the universe, and the identity of dark matter which matches the criteria for the structure of galaxies. In a special case wherein the gravitational potential energy density of a blackhole equals that of the Plank mass, matter converts to energy and spacetime expands with the release of a gamma ray burst. The singularity in the SM is eliminated.

5. R. Mills, "The Grand Unified Theory of Classical Quantum Mechanics", II
Nuovo Cimento, submitted.

A theory of classical quantum mechanics (CQM) is derived from first principles that successfully applies physical laws on all scales. Using Maxwell's equations, the classical wave equation is solved with the constraint that a bound electron cannot radiate energy. By further application of Maxwell's equations to electromagnetic and gravitational fields at particle production, the Schwarzschild metric (SM) is derived from the classical wave equation which modifies general relativity to include conservation of spacetime in addition to momentum and matter/energy. The result gives a natural relationship between Maxwell's equations, special relativity, and general relativity. It gives gravitation from the atom to the cosmos.

THIS PAGE BLANK (USPTO)

**6. R. Mills and M. Nansteel, "Anomalous Argon-Hydrogen-Strontium Discharge",
IEEE Transactions of Plasma Science, submitted.**

We report the observation of intense extreme ultraviolet (EUV) emission from incandescently heated atomic hydrogen and atomized strontium that increased with argon. Typically the emission of extreme ultraviolet light from hydrogen gas is achieved via a discharge at high voltage, a high power inductively coupled plasma, or a plasma created and heated to extreme temperatures by RF coupling (e.g. $>10^6 K$) with confinement provided by a toroidal magnetic field. The observed plasma formed at low temperatures (e.g. $\approx 10^3 K$) from atomic hydrogen generated at a tungsten filament that heated a titanium dissociator and atomic strontium which was vaporized from the metal by heating. The emission intensity of the plasma generated by atomic strontium increased significantly with the introduction of argon gas only when Ar^+ emission was observed. No emission was observed with hydrogen when sodium, magnesium, or barium replaced strontium or with hydrogen, hydrogen-argon mixtures, or strontium alone. The power balance of a gas cell having vaporized strontium and atomized hydrogen from pure hydrogen or argon-hydrogen mixture (77/23%) was measured by integrating the total light output corrected for spectrometer system response and energy over the visible range. Hydrogen control cell experiments were identical except that sodium, magnesium, or barium replaced strontium. In the case of hydrogen-sodium, hydrogen-magnesium, and hydrogen-barium mixtures, 4000, 7000, and 6500 times the power of the hydrogen-strontium mixture was required, respectively, in order to achieve that same optically measured light output power. With the addition of argon to the hydrogen-strontium plasma, the power required to achieve that same optically measured light output power was reduced by a factor of about two. The power required to maintain a plasma of equivalent optical brightness with strontium atoms present was 8600 and 6300 times less than that required for argon-hydrogen and argon control, respectively. A plasma formed at a cell voltage of about 250 V for hydrogen alone and sodium-hydrogen mixtures, 140-150 V for hydrogen-magnesium and hydrogen-barium mixtures, 224 V for an argon-hydrogen mixture, and 190 V for argon alone; whereas, a plasma formed for hydrogen-strontium mixtures and argon-hydrogen-strontium mixtures at extremely low voltages of about 2 V and 6.6 V, respectively.

**7. R. Mills, B. Dhandapani, M. Nansteel, J. He, A. Voigt, Identification of
Compounds Containing Novel Hydride Ions by Nuclear Magnetic Resonance
Spectroscopy, Int. J. Hydrogen Energy, submitted.**

THIS PAGE BLANK (USPTO)

Novel inorganic alkali and alkaline earth hydrides of the formula MH^+ , MH_2^+ , and MH^+X wherein M is the metal, X is a halide, and H^+ comprises a novel high binding energy hydride ion were synthesized in a high temperature gas cell by reaction of atomic hydrogen with a catalyst and MH , MH_2 , or MX corresponding to an alkali metal or alkaline earth metal compound, respectively. Novel hydride ions of the corresponding novel hydride compounds were characterized by an extraordinary upfield shifted peak observed by 1H nuclear magnetic resonance spectroscopy.

8. R. Mills, "BlackLight Power Technology-A New Clean Energy Source with the Potential for Direct Conversion to Electricity", Global Foundation International Conference on "Global Warming and Energy Policy", Dr. Behram N. Kursunoglu, Chairman, Fort Lauderdale, FL, November 26-28, 2000, in press.

BlackLight Power, Inc. (the Company), a Delaware corporation based in its 53,000 sq. ft. headquarters in Cranbury, New Jersey, believes it has developed a new hydrogen chemical process that generates power, plasma (a hot ionized glowing gas), and a vast class of new compositions of matter. Specifically, the Company has designed and tested a new proprietary energy-producing chemical process. The Company has developed high-power density, high-temperature, hydrogen gas cells that produce intense light, power of orders of magnitude greater than that of the combustion of hydrogen at high temperatures, and power densities equal to those of many electric power plants. The Company is focusing on cells for generating light and plasma for lighting applications and direct conversion to electricity, respectively.

The cells generate energy through a chemical process (BlackLight Process) which the Company believes causes the electrons of hydrogen atoms to drop to lower orbits thus releasing energy in excess of the energy required to start the process. The lower-energy atomic hydrogen product of the BlackLight Process reacts with an electron to form a hydride ion which further reacts with elements other than hydrogen to form novel compounds called hydrino hydride compounds (HHCs) which are proprietary to the Company. The Company is developing the vast class of proprietary chemical compounds formed via the BlackLight Process. Its technology has far-reaching applications in many industries.

The power may be in the form of a plasma, a hot ionized glowing gas. The plasma may be converted directly to electricity with high efficiency using a known microwave device called a gyrotron, thus, avoiding a heat engine such as a turbine. The Company is working on direct plasma to electricity conversion. The device is

THIS PAGE BLANK (USPTO)

linearly scaleable from the size of hand held units to large units which could replace large turbines.

There are many advantages of the technology. The energy balance permits the use of electrolysis of water to split water into its elemental constituents of hydrogen and oxygen as the source of hydrogen fuel using a small fraction of the output electricity. Additionally, pollution produced by fossil and nuclear fuels should be eliminated since no green house gases, air pollutants, or hazardous wastes are produced. As no fossil fuels are required, the projected commercial operating costs are much less than that of any known competing energy source.

The Company's process may start with water as the hydrogen source and convert it to HHCs; whereas, fuel cells typically require a hydrocarbon fuel and an expensive reformer to convert hydrocarbons to hydrogen and carbon dioxide. The Company's plasma to electric conversion technology with no reformer, no fuel cost, creation of a valuable chemical by-product rather than pollutants such as carbon dioxide, and significantly lower capital costs and operating and maintenance (O&M) costs are anticipated to result in household units that are competitive with central power and significantly superior to competing microdistributed power technologies such as fuel cells.

9. R. Mills, The Nature of Free Electrons in Superfluid Helium--a Test of Quantum Mechanics and a Basis to Review its Foundations and Make a Comparison to Classical Theory, Int. J. Hydrogen Energy, submitted.

The Schrödinger equation was originally postulated in 1926 as having a solution of the one electron atom. It gives the principal energy levels of the hydrogen atom as eigenvalues of eigenfunction solutions of the Laguerre differential equation. But, as the principal quantum number $n \gg 1$, the eigenfunctions become nonsensical. Despite its wide acceptance, on deeper inspection, the Schrödinger solution is plagued with many failings as well as difficulties in terms of a physical interpretation that have caused it to remain controversial since its inception. Only the one electron atom may be solved without approximations, but it fails to predict electron spin and leads to models with nonsensical consequences such as negative energy states of the vacuum, infinities, and negative kinetic energy. In addition to many predictions which simply do not agree with observations, the Schrödinger equation predicts noncausality, nonlocality, spook actions at a distance or quantum telepathy, perpetual motion, and many internal inconsistencies where contradicting statements have to be taken true simultaneously. Recently, the behavior of free electrons in superfluid

THIS PAGE BLANK (USPTO)

helium has again forced the issue of the meaning of the wavefunction. Electrons form bubbles in superfluid helium which reveal that the electron is real and that a physical interpretation of the wavefunction is necessary. Furthermore, when irradiated with light of energy of about a 0.5 to several electron volts [1], the electrons carry current at different rates as if they exist with different sizes. It has been proposed that the behavior of free electrons in superfluid helium can be explained in terms of the electron breaking into pieces at superfluid helium temperatures [1]. Yet, the electron has proven to be indivisible even under particle accelerator collisions at 90 GeV (LEPII). The nature of the wavefunction must now be addressed. It is time for the physical rather than the mathematical nature of the wavefunction to be determined. A theory of classical quantum mechanics (CQM) was derived from first principles by Mills [2] that successfully applies physical laws on all scales. Using the classical wave equation with the constraint of nonradiation based on Maxwell's equations, CQM gives closed form physical solutions for the electron in atoms, the free electron, and the free electron in superfluid helium. The prediction of fractional principal quantum energy states of the electron in liquid helium match the photoconductivity and mobility observations without requiring that the electron is divisible.

10. R. Mills, M. Nansteel, and Y. Lu, "Anomalous Hydrogen-Strontium Discharge", European Journal of Physics D, submitted.

We report the observation of intense extreme ultraviolet (EUV) emission from incandescently heated atomic hydrogen and atomized strontium. Typically the emission of extreme ultraviolet light from hydrogen gas is achieved via a discharge at high voltage, a high power inductively coupled plasma, or a plasma created and heated to extreme temperatures by RF coupling (e.g. $>10^6 K$) with confinement provided by a toroidal magnetic field. The observed plasma formed at low temperatures (e.g. $\approx 10^3 K$) from atomic hydrogen generated at a tungsten filament that heated a titanium dissociator and atomic strontium which was vaporized from the metal by heating. No emission was observed when sodium, magnesium, or barium replaced strontium or with hydrogen or strontium alone. The power balance of a gas cell having atomized hydrogen and strontium was measured by integrating the total light output corrected for spectrometer system response and energy over the visible range. Control cell experiments were identical except that sodium, magnesium, or barium replaced strontium. In the case of hydrogen-sodium, hydrogen-magnesium, and hydrogen-barium mixtures, 4000, 7000, and 6500 times the power of the hydrogen-strontium mixture was required, respectively, in order to achieve that same

THIS PAGE BLANK (USPTO)

optically measured light output power. A plasma formed at a cell voltage of about 250 V for hydrogen alone and sodium-hydrogen mixtures, and 140-150 V for hydrogen-magnesium and hydrogen-barium mixtures; whereas, a plasma formed for hydrogen-strontium mixtures at an extremely low voltage of about 2 V.

11. R. Mills, J. Dong, Y. Lu, "Observation of Extreme Ultraviolet Hydrogen Emission from Incandescently Heated Hydrogen Gas with Certain Catalysts", *Int. J. Hydrogen Energy*, Vol. 25, (2000), pp. 919-943.

Typically the emission of extreme ultraviolet light from hydrogen gas is achieved via a discharge at high voltage, a high power inductively coupled plasma, or a plasma created and heated to extreme temperatures by RF coupling (e.g. $>10^4\text{ K}$) with confinement provided by a toroidal magnetic field. We report the observation of intense EUV emission at low temperatures (e.g. $<10^3\text{ K}$) from atomic hydrogen and certain atomized pure elements or certain gaseous ions which ionize at integer multiples of the potential energy of atomic hydrogen.

12. R. Mills, "Observation of Extreme Ultraviolet Emission from Hydrogen-KI Plasmas Produced by a Hollow Cathode Discharge", *Int. J. Hydrogen Energy*, in press.

A high voltage discharge of hydrogen with and without the presence of a source of potassium, potassium iodide, in the discharge was performed at INP Greifswald, Germany with a hollow cathode. It has been reported that intense extreme ultraviolet (EUV) emission was observed at low temperatures (e.g. $<10^3\text{ K}$) from atomic hydrogen and certain atomized elements or certain gaseous ions which ionize at integer multiples of the potential energy of atomic hydrogen, 27.2 eV [1, 3-5]. Two potassium ions or a potassium atom may each provide an electron ionization or transfer reaction that has a net enthalpy equal to an integer multiple of 27.2 eV . The spectral lines of atomic hydrogen were intense enough to be recorded on photographic films only when KI was present. EUV lines not assignable to potassium, iodine, or hydrogen were observed at 73.0, 132.6, 513.6, 677.8, 885.9, and 1032.9 Å. The lines are assigned to transitions of atomic hydrogen to lower energy levels corresponding to lower energy hydrogen atoms called hydrino atoms and the emission from the excitation of the corresponding hydride ions formed from the hydrino atoms.

13. R. Mills, "Temporal Behavior of Light-Emission in the Visible Spectral Range from a Ti-K₂CO₃-H-Cell", *Int. J. Hydrogen Energy*, in press.

THIS PAGE BLANK (USPTO)

INP Greifswald, Germany reports the generation of a hydrogen plasma and extreme ultraviolet emission as recorded via the hydrogen Balmer emission in the visible range. Typically a hydrogen plasma is generated and the emission of extreme ultraviolet light from hydrogen gas is achieved via a discharge at high voltage, a high power inductively coupled plasma, or a plasma created and heated to extreme temperatures by RF coupling (e.g. $>10^6 K$) with confinement provided by a toroidal magnetic field. The observed plasma formed at low temperatures (e.g. $\approx 10^3 K$) from atomic hydrogen generated at a tungsten filament that heated a titanium dissociator coated with potassium carbonate. The temporal behavior of the plasma was recorded via hydrogen Balmer alpha line emission when all power into the cell was terminated. A two second decay of the plasma was observed after a fast decay of the electric field to zero. The persistence of emission following the removal of all of the power to the cell indicates that a novel chemical power source is present that forms an energetic plasma in hydrogen. No unusual behavior was observed with the control sodium carbonate.

14. R. Mills, T. Onuma, and Y. Lu, "Formation of a Hydrogen Plasma from an Incandescently Heated Hydrogen-Catalyst Gas Mixture with an Anomalous Afterglow Duration", Int. J. Hydrogen Energy, in press.

We report the generation of a plasma of hydrogen and certain alkali ions as recorded via EUV spectroscopy and the hydrogen Balmer and alkali line emissions in the visible range. Typically a hydrogen plasma is generated and the emission of extreme ultraviolet light from hydrogen gas is achieved via a discharge at high voltage, a high power inductively coupled plasma, or a plasma created and heated to extreme temperatures by RF coupling (e.g. $>10^6 K$) with confinement provided by a toroidal magnetic field. The observed plasma formed at low temperatures (e.g. $\approx 10^3 K$) from atomic hydrogen generated at a tungsten filament that heated a titanium dissociator and a catalyst comprising one of potassium, rubidium, cesium, and their carbonates and nitrates. These atoms and ions ionize to provide a catalyst with a net enthalpy of reaction of an integer multiple of the potential energy of atomic hydrogen ($m \cdot 27.2 \text{ eV}$ $m = \text{integer}$) to within 0.17 eV and comprise only a single ionization in the case of a potassium or rubidium ion. Whereas, the chemically similar atoms of sodium and lithium carbonates and nitrates which do not ionize with these constraints caused no emission. To test the electric dependence of the emission, the weak electric field of about 1 V/cm was set and measured to be zero in $<0.5 \times 10^{-4} \text{ sec}$. An anomalous afterglow duration of about one to two seconds was recorded in the case

THIS PAGE BLANK (USPTO)

of potassium, rubidium, cesium, K_2CO_3 , $RbNO_3$, and $CsNO_3$. Hydrogen line or alkali line emission was occurring even though the voltage between the heater wires was set to and measured to be zero. These atoms and ions ionize to provide a catalyst with a net enthalpy of reaction of an integer multiple of the potential energy of atomic hydrogen to within less than the thermal energies at $\approx 10^3 K$ and comprise only a single ionization in the case of a potassium or rubidium ion. Since the thermal decay time of the filament for dissociation of molecular hydrogen to atomic hydrogen was similar to the anomalous plasma afterglow duration, the emission was determined to be due to a reaction of atomic hydrogen with a catalyst that did not require the presence of an electric field to be functional.

15. R. Mills, M. Nansteel, and Y. Lu, "Observation of Extreme Ultraviolet Hydrogen Emission from Incandescently Heated Hydrogen Gas with Strontium that Produced an Anomalous Optically Measured Power Balance", *Int. J. Hydrogen Energy*, in press.

We report the observation of intense extreme ultraviolet (EUV) emission from incandescently heated atomic hydrogen and atomized strontium. It has been reported that intense EUV emission was observed at low temperatures (e.g. $\approx 10^3 K$) from atomic hydrogen and certain atomized elements or certain gaseous ions which ionize at integer multiples of the potential energy of atomic hydrogen, $27.2 eV$ [1-4]. Strontium ionizes at integer multiples of the potential energy of atomic hydrogen. Typically the emission of extreme ultraviolet light from hydrogen gas is achieved via a discharge at high voltage, a high power inductively coupled plasma, or a plasma created and heated to extreme temperatures by RF coupling (e.g. $> 10^6 K$) with confinement provided by a toroidal magnetic field. The observed plasma formed at low temperatures (e.g. $\approx 10^3 K$) from atomic hydrogen generated at a tungsten filament that heated a titanium dissociator and atomic strontium which was vaporized from the metal by heating. No emission was observed when sodium, magnesium, or barium replaced strontium or when argon replaced hydrogen with strontium. The power balance of a gas cell having atomized hydrogen and strontium was measured by integrating the total light output corrected for spectrometer system response and energy over the visible range. A control cell was identical except that sodium replaced strontium. In this case, 4000 times the power of the strontium cell was required in order to achieve that same optically measured light output power. A plasma formed at a cell voltage of about 250 volts in the cell with hydrogen alone and in the cell with hydrogen and sodium; whereas, a plasma formed in the strontium cell at the extremely

THIS PAGE BLANK (USPTO)

low voltage of about 2 volts. The starting and maintenance discharge voltages were two orders of magnitude of that predicted by current theory or observed experimentally.

16. R. Mills, *The Grand Unified Theory of Classical Quantum Mechanics*, January 2000 Edition, BlackLight Power, Inc., Cranbury, New Jersey, Distributed by Amazon.com.

In 1926, Schrödinger postulated the equation, $H\Psi = E\Psi$, where Ψ is the wave function, H is the wave operator, and E is the energy of the wave. Mills has solved and published a solution of a Schrödinger type equation based on first principles. The central feature of this theory is that all particles (atomic-size and macroscopic particles) obey the same physical laws. Whereas Schrödinger postulated a boundary condition: $\Psi \rightarrow 0$ as $r \rightarrow \infty$, the boundary condition in Mills' theory was derived from Maxwell's equations [8]:

For non-radiative states, the current-density function must not possess space-time Fourier components that are synchronous with waves traveling at the speed of light.

Application of this boundary condition leads to a physical model of particles, atoms, molecules, and, in the final analysis, cosmology. The closed-form mathematical solutions contain fundamental constants only, and the calculated values for physical quantities agree with experimental observations.

An important feature of Mills theory is that it predicts that the Rydberg's equation given by

$$E_n = -\frac{e^2}{n^2 8\pi\epsilon_0 a_H} = -\frac{13.598 eV}{n^2} \quad (1)$$

$$n = 1, 2, 3, \dots \quad (2)$$

where a_H is the Bohr radius for the hydrogen atom (52.947 pm), e is the magnitude of the charge of the electron, and ϵ_0 is the vacuum permittivity should be extended. Eq. (2), should be replaced by Eq. (3).

$$n = 1, 2, 3, \dots, \text{and}, n = \frac{1}{2}, \frac{1}{3}, \frac{1}{4}, \dots \quad (3)$$

Some revisions to standard quantum theory are implied. Quantum mechanics becomes a real physical description as opposed to a purely mathematical model

THIS PAGE BLANK (USPTO)

where the old and the revised versions are interchangeable by a Fourier Transform operation.

The theories of Bohr, Schrödinger, and presently Mills all give the identical equation for the principal energy levels of the one electron atom (Eq. (1)). The Mills theory solves the two dimensional wave equation for the charge density function of the electron. And, the Fourier transform of the charge density function is a solution of the three dimensional wave equation in frequency (k, ω) space. Whereas, the Schrödinger equation solutions are three dimensional in spacetime. The energy is given by

$$\int_{-\infty}^{\infty} \psi H \psi d\nu = E \int_{-\infty}^{\infty} \psi^2 d\nu \quad (4)$$

$$\int_{-\infty}^{\infty} \psi^2 d\nu = 1 \quad (5)$$

Thus,

$$\int_{-\infty}^{\infty} \psi H \psi d\nu = E \quad (6)$$

In the case that the potential energy of the Hamiltonian, H , is a constant times the wavenumber, the Schrödinger equation is the well known Bessel equation. Then with one of the solutions for ψ , Eq. (6) is equivalent to an inverse Fourier transform. According to the duality and scale change properties of Fourier transforms, the energy equation of the present theory and that of quantum mechanics are identical, the energy of a radial Dirac delta function of radius equal to an integer multiple of the radius of the hydrogen atom (Eq. (1)). And, Bohr obtained the same energy formula by postulating nonradiative states with angular momentum $L_z = m\hbar$ and solving the energy equation classically.

Mills revisions transform Schrödinger's quantum theory into what may be termed a *classical quantum theory*. Physical descriptions flow readily from the theory. For example, in the old quantum theory the spin angular momentum of the electron is called the "intrinsic angular momentum". This term arises because it is difficult to provide a physical interpretation for the electron's spin angular momentum. Quantum Electrodynamics provides somewhat of a physical interpretation by proposing that the "vacuum" contains fluctuating electric and magnetic fields. In contrast, in Mills' theory, spin angular momentum results from the motion of negatively charged mass moving systematically, and the equation for angular momentum, $r \times p$, can be applied directly to the wave function (a current density function) that describes the electron. And, quantization is carried by the photon, rather than probability waves of the electron.

THIS PAGE BLANK (USPTO)

Physics, 54, (1986), pp. 1126-1129.

18. R. Mills, B. Dhandapani, N. Greenig, J. He, "Synthesis and Characterization of Potassium Iodo Hydride", **Int. J. of Hydrogen Energy**, Vol. 25, Issue 12, December, (2000), pp. 1185-1203.

A novel inorganic hydride compound KH which comprises a high binding energy hydride ion was synthesized by reaction of atomic hydrogen with potassium metal and potassium iodide. Potassium iodo hydride was identified by time of flight secondary ion mass spectroscopy, X-ray photoelectron spectroscopy, 1H and ^{13}K nuclear magnetic resonance spectroscopy, Fourier transform infrared spectroscopy, electrospray ionization time of flight mass spectroscopy, liquid chromatography/mass spectroscopy, thermal decomposition with analysis by gas chromatography, and mass spectroscopy, and elemental analysis. Hydride ions with increased binding energies may form many novel compounds with broad applications.

19. R. Mills, "Novel Inorganic Hydride", **Int. J. of Hydrogen Energy**, Vol. 25, (2000), pp. 669-683.

A novel inorganic hydride compound $KH\text{KHCO}$, which is stable in water and comprises a high binding energy hydride ion was isolated following the electrolysis of a K_2CO_3 electrolyte. Inorganic hydride clusters $K[KH\text{KHCO}_3]$ were identified by Time of Flight Secondary Ion Mass Spectroscopy. Moreover, the existence of a novel hydride ion has been determined using X-ray photoelectron spectroscopy, and proton nuclear magnetic resonance spectroscopy. Hydride ions with increased binding energies may be the basis of a high voltage battery for electric vehicles.

20. R. Mills, B. Dhandapani, M. Nansteel, J. He, "Synthesis and Characterization of Novel Hydride Compounds", **Int. J. of Hydrogen Energy**, in press.

Novel inorganic alkali and alkaline earth hydrides of the formula MH_x and MHM_x wherein M is the metal, x , is a singly negatively charged anion, and H comprises a novel high binding energy hydride ion were synthesized in a high temperature gas cell by reaction of atomic hydrogen with a catalyst and MX or M_x , corresponding to an alkali metal or alkaline earth metal, respectively. It has been reported that intense extreme ultraviolet (EUV) emission was observed at low temperatures (e.g. $\approx 10^3 K$) from atomic hydrogen and certain atomized elements or certain gaseous ions which ionize at integer multiples of the potential energy of atomic hydrogen, $27.2 eV$ [1-5]. These atomized elements or certain gaseous ions comprised

THIS PAGE BLANK (USPTO)

the catalyst to form MHX and $MHMX$. For example, atomic hydrogen was reacted with strontium vapor and $SrBr_2$ to form $SrHBr$. Novel hydride compounds such as $SrHBr$ were identified by time of flight secondary ion mass spectroscopy, X-ray photoelectron spectroscopy, proton nuclear magnetic resonance spectroscopy, and thermal decomposition with analysis by gas chromatography, and mass spectroscopy. Hydride ions with increased binding energies form novel compounds with potential broad applications such as a high voltage battery for consumer electronics and electric vehicles. In addition, these novel compositions of matter and associated technologies may have far-reaching applications in many industries including chemical, electronics, computer, military, energy, and aerospace in the form of products such as propellants, solid fuels, surface coatings, structural materials, and chemical processes.

21. R. Mills, "Highly Stable Novel Inorganic Hydrides", Journal of Materials Research, submitted.

Novel inorganic hydride compounds $KH KHCO_3$, and KH were isolated following the electrolysis of a K_2CO_3 electrolyte. The compounds which comprised high binding energy hydride ions were stable in water, and KH was stable at elevated temperature (600 °C). Inorganic hydride clusters $K[KH KHCO_3]_n$ were identified by positive Time of Flight Secondary Ion Mass Spectroscopy (ToF-SIMS) of $KH KHCO_3$. The negative ToF-SIMS was dominated by hydride ion. The positive and negative ToF-SIMS of KH showed essentially K^+ and H^- only, respectively. Moreover, the existence of novel hydride ions was determined using X-ray photoelectron spectroscopy, and proton nuclear magnetic resonance spectroscopy. Hydride ions with increased binding energies may be the basis of a high voltage battery for electric vehicles.

22. R. Mills, "Novel Hydrogen Compounds from a Potassium Carbonate Electrolytic Cell", Fusion Technology, Vol. 37, No. 2, March, (2000), pp. 157-182.

Novel compounds containing hydrogen in new hydride and polymeric states which demonstrate novel hydrogen chemistry have been isolated following the electrolysis of a K_2CO_3 electrolyte with the production of excess energy. Inorganic hydride clusters $K[KH KHCO_3]_n$ and hydrogen polymer ions such as OH_{12}^- and H_{16}^- were identified by time of flight secondary ion mass spectroscopy. The presence of compounds containing new states of hydrogen were confirmed by X-ray photoelectron spectroscopy, X-ray diffraction, Fourier transform infrared spectroscopy, Raman spectroscopy, and proton nuclear magnetic resonance spectroscopy.

THIS PAGE BLANK (USPTO)

23. R. Mills, "The Hydrogen Atom Revisited", Int. J. of Hydrogen Energy, Vol. 25, Issue 12, December, (2000), pp. 1171-1183.

Several myths about quantum mechanics exist due to a loss of awareness of its details since its inception in the beginning of the last century or based on recent experimental evidence. It is taught in textbooks that atomic hydrogen cannot go below the ground state. Atomic hydrogen having an experimental ground state of 13.6 eV can only exist in a vacuum or in isolation, and atomic hydrogen cannot go below this ground state in isolation. However, there is no known composition of matter containing hydrogen in the ground state of 13.6 eV. It is a myth that hydrogen has a theoretical ground state based on first principles. Historically there were many directions in which to proceed to solve a wave equation for hydrogen. The Schrödinger equation gives the observed spontaneously radiative states and the nonradiative energy level of atomic hydrogen. On this basis alone, it is justified despite its inconsistency with physical laws as well as with many experiments. A solution compatible with first principles and having first principles as the basis of quantization was never found. Scattering results required the solution to be interpreted as probability waves that give rise to the uncertainty principle which in turn forms the basis of the wave particle duality. The correspondence principal predicts that quantum predictions must approach classical predictions on a large scale. However, recent data has shown that the Heisenberg uncertainty principle as the basis of the wave particle duality and the correspondence principle taught in textbooks are experimentally incorrect. Recently, a reconsideration of the postulates of quantum mechanics, has given rise to a closed form solution of a Schrödinger-like wave equation based on first principles. Hydrogen at predicted lower energy levels has been identified in the extreme ultraviolet emission spectrum from interstellar medium. In addition, new compositions of matter containing hydrogen at predicted lower energy levels have recently been observed in the laboratory, which energy levels are achieved using the novel catalysts.

24. Labov, S., Bowyer, S., "Spectral observations of the extreme ultraviolet background", The Astrophysical Journal, 371, (1991), pp. 810-819.

25. Mills, R., Good, W., "Fractional Quantum Energy Levels of Hydrogen", Fusion Technology, Vol. 28, No. 4, November, (1995), pp. 1697-1719.

Determination of excess heat release during the electrolysis of aqueous

THIS PAGE BLANK (USPTO)

potassium carbonate by the very accurate and reliable method of heat measurement, flow calorimetry; describes the experimental identification of hydrogen atoms in fractional quantum energy levels—hydrinos—by X-ray Photoelectron Spectroscopy (XPS); describes the experimental identification of hydrogen atoms in fractional quantum energy levels—hydrinos—by emissions of soft X-rays from dark matter; describes the experimental identification of hydrogen molecules in fractional quantum energy levels—dihydrino molecules by high resolution magnetic sector mass spectroscopy with ionization energy determination, and gives a summary.

In summary:

Excess power and heat were observed during the electrolysis of aqueous potassium carbonate. Flow calorimetry of pulsed current electrolysis of aqueous potassium carbonate at a nickel cathode was performed in a single-cell dewar. The average power out of 24.6 watts exceeded the average input power (voltage times current) of 4.73 watts by a factor greater than 5. The total input energy (integration of voltage times current) over the entire duration of the experiment was 5.72 MJ; whereas, the total output energy was 29.8 MJ. No excess heat was observed when the electrolyte was changed from potassium carbonate to sodium carbonate. The source of heat is assigned to the electrocatalytic, exothermic reaction whereby the electrons of hydrogen atoms are induced to undergo transitions to quantized energy levels below the conventional "ground state". These lower energy states correspond to fractional quantum numbers: $n = 1/2, 1/3, 1/4, \dots$. Transitions to these lower energy states are stimulated in the presence of pairs of potassium ions (K^+/K^+ electrocatalytic couple) which provide 27.2 eV energy sinks.

The identification of the $n = 1/2$ hydrogen atom, $H(n = 1/2)$ is reported. Samples of the nickel cathodes of aqueous potassium carbonate electrolytic cells and aqueous sodium carbonate electrolytic cells were analyzed by XPS (Zettlemoyer Center for Surface Studies, Sinclair Laboratory, Lehigh University). A broad peak centered at 54.6 eV was present only in the cases of the potassium carbonate cells. The binding energy (in vacuum) of $H(n = 1/2)$ is 54.4 eV. Thus, the theoretical and measured binding energies for $H(n = 1/2)$ are in excellent agreement.

Further experimental identification of hydrinos—down to $H(n = 1/8)$ —can be found in the alternative explanation by Mills et al. for the soft X-ray emissions of the dark interstellar medium observed by Labov and Bowyer [15] of the Extreme UV Center of the University of California, Berkeley. The agreement between the experimental spectrum and the energy values predicted for the proposed transitions is

THIS PAGE BLANK (USPTO)

remarkable.

The reaction product of two H($n=1/2$) atoms, the dihydrino molecule, was identified by mass spectroscopy (Shrader Analytical & Consulting Laboratories). The mass spectrum of the cryofiltered gases evolved during the electrolysis of a light water K_2CO_3 electrolyte with a nickel cathode demonstrated that the dihydrino molecule, $H_2(n = 1/2)$, has a higher ionization energy, about 63 eV, than normal molecular hydrogen, $H_2(n = 1)$, 15.46 eV. The high resolution (0.001 AMU) magnetic sector mass spectroscopic analysis of the postcombustion gases indicated the presence of two peaks of nominal mass two-- one peak at 70 eV and one peak at 25 eV. The same analysis of molecular hydrogen indicates only one peak at 25 eV and one peak at 70 eV. In the case of the postcombustion sample at 70 eV, one peak was assigned as the hydrogen molecular ion peak, $H_2^+(n = 1)$, and one peak was assigned as the dihydrino molecular peak, $H_2^+(n = 1/2)$ which has a slightly larger magnetic moment.

26. Mills, R., Good, W., Shaubach, R., "Dihydrino Molecule Identification", Fusion Technology, Vol. 25, 103 (1994).

Calorimetry of pulsed current and continuous electrolysis of aqueous potassium carbonate (K^+/K^+ electrocatalytic couple) at a nickel cathode was performed by Thermacore, Inc. The excess power out of 41 watts exceeded the total input power given by the product of the electrolysis voltage and current by a factor greater than 8. Elemental analysis of the electrolyte and metallurgical analysis of the cathode showed no evidence of chemical reactions. The pH, specific gravity, concentration of K_2CO_3 , and the elemental analysis of the electrolyte sample taken after 42 days of continuous operation were unchanged from that of the values obtained for the electrolyte sample taken before operation. Elemental analysis and scanning electron microscopy of metallurgical samples of the nickel cathode taken before operation and at day 56 of continuous operation were identical indicating that the nickel cathode had not changed chemically or physically. Scintillation counter and photographic film measurements showed that no radiation above background was detected indicating that nuclear reactions did not occur.

The "ash" of the exothermic reaction is atoms having electrons of energy below the "ground state" which are predicted to form molecules. The predicted molecules were identified by lack of reactivity with oxygen, by separation from molecular deuterium by cryofiltration, and by mass spectroscopic analysis. The combustion of the gases evolved during the electrolysis of a light water K_2CO_3 electrolyte (K^+/K^+

THIS PAGE BLANK (USPTO)

electrocatalytic couple) with a nickel cathode was incomplete. The mass spectroscopic analysis (Dr. David Parees of Air Products & Chemicals, Inc.) of the m/e = 2 peak of the combusted gas demonstrated that the dihydrino molecule, $H_2(n = 1/2)$, has a higher ionization energy than H_2 .

Calorimetry of pulsed current and continuous electrolysis of aqueous potassium carbonate (K^+/K^+ electrocatalytic couple) at a nickel cathode was performed in single cell dewar calorimetry cells by HydroCatalysis Power Corporation. Excess power out exceeded input power by a factor greater than 16. No excess heat was observed when the electrolyte was changed from potassium carbonate to the control sodium carbonate. The faraday efficiency was measured volumetrically to be 100%.

27. R. Mills and S. Kneizys, **Fusion Technol.** Vol. 20, 65 (1991).

Calorimetry of pulsed current and continuous electrolysis of aqueous potassium carbonate (K^+/K^+ electrocatalytic couple) at a nickel cathode was performed in single cell dewar calorimetry cells by Mills of Franklin and Marshall College and Kneizys of Ursinus College. Excess power out exceeded the input power by a factor greater than 37. No excess heat was observed when the electrolyte was changed from potassium carbonate to the control sodium carbonate.

28. V. Noninski, **Fusion Technol.**, Vol. 21, 163 (1992).

Dr. Noninski of the Laboratory for Electrochemistry of Renewed Electrode-Solution Interface (LEPGER) successfully reproduced the results of Mills and Kneizys [17] as a visiting professor at Franklin and Marshall College. A significant increase in temperature with every watt input, compared with the calibration experiment ($\approx 50^\circ C/W$ versus $\approx 30^\circ C/W$), was observed during the electrolysis of potassium carbonate. This effect was not observed when sodium carbonate was electrolyzed. No trivial explanation (in terms of chemical reactions, change in heat transfer properties, etc.) of this effect were found.

29. Niedra, J., Meyers, I., Fralick, G. C., and Baldwin, R., "Replication of the Apparent Excess Heat Effect in a Light Water-Potassium Carbonate-Nickel Electrolytic Cell, NASA Technical Memorandum 107167, February, (1996). pp. 1-20.; Niedra, J., Baldwin, R., Meyers, I., NASA Presentation of Light Water Electrolytic Tests, May 15, 1994.

NASA Lewis tested a cell identical to that of Thermacore [16] with the exception that it was minus the central cathode. A cell identical to the test cell with heater power

THIS PAGE BLANK (USPTO)

only (no electrolysis) was the calibration control and the blank cell with the heater power equal to zero. The test cell was also calibrated "on the fly" by measuring the temperature relative to the blank cell at several values of heater input power of the test cell. "Replication of experiments claiming to demonstrate excess heat production in light water-Ni-K₂CO₃ electrolytic cells was found to produce an apparent excess heat of 11 W maximum, for 60 W electrical power into the cell. Power gains ranged from 1.06 to 1.68." The production of excess energy with a power gain of 1.68 would require 0% Faraday efficiency to account for the observed excess power.

THIS PAGE BLANK (USPTO)

Minimum Heat of Formation of Potassium Iodo Hydride

Randell L. Mills

Jinquan Dong

William Good

Andreas Voigt

BlackLight Power, Inc.

493 Old Trenton Road

Cranbury, NJ 08512

It was previously reported [R. Mills, B. Dhandapani, N. Greenig, J. He, "Synthesis and Characterization of Potassium Iodo Hydride", Int. J. of Hydrogen Energy, Vol. 25, Issue 12, December, (2000), pp. 1185-1203.] that a novel inorganic hydride compound *KHI* which comprised a high binding energy hydride ion was synthesized by reaction of atomic hydrogen with potassium metal and potassium iodide. Potassium iodo hydride was identified by time of flight secondary ion mass spectroscopy, X-ray photoelectron spectroscopy, 1H and ^{39}K nuclear magnetic resonance spectroscopy, Fourier transform infrared spectroscopy, electrospray ionization time of flight mass spectroscopy, liquid chromatography/mass spectroscopy, thermal decomposition with analysis by gas chromatography, and mass spectroscopy, and elemental analysis. We report measurements of heats of formation of *KHI* by differential scanning calorimetry (DSC) on a very reliable commercial instrument, a Setaram HT 1000 DSC. With reactant *KI* present, potassium metal catalyst and atomic hydrogen were produced by decomposition of *KH* at an extremely slow rate under a helium atmosphere to increase the amount of atomic hydrogen by slowing the rate of molecular hydrogen formation. Since not all of the starting materials reacted, the observed minimum heats of formation were over -2000 kJ/mole H_2 compared to the enthalpy of combustion of hydrogen of -241.8 kJ/mole H_2 .

INTRODUCTION

Based on the solution of a Schrödinger-type wave equation with a nonradiative boundary condition based on Maxwell's equations, Mills [1-36] predicts that atomic hydrogen may undergo a catalytic reaction with certain atomized elements or certain gaseous ions which singly or multiply ionize at integer multiples of the potential energy of atomic hydrogen, 27.2 eV , $m \cdot 27.28\text{ eV}$ wherein m is a integer. One such atomic catalytic system involves potassium metal. The first, second, and third ionization energies of potassium are 4.34066 eV , 31.63 eV , 45.806 eV , respectively [37]. The triple ionization ($t=3$) reaction of K to K^{3+} , then, has a net enthalpy of reaction of 81.7766 eV , which is equivalent to $3 \cdot 27.2\text{ eV}$. Potassium ions can also provide a net enthalpy of a multiple of that of the potential energy of the hydrogen atom. The second ionization energy of potassium is 31.63 eV ; and K^+ releases 4.34 eV when it is reduced to K [37]. The combination of reactions K^+ to K^{2+} and K^+ to K , then, has a net enthalpy of reaction of 27.28 eV , which is equivalent to $1 \cdot 27.2\text{ eV}$.

Observation of intense extreme ultraviolet (EUV) emission at low temperatures (e.g. $\approx 10^3\text{ K}$) from atomic hydrogen and certain atomized elements or certain gaseous ions [6-21] has been reported previously. The only pure elements that were observed to emit EUV were those wherein the ionization of t electrons from an atom to a continuum energy level is such that the sum of the ionization energies of the t electrons is approximately $m \cdot 27.2\text{ eV}$ where t and m are each an integer. Potassium, cesium, and strontium atoms and Rb^+ ion ionize at integer multiples of the potential energy of atomic hydrogen and caused emission. Whereas, the chemically similar atoms, sodium, magnesium and barium, do not ionize at integer multiples of the potential energy of atomic hydrogen and caused no emission. Additional prior studies that support the possibility of a novel reaction of atomic hydrogen which produces an anomalous discharge and produces novel hydride compounds [6-35] include: 1.) the recent analysis of mobility and spectroscopy data of individual electrons in liquid helium which shows direct experimental confirmation that electrons may have fractional principal quantum energy levels [36], 2.) the observation of continuum state emission of Cs^{2+} and Ar^{2+} at 53.3 nm

and 45.6 nm, respectively, with the absence of the other corresponding Rydberg series of lines from these species which confirmed the resonant nonradiative energy transfer of 27.2 eV from atomic hydrogen to the catalysts atomic cesium or Ar⁺ [6], 3.) the spectroscopic observation of the predicted hydride ion H⁻(1/2) of hydrogen catalysis by either cesium atom or Ar⁺ catalyst at 407 nm corresponding to its predicted binding energy of 3.05 eV [6], 4.) the identification of transitions of atomic hydrogen to lower energy levels corresponding to lower energy hydrogen atoms in the extreme ultraviolet emission spectrum from interstellar medium [1, 5], 5.) the EUV spectroscopic observation of lines by the Institut Fur Niedertemperatur-Plasmaphysik e.V. that could be assigned to transitions of atomic hydrogen to lower energy levels corresponding to lower energy hydrogen atoms and the emission from the excitation of the corresponding hydride ions [11], 6.) the observation by the Institut Fur Niedertemperatur-Plasmaphysik e.V. of an anomalous plasma and plasma afterglow duration formed with hydrogen-potassium mixtures [12], 7.) the observation of anomalous afterglow durations of plasmas formed by catalysts providing a net enthalpy of reaction within thermal energies of $m \cdot 27.28$ eV [12-13], 8.) the observation of Lyman series in the EUV that represents an energy release 10 times hydrogen combustion which is greater than that of any known chemical reaction [6-21], 9.) the observation of line emission by the Institut Fur Niedertemperatur-Plasmaphysik e.V. with a 4 ° grazing incidence EUV spectrometer that was 100 times more energetic than the combustion of hydrogen [11], 10.) the observation of anomalous plasmas formed with strontium and argon catalysts at 1% of the theoretical or prior known voltage requirement with a light output for power input up to 8600 times that of the control standard light source [8-9, 14], 11.) the observation that the optically measured output power of gas cells for power supplied to the glow discharge increased by over two orders of magnitude depending on the presence of less than 1% partial pressure of certain of catalysts in hydrogen gas or argon-hydrogen gas mixtures [7], 12.) the isolation of novel hydrogen compounds as products of the reaction of atomic hydrogen with atoms and ions which formed an anomalous plasma as reported in the EUV studies [17, 19-35], 13.) the identification of novel hydride compounds by i.) time of flight secondary ion mass spectroscopy

which showed a dominant hydride ion in the negative ion spectrum, ii.) X-ray photoelectron spectroscopy which showed novel hydride peaks and significant shifts of the core levels of the primary elements bound to the novel hydride ions, iii.) 1H nuclear magnetic resonance spectroscopy (NMR) which showed extraordinary upfield chemical shifts compared to the NMR of the corresponding ordinary hydrides, and iv.) thermal decomposition with analysis by gas chromatography, and mass spectroscopy which identified the compounds as hydrides [17, 19-35], 14.) the NMR identification of novel hydride compounds MH^*X wherein M is the metal, X , is a halide, and H^* comprises a novel high binding energy hydride ion identified by a large distinct upfield resonance [22-23, 26], 15.) the replication of the NMR results of the identification of novel hydride compounds by large distinct upfield resonances at Spectral Data Services, University of Massachusetts Amherst, University of Delaware, Grace Davison, and National Research Council of Canada [22], 16.) the NMR identification of novel hydride compounds MH^* and MH_2^* wherein M is the metal and H^* comprises a novel high binding energy hydride ion identified by a large distinct upfield resonance that proves the hydride ion is different from the hydride ion of the corresponding known compound of the same composition [22].

A novel inorganic hydride compound KHI which comprises a high binding energy hydride ion was previously synthesized by a catalytic reaction of atomic hydrogen with potassium metal and potassium iodide [22-23, 26]. Potassium iodo hydride was prepared in a stainless steel gas cell comprising a Ti screen hydrogen dissociator and KI . Potassium metal was added to the cell under an argon atmosphere. The cell was then continuously evacuated with a high vacuum turbo pump and heated to 650 °C. The hydrogen pressure was then maintained at 1500 torr for 48 hours after which time the cell was cooled, and blue crystals of the KHI product were removed and analyzed. The synthesis was repeated with the exception that the hydrogen was slowly added to maintain a pressure within the range of 1 torr to 10 torr and green crystals of KHI formed.

The reported [23] time of flight secondary ion mass spectroscopy (ToF-SIMS), X-ray photoelectron spectroscopy (XPS), 1H and ^{39}K nuclear magnetic resonance spectroscopy (1H and ^{39}K NMR), Fourier transform infrared spectroscopy (FTIR), electrospray ionization time of flight mass

spectroscopy (ESITOFMS), liquid chromatography/mass spectroscopy (LC/MS), thermal decomposition with analysis by gas chromatography (GC), and mass spectroscopy (MS), and elemental analysis results confirm the identification of *KHI* having hydride ions, $H^-(1/2) E_b = 3.05 \text{ eV}$, $H^-(1/4) E_b = 11.2 \text{ eV}$, and $H^-(1/6) E_b = 22.8 \text{ eV}$ predicted by Mills [1]. Two forms of hydride ion ($H^-(1/2)$ and $H^-(1/4)$) may be formed with two potassium ions or potassium metal as the catalyst, respectively, which was supported by the XPS, NMR, and LC/MS data of the blue crystals. The ToF-SIMS, XPS, and NMR results of the green crystals indicated that a higher binding energy hydride $H^-(1/6)$ formed by running the catalysis reaction at lower hydrogen pressure.

The LC/MS data indicated that the blue crystal comprised a novel compound *KHI* which contained two different hydride ions that gave rise to different mass fragmentation patterns. One *KHI* compound with a retention time of $RT = 11.42 \text{ min.}$ gave rise to a $K(KI)_2^+$ mass fragment. Whereas, a second *KHI* compound with a retention of about $RT = 23 \text{ min.}$ gave rise to a $K(KI)_2^+$ and a $K(KI)_2^+$ mass fragment.

The positive ion ESITOFMS spectrum of the blue crystals and that of the *KI* control were dominated by the K^+ ion. A series of positive ions $K[KI]_n^+ m/z = (39 + 166n)$ were also observed. In addition, KHI^+ was only observed from the blue crystals.

The positive and negative ToF-SIMS results of the blue crystals were consistent with the proposed structure *KHI*. The positive ion spectrum of the blue crystals and that of the *KI* control were dominated by the K^+ ion. The comparison of the positive ToF-SIMS spectrum of the *KI* control with the blue crystals demonstrated that the $^{39}K^+$ peak of the blue crystals saturated the detector and gave rise to a peak that was atypical of the natural abundance of ^{41}K which was indicative of a unique crystalline matrix. The negative ion ToF-SIMS of the blue crystals was dominated by H^- and I^- peaks of about equal intensity. Iodide alone dominated the negative ion ToF-SIMS of the *KI* control.

The positive and negative ToF-SIMS spectrum obtained from the green crystals was similar to that obtained from the blue crystals except that the hydride ion peak of the negative ToF-SIMS spectrum obtained from the green crystals was much larger than that obtained from the blue crystals. This result was consistent with the formation of a higher

hydride content or a higher hydride ion yield in the green crystals which indicated that a higher binding energy hydride was formed by running the catalysis reaction at lower hydrogen pressure.

The XPS data of the core levels clearly indicated a change in the electronic structure and different bonding in *KHI* relative to that in the corresponding *KI*. This binding influenced the metal core level with little perturbation of the halogen core level. Comparing the alterations in the *K* core levels versus the *I* core level indicated that the lower-energy hydrogen species binds to the metal center of *KI*. An additional spin-orbit splitting component had to be added to each potassium iodo hydride in order to obtain a good curve fit of the *K2p* spectra. In each case, the second component of spin-orbit splitting was assigned to the formation of the alkali metal halido hydride, *KHI*. The presence of the novel hydride ion shifted the *K2p* peaks to lower binding energies relative to the corresponding peaks of *KI*. The change in electronic structure was greatest with the green crystals which indicates that a higher binding energy hydride was formed by running the catalysis reaction at lower hydrogen pressure.

The 0-100 eV binding energy region of a high resolution XPS spectra of the blue and green crystals indicated the presence of the hydride ions $H^{-}(1/2)$ and $H^{-}(1/4)$ in the case of the blue crystals and the presence of the higher binding energy hydride ion $H^{-}(1/6)$ in the case of the green crystals. This product was predicted by an autocatalysis reaction of two $H(1/4)$ atoms which has been confirmed by extreme ultraviolet spectroscopy [11].

The upfield peak in the NMR spectrum of the green crystals at -2.5 ppm was assigned to a novel hydride ion that has a smaller radius than that of the hydride ions observed in the case of the blue crystals corresponding to resonances at -0.376 ppm and -1.209 ppm since the upfield shift was larger in the case of the green crystals. A smaller radius corresponds to a higher binding energy. The NMR results of the identification of *KHI* by large distinct upfield resonances have been reproduced at Spectral Data Services, University of Delaware, Grace Davison, and National Research Council of Canada [22].

In the present study, the heats of formation of *KHI* was measured by differential scanning calorimetry (DSC) on a very reliable commercial

instrument, a Setaram HT 1000 DSC. With reactant *KI* present, potassium metal catalyst and atomic hydrogen were produced by decomposition of *KH* at an extremely slow rate under a helium atmosphere to increase the amount of atomic hydrogen by slowing the rate of molecular hydrogen formation. *MgH₂* was run as a control since no ionization reaction is possible for magnesium metal or magnesium ions with a net positive enthalpy of an integer multiple of the potential energy of atomic hydrogen, *m*>27.28 eV. No emission was observed for magnesium in previous EUV and visible spectroscopy studies of vaporized magnesium metal with atomic hydrogen [6-10]. As further controls to test the dependence of the reaction on atomic hydrogen, a hydrogen atmosphere replaced the helium atmosphere, or the heating ramp rate was increased.

EXPERIMENTAL

Potassium hydride (*KH*, Aldrich, 30 wt. % dispersion in mineral oil, Catalog #21,581-3, Lot # E107116JU) was cleaned by washing with hexane. The *KH*/mineral oil suspension was allowed to settle inside the glove box. The layer of mineral oil was separated from the *KH* layer. 10 g of the unwashed *KH* containing mineral oil was placed in a 100 ml Schlenk tube. The Schlenk tube was connected to a vacuum manifold outside the glove box. 20 ml of hexane (Aldrich, anhydrous, Catalog # 22,706-4, used as supplied by manufacturer) was added under argon flow. After stirring for 5 minutes, the *KH* was allowed to settle, and the supernatant liquid was removed with a syringe. The hexane washing procedure was repeated 4 additional times. The *KH* was dried under vacuum for 3 hours and stored in a glove box prior to use.

Differential scanning calorimeter (DSC) measurements were performed using the DSC mode of a Setaram HT-1000 calorimeter (Setaram, France). Two matched Alumina glove fingers were used as the sample compartment and the reference compartment. The fingers permitted the control of the reaction atmosphere. 0.050 g of washed *KH* was placed in a flat-base Al-23 crucible (Alfa-Aesar, 15 mm high x 10 mm OD x 8 mm ID) and covered with 0.500 g of *KI* (Alfa-Aesar, 99.99%). The crucible was then placed in the bottom of the sample Alumina glove

finger cell. As a reference, an aluminum oxide sample (Alfa-Aesar, -400 Mesh powder, 99.9%) with similar weight as the sample was placed in a matched Al-23 crucible. All samples were handled in a dry box. Each Alumina glove finger cell was sealed in the glove box, removed from the glove box, and then quickly attached to the Setaram calorimeter. The system was immediately evacuated to pressure of 1 mtorr or less. The cell was back filled with one atmosphere of helium and evacuated again. The cell was then refilled with helium to 760 torr. The cells were then inserted into the oven, and secured to their positions in the DSC instrument. The oven temperature was brought to the desired starting temperature of 100 °C. The oven temperature was scanned from 100 °C to 750 °C at a ramp rate of 0.1 degree/minute.

As a control, one atmosphere of hydrogen replaced the one atmosphere of helium. As a second control, MgH_2 replaced KH and KI . A 50 mg MgH_2 sample (Alfa-Aesar, 90%, remainder Mg) was added to the sample cell, while a similar weight of aluminum oxide (Alfa-Aesar) was added to the reference cell. Both samples were also handled in a dry box. As a third control, the ramp rate was doubled to 0.2 degree/minute for the DSC of the mixture of KH and KI . As a fourth control with 0.500 g of KI and 760 torr helium, 0.050 g of potassium metal replaced the 0.050 g of KH .

A DSC of a sample comprising a majority KI and containing some KHI synthesized previously [23] and a DSC of KI were run in order assist in the identification of the reaction product which may have occurred during the DSC experiment.

RESULTS AND DISCUSSION

The DSC (100-750 °C) results of KH and KI mixtures are shown in Figures 1-2. In Figure 1, a broad endotherm was observed at 300 to 400 °C which corresponded to 105.2 kJ/mole H_2 . Potassium hydride decomposes in this temperature range (288 to 415 °C) with a corresponding enthalpy of 118.2 kJ/mole H_2 [38]. A large exotherm was observed in the region 435 to 675 °C which corresponded to -2306 kJ/mole H_2 . A feature was observed within the exotherm at 410 to 475 °C that may correspond to an endothermic component due to the vaporization of potassium metal. The

boiling point of potassium metal is 756.5 °C with a corresponding enthalpy of vaporization of 81.1 kJ/mole K(m) [39]. Another endotherm within the exothermic feature was observed at 673 °C. This is close to the known melting point of *KI* of 681 °C with a corresponding enthalpy of fusion of 24.0 kJ/mole *KI* [40]. The difference in temperatures may be due to the presence of *KHI* product. A DSC of a sample from the *KHI* synthesis reported previously [23] is shown in Figure 3. The same endothermic feature was observed at 673 °C corresponding to an enthalpy of 16.84 kJ/mole *KHI* as well as a new feature at 537 °C corresponding to an enthalpy of 1.52 kJ/mole *KHI*. The DSC of pure *KI* is shown in Figure 4. Only a sharp endotherm at 681 °C corresponding to an enthalpy of 23.90 kJ/mole *KI* was observed. The control *KI* DSC results closely matched the published melting point and heat of fusion of *KI* [40].

In repeat DSC experiments of *KH* and *KI* mixtures, the heat balance features were very similar. In Figure 2, a broad endotherm was observed at 300 to 400 °C which corresponded to 90.4 kJ/mole *H₂*. A large exotherm was observed in the region 435 to 675 °C which corresponded to -2332 kJ/mole *H₂*. Within the exotherm the endothermic components at 410 to 475 °C and 673 °C were also observed.

Flames from potassium metal were observed upon exposure of the contents of the sample glove finger to air following the DSC run; whereas, *KHI* was reported to be nonflammable [23]. Since not all of the starting materials reacted, the observed minimum heats of formation of *KHI* were -2306 kJ/mole *H₂* compared to the enthalpy of combustion of hydrogen of -241.8 kJ/mole *H₂* [41].

The DSC (100-750 °C) results of *MgH₂* are shown in Figures 5-6. In both cases, two sharp endothermic peaks were observed. In Figures 5 and 6, a first peak was observed centered at 351.75 °C corresponding to 68.61 kJ/mole *MgH₂* and at 368.52 °C corresponding to 59.11 kJ/mole *MgH₂*, respectively. The decomposition of *MgH₂* is observed at 440 to 560 °C corresponding to 74.4 kJ/mole *MgH₂* [38]. In Figures 5 and 6, a second peak was observed centered at 648.46 °C corresponding to 6.65 kJ/mole *MgH₂*, and at 648.32 °C corresponding to 5.10 kJ/mole *MgH₂*, respectively. The known melting point of *Mg(m)* is 650 °C corresponding to an enthalpy of fusion of 8.48 kJ/mole *Mg(m)* [42].

When the DSC reactions of *KH* and *KI* mixtures were repeated with one atmosphere of hydrogen replacing helium, only the known endothermic peaks of *KH* decomposition and *KI* melting were observed. The same result was observed when the heating rate was changed from 0.1 degree/minute to 0.2 degree/minute. The addition of an inert gas such as helium decreases the rate decomposition of a hydride by reducing the rate of molecular hydrogen formation from atomic hydrogen [43]. The rate of molecular hydrogen formation from atomic hydrogen is also decreased by decreasing the partial pressure of atomic hydrogen [44]. The partial pressure of atomic hydrogen is dependent on the hydride decomposition rate. In addition, when *MgH₂* replaced *KH*, only the known endothermic peaks of *MgH₂* decomposition and *Mg(m)* melting were observed. No exotherm was observed for the control with 0.500 g of *KI*, 760 torr helium, and 0.050 g of potassium metal which replaced the 0.050 g of *KH*. The results indicate that the exothermic reaction requires atomic hydrogen and potassium metal which supports the catalysis of atomic hydrogen by potassium atoms as the source of the large exotherm. These results are consistent with the previous reports of the formation of an anomalous plasma with atomic hydrogen and potassium but not with magnesium [6-10].

CONCLUSION

The observed minimum heats of formation of *KHI* by the catalytic reaction of potassium with atomic hydrogen and *KI* were over -2000 kJ/mole *H₂* compared to the enthalpy of combustion of hydrogen of -241.8 kJ/mole *H₂*. Since the net enthalpy released is essentially an order of magnitude that of combustion, the catalysis of atomic hydrogen represents a new source of energy with *H₂O* as the source of hydrogen fuel. Moreover, rather than air pollutants or radioactive waste, novel hydride compounds with potential commercial applications are the products [45-46].

ACKNOWLEDGMENT

Special thanks to Mark Nansteel and Nelson Greenig for engineering support and Bala Dhandapani for assisting with logistics and reviewing this manuscript.

REFERENCES

1. R. Mills, *The Grand Unified Theory of Classical Quantum Mechanics*, January 2000 Edition, BlackLight Power, Inc., Cranbury, New Jersey, Distributed by Amazon.com.
2. R. Mills, "The Grand Unified Theory of Classical Quantum Mechanics", Global Foundation, Inc. Orbis Scientiae entitled *The Role of Attractive and Repulsive Gravitational Forces in Cosmic Acceleration of Particles The Origin of the Cosmic Gamma Ray Bursts*, (29th Conference on High Energy Physics and Cosmology Since 1964) Dr. Behram N. Kursunoglu, Chairman., December 14-17, 2000, Lago Mar Resort, Fort Lauderdale, FL.
3. R. Mills, "The Grand Unified Theory of Classical Quantum Mechanics", Global Foundation, Inc. Orbis Scientiae entitled *The Role of Attractive and Repulsive Gravitational Forces in Cosmic Accélération of Particles The Origin of the Cosmic Gamma Ray Bursts*, (29th Conference on High Energy Physics and Cosmology Since 1964) Dr. Behram N. Kursunoglu, Chairman., December 14-17, 2000, Lago Mar Resort, Fort Lauderdale, FL, in press.
4. R. Mills, "The Grand Unified Theory of Classical Quantum Mechanics", *Il Nuovo Cimento*, submitted.
5. R. Mills, "The Hydrogen Atom Revisited", *Int. J. of Hydrogen Energy*, Vol. 25, Issue 12, December, (2000), pp. 1171-1183.
6. R. Mills, "Spectroscopic Identification of a Novel Catalytic Reaction of Atomic Hydrogen and the Hydride Ion Product", *Int. J. Hydrogen Energy*, submitted.
7. R. Mills, N. Greenig, S. Hicks, "Optically Measured Power Balances of Anomalous Discharges of Mixtures of Argon, Hydrogen, and Potassium, Rubidium, Cesium, or Strontium Vapor", *Int. J. Hydrogen Energy*, submitted.

8. R. Mills and M. Nansteel, "Anomalous Argon-Hydrogen-Strontium Discharge", IEEE Transactions of Plasma Science, submitted.
9. R. Mills, M. Nansteel, and Y. Lu, "Anomalous Hydrogen/Strontium Discharge", European Journal of Physics D, submitted.
10. R. Mills, J. Dong, Y. Lu, "Observation of Extreme Ultraviolet Hydrogen Emission from Incandescently Heated Hydrogen Gas with Certain Catalysts", Int. J. Hydrogen Energy, Vol. 25, (2000), pp. 919-943.
11. R. Mills, "Observation of Extreme Ultraviolet Emission from Hydrogen-KI Plasmas Produced by a Hollow Cathode Discharge", Int. J. Hydrogen Energy, in press.
12. R. Mills, "Temporal Behavior of Light-Emission in the Visible Spectral Range from a Ti-K₂CO₃-H-Cell", Int. J. Hydrogen Energy, in press.
13. R. Mills, T. Onuma, and Y. Lu, "Formation of a Hydrogen Plasma from an Incandescently Heated Hydrogen-Catalyst Gas Mixture with an Anomalous Afterglow Duration", Int. J. Hydrogen Energy, in press.
14. R. Mills, M. Nansteel, and Y. Lu, "Observation of Extreme Ultraviolet Hydrogen Emission from Incandescently Heated Hydrogen Gas with Strontium that Produced an Anomalous Optically Measured Power Balance", Int. J. Hydrogen Energy, in press.
15. R. Mills, J. Dong, Y. Lu, J. Conrads, "Observation of Extreme Ultraviolet Hydrogen Emission from Incandescently Heated Hydrogen Gas with Certain Catalysts", 1999 Pacific Conference on Chemistry and Spectroscopy and the 35th ACS Western Regional Meeting, Ontario Convention Center, California, (October 6-8, 1999).
16. R. Mills, J. Dong, N. Greenig, and Y. Lu, "Observation of Extreme Ultraviolet Hydrogen Emission from Incandescently Heated Hydrogen Gas with Certain Catalysts", National Hydrogen Association, 11 th Annual U.S. Hydrogen Meeting, Vienna, VA, (February 29-March 2, 2000).
17. R. Mills, B. Dhandapani, N. Greenig, J. He, J. Dong, Y. Lu, and H. Conrads, "Formation of an Energetic Plasma and Novel Hydrides from Incandescently Heated Hydrogen Gas with Certain Catalysts", National Hydrogen Association, 11 th Annual U.S. Hydrogen Meeting, Vienna, VA, (February 29-March 2, 2000).
18. Mills, J. Dong, N. Greenig, and Y. Lu, "Observation of Extreme Ultraviolet Hydrogen Emission from Incandescently Heated Hydrogen

- Gas with Certain Catalysts", 219 th National ACS Meeting, San Francisco, California, (March 26-30, 2000).
19. R. Mills, B. Dhandapani, N. Greenig, J. He, J. Dong, Y. Lu, and H. Conrads, "Formation of an Energetic Plasma and Novel Hydrides from Incandescently Heated Hydrogen Gas with Certain Catalysts", 219 th National ACS Meeting, San Francisco, California, (March 26-30, 2000).
20. R. Mills, B. Dhandapani, N. Greenig, J. He, J. Dong, Y. Lu, and H. Conrads, "Formation of an Energetic Plasma and Novel Hydrides from Incandescently Heated Hydrogen Gas with Certain Catalysts", June ACS Meeting (29th Northeast Regional Meeting, University of Connecticut, Storrs, CT, (June 18-21, 2000)).
21. R. Mills, B. Dhandapani, N. Greenig, J. He, J. Dong, Y. Lu, and H. Conrads, "Formation of an Energetic Plasma and Novel Hydrides from Incandescently Heated Hydrogen Gas with Certain Catalysts", August National ACS Meeting (220th ACS National Meeting, Washington, DC, (August 20-24, 2000)).
22. R. Mills, B. Dhandapani, M. Nansteel, J. He, A. Voigt, Identification of Compounds Containing Novel Hydride Ions by Nuclear Magnetic Resonance Spectroscopy, Int. J. Hydrogen Energy, submitted.
23. R. Mills, B. Dhandapani, N. Greenig, J. He, "Synthesis and Characterization of Potassium Iodo Hydride", Int. J. of Hydrogen Energy, Vol. 25, Issue 12, December, (2000), pp. 1185-1203.
24. R. Mills, "Novel Inorganic Hydride", Int. J. of Hydrogen Energy, Vol. 25, (2000), pp. 669-683.
25. R. Mills, "Novel Hydrogen Compounds from a Potassium Carbonate Electrolytic Cell", Fusion Technology, Vol. 37, No. 2, March, (2000), pp. 157-182.
26. R. Mills, B. Dhandapani, M. Nansteel, J. He, "Synthesis and Characterization of Novel Hydride Compounds", Int. J. of Hydrogen Energy, in press.
27. R. Mills, "Highly Stable Novel Inorganic Hydrides", Journal of Materials Research, submitted.
28. R. Mills, "Novel Hydride Compound", 1999 Pacific Conference on Chemistry and Spectroscopy and the 35th ACS Western Regional Meeting, Ontario Convention Center, California, (October 6-8, 1999).

29. R. Mills, B. Dhandapani, N. Greenig, J. He, "Synthesis and Characterization of Potassium Iodo Hydride", 1999 Pacific Conference on Chemistry and Spectroscopy and the 35th ACS Western Regional Meeting, Ontario Convention Center, California, (October 6-8, 1999).
30. R. Mills, J. He, and B. Dhandapani, "Novel Hydrogen Compounds", 1999 Pacific Conference on Chemistry and Spectroscopy and the 35th ACS Western Regional Meeting, Ontario Convention Center, California, (October 6-8, 1999).
31. R. Mills, "Novel Hydride Compound", National Hydrogen Association, 11 th Annual U.S. Hydrogen Meeting, Vienna, VA, (February 29-March 2, 2000).
32. R. Mills, J. He, and B. Dhandapani, "Novel Alkali and Alkaline Earth Hydrides", National Hydrogen Association, 11 th Annual U.S. Hydrogen Meeting, Vienna, VA, (February 29-March 2, 2000).
33. R. Mills, "Novel Hydride Compound", 219 th National ACS Meeting, San Francisco, California, (March 26-30, 2000).
34. R. Mills, J. He, and B. Dhandapani, "Novel Alkali and Alkaline Earth Hydrides", 219 th National ACS Meeting, San Francisco, California, (March 26-30, 2000).
35. R. Mills, J. He, and B. Dhandapani, "Novel Alkali and Alkaline Earth Hydrides", August National ACS Meeting (220th ACS National Meeting, Washington, DC, (August 20-24, 2000)).
36. R. Mills, The Nature of Free Electrons in Superfluid Helium--a Test of Quantum Mechanics and a Basis to Review its Foundations and Make a Comparison to Classical Theory, Int. J. Hydrogen Energy, in press.
37. David R. Linde, *CRC Handbook of Chemistry and Physics*, 79 th Edition, CRC Press, Boca Raton, Florida, (1998-9), p. 10-175 to p. 10-177.
38. W. M. Muller, J. P. Blackledge, G. G. Libowitz, *Metal Hydrides*, Academic Press, New York, (1968), p 201.
39. J. C. Bailar, H. J. Emeleus, R. Nyholm, A. F. Trotman-Dickenson, Editors, *Comprehensive Inorganic Chemistry*, Pergamon Press, Oxford, UK, (1973), 1st Edition, p. 381.
40. G. J. Janz, *Molten Salts Handbook*, Academic Press, New York, (1967), p. 184.
41. David R. Linde, *CRC Handbook of Chemistry and Physics*, 79 th Edition, CRC Press, Boca Raton, Florida, (1998-9), p. 5-18.

42. David R. Linde, *CRC Handbook of Chemistry and Physics*, 79 th Edition, CRC Press, Boca Raton, Florida, (1998-9), p. 12-191.
43. Schoenfelder, C. W., Swisher, J. H., *J. Vac. Sci. Tech.*, Vol. 10, No. 5, (1973), pp. 862-870.
44. N. V. Sidgwick, *The Chemical Elements and Their Compounds*, Volume I, Oxford, Clarendon Press, (1950), p.17.
45. R. Mills, "BlackLight Power Technology-A New Clean Energy Source with the Potential for Direct Conversion to Electricity", Global Foundation, Inc. conference entitled *Global Warming and Energy Policy*, Fort Lauderdale, FL, November 26-28, 2000.
46. R. Mills, "BlackLight Power Technology-A New Clean Energy Source with the Potential for Direct Conversion to Electricity", Global Foundation International Conference on "Global Warming and Energy Policy", Dr. Behram N. Kursunoglu, Chairman, Fort Lauderdale, FL, November 26-28, 2000, in press.

Figure Captions

- Figure 1. The results of the DSC (100-750 °C) of *KH* and *KI* at a scan rate of 0.1 degree/minute.
- Figure 2. The repeat results of the DSC (100-750 °C) of *KH* and *KI* at a scan rate of 0.1 degree/minute.
- Figure 3. The results of the DSC (100-750 °C) of *KI* with some *KHI* at a scan rate of 0.1 degree/minute.
- Figure 4. The results of the DSC (100-750 °C) of *KI* at a scan rate of 0.1 degree/minute.
- Figure 5. The results of the DSC (100-750 °C) of MgH_2 at a scan rate of 0.1 degree/minute.
- Figure 6. The repeat results of the DSC (100-750 °C) of MgH_2 at a scan rate of 0.1 degree/minute.

Fig. 1

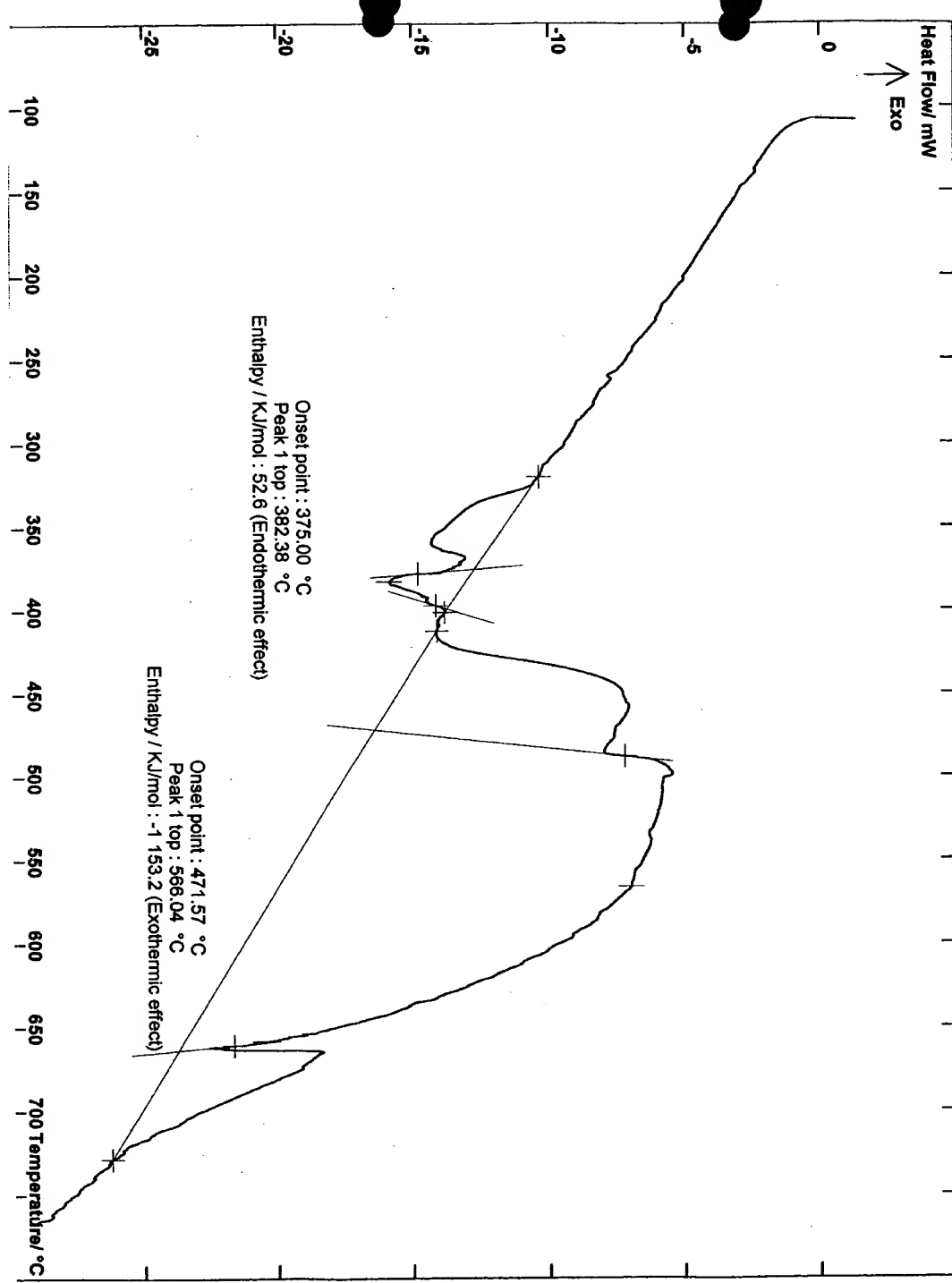


Fig. 2

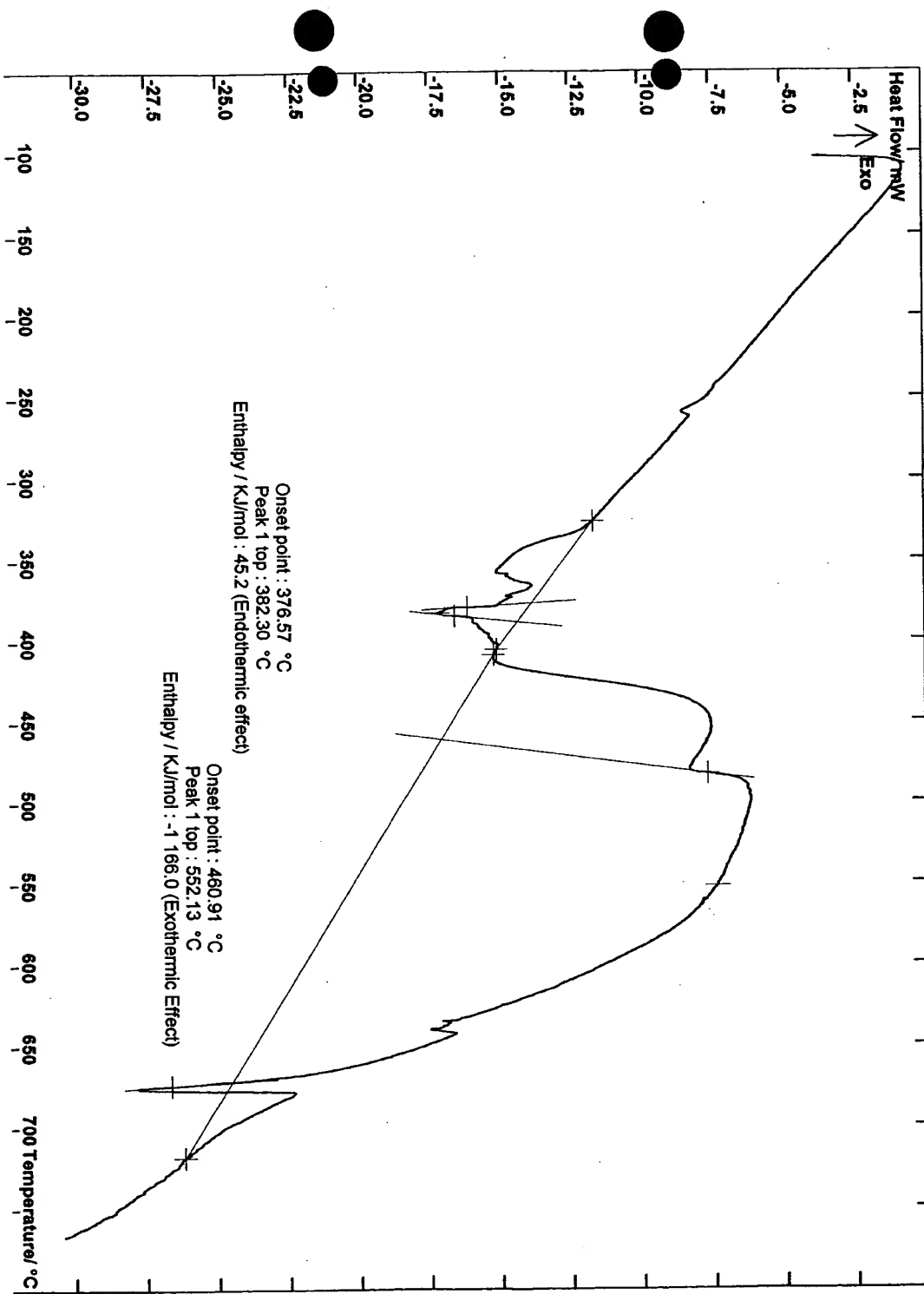


Fig. 3

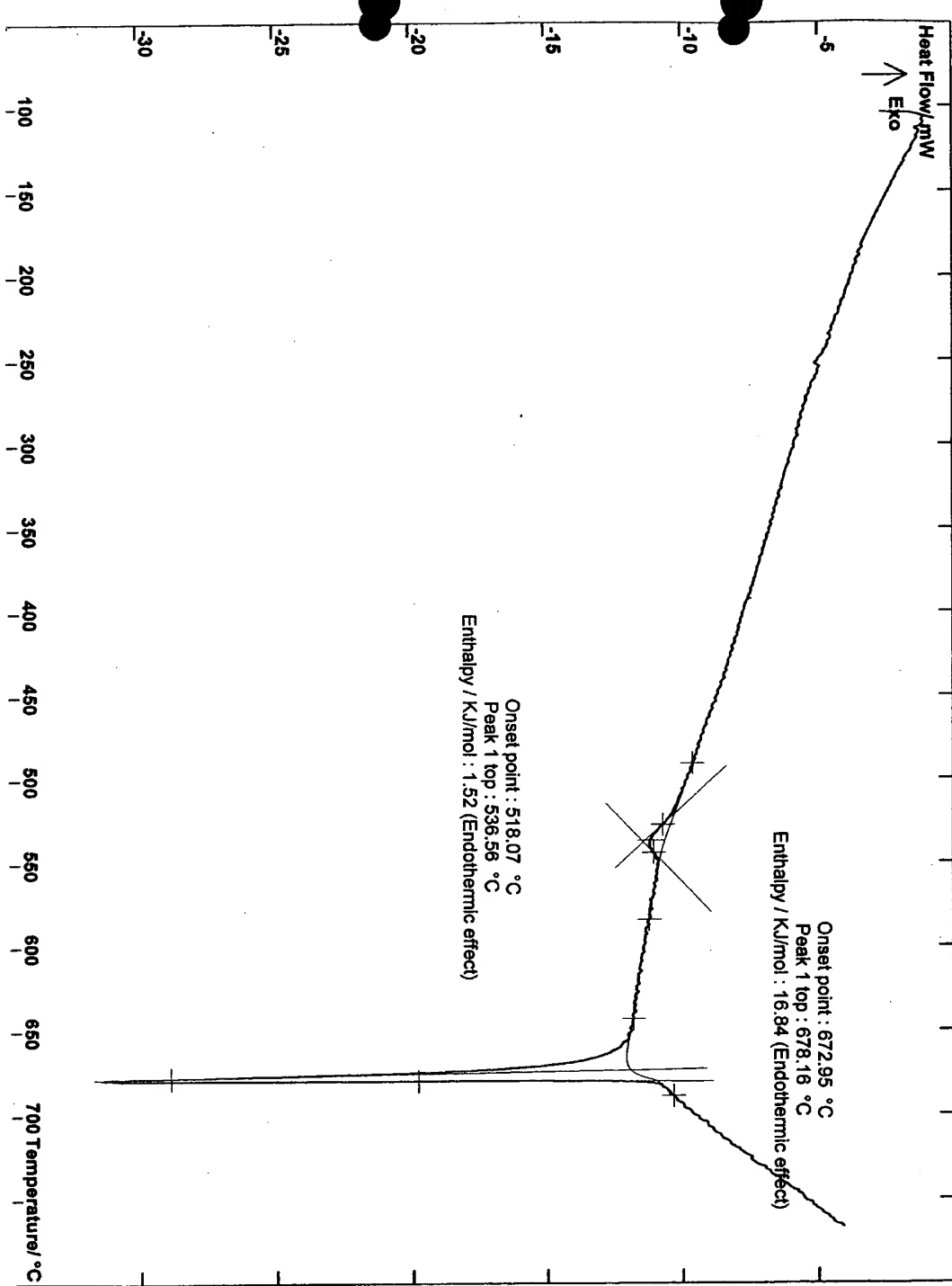


Fig. 4

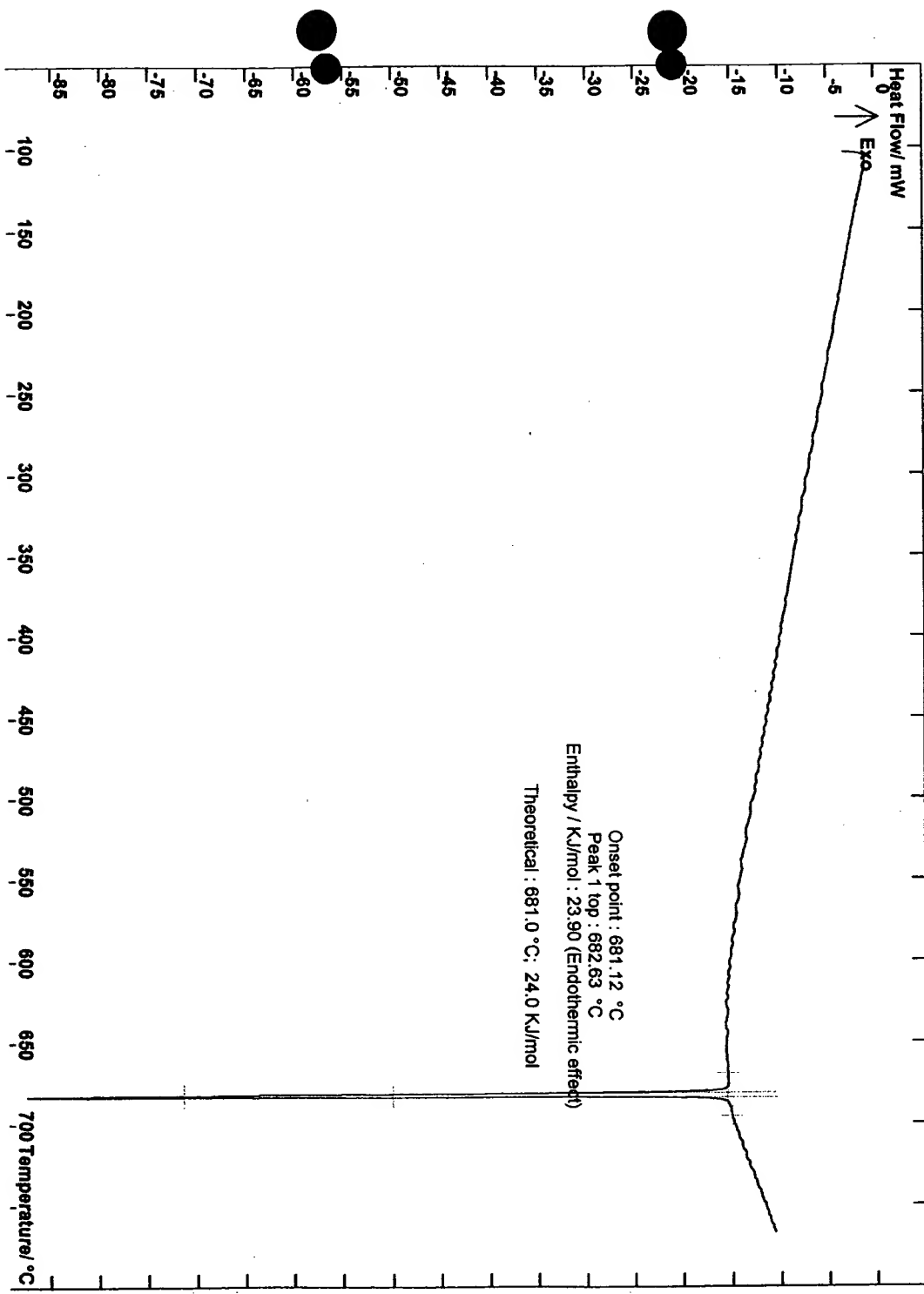


Fig. 5

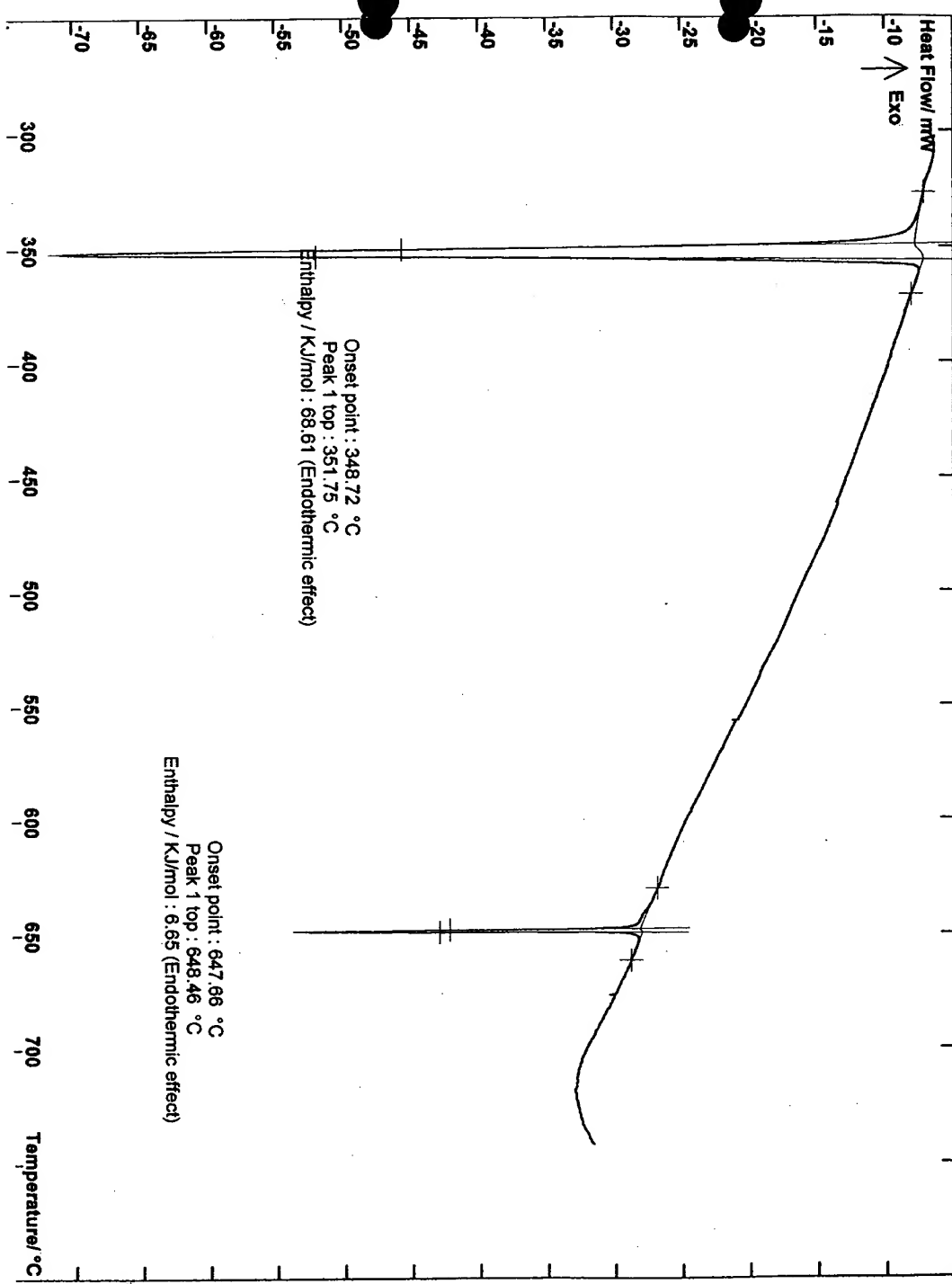
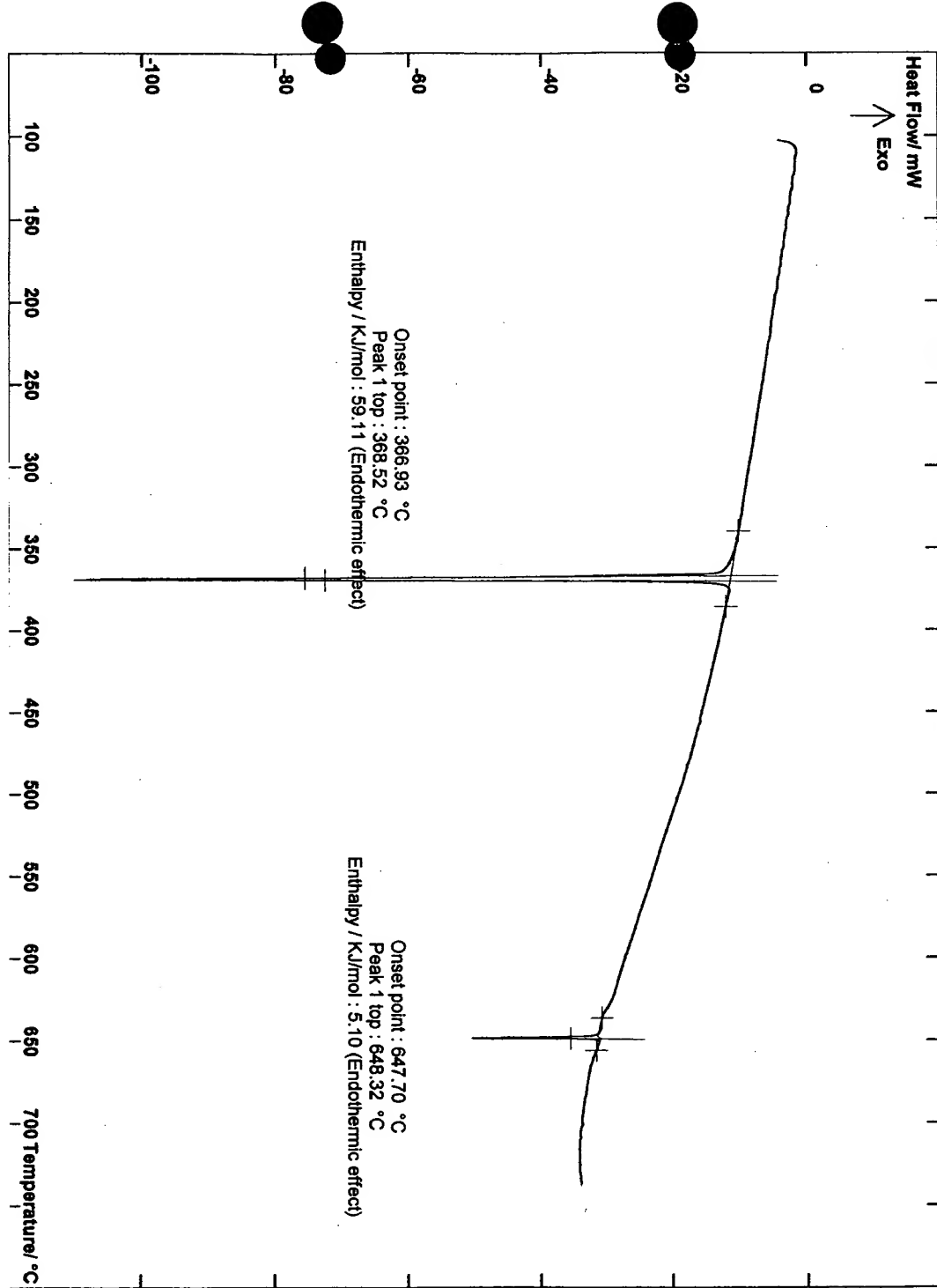


Fig. 6



Spectroscopic Identification of a Novel Catalytic Reaction of Atomic Hydrogen and the Hydride Ion Product

Randell L. Mills
BlackLight Power, Inc.
493 Old Trenton Road
Cranbury, NJ 08512

From a solution of a Schrödinger-type wave equation with a nonradiative boundary condition based on Maxwell's equations, Mills predicts that atomic hydrogen may undergo a catalytic reaction with certain atomized elements such as cesium and strontium atoms or certain gaseous ions such as Ar^+ which singly or multiply ionize at integer multiples of the potential energy of atomic hydrogen, 27.2 eV. The reaction involves a nonradiative energy transfer to form a hydrogen atom that is lower in energy than unreacted atomic hydrogen with the release of energy. Intense extreme ultraviolet (EUV) emission was observed from incandescently heated atomic hydrogen and the atomized catalysts that generated the plasma at low temperatures (e.g. $\approx 10^3 K$). No emission was observed with cesium, strontium, argon, hydrogen, or an argon-hydrogen mixture (97/3%) alone or when sodium, magnesium, or barium replaced strontium or cesium with hydrogen or with an argon-hydrogen mixture. The emission intensity of the plasma generated by the cesium or strontium catalyst increased significantly with the introduction of argon gas only when Ar^+ emission was observed. Ar^+ which served as a second catalyst was generated by the formation of a plasma with cesium or strontium catalyst. Emission was observed from a continuum state of Cs^{2+} and Ar^{2+} at 53.3 nm and 45.6 nm, respectively. The single emission feature with the absence of the other corresponding Rydberg series of lines from these species confirmed the resonant nonradiative energy transfer of 27.2 eV from atomic hydrogen to atomic cesium or Ar^+ . The catalysis product, a lower-energy hydrogen atom, was predicted to be a highly reactive intermediate which further reacts to form a novel hydride ion. The predicted hydride ion of hydrogen catalysis by either cesium atom or Ar^+ catalyst is the hydride ion $H^- (1/2)$. This ion was observed spectroscopically at 407 nm corresponding to its predicted binding energy of 3.05 eV.

I. INTRODUCTION

A. Novel Hydrogen Chemistry

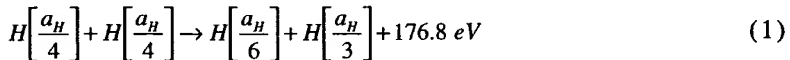
Based on the solution of a Schrödinger-type wave equation with a nonradiative boundary condition based on Maxwell's equations, Mills [1-31] predicts that atomic hydrogen may undergo a catalytic reaction with certain atomized elements or certain gaseous ions which singly or multiply ionize at integer multiples of the potential energy of atomic hydrogen, 27.2 eV. For example, cesium atoms ionize at an integer multiple of the potential energy of atomic hydrogen, $m \cdot 27.2$ eV. The enthalpy of ionization of Cs to Cs^{2+} has a net enthalpy of reaction of 27.05135 eV, which is equivalent to $m=1$ [32]. And, the reaction Ar^+ to Ar^{2+} has a net enthalpy of reaction of 27.63 eV, which is equivalent to $m=1$ [32]. In each case, the reaction involves a nonradiative energy transfer to form a hydrogen atom that is lower in energy than unreacted atomic hydrogen. The product hydrogen atom has an energy state that corresponds to a fractional principal quantum number. Recent analysis of mobility and spectroscopy data of individual electrons in liquid helium show direct experimental confirmation that electrons may have fractional principal quantum energy levels [33]. The lower-energy hydrogen atom is a highly reactive intermediate which further reacts to form a novel hydride ion. We report single line emission from the excited catalyst ion formed by nonradiatively accepting the energy of 27.2 eV from atomic hydrogen. Furthermore, the emission from the predicted hydride ion product was observed spectroscopically. The catalytic reaction with the formation of the hydride ions produces an intense hydrogen plasma which was observed by EUV and visible emission.

Typically the emission of extreme ultraviolet light from hydrogen gas is achieved via a discharge at high voltage, a high power inductively coupled plasma, or a plasma created and heated to extreme temperatures by RF coupling (e.g. $>10^6$ K) with confinement provided by a toroidal magnetic field. Observation of intense extreme ultraviolet (EUV) emission at low temperatures (e.g. $\approx 10^3$ K) from atomic hydrogen and certain atomized elements or certain gaseous ions [2-16] has been reported previously. The only pure elements that were observed to emit

EUV were those wherein the ionization of t electrons from an atom to a continuum energy level is such that the sum of the ionization energies of the t electrons is approximately $m \cdot 27.2 \text{ eV}$ where t and m are each an integer. Potassium, cesium, and strontium atoms and Rb^+ ion ionize at integer multiples of the potential energy of atomic hydrogen and caused emission. Whereas, the chemically similar atoms, sodium, magnesium and barium, do not ionize at integer multiples of the potential energy of atomic hydrogen and caused no emission.

Prior studies that support the possibility of a novel reaction of atomic hydrogen which produces an anomalous discharge and produces novel hydride compounds include extreme ultraviolet (EUV) spectroscopy [3-6, 8-16], plasma formation [2-16], power generation [2-4, 9, 31], and analysis of chemical compounds [12, 14-31].

1.) Lines observed at the Institut Fur Niedertemperatur-Plasmaphysik e.V. by EUV spectroscopy could be assigned to transitions of atomic hydrogen to lower energy levels corresponding to lower energy hydrogen atoms and the emission from the excitation of the corresponding hydride ions [6]. For example, the product of the catalysis of atomic hydrogen with potassium metal, $H\left[\frac{a_H}{4}\right]$ may serve as both a catalyst and a reactant to form $H\left[\frac{a_H}{3}\right]$ and $H\left[\frac{a_H}{6}\right]$. The transition of $H\left[\frac{a_H}{4}\right]$ to $H\left[\frac{a_H}{6}\right]$ induced by a multipole resonance transfer of 54.4 eV ($2 \cdot 27.2 \text{ eV}$) and a transfer of 40.8 eV with a resonance state of $H\left[\frac{a_H}{3}\right]$ excited in $H\left[\frac{a_H}{4}\right]$ is represented by



The predicted 176.8 eV (70.2 \AA) photon is a close match with the observed 73.0 \AA line. The energy of this line emission corresponds to an equivalent temperature of $1,000,000 \text{ }^\circ\text{C}$ and an energy over 100 times the energy of combustion of hydrogen.

2.) Transitions of atomic hydrogen to lower energy levels corresponding to lower energy hydrogen atoms has been identified in the extreme ultraviolet emission spectrum from interstellar medium [34].

3.) Observation of intense extreme ultraviolet (EUV) emission has been reported at low temperatures (e.g. $\approx 10^3 K$) from atomic hydrogen and certain atomized elements or certain gaseous ions [2-16]. The only pure elements that were observed to emit EUV were those wherein the ionization of t electrons from an atom to a continuum energy level is such that the sum of the ionization energies of the t electrons is approximately $m \cdot 27.2 eV$ where t and m are each an integer. Potassium, cesium, and strontium atoms and Rb^+ ion ionize at integer multiples of the potential energy of atomic hydrogen and caused emission. Whereas, the chemically similar atoms, sodium, magnesium, and barium do not ionize at integer multiples of the potential energy of atomic hydrogen and caused no emission.

4.) An energetic plasma in hydrogen was generated using strontium atoms as the catalyst. The plasma formed at 1% of the theoretical or prior known voltage requirement with 4,000-7,000 times less power input power compared to noncatalyst controls, sodium, magnesium, or barium atoms, wherein the plasma reaction was controlled with a weak electric field [4, 9]. The light output for power input increased to 8600 times that of the control when argon was added to the hydrogen strontium plasma to form catalyst Ar^+ [3].

5.) The optically measured output power of gas cells for power supplied to the glow discharge increased by over two orders of magnitude depending on the presence of less than 1% partial pressure of certain of catalysts in hydrogen gas or argon-hydrogen gas mixtures [2].

6.) In experiments performed at the Institut Fur Niedertemperatur-Plasmaphysik e.V., an anomalous plasma formed with hydrogen-potassium mixtures wherein the plasma decayed with a two second half-life which was the thermal decay time of the filament which dissociated molecular hydrogen to atomic hydrogen when the electric field was set to zero [7, 10]. This experiment showed that hydrogen line emission was occurring even though the voltage between the heater wires was set to and measured to be zero and indicated that the emission was due to a

reaction of potassium catalyst with atomic hydrogen which confirms a new chemical source of power.

7.) A plasma of hydrogen and certain alkali ions formed at low temperatures (e.g. $\approx 10^3 K$) as recorded via EUV spectroscopy and the hydrogen Balmer and alkali line emissions in the visible range. The observed plasma formed at low temperatures (e.g. $\approx 10^3 K$) from atomic hydrogen generated at a tungsten filament that heated a titanium dissociator and a catalyst comprising one of potassium, rubidium, cesium, and their carbonates and nitrates. These atoms and ions ionize to provide a catalyst with a net enthalpy of reaction of an integer multiple of the potential energy of atomic hydrogen ($m \cdot 27.2 \text{ eV}$ $m = \text{integer}$) to within 0.17 eV and comprise only a single ionization in the case of a potassium or rubidium ion. Whereas, the chemically similar atoms of sodium and sodium and lithium carbonates and nitrates which do not ionize with these constraints caused no emission. To test the electric dependence of the emission, the weak electric field of about 1 V/cm was set and measured to be zero in $< 0.5 \times 10^{-6} \text{ sec}$. An anomalous afterglow duration of about one to two seconds was recorded in the case of potassium, rubidium, cesium, K_2CO_3 , $RbNO_3$, and $CsNO_3$. Hydrogen line or alkali line emission was occurring even though the voltage between the heater wires was set to and measured to be zero. These atoms and ions ionize to provide a catalyst with a net enthalpy of reaction of an integer multiple of the potential energy of atomic hydrogen to within less than the thermal energies at $\approx 10^3 K$ and comprise only a single ionization in the case of a potassium or rubidium ion. Since the thermal decay time of the filament for dissociation of molecular hydrogen to atomic hydrogen was similar to the anomalous plasma afterglow duration, the emission was determined to be due to a reaction of atomic hydrogen with a catalyst that did not require the presence of an electric field to be functional.

8.) Reports of the formation of novel compounds provide substantial evidence supporting a novel reaction of hydrogen as the mechanism of the observed EUV emission and anomalous discharge. Novel hydrogen compounds have been isolated as products of the reaction of atomic hydrogen with atoms and ions identified as catalysts in the reported EUV studies [2-31]. Novel inorganic alkali and alkaline earth hydrides of the formula MH^* and MH^*X wherein M is the metal,

X , is a singly negatively charged anion, and H^* comprises a novel high binding energy hydride ion were synthesized in a high temperature gas cell by reaction of atomic hydrogen with a catalyst such as potassium metal and MH , MX or MX_2 corresponding to an alkali metal or alkaline earth metal compound, respectively [17, 20-21]. Novel hydride compounds were identified by 1.) time of flight secondary ion mass spectroscopy which showed a dominant hydride ion in the negative ion spectrum, 2.) X-ray photoelectron spectroscopy which showed novel hydride peaks and significant shifts of the core levels of the primary elements bound to the novel hydride ions, 3.) 1H nuclear magnetic resonance spectroscopy (NMR) which showed extraordinary upfield chemical shifts compared to the NMR of the corresponding ordinary hydrides, and 4.) thermal decomposition with analysis by gas chromatography, and mass spectroscopy which identified the compounds as hydrides [17, 20].

An upfield shifted NMR peak is consistent with a hydride ion with a smaller radius as compared with ordinary hydride since a smaller radius increases the shielding or diamagnetism. Thus, the NMR shows that the hydride formed in the catalytic reaction has been reduced in distance to the nucleus indicating that the electrons are in a lower-energy state. Compared to the shift of known corresponding hydrides the NMR provides direct evidence of reduced energy state hydride ions.

The NMR results confirm the identification of novel hydride compounds MH^*X , MH^* , and MH_2^* wherein M is the metal, X , is a halide, and H^* comprises a novel high binding energy hydride ion. For example, large distinct upfield resonances were observed at -4.6 ppm and -2.8 ppm in the case of KH^*Cl and KH^* , respectively. Whereas, the resonances for the ordinary hydride ion of KH were observed at 0.8 and 1.1 ppm. The presence of a halide in each compound MH^*X does not explain the upfield shifted NMR peak since the same NMR spectrum was observed for an equimolar mixture of the pure hydride and the corresponding alkali halide (MH/MX) as was observed for the pure hydride, MH . The synthesis of novel hydrides such as KH^* with upfield shifted peaks prove that the hydride ion is different from the hydride ion of the corresponding known compound of the same composition. The

reproducibility of the syntheses and the results from five independent laboratories confirm the formation of novel hydride ions.

The mechanism of EUV emission and formation of novel hydrides can not be explained by the conventional chemistry of hydrogen, but it is predicted by a solution of the Schrödinger equation with a nonradiative boundary constraint put forward by Mills [1]. Mills predicts that certain atoms or ions serve as catalysts to release energy from hydrogen to produce an increased binding energy hydrogen atom called a *hydrino atom* having a binding energy of

$$\text{Binding Energy} = \frac{13.6 \text{ eV}}{n^2} \quad (2)$$

where

$$n = \frac{1}{2}, \frac{1}{3}, \frac{1}{4}, \dots, \frac{1}{p} \quad (3)$$

and p is an integer greater than 1, designated as $H\left[\frac{a_H}{p}\right]$ where a_H is the radius of the hydrogen atom. Hydrinos are predicted to form by reacting an ordinary hydrogen atom with a catalyst having a net enthalpy of reaction of about

$$m \cdot 27.2 \text{ eV} \quad (4)$$

where m is an integer. This catalysis releases energy from the hydrogen atom with a commensurate decrease in size of the hydrogen atom, $r_n = n a_H$. For example, the catalysis of $H(n=1)$ to $H(n=1/2)$ releases 40.8 eV, and the hydrogen radius decreases from a_H to $\frac{1}{2}a_H$.

The excited energy states of atomic hydrogen are also given by Eq. (2) except that

$$n = 1, 2, 3, \dots \quad (5)$$

The $n=1$ state is the "ground" state for "pure" photon transitions (the $n=1$ state can absorb a photon and go to an excited electronic state, but it cannot release a photon and go to a lower-energy electronic state). However, an electron transition from the ground state to a lower-energy state is possible by a nonradiative energy transfer such as multipole coupling or a resonant collision mechanism. These lower-energy states have fractional quantum numbers, $n = \frac{1}{\text{integer}}$. Processes that occur without photons and that require collisions are common. For example,

the exothermic chemical reaction of $H + H$ to form H_2 does not occur with the emission of a photon. Rather, the reaction requires a collision with a third body, M , to remove the bond energy- $H + H + M \rightarrow H_2 + M^*$ [35]. The third body distributes the energy from the exothermic reaction, and the end result is the H_2 molecule and an increase in the temperature of the system. Some commercial phosphors are based on nonradiative energy transfer involving multipole coupling. For example, the strong absorption strength of Sb^{3+} ions along with the efficient nonradiative transfer of excitation from Sb^{3+} to Mn^{2+} , are responsible for the strong manganese luminescence from phosphors containing these ions [36]. Similarly, the $n=1$ state of hydrogen and the $n=\frac{1}{\text{integer}}$ states of hydrogen are

nonradiative, but a transition between two nonradiative states is possible via a nonradiative energy transfer, say $n=1$ to $n=1/2$. In these cases, during the transition the electron couples to another electron transition, electron transfer reaction, or inelastic scattering reaction which can absorb the exact amount of energy that must be removed from the hydrogen atom. Thus, a catalyst provides a net positive enthalpy of reaction of $m \cdot 27.2 \text{ eV}$ (i.e. it absorbs $m \cdot 27.2 \text{ eV}$ where m is an integer). Certain atoms or ions serve as catalysts which resonantly accept energy from hydrogen atoms and release the energy to the surroundings to effect electronic transitions to fractional quantum energy levels. Recent analysis of mobility and spectroscopy data of individual electrons in liquid helium show direct experimental evidence that electrons may have fractional principal quantum energy levels [33].

The catalysis of hydrogen involves the nonradiative transfer of energy from atomic hydrogen to a catalyst which may then release the transferred energy by radiative and nonradiative mechanisms. As a consequence of the nonradiative energy transfer, the hydrogen atom becomes unstable and emits further energy until it achieves a lower-energy nonradiative state having a principal energy level given by Eq. (2-3).

The energy released during catalysis may undergo internal conversion and ionize or excite molecular and atomic hydrogen resulting in hydrogen emission which includes well characterized ultraviolet lines such as the Lyman series. Lyman α emission was sought by EUV

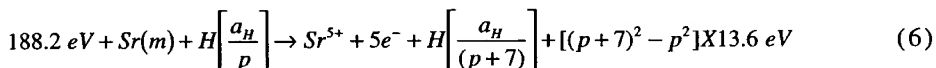
spectroscopy. The energy released during catalysis may also undergo internal conversion and cause alkali line emission. The existence of Balmer emission requires that Lyman emission is also generated. This confirms that a hydrogen plasma exists. Lyman α emission was sought by EUV spectroscopy, and Balmer and alkali line emission was sought by visible spectroscopy.

B. Catalysts

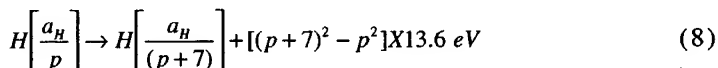
The emission observed EUV emission could not be explained by conventional chemistry; rather it must have been due to a novel chemical reaction between catalyst and atomic hydrogen. According to Mills [1], a catalytic system is provided by the ionization of t electrons from an atom or ion to a continuum energy level such that the sum of the ionization energies of the t electrons is approximately $m \times 27.2 \text{ eV}$ where m is an integer.

Strontium

One such catalytic system involves strontium. The first through the fifth ionization energies of strontium are 5.69484 eV , 11.03013 eV , 42.89 eV , 57 eV , and 71.6 eV , respectively [32]. The ionization reaction of Sr to Sr^{5+} , ($t=5$), then, has a net enthalpy of reaction of 188.2 eV , which is equivalent to $m=7$ in Eq. (4).

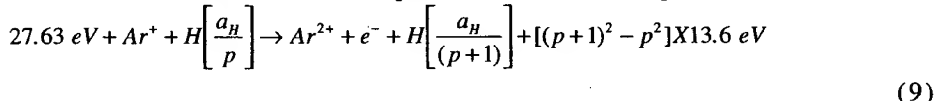


And, the overall reaction is

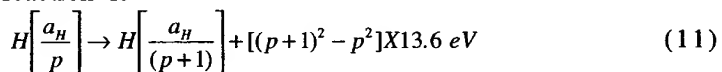


Argon Ion

Argon ions can also provide a net enthalpy of a multiple of that of the potential energy of the hydrogen atom. The second ionization energy of argon is 27.63 eV. The reaction Ar^+ to Ar^{2+} has a net enthalpy of reaction of 27.63 eV, which is equivalent to $m=1$ in Eq. (4).

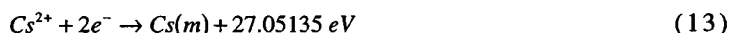
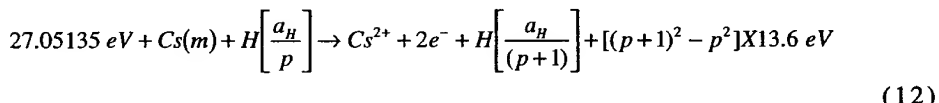


And, the overall reaction is

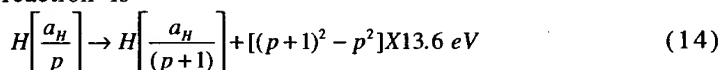


Cesium

A catalytic system is provided by the ionization of 2 electrons from a cesium atom each to a continuum energy level such that the sum of the ionization energies of the 2 electrons is approximately 27.2 eV. The first and second ionization energies of cesium are 3.89390 eV and 23.15745 eV, respectively [32]. The double ionization ($t=2$) reaction of Cs to Cs^{2+} , then, has a net enthalpy of reaction of 27.05135 eV, which is equivalent to $m=1$ in Eq. (4).



And, the overall reaction is



C. Hydride Ion

A novel hydride ion having extraordinary chemical properties given by Mills [1] is predicted to form by the reaction of an electron with

a hydrino (Eq. (15)). The resulting hydride ion is referred to as a hydrino hydride ion, designated as $H^-(1/p)$.



The hydrino hydride ion is distinguished from an ordinary hydride ion having a binding energy of 0.8 eV. The hydrino hydride ion is predicted [1] to comprise a hydrogen nucleus and two indistinguishable electrons at a binding energy according to the following formula:

$$\text{Binding Energy} = \frac{\hbar^2 \sqrt{s(s+1)}}{8\mu_e a_0^2 \left[\frac{1+\sqrt{s(s+1)}}{p} \right]^2} - \frac{\pi \mu_0 e^2 \hbar^2}{m_e^2 a_0^3} \left(1 + \frac{2^2}{\left[\frac{1+\sqrt{s(s+1)}}{p} \right]^3} \right) \quad (16)$$

where p is an integer greater than one, $s=1/2$, π is pi, \hbar is Planck's constant bar, μ_0 is the permeability of vacuum, m_e is the mass of the electron, μ_e is the reduced electron mass, a_0 is the Bohr radius, and e is the elementary charge. The ionic radius is

$$r_i = \frac{a_0}{p} \left(1 + \sqrt{s(s+1)} \right); s = \frac{1}{2} \quad (17)$$

From Eq. (17), the radius of the hydrino hydride ion $H^-(1/p)$; p = integer is $\frac{1}{p}$ that of ordinary hydride ion, $H^-(1/1)$. Compounds containing hydrino hydride ions have been isolated as products of the reaction of atomic hydrogen with atoms and ions identified as catalysts by EUV emission [2-31].

We report that plasma that emitted intense EUV formed at low temperatures (e.g. $\approx 10^3 K$) from atomic hydrogen generated at a tungsten filament and atomic strontium or cesium catalyst (Eqs. (6-8) and (12-14), respectively) which were vaporized from the metal by heating. A first catalyst may produce a second catalyst from a source of the second catalyst. For example, a plasma may be formed using atomic hydrogen

and strontium catalyst (Eqs. (6-8)). If argon was added to the plasma, then catalyst Ar^+ (Eqs. (9-11)) would be produced from argon. Second catalyst Ar^+ would in turn generate more Ar^+ which may dominate the catalysis reaction. The emission intensity of the plasma generated by the strontium catalyst increased significantly with the introduction of argon gas only when Ar^+ emission was observed. No emission was observed with cesium, strontium, argon, or hydrogen alone or when sodium, magnesium, or barium replaced strontium or cesium with hydrogen or with an argon-hydrogen mixture.

Characteristic emission was observed from a continuum state of Cs^{2+} and Ar^{2+} which confirmed the resonant nonradiative energy transfer of 27.2 eV from atomic hydrogen to atomic cesium or Ar^+ , respectively. The predicted $H^-(1/2)$ hydride ion of hydrogen catalysis by either cesium atom or Ar^+ catalyst given by Eqs. (12-14) and Eqs. (9-11), respectively and Eq. (16) was observed spectroscopically at 407 nm corresponding to its predicted binding energy of 3.05 eV.

II. EXPERIMENTAL

A. EUV, UV, and Visible Spectroscopy

Due to the extremely short wavelength of this radiation, "transparent" optics do not exist for EUV spectroscopy. Therefore, a windowless arrangement was used wherein the source was connected to the same vacuum vessel as the grating and detectors of the EUV spectrometer. Windowless EUV spectroscopy was performed with an extreme ultraviolet spectrometer that was mated with the cell. Differential pumping permitted a high pressure in the cell as compared to that in the spectrometer. This was achieved by pumping on the cell outlet and pumping on the grating side of the collimator that served as a pin-hole inlet to the optics. The cell was operated under gas flow conditions while maintaining a constant gas pressure in the cell with a mass flow controller.

The experimental set up shown in Figure 1 comprised a quartz cell which was 500 mm in length and 50 mm in diameter. The cell had three ports for gas inlet, outlet, and photon detection. The cell pump was a

mechanical pump. A second gas port from a line common with the cell inlet could supply gas to the cell from the monochromator of the spectrometer according to a special method described below. The spectrometer was continuously evacuated to 10^{-4} – 10^{-6} torr by a turbomolecular pump with the pressure read by a cold cathode pressure gauge. The EUV spectrometer was connected to the cell light source with a 1.5 mm X 5 mm collimator which provided a light path to the slits of the EUV spectrometer. The collimator also served as a flow constrictor of gas from the cell. Valves were between the cell and the mechanical pump, the cell and the monochromator, the monochromator and the gas supply, and the monochromator and its turbo pump.

A tungsten filament heater and hydrogen dissociator (0.508 mm in diameter and 800 cm in length, total resistance ~2.5 ohm) and, in the case of the control hydrogen gas experiments, a titanium cylindrical screen (300 mm long and 40 mm in diameter) that performed as a second hydrogen dissociator were inside the quartz cell. A new dissociator was used for each control hydrogen gas experiment. The filament was coiled on a grooved ceramic tube support to maintain its shape when heated. The return lead passed through the inside of the ceramic tube. The titanium screen was electrically floated. The power was applied to the filament by a Sorensen 80-13 power supply which was controlled by a constant power controller. The temperature of the tungsten filament was estimated to be in the range of 1100 to 1500 °C. The external cell wall temperature was about 700 °C. Except where indicated, the gas was ultrahigh purity hydrogen, argon-hydrogen mixture (97/3%), or an argon-hydrogen mixture (95/5%). Except where indicated, the gas pressure inside the cell was maintained at about 300 mtorr with a hydrogen flow rate of 5.5 sccm, an argon-hydrogen mixture (97/3%) flow rate of 5.5 sccm, or an argon flow rate of 5.2 sccm and a hydrogen flow rate of 0.3 sccm, respectively. Each gas flow was controlled by a 20 sccm range mass flow controller (MKS 1179A21CS1BB) with a readout (MKS type 246). The entire quartz cell was enclosed inside an insulation package comprised of Zircar AL-30 insulation. Several K type thermocouples were placed in the insulation to measure key temperatures of the cell and insulation. The thermocouples were read with a multichannel computer data acquisition system.

In the present study, the light emission phenomena was studied for 1.) hydrogen, argon, neon, and helium alone; 2.) sodium, magnesium, barium, cesium, and strontium metals alone; 3.) sodium, magnesium, barium, cesium, and strontium with hydrogen; 4.) sodium, magnesium, barium, cesium, and strontium with an argon-hydrogen mixture (97/3%), and 5.) cesium and strontium with argon-hydrogen mixtures. The pure elements of sodium, magnesium, barium, cesium, and strontium were placed in the bottom of the cell and vaporized by filament heating. The power applied to the filament was 300 W in the case of strontium and up to 600 W in the case of magnesium, barium, and sodium metals. The voltage across the filament was about 55 V and the current was about 5.5 A at 300 W. For the controls, magnesium, barium, and sodium metals, the cell was increased in temperature to the maximum permissible with the power supply.

The light emission was introduced to an EUV spectrometer for spectral measurement. The spectrometer was a McPherson 0.2 meter monochromator (Model 302, Seya-Namioka type) equipped with a 1200 lines/mm holographic grating with a platinum coating (except that a MgF_2 coated grating was used for an experiment with a cesium- argon-hydrogen mixture as indicated in the figure caption of Figure 31). This grating has a very low efficiency at the region of hydrogen Lyman α . The wavelength region covered by the monochromator was 30–560 nm. A channel electron multiplier (CEM) was used to detect the EUV light. The wavelength resolution was about 1 nm (FWHM) with an entrance and exit slit width of 300 μm . The vacuum inside the monochromator was maintained below 5×10^{-4} torr by a turbo pump. The EUV spectrum (40–160 nm) of the cell emission with cesium or strontium present was recorded at about the point of the maximum Lyman α emission.

To achieve higher sensitivity at the shorter EUV wavelengths, the light emission was recorded with a McPherson 4° grazing incidence EUV spectrometer (Model 248/310G) equipped with a grating having 600 G/mm with a radius of curvature of $\approx 1\text{ m}$. The angle of incidence was 87°. The wavelength region covered by the monochromator was 1–65 nm. The wavelength resolution was about 0.1 nm (FWHM) with an entrance and exit slit width of 50 μm . A channel electron multiplier (CEM) was

used to detect the EUV light. The vacuum inside the monochromator was maintained below 5×10^{-4} torr by a turbo pump.

The EUV/UV/VIS spectrum (40–560 nm) of the cell emission with hydrogen alone was recorded with a photomultiplier tube (PMT) and a sodium salicylate scintillator. The PMT (Model R1527P, Hamamatsu) used has a spectral response in the range of 185–680 nm with a peak efficiency at about 400 nm. The scan interval was 0.4 nm. The inlet and outlet slit were 500 μm with a corresponding wavelength resolution of 2 nm.

B. Standard Hydrogen, Argon, and Cesium Emission Spectrum

Standard extreme ultraviolet emission spectra of atomic and molecular hydrogen, argon, and cesium were obtained with a microwave plasma system and an EUV spectrometer. The microwave generator was a Ophos model MPG-4M generator (Frequency: 2450 MHz). The output power was set at about 85 W. Hydrogen or argon was flowed through a quartz tube (1.25 cm ID, 20 cm long) at 500 mtorr. The tube was fitted with an Ophos coaxial microwave cavity (Evenson cavity), and was directly connected to the collimator port of an EUV spectrometer. The EUV spectrometer was a McPherson model 302 (Seya-Namioka type) normal incidence monochromator. The monochromator slits were 100X100 μm . A sodium salicylate converter was used, and the emission was detected with a photomultiplier tube detector (Hamamatsu R1527P).

In order to record the standard cesium spectrum, a cesium side-arm reservoir was joined to the quartz tube. The reservoir comprised a 1.25 cm ID Pyrex tube with a sealed capillary tip at the end that attached to the microwave plasma quartz tube. In a drybox, about 0.5 g of cesium metal was placed in the reservoir through the other open end of the Pyrex tube. The Pyrex tube was then capped with a septum and was flame-sealed outside the drybox. A glass-capped magnetic bar was placed inside the quartz tube, which was then connected to EUV spectrometer and a gas/vacuum line. After a good vacuum ($\sim 10^{-5}$ torr) was obtained, the capillary tip on the cesium reservoir was broken through by moving the magnetic bar with an external magnet. The cesium was heated until it liquefied and flowed into the quartz tube.

Hydrogen gas was flowed through the quartz tube at 500 mtorr to generate a plasma with cesium vapor.

C. 407 nm Emission from Strontium and Ar⁺ Catalyst

1.) The monochromator was under high vacuum with the valve to the cell closed. The cell was heated overnight at 275 °C corresponding to a filament power of 100 W. An argon-hydrogen mixture (97/3%) was flowed at 4 sccm through the cell port which maintained a total pressure of 1.5 torr. 2.) Next, the gas flow was stopped, and the cell pressure was reduced to less than 500 mtorr with the cell pump. The valve to the monochromator was opened. Both the cell pump and the spectrometer turbo pump were stopped so that the cell was no longer pumped. The argon-hydrogen mixture gas was added from the monochromator port. The flow rate was adjusted to achieve a pressure of 1 torr, and a 100 mtorr partial pressure of pure hydrogen was added by flowing the gas into the cell from the monochromator port until the total pressure was 1.1 torr. Since the valve to the monochromator was open, the entire light detection system was also at under the same gas as the cell. 3.) The filament power was increased to 200 W without pumping. When the temperature reached a steady state at 400 °C, the UV/VIS spectrum (300–560 nm) was recorded with the photomultiplier tube (PMT) and the sodium salicylate scintillator (spectrum shown in Figure 20). 4.) Then the hydrogen pressure was increased to 10 torr by flowing pure hydrogen into the cell from the monochromator port. 5.) The power was increased to 300 W, and the cell was maintained at 600 °C overnight. 6.) Next, the cell pressure was reduced by pumping with the cell pump. When a pressure of 400 mtorr was achieved, the pumping was stopped. A strong blue-green plasma was observed. The UV/VIS spectrum (300–560 nm) was recorded with the photomultiplier tube (PMT) and the sodium salicylate scintillator (spectrum shown in Figure 21). Without pumping the pressure gradually increased to about 1 torr. The plasma then ceased.

III. RESULTS

A. EUV Spectroscopy

The cell without any test material present was run to establish the baseline of the spectrometer. The intensity of the Lyman α emission as a function of time from the gas cell at a cell temperature of 700 °C comprising a tungsten filament, a titanium dissociator, and 300 mtorr hydrogen with a flow rate of 5.5 sccm is shown in Figure 2. The corresponding UV/VIS spectrum (40–560 nm) is shown in Figure 3. The spectrum was recorded with a photomultiplier tube (PMT) and a sodium salicylate scintillator. No emission was observed except for the blackbody filament radiation at the longer wavelengths. No emission was also observed for the pure elements alone or when argon, neon, or helium replaced hydrogen.

The intensity of the Lyman α emission as a function of time from the gas cell at a cell temperature of 700 °C comprising a tungsten filament, a titanium dissociator, vaporized sodium, magnesium, or barium metal, and 300 mtorr hydrogen with a flow rate of 5.5 sccm are shown in Figures 4, 5, and 6, respectively. Sodium, magnesium, or barium metal was vaporized by filament heating. No emission was observed in any case. The maximum filament power was greater than 500 W. A metal coating formed in the cap of the cell over the course of the experiment in all cases.

The intensity of the Lyman α emission as a function of time from the gas cell at a cell temperature of 700 °C comprising a tungsten filament, a titanium dissociator, vaporized cesium or strontium metal, and 300 mtorr hydrogen with a flow rate of 5.5 sccm are shown in Figures 7 and 8, respectively. Strong emission was observed from both vaporized cesium and strontium with hydrogen. The EUV spectrum (60–140 nm) of the cell emission recorded at about the point of the maximum Lyman α emission for cesium is shown in Figure 9. The EUV spectrum (40–160 nm) of the cell emission recorded at about the point of the maximum Lyman α emission for strontium is shown in Figure 10. In each case, no emission was observed in the absence of hydrogen, and no emission occurred until

the catalyst was vaporized as indicated by the appearance of a metal coating in the cap of the cell over the course of the experiment.

Hydrogen was replaced by a 97% argon and 3% hydrogen mixture. The intensity of the Lyman α emission as a function of time from each gas cell was recorded. The intensity of the Lyman α emission as a function of time from the gas cell at a cell temperature of 700 °C comprising a tungsten filament, and 300 mtorr argon-hydrogen mixture (97/3%) that was recorded with a CEM is shown in Figure 11. No emission was observed with argon-hydrogen mixtures alone. The EUV spectrum (40–160 nm) of the sodium, magnesium, and barium gas cell emission that was recorded with a PMT and a sodium salicylate scintillator two hours after the cell reached 700 °C are shown in Figures 12, 13, and 14, respectively. Each cell comprised a tungsten filament, vaporized metal, and 300 mtorr argon-hydrogen mixture (97/3%). No emission was observed in any case.

The EUV spectrum (40–160 nm) of the cell emission recorded at about the point of the maximum Lyman α emission from the gas cell at a cell temperature of 700 °C comprising a tungsten filament, vaporized cesium or strontium metal, and 300 mtorr argon-hydrogen mixture (97/3%) with a flow rate of 5.5 sccm that was recorded with a PMT and a sodium salicylate scintillator are shown in Figures 15 and 16, respectively. Cesium or strontium metal was vaporized by filament heating. Strong emission was observed from both cesium and strontium with an argon-hydrogen mixture that was more intense than with hydrogen and cesium or strontium. The Lyman series corresponded to atomic hydrogen emission and strong Ar^+ ion emission was observed at 92.0 nm and 93.2 nm. The emission intensity of the plasma generated by the cesium or strontium catalyst increased significantly with the introduction of argon gas only when Ar^+ emission was observed.

The anomalous plasma required the presence of hydrogen. It was found that increasing the hydrogen pressure initially increased the atomic hydrogen emission lines, but with increasing hydrogen partial pressure at a constant total pressure, the Ar^+ emission in the EUV at 92.0 nm and 93.2 nm decreased which resulted in a decrease of the plasma intensity including the hydrogen emission. The zero order emission in the EUV was observed with titration of increasing partial pressure of

hydrogen added to argon gas. The optimum argon-hydrogen gas mixture which produced the greatest emission was determined to be 95% argon and 5% hydrogen.

Kuraica and Konjevic [38] observed intense 50 eV anomalous thermal broadening of the Balmer lines with argon present in the negative glow of a glow discharge of an argon-hydrogen mixture irrespective of cathode material (carbon, copper, and silver), and an observed anomalous discharge was not observed in neon-hydrogen and pure hydrogen mixtures. The optimum argon-hydrogen gas mixture which produced the greatest emission in the present EUV study was similar to the 97% argon and 3% hydrogen mixture of Kuraica and Konjevic [38]. The optimum ratio was consistent with an anomalous discharge mechanism which required maximum concentrations of both atomic hydrogen and Ar^+ .

B. EUV Emission of Ar^+ Catalyst Formed with Strontium

The EUV spectra (40–160 nm) of the emission of a strontium-argon-hydrogen gas cell and a control hydrogen microwave plasma are shown in Figures 17, and 18, respectively. The standard EUV emission spectrum (20–65 nm) of an argon microwave plasma recorded on the McPherson 4° grazing incidence EUV spectrometer (Model 248/310G) with a CEM is shown in Figure 19. A broad continuum radiation in the region of 45.6 nm was observed in the strontium-argon-hydrogen gas cell emission that was not present in the control hydrogen or argon plasmas. (The broad continuum radiation in the region of 45.6 nm shown in Figure 17 is actually significantly larger than shown due to the low grating efficiency at the short wavelengths.) This emission was dramatically different from that given by a microwave plasma of argon wherein the entire Rydberg series of lines of Ar^+ was observed with a discontinuity of the series at the limit of the ionization energy of Ar^+ to Ar^{2+} at 44.9 nm. In addition, an intense Rydberg series of lines in the region 110-130 nm was observed in the strontium-argon-hydrogen gas cell emission as shown in Figure 17. The lines were not present in the control hydrogen or argon plasmas, and were only observed with strontium present with argon and hydrogen.

The series was assigned to forbidden transitions of strontium which are not reported in the NIST Tables [39].

C. 407 nm Emission with Ar⁺ Catalyst Formed with Strontium

The UV/VIS spectra (300–560 nm) of the cell emission from the gas cell at a cell temperature of 400 °C comprising a tungsten filament, vaporized strontium metal, and 1.1 torr argon-hydrogen mixture (97/3%) following step #3 of the 407 Emission Protocol and step #5 of the 407 Emission Protocol are shown in Figures 20 and 21, respectively. The EUV spectra (300–560 nm) of the cell emission from the strontium-argon-hydrogen gas cell following step #3 and step #5 of the 407 are superimposed in Figure 22. From the comparison, a novel continuum feature is observed at 407 nm which was not due to strontium emission. The standard UV/VIS emission spectrum (300–560 nm) of a hydrogen microwave plasma recorded on the McPherson model 302 (Seya-Namioka type) EUV spectrometer with a PMT and a sodium salicylate scintillator is shown in Figure 23. The EUV spectra (300–560 nm) of the cell emission from the strontium-argon-hydrogen gas cell following step #5 of the 407 Emission Protocol and the standard hydrogen microwave plasma spectrum are superimposed in Figure 24. From the comparison, the novel 407 nm continuum feature was not due to hydrogen emission. The novel 407 nm continuum peak was observed by allowing the gas cell to react overnight under static conditions with strontium catalyst, a source of Ar⁺ catalyst (argon gas), and excess hydrogen reactant. These results are consistent with the formation of H⁻(1/2) from the catalysis of atomic hydrogen by Ar⁺. Unidentified continuum lines at 427.2 nm and 434.4 nm are indicated in Figure 21. These lines which are close to the 407 nm peak assigned to H⁻(1/2) may be due to resonant transfer from the hydride continuum emission to otherwise very weak strontium or hydrogen lines.

D. Broad 35-40 nm Peak with Ar⁺ Catalyst

The EUV spectrum (25–70 nm) of the cell emission from the gas cell at a cell temperature of 700 °C comprising a tungsten filament, vaporized

strontium metal, and 300 mtorr argon-hydrogen mixture (97/3%) is shown in Figure 25. A broad peak was observed in the 35-40 nm region. It coincided with strong Ar^+ emission wherein the Ar^+ was generated in the anomalous plasma formed by the atomic strontium catalyst. This peak may be due to an excimer of a highly excited argon ion, Ar^+ , corresponding to the emission observed at 46 nm and the novel hydride ion, H^- (1/2), corresponding to the emission observed at 407 nm. (See Discussion section.)

E. EUV Emission of Cesium Catalyst

The EUV spectrum (40–160 nm) of the emission of the cesium-hydrogen gas cell is shown in Figures 26. Line emission corresponding to the second ionization energy of cesium, 23.15745 eV [32], for the decay transition Cs^{2+} to Cs^+ was observed at 53.3 nm. (The 53.3 nm emission shown in Figure 26 is actually significantly larger than shown due to the low grating efficiency at the short wavelengths.) The only cesium lines observed for the standard cesium microwave plasma were in the visible region, and no lines were observed at wavelengths shorter than 80 nm in the case of the standard hydrogen microwave plasma as shown in Figure 18. The resonance lines of Cs II were observed with a sliding spark on the 10.7 m normal incidence vacuum spectrometer at the National Bureau of Standards (NBS) [40] as given in Table 1. The 53.3 nm emission of the hydrogen catalysis reaction with cesium shown in Figure 26 is dramatically different from the NBS standard cesium spectrum wherein a series of lines of Cs^+ was observed that vanished at the limit of the ionization energy of Cs^+ to Cs^{2+} . In fact, the ionization limit was not observed; rather, it was derived by NBS to be 23.17(4) eV [40]. Furthermore, I. S. Aleksakhin et al. recorded the emission of cesium in the 45-75 nm region during electron-atom collisions [41]. The ionization energy limit at 53.3 nm was not observed by I. S. Aleksakhin et al. either.

F. 407 nm Emission with Cesium Catalyst

The UV/VIS spectra (300–560 nm) of the cesium-hydrogen gas cell ten minutes after the formation of a strong plasma and running

continuously for four hours since the formation of a strong plasma are shown in Figures 27 and 28, respectively. The noise features in Figure 27 at 425 nm and 480 nm were due to initial instabilities in the plasma as function of time. The UV/VIS spectra (300–560 nm) of the cesium-hydrogen gas cell at the ten minute time point and the same cell at the four hour time point are superimposed in Figure 29. The UV/VIS spectrum (300–560 nm) of the standard hydrogen microwave plasma is shown in Figure 23. The UV/VIS spectra (300–560 nm) of the cesium-hydrogen gas cell at the four hour time point and the standard hydrogen microwave plasma are superimposed in Figure 30. From the comparison, a novel continuum feature is observed at 407 nm which was not due to hydrogen or cesium emission. The novel 407 nm continuum peak was observed only with cesium and atomic hydrogen present over an extended reaction time. These results are consistent with the formation of $H^-(1/2)$ from the catalysis of atomic hydrogen by $Cs(m)$.

G. 46 nm Emission with Ar^+ Catalyst Formed with Cesium

The EUV spectrum (40–160 nm) of the emission of the cesium-argon-hydrogen gas cell, the cesium-hydrogen gas cell, and the hydrogen microwave plasma are shown in Figures 31, 26, and 18, respectively. The standard EUV emission spectrum (20–65 nm) of an argon microwave plasma recorded on the McPherson 4° grazing incidence EUV spectrometer with a CEM is shown in Figure 19. A broad continuum radiation in the region of 45.6 nm was observed in the cesium-argon-hydrogen gas cell emission that was not present in the cesium-hydrogen or control plasmas. This emission was dramatically different from that given by the argon microwave plasma wherein the entire Rydberg series of lines of Ar^+ was observed with a discontinuity of the series at the limit of the ionization energy of Ar^+ to Ar^{2+} at 44.9 nm as shown in Figure 19. Thus, the novel 45.6 nm continuum peak shown in Figure 31 for the case of Ar^+ catalyst formed by the anomalous plasma generated by strontium catalyst was observed with the addition of argon to the cesium-hydrogen plasma as shown in Figure 26. These results are consistent with the formation of Ar^+ which served as a second catalyst that was generated by the formation of a plasma with cesium catalyst.

IV. DISCUSSION

A plasma that emitted intense EUV formed at low temperatures (e.g. $\approx 10^3$ K) from atomic hydrogen and atomic cesium or strontium catalyst which was vaporized from the metal by heating. The emission intensity of the plasma generated by the cesium or strontium catalyst increased significantly with the introduction of argon gas only when Ar^+ emission was observed. Ar^+ which served as a second catalyst was generated by the formation of a plasma with cesium or strontium catalyst. An intense Rydberg series of lines in the region 110-130 nm was assigned to forbidden transitions of strontium which are not reported in the NIST Tables [39]. The reason for the observation of the intense forbidden transitions may involve the strontium catalyst mechanism.

In the cases where Lyman α emission was observed, no possible chemical reactions of the tungsten filament, the dissociator, the vaporized test material, and 300 mtorr hydrogen or argon-hydrogen mixture gas at a cell temperature of 700 °C could be found which accounted for the hydrogen Lyman α line emission. In fact, no known chemical reaction releases enough energy to excite Lyman α emission from hydrogen. The emission was not observed with cesium, strontium, argon, hydrogen, or an argon-hydrogen mixture (97/3%) alone. Intense emission was observed for cesium and strontium with hydrogen gas and the argon-hydrogen mixture gas, but no emission was observed when sodium, magnesium, or barium replaced strontium or cesium with hydrogen or with the argon-hydrogen mixture. This result indicates that the emission was due to a reaction of the catalyst with hydrogen.

The only pure elements that were observed to emit EUV were those wherein the ionization of t electrons from an atom to a continuum energy level is such that the sum of the ionization energies of the t electrons is approximately $m \cdot 27.2$ eV where t and m are each an integer. Argon ions and cesium atoms ionize at an integer multiple of the potential energy of atomic hydrogen, $m \cdot 27.2$ eV. The single ionization reaction ($t=1$) of Ar^+ to Ar^{2+} has a net enthalpy of reaction of 27.63 eV, which is equivalent to $m=1$. And, the double ionization ($t=2$) of Cs to Cs^{2+} has a net enthalpy of

reaction of 27.05135 eV, which is equivalent to $m=1$ [32]. In each case, the reaction involves a nonradiative energy transfer to form a hydrogen atom that is lower in energy than unreacted atomic hydrogen.

Characteristic emission was observed from a continuum state of Ar^{2+} which confirmed the resonant nonradiative energy transfer of 27.2 eV from atomic hydrogen Ar^+ . In the anomalous discharge of hydrogen due to the presence of Ar^+ , atomic hydrogen may resonantly transfer energy to Ar^+ to cause its ionization to Ar^{2+} which may then decay and emit the radiation. The vacuum reaction in the absence of an electric field is



In the catalysis of atomic hydrogen by Ar^+ , a weak electric field may adjust the energy of ionizing Ar^+ to Ar^{2+} to match the energy of 27.2 eV to permit the catalysis. The transfer of 27.2 eV from atomic hydrogen to Ar^+ in the presence of the weak field of the filament results in its excitation to a continuum state. Then, the energy for the transition from essentially the Ar^{2+} state to the lowest state of Ar^+ is predicted to give a broad continuum radiation in the region of 45.6 nm. This broad continuum emission was observed. This emission was dramatically different from that given by an argon microwave plasma wherein the entire Rydberg series of lines of Ar^+ was observed with a discontinuity of the series at the limit of the ionization energy of Ar^+ to Ar^{2+} . The observed Ar^+ continuum in the region of 45.6 nm confirms the catalyst mechanism of the anomalous discharge.

A broad peak observed in the 35-40 nm region is shown in Figure 25. It coincided with strong Ar^+ emission wherein the Ar^+ was generated in the anomalous plasma formed by the atomic strontium catalyst. This peak may be due to an excimer of a highly excited argon ion, Ar^+ , corresponding to the emission observed at 46 nm and the novel hydride ion, $H^-(1/2)$, corresponding to the emission observed at 407 nm. Ar^+ is excited to the bound-free limit during the catalysis of atomic hydrogen, and $H^-(1/2)$ is formed in its bound-free state by the reaction of the hydrogen catalysis product with an electron.



In addition, the hydride high energy states are easily excited due to the continuum absorption feature of any hydride ion. The argon ion and the

high binding energy hydride ion may form an excimer that is similar to an argon monohalide excimer.

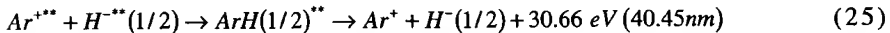
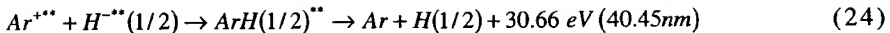
Broad peaks due to excimers of argon and the halides chlorine and fluorine are known to emit at much longer wavelengths and are the basis of argon halogen excimer lasers [42]. Excimer lasers involve emission from an excited molecule which dissociates following the emission due to a repulsive potential curve between the unexcited atoms. For the hypothetical excimer molecule AB , collision of unexcited A and B atoms occurs along a repulsive potential curve. However, if the electrons in one atom such as B are excited, creating a state labeled B^* , B^* may combine with atom A to produce an excited state of the molecule AB^* . Binding energies, relative to excited atoms, for such excited state complexes range from 0.1 eV for many rare gas-metal atom combinations, to about 5 eV for noble gas monohalides [42].

In excimer lasers, the pumping is by direct electron beam pumping, electron-beam-controlled-discharge pumping, and self-sustained-discharge pumping [43]. Pumping reactions include



where $ArF^{*''}$ denotes the ionic excited states of ArF with large amounts of vibrational excitation. In the case of the $ArCl$ excimer laser, the 170 nm continuum band emission has been determined to be due to an ionic excited state of argon monochloride, Ar^+Cl^- , emitting to the repulsive $ArCl$ ground state [42].

The broad peak starting at 40 and ending at about 35 nm may be the ionic pair excimer emission of $Ar^{*''}$ and $H^{*''}(1/2)$. (A highly excited state of a species M at the bound-free limit is represented by the $M^{*''}$.) This peak has an energy width of about 4.5 eV which is about the typical binding energy, relative to excited atoms, for such excited state noble gas monohalides complexes. Possible excimer reactions with emission that match the observed peak starting at 40 nm are



Rather than requiring energy intensive electron beam or discharge pumping schemes, the plasma and the excimer are formed by the catalysis of atomic hydrogen with the potential for a very short wavelength, energy efficient excimer laser.

Characteristic Cs^{2+} line emission was observed which confirmed the resonate nonradiative energy transfer of 27.2 eV from atomic hydrogen to atomic cesium. In the anomalous discharge of hydrogen due to the presence of atomic cesium, atomic hydrogen may resonantly transfer energy to cesium to cause its double ionization to Cs^{2+} which may then decay and emit the radiation. The vacuum reaction is



In the catalysis of atomic hydrogen by cesium, thermal energies may broaden the enthalpy of reaction. The relationship between kinetic energy and temperature is given by

$$E_{kinetic} = \frac{3}{2} kT \quad (27)$$

For a temperature of 1200 K, the thermal energy is 0.16 eV, and the net enthalpy of reaction provided by cesium metal is 27.21 eV which matches the energy of 27.2 eV to permit the catalysis. Following the resonant transfer, the decay energy for the transition Cs^{2+} to Cs^+ is predicted to give 27.2 eV line emission corresponding to the second ionization energy of cesium, 23.15745 eV. This line emission was observed. This emission was dramatically different from that given by a microwave plasma of argon wherein the entire Rydberg series of lines of Cs^+ was observed with a discontinuity of the series at the limit of the ionization energy of Cs^+ to Cs^{2+} . The observed Cs^{2+} single line emission at 53.3 nm confirms the catalyst mechanism of the anomalous discharge.

$Cs(m)$ and Ar^{+*} are predicted to catalyze hydrogen to form $H\left[\frac{a_H}{2}\right]$

which reacts with and electron to form $H^-(1/2)$. The predicted $H^-(1/2)$ hydride ion of hydrogen catalysis by either cesium atom or Ar^+ catalyst

was observed spectroscopically at 407 nm corresponding to its predicted binding energy of 3.05 eV. The hydride reaction product formed over time.

The release of energy from hydrogen as evidenced by the EUV emission must result in a lower-energy state of hydrogen. The present study identified the formation of a novel hydride ion. The formation of novel compounds based on novel hydride ions would be substantial evidence supporting catalysis of hydrogen as the mechanism of the observed EUV emission and further support the present spectroscopic identification of H^- (1/2). Compounds containing hydrino hydride ions have been isolated as products of the reaction of atomic hydrogen with atoms and ions identified as catalysts in this and previously reported EUV studies [12, 14-31]. The novel hydride compounds were identified analytically by techniques such as time of flight secondary ion mass spectroscopy, X-ray photoelectron spectroscopy, and 1H nuclear magnetic resonance spectroscopy. For example, the time of flight secondary ion mass spectroscopy showed a large hydride peak in the negative spectrum. The X-ray photoelectron spectrum showed large metal core level shifts due to binding with the hydride as well as novel hydride peaks. The 1H nuclear magnetic resonance spectrum showed significantly upfield shifted peaks which corresponded to and identified novel hydride ions. The implications are that a new field of novel hydrogen chemistry has been discovered.

ACKNOWLEDGMENT

Special thanks to Ying Lu, Takeyoshi Onuma, and Jiliang He for recording the spectra and Bala Dhandapani for assisting with logistics and reviewing this manuscript.

REFERENCES

1. R. Mills, The Grand Unified Theory of Classical Quantum Mechanics, January 2000 Edition, BlackLight Power, Inc., Cranbury, New Jersey, Distributed by Amazon.com.

2. R. Mills, N. Greenig, S. Hicks, "Optically Measured Power Balances of Anomalous Discharges of Mixtures of Argon, Hydrogen, and Potassium, Rubidium, Cesium, or Strontium Vapor", Int. J. Hydrogen Energy, submitted.
3. R. Mills and M. Nansteel, "Anomalous Argon-Hydrogen-Strontium Discharge", IEEE Transactions of Plasma Science, submitted.
4. R. Mills, M. Nansteel, and Y. Lu, "Anomalous Hydrogen-Strontium Discharge", European Journal of Physics D, submitted.
5. R. Mills, J. Dong, Y. Lu, "Observation of Extreme Ultraviolet Hydrogen Emission from Incandescently Heated Hydrogen Gas with Certain Catalysts", Int. J. Hydrogen Energy, Vol. 25, (2000), pp. 919-943.
6. R. Mills, "Observation of Extreme Ultraviolet Emission from Hydrogen-KI Plasmas Produced by a Hollow Cathode Discharge", Int. J. Hydrogen Energy, in press.
7. R. Mills, "Temporal Behavior of Light-Emission in the Visible Spectral Range from a Ti-K₂CO₃-H-Cell", Int. J. Hydrogen Energy, in press.
8. R. Mills, Y. Lu, and T. Onuma, "Formation of a Hydrogen Plasma from an Incandescently Heated Hydrogen-Catalyst Gas Mixture with an Anomalous Afterglow Duration", Int. J. Hydrogen Energy, in press.
9. R. Mills, M. Nansteel, and Y. Lu, "Observation of Extreme Ultraviolet Hydrogen Emission from Incandescently Heated Hydrogen Gas with Strontium that Produced an Anomalous Optically Measured Power Balance", Int. J. Hydrogen Energy, in press.
10. R. Mills, J. Dong, Y. Lu, J. Conrads, "Observation of Extreme Ultraviolet Hydrogen Emission from Incandescently Heated Hydrogen Gas with Certain Catalysts", 1999 Pacific Conference on Chemistry and Spectroscopy and the 35th ACS Western Regional Meeting, Ontario Convention Center, California, (October 6-8, 1999).
11. R. Mills, J. Dong, N. Greenig, and Y. Lu, "Observation of Extreme Ultraviolet Hydrogen Emission from Incandescently Heated Hydrogen Gas with Certain Catalysts", National Hydrogen Association, 11 th Annual U.S. Hydrogen Meeting, Vienna, VA, (February 29-March 2, 2000).
12. R. Mills, B. Dhandapani, N. Greenig, J. He, J. Dong, Y. Lu, and H. Conrads, "Formation of an Energetic Plasma and Novel Hydrides from Incandescently Heated Hydrogen Gas with Certain Catalysts", National

- Hydrogen Association, 11 th Annual U.S. Hydrogen Meeting, Vienna, VA, (February 29-March 2, 2000).
13. Mills, J. Dong, N. Greenig, and Y. Lu, "Observation of Extreme Ultraviolet Hydrogen Emission from Incandescently Heated Hydrogen Gas with Certain Catalysts", 219 th National ACS Meeting, San Francisco, California, (March 26-30, 2000).
 14. R. Mills, B. Dhandapani, N. Greenig, J. He, J. Dong, Y. Lu, and H. Conrads, "Formation of an Energetic Plasma and Novel Hydrides from Incandescently Heated Hydrogen Gas with Certain Catalysts", 219 th National ACS Meeting, San Francisco, California, (March 26-30, 2000).
 15. R. Mills, B. Dhandapani, N. Greenig, J. He, J. Dong, Y. Lu, and H. Conrads, "Formation of an Energetic Plasma and Novel Hydrides from Incandescently Heated Hydrogen Gas with Certain Catalysts", June ACS Meeting (29th Northeast Regional Meeting, University of Connecticut, Storrs, CT, (June 18-21, 2000)).
 16. R. Mills, B. Dhandapani, N. Greenig, J. He, J. Dong, Y. Lu, and H. Conrads, "Formation of an Energetic Plasma and Novel Hydrides from Incandescently Heated Hydrogen Gas with Certain Catalysts", August National ACS Meeting (220th ACS National Meeting, Washington, DC, (August 20-24, 2000)).
 17. R. Mills, B. Dhandapani, N. Greenig, J. He, "Synthesis and Characterization of Potassium Iodo Hydride", Int. J. of Hydrogen Energy, Vol. 25, Issue 12, December, (2000), pp. 1185-1203.
 18. R. Mills, "Novel Inorganic Hydride", Int. J. of Hydrogen Energy, Vol. 25, (2000), pp. 669-683.
 19. R. Mills, "Novel Hydrogen Compounds from a Potassium Carbonate Electrolytic Cell", Fusion Technology, Vol. 37, No. 2, March, (2000), pp. 157-182.
 20. R. Mills, B. Dhandapani, M. Nansteel, J. He, T. Shannon, A. Echezuria, "Synthesis and Characterization of Novel Hydride Compounds", Int. J. of Hydrogen Energy, in press.
 21. R. Mills, B. Dhandapani, M. Nansteel, J. He, A. Voigt, "Identification of Compounds Containing Novel Hydride Ions by Nuclear Magnetic Resonance Spectroscopy", Int. J. Hydrogen Energy, submitted.
 22. R. Mills, "Highly Stable Novel Inorganic Hydrides", Journal of Materials Research, submitted.

23. R. Mills, "Novel Hydride Compound", 1999 Pacific Conference on Chemistry and Spectroscopy and the 35th ACS Western Regional Meeting, Ontario Convention Center, California, (October 6-8, 1999).
24. R. Mills, B. Dhandapani, N. Greenig, J. He, "Synthesis and Characterization of Potassium Iodo Hydride", 1999 Pacific Conference on Chemistry and Spectroscopy and the 35th ACS Western Regional Meeting, Ontario Convention Center, California, (October 6-8, 1999).
25. R. Mills, J. He, and B. Dhandapani, "Novel Hydrogen Compounds", 1999 Pacific Conference on Chemistry and Spectroscopy and the 35th ACS Western Regional Meeting, Ontario Convention Center, California, (October 6-8, 1999).
26. R. Mills, "Novel Hydride Compound", National Hydrogen Association, 11 th Annual U.S. Hydrogen Meeting, Vienna, VA, (February 29-March 2, 2000).
27. R. Mills, J. He, and B. Dhandapani, "Novel Alkali and Alkaline Earth Hydrides", National Hydrogen Association, 11 th Annual U.S. Hydrogen Meeting, Vienna, VA, (February 29-March 2, 2000).
28. R. Mills, "Novel Hydride Compound", 219 th National ACS Meeting, San Francisco, California, (March 26-30, 2000).
29. R. Mills, J. He, and B. Dhandapani, "Novel Alkali and Alkaline Earth Hydrides", 219 th National ACS Meeting, San Francisco, California, (March 26-30, 2000).
30. R. Mills, J. He, and B. Dhandapani, "Novel Alkali and Alkaline Earth Hydrides", August National ACS Meeting (220 th ACS National Meeting, Washington, DC, (August 20-24, 2000)).
31. R. Mills, W. Good, A. Voigt, Jinquan Dong, "Minimum Heat of Formation of Potassium Iodo Hydride", Int. J. Hydrogen Energy, submitted.
32. David R. Linde, *CRC Handbook of Chemistry and Physics*, 79 th Edition, CRC Press, Boca Raton, Florida, (1998-9), p. 10-175 to p. 10-177.
33. R. Mills, The Nature of Free Electrons in Superfluid Helium--a Test of Quantum Mechanics and a Basis to Review its Foundations and Make a Comparison to Classical Theory, Int. J. Hydrogen Energy, in press.
34. R. Mills, "The Hydrogen Atom Revisited", Int. J. of Hydrogen Energy, Vol. 25, Issue 12, December, (2000), pp. 1171-1183.
35. N. V. Sidgwick, *The Chemical Elements and Their Compounds*, Volume I, Oxford, Clarendon Press, (1950), p.17.

36. M. D. Lamb, *Luminescence Spectroscopy*, Academic Press, London, (1978), p. 68.
37. C. L. Yaws, *Chemical Properties Handbook*, McGraw-Hill, (1999).
38. Kuraica, M., Konjevic, N., Physical Review A, Volume 46, No. 7, October (1992), pp. 4429-4432.
39. NIST Atomic Spectra Database, www.physics.nist.gov/cgi-bin/AtData/display.ksh.
40. J. Reader, G. L. Epstein, "Resonance lines of Cs II, Ba III, and La IV", Journal of the Optical Society of America, Vol. 65, No. 6, June, (1975), pp. 638-641.
41. I. S. Aleksakhin, G. G. Bogachev, A. I. Zapesochnyi, "Study of the emission of potassium, rubidium, and cesium in the 45-75 nm region during electron-atom collisions", J. Applied Spectroscopy, Vol. 23, No. 6, December, (1975), pp. 1666-1668. Translated from Zh. Prikl. Spektrosk. (USSR), Vol. 23, No. 6, December (1975), pp. 1103-1105.
42. J. J. Ewing. "Excimer Lasers", *Laser Handbook*, Edited by M. L. Stitch, North-Holland Publishing Company, Vol. A4, (1979) , pp. 135-197.
43. H. Shimazaki, S. Nakamura, M. Obara, T. Fujioka, AIP Conference Proceedings, Series Editor: H. C. Wolfe, No. 100, Subseries in Optical Science and Engineering, No. 3, Excimer Lasers-1983, Edited by C. I. Rhodes, H. Egger, H. Pummer, OSA, Lake Tahoe, Nevada, American Institute of Physics, New York, (1983), pp. 12-18.

Table 1. Resonance lines of Cs II observed with a sliding spark on the 10.7 m normal incidence vacuum spectrometer at NBS [40]. The uncertainty of the wavelengths is $\pm 0.005 \text{ \AA}$.

$\lambda (\text{\AA})$	Intensity	$\sigma (\text{cm}^{-1})$	Upper Level
926.657	40000	107914.8	$6p^6 5d\ ^3P_1$
901.270	35000	110954.5	$6s3/2[3/2]_1$
813.837	15000	122874.7	$6s1/2[1/2]_1$
808.761	15000	123645.9	$5d\ ^3D_1$
718.138	15000	139249.0	$5d^1 P_1$
668.386	500	149614	$7s3/2[3/2]_1$
657.112	100	152181	$6d\ ^3P_1$
639.356	2000	156407	$6d\ ^3D_1$
612.756	35	163189	$7s1/2[1/2]_1$
591.044	250	169192	$6d^1 P_1$
607.291	50	164666	$8s3/2[3/2]_1$
575.320	10	173816	$6d\ ^3D_1$
564.158	1	177256	$7d^1 P_1$

Figure Captions

Figure 1. The experimental set up comprising a gas cell light source and an EUV spectrometer which was differentially pumped.

Figure 2. The intensity of the Lyman α emission as a function of time from the gas cell at a cell temperature of 700 °C comprising a tungsten filament, a titanium dissociator, and 300 mtorr hydrogen that was recorded with a CEM.

Figure 3. The UV/VIS spectrum (40–560 nm) of the cell emission from the gas cell at a cell temperature of 700 °C comprising a tungsten filament, a titanium dissociator, and 300 mtorr hydrogen that was recorded with a photomultiplier tube (PMT) and a sodium salicylate scintillator with slit widths of 500X500 μm .

Figure 4. The intensity of the Lyman α emission as a function of time from the gas cell at a cell temperature of 700 °C comprising a tungsten filament, a titanium dissociator, vaporized sodium metal, and 300 mtorr hydrogen that was recorded with a CEM.

Figure 5. The intensity of the Lyman α emission as a function of time from the gas cell at a cell temperature of 700 °C comprising a tungsten filament, a titanium dissociator, vaporized magnesium, and 300 mtorr hydrogen that was recorded with a CEM.

Figure 6. The intensity of the Lyman α emission as a function of time from the gas cell at a cell temperature of 700 °C comprising a tungsten filament, a titanium dissociator, vaporized barium metal, and 300 mtorr hydrogen that was recorded with a CEM.

Figure 7. The intensity of the Lyman α emission as a function of time from the gas cell at a cell temperature of 700 °C comprising a tungsten filament, a titanium dissociator, vaporized cesium metal, and 300 mtorr hydrogen that was recorded with a CEM.

Figure 8. The intensity of the Lyman α emission as a function of time from the gas cell at a cell temperature of 700 °C comprising a tungsten filament, a titanium dissociator, vaporized strontium metal, and 300 mtorr hydrogen that was recorded with a CEM.

Figure 9. The EUV spectrum (60–140 nm) of the cell emission recorded at about the point of the maximum Lyman α emission from the gas cell at a cell temperature of 700 °C comprising a tungsten filament, a

titanium dissociator, vaporized cesium metal, and 300 mtorr hydrogen that was recorded with a CEM.

Figure 10. The EUV spectrum (40–160 nm) of the cell emission recorded at about the point of the maximum Lyman α emission from the gas cell at a cell temperature of 700 °C comprising a tungsten filament, a titanium dissociator, vaporized strontium metal, and 300 mtorr hydrogen that was recorded with a CEM.

Figure 11. The intensity of the Lyman α emission as a function of time from the gas cell at a cell temperature of 700 °C comprising a tungsten filament, and 300 mtorr argon-hydrogen mixture (97/3%) that was recorded with a CEM.

Figure 12. The EUV emission spectrum (40–160 nm) from a gas cell comprising a tungsten filament, vaporized sodium metal, and 300 mtorr argon-hydrogen mixture (97/3%) that was recorded with a PMT and a sodium salicylate scintillator two hours after the cell reached 700 °C.

Figure 13. The EUV emission spectrum (40–160 nm) from a gas cell comprising a tungsten filament, vaporized magnesium metal, and 300 mtorr argon-hydrogen mixture (97/3%) that was recorded with a PMT and a sodium salicylate scintillator two hours after the cell reached 700 °C.

Figure 14. The EUV emission spectrum (40–160 nm) from a gas cell comprising a tungsten filament, vaporized barium metal, and 300 mtorr argon-hydrogen mixture (97/3%) that was recorded with a PMT and a sodium salicylate scintillator two hours after the cell reached 700 °C.

Figure 15. The EUV spectrum (40–160 nm) of the cell emission recorded at about the point of the maximum Lyman α emission from the gas cell at a cell temperature of 700 °C comprising a tungsten filament, vaporized cesium metal, and 300 mtorr argon-hydrogen mixture (97/3%) that was recorded with a PMT and a sodium salicylate scintillator.

Figure 16. The EUV spectrum (40–160 nm) of the cell emission recorded at about the point of the maximum Lyman α emission from the gas cell at a cell temperature of 700 °C comprising a tungsten filament, vaporized strontium metal, and 300 mtorr argon-hydrogen mixture (97/3%) that was recorded with a PMT and a sodium salicylate scintillator.

Figure 17. The EUV spectrum (40–160 nm) of the cell emission from

the gas cell at a cell temperature of 700 °C comprising a tungsten filament, vaporized strontium metal, and 300 mtorr argon-hydrogen mixture (97/3%) that showed novel catalysts features and spectral lines.

Figure 18. Standard EUV emission spectrum (40–160 nm) of a hydrogen microwave plasma recorded on the McPherson model 302 (Seya-Namioka type) EUV spectrometer with a PMT and a sodium salicylate scintillator.

Figure 19. Standard EUV emission spectrum (20–65 nm) of an argon microwave plasma recorded on the McPherson 4° grazing incidence EUV spectrometer (Model 248/310G) with a CEM.

Figure 20. The EUV spectrum (300–560 nm) of the cell emission from the gas cell at a cell temperature of 400 °C comprising a tungsten filament, vaporized strontium metal, and 1.1 torr argon-hydrogen mixture (97/3%) following step #3 of the 407 Emission Protocol that was recorded with a PMT and a sodium salicylate scintillator.

Figure 21. The UV/VIS spectrum (300–560 nm) of the cell emission from the gas cell at a cell temperature of 600 °C comprising a tungsten filament, vaporized strontium metal, and 400 mtorr argon-hydrogen mixture (97/3%) following step #5 of the 407 Emission Protocol that was recorded with a PMT and a sodium salicylate scintillator.

Figure 22. The EUV spectra (300–560 nm) of the cell emission from the strontium-argon-hydrogen gas cell following step #3 (dotted line) and step #5 (solid line) of the 407 Emission Protocol.

Figure 23. Standard UV/VIS emission spectrum (300–560 nm) of a hydrogen microwave plasma recorded on the McPherson model 302 (Seya-Namioka type) EUV spectrometer with a PMT and a sodium salicylate scintillator.

Figure 24. The UV/VIS spectra (300–560 nm) of the cell emission from strontium-argon-hydrogen gas cell following step #5 (solid line) of the 407 Emission Protocol and the standard hydrogen microwave plasma (dotted line).

Figure 25. The EUV spectrum (25–70 nm) of the cell emission from the gas cell at a cell temperature of 700 °C comprising a tungsten filament, vaporized strontium metal, and 300 mtorr argon-hydrogen mixture (97/3%) that was recorded with a CEM.

Figure 26. The EUV spectrum (40–160 nm) of the cell emission from

the gas cell at a cell temperature of 700 °C comprising a tungsten filament, vaporized cesium metal, and 300 mtorr hydrogen that was recorded with a PMT and a sodium salicylate scintillator.

Figure 27. The UV/VIS spectrum (300–560 nm) of the cell emission from the gas cell that was recorded with a PMT and a sodium salicylate scintillator ten minutes after the formation of a strong plasma. The cell at 700 °C comprised a tungsten filament, vaporized cesium metal, and 300 mtorr hydrogen.

Figure 28. The UV/VIS spectrum (300–560 nm) of the cell emission from the gas cell that was recorded with a PMT and a sodium salicylate scintillator four hours after the formation of a sustained strong plasma. The cell at 700 °C comprised a tungsten filament, vaporized cesium metal, and 300 mtorr hydrogen.

Figure 29. The UV/VIS spectra (300–560 nm) of the cesium-hydrogen gas cell at the ten minute time point (dotted line) and same the cell at the four hour time point (solid line).

Figure 30. The UV/VIS spectra (300–560 nm) of the cell emission from cesium-hydrogen gas cell at the four hour time point and the standard hydrogen microwave plasma.

Figure 31. The EUV spectrum (40–160 nm) of the cell emission from the gas cell at a cell temperature of 700 °C comprising a tungsten filament, vaporized cesium metal, and 300 mtorr argon-hydrogen mixture (97/3%) that was recorded with a CEM with a MgF_2 coated grating.

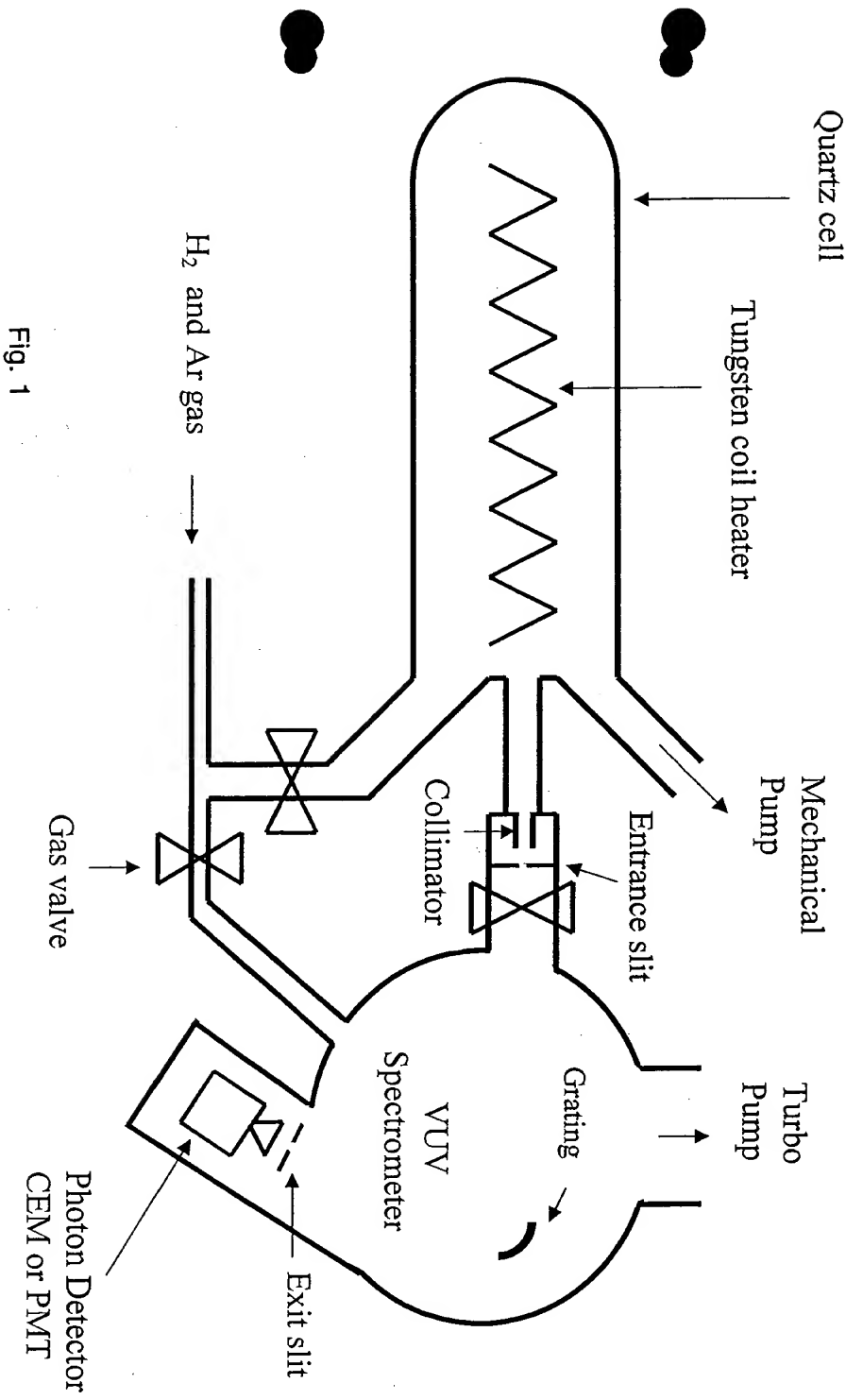


Fig. 1

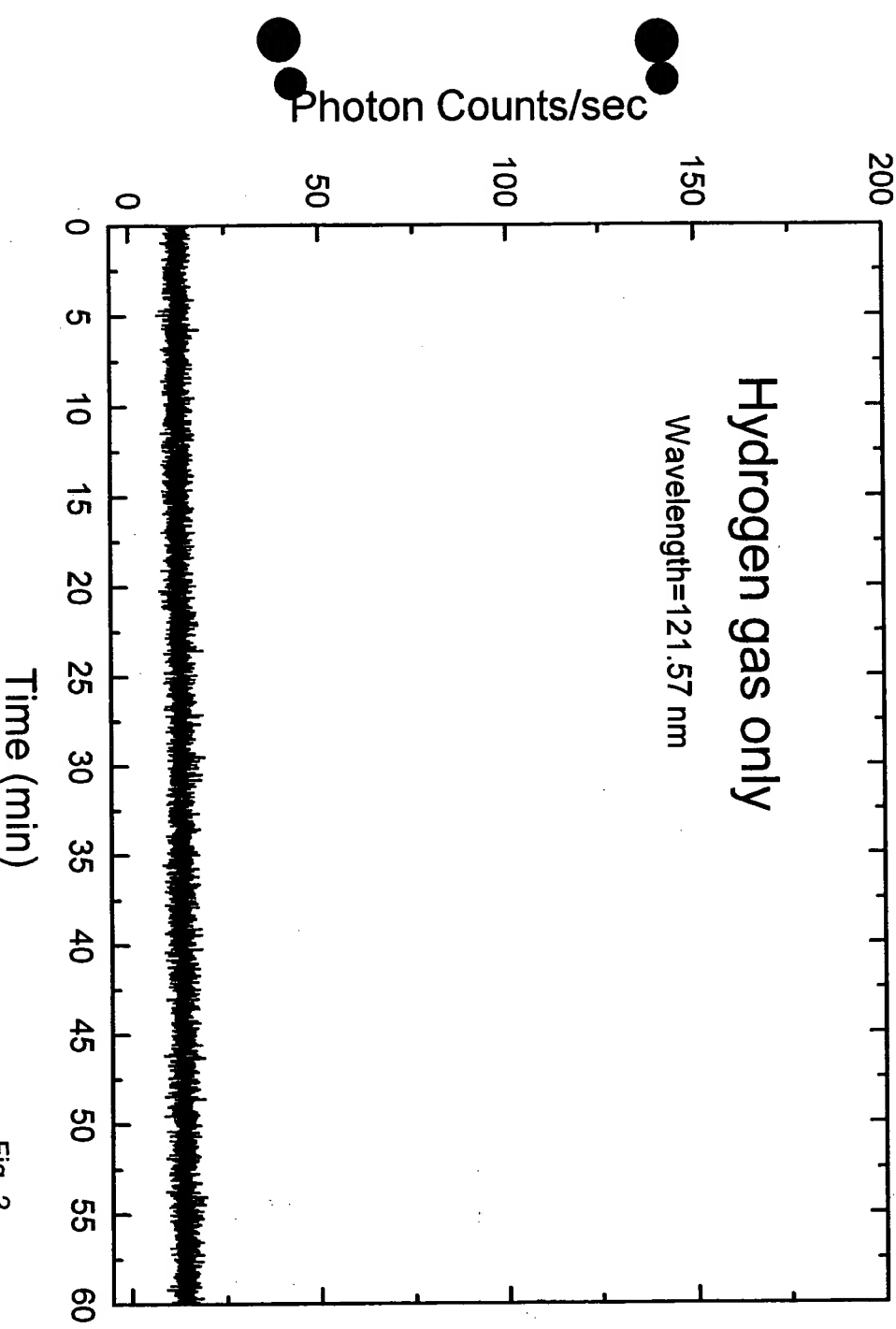


Fig. 2

Wavelength (nm)

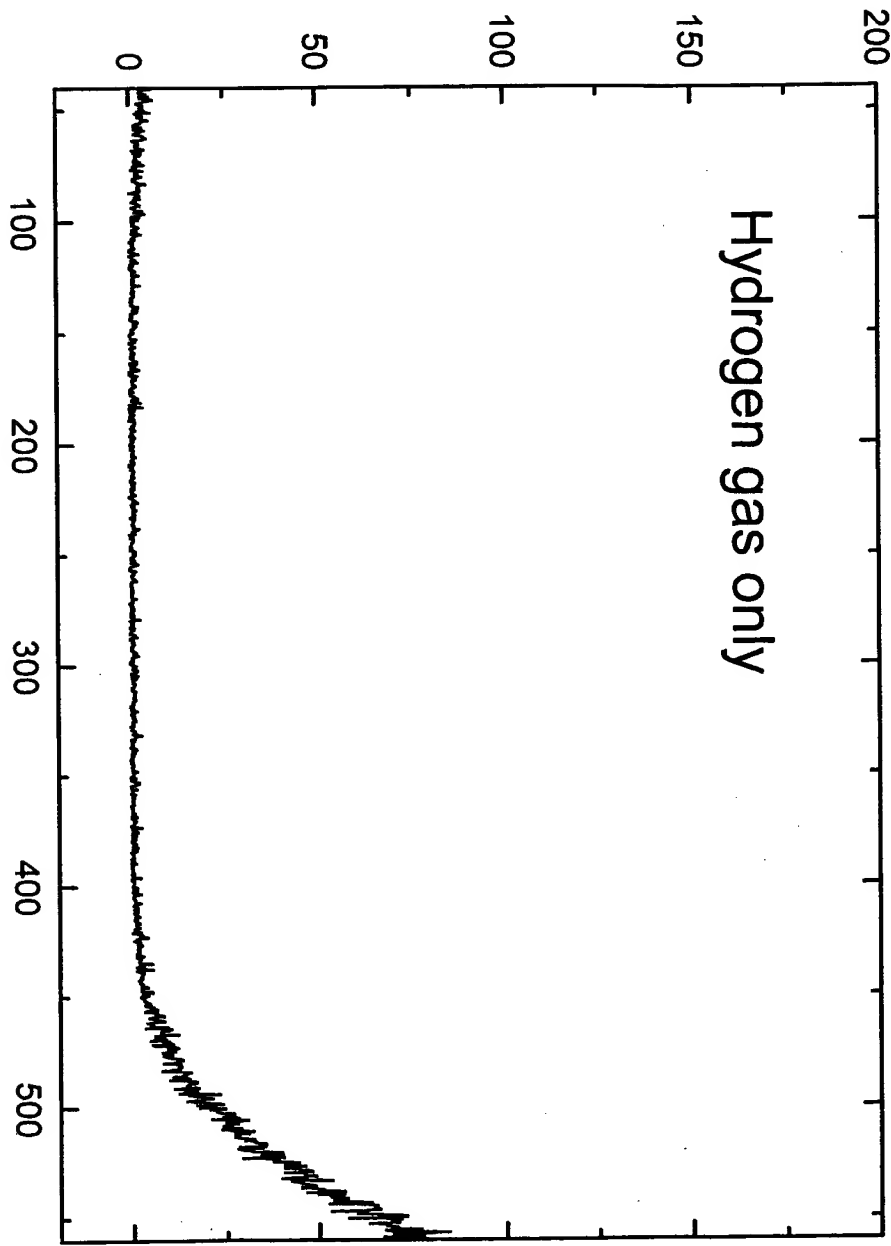


Fig. 3

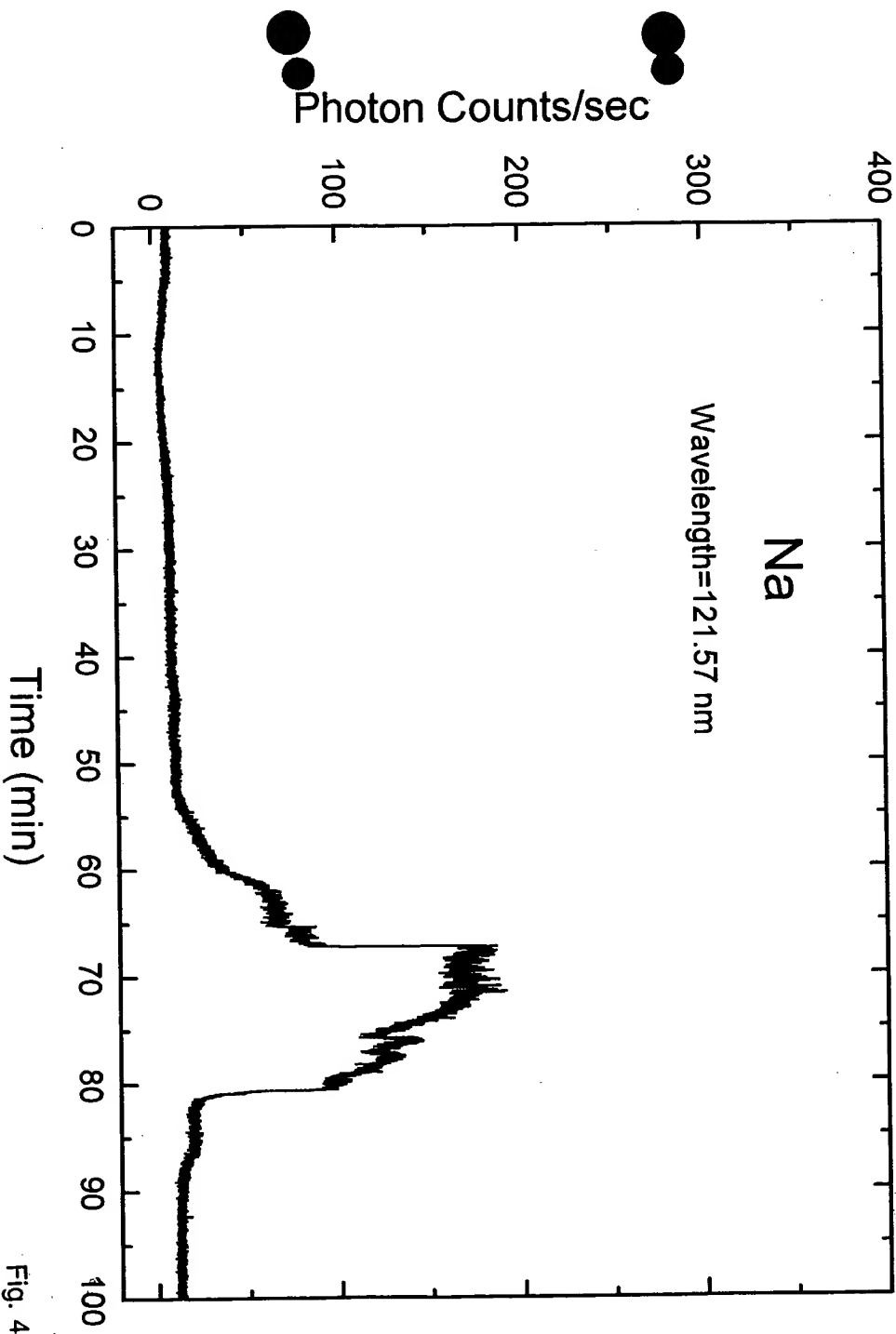


Fig. 4

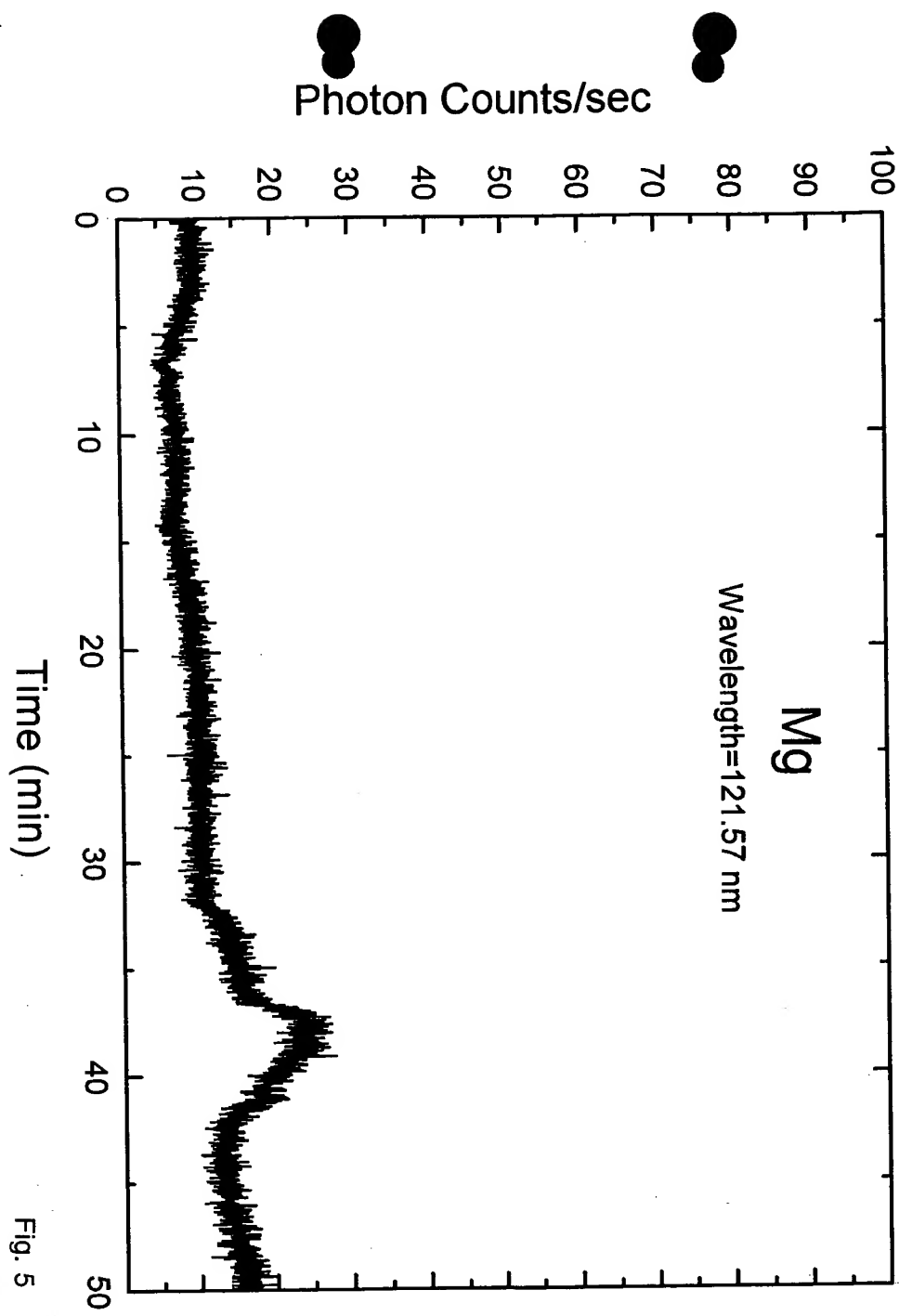


Fig. 5

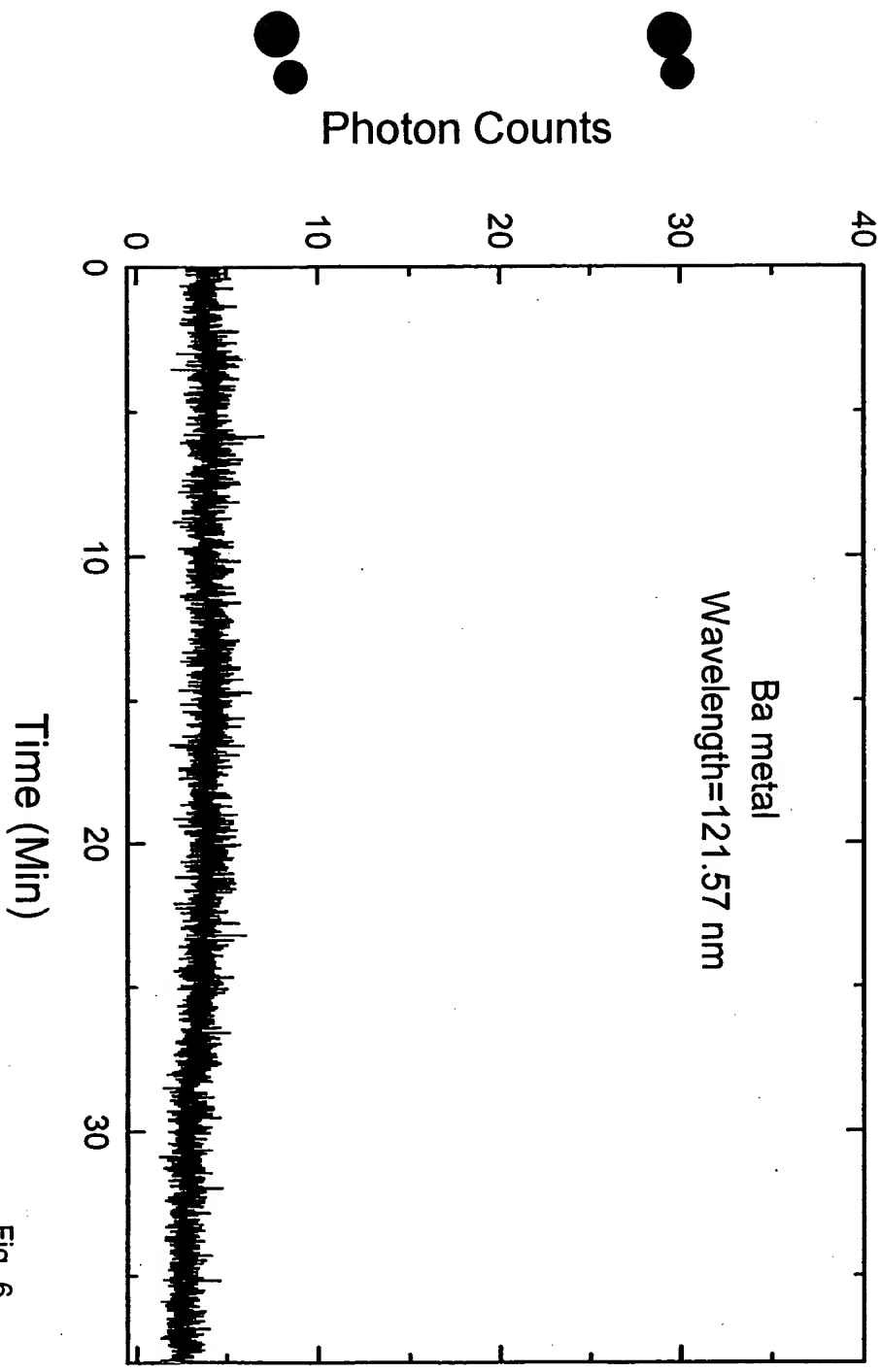
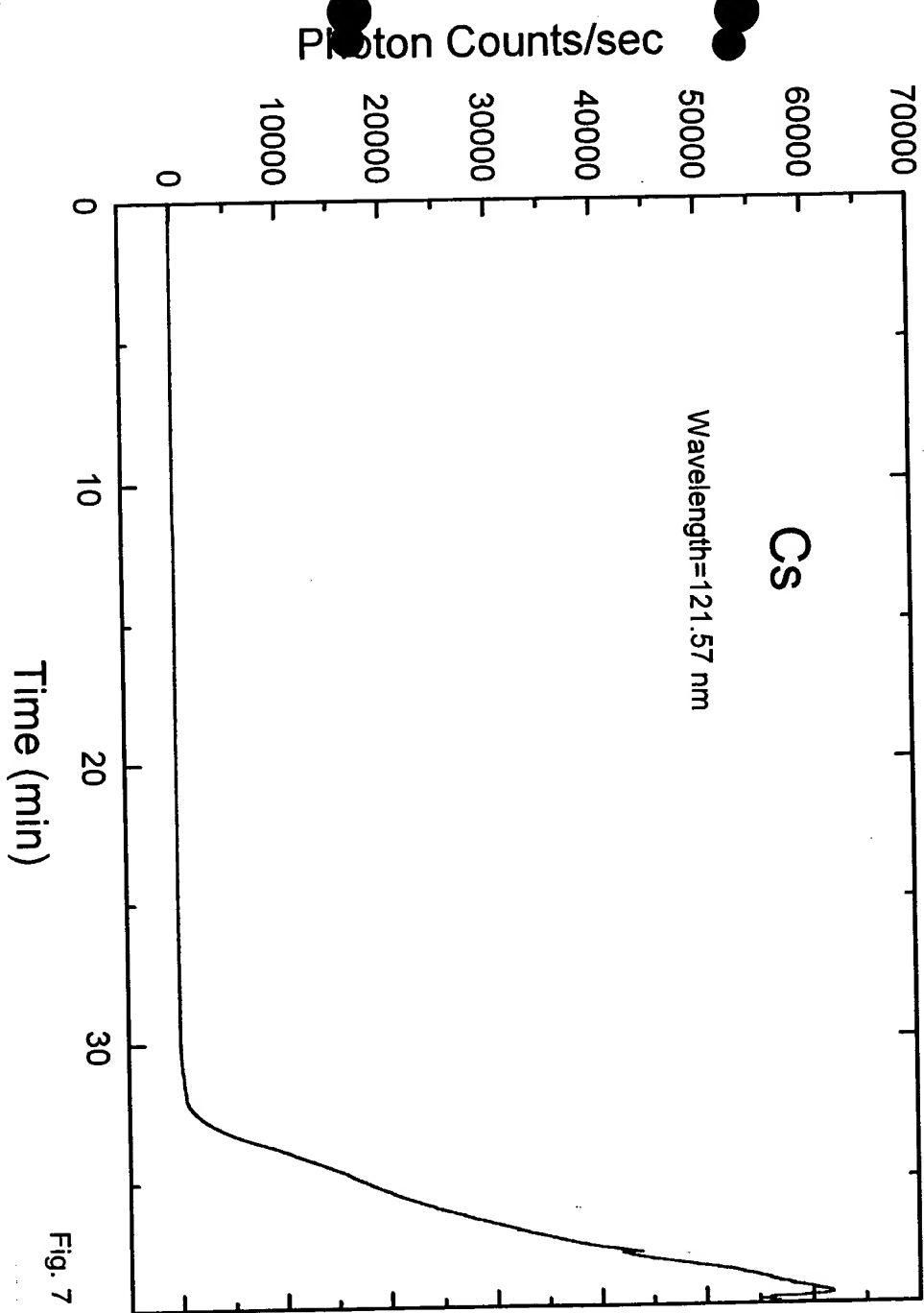


Fig. 6



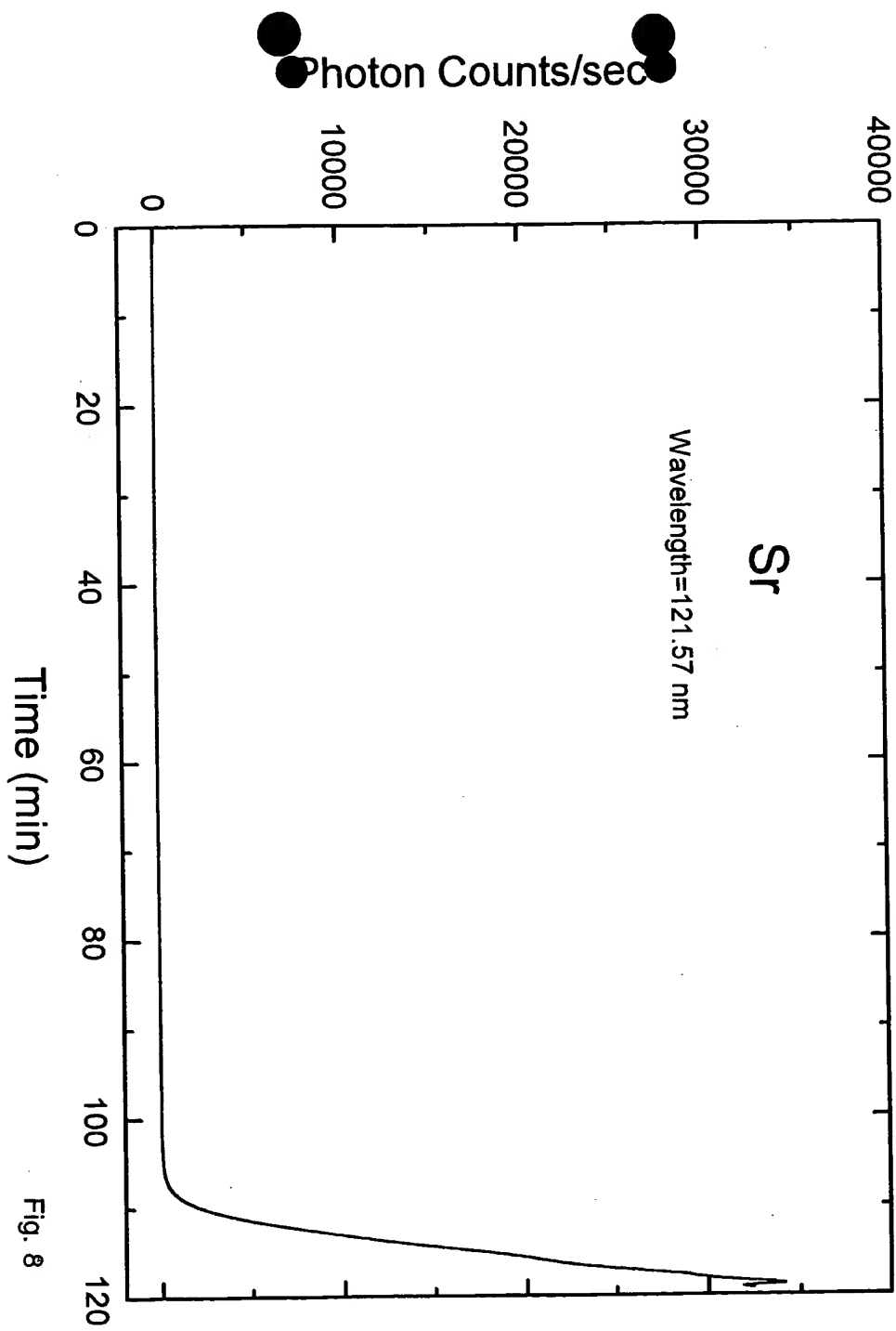


Fig. 8

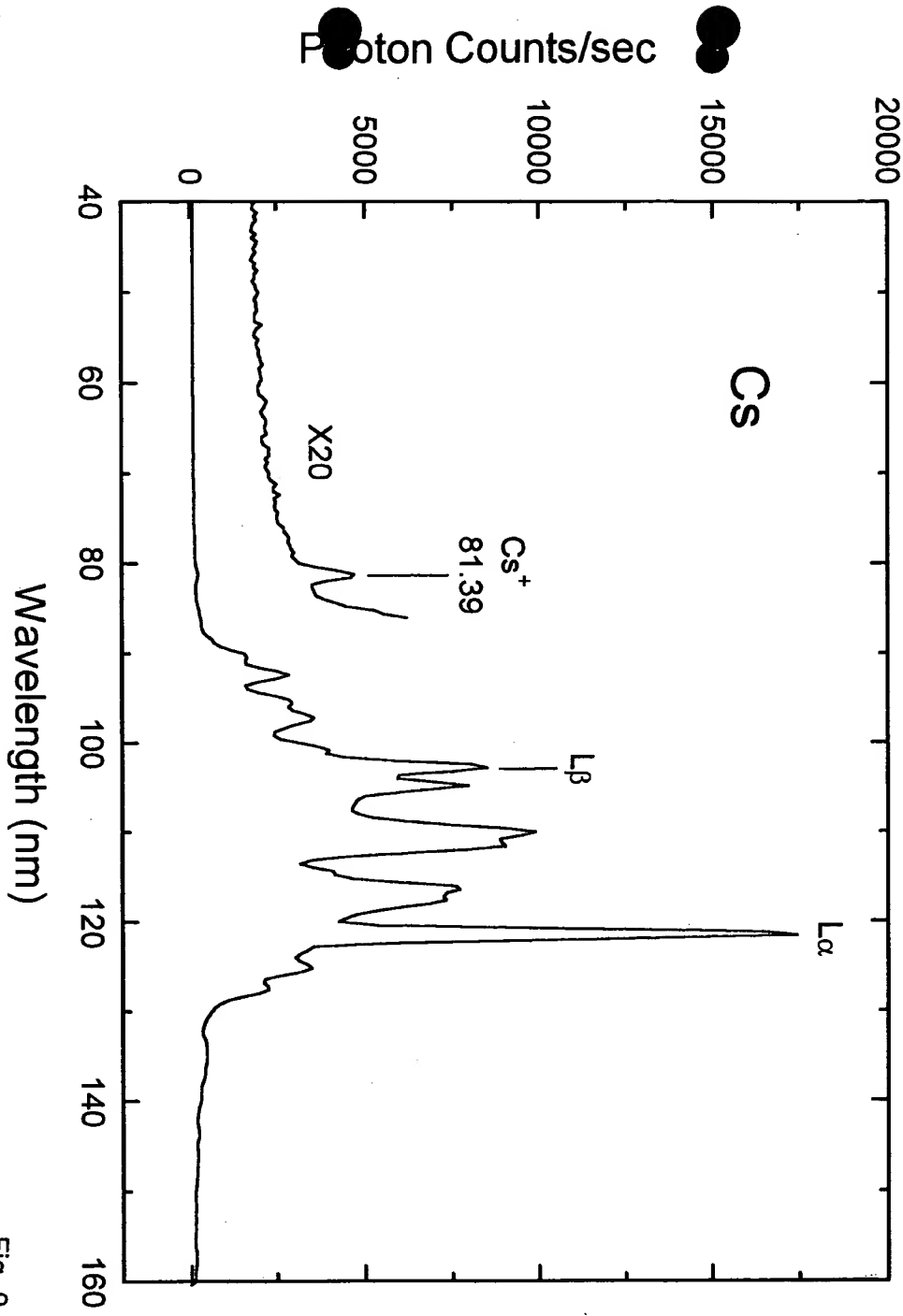


Fig. 9

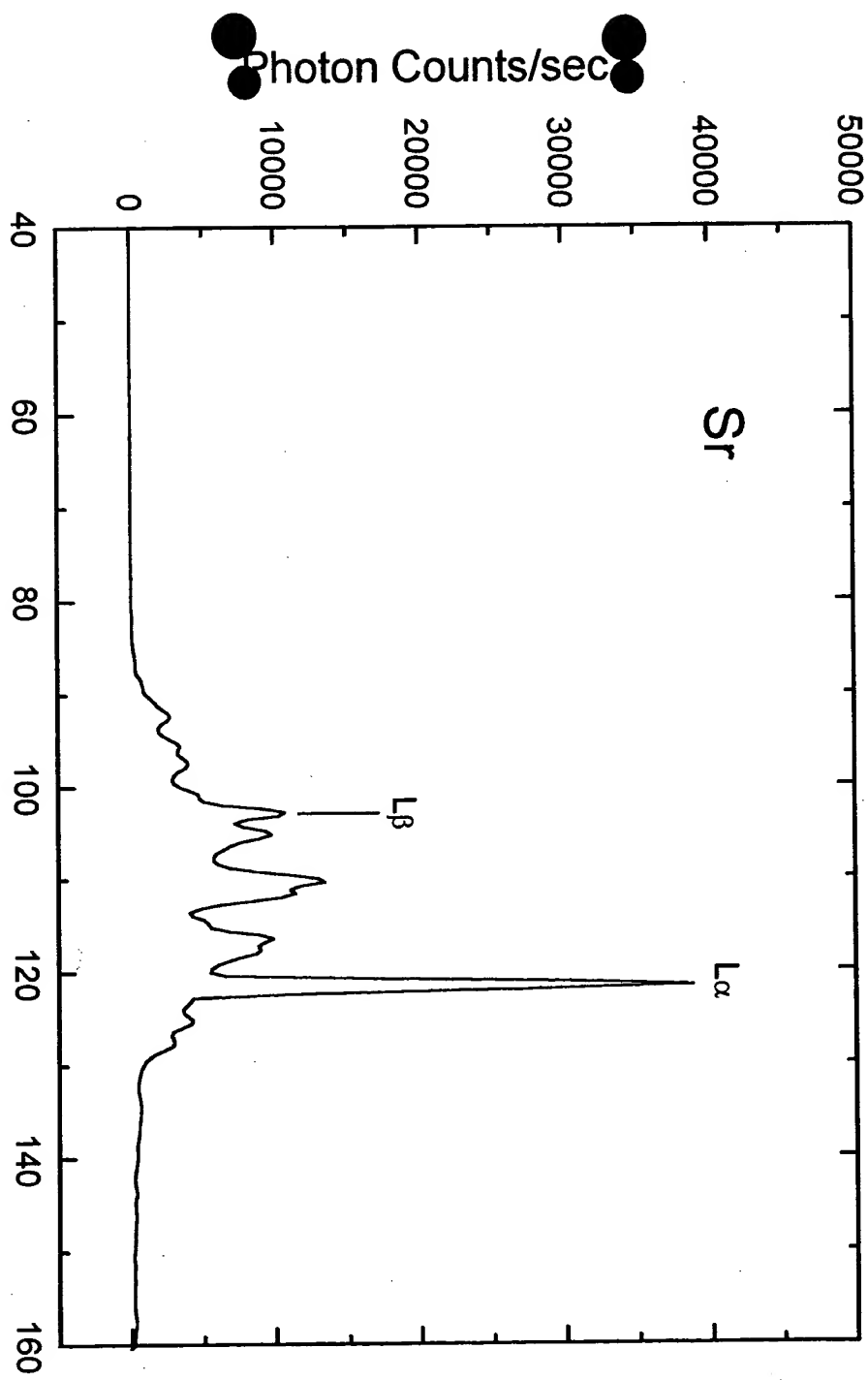


Fig. 10.

Fig. 11

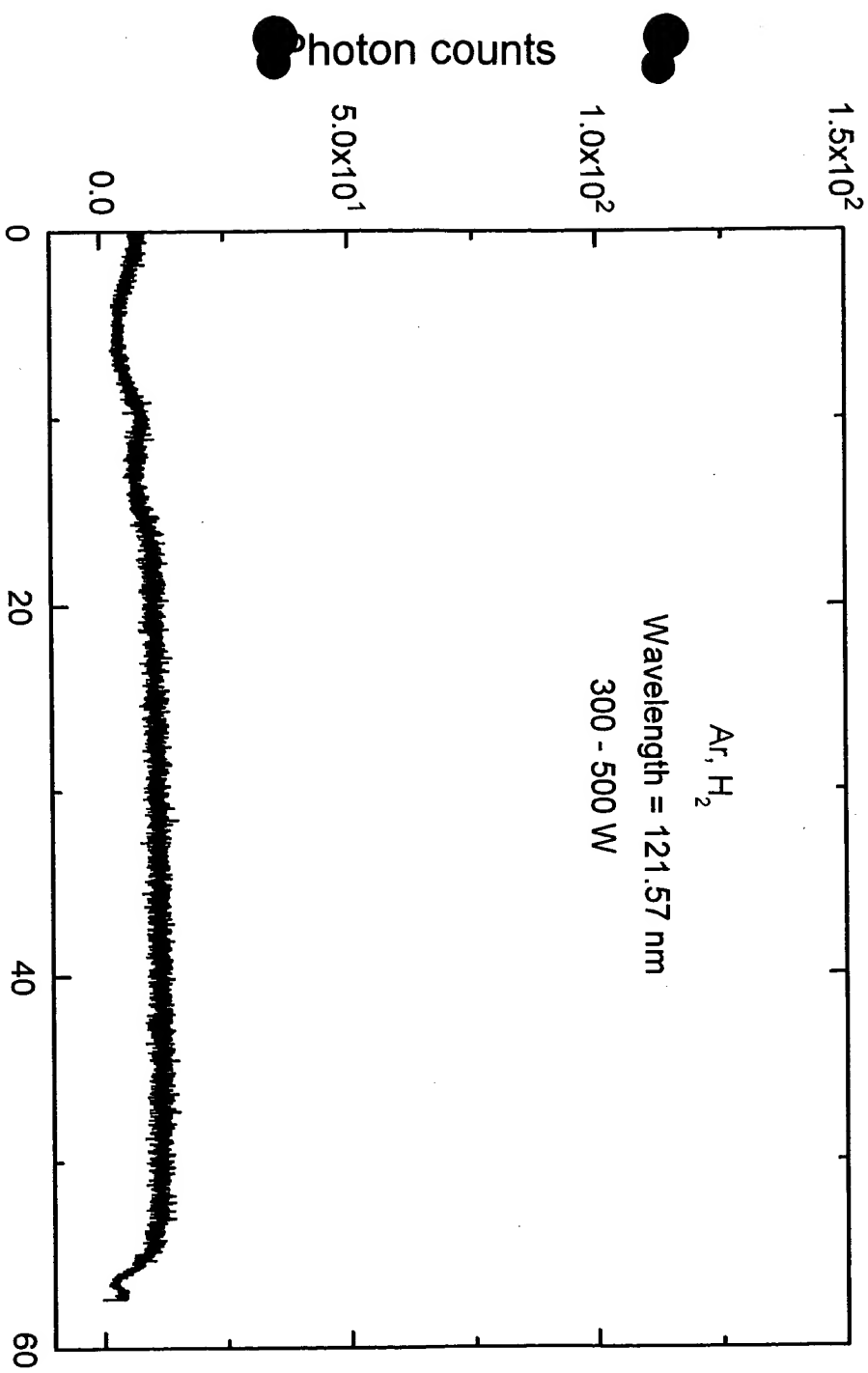


Fig. 12

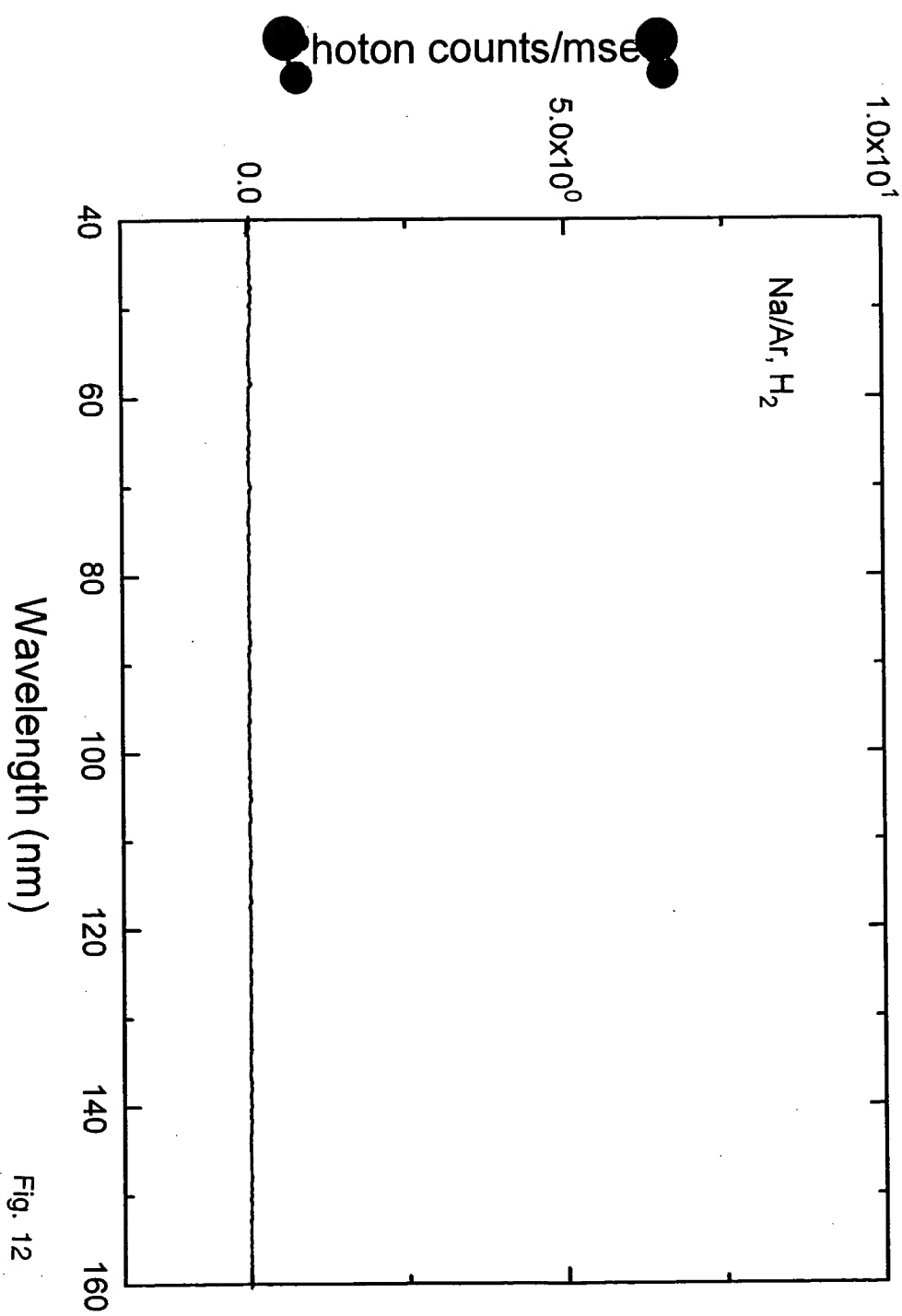
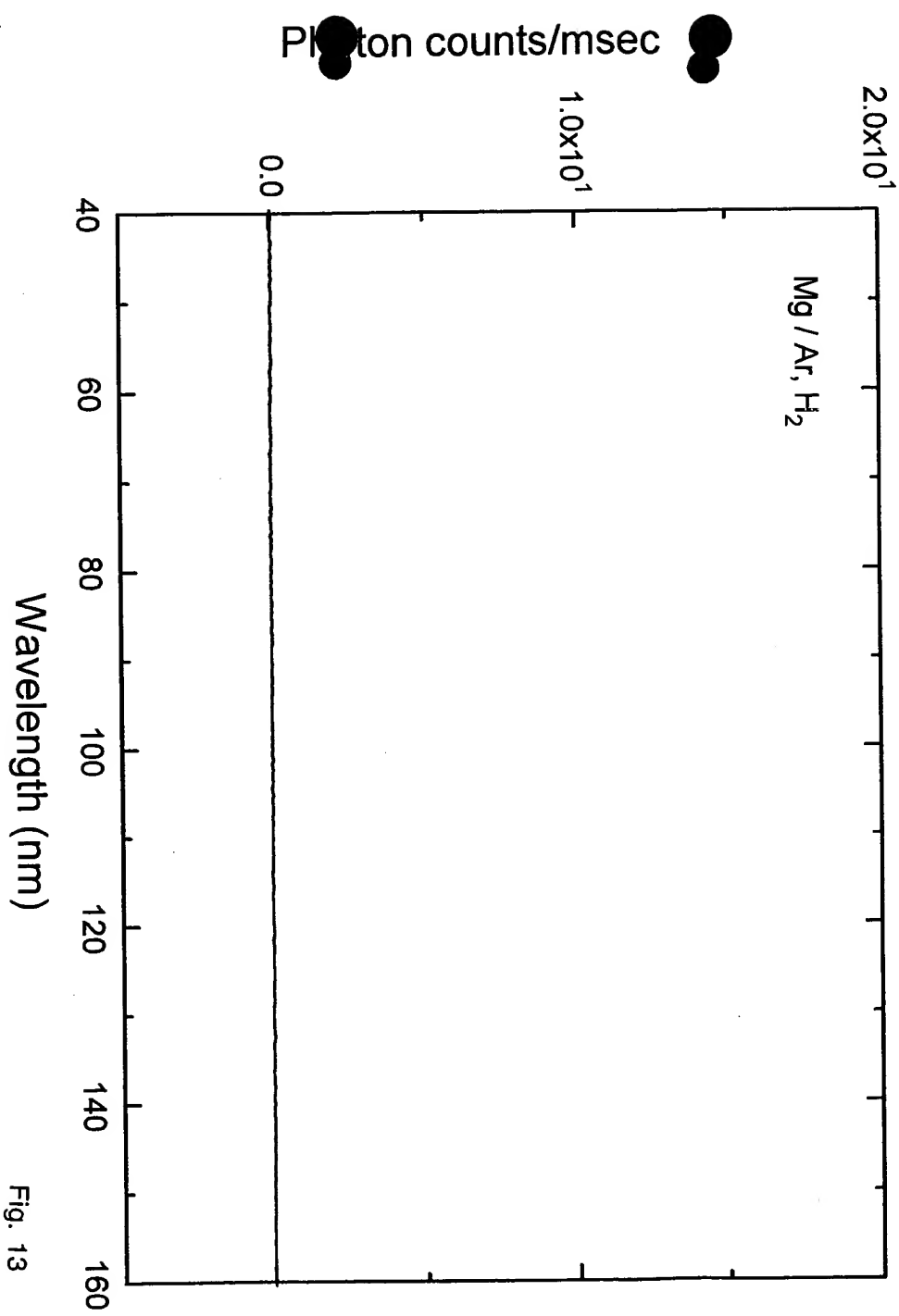


Fig. 13



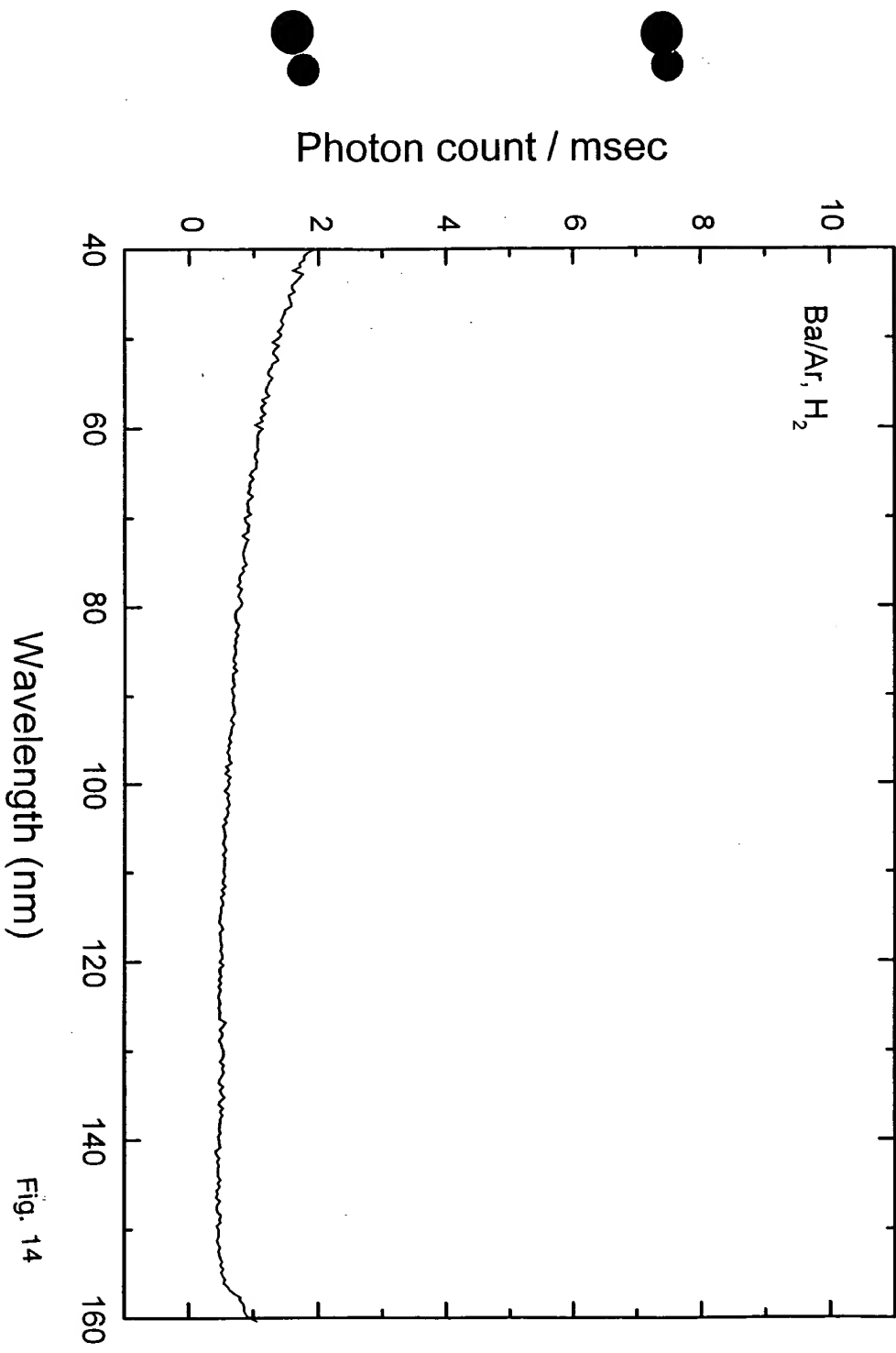


Fig. 14

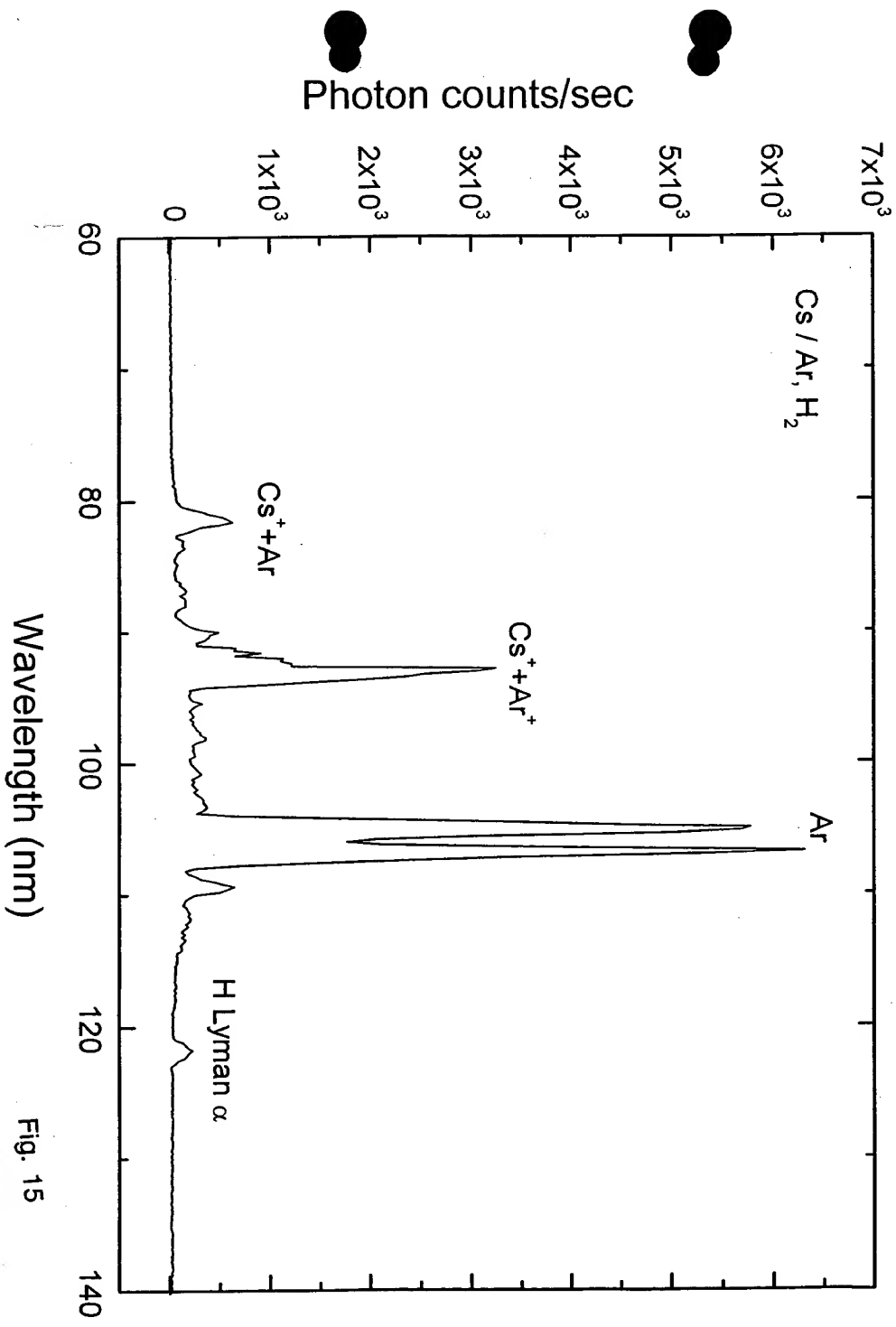


Fig. 15

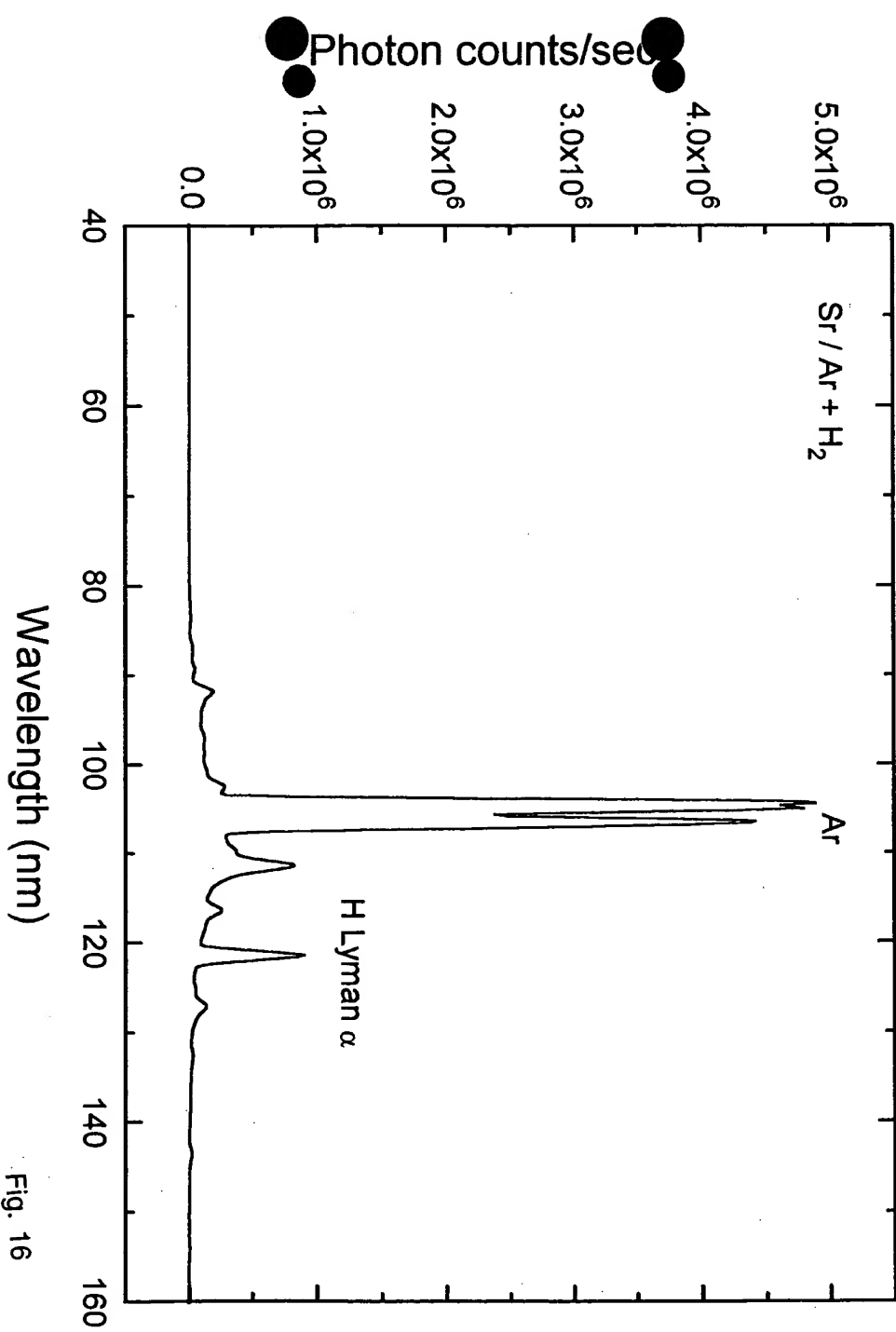


Fig. 16

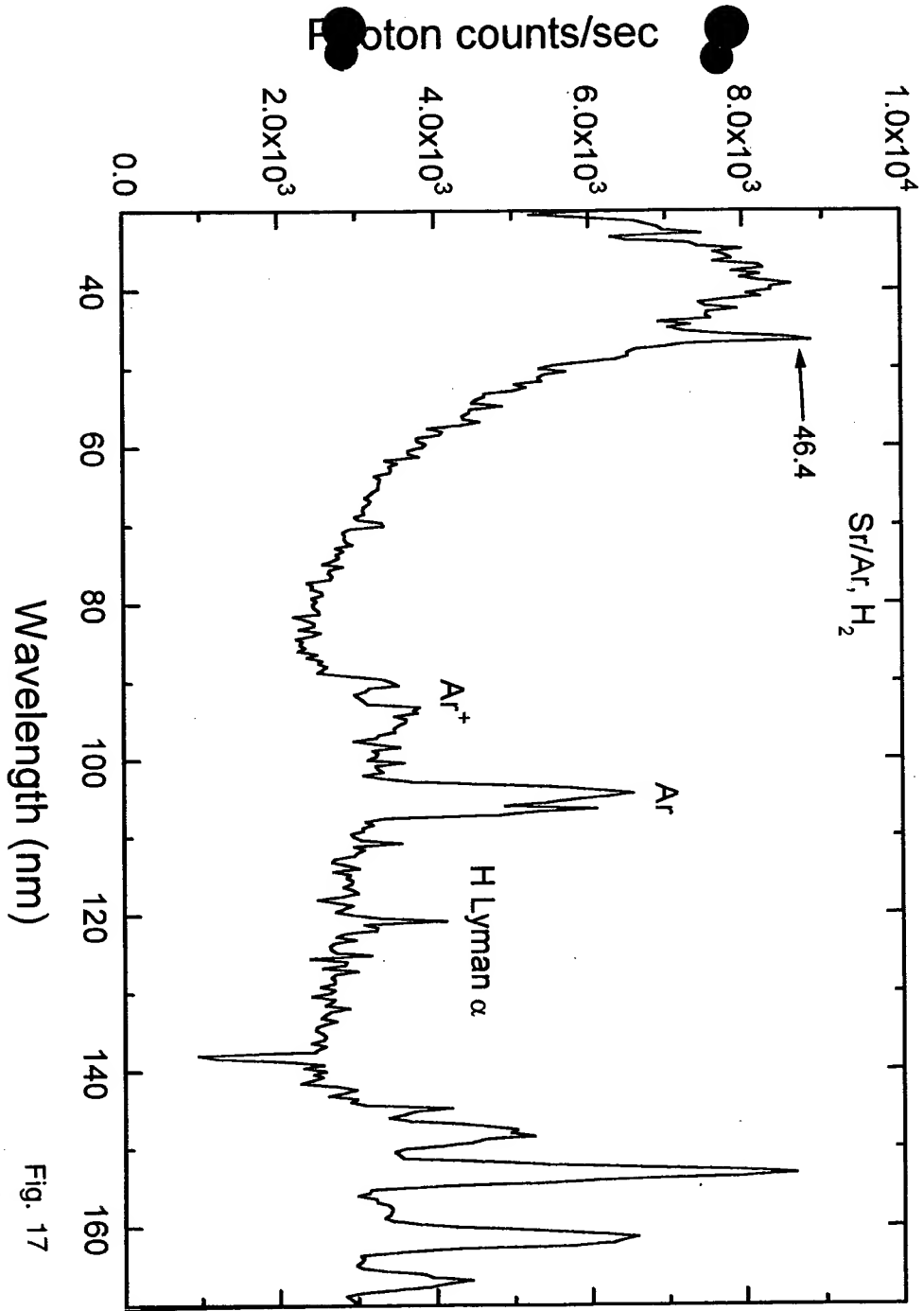


Fig. 17

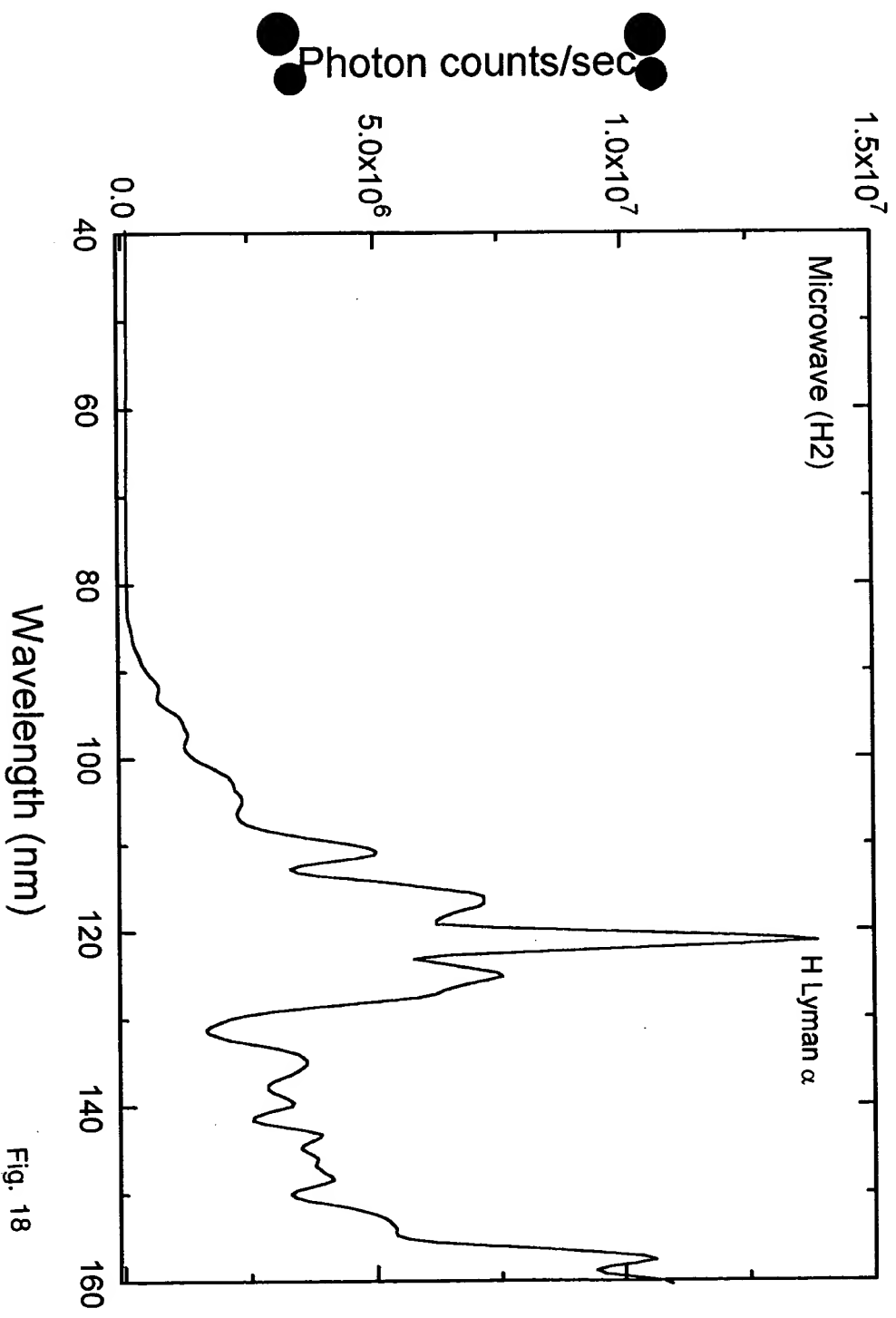
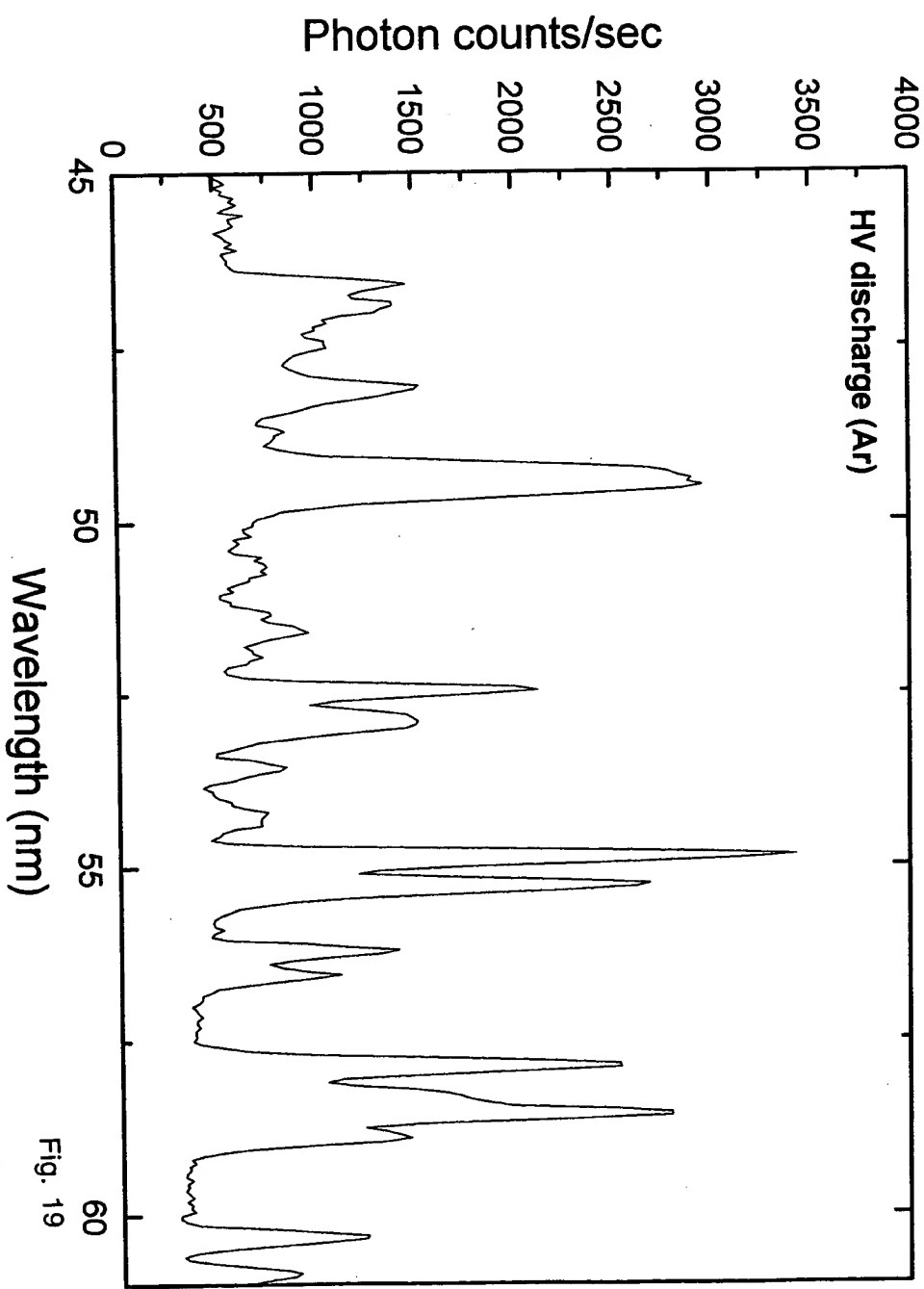


Fig. 18



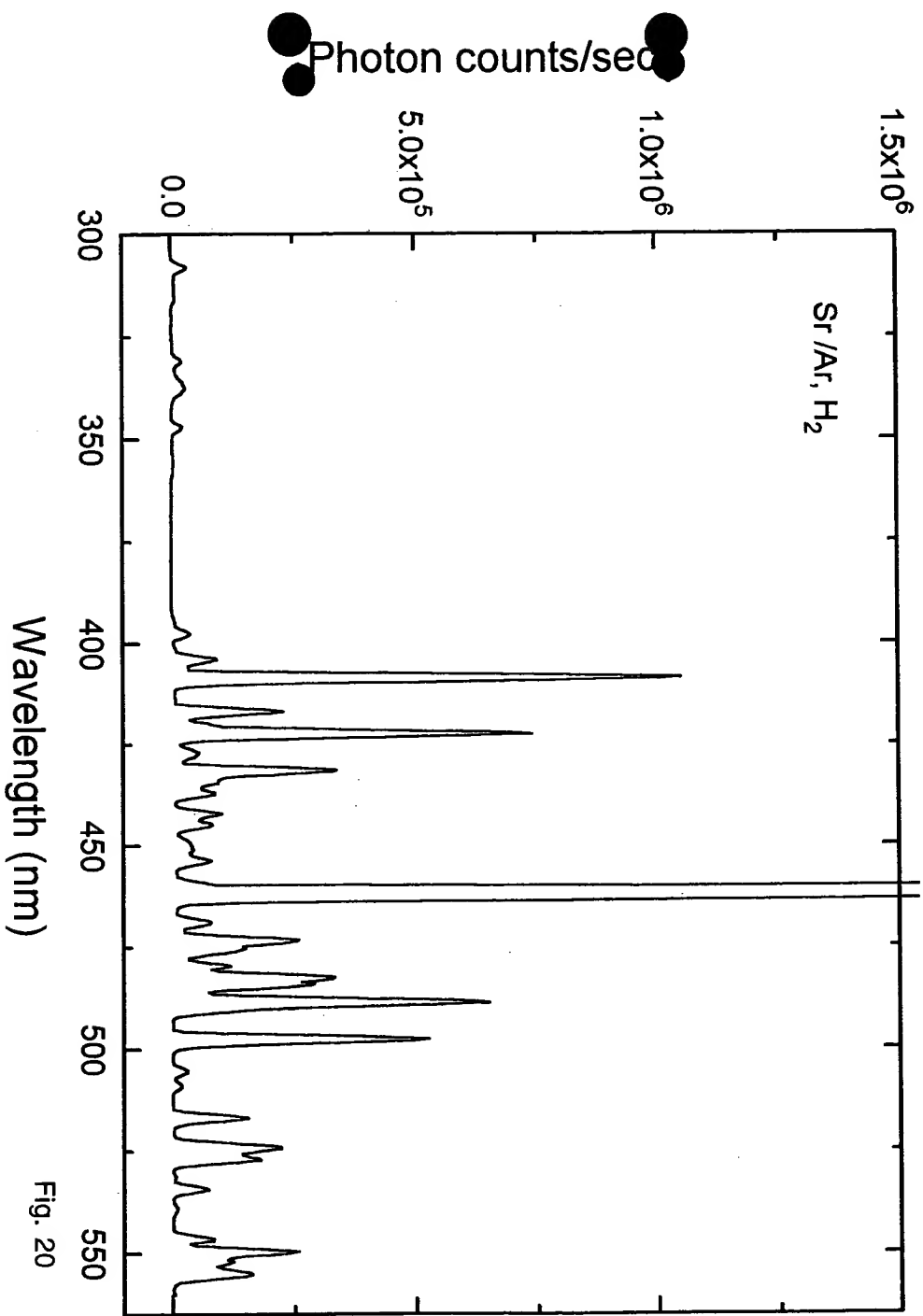


Fig. 20

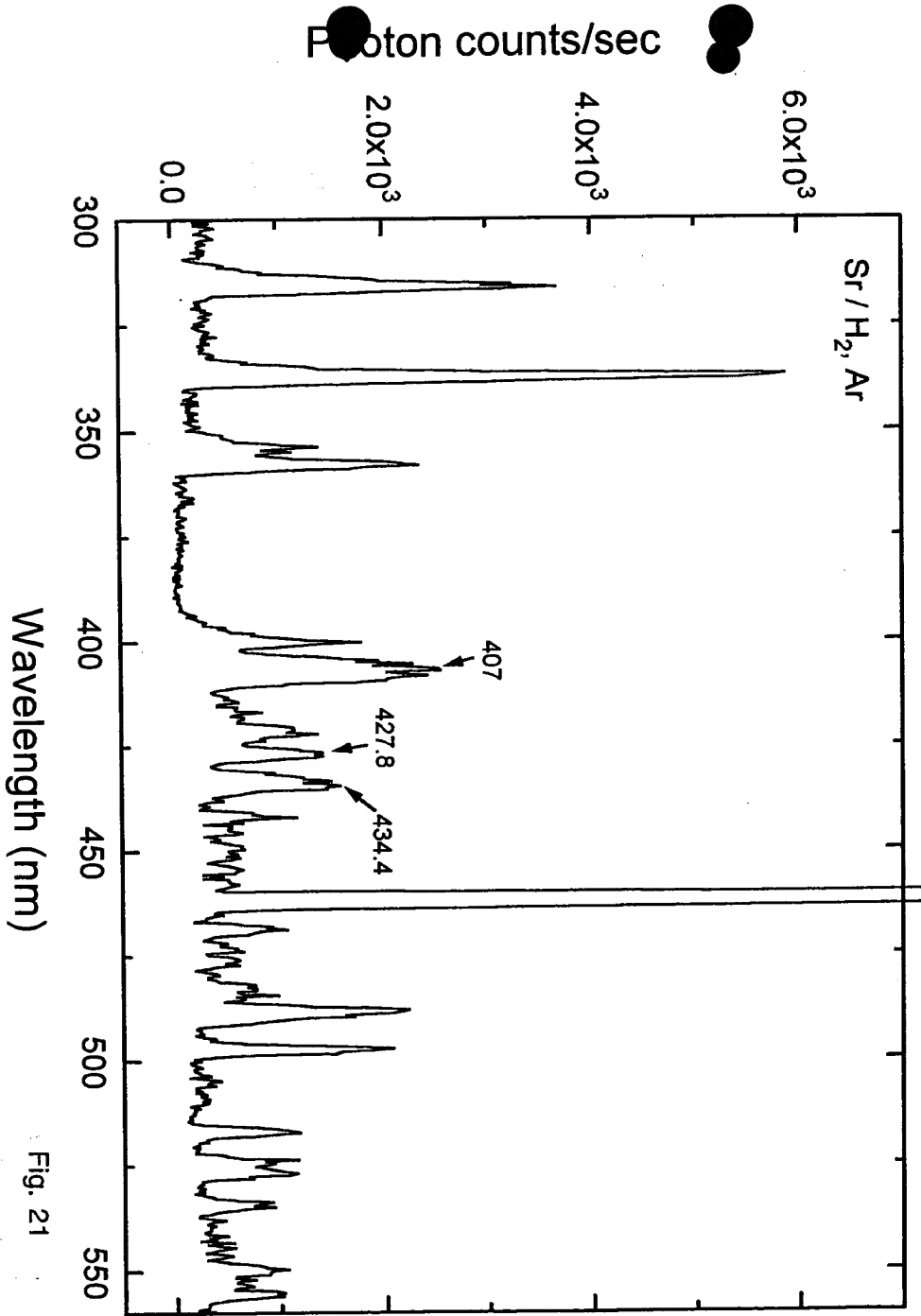


Fig. 21

Photon counts (arb)

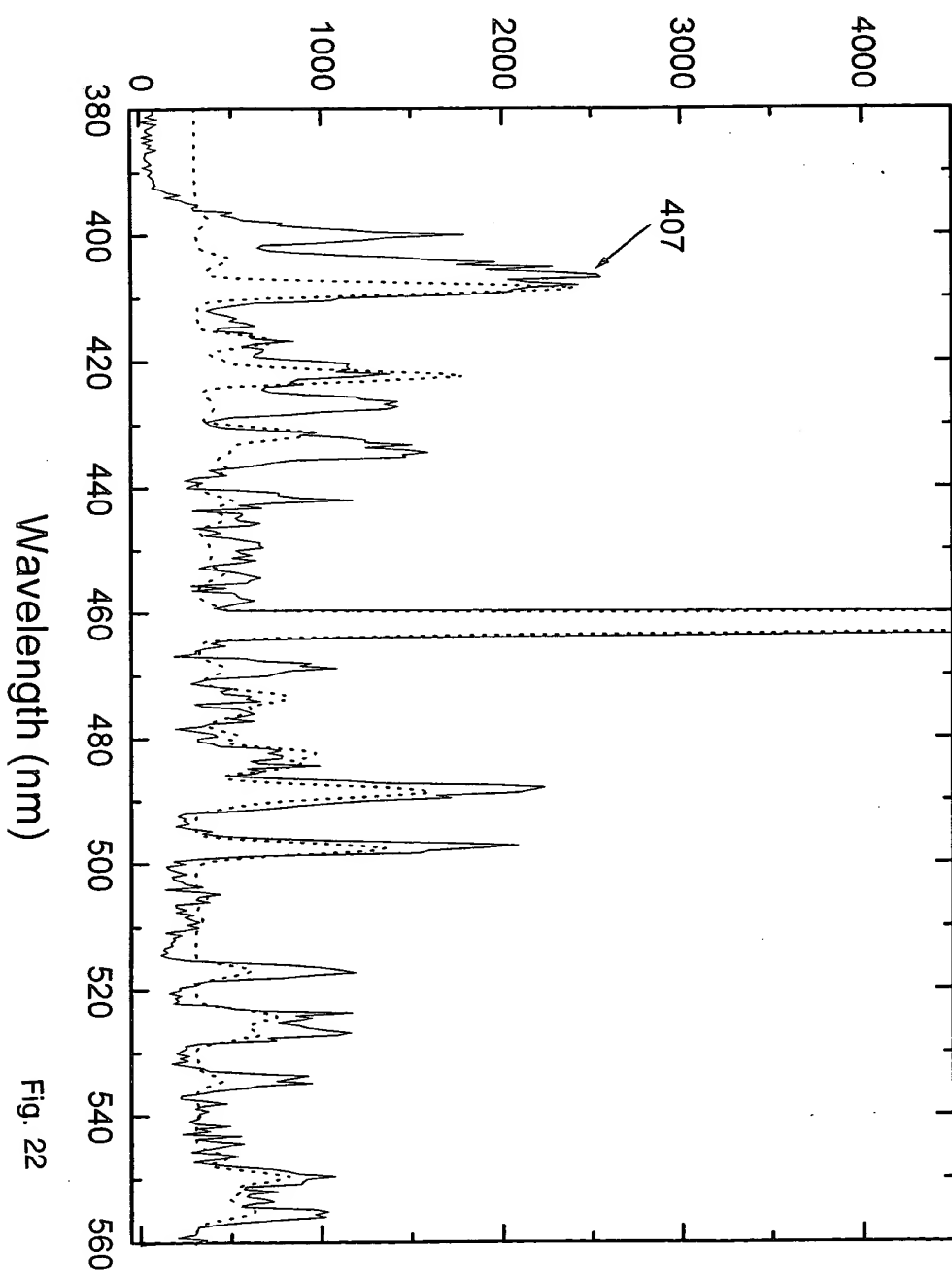


Fig. 22

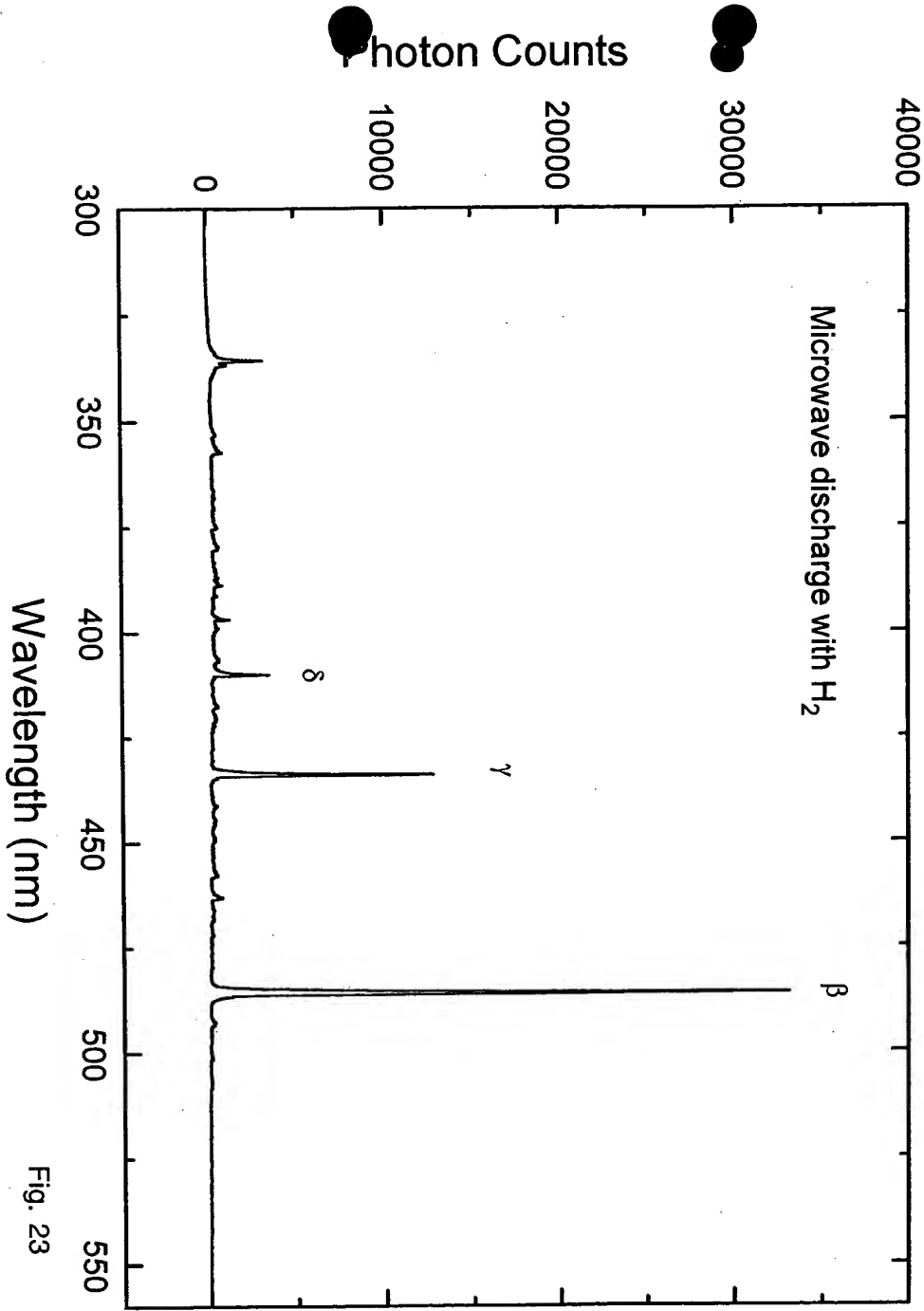


Fig. 23

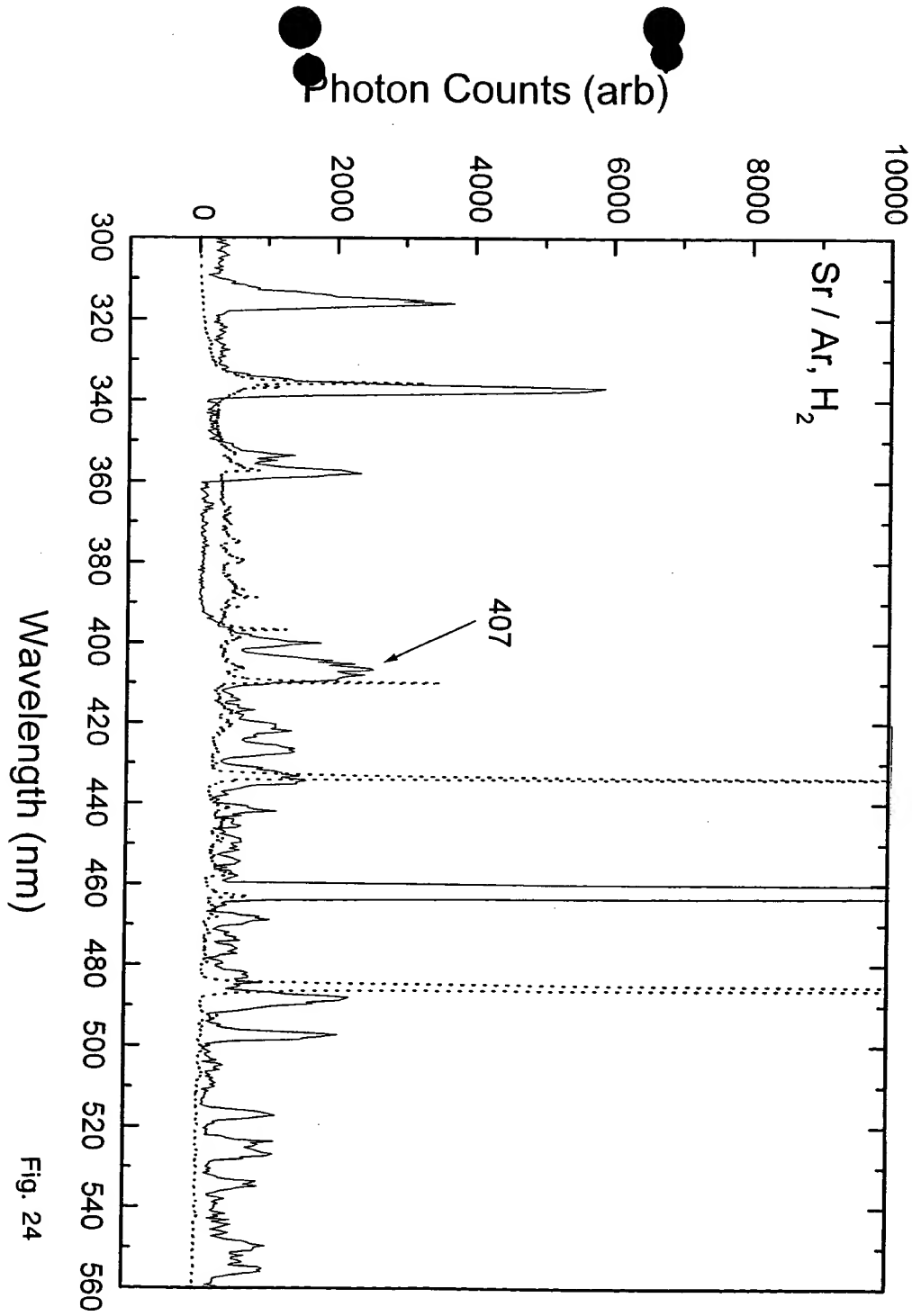


Fig. 24

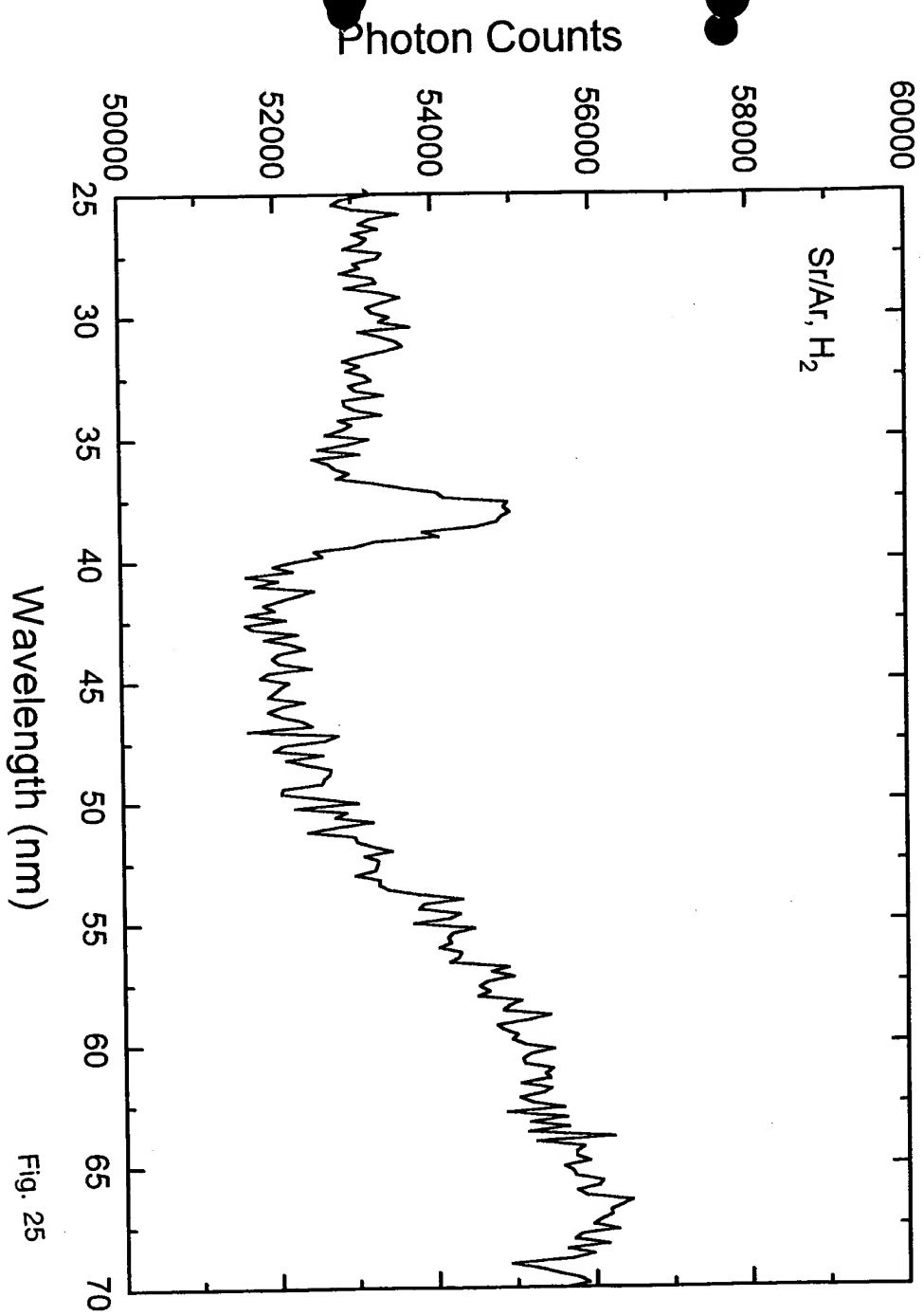


Fig. 25

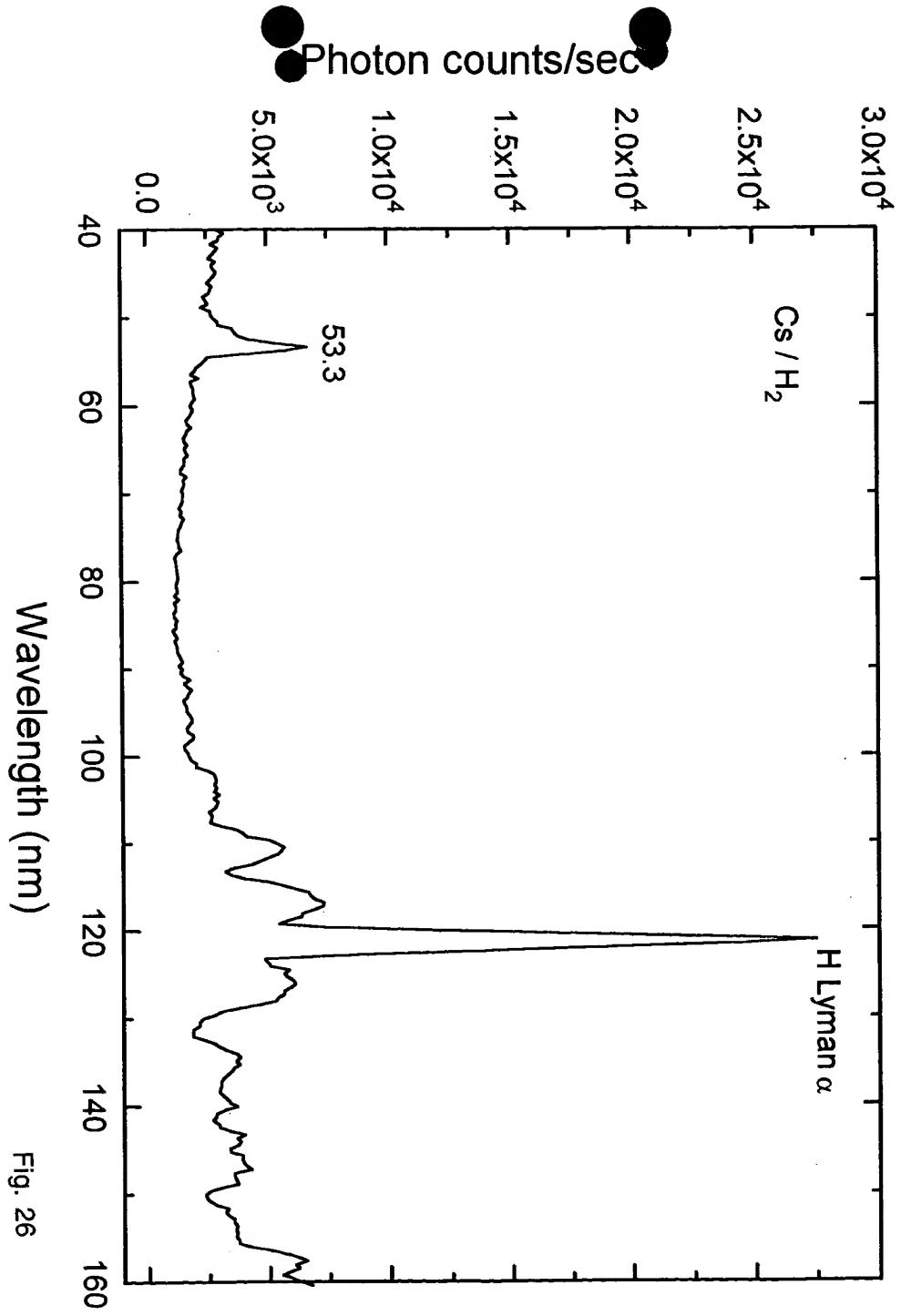


Fig. 26

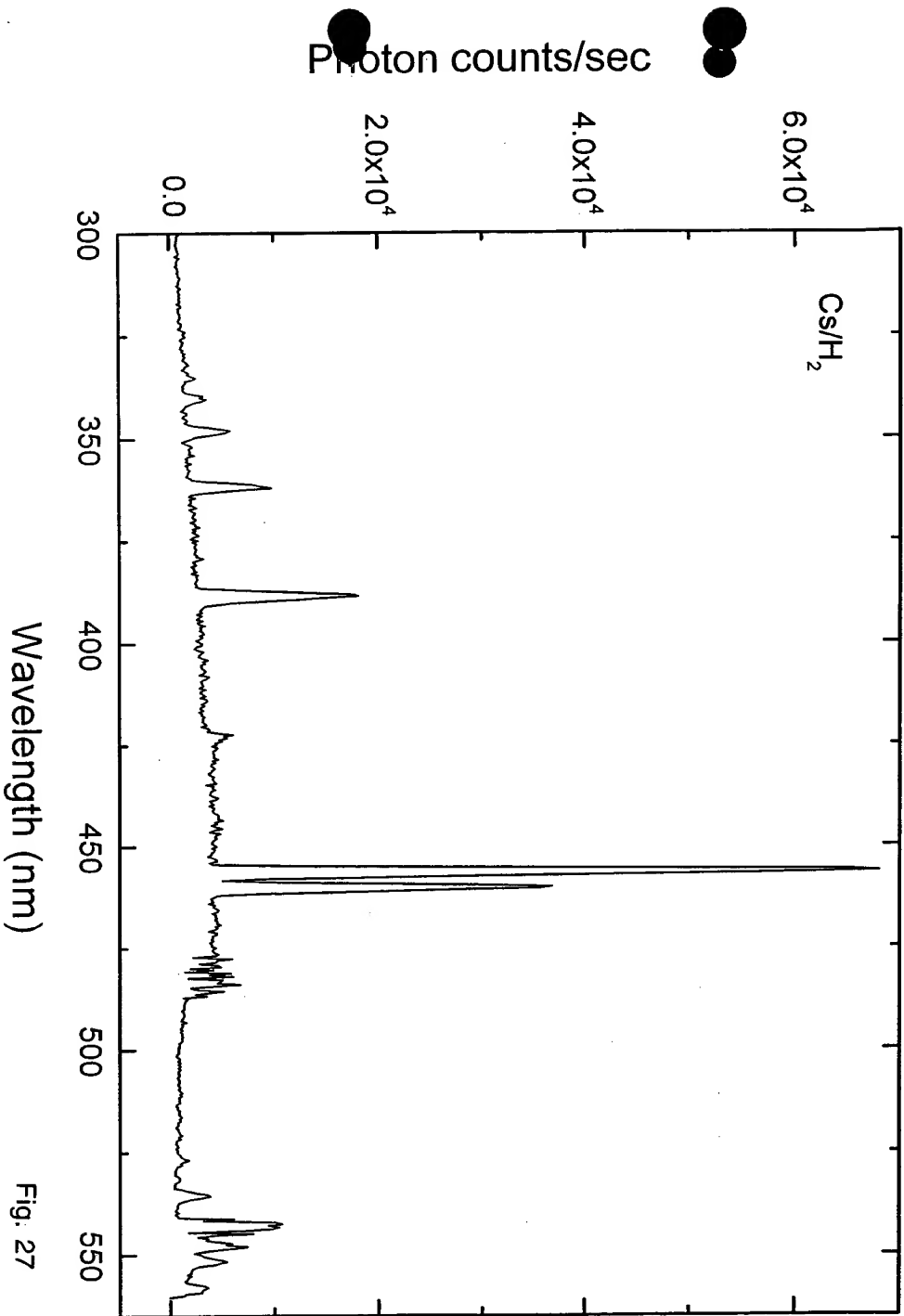


Fig. 27

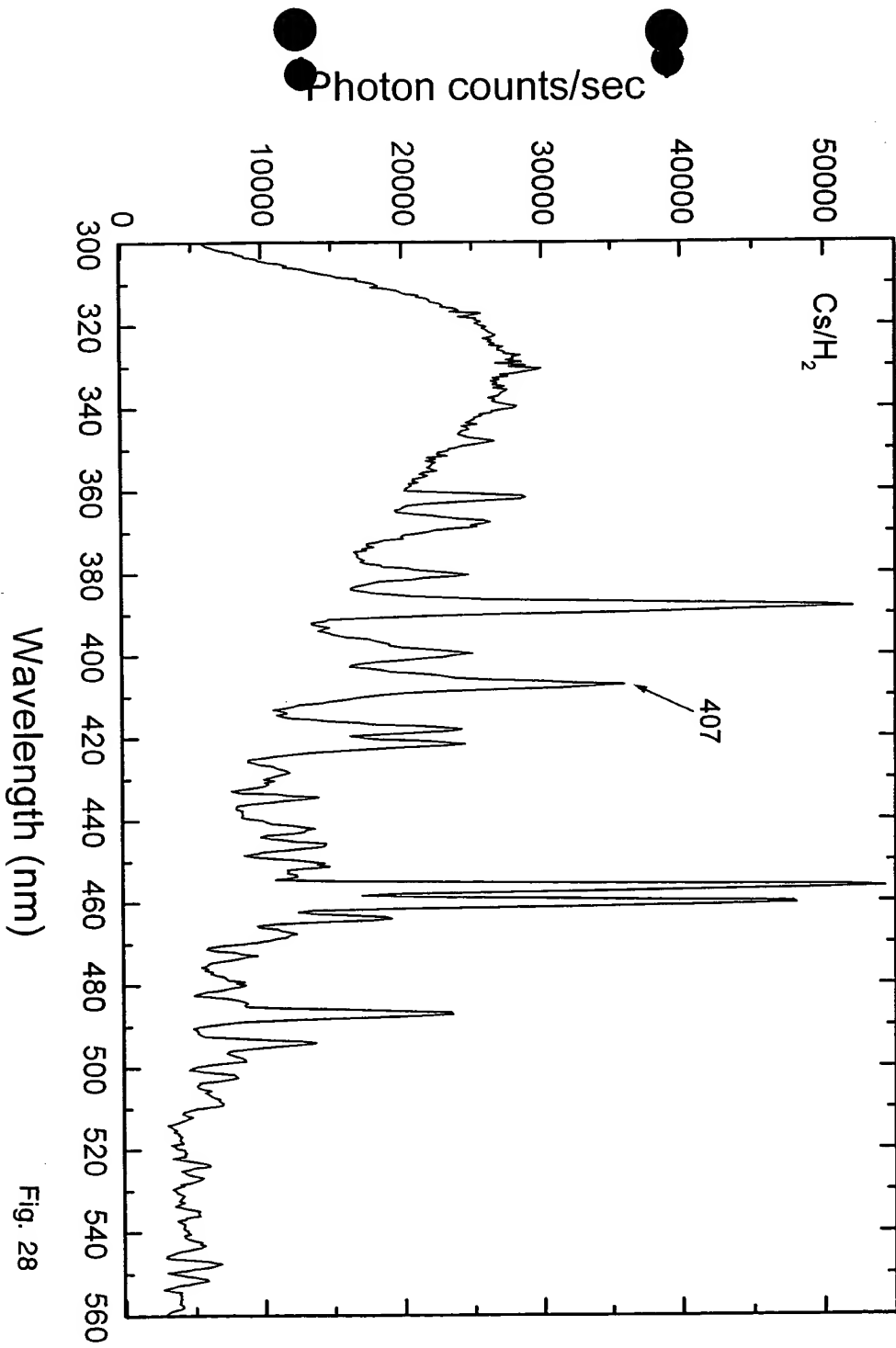
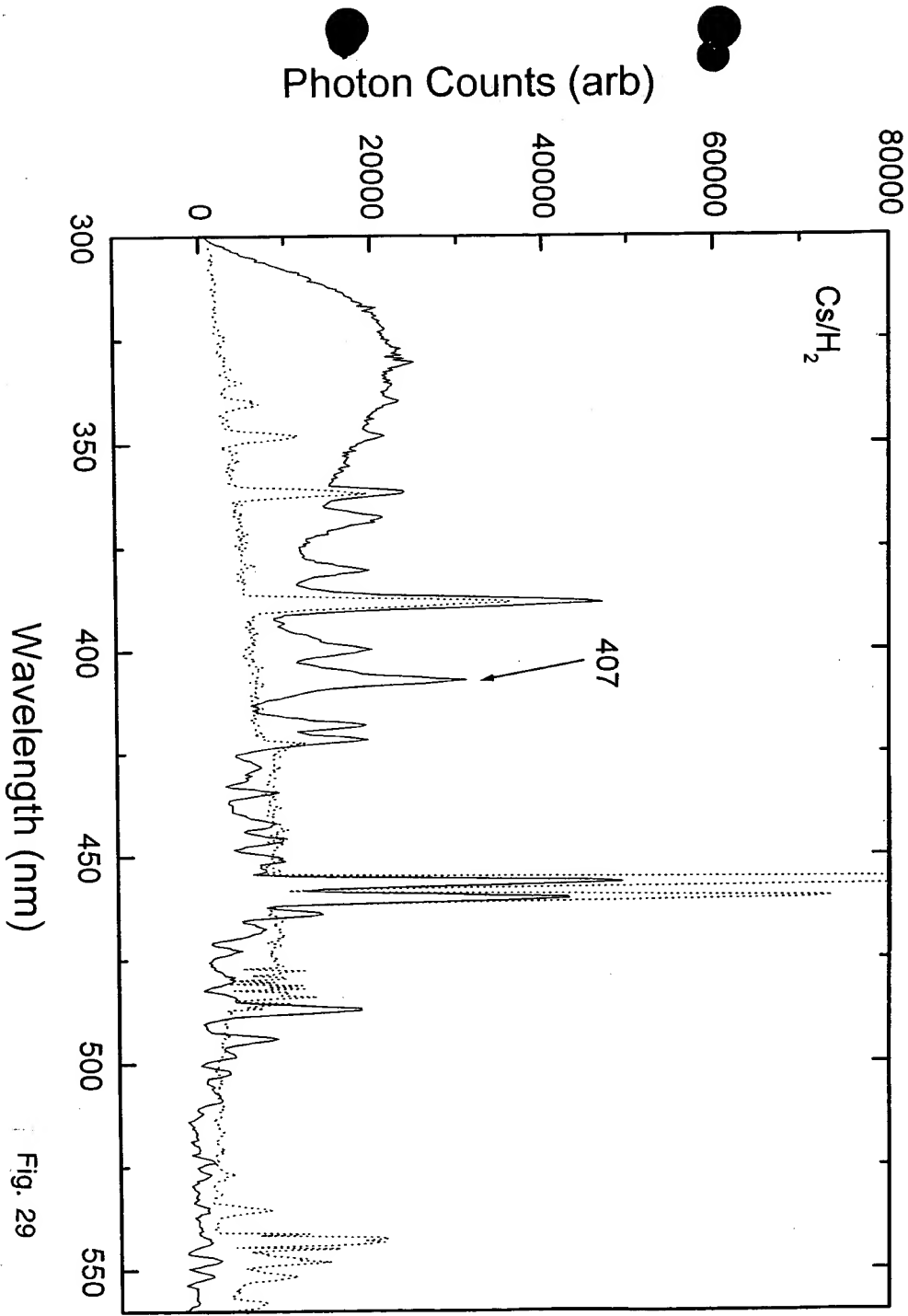


Fig. 28



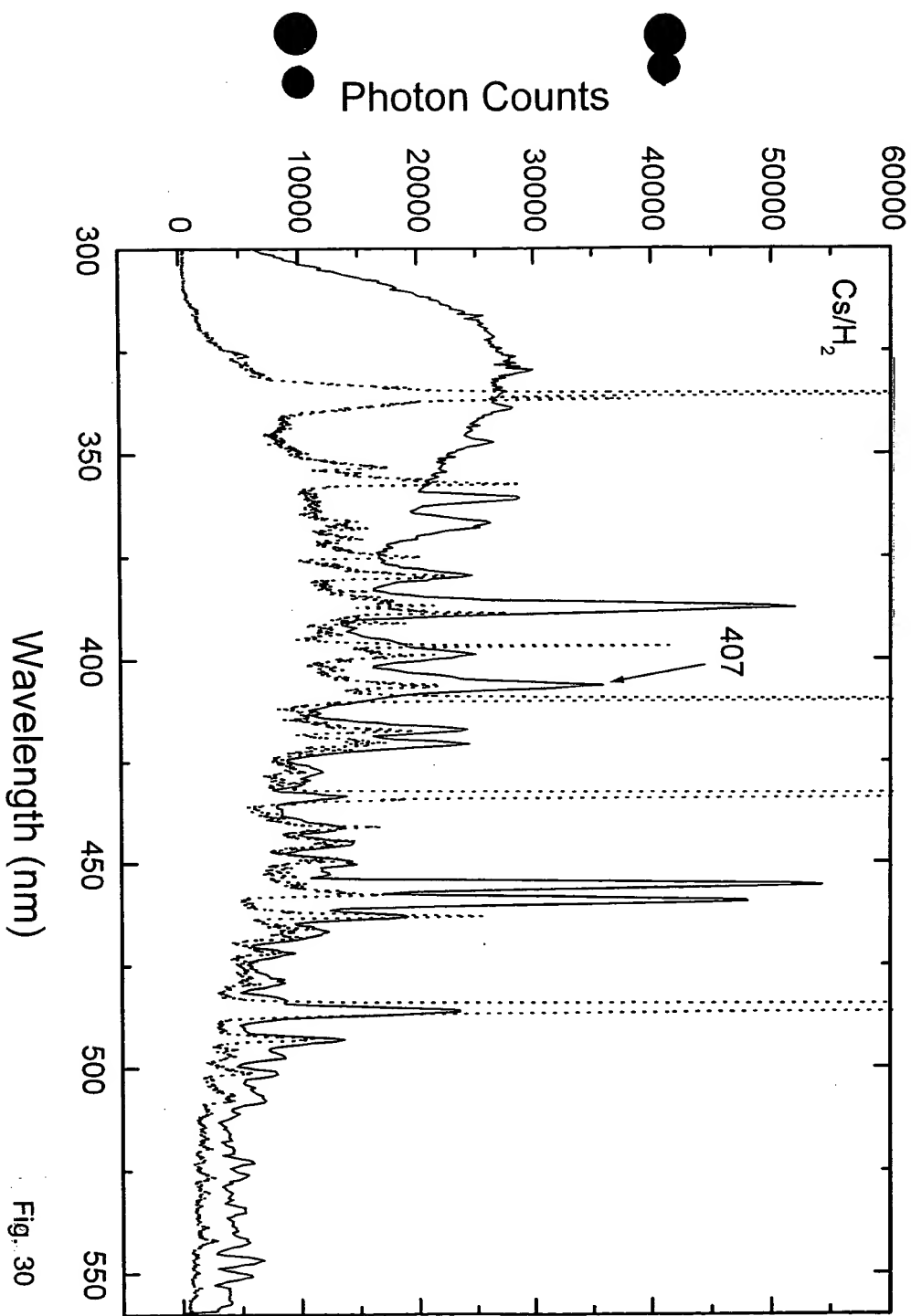


Fig. 30

Photon counts/sec

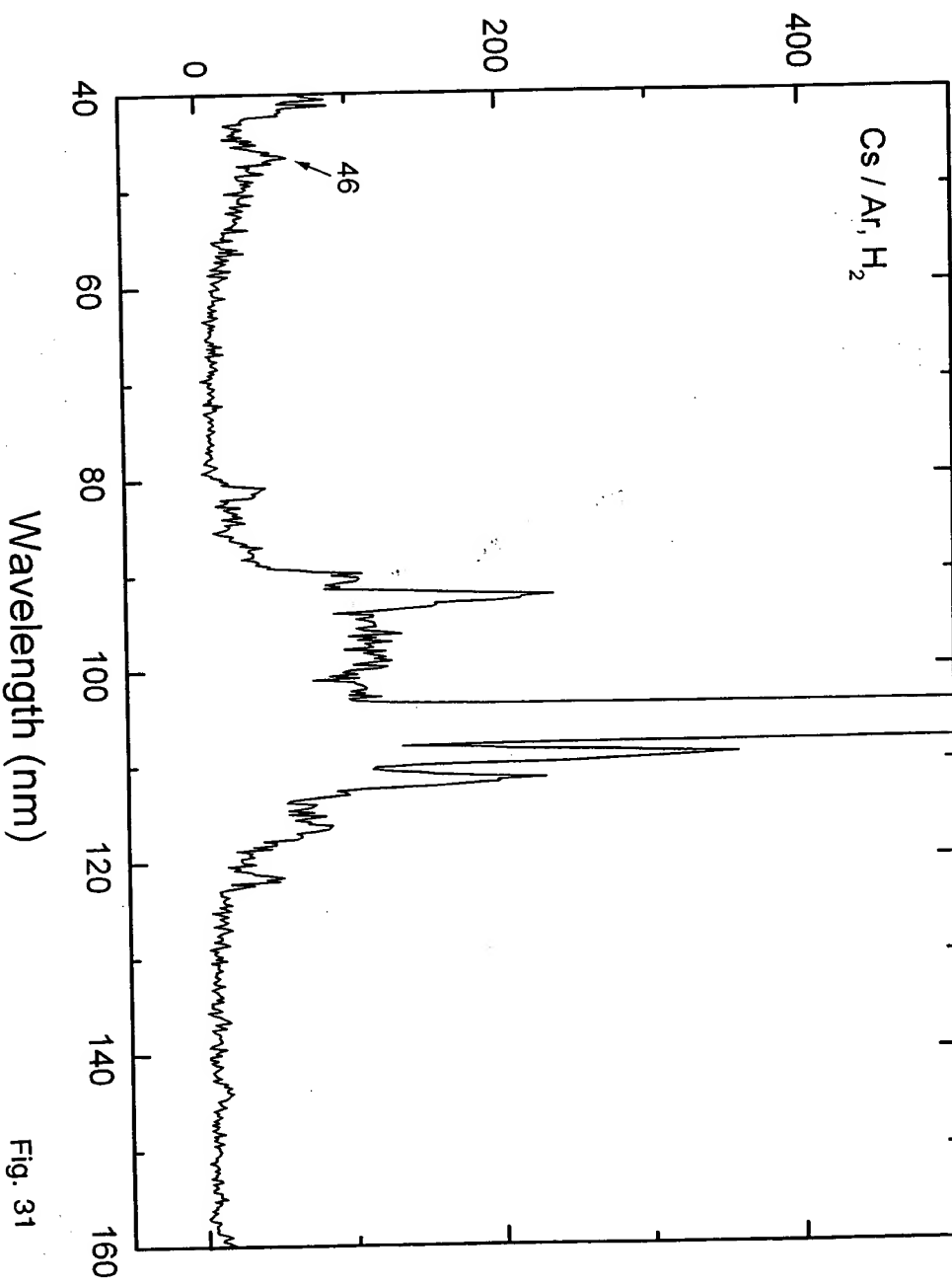


Fig. 31

THIS PAGE BLANK (USPTO)

Optically Measured Power Balances of Anomalous Discharges of Mixtures of Argon, Hydrogen, and Potassium, Rubidium, Cesium, or Strontium Vapor

Randell L. Mills

Nelson Greenig

Steven Hicks

BlackLight Power, Inc.

493 Old Trenton Road

Cranbury, NJ 08512

The power balances of gas cells having atomized hydrogen from pure hydrogen alone, an argon-hydrogen mixture alone, or pure hydrogen or an argon-hydrogen mixture with vaporized potassium, rubidium, cesium, strontium, sodium, or magnesium were measured by integrating the total light output corrected for spectrometer system response and energy over the visible range as the input power was varied. The light emitted for power supplied to the glow discharge increased by over two orders of magnitude depending on the presence of less than 1% partial pressure of certain of the alkali or alkaline earth metals in hydrogen gas or argon-hydrogen gas mixtures. Whereas, other chemically similar metals had no effect on the plasma. The metal vapor enhancement of the emission was dramatically greater with an argon-hydrogen mixture versus pure hydrogen, and a 97% argon and 3% hydrogen mixture had greater emission than either gas alone. Only those atoms or ions which ionize at integer multiples of the potential energy of atomic hydrogen, potassium, cesium, Rb^+ , strontium, and Ar^+ caused an anomalous increase in emission; whereas, no anomalous behavior was observed in the case of $Mg(m)$ and $Na(m)$ which do not provide a reaction with a net enthalpy of a multiple of the potential energy of atomic hydrogen. The light intensity versus power input of a mixture of these metals with hydrogen, argon, or argon-hydrogen gas was the same as that of the corresponding gas alone. At an input power to the glow discharge of 10 watts, the optically measured light output power of a mixture of strontium, cesium, potassium, or rubidium with 97% argon and 3% hydrogen was 750, 70, 16, and 13 $\mu W/cm^2$, respectively. Whereas, the optically measured light output power of the argon-hydrogen mixture (97/3%) alone or with sodium or magnesium was about 11 $\mu W/cm^2$, and the result for hydrogen or argon alone was 1.5 $\mu W/cm^2$. A temperature dependence of some of the anomalous plasmas was determined corresponding to the metal's partial pressure dependence on temperature. These studies provide useful parameters for the optimization of the catalytic reaction of atomic hydrogen.

I. INTRODUCTION

Based on the solution of a Schrödinger-type wave equation with a nonradiative boundary condition based on Maxwell's equations, Mills [1-31] predicts that atomic hydrogen may undergo a catalytic reaction with certain atomized elements or certain gaseous ions which singly or multiply ionize at integer multiples of the potential energy of atomic hydrogen, 27.2 eV. For example, cesium atoms ionize at an integer multiple of the potential energy of atomic hydrogen, $m \cdot 27.2$ eV. The enthalpy of ionization of Cs to Cs^{2+} has a net enthalpy of reaction of 27.05135 eV, which is equivalent to $m=1$ [32]. And, the reaction Ar^+ to Ar^{2+} has a net enthalpy of reaction of 27.63 eV, which is equivalent to $m=1$ [32]. In each case, the reaction involves a nonradiative energy transfer to form a hydrogen atom that is lower in energy than unreacted atomic hydrogen. The product hydrogen atom has an energy state that corresponds to a fractional principal quantum number. Recent analysis of mobility and spectroscopy data of individual electrons in liquid helium show direct experimental confirmation that electrons may have fractional principal quantum energy levels [33]. The lower-energy hydrogen atom is a highly reactive intermediate which further reacts to form a novel hydride ion. Emission was observed previously from a continuum state of Cs^{2+} and Ar^{2+} at 53.3 nm and 45.6 nm, respectively [2]. The single emission feature with the absence of the other corresponding Rydberg series of lines from these species confirmed the resonate nonradiative energy transfer of 27.2 eV from atomic hydrogen to atomic cesium or Ar^+ . The catalysis product, a lower-energy hydrogen atom, was predicted to be a highly reactive intermediate which further reacts to form a novel hydride ion. The predicted hydride ion of hydrogen catalysis by either cesium atom or Ar^+ catalyst is the hydride ion $H^-(1/2)$. This ion was observed spectroscopically at 407 nm corresponding to its predicted binding energy of 3.05 eV. The catalytic reaction with the formation the hydride ions are given in the Appendix.

Typically the emission of extreme ultraviolet light from hydrogen gas is achieved via a discharge at high voltage, a high power inductively coupled plasma, or a plasma created and heated to extreme temperatures by RF coupling (e.g. $> 10^6$ K) with confinement provided by a toroidal

magnetic field. Observation of intense extreme ultraviolet (EUV) emission at low temperatures (e.g. $\approx 10^3$ K) from atomic hydrogen and certain atomized elements or certain gaseous ions [2-16] has been reported previously. The only pure elements that were observed to emit EUV were those wherein the ionization of t electrons from an atom to a continuum energy level is such that the sum of the ionization energies of the t electrons is approximately $m \cdot 27.2$ eV where t and m are each an integer. Potassium, cesium, and strontium atoms and Rb^+ ion ionize at integer multiples of the potential energy of atomic hydrogen and caused emission. Whereas, the chemically similar atoms, sodium, magnesium and barium, do not ionize at integer multiples of the potential energy of atomic hydrogen and caused no emission.

Additional prior studies that support the possibility of a novel reaction of atomic hydrogen which produces an anomalous discharge and produces novel hydride compounds include extreme ultraviolet (EUV) spectroscopy [2-6, 9-16], plasma formation [2-16], power generation [3-4, 9, 31], and analysis of chemical compounds [17-31].

1.) Lines observed at the Institut Fur Niedertemperatur-Plasmaphysik e.V. by EUV spectroscopy could be assigned to transitions of atomic hydrogen to lower energy levels corresponding to lower energy hydrogen atoms and the emission from the excitation of the corresponding hydride ions [6]. For example, the product of the catalysis of atomic hydrogen with potassium metal, $H\left[\frac{a_H}{4}\right]$ may serve as both a catalyst and a reactant to form $H\left[\frac{a_H}{3}\right]$ and $H\left[\frac{a_H}{6}\right]$. The transition of $H\left[\frac{a_H}{4}\right]$ to $H\left[\frac{a_H}{6}\right]$ induced by a multipole resonance transfer of 54.4 eV ($2 \cdot 27.2$ eV) and a transfer of 40.8 eV with a resonance state of $H\left[\frac{a_H}{3}\right]$ excited in $H\left[\frac{a_H}{4}\right]$ is represented by

$$H\left[\frac{a_H}{4}\right] + H\left[\frac{a_H}{4}\right] \rightarrow H\left[\frac{a_H}{6}\right] + H\left[\frac{a_H}{3}\right] + 176.8 \text{ eV} \quad (1)$$

The predicted 176.8 eV (70.2 Å) photon is a close match with the observed 73.0 Å line. The energy of this line emission corresponds to an

equivalent temperature of 1,000,000 °C and an energy over 100 times the energy of combustion of hydrogen.

2.) Transitions of atomic hydrogen to lower energy levels corresponding to lower energy hydrogen atoms has been identified in the extreme ultraviolet emission spectrum from interstellar medium [34].

3.) An anomalous plasma with hydrogen-potassium mixtures has been reported in an experiment similar to the present plasma experiments [7-8, 10]. In experiments performed at the Institut Fur Niedertemperatur-Plasmaphysik e.V., an anomalous plasma formed with hydrogen-potassium mixtures wherein the plasma decayed with a two second half-life which was the thermal decay time of the filament which dissociated molecular hydrogen to atomic hydrogen when the electric field was set to zero [7, 10]. This experiment showed that hydrogen line emission was occurring even though the voltage between the heater wires was set to and measured to be zero and indicated that the emission was due to a reaction of potassium atoms with atomic hydrogen which confirms a new chemical source of power. Potassium atoms ionize at an integer multiple of the potential energy of atomic hydrogen, $m \cdot 27.2 \text{ eV}$. The enthalpy of ionization of K to K^{3+} has a net enthalpy of reaction of 81.7426 eV , which is equivalent to $m = 3$.

4.) An anomalous plasma of hydrogen and certain alkali ions formed at low temperatures (e.g. $\approx 10^3 \text{ K}$) as recorded via EUV spectroscopy and the hydrogen Balmer and alkali line emissions in the visible range. The observed plasma formed at low temperatures (e.g. $\approx 10^3 \text{ K}$) from atomic hydrogen generated at a tungsten filament that heated a titanium dissociator and a catalyst comprising one of potassium, rubidium, cesium, and their carbonates and nitrates. These atoms and ions ionize to provide a catalyst with a net enthalpy of reaction of an integer multiple of the potential energy of atomic hydrogen ($m \cdot 27.2 \text{ eV}$, $m = \text{integer}$) to within 0.17 eV and comprise only a single ionization in the case of a potassium or rubidium ion. Whereas, the chemically similar atoms of sodium and sodium and lithium carbonates and nitrates which do not ionize with these constraints caused no emission. To test the electric dependence of the emission, a weak electric field of about 1 V/cm was set and measured to be zero in $< 0.5 \times 10^{-6} \text{ sec}$. An anomalous afterglow duration of about one to two seconds was

recorded in the case of potassium, rubidium, cesium, K_2CO_3 , $RbNO_3$, and $CsNO_3$. Hydrogen line or alkali line emission was occurring even though the voltage between the heater wires was set to and measured to be zero. These atoms and ions ionize to provide a catalyst with a net enthalpy of reaction of an integer multiple of the potential energy of atomic hydrogen to within less than the thermal energies at $\approx 10^3 K$ and comprise only a single ionization in the case of a potassium or rubidium ion. Since the thermal decay time of the filament for dissociation of molecular hydrogen to atomic hydrogen was similar to the anomalous plasma afterglow duration, the emission was determined to be due to a reaction of atomic hydrogen with a catalyst that did not require the presence of an electric field to be functional.

5.) An energetic plasma in hydrogen was generated using strontium atoms as the catalyst. The plasma formed at 1% of the theoretical (Townsend theory) or prior known voltage requirement with 4,000-7,000 times less power input power compared to noncatalyst controls, sodium, magnesium, or barium atoms, wherein the plasma reaction was controlled with a weak electric field [4, 9]. The light output for power input increased to 8600 times that of the control when argon was added to the hydrogen strontium plasma [3].

In the present study, the alkali and alkaline earth metal catalysts and argon ion catalyst which were previously reported to produce anomalous discharges [2-16] were studied with controls to determine their relative performance. Anomalous and normal discharges were observed by visible emission. The anomalous power balances of gas cells were measured by integrating the total light output corrected for spectrometer system response and energy over the visible range as the input power was varied. The measurements were performed on hydrogen, argon, or argon-hydrogen mixtures alone and with vaporized alkali and alkaline earth metals in a stainless steel glow discharge cell. The cathode of the discharge cell was a central tungsten filament. The anode was a cylindrical nickel mesh. A radial electric field existed between the cathode and anode. Power was applied to the electrode to achieve a bright plasma which was recorded over the wavelength range $350 \leq \lambda \leq 750 nm$. In addition, the optimum argon to hydrogen ratio for producing the maximum anomalous emission with potassium was

determined. Some of the anomalous plasmas were further studied for temperature dependence corresponding to the catalyst metal's partial pressure dependence on temperature.

II. EXPERIMENTAL

A. Power cell apparatus and procedure

Plasma studies with 1.) hydrogen, argon, argon-hydrogen mixture (97/3%), and argon-hydrogen mixture (90/10%), 2.) sodium, magnesium, cesium, potassium, rubidium, and strontium with hydrogen, 3.) sodium, magnesium, cesium, potassium, rubidium, and strontium with argon, 4.) sodium, magnesium, cesium, potassium, rubidium, and strontium with argon-hydrogen mixture (97/3%), and 5.) potassium with argon-hydrogen mixture (90/10%) were carried out in the cylindrical stainless steel gas cell shown in Figure 1. All experiments were conducted at 650 °C except for studies on the temperature dependence of the light emission versus input power performed on cesium with argon-hydrogen mixture (97/3%), and rubidium with argon-hydrogen mixture (97/3%).

The experimental setup for generating a glow discharge hydrogen plasma and for optically measuring the power balance is shown in Figures 1 and 2. The 304-stainless steel cell was in the form of a tube having an internal cavity of 35.9 cm in length and 7.4 cm in diameter. The top end of the cell was welded to a high vacuum 11.75 cm diameter conflat flange. A silver plated copper gasket was placed between a mating flange and the cell flange. The two flanges were held together with 10 circumferential bolts. The mating flange contained five penetrations comprising 1&2.) two stainless steel thermocouple wells which placed thermocouples in the cell interior 2 cm from the discharge gap and 2 cm from the cell axis, 3.) a 1 cm diameter stainless steel light path tube located 2 cm off-axis that passed through the flange, extended 10 cm into the cell to a location 1 cm from a discharge volume between two electrodes, and had a saphire window view port at the interior tube end, 4.) a 1 cm stainless steel catalyst delivery tube welded flush with the flange top, and 5.) a stainless steel tube (1 cm diameter and 100 cm in length) welded flush with the bottom surface of the top flange that

served as a vacuum line from the cell and contained a center coaxial assembly that extended 35 cm into the cell. The assembly comprised a 0.15 cm ID stainless steel hydrogen or argon-hydrogen supply tube, anode power connection, and electrode assembly support surrounded by a high density Alumina tube electrical insulator (0.4 cm ID and 0.7 OD).

The glow discharge electrode assembly shown in Figure 1 comprised an axial inner tungsten spiral wire (1.9 mm OD by 200 cm long) anode (2.1 cm by 10 cm long) and a circumferential nickel mesh cathode (60 cm ID by 20 cm long, Belleville Wire Cloth Co., Inc.) supported by an Alumina frame comprising a top and bottom Alumina disc (6 cm OD Alpha Aesar 3318). The Alumina tube electrical insulator of the coaxial assembly stopped at the bottom Alumina disc. A second spirally grooved Alumina tube (2.1 cm OD by 10 cm long Alpha Aesar 33204) was concentric to the insulator and supported the tungsten anode which terminated at the top without a connection. The bottom of the tungsten wire anode passed through a hole in the Alumina tube electrical insulator and a hole in the bottom Alumina disc to connect with the anode power connection. The connection was made by compressing the tungsten wire between two collar clamps wherein the top clamp also served to connect the electrode assembly to the electrode assembly support. The cathode was connected to the top flange by a stainless steel wire.

Concentrated aqueous solutions ($\approx 0.6 M$) of sodium carbonate (Alfa Aesar ACS grade 99+ %), potassium carbonate (Alfa Aesar ACS grade 99+ %), rubidium carbonate (Alfa Aesar 99 %), cesium carbonate (Alfa Aesar 99 %), and magnesium carbonate (Alfa Aesar Puratronic grade 99.996 %) were sprayed onto the nickel mesh cathode and dried with a hot air gun. The application of the metal carbonate was carried out until the surface was completely covered with an inorganic film. The electrode assembly comprising the cathode and central anode was placed in the cell as shown in Figure 2. The cell was evacuated through the outer vacuum line with a high vacuum molecular drag pump (Hovac DRI-2) to reach 50 mtorr measured by a 100 torr pressure gauge (MKS Baratron). The vacuum pump valve was then closed. The cell was surrounded by a temperature controlled oven ($\pm 0.3^\circ\text{C}$ at 650°C) as shown in Figure 2 having high temperature insulation (AL 30 Zircar), a controller (Omega) type 76000),

and a regulated power supply. Type K thermocouples (Omega) housed in the two stainless steel wells read the cell temperature. The cell was heated and maintained at a temperature of 650 °C except for studies on the temperature dependence of the light emission versus input power. The cell was then pressurized with hydrogen (99.999% purity) to approximately 100 torr that was flowed through the inner supply tube. The pressure in the supply tube was measured by a 100 torr pressure gauge (MKS Baratron). The cell was then subsequently evacuated through the outer vacuum line to purge CO_2 and gaseous contaminants from the system. The decomposition of the metal carbonate to the corresponding metal was repeated until no further CO_2 was observed with a visible spectrometer (Ocean Optics S2000).

Strontium (Aldrich Chemical Company 99.9 %) metal was supplied to the cell using a transfer apparatus to avoid exposure of the metal to air. The transfer apparatus comprised a reservoir and a ball valve (Swagelok SS-45S8). The strontium was loaded into the reservoir in a glove box under a dry argon atmosphere through the valve passage. The valve was then closed. The transfer assembly was then attached to the catalyst delivery tube. The cell was evacuated through the outer vacuum line to reach 50 mtorr. The vacuum pump valve was then closed. The cell was heated and maintained at a temperature of 300 °C. The strontium was loaded into the cell through the ball valve. The cell was then pressurized with hydrogen (99.999% purity) to approximately 100 torr that was flowed through the inner supply tube. The cell was then subsequently evacuated through the outer vacuum line to purge gaseous contaminants from the system. The cell was heated and maintained at a temperature of 650 °C.

After the metal was formed or loaded into the cell, the cell was operated under gas flow conditions while maintaining a constant gas pressure in the cell with a mass flow controller where the pressure in the hydrogen and argon supply tube outside the furnace was monitored by the 100 torr MKS Baratron absolute pressure gauge. Except where indicated, the gas was ultrahigh purity hydrogen, argon-hydrogen mixture (97/3%), or an argon-hydrogen mixture (90/10%). The gas pressure inside the cell was maintained at about 300 mtorr with a hydrogen flow rate of 5.5 sccm, an argon-hydrogen mixture (97/3%) flow

rate of 5.5 sccm, or an argon flow rate of 5.0 sccm and a hydrogen flow rate of 0.6 sccm, respectively. Each gas flow was controlled by a 20 sccm range mass flow controller (MKS 1179A21CS1BB) with a readout (MKS type 247C). The partial pressure of the metal was determined by its equilibrium vapor pressure at the operating temperature of the cell as given in Table 1.

The field voltage was increased until breakdown occurred. This was confirmed by the spectrometer response to visible light emitted from the cell. The discharge was started and maintained by a DC electric field in the 1.9 cm annular gap between an axial anode and a cylindrical circumferential cathode. The glow discharge power was 0.300 A constant current provided by a custom built (BlackLight Power, Inc.) constant current controller with a response time of $<0.5 \times 10^{-6}$ sec. The quick response time assured the maintenance of a stable plasma as determined by using an oscilloscope to monitor the DC voltage and current. With the current fixed, the power was given by the constant current times the driving voltage. The power was increased by ramping the voltage at constant current and the optical power output was recorded.

B. Optical measurements

A glow discharge was produced in a stainless steel gas cell shown in Figure 2 comprising the axial inner tungsten wire anode and the circumferential nickel mesh cathode shown in Figure 1. An essentially uniform radial electric field existed between the anode and cathode. A 1.6 mm thick UV-grade sapphire window with a 1 cm view diameter provided a visible light path from inside the cell. The viewing direction was parallel to the cell axis. The 1 cm diameter stainless steel light path tube passed through the furnace wall to provide an optical light path from the sapphire window to the furnace exterior. An 0.63 cm diameter quartz rod channeled the light from the window through the light path tube to a collimating lens which was focused on a 100 μm optical fiber located outside the furnace. Spectral data was recorded with a visible spectrometer (Ocean Optics S2000) and stored by a personal computer. To correct for the nonuniform response of the spectrometer system as a function of wavelength and the dependence of energy on wavelength, the

system was calibrated against a reference light source (Ocean Optics LS-1-CAL). A spectral calibration factor was applied to the count rate data at each wavelength to yield the irradiation of the detector in units of energy/time/area/wavelength. The total visible radiant flux incident on the detector was calculated by integrating the spectral irradiation between 400 and 700 nm.

III. RESULTS

A. Comparison of catalysts by optically measured power balance

The optically measured light output power was determined by integrating the total light output corrected for spectrometer system response and energy over the visible range, $350 \leq \lambda \leq 750 \text{ nm}$ as the input power was varied. Comparison of hydrogen, argon, and various mixtures of hydrogen and argon with catalysts and noncatalyst controls are given in Figures 3-7 which plot the output light intensity versus power input to the glow discharge. Since the current remained constant at 0.300 A, the voltage can be determined from the power in these figures by multiplying by 3. In Figures 3-5, the results of the test gas alone, sodium or magnesium with hydrogen, and potassium, rubidium, cesium, strontium, sodium, or magnesium with argon are plotted together for convenience since no difference was observed with the metal present. In the case that a plasma could not be achieved at low power, the curve at higher input power was fitted (dotted line) and extended to the lower input power region.

The comparison of the light output power ($\mu\text{W}/\text{cm}^2$) of 1.) hydrogen, argon, argon-hydrogen mixture (97/3%), and argon-hydrogen mixture (90/10%), 2.) sodium, magnesium, and potassium with hydrogen, 3.) sodium, magnesium, cesium, potassium, rubidium, and strontium with argon, 4.) sodium, magnesium, cesium, potassium, rubidium, and strontium with argon-hydrogen mixture (97/3%), and 5.) potassium with argon-hydrogen mixture (90/10%) is shown in Figures 3-5. The $0-50 \mu\text{W}/\text{cm}^2$ range is shown in Figure 3. At an input power to the glow discharge of 10 watts, the optically measured light output power of both

of a mixture of cesium and argon-hydrogen (97/3%) and a mixture of strontium and argon-hydrogen (97/3%) were off-scale, and the optically measured light output power of a mixture of potassium and argon-hydrogen (90/10%), potassium and argon-hydrogen (97/3%), rubidium and argon-hydrogen (97/3%), argon-hydrogen (97/3%), argon-hydrogen (90/10%), and potassium and hydrogen was 27, 16, 13, 11, 10, and $5 \mu\text{W}/\text{cm}^2$, respectively. Whereas, the optically measured light output power of hydrogen or argon alone was $1.5 \mu\text{W}/\text{cm}^2$. Thus, at 10 watts, the optically measured light output power trend for these on-scale mixtures was $\text{K} + \text{Ar} + \text{H}_2$ (90/10%) > $\text{K} + \text{Ar} + \text{H}_2$ (97/3%) > $\text{Rb} + \text{Ar} + \text{H}_2$ (97/3%) > $\text{Ar} + \text{H}_2$ (97/3%) > $\text{Ar} + \text{H}_2$ (90/10%) > $\text{K} + \text{H}_2$ > H_2 alone = $\text{Na} + \text{H}_2$, $\text{Mg} + \text{H}_2$, Ar alone, $\text{Na} + \text{Ar}$, $\text{Mg} + \text{Ar}$, $\text{K} + \text{Ar}$, $\text{Rb} + \text{Ar}$, $\text{Cs} + \text{Ar}$, $\text{Sr} + \text{Ar}$. Magnesium and sodium had no effect on the hydrogen plasma, and no metal had an effect on the argon plasma. For potassium which significantly increased the light output of an argon-hydrogen mixture, the ratio of argon to hydrogen was varied, and the ratio which maximized the optical output power in the visible was determined to be about 90 % argon and 10% hydrogen. Strontium and hydrogen produced a bright plasma which was comparable to the plasma formed with cesium and argon-hydrogen (97%/3%), but was not as stable. Cesium and hydrogen also formed a bright plasma with hydrogen that was less intense and stable than in the case of the plasma formed with argon present. Rubidium and hydrogen showed slightly weaker anomalous emission than potassium and hydrogen.

The comparison of the optically measured light output powers in the range the $0 - 200 \mu\text{W}/\text{cm}^2$ and $0 - 800 \mu\text{W}/\text{cm}^2$ are shown in Figures 4 and 5, respectively. In Figure 4, at an input power to the glow discharge of 10 watts, the optically measured light output power of a mixture of strontium and argon-hydrogen (97/3%) was off-scale. From Figure 5, the optically measured light output power of a mixture of strontium or cesium with 97 % argon and 3 % hydrogen was 750 and $70 \mu\text{W}/\text{cm}^2$, respectively. Thus, from the combined results shown in Figures 3-5, the optically measured light output power trend at 10 watts was $\text{Sr} + \text{Ar} + \text{H}_2$ (97/3%) >> $\text{Cs} + \text{Ar} + \text{H}_2$ (97/3%) > $\text{K} + \text{Ar} + \text{H}_2$ (90/10%) > $\text{K} + \text{Ar} + \text{H}_2$ (97/3%) > $\text{Rb} + \text{Ar} + \text{H}_2$ (97/3%) > $\text{Ar} + \text{H}_2$ (97/3%) > $\text{Ar} + \text{H}_2$ (90/10%) > $\text{K} + \text{H}_2$ > H_2 alone = $\text{Na} + \text{H}_2$, $\text{Mg} + \text{H}_2$, Ar alone, $\text{Na} + \text{Ar}$, $\text{Mg} + \text{Ar}$, $\text{K} + \text{Ar}$, $\text{Rb} + \text{Ar}$.

Ar, Cs + Ar, Sr + Ar. With the addition of strontium to argon-hydrogen (97/3%), the light output was about 75 times higher compared to argon-hydrogen alone and about 500 times higher compared to hydrogen or argon alone.

B. Temperature dependence of catalysts by optically measured power balance

The temperature dependence of the light emission of cesium-argon-hydrogen mixture (97/3%) as a function of input power was studied and compared with the emission of potassium and rubidium with argon-hydrogen mixture (97/3%) at a cell temperature of 650 °C. The comparison of the light output power ($\mu W/cm^2$) of 1.) potassium and argon-hydrogen mixture (97/3%) at a cell temperature of 650 °C, 2.) rubidium and argon-hydrogen mixture (97/3%) at a cell temperature of 650 °C, and 3.) cesium and argon-hydrogen mixture (97/3%) at a cell temperature of 480 °C, 500 °C, 520 °C, 540 °C, 565 °C, and 600 °C is shown in Figure 6. The input power to the glow discharge to achieve an optically measured light output power of $30 mW/cm^2$ from a mixture of cesium and argon-hydrogen (97/3%) at 480 °C, 500 °C, 520 °C, 540 °C, 565 °C, and 600 °C was 2, 3, 4, 5, 7, and 18 W, respectively. In comparison, the input power to the glow discharge to achieve an optically measured light output power of $30 mW/cm^2$ from a mixture of potassium or rubidium with argon-hydrogen mixture (97/3%) at 650 °C was 15 and about 33 W, respectively. The optically measured trend of the temperature dependence of the cesium light output power was in order of decreasing temperature. The light output for cesium at the lowest temperature of 480 °C was the greatest at the lowest input powers, but the output was asymptotic at about 4 W input. The cause may be due to a shortage of cesium metal catalyst from the decomposition reaction of the source, Cs_2CO_3 . The light output for cesium at the highest temperature of 600 °C was distinguishably lower than the emission for any other temperature. The cause may be due to an excessive cesium vapor pressure which decreased the catalysis rate and excessively increased the conductivity of the plasma.

The data indicates that the catalysis reaction is sensitive to the

cesium vapor pressure with a decrease in rate due to excess cesium vapor pressure. The vapor pressure of cesium as a function of temperature is given in Table 1.

The comparison of the light output power ($\mu\text{W}/\text{cm}^2$) of 1.) cesium and argon-hydrogen mixture (97/3%) at a cell temperature of 565 °C, and 2.) rubidium and argon-hydrogen mixture (97/3%) at a cell temperature of 470 °C, 500 °C, 535 °C, 560 °C, 600 °C, 620 °C, and 650 °C is shown in Figure 7. The light output for rubidium at the lowest temperature of 470 °C was distinguishably lower than the emission for any other temperature. The cause may be due to a shortage of metal from the decomposition reaction of the source, Rb_2CO_3 . The outputs for the cases at the higher temperatures, 560 °C, 600 °C, 620 °C, and 650 °C are very similar in magnitude and behavior showing essentially linear output with input.

The cesium and argon-hydrogen mixture (97/3%) at 565 °C produced the highest output for input at about 7 watt at which point the emission becomes essentially linear with input power. An asymptotic behavior was observed to a lesser extent for rubidium for the intermediate the temperatures, 500 °C and 535 °C. Rubidium at a cell temperature of 500 °C produced the highest output for an input power less than 10 watts. But, the highest difference of about 70 % more emission relative to other cell temperatures was observed from the 535 °C cell which showed a peak emission at 12 W input.

The data indicates that the catalysis reaction is sensitive to the rubidium vapor pressure with a decrease in rate due deviation from an optimum. The vapor pressure of rubidium as a function of temperature is given in Table 1. At 10 watts input, cesium produced about 6 times the output of rubidium at any temperature. This indicates that the reaction is much more dependent on the activity of the particular catalyst then on temperature within a reasonably broad temperature range.

IV. DISCUSSION

The optical power balances of gas cells having atomized hydrogen from an argon-hydrogen mixture alone or pure hydrogen or an argon-hydrogen mixture with vaporized potassium, rubidium as a source of Rb^+

in the glow discharge, cesium, or strontium were measured by integrating the total light output corrected for spectrometer system response and energy over the visible range as the input power was varied. Control experiments were identical except that the pure gas was run alone, or sodium or magnesium replaced the metal catalyst in the case of a metal mixture with hydrogen gas or an argon-hydrogen mixture. The light emitted for power supplied to the glow discharge increased by over two orders of magnitude depending on the presence of less than 1% partial pressure of certain of the alkali or alkaline earth metals in hydrogen gas or argon-hydrogen gas mixtures. Whereas, other chemically similar metals had no effect on the plasma. The metal vapor enhancement of the emission was dramatically greater with an argon-hydrogen mixture versus pure hydrogen, and a 97 % argon and 3 % hydrogen mixture had greater emission than either gas alone. Only those atoms or ions which ionize at integer multiples of the potential energy of atomic hydrogen, potassium, cesium, Rb^+ , strontium, and Ar^+ caused an anomalous increase in emission; whereas, no anomalous behavior was observed in the case of $Mg(m)$ and $Na(m)$ which do not provide a reaction with a net enthalpy of a multiple of the potential energy of atomic hydrogen. The light intensity versus power input with these metals were the same as that of the hydrogen gas or argon-hydrogen gas mixture alone.

At an input power to the glow discharge of 10 watts, the optically measured light output power of a mixture of strontium, cesium, potassium, or rubidium with 97 % argon and 3 % hydrogen was 750, 70, 16, and $13 \mu\text{W}/\text{cm}^2$, respectively. The emission from potassium with argon-hydrogen mixtures was maximized at a ratio of 90% argon and 10% hydrogen that output $27 \mu\text{W}/\text{cm}^2$ of light with 10 W input. The optically measured light output power of the argon-hydrogen mixture (97/3%) and (90/10%) was $11 \mu\text{W}/\text{cm}^2$ and $10 \mu\text{W}/\text{cm}^2$, respectively. Whereas, the optically measured light output power of a mixture of potassium with hydrogen was $5 \mu\text{W}/\text{cm}^2$, and the result for hydrogen or argon alone was $1.5 \mu\text{W}/\text{cm}^2$. Thus, at 10 watts, the optically measured light output power trend was $Sr + Ar + H_2$ (97/3%) $>> Cs + Ar + H_2$ (97/3%) $> K + Ar + H_2$ (90/10%) $> K + Ar + H_2$ (97/3%) $> Rb + Ar + H_2$ (97/3%) $> Ar + H_2$ (97/3%) $> Ar + H_2$ (90/10%) $> K + H_2 > H_2$ alone = $Na + H_2$, $Mg + H_2$, Ar alone, $Na + Ar$, $Mg + Ar$, $K + Ar$, $Rb + Ar$, $Cs + Ar$, $Sr + Ar$. Magnesium and sodium had no

effect on the hydrogen or argon-hydrogen plasma; whereas, addition of potassium to hydrogen or an argon-hydrogen mixture increased the optical output power. At 10 watts input, the addition of argon to the potassium-hydrogen mixture to provide Ar^+ catalyst increased the output by a factor of 3 and 6 for an argon-hydrogen mixture of 97/3% and 90/10%, respectively. The data indicate that the combination of potassium and argon catalyst is not simply additive. This implies that potassium catalyst may increase the amount of Ar^+ catalyst to enhance the catalysis of hydrogen. With the addition of strontium to argon-hydrogen (97/3%), the light output was about 75 times higher compared to argon-hydrogen alone and about 500 times higher compared to hydrogen or argon alone. Thus, strontium catalyst may increase the amount of Ar^+ catalyst to a greater extent than potassium to enhance the catalysis of hydrogen.

Compared to the output of $200 \mu W/cm^2$ with 10 watts input to the strontium-argon-hydrogen mixture, the power to achieve the same optically measured light output power from the hydrogen controls was estimated to be at a factor of 1000 times greater based on the slope of the light output versus power input plots. The projected kilowatts of input power was not achievable with the experimental apparatus. The results indicate that an extraordinary anomalous plasma formed with a strontium-argon-hydrogen mixture.

A temperature dependence of some of the anomalous plasmas was determined corresponding to the metal's partial pressure dependence on temperature. The optically measured trend of the temperature dependence of the cesium light output power was in order of decreasing temperature. The optimum operating temperature for cesium-argon-hydrogen over the range $480^\circ C - 600^\circ C$ was determined to be $480^\circ C$. The light output for cesium at the highest temperature of $600^\circ C$ was distinguishably lower than the emission for any other temperature. The optimum operating temperature for rubidium-argon-hydrogen over the range $470^\circ C - 650^\circ C$ was determined to be $535^\circ C$. The data indicates that the catalysis reaction is sensitive to the cesium or rubidium vapor pressure with a decrease in rate due deviation from an optimum. At 10 watts input, cesium at $565^\circ C$ produced about 6 times the light output power of rubidium at any temperature. This indicates that the reaction is

much more dependent on the activity of the particular catalyst than on temperature within a reasonably broad temperature range.

In the cases where an anomalous optically measured power balance was observed, no possible chemical reactions of the tungsten filament cathode, the nickel mesh anode, the vaporized metal, and hydrogen or argon-hydrogen mixture gas at a cell temperature of about 650 °C could be found which accounted for the increased emission. In fact, no known chemical reaction releases enough energy to cause an anomalous plasma of hydrogen. Intense anomalous emission was observed for catalysts in the presence of hydrogen and no unusual behavior was observed for noncatalysts. This result indicates that the emission was due to a reaction of the catalyst with hydrogen. The catalyst enhancement of the emission was dramatically greater with an argon-hydrogen mixture versus pure hydrogen. This implies that the catalyst may increase the amount of Ar^+ catalyst to enhance the catalysis of hydrogen.

The most intense plasma was formed by a mixture of strontium and argon with hydrogen. The presence of a weak electric field may be necessary in order for strontium and Ar^+ to produce an anomalous discharge of hydrogen. In the case that electrons are ionized to a continuum energy level, the presence of a low strength electric field alters the continuum energy levels. The ionization energy of 188.2 eV is 1% less than $m \cdot 27.2$ eV where $m = 7$, and the ionization energy of Ar^+ to Ar^{2+} is 27.6 eV. In the anomalous discharge of hydrogen due to the presence of strontium and Ar^+ , the weak field may adjust the energy of ionizing strontium and Ar^+ to match the energy of 7 · 27.2 eV and 27.2 eV, respectively, to permit a novel reaction of atomic hydrogen.

The release of energy from hydrogen as evidenced by the anomalous emission must result in a lower-energy state of hydrogen. The theory is given in the Appendix. The lower-energy hydrogen atom called a hydrino atom by Mills [1] would be expected to demonstrate novel chemistry. Reports of the formation of novel compounds provide substantial evidence supporting a novel reaction of hydrogen as the mechanism of the observed anomalous discharge. Novel hydrogen compounds have been isolated as products of the reaction of atomic hydrogen with atoms and ions which formed an anomalous plasma in the present studies and previously reported in EUV studies [2-16]. Novel

inorganic alkali and alkaline earth hydrides of the formula MH^* and MH^*X wherein M is the metal, X , is a singly negatively charged anion, and H^* comprises a novel high binding energy hydride ion were synthesized in a high temperature gas cell by reaction of atomic hydrogen with a catalyst such as potassium metal and MH , MX or MX_2 corresponding to an alkali metal or alkaline earth metal compound, respectively [17, 20-21]. Novel hydride compounds were identified by 1.) time of flight secondary ion mass spectroscopy which showed a dominant hydride ion in the negative ion spectrum, 2.) X-ray photoelectron spectroscopy which showed novel hydride peaks and significant shifts of the core levels of the primary elements bound to the novel hydride ions, 3.) 1H nuclear magnetic resonance spectroscopy (NMR) which showed extraordinary upfield chemical shifts compared to the NMR of the corresponding ordinary hydrides, and 4.) thermal decomposition with analysis by gas chromatography, and mass spectroscopy which identified the compounds as hydrides [17, 20].

The implications are that a new field of novel hydrogen chemistry has been discovered which may be a new power source that creates an energetic plasma. The plasma may be converted directly to electricity with high efficiency using a known microwave device called a gyrotron, thus, avoiding a heat engine such as a turbine. Plasma to electric conversion technology with no reformer, no fuel cost, creation of a valuable chemical by-product rather than pollutants such as carbon dioxide, and significantly lower capital costs and operating and maintenance (O&M) costs are anticipated to result in microdistributed units that are competitive with central power and significantly superior to competing microdistributed power technologies such as fuel cells [36].

APPENDIX

Mills [1] predicts that certain atoms or ions serve as catalysts to release energy from hydrogen to produce an increased binding energy hydrogen atom called a *hydrino atom* having a binding energy of

$$\text{Binding Energy} = \frac{13.6 \text{ eV}}{n^2} \quad (2)$$

where

$$n = \frac{1}{2}, \frac{1}{3}, \frac{1}{4}, \dots, \frac{1}{p} \quad (3)$$

and p is an integer greater than 1, designated as $H\left[\frac{a_H}{p}\right]$ where a_H is the radius of the hydrogen atom. Hydrinos are predicted to form by reacting an ordinary hydrogen atom with a catalyst having a net enthalpy of reaction of about

$$m \cdot 27.2 \text{ eV} \quad (4)$$

where m is an integer. This catalysis releases energy from the hydrogen atom with a commensurate decrease in size of the hydrogen atom, $r_n = n a_H$. For example, the catalysis of $H(n=1)$ to $H(n=1/2)$ releases 40.8 eV, and the hydrogen radius decreases from a_H to $\frac{1}{2}a_H$.

The excited energy states of atomic hydrogen are also given by Eq. (2) except that

$$n = 1, 2, 3, \dots \quad (5)$$

The $n=1$ state is the "ground" state for "pure" photon transitions (the $n=1$ state can absorb a photon and go to an excited electronic state, but it cannot release a photon and go to a lower-energy electronic state).

However, an electron transition from the ground state to a lower-energy state is possible by a nonradiative energy transfer such as multipole coupling or a resonant collision mechanism. These lower-energy states have fractional quantum numbers, $n = \frac{1}{\text{integer}}$. Processes that occur

without photons and that require collisions are common. For example, the exothermic chemical reaction of $H + H$ to form H_2 does not occur with the emission of a photon. Rather, the reaction requires a collision with a third body, M , to remove the bond energy $H + H + M \rightarrow H_2 + M^*$ [37]. The third body distributes the energy from the exothermic reaction, and the end result is the H_2 molecule and an increase in the temperature of the system. Some commercial phosphors are based on nonradiative energy transfer involving multipole coupling. For example, the strong absorption strength of Sb^{3+} ions along with the efficient nonradiative transfer of excitation from Sb^{3+} to Mn^{2+} , are responsible for the strong manganese luminescence from phosphors containing these ions [38]. Similarly, the $n=1$ state of hydrogen and the $n = \frac{1}{\text{integer}}$ states of hydrogen are

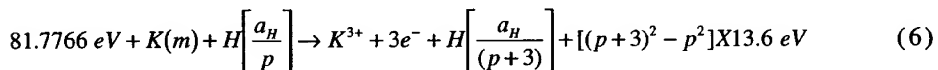
nonradiative, but a transition between two nonradiative states is possible via a nonradiative energy transfer, say $n=1$ to $n=1/2$. In these cases, during the transition the electron couples to another electron transition, electron transfer reaction, or inelastic scattering reaction which can absorb the exact amount of energy that must be removed from the hydrogen atom. Thus, a catalyst provides a net positive enthalpy of reaction of $m \cdot 27.2 \text{ eV}$ (i.e. it absorbs $m \cdot 27.2 \text{ eV}$ where m is an integer). Certain atoms or ions serve as catalysts which resonantly accept energy from hydrogen atoms and release the energy to the surroundings to effect electronic transitions to fractional quantum energy levels.

Catalysts

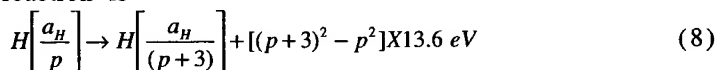
The emission must have been due to a novel chemical reaction between catalyst and atomic hydrogen. According to Mills [1], a catalytic system is provided by the ionization of t electrons from an atom or ion to a continuum energy level such that the sum of the ionization energies of the t electrons is approximately $m \cdot X 27.2 \text{ eV}$ where m is an integer.

Potassium Metal

One such atomic catalytic system involves potassium metal. The first, second, and third ionization energies of potassium are 4.34066 eV , 31.63 eV , 45.806 eV , respectively [32]. The triple ionization ($t=3$) reaction of K to K^{3+} , then, has a net enthalpy of reaction of 81.7766 eV , which is equivalent to $m=3$ in Eq. (4).



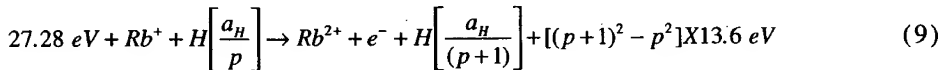
And, the overall reaction is



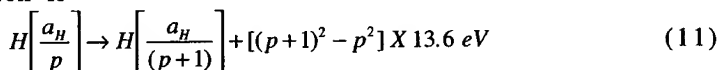
Rubidium Ion

Rubidium ions formed in the glow discharge can also provide a net enthalpy of a multiple of that of the potential energy of the hydrogen

atom. The second ionization energy of rubidium is 27.28 eV . The reaction Rb^+ to Rb^{2+} has a net enthalpy of reaction of 27.28 eV , which is equivalent to $m=1$ in Eq. (4).

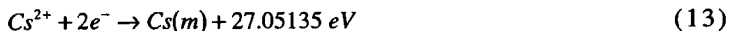
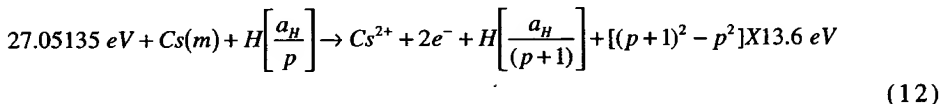


The overall reaction is

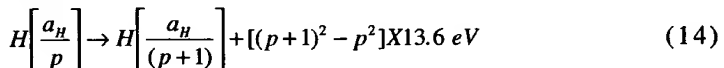


Cesium Metal

A catalytic system is provided by the ionization of 2 electrons from a cesium atom each to a continuum energy level such that the sum of the ionization energies of the 2 electrons is approximately 27.2 eV . The first and second ionization energies of cesium are 3.89390 eV and 23.15745 eV , respectively [32]. The double ionization reaction of Cs to Cs^{2+} , then, has a net enthalpy of reaction of 27.05135 eV , which is equivalent to $m=1$ in Eq. (4).

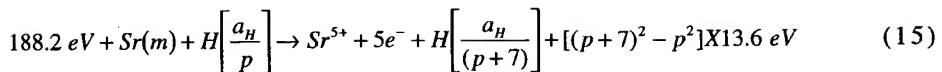


And, the overall reaction is

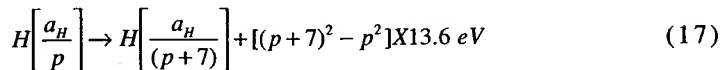


Strontium Metal

Another catalytic system involves strontium. The first through the fifth ionization energies of strontium are 5.69484 eV , 11.03013 eV , 42.89 eV , 57 eV , and 71.6 eV , respectively [32]. The ionization reaction of Sr to Sr^{5+} , ($t=5$), then, has a net enthalpy of reaction of 188.2 eV , which is equivalent to $m=7$ in Eq. (4).

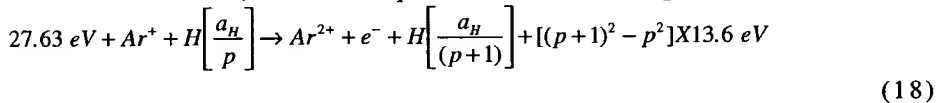


And, the overall reaction is

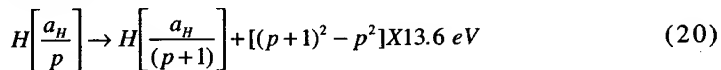


Argon Ion

Argon ions can also provide a net enthalpy of a multiple of that of the potential energy of the hydrogen atom. The second ionization energy of argon is 27.63 eV. The reaction Ar^+ to Ar^{2+} has a net enthalpy of reaction of 27.63 eV, which is equivalent to $m=1$ in Eq. (4).



And, the overall reaction is



Hydride Ion

A novel hydride ion having extraordinary chemical properties given by Mills [1] is predicted to form by the reaction of an electron with a hydrino (Eq. (21)). The resulting hydride ion is referred to as a hydrino hydride ion, designated as $H^-(1/p)$.



The hydrino hydride ion is distinguished from an ordinary hydride ion having a binding energy of 0.8 eV. The hydrino hydride ion is predicted [1] to comprise a hydrogen nucleus and two indistinguishable electrons at a binding energy according to the following formula:

$$Binding\ Energy = \frac{\hbar^2 \sqrt{s(s+1)}}{8\mu_e a_0^2 \left[\frac{1 + \sqrt{s(s+1)}}{p} \right]^2} - \frac{\pi \mu_0 e^2 \hbar^2}{m_e^2 a_0^3} \left(1 + \frac{2^2}{\left[\frac{1 + \sqrt{s(s+1)}}{p} \right]^3} \right) \quad (22)$$

where p is an integer greater than one, $s=1/2$, π is pi, \hbar is Planck's constant bar, μ_0 is the permeability of vacuum, m_e is the mass of the electron, μ_e is the reduced electron mass, a_0 is the Bohr radius, and e is the elementary charge. The ionic radius is

$$r_1 = \frac{a_0}{p} \left(1 + \sqrt{s(s+1)} \right); s = \frac{1}{2} \quad (23)$$

From Eq. (23), the radius of the hydrino hydride ion $H^-(1/p)$; $p = \text{integer}$ is $\frac{1}{p}$ that of ordinary hydride ion, $H^-(1/1)$. Compounds containing hydrino hydride ions have been isolated as products of the reaction of atomic hydrogen with atoms and ions identified as catalysts by EUV emission [2-31].

ACKNOWLEDGMENT

Special thanks to Mark Nanstell for developing some of the glow discharge and visible spectroscopy methods and to Bala Dhandapani for logistics and for reviewing this manuscript.

REFERENCES

1. R. Mills, The Grand Unified Theory of Classical Quantum Mechanics, January 2000 Edition, BlackLight Power, Inc., Cranbury, New Jersey, Distributed by Amazon.com.
2. R. Mills, "Spectroscopic Identification of a Novel Catalytic Reaction of Atomic Hydrogen and the Hydride Ion Product", Int. J. Hydrogen Energy, submitted.
3. R. Mills and M. Nansteel, "Anomalous Argon-Hydrogen-Strontium

- Discharge", IEEE Transactions of Plasma Science, submitted.
4. R. Mills, M. Nansteel, and Y. Lu, "Anomalous Hydrogen-Strontium Discharge", European Journal of Physics D, submitted.
 5. R. Mills, J. Dong, Y. Lu, "Observation of Extreme Ultraviolet Hydrogen Emission from Incandescently Heated Hydrogen Gas with Certain Catalysts", Int. J. Hydrogen Energy, Vol. 25, (2000), pp. 919-943.
 6. R. Mills, "Observation of Extreme Ultraviolet Emission from Hydrogen-KI Plasmas Produced by a Hollow Cathode Discharge", Int. J. Hydrogen Energy, in press.
 7. R. Mills, "Temporal Behavior of Light-Emission in the Visible Spectral Range from a Ti-K₂CO₃-H-Cell", Int. J. Hydrogen Energy, in press.
 8. R. Mills, Y. Lu, and T. Onuma, "Formation of a Hydrogen Plasma from an Incandescently Heated Hydrogen-Catalyst Gas Mixture with an Anomalous Afterglow Duration", Int. J. Hydrogen Energy, in press.
 9. R. Mills, M. Nansteel, and Y. Lu, "Observation of Extreme Ultraviolet Hydrogen Emission from Incandescently Heated Hydrogen Gas with Strontium that Produced an Anomalous Optically Measured Power Balance", Int. J. Hydrogen Energy, in press.
 10. R. Mills, J. Dong, Y. Lu, J. Conrads, "Observation of Extreme Ultraviolet Hydrogen Emission from Incandescently Heated Hydrogen Gas with Certain Catalysts", 1999 Pacific Conference on Chemistry and Spectroscopy and the 35th ACS Western Regional Meeting, Ontario Convention Center, California, (October 6-8, 1999).
 11. R. Mills, J. Dong, N. Greenig, and Y. Lu, "Observation of Extreme Ultraviolet Hydrogen Emission from Incandescently Heated Hydrogen Gas with Certain Catalysts", National Hydrogen Association, 11 th Annual U.S. Hydrogen Meeting, Vienna, VA, (February 29-March 2, 2000).
 12. R. Mills, B. Dhandapani, N. Greenig, J. He, J. Dong, Y. Lu, and H. Conrads, "Formation of an Energetic Plasma and Novel Hydrides from Incandescently Heated Hydrogen Gas with Certain Catalysts", National Hydrogen Association, 11 th Annual U.S. Hydrogen Meeting, Vienna, VA, (February 29-March 2, 2000).
 13. Mills, J. Dong, N. Greenig, and Y. Lu, "Observation of Extreme Ultraviolet Hydrogen Emission from Incandescently Heated Hydrogen Gas with Certain Catalysts", 219 th National ACS Meeting, San

Francisco, California, (March 26-30, 2000).

14. R. Mills, B. Dhandapani, N. Greenig, J. He, J. Dong, Y. Lu, and H. Conrads, "Formation of an Energetic Plasma and Novel Hydrides from Incandescently Heated Hydrogen Gas with Certain Catalysts", 219 th National ACS Meeting, San Francisco, California, (March 26-30, 2000).
15. R. Mills, B. Dhandapani, N. Greenig, J. He, J. Dong, Y. Lu, and H. Conrads, "Formation of an Energetic Plasma and Novel Hydrides from Incandescently Heated Hydrogen Gas with Certain Catalysts", June ACS Meeting (29th Northeast Regional Meeting, University of Connecticut, Storrs, CT, (June 18-21, 2000)).
16. R. Mills, B. Dhandapani, N. Greenig, J. He, J. Dong, Y. Lu, and H. Conrads, "Formation of an Energetic Plasma and Novel Hydrides from Incandescently Heated Hydrogen Gas with Certain Catalysts", August National ACS Meeting (220th ACS National Meeting, Washington, DC, (August 20-24, 2000)).
17. R. Mills, B. Dhandapani, N. Greenig, J. He, "Synthesis and Characterization of Potassium Iodo Hydride", Int. J. of Hydrogen Energy, Vol. 25, Issue 12, December, (2000), pp. 1185-1203.
18. R. Mills, "Novel Inorganic Hydride", Int. J. of Hydrogen Energy, Vol. 25, (2000), pp. 669-683.
19. R. Mills, "Novel Hydrogen Compounds from a Potassium Carbonate Electrolytic Cell", Fusion Technology, Vol. 37, No. 2, March, (2000), pp. 157-182.
20. R. Mills, B. Dhandapani, M. Nansteel, J. He, T. Shannon, A. Echezuria, "Synthesis and Characterization of Novel Hydride Compounds", Int. J. of Hydrogen Energy, in press.
21. R. Mills, B. Dhandapani, M. Nansteel, J. He, A. Voigt, Identification of Compounds Containing Novel Hydride Ions by Nuclear Magnetic Resonance Spectroscopy, Int. J. Hydrogen Energy, submitted.
22. R. Mills, "Highly Stable Novel Inorganic Hydrides", Journal of Materials Research, submitted.
23. R. Mills, "Novel Hydride Compound", 1999 Pacific Conference on Chemistry and Spectroscopy and the 35th ACS Western Regional Meeting, Ontario Convention Center, California, (October 6-8, 1999).
24. R. Mills, B. Dhandapani, N. Greenig, J. He, "Synthesis and Characterization of Potassium Iodo Hydride", 1999 Pacific Conference

- on Chemistry and Spectroscopy and the 35th ACS Western Regional Meeting, Ontario Convention Center, California, (October 6-8, 1999).
- 25. R. Mills, J. He, and B. Dhandapani, "Novel Hydrogen Compounds", 1999 Pacific Conference on Chemistry and Spectroscopy and the 35th ACS Western Regional Meeting, Ontario Convention Center, California, (October 6-8, 1999).
 - 26. R. Mills, "Novel Hydride Compound", National Hydrogen Association, 11 th Annual U.S. Hydrogen Meeting, Vienna, VA, (February 29-March 2, 2000).
 - 27. R. Mills, J. He, and B. Dhandapani, "Novel Alkali and Alkaline Earth Hydrides", National Hydrogen Association, 11 th Annual U.S. Hydrogen Meeting, Vienna, VA, (February 29-March 2, 2000).
 - 28. R. Mills, "Novel Hydride Compound", 219 th National ACS Meeting, San Francisco, California, (March 26-30, 2000).
 - 29. R. Mills, J. He, and B. Dhandapani, "Novel Alkali and Alkaline Earth Hydrides", 219 th National ACS Meeting, San Francisco, California, (March 26-30, 2000).
 - 30. R. Mills, J. He, and B. Dhandapani, "Novel Alkali and Alkaline Earth Hydrides", August National ACS Meeting (220 th ACS National Meeting, Washington, DC, (August 20-24, 2000)).
 - 31. R. Mills, W. Good, A. Voigt, Jinquan Dong, "Minimum Heat of Formation of Potassium Iodo Hydride", Int. J. Hydrogen Energy, submitted.
 - 32. David R. Linde, *CRC Handbook of Chemistry and Physics*, 79 th Edition, CRC Press, Boca Raton, Florida, (1998-9), p. 10-175 to p. 10-177.
 - 33. R. Mills, The Nature of Free Electrons in Superfluid Helium--a Test of Quantum Mechanics and a Basis to Review its Foundations and Make a Comparison to Classical Theory, Int. J. Hydrogen Energy, in press.
 - 34. R. Mills, "The Hydrogen Atom Revisited", Int. J. of Hydrogen Energy, Vol. 25, Issue 12, December, (2000), pp. 1171-1183.
 - 35. C. L. Yaws, *Chemical Properties Handbook*, McGraw-Hill, (1999).
 - 36. R. Mills, "BlackLight Power Technology-A New Clean Energy Source with the Potential for Direct Conversion to Electricity", Global Foundation, Inc. conference entitled *Global Warming and Energy Policy*, Fort Lauderdale, FL, November 26-28, 2000.
 - 37. N. V. Sidgwick, *The Chemical Elements and Their Compounds*, Volume I, Oxford, Clarendon Press, (1950), p.17.

38. M. D. Lamb, *Luminescence Spectroscopy*, Academic Press, London, (1978), p. 68.

TABLE 1. Vapor pressure of metals versus temperature.

T (°C)	Na P _v (Torr) ^a	K P _v (Torr) ^a	Rb P _v (Torr) ^a	Cs P _v (Torr) ^a	Mg P _v (Torr) ^a	Sr P _v (Torr) ^a
470	2.0	16.7	43.2	65.9	0.030	0.001
500	3.8	28.3	68.9	101.5	0.075	0.004
520	5.6	39.3	92.1	132.6	0.132	0.007
535	7.5	49.8	113.4	160.5	0.197	0.011
540	8.3	53.8	121.3	170.8	0.225	0.012
560	12.0	72.4	157.7	217.0	0.372	0.022
600	23.6	125.8	256.8	337.7	0.947	0.061
620	32.4	162.8	322.2	414.4	1.459	0.100
650	50.9	234.4	444.5	552.9	2.682	0.197

^a Calculated [35]

Figure Captions

Figure 1. The electrode assembly of the glow discharge cell.

Figure 2. The stainless steel cell and experimental setup for generating a glow discharge plasma and optically measuring the power balance from 1.) hydrogen, argon, argon-hydrogen mixture (97/3%), and argon-hydrogen mixture (90/10%), 2.) sodium, magnesium, cesium, potassium, rubidium, and strontium with hydrogen, 3.) sodium, magnesium, cesium, potassium, rubidium, and strontium with argon, 4.) sodium, magnesium, cesium, potassium, rubidium, and strontium with argon-hydrogen mixture (97/3%), and 5.) potassium with argon-hydrogen mixture (90/10%).

Figure 3. The comparison of the light output power ($\mu\text{W}/\text{cm}^2$) of H_2 alone \blacktriangle , Ar alone \triangle , $\text{Ar} + H_2$ (97/3%) \times , $\text{Ar} + H_2$ (90/10%) \blacksquare , $\text{Na} + H_2$ \blacktriangle , $\text{Mg} + H_2$ \blacktriangle , $\text{K} + H_2$ \blacklozenge , $\text{Na} + \text{Ar}$ \triangle , $\text{Mg} + \text{Ar}$ \triangle , $\text{K} + \text{Ar}$ \triangle , $\text{Rb} + \text{Ar}$ \triangle , $\text{Cs} + \text{Ar}$ \triangle , $\text{Sr} + \text{Ar}$ \triangle , $\text{Na} + \text{Ar} + H_2$ (97/3%) \times , $\text{Mg} + \text{Ar} + H_2$ (97/3%) \times , $\text{K} + \text{Ar} + H_2$ (97/3%) \times , $\text{Rb} + \text{Ar} + H_2$ (97/3%) \square , $\text{Cs} + \text{Ar} + H_2$ (97/3%) \square , $\text{Sr} + \text{Ar} + H_2$ (97/3%) \diamond , and $\text{K} + \text{Ar} + H_2$ (90/10%) \blacksquare showing the $0 - 50 \mu\text{W}/\text{cm}^2$ range with $\text{Cs} + \text{Ar} + H_2$ (97/3%) \square and $\text{Sr} + \text{Ar} + H_2$ (97/3%) \diamond off-scale.

Figure 4. The comparison of the light output power ($\mu\text{W}/\text{cm}^2$) of H_2 alone \blacktriangle , Ar alone \triangle , $\text{Ar} + H_2$ (97/3%) \times , $\text{Ar} + H_2$ (90/10%) \blacksquare , $\text{Na} + H_2$ \blacktriangle , $\text{Mg} + H_2$ \blacktriangle , $\text{K} + H_2$ \blacklozenge , $\text{Na} + \text{Ar}$ \triangle , $\text{Mg} + \text{Ar}$ \triangle , $\text{K} + \text{Ar}$ \triangle , $\text{Rb} + \text{Ar}$ \triangle , $\text{Cs} + \text{Ar}$ \triangle , $\text{Sr} + \text{Ar}$ \triangle , $\text{Na} + \text{Ar} + H_2$ (97/3%) \times , $\text{Mg} + \text{Ar} + H_2$ (97/3%) \times , $\text{K} + \text{Ar} + H_2$ (97/3%) \blacksquare , $\text{Rb} + \text{Ar} + H_2$ (97/3%) \square , $\text{Cs} + \text{Ar} + H_2$ (97/3%) \square , $\text{Sr} + \text{Ar} + H_2$ (97/3%) \diamond , and $\text{K} + \text{Ar} + H_2$ (90/10%) \blacksquare showing the $0 - 200 \mu\text{W}/\text{cm}^2$ range with $\text{Sr} + \text{Ar} + H_2$ (97/3%) \diamond off-scale.

Figure 5. The comparison of the light output power ($\mu\text{W}/\text{cm}^2$) of H_2 alone \blacktriangle , Ar alone \triangle , $\text{Ar} + H_2$ (97/3%) \times , $\text{Ar} + H_2$ (90/10%) \blacksquare , $\text{Na} + H_2$ \blacktriangle , $\text{Mg} + H_2$ \blacktriangle , $\text{K} + H_2$ \blacklozenge , $\text{Na} + \text{Ar}$ \triangle , $\text{Mg} + \text{Ar}$ \triangle , $\text{K} + \text{Ar}$ \triangle , $\text{Rb} + \text{Ar}$ \triangle , $\text{Cs} + \text{Ar}$ \triangle , $\text{Sr} + \text{Ar}$ \triangle , $\text{Na} + \text{Ar} + H_2$ (97/3%) \times , $\text{Mg} + \text{Ar} + H_2$ (97/3%) \times , $\text{K} + \text{Ar} + H_2$ (97/3%) \blacksquare , $\text{Rb} + \text{Ar} + H_2$ (97/3%) \square , $\text{Cs} + \text{Ar} + H_2$ (97/3%) \square , $\text{Sr} + \text{Ar} + H_2$ (97/3%) \diamond , and $\text{K} + \text{Ar} + H_2$ (90/10%) \blacksquare showing the $0 - 800 \mu\text{W}/\text{cm}^2$

range.

Figure 6. The comparison of the light output power ($\mu W/cm^2$) of K + Ar + H₂ (97/3%) at a cell temperature of 650 °C —+—, Rb + Ar + H₂ (97/3%) at a cell temperature of 650 °C ———, Cs + Ar + H₂ (97/3%) at a cell temperature of 480 °C —*—, Cs + Ar + H₂ (97/3%) at a cell temperature of 500 °C —■—, Cs + Ar + H₂ (97/3%) at a cell temperature of 520 °C —▲—, Cs + Ar + H₂ (97/3%) at a cell temperature of 540 °C —×—, Cs + Ar + H₂ (97/3%) at a cell temperature of 565 °C —◆—, and Cs + Ar + H₂ (97/3%) at a cell temperature of 600 °C —□—.

Figure 7. The comparison of the light output power ($\mu W/cm^2$) of Cs + Ar + H₂ (97/3%) at a cell temperature of 565 °C ———, Rb + Ar + H₂ (97/3%) at a cell temperature of 470 °C —◆—, Rb + Ar + H₂ (97/3%) at a cell temperature of 500 °C —■—, Rb + Ar + H₂ (97/3%) at a cell temperature of 535 °C —▲—, Rb + Ar + H₂ (97/3%) at a cell temperature of 560 °C —×—, Rb + Ar + H₂ (97/3%) at a cell temperature of 600 °C —*—, Rb + Ar + H₂ (97/3%) at a cell temperature of 620 °C —◊—, and Rb + Ar + H₂ (97/3%) at a cell temperature of 650 °C —+—.

FIGURE 1.

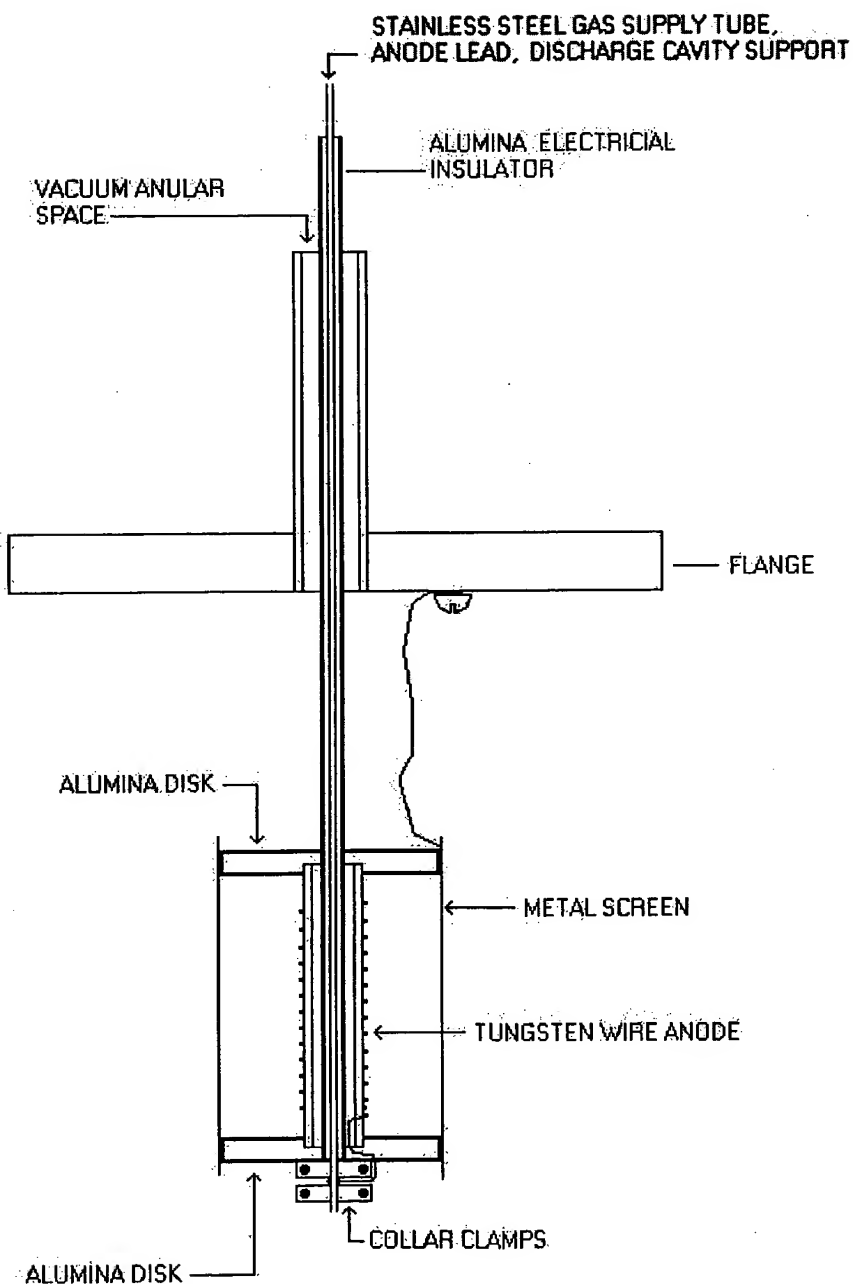


FIGURE 2.

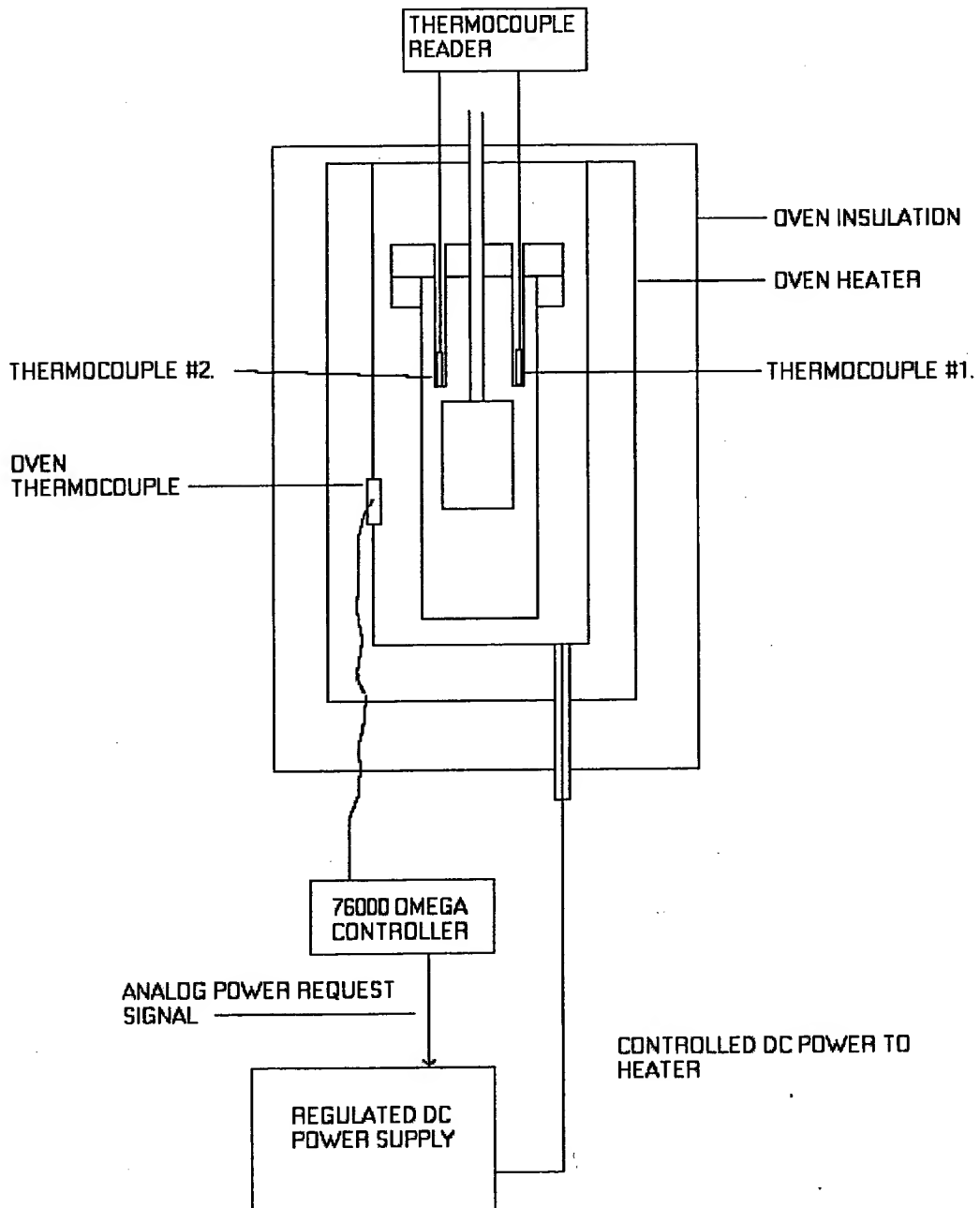
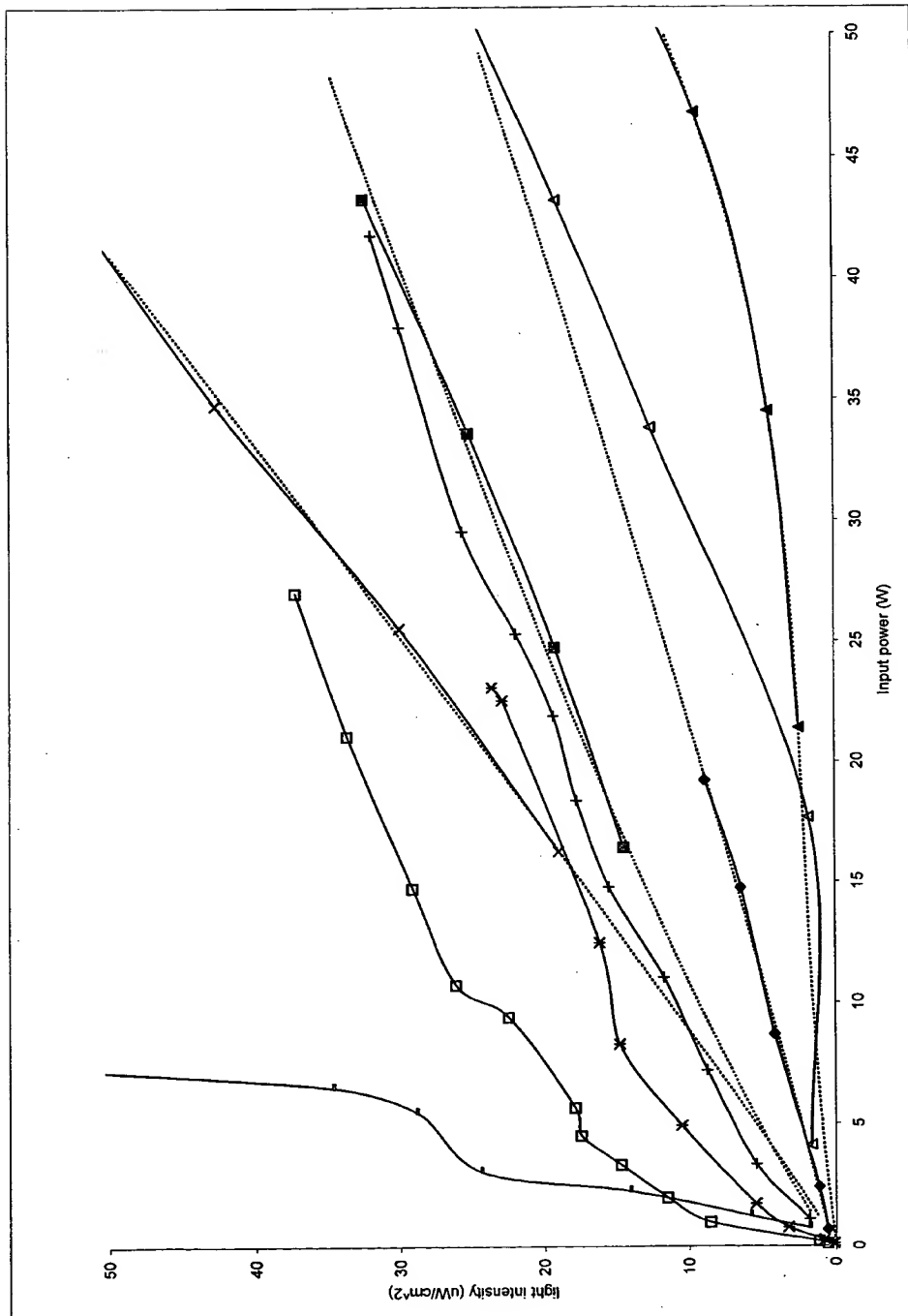


Fig. 3



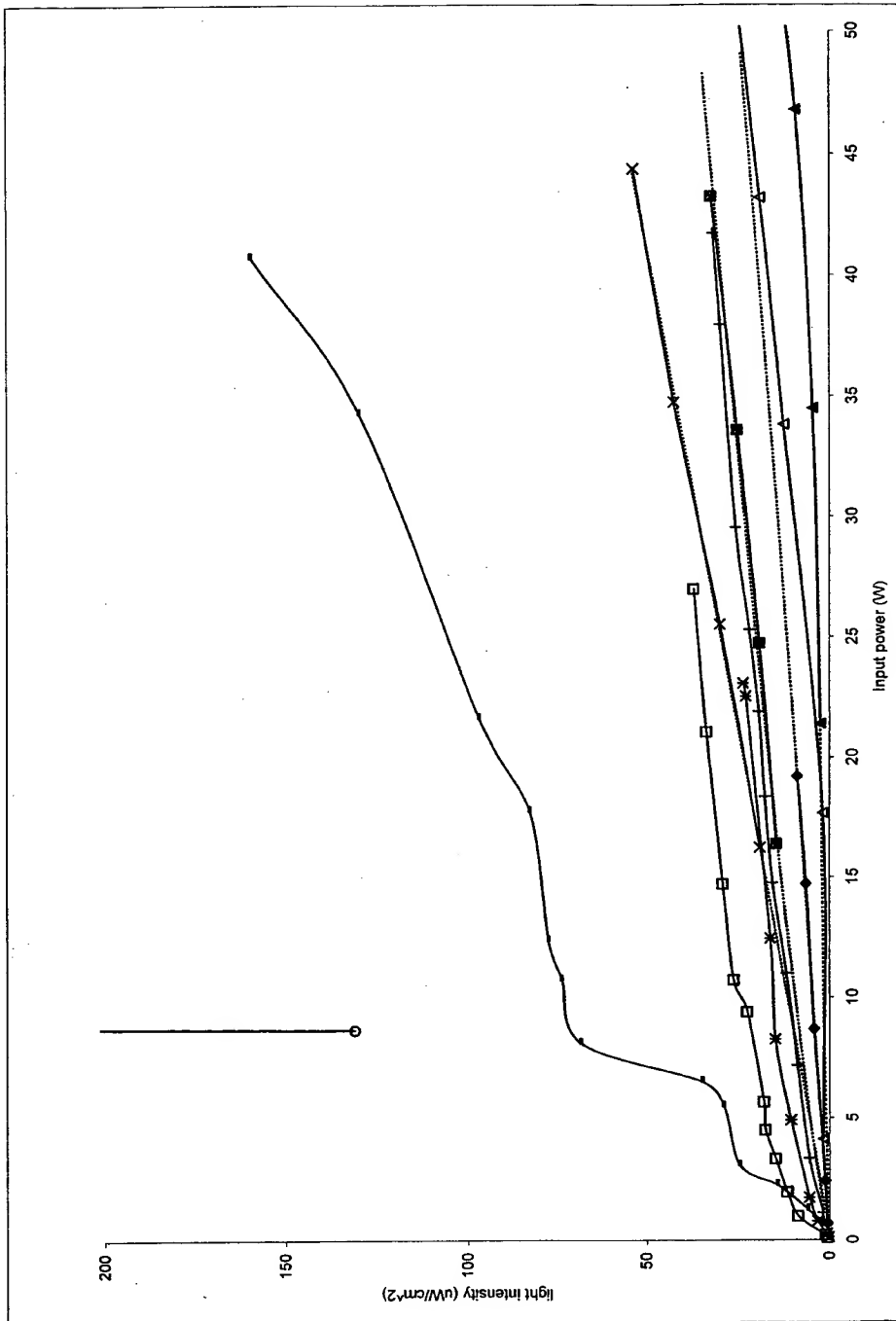


Fig. 4

Fig. 5

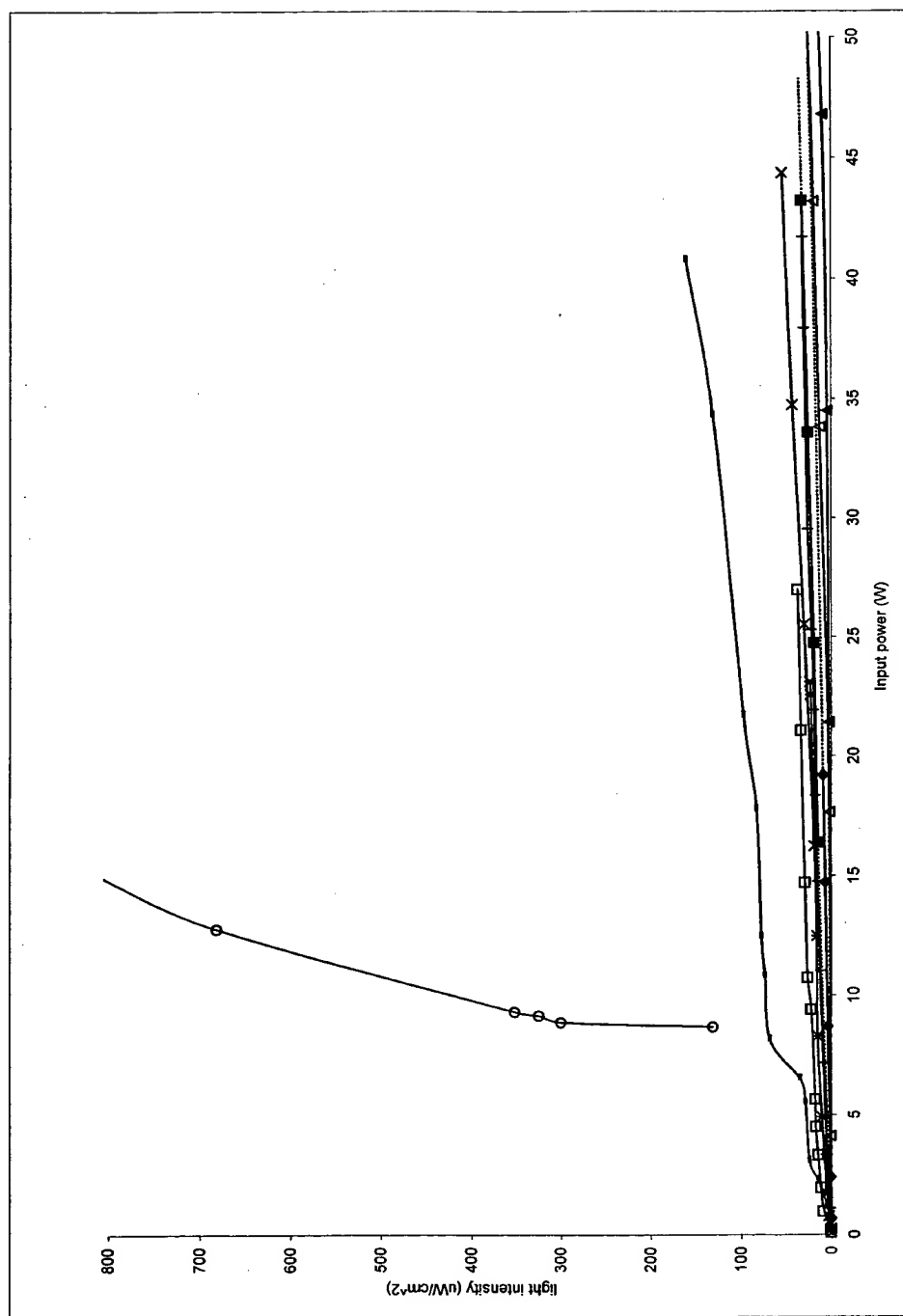


Fig. 6

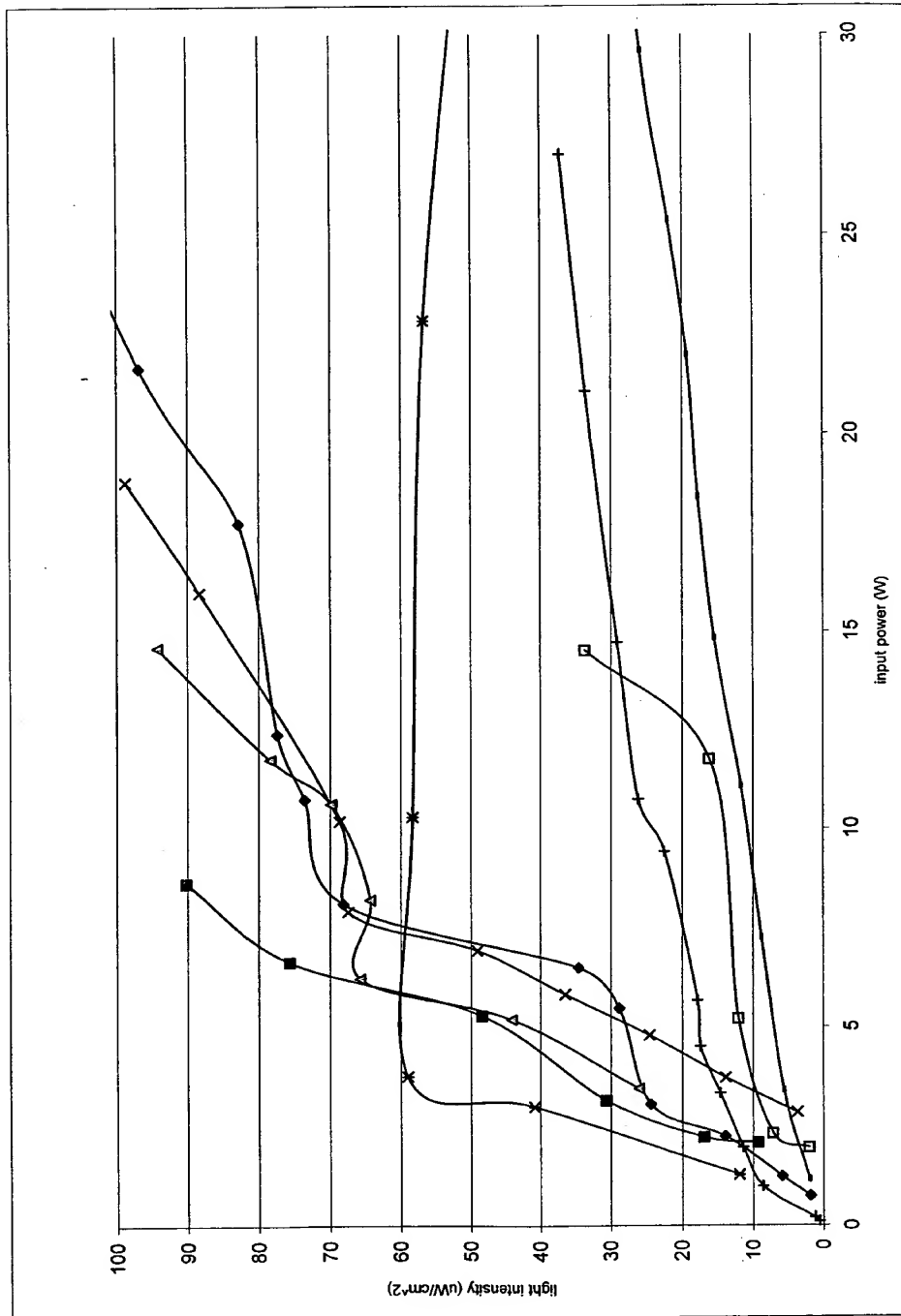
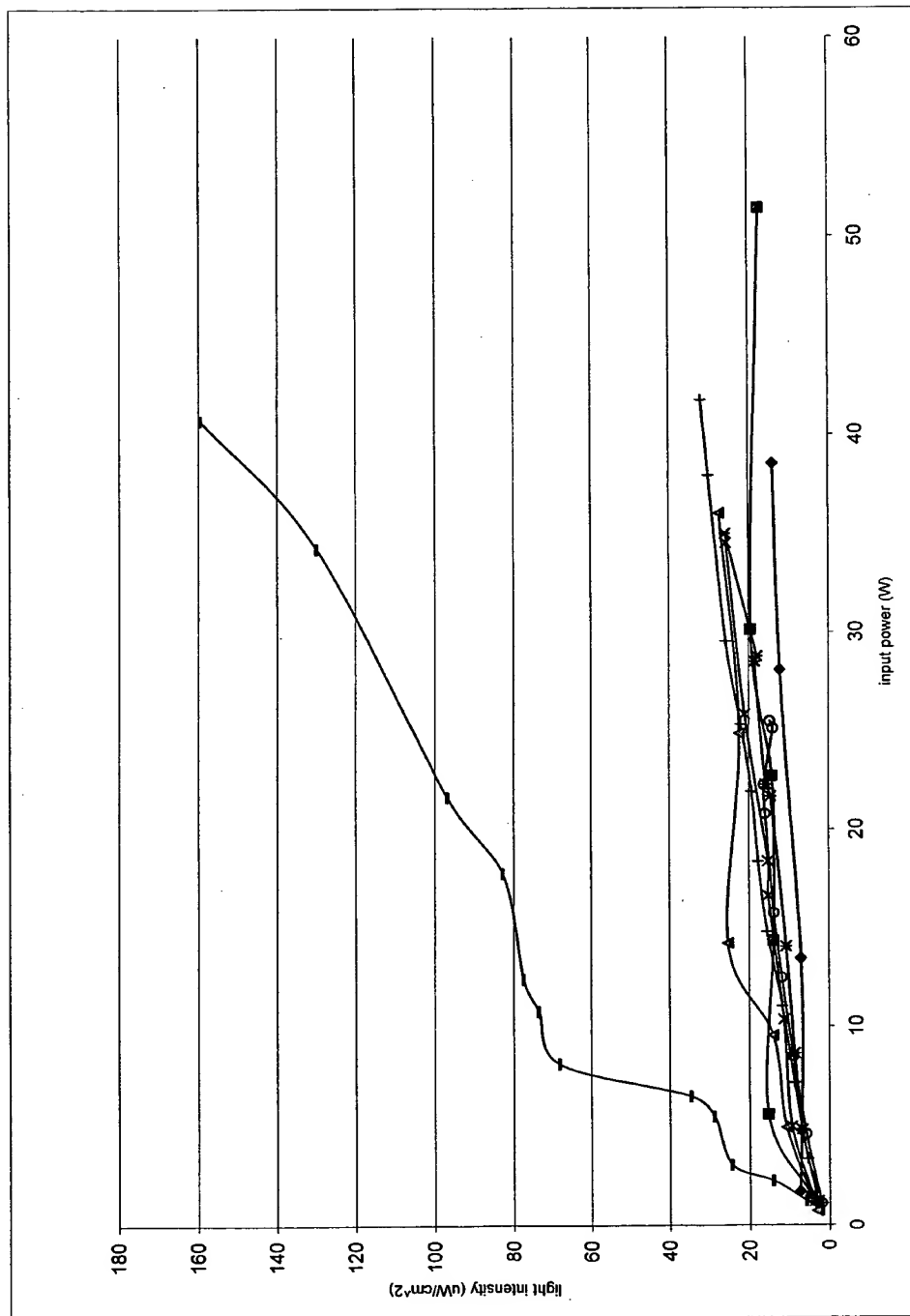


Fig. 7



Presented at the Global Foundation, Inc. Conference
The Role of Attractive and Repulsive Gravitational Forces
in Cosmic Acceleration of Particles
The Origin of the Cosmic Gamma Ray Bursts
(29th Conference on High Energy Physics and Cosmology)
Ft. Lauderdale, FL
December 14-17, 2000
Dr. Behram Kursunoglu, Chairman

THE GRAND UNIFIED THEORY OF CLASSICAL QUANTUM MECHANICS

Randell L. Mills

1. INTRODUCTION

A theory of classical quantum mechanics (CQM), derived from first principles,¹ successfully applies physical laws on all scales. The classical wave equation is solved with the constraint that a bound electron cannot radiate energy. The mathematical formulation for zero radiation based on Maxwell's equations follows from a derivation by Haus.² The function that describes the motion of the electron must not possess spacetime Fourier components that are synchronous with waves traveling at the speed of light. CQM gives closed form solutions for the atom, including the stability of the $n=1$ state and the instability of the excited states, the equation of the photon and electron in excited states, the equation of the free electron, and photon which predict the wave particle duality behavior of particles and light. The current and charge density functions of the electron may be directly physically interpreted. For example, spin angular momentum results from the motion of negatively charged mass moving systematically, and the equation for angular momentum, $\mathbf{r} \times \mathbf{p}$, can be applied directly to the wave function, called an orbitsphere (a current density function), that describes the electron. The magnetic moment of a Bohr magneton, Stern Gerlach experiment, g factor, Lamb shift, resonant line width and shape, selection rules, correspondence principle, wave particle duality, excited states, reduced mass, rotational energies, and momenta, orbital and spin splitting, spin-orbital coupling, Knight shift, and spin-nuclear coupling are derived in closed form equations based on Maxwell's equations. The calculations agree with experimental observations.

For or any kind of wave advancing with limiting velocity and capable of transmitting signals, the equation of front propagation is the same as the equation for the front of a light wave. By applying this condition to electromagnetic and gravitational fields at

Randell L Mills, President, BlackLight Power, Inc., 493 Old Trenton Road, Cranbury, NJ 08512, Phone: 609-490-1090, e-mail: rmills@blacklightpower.com; www.blacklightpower.com

particle production, the Schwarzschild metric (SM) is derived from the classical wave equation which modifies general relativity to include conservation of spacetime in addition to momentum and matter/energy. The result gives a natural relationship between Maxwell's equations, special relativity, and general relativity. It gives gravitation from the atom to the cosmos. The Universe is time harmonically oscillatory in matter energy and spacetime expansion and contraction with a minimum radius that is the gravitational radius. In closed form equations with fundamental constants only, CQM gives the deflection of light by stars, the precession of the perihelion of Mercury, the particle masses, the Hubble constant, the age of the Universe, the observed acceleration of the expansion, the power of the Universe, the power spectrum of the Universe, the microwave background temperature, the uniformity of the microwave background radiation, the microkelvin spatial variation of the microwave background radiation, the observed violation of the GZK cutoff, the mass density, the large scale structure of the Universe, and the identity of dark matter which matches the criteria for the structure of galaxies. In a special case wherein the gravitational potential energy density of a blackhole equals that of the Plank mass, matter converts to energy and spacetime expands with the release of a gamma-ray burst. The singularity in the SM is eliminated.

2. COSMOLOGICAL THEORY BASED ON MAXWELL'S EQUATIONS

Maxwell's equations and special relativity are based on the law of propagation of a electromagnetic wave front in the form

$$1/c^2 (\delta\omega/\delta t)^2 - [(\delta\omega/\delta x)^2 + (\delta\omega/\delta y)^2 + (\delta\omega/\delta z)^2] = 0 \quad (1)$$

For any kind of wave advancing with limiting velocity and capable of transmitting signals, the equation of front propagation is the same as the equation for the front of a light wave. Thus, the equation $1/c^2 (\delta\omega/\delta t)^2 - (\text{grad}\omega)^2 = 0$ acquires a general character; it is more general than Maxwell's equations from which Maxwell originally derived it.

A discovery of the present work is that the classical wave equation governs: (1) the motion of bound electrons, (2) the propagation of any form of energy, (3) measurements between inertial frames of reference such as time, mass, momentum, and length (Minkowski tensor), (4) fundamental particle production and the conversion of matter to energy, (5) a relativistic correction of spacetime due to particle production or annihilation (Schwarzschild metric), (6) the expansion and contraction of the Universe, (7) the basis of the relationship between Maxwell's equations, Planck's equation, the de Broglie equation, Newton's laws, and special, and general relativity.

The relationship between the time interval between ticks t of a clock in motion with velocity v relative to an observer and the time interval t_0 between ticks on a clock at rest relative to an observer²⁴ is

$$(ct)^2 = (ct_0)^2 + (vt)^2. \quad (2)$$

Thus, the time dilation relationship based on the constant maximum speed of light c in any inertial frame is $t = t_0 / \sqrt{1 - (v^2/c^2)}$. The metric $g_{\mu\nu}$ for Euclidean space is the

Minkowski tensor $\eta_{\mu\nu}$. In this case, the separation of proper time between two events x^{μ} and $x^{\mu} + dx^{\mu}$ is $d\tau^2 = -\eta_{\mu\nu}dx^{\mu}dx^{\nu}$.

3. THE EQUIVALENCE OF THE GRAVITATIONAL MASS AND THE INERTIAL MASS

The equivalence of the gravitational mass and the inertial mass $m_g/m_i = \text{universal constant}$ which is predicted by Newton's law of mechanics and gravitation is experimentally confirmed to less 1×10^{-11} .³ In physics, the discovery of a universal constant often leads to the development of an entirely new theory. From the universal constancy of the velocity of light c , the special theory of relativity was derived; and from Planck's constant h , the quantum theory was deduced. Therefore, the universal constant m_g/m_i should be the key to the gravitational problem. The energy equation of Newtonian gravitation is

$$E = \frac{1}{2}mv^2 - \frac{GMm}{r} = \frac{1}{2}mv_0^2 - \frac{GMm}{r_0} = \text{constant} \quad (3)$$

Since h , the angular momentum per unit mass, is $h = L/m = |\mathbf{r} \times \mathbf{v}| = r_0 v_0 \sin \phi$, the eccentricity e may be written as

$$e = \left[1 + \left(v_0^2 - \frac{2GM}{r_0} \right) \frac{r_0^2 v_0^2 \sin^2 \phi}{G^2 M^2} \right]^{1/2}, \quad (4)$$

where m is the inertial mass of a particle, v_0 is the speed of the particle, r_0 is the distance of the particle from a massive object, ϕ is the angle between the direction of motion of the particle and the radius vector from the object, and M is the total mass of the object (including a particle). The eccentricity e given by Newton's differential equations of motion in the case of the central field permits the classification of the orbits according to the total energy E ⁴ (column 1) and the orbital velocity squared, v_0^2 , relative to the gravitational velocity squared, $2GM/r_0$ ⁴ (column 2):

$E < 0$	$v_0^2 < 2GM/r_0$	$e < 1$	ellipse
$E < 0$	$v_0^2 < 2GM/r_0$	$e = 0$	circle (special case of ellipse)
$E = 0$	$v_0^2 = 2GM/r_0$	$e = 1$	parabolic orbit
$E > 0$	$v_0^2 > 2GM/r_0$	$e > 1$	hyperbolic orbit

4. CONTINUITY CONDITIONS FOR THE PRODUCTION OF A PARTICLE FROM A PHOTON TRAVELING AT LIGHT SPEED

A photon traveling at the speed of light gives rise to a particle with an initial radius equal to its Compton wavelength bar.

$$r = \lambda_c = \frac{\hbar}{m_0 c} = r_a, \quad (5)$$

The particle must have an orbital velocity equal to Newtonian gravitational escape velocity v_g of the antiparticle.

$$v_g = \sqrt{\frac{2Gm}{r}} = \sqrt{\frac{2Gm_0}{\lambda_c}}. \quad (6)$$

The eccentricity is one. The orbital energy is zero. The particle production trajectory is a parabola relative to the center of mass of the antiparticle.

4.1 A Gravitational Field as a Front Equivalent to Light Wave Front

The particle with a finite gravitational mass gives rise to a gravitational field that travels out as a front equivalent to a light wave front. The form of the outgoing gravitational field front traveling at the speed of light is $f(t - r/c)$ and $d\tau^2$ is given by

$$d\tau^2 = f(r)dt^2 - \frac{1}{c^2} [f(r)^2 dr^2 + r^2 d\theta^2 + r^2 \sin^2 \theta d\phi^2]. \quad (7)$$

The speed of light as a constant maximum as well as phase matching and continuity conditions of the electromagnetic and gravitational waves require the following form of the squared displacements:

$$(ct)^2 + (v_g t)^2 = (ct)^2, \quad (8)$$

$$f(r) = \left(1 - \left(\frac{v_g}{c} \right)^2 \right). \quad (9)$$

In order that the wave front velocity does not exceed c in any frame, spacetime must undergo time dilation and length contraction due to the particle production event. *The derivation and result of spacetime time dilation is analogous to the derivation and result of special relativistic time dilation* wherein the relative velocity of two inertial frames replaces the gravitational velocity.

The general form of the metric due to the relativistic effect on spacetime due to mass m_0 with v_g given by Eq. (6) is

$$d\tau^2 = \left(1 - \left(\frac{v_g}{c} \right)^2 \right) dt^2 - \frac{1}{c^2} \left[\left(1 - \left(\frac{v_g}{c} \right)^2 \right)^{-1} dr^2 + r^2 d\theta^2 + r^2 \sin^2 \theta d\phi^2 \right]. \quad (10)$$

The gravitational radius, r_g , of each orbitsphere of the particle production event, each of

mass m_0 and the corresponding general form of the metric are respectively

$$r_s = \frac{2Gm_0}{c^2}, \quad (11)$$

$$d\tau^2 = \left(1 - \frac{r_s}{r}\right)dt^2 - \frac{1}{c^2} \left[\left(1 - \frac{r_s}{r}\right)^{-1} dr^2 + r^2 d\theta^2 + r^2 \sin^2 \theta d\phi^2 \right]. \quad (12)$$

Masses and their effects on spacetime *superimpose*. The separation of proper time between two events x^μ and $x^\mu + dx^\mu$ is

$$d\tau^2 = \left(1 - \frac{2GM}{c^2 r}\right)dt^2 - \frac{1}{c^2} \left[\left(1 - \frac{2GM}{c^2 r}\right)^{-1} dr^2 + r^2 d\theta^2 + r^2 \sin^2 \theta d\phi^2 \right]. \quad (13)$$

The metric $g_{\mu\nu}$ for non-Euclidean space due to the relativistic effect on spacetime due to mass M is the *Schwarzschild metric* which gives the relationship whereby matter causes relativistic corrections to spacetime that determines the curvature of spacetime and is the origin of gravity.

4.2. Particle Production Continuity Conditions from Maxwell's Equations, and the Schwarzschild Metric

The photon to particle event requires a transition state that is continuous wherein the velocity of a transition state orbitsphere is the speed of light. The radius, r , is the Compton wavelength bar, λ_c , given by Eq. (5). At production, the Planck equation energy, the electric potential energy, and the magnetic energy are equal to $m_0 c^2$.

The Schwarzschild metric gives the relationship whereby matter causes relativistic corrections to spacetime that determines the masses of fundamental particles. Substitution of $r = \lambda_c$; $dr = 0$; $d\theta = 0$; $\sin^2 \theta = 1$ into the Schwarzschild metric gives

$$d\tau = dt \left(1 - \frac{2Gm_0}{c^2 r_c} - \frac{v^2}{c^2}\right)^{\frac{1}{2}}, \quad (14)$$

with $v^2 = c^2$, the relationship between the proper time and the coordinate time is

$$\tau = ti \sqrt{\frac{2GM}{c^2 r_c}} = ti \sqrt{\frac{2GM}{c^2 \lambda_c}} = ti \frac{v_s}{c}. \quad (15)$$

When the orbitsphere velocity is the speed of light, continuity conditions based on the constant maximum speed of light given by Maxwell's equations are mass energy = Planck equation energy = electric potential energy = magnetic energy = mass/spacetime metric energy. Therefore, $m_0 c^2 = \hbar\omega = V = E_{mag} = E_{spacetime}$

$$m_0 c^2 = \hbar \omega = \frac{\hbar^2}{m_0 \lambda_c^2} = \alpha^{-1} \frac{e^2}{4\pi e_0 \lambda_c} = \alpha^{-1} \frac{\pi \mu_0 e^2 \hbar^2}{(2\pi m_0) \lambda_c^3} = \frac{\alpha \hbar}{1 \text{ sec}} \sqrt{\lambda_c c^2} . \quad (16)$$

The continuity conditions based on the constant maximum speed of light given by the Schwarzschild metric are:

$$\frac{\text{proper time}}{\text{coordinate time}} = \frac{\text{gravitational wave condition}}{\text{electromagnetic wave condition}} = \frac{\text{gravitational mass phase matching}}{\text{charge/inertial mass phase matching}} , \quad (17)$$

$$\frac{\text{proper time}}{\text{coordinate time}} = i \sqrt{\frac{2Gm}{c^2 \lambda_c}} = i \frac{v_g}{\alpha c} . \quad (18)$$

5. MASSES OF FUNDAMENTAL PARTICLES

Each of the Planck equation energy, electric energy, and magnetic energy corresponds to a particle given by the relationship between the proper time and the coordinate time. The electron and down-down-up neutron correspond to the Planck equation energy. The muon and strange-strange-charmed neutron correspond to the electric energy. The tau and bottom-bottom-top neutron correspond to the magnetic energy. The particle must possess the escape velocity v_g relative to the antiparticle where $v_g < c$. According to Newton's law of gravitation, the eccentricity is one and the particle production trajectory is a parabola relative to the center of mass of the antiparticle.

5.1. The Electron-Antielectron Lepton Pair

A clock is defined in terms of a self consistent system of units used to measure the particle mass. The proper time of the particle is equated with the coordinate time according to the Schwarzschild metric corresponding to light speed. The special relativistic condition corresponding to the Planck energy gives the mass of the electron.

$$2\pi \frac{\hbar}{mc^2} = \text{sec} \sqrt{\frac{2Gm^2}{ca^2 \hbar}} , \quad (19)$$

$$m_e = \left(\frac{\hbar \alpha}{\text{sec} c^2} \right)^{\frac{1}{2}} \left(\frac{ch}{2G} \right)^{\frac{1}{2}} = 9.1097 \times 10^{-31} \text{ kg} , \quad (20)$$

$$m_e = 9.1097 \times 10^{-31} \text{ kg} - 18 \text{ eV} / c^2 (v_e) = 9.1094 \times 10^{-31} \text{ kg} , \quad (21)$$

$$m_{e \text{ experimental}} = 9.1095 \times 10^{-31} \text{ kg} . \quad (22)$$

5.2. Down-Down-Up Neutron (DDU)

The corresponding equation for production of the neutron is

7. RELATIONSHIP OF MATTER TO ENERGY AND SPACETIME EXPANSION

The Schwarzschild metric gives the relationship whereby matter causes relativistic corrections to spacetime. The limiting velocity c results in the contraction of spacetime due to particle production, which is given by $2\pi r_g$, where r_g is the gravitational radius of the particle. This has implications for the expansion of spacetime when matter converts to energy. Q the mass/energy to expansion/contraction quotient of spacetime is given by the ratio of the mass of a particle at production divided by T the period of production.

$$Q = \frac{m_0}{T} = \frac{m_0}{\frac{2\pi r_g}{c}} = \frac{m_0}{\frac{2\pi 2Gm_0}{c^2}} = \frac{c^3}{4\pi G} = 3.22 \times 10^{34} \frac{\text{kg}}{\text{sec}}. \quad (34)$$

The gravitational equations with the equivalence of the particle production energies [Eq. (16)] permit the conservation of mass/energy ($E=mc^2$) and spacetime ($c^3/4\pi G=3.22 \times 10^{34} \text{ kg/sec}$). With the conversion of $3.22 \times 10^{34} \text{ kg}$ of matter to energy, spacetime expands by 1 sec. The photon has inertial mass and angular momentum, but due to Maxwell's equations and the implicit special relativity it does not have a gravitational mass.

7.1. Cosmological Consequences

The Universe is closed (it is finite but with no boundary). It is a 3-sphere Universe-Riemannian three dimensional hyperspace plus time of constant positive curvature at each r-sphere. The *Universe is oscillatory in matter/energy and spacetime* with a finite minimum radius, the gravitational radius. Spacetime expands as mass is released as energy which provides the basis of the atomic, thermodynamic, and cosmological arrows of time. Different regions of space are isothermal even though they are separated by greater distances than that over which light could travel during the time of the expansion of the Universe.⁹ Presently, stars and large scale structures exist which are older than the elapsed time of the present expansion as stellar, galaxy, and supercluster evolution occurred during the contraction phase.¹⁰⁻¹⁶ The maximum power radiated by the Universe which occurs at the beginning of the expansion phase is $P_U=c^3/4\pi G = 2.89 \times 10^{71} W$. Observations beyond the beginning of the expansion phase are not possible since the Universe is entirely matter filled.

7.2. The Period of Oscillation of the Universe Based on Closed Propagation of Light

Mass/energy is conserved during harmonic expansion and contraction. The gravitational potential energy E_{grav} given by Eq. (28) with $m_0 = m_U$ is equal to $m_U c^2$ when the radius of the Universe r is the gravitational radius r_G . The gravitational velocity v_G [Eq. (30) with $r=r_G$ and $m_0 = m_U$] is the speed of light in a circular orbit wherein the eccentricity is equal to zero and the escape velocity from the Universe can never be reached. The period of the oscillation of the Universe and the period for light to transverse the Universe corresponding to the gravitational radius r_G must be equal. The harmonic oscillation period, T , is

$$T = \frac{2\pi r_G}{c} = \frac{2\pi G m_U}{c^3} = \frac{2\pi G (2 \times 10^{54} \text{ kg})}{c^3} = 3.10 \times 10^{19} \text{ sec} = 9.83 \times 10^{11} \text{ years}, \quad (35)$$

where the mass of the Universe, m_U , is approximately $2 \times 10^{54} \text{ kg}$. (The initial mass of the Universe of $2 \times 10^{54} \text{ kg}$ is based on internal consistency with the size, age, Hubble constant, temperature, density of matter, and power spectrum.) Thus, the observed Universe will expand as mass is released as photons for $4.92 \times 10^{11} \text{ years}$. At this point in its world line, the Universe will obtain its maximum size and begin to contract.

8. THE DIFFERENTIAL EQUATION OF THE RADIUS OF THE UNIVERSE

Based on conservation of mass/energy ($E=mc^2$) and spacetime ($c^3/4\pi G=3.22 \times 10^{34} \text{ kg/sec}$). The Universe behaves as a simple harmonic oscillator having a restoring force, F , which is proportional to the radius. The proportionality constant, k , is given in terms of the potential energy, E , gained as the radius decreases from the maximum expansion to the minimum contraction.

$$\frac{E}{N^2} = k. \quad (36)$$

Since the gravitational potential energy E_{grav} is equal to $m_U c^2$ when the radius of the Universe r is the gravitational radius r_G

$$F = -kN = -\frac{m_U c^2}{r_0^2} N = -\frac{m_U c^2}{\left(\frac{G m_U}{c^2}\right)^2} N. \quad (37)$$

And, the differential equation of the radius of the Universe, N is

$$m_U \ddot{N} + \frac{m_U c^2}{r_G^2} N = m_U \ddot{N} + \frac{m_U c^2}{\left(\frac{G m_U}{c^2}\right)^2} N = 0. \quad (38)$$

The *maximum radius of the Universe*, the amplitude, r_0 , of the time harmonic variation in the radius of the Universe, is given by the quotient of the total mass of the Universe and Q , the mass/energy to expansion/contraction quotient.

$$r_0 = \frac{m_U}{Q} = \frac{m_U}{\frac{c^3}{4\pi G}} = \frac{2 \times 10^{54} \text{ kg}}{\frac{c^3}{4\pi G}} = 1.97 \times 10^{12} \text{ light years}. \quad (39)$$

The *minimum radius* which corresponds to the gravitational radius r_g , given by Eq. (11) with $m_0=m_U$ is $3.12 \times 10^{11} \text{ light years}$. When the radius of the Universe is the gravitational radius, r_g , the proper time is equal to the coordinate time by Eq. (15) and the gravitational escape velocity v_g of the Universe is the speed of light. The radius of the Universe as a function of time is

$$N = \left(r_s + \frac{cm_u}{Q} \right) - \frac{cm_u}{Q} \cos \left(\frac{2\pi t}{\frac{2\pi G}{c}} \right) = \left(\frac{2Gm_u}{c^2} + \frac{cm_u}{4\pi G} \right) - \frac{cm_u}{4\pi G} \cos \left(\frac{2\pi t}{\frac{2\pi Gm_u}{c^3}} \right). \quad (40)$$

The expansion/contraction rate, \dot{N} , is given by time derivative of Eq. (40)

$$\dot{N} = 4\pi c X 10^{-3} \sin \left(\frac{2\pi t}{\frac{2\pi Gm_u}{c^3}} \right) \frac{km}{sec}. \quad (41)$$

9. THE HUBBLE CONSTANT

The *Hubble constant* is given by the ratio of the expansion rate given in units of km/sec divided by the radius of the expansion in Mpc . The radius of expansion is equivalent to the radius of the light sphere with an origin at the time point when the Universe stopped contracting and started to expand.

$$H = \frac{\dot{N}}{t Mpc} = \frac{4\pi c X 10^{-3} \sin \left(\frac{2\pi t}{\frac{2\pi Gm_u}{c^3}} \right) \frac{km}{sec}}{t Mpc}, \quad (42)$$

for $t = 10^{10} \text{ light years} = 3.069 X 10^3 \text{ Mpc}$, the Hubble constant, H_0 , is $78.6 \text{ km/sec}\cdot\text{Mpc}$. The experimental value is¹⁷ $H_0 = 80 \pm 17 \text{ km/sec}\cdot\text{Mpc}$.

10. THE DENSITY OF THE UNIVERSE AS A FUNCTION OF TIME

The density of the Universe as a function of time $\rho_U(t)$ is given by the ratio of the mass as a function of time and the volume as a function of time.

$$\rho_U(t) = \frac{m_U(t)}{V(t)} = \frac{m_U(t)}{\frac{4}{3}\pi N(t)^3} = \frac{\frac{m_u}{2} \left(1 + \cos \left(\frac{2\pi t}{\frac{2\pi Gm_u}{c^3}} \right) \right)}{\frac{4}{3}\pi \left(\left(\frac{2Gm_u}{c^2} + \frac{cm_u}{4\pi G} \right) - \frac{cm_u}{4\pi G} \cos \left(\frac{2\pi t}{\frac{2\pi Gm_u}{c^3}} \right) \right)^3}, \quad (43)$$

for $t = 10^{10} \text{ light years}$, $\rho_U = 1.7 X 10^{-22} \text{ g/cm}^3$ The density of luminous matter of stars and gas of galaxies is about $\rho_U = 2 X 10^{-31} \text{ g/cm}^3$.¹⁸⁻¹⁹

11. THE POWER OF THE UNIVERSE AS A FUNCTION OF TIME, $P_U(t)$

From $E = mc^2$ and Eq. (34),

$$P_U(t) = \frac{c^5}{8\pi G} \left(1 + \cos \left(\frac{2\pi t}{2\pi r_c} \right) \right) \quad (44)$$

For $t = 10^{10}$ light years, $P_U(t) = 2.88 \times 10^{31} W$. The observed power is consistent with that predicted.

12. THE TEMPERATURE OF THE UNIVERSE AS A FUNCTION OF TIME

The temperature of the Universe as a function of time, $T_U(t)$, follows from the Stefan-Boltzmann law.

$$T_U(t) = \left(\frac{1}{1 + \frac{Gm_U(t)}{c^3 N(t)}} \right)^{\frac{1}{4}} \left[\frac{R_U(t)}{e\sigma} \right]^{\frac{1}{4}} = \left(\frac{1}{1 + \frac{Gm_U(t)}{c^3 N(t)}} \right)^{\frac{1}{4}} \left[\frac{\frac{P_U(t)}{4\pi N(t)}}{e\sigma} \right]^{\frac{1}{4}}. \quad (45)$$

The calculated uniform temperature is about 2.7 K which is in agreement with the observed microwave background temperature.⁹

13. POWER SPECTRUM OF THE COSMOS

The power spectrum of the cosmos, as measured by the Las Campanas Survey, generally follows the prediction of cold dark matter on the scales of 200 million to 600 million light-years. However, the power increases dramatically on scales of 600 million to 900 million light-years. The infinitesimal temporal displacement, $d\tau^2$, is given by Eq. (13).

The relationship between the proper time and the coordinate time is

$$\tau = t \sqrt{1 - \frac{2Gm_U}{c^2 r}} = t \sqrt{1 - \frac{r_x}{r}}. \quad (46)$$

The power maximum in the proper frame occurs at

$$\tau = 5 \times 10^9 \text{ light years} \sqrt{1 - \frac{3.12 \times 10^{11} \text{ light years}}{3.22 \times 10^{11} \text{ light years}}} = 880 \times 10^6 \text{ light years}. \quad (47)$$

The power maximum of the current observable Universe is predicted to occur on the

scale of 880×10^6 light years. There is excellent agreement between the predicted value and the experimental value of $600\text{--}900 \times 10^6$ light years.¹⁶

14. THE EXPANSION/CONTRACTION ACCELERATION, \ddot{N}

The expansion/contraction acceleration rate, \ddot{N} , is given by the time derivative of Eq. (41).

$$\ddot{N} = 2\pi \frac{c^4}{Gm_u} \cos \left(\frac{2\pi t}{\frac{2\pi Gm_u}{c^3} \sec} \right) = \ddot{N} = H_o = 78.7 \cos \left(\frac{2\pi t}{3.01 \times 10^3 \text{ Mpc}} \right) \frac{\text{km}}{\text{sec} \cdot \text{Mpc}} \quad (48)$$

The differential in the radius of the Universe, ΔN , due to its acceleration is given by $\Delta N = 1/2\ddot{N}t^2$. The differential in expanded radius for the elapsed time of expansion, $t = 10^{10}$ light years corresponds to a decease in brightness of a supernovae standard candle of about an order of magnitude of that expected where the distance is taken as ΔN . This result based on the predicted rate of acceleration of the expansion is consistent with the experimental observation.²⁰⁻²²

Furthermore, the microwave background radiation image obtained by the Boomerang telescope²³ is consistent with a Universe of nearly flat geometry since the commencement of its expansion. The data is consistent with a large offset radius of the Universe with a fractional increase in size since the commencement of expansion about 10 billion years ago.

15. THE PERIODS OF SPACETIME EXPANSION/CONTRACTION AND PARTICLE DECAY/PRODUCTION FOR THE UNIVERSE ARE EQUAL

The period of the expansion/contraction cycle of the radius of the Universe, T , is given by Eq. (35). It follows from the Poynting power theorem with spherical radiation that the transition lifetimes are given by the ratio of energy and the power of the transition.

$$\begin{aligned} \tau &= \frac{\text{energy}}{\text{power}} = \frac{[\hbar\omega]}{\left[\frac{2\pi c}{[(2l+1)\gamma!]} \left(\frac{l+1}{l} \right) k^{2l+1} |Q_{lm} + Q'_{lm}|^2 \right]} \\ &= \frac{1}{2\pi} \left(\frac{\hbar}{e^2} \right) \sqrt{\frac{\mu_e}{\epsilon_e}} \frac{[(2l+1)\gamma!]}{2\pi} \left(\frac{l}{l+1} \right) \left(\frac{l+3}{3} \right)^2 \frac{1}{(\sigma_n)^2 \omega} \end{aligned} \quad (49)$$

Exponential decay applies to electromagnetic energy decay $h(t) = e^{-\frac{1}{T}} u(t)$. The

coordinate time is imaginary because energy transitions are spacelike due spacetime expansion from matter to energy conversion. For example, the mass of the electron (a fundamental particle) is given by

$$\frac{2\pi\lambda_c}{\sqrt{\frac{2Gm_e}{\lambda_c}}} = \frac{2\pi\lambda_c}{v_g} = i\alpha^{-1} sec, \quad (50)$$

where v_g is Newtonian gravitational velocity [Eq. (6)]. When the gravitational radius r_g is the radius of the Universe, the proper time is equal to the coordinate time by Eq. (15), and the gravitational escape velocity v_g of the Universe is the speed of light. Replacement of the coordinate time, t , by the spacelike time, it , gives

$$h(t) = Re \left[e^{\frac{-i}{T}t} \right] = \cos \frac{2\pi}{T} t, \quad (51)$$

where the period is T [Eq. (35)]. The continuity conditions based on the constant maximum speed of light (Maxwell's equations) are given by Eqs. (16). The continuity conditions based on the constant maximum speed of light (Schwarzschild metric) are given by Eqs. (17-18). The periods of spacetime expansion/contraction and particle decay/production for the Universe are equal because only the particles which satisfy Maxwell's equations and the relationship between proper time and coordinate time imposed by the Schwarzschild metric may exist.

16. WAVE EQUATION

The general form of the light front wave equations is given by Eq. (1). The equation of the radius of the Universe, N , may be written as

$$N = \left(\frac{2Gm_u}{c^2} + \frac{cm_u}{c^3} \right) - \frac{cm_u}{4\pi G} \cos \left(\frac{2\pi}{2\pi Gm_u} \sec \left(t - \frac{N}{c} \right) \right) m, \quad (52)$$

which is a solution of the wave equation for a light wave front.

17. CONCLUSION

Maxwell's equations, Planck's equation, the de Broglie equation, Newton's laws, and special, and general relativity are unified.

REFERENCES

1. R. Mills, *The Grand Unified Theory of Classical Quantum Mechanics*, January 2000 Edition, BlackLight Power, Inc., Cranbury, New Jersey, Distributed by Amazon.com.
2. H. A. Haus, On the radiation from point charges, *American Journal of Physics*, **54**, 1126–1129 (1986).
3. E. G. Adelberger, C. W. Stubbs, B. R. Heckel, Y. Su, H. E. Swanson, G. Smith, J. H. Gundlach, *Phys. Rev. D*, **42**(10), 3267–3292 (1990).
4. G. R. Fowles, *Analytical Mechanics*, Third Edition, Holt, Rinehart, and Winston, New York, (1977), pp. 154–155.
5. T. Van Flandern, The Speed of Gravity—What the Experiments Say, *Physics Letters A*, **250**, 1–11 (1998).
6. R Cowen, Gamma-ray burst makes quite a bang, *Science News*, **153**(19), 292(1998).
7. M. Chown, The ultimate free lunch, *New Scientist*, **154**(2081), 50–51 (1997)/
8. B. Schwarzschild, Giant air shower array shows cosmic-ray spectrum violating greisen cutoff, *Physics Today*, **51**(10), 19–21 (1998).
9. J. C. Mather, E. S. Cheng, A preliminary measurement of the cosmic microwave background spectrum by the Cosmic Background Explorer (COBE) satellite, *Astrophysical Journal Letters*, **354**, L37–L40 (May 10, 1990).
10. W. Saunders, C. Frenk, et al; The density field of the local universe; *Nature*, **349**(6304), 32–38 (1991).
11. R. P. Kirshner, A. Oemler, Jr., P.L. Schechter, S.A. Shectman, A deep survey of galaxies, *Astronomical Journal*, **88**, 1285–1300 (September 1983).
12. V. de Lapparent, M.J. Geller, J.P. Huchra, The mean density and two-point correlation function for the CfA redshift survey slices, *Astrophysical Journal*, **332**(9) 44–56 (September 1, 1988).
13. A. Dressler, D. Lynden-Bell, D. Burstein, et. al., Spectroscopy and photometry of elliptical galaxies. I–A new distance estimator, *Astrophysical Journal*, **313**(2), 42–58 (1987).
14. S. Flamsteed, Crisis in the Cosmos, *Discover*, **16**(3), 66(1995).
15. J. Glanz, CO the early universe clouds cosmologists' views, *Science*, **273**(5275), 581 (1996).
16. S. D. Landy, Mapping the Universe, *Scientific American*, **280**(6), 38–45 (1999).
17. W.L. Freeman, et al., Distance to the Virgo cluster galaxy M100 from Hubble Space, *Nature*, **371**(6500), 757–762 (1994).
18. R. M. Wald, *General Relativity*, University of Chicago Press, Chicago, (1984), pp. 114–116.
19. P. J. E. Peebles, J. Silk, Joseph, A cosmic book of phenomena, *Nature*, **346**(6281), 233 (1990).
20. J. Glanz; Astronomers see a cosmic antigravity force at work, *Science*, **279**(5355), 1298–1299 (1998).
21. R. Cowen, Living with lambda, *Science News*, **153**(22), 344 (1998).
22. R. Cowen, Studies support an accelerating Universe, *Science News*, **154**(18), 277 (1998).
23. P. de Bernardi et al., A flat Universe from high-resolution maps of the cosmic microwave background radiation, *Nature*, Vol. 404, (2000), p. 955; <http://www.physics.ucsb.edu/~boomerang>.
24. A. Beiser, *Concepts of Modern Physics*, 4th Edition, McGraw-Hill Book Company, New York, (1978), 2–10.

THIS PAGE BLANK (USPTO)

The Grand Unified Theory of Classical Quantum Mechanics

Dr. Randell L. Mills
BlackLight Power, Inc.
493 Old Trenton Road
Cranbury, NJ 08512
609-490-1090
rmills@blacklightpower.com

Presented at
the Global Foundation, Inc.

The Role of Attractive and Repulsive Gravitational Forces
in Cosmic Acceleration of Particles

The Origin of the Cosmic Gamma Ray Bursts
(29th Conference)

on High Energy Physics and Cosmology Since 1964)

Ft. Lauderdale, FL

Lago Mar Resort

December 14-17, 2000

Dr. Behram Kursunoglu, Chairman

THIS PAGE BLANK (USPTO)

The Grand Unified Theory of Classical Quantum Mechanics

A theory of classical quantum mechanics (CQM) is derived from first principles that successfully applies physical laws on all scales. Using the classical wave equation with the constraint of nonradiation based on Maxwell's equations, CQM gives closed form solutions for the atom including the stability of the $n=1$ state and the instability of the excited states, the equation of the photon and electron in excited states, the equation of the free electron, and photon which predict the wave particle duality behavior of particles and light. The current and charge density functions of the electron may be directly physically interpreted. For example, spin angular momentum results from the motion of negatively charged mass moving systematically, and the equation for angular momentum, $\mathbf{r} \times \mathbf{p}$, can be applied directly to the wave function (a current density function) that describes the electron. The magnetic moment of a Bohr magneton, Stern Gerlach experiment, g factor, Lamb shift, resonant line width and shape, selection rules, correspondence principle, wave particle duality, excited states, reduced mass, rotational energies, and momenta, orbital and spin splitting, spin-orbital coupling, Knight shift, and spin-nuclear coupling are derived in closed form equations based on Maxwell's equations. The calculations agree with experimental observations.

For or any kind of wave advancing with limiting velocity and capable of transmitting signals, the equation of front propagation is the same as the equation for the front of a light wave. By applying this condition to electromagnetic and gravitational fields at particle production, the Schwarzschild metric (SM) is derived from the classical wave equation which modifies general relativity to include conservation of spacetime in addition to momentum and matter/energy. The result gives a natural relationship between Maxwell's equations, special relativity, and general relativity. It gives gravitation from the atom to the cosmos. The universe is time harmonically oscillatory in matter energy and spacetime expansion and contraction with a minimum radius that is the gravitational radius. In closed form equations with fundamental constants only, CQM gives the deflection of light by stars, the precession of the perihelion of Mercury, the particle masses, the Hubble constant, the age of the universe, the observed acceleration of the expansion, the power of the universe, the power spectrum of the universe, the microwave background temperature, the uniformity of the microwave background radiation, the microkelvin spatial variation of the microwave background radiation, the observed violation of the GZK cutoff, the mass density, the large scale structure of the universe, and the identity of dark matter which matches the criteria for the structure of galaxies. In a special case wherein the gravitational potential energy density of a blackhole equals that of the Plank mass, matter converts to energy and spacetime expands with the release of a gamma ray burst. The singularity in the SM is eliminated.

THIS PAGE BLANK (USPTO)

The Grand Unified Theory of Classical Quantum Mechanics

Dr. Randell L. Mills
 Blacklight Power, Inc.
 493 Old Trenton Road
 Cranbury, NJ 08512
 609-490-1090
 rmills@blacklightpower.com

Presented at
 the Global Foundation, Inc.
 The Role of Attractive and Repulsive Gravitational Forces
 In Cosmic Acceleration of Particles
 The Origin of the Cosmic Gamma Ray Bursts
 (29 th Conference on High Energy Physics and Cosmology Since 1964)
 Ft. Lauderdale, FL
 Lago Mar Resort
 December 14-17, 2000
 Dr. Behram Kursunoglu, Chairman

Wave Equation

$$\left[\nabla^2 - \frac{1}{v^2} \frac{\delta^2}{\delta t^2} \right] \rho(r, \theta, \phi, t) = 0$$

Boundary Constraint from Maxwell's Equations

For non-radiative states, the current-density function must NOT possess spacetime Fourier components that are synchronous with waves traveling at the speed of light.

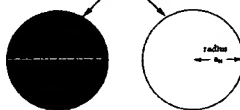
The solution for the radial function which satisfies the boundary condition is a delta function

$$f(r) = \frac{1}{r^2} \delta(r - r_n)$$

where $r_n = nr_1$

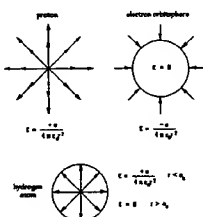
The Orbitosphere

The orbitosphere has zero thickness.
 It is a two-dimensional surface.



The orbitosphere is a two dimensional spherical shell with the Bohr radius of the hydrogen atom.

Electric Fields of Proton, Electron, and Hydrogen Atom



The Wavelength of the Free Electron

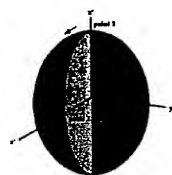
$$\lambda_n = \frac{\hbar}{p_n} = \frac{\hbar}{m_e v_n}$$

$$v_n = \frac{\hbar}{m_e r_n}$$

$$\sum |L_i| = \sum |\mathbf{r} \times m_i \mathbf{v}| = m_e r_n \frac{\hbar}{m_e r_n} = \hbar$$

the de Broglie wavelength is observed for the electron

Spin Function



Two infinitesimal point masses (charges) of two orthogonal great circle current loops in the orbitsphere frame.

Time Dependence of Representative Point of Each Great Circle Current Loop

point one:

$$\dot{x}_1 = 0 \quad \dot{y}_1 = -r_n \sin(\omega_n t) \quad \dot{z}_1 = r_n \cos(\omega_n t)$$

point two:

$$\dot{x}_2 = r_n \cos(\omega_n t) \quad \dot{y}_2 = 0 \quad \dot{z}_2 = r_n \sin(\omega_n t)$$

Nested Series of Great Circle Current Loops

point one:

$$\begin{bmatrix} x_1 \\ y_1 \\ z_1 \end{bmatrix} = \begin{bmatrix} \cos(\Delta\alpha) & -\sin^2(\Delta\alpha) & -\sin(\Delta\alpha)\cos(\Delta\alpha) \\ 0 & \cos(\Delta\alpha) & -\sin(\Delta\alpha) \\ \sin(\Delta\alpha) & \cos(\Delta\alpha)\sin(\Delta\alpha) & \cos^2(\Delta\alpha) \end{bmatrix} \begin{bmatrix} \dot{x}_1 \\ \dot{y}_1 \\ \dot{z}_1 \end{bmatrix}$$

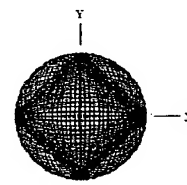
and $\Delta\alpha = -\Delta\alpha$ replaces $\Delta\alpha$ for $\sum_{n=1}^{\infty} \Delta\alpha = \sqrt{2}\pi$; $\sum_{n=1}^{\infty} |\Delta\alpha| = \sqrt{2}\pi$

point two:

$$\begin{bmatrix} x_2 \\ y_2 \\ z_2 \end{bmatrix} = \begin{bmatrix} \cos(\Delta\alpha) & -\sin^2(\Delta\alpha) & -\sin(\Delta\alpha)\cos(\Delta\alpha) \\ 0 & \cos(\Delta\alpha) & -\sin(\Delta\alpha) \\ \sin(\Delta\alpha) & \cos(\Delta\alpha)\sin(\Delta\alpha) & \cos^2(\Delta\alpha) \end{bmatrix} \begin{bmatrix} \dot{x}_2 \\ \dot{y}_2 \\ \dot{z}_2 \end{bmatrix}$$

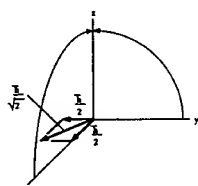
and $\Delta\alpha = -\Delta\alpha$ replaces $\Delta\alpha$ for $\sum_{n=1}^{\infty} \Delta\alpha = \sqrt{2}\pi$; $\sum_{n=1}^{\infty} |\Delta\alpha| = \sqrt{2}\pi$

Current Pattern of the Orbitsphere

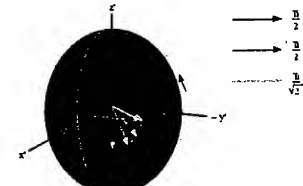


VIEW ALONG THE Z AXIS

Resultant Angular Momentum Vector



Projection of the Resultant Angular Momentum Vector over the Orbitsphere



Stern-Gerlach Experiment

Spin Quantum Number, $s \left(z = \frac{1}{2}; m_s = \pm \frac{1}{2} \right)$

$$\sum_{\alpha=1}^{\infty} \Delta \alpha = \sqrt{2}\pi$$

$$\langle L_z \rangle_{z \text{ axis}} = \frac{1}{2} \frac{\hbar}{\sqrt{2}} \frac{1}{\sqrt{2}} = \frac{\hbar}{4}$$

$$\langle L_z \rangle_{z \text{ axis}} = \frac{1}{2} \frac{\hbar}{\sqrt{2}} \frac{1}{\sqrt{2}} = \frac{\hbar}{4}$$

$$\sum_{\alpha=1}^{\infty} |\Delta \alpha| = \sqrt{2}\pi$$

$$\langle L_z \rangle_{z \text{ axis}} = 0$$

$$\langle L_z \rangle_{z \text{ axis}} = \frac{1}{2} \frac{\hbar}{\sqrt{2}} \frac{1}{\sqrt{2}} = \frac{\hbar}{4}$$

Total Component Angular Momentum

$$\langle L_z \rangle_{\Sigma \Delta \alpha} = \frac{\hbar}{4} + 0 = \frac{\hbar}{4}$$

$$\langle L_z \rangle_{\Sigma \Delta \alpha} = \frac{\hbar}{4} + \frac{\hbar}{4} = \frac{\hbar}{2}$$

Projection of the Angular Momentum onto a Vector S that Precesses about the Z-Axis

S the projection of the orbitsphere angular momentum that precesses about the z-axis called the spin axis at an angle of $\theta = \frac{\pi}{3}$ and an angle of $\phi = \pi$ with respect to $\langle L_z \rangle_{\Sigma \Delta \alpha}$ is

$$S = \pm \frac{\sqrt{3}}{4} \hbar$$

S rotates about the z-axis at the Larmor frequency

$\langle S_z \rangle$, the time averaged projection of the orbitsphere angular momentum onto the axis of the applied magnetic field is

$$\langle S_z \rangle_{\Sigma \Delta \alpha} = \pm \frac{\hbar}{2}$$

Electron g Factor

Conservation of angular momentum of the orbitsphere permits a discrete change of its "kinetic angular momentum" ($r \times mv$) by the the applied magnetic field of $\frac{\hbar}{2}$, and concomitantly the "potential angular momentum" ($r \times eA$) must change by $\frac{\hbar}{2}$.

$$\begin{aligned} \Delta L &= \frac{\hbar}{2} - r \times eA \\ &= \frac{\hbar}{2} - \frac{e\phi}{2\pi} \end{aligned}$$

In order that the change of angular momentum, ΔL , equals zero, ϕ must be $\Phi_0 = \frac{\hbar}{2e}$, the magnetic flux quantum.

Electron g Factor cont'd

The magnetic moment of the electron is parallel or antiparallel to the applied field only.

The total energy of the flip transition is the sum of the energy of a fluxon braiding the orbitsphere and the energy of reorientation of the magnetic moment.

$$\Delta E_{\text{mag}}^{\text{flip}} = \frac{1}{2} (\mu_s B + \frac{\alpha}{2\pi} \mu_p B)$$

$$\Delta E_{\text{mag}}^{\text{flip}} = 2(1 + \frac{\alpha}{2\pi}) \mu_s B$$

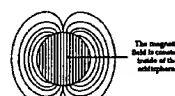
$$\Delta E_{\text{mag}}^{\text{flip}} = 2g \mu_s B$$

The spin-flip transition can be considered as involving a magnetic moment of g times that of a bohr magneton. The predicted value of the g factor is 1.00116. The experimental value is 1.00116.

Magnetic Fields of the Electron

$$\mathbf{H} = \frac{e\hbar}{m_e r_a^2} (I_x \cos \theta - I_y \sin \theta) \quad \text{for } r < r_a$$

$$\mathbf{H} = \frac{e\hbar}{2m_e r^2} (I_x 2 \cos \theta - I_y \sin \theta) \quad \text{for } r > r_a$$



Derivation of the Magnetic Energy

The energy stored in the magnetic field of the electron is

$$E_{mag} = \frac{1}{2} \mu_0 \int_0^{2\pi} \int_0^{\pi} \int_0^{\infty} H^2 r^2 \sin \theta dr d\theta d\phi$$

$$E_{mag \text{ total}} = \frac{\pi \mu_0 e^2 \hbar^2}{m_e^2 r_i^3}$$

Angular Functions

Based on the radial solution, the angular charge and current-density functions of the electron, $A(\theta, \phi, t)$, must be a solution of the wave equation in two dimensions (plus time),

$$\left[\nabla^2 - \frac{1}{v^2} \frac{\partial^2}{\partial t^2} \right] A(\theta, \phi, t) = 0$$

$$\text{where } \rho(r, \theta, \phi, t) = f(r) A(\theta, \phi, t) = \frac{1}{r^2} \delta(r - r_i) A(\theta, \phi, t)$$

$$\text{and } A(\theta, \phi, t) = Y(\theta, \phi) \zeta(t)$$

$$\left[\frac{1}{r^2 \sin \theta} \frac{\partial}{\partial \theta} \left(\frac{\sin \theta}{\partial \theta} \right)_{,r} + \frac{1}{r^2 \sin^2 \theta} \frac{\partial}{\partial \phi^2} \right]_{,r} - \frac{1}{v^2} \frac{\partial^2}{\partial t^2} A(\theta, \phi, t) = 0$$

where v is the linear velocity of the electron

Charge-Density Functions

The charge-density functions including the time-function factor are

$$\ell = 0 \\ \rho(r, \theta, \phi, t) = \frac{e}{8\pi r^2} [\delta(r - r_i) [Y_0^0(\theta, \phi) + Y_0^0(\theta, \phi)]]$$

$$\ell \neq 0 \\ \rho(r, \theta, \phi, t) = \frac{e}{4\pi r^2} [\delta(r - r_i) [Y_m^0(\theta, \phi) + \text{Re}[Y_m^m(\theta, \phi)[1 + e^{i\omega t}]]]]$$

where

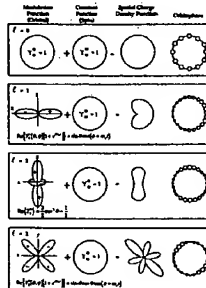
$$\text{Re}[Y_m^m(\theta, \phi)[1 + e^{i\omega t}]] = \text{Re}[Y_m^m(\theta, \phi) + Y_m^m(\theta, \phi)e^{i\omega t}] = P_m^m(\cos \theta) \cos m\phi + Q_m^m(\cos \theta) \cos(m\phi + \omega_t t)$$

and $\omega_t = 0$ for $m = 0$

Spin and Orbital Parameters

- The constant spin function is modulated by a time and spherical harmonic function.
- The modulation or traveling charge density wave corresponds to an orbital angular momentum in addition to a spin angular momentum.
- These states are typically referred to as p, d, f, etc. states or orbitals and correspond to an ℓ quantum number not equal to zero.

Orbital and Spin Functions

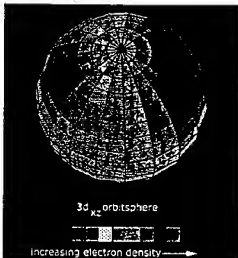


The orbital function modulates the constant (spin) function. (shown for $t=0$; cross-sectional view)

Charge Density Wave Moves on the Surface About the Z-Axis



Charge Density Wave Moves on the Surface About the Z-Axis



Moment of Inertia and Spin and Rotational Energies

$$\ell = 0$$

$$I_0 = I_{\text{spin}} = \frac{m_e r_e^2}{2}$$

$$L_z = I_0 \omega_z = \frac{\hbar}{2}$$

$$E_{\text{rotational}} = E_{\text{rotational, spin}} = \frac{1}{2} \left[I_{\text{spin}} \left(\frac{\hbar}{m_e r_e^2} \right)^2 \right] = \frac{1}{2} \left[\frac{m_e r_e^2}{2} \left(\frac{\hbar}{m_e r_e^2} \right)^2 \right] = \frac{1}{4} \left[\frac{\hbar^2}{2 m_e r_e^2} \right]$$

Moment of Inertia and Spin and Rotational Energies cont'd

$$\ell \neq 0$$

$$I_{\text{orbital}} = m_e r_e^2 \left[\frac{\ell(\ell+1)}{\ell^2 + \ell + 1} \right]^{\frac{1}{2}}$$

$$L_z = m\hbar$$

$$E_{\text{rotational, orbital}} = \frac{\hbar^2}{2I} \left[\frac{\ell(\ell+1)}{\ell^2 + 2\ell + 1} \right]$$

$$T = \frac{\hbar^2}{2m_e r_e^2}$$

$$\langle E_{\text{rotational, orbital}} \rangle = 0$$

Nonradiation Condition (Acceleration Without Radiation)

$$X(v, \theta, \Phi, \omega) = 4\pi v \frac{\sin(2v, \epsilon_c)}{2r_e r_i} \otimes 2\pi \sum_{n=1}^{\infty} \frac{(-1)^{n-1} (\pi \sin \theta)^{n-1}}{(v-1)(v-1)!} \frac{\Gamma\left(\frac{1}{2}\right)\Gamma\left(\frac{v+1}{2}\right)}{(\pi \cos \theta)^{n-1} 2^{n-1} (v-1)!}$$

$$\otimes 2\pi \sum_{n=1}^{\infty} \frac{(-1)^{n-1} (\pi \sin \theta)^{n-1}}{(v-1)(v-1)!} \frac{\Gamma\left(\frac{1}{2}\right)\Gamma\left(\frac{v+1}{2}\right)}{(\pi \cos \theta)^{n-1} 2^{n-1} (v-1)!} \frac{2v!}{4\pi} e^{-2v} \frac{1}{4\pi} [\delta(\omega - \omega_r) + \delta(\omega + \omega_r)]$$

$$s_v * v_n = s_v * c = \alpha_v$$

$$r_v = \lambda_v$$

Spacetime harmonics of $\frac{\partial v}{c} = k$ or $\frac{\partial v}{c} \sqrt{\frac{E}{\epsilon_c}} = k$ for which the Fourier transform of the current-density function is nonzero do not exist. Radiation due to charge motion does not occur in any medium when this boundary condition is met.

Force Balance Equation

$$\frac{m_e v_1^2}{4\pi r_1^2} = \frac{e}{4\pi r_1^2} \frac{Ze}{4\pi \epsilon_o r_1^2} - \frac{1}{4\pi r_1^2} \frac{\hbar^2}{mr_1^3}$$

$$r_1 = \frac{a_H}{Z}$$

Energy Calculations

Potential Energy

$$V = \frac{-Ze^2}{4\pi \epsilon_o r_1} = \frac{-Z^2 e^2}{4\pi \epsilon_o a_H} = -Z^2 X 4.3675 X 10^{-11} J = -Z^2 X 27.2 eV$$

Kinetic Energy

$$T = \frac{Z^2 e^2}{8\pi \epsilon_o a_H} = Z^2 X 13.59 eV \quad T = E_{ele} = -\frac{1}{2} \epsilon_o \int \mathbf{E}^2 d\mathbf{v}$$

where $\mathbf{E} = -\frac{Ze}{4\pi \epsilon_o r^2}$

Electric Energy

$$E_{ele} = -\frac{Z^2 e^2}{8\pi \epsilon_o a_H} = -Z^2 X 2.1786 X 10^{-11} J = -Z^2 X 13.598 eV$$

Some Calculated Parameters for the Hydrogen Atom (n=1)

radius	$r_1 = a_0$	$5.2918 \times 10^{-11} \text{ m}$
potential energy	$V = \frac{-e^2}{4\pi\epsilon_0 r_1}$	-27.196 eV
kinetic energy	$T = \frac{1}{2}mv_1^2$	13.598 eV
angular velocity (spin)	$\omega_1 = \frac{\hbar}{mr_1^2}$	$4.13 \times 10^{15} \text{ rad/s}$
linear velocity	$v_1 = r_1\omega_1$	$2.19 \times 10^6 \text{ m/s}$
wavelength	$\lambda_1 = 2\pi r_1$	$3.225 \times 10^{-10} \text{ m}$
spin quantum number	$m = \frac{1}{2}$	$\frac{1}{2}$
moment of inertia	$I = mr_1^2(\sqrt{\omega_1})^2$	$2.309 \times 10^{-40} \text{ kgm}^2$
angular kinetic energy	$E_{\text{spin}} = \frac{1}{2}I\omega_1^2$	11.78 eV

Some Calculated Parameters for the Hydrogen Atom (n=1) cont'd

magnitude of the angular momentum	\hbar	$1.0545 \times 10^{-34} \text{ Js}$
projection of the angular momentum onto the S-axis	$S_z = \hbar\sqrt{x(x+1)}$	$9.133 \times 10^{-35} \text{ Js}$
projection of the angular momentum onto the Z-axis	$S_z = \frac{\hbar}{2}$	$5.275 \times 10^{-35} \text{ Js}$
mass density	$\frac{m}{4\pi r_1^3}$	$2.589 \times 10^{-31} \text{ kgm}^{-3}$
charge-density	$\frac{e}{4\pi r_1^2}$	4.553 Cm^{-2}

Calculated Energies (Non-Relativistic) and Calculated Ionization Energies for Some One-electron Atoms

Atom	Calculated a_0 (Å)	Calculated Kinetic Energy (eV)	Calculated Potential Energy (eV)	Calculated Ionization Energy (eV)	Experimental Ionization Energy (eV)
H	1.000	13.59	-47.18	13.59	13.59
H ⁺	0.630	54.33	-108.70	54.33	54.33
Li ⁺	0.533	122.23	-244.56	122.23	122.43
B ⁺	0.450	217.40	-436.80	217.40	217.71
F ⁺	0.300	339.68	-679.38	339.68	340.22
C ⁺	0.187	489.14	-787.28	489.14	489.90
P ⁺	0.143	685.77	-1321.04	685.77	687.00
O ⁺	0.125	848.58	-1738.16	848.58	871.38

Excited States

- The orbitsphere is a dynamic spherical resonator cavity which traps photons of discrete frequencies.
- The relationship between an allowed radius and the "photon standing wave" wavelength is $2\pi r = n\lambda$ where n is an integer.
- The relationship between an allowed radius and the electron wavelength is $2\pi r = n\lambda_e$ where $n=1, 2, 3, 4, \dots$
- The radius of an orbitsphere increases with the absorption of electromagnetic energy.
- The solutions to Maxwell's equations for modes that can be excited in the orbitsphere resonator cavity give rise to four quantum numbers, and the energies of the modes are the experimentally known hydrogen spectrum.

Excited States cont'd

The relationship between the electric field equation and the "trapped photon" source charge-density function is given by Maxwell's equation in two dimensions

$$n(E_x - E_y) = \frac{\sigma}{\epsilon_0}$$

The photon standing electromagnetic wave is phase matched to with the electron

$$E_{\text{resonant}} = \frac{4\pi\lambda^2}{4\pi\epsilon_0 c^2} \left[-E_x(k, r) + \frac{1}{2} [E_x(k, r) + E_y(k, r)] [E_x(k, r) + E_y(k, r)] \right]$$

$$\frac{1}{2} E_x(k, r) + E_y(k, r) = 0$$

$$E_{\text{resonant}} = \frac{4\pi\lambda^2}{4\pi\epsilon_0 c^2} \left[-E_x(k, r) + \frac{1}{2} [E_x(k, r) + E_y(k, r)] [E_x(k, r) + E_y(k, r)] \right]$$

$$E_{\text{resonant}} = \frac{4\pi\lambda^2}{4\pi\epsilon_0 c^2} \left[-E_x(k, r) + \frac{1}{2} [E_x(k, r) + E_y(k, r)] [E_x(k, r) + E_y(k, r)] \right]$$

For $r=n a_0$ and $m=0$, the total radial electric field is

$$E_{\text{resonant}} = \frac{1}{4\pi\epsilon_0 c^2}$$

Photon Absorption

- The energy of the photon which excites a mode in the electron spherical resonator cavity from radius a_0 to radius na_0 is

$$E_{\text{photon}} = \frac{\sigma^2}{8\pi\epsilon_0 c^2} \left[\frac{1}{a_0} - \frac{1}{na_0} \right] \Delta\nu = \hbar\nu$$
- The change in angular velocity of the orbitsphere for an excitation from $n=1$ to n is

$$\Delta\omega = \frac{n}{(na_0)^2} - \frac{1}{a_0^2} = \frac{n}{(na_0)^2} \left[1 - \frac{1}{n^2} \right]$$
- The kinetic energy change of the transition is

$$\frac{1}{2} m_e (\Delta\nu)^2 = \frac{\sigma^2}{8\pi\epsilon_0 c^2} \left[1 - \frac{1}{n^2} \right] = \hbar\nu_{\text{photon}}$$
- The change in angular velocity of the electron orbitsphere is identical to the angular velocity of the photon necessary for the excitation, ω_{photon}
- The correspondence principle holds

Orbital and Spin Splitting

The ratio of the square of the angular momentum, M^2 , to the square of the energy, E^2 , for a pure (l, m) multipole

$$\frac{M^2}{E^2} = \frac{m^2}{\omega^2}$$

The magnetic moment is defined as $\mu = \frac{\text{charge} \times \text{angular momentum}}{2 \times \text{mass}}$

The radiation of a multipole of order (l, m) carries $m\hbar$ units of the z component of angular momentum per photon of energy $\hbar\omega$. Thus, the z component of the angular momentum of the corresponding excited state electron orbitalsphere is $L_z = m\hbar$

Therefore, $\mu_s = \frac{e m \hbar}{2 m_e} = m \mu_B$ where μ_B is the Bohr magneton.

The orbital splitting energy is

$$E_{\text{split}} = m \mu_B B$$

Orbital and Spin Splitting cont'd

The spin and orbital splitting energies superimpose; thus, the principal excited state energy levels of the hydrogen atom are split by the energy $E_{\text{split}}^{orb+sp}$

$$E_{\text{split}}^{orb+sp} = m \frac{e\hbar}{2m_e} B + m_s g \frac{e\hbar}{m_e} B$$

where

$$n = 2, 3, 4, \dots$$

$$\ell = 1, 2, \dots, n-1$$

$$m = -\ell, -\ell+1, \dots, 0, \dots, +\ell$$

$$m_s = +\frac{1}{2}$$

Selection Rules for the Electric Dipole Transition

$$\Delta m = 0, \pm 1$$

$$\Delta m_s = 0$$

Resonant Line Shape

$$\frac{1}{\tau} = \frac{\text{power}}{\text{energy}} = \frac{\left[\frac{2\pi}{[(2l+1)\hbar]} \right] \left(\frac{(-1)^{2l+1}}{l+1} (2l+1) \right)^2}{[\hbar\omega]} = 2\pi \left(\frac{c^2}{\lambda} \right) \frac{2\pi}{\hbar} \frac{(-1)^{2l+1}}{[(2l+1)\hbar]} \left(\frac{l+1}{l} \right)^2 \left(\frac{3}{l+3} \right)^2 (4m_e)^2 =$$

$$E(\omega) = \int e^{-\alpha t} e^{-i\omega t} dt = \frac{1}{\alpha - i\omega}$$

The relationship between the rise-time and the bandwidth for exponential decay is

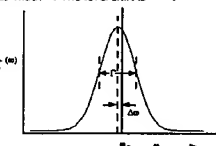
$$\tau^2 = \frac{1}{\alpha}$$

The energy radiated per unit frequency interval is

$$\frac{dE(\omega)}{d\omega} = \frac{1}{2\pi} \frac{1}{(\omega - \omega_0 - \Delta\omega)^2 + (\Gamma/2)^2}$$

Broadening of the Spectral Line and the Radiative Reaction

Broadening of the spectral line due to the rise-time and shifting of the spectral line due to the radiative reaction. The resonant line shape has width Γ . The level shift is $\Delta\omega$.



Lamb Shift

The Lamb Shift of the $^3P_{1/2}$ state of the hydrogen atom is due to conservation of linear momentum of the electron, atom, and photon.

Electron Component

$$\Delta' = \frac{\Delta\sigma}{2\pi} = \frac{E_{\text{in}}}{\hbar} = 3 \frac{(E_{\text{in}})^2}{\hbar 2m_e c^2} = 1052 \text{ MHz}$$

where E_{in} is

$$E_{\text{in}} = 13.6 \left(1 - \frac{1}{n^2} \right) \frac{1}{[X_m]_{l=1}} - \Delta\omega$$

$$E_{\text{in}} = 13.6 \left(1 - \frac{1}{n^2} \right) \frac{3}{8\pi} - \Delta\omega;$$

$$\Delta\omega \ll \ll 1$$

$$\therefore E_{\text{in}} = 13.6 \left(1 - \frac{1}{n^2} \right) \frac{3}{8\pi}$$

Lamb Shift cont'd

Atom Component

$$\Delta' = \frac{\Delta\sigma}{2\pi} = \frac{E_{\text{in}}}{\hbar} = \frac{1}{2} \frac{(E_{\text{in}})^2}{2m_e c^2} = 6.5 \text{ MHz}$$

Sum of the Components

$$\Delta\omega = 1052 \text{ MHz} + 6.5 \text{ MHz} = 1058.5 \text{ MHz}$$

The experimental Lamb Shift is 1058 MHz.

Instability of Excited States

$n = 2, 3, 4, \dots$

$$\sigma_{\text{photon}} = \frac{e}{4\pi(r_s)^2} \left[Y_0^0(\theta, \phi) - \frac{1}{n} \left[Y_0^0(\theta, \phi) + Y_n^m(\theta, \phi) R e^{i[m\phi]} \right] \right] \delta(r - r_s)$$

$$\sigma_{\text{electron}} = \frac{-e}{4\pi(r_s)^2} \left[Y_0^0(\theta, \phi) + Y_n^m(\theta, \phi) R e^{i[m\phi]} \right] \delta(r - r_s)$$

$$\sigma_{\text{photon}} + \sigma_{\text{electron}} = \frac{e}{4\pi(r_s)^2}$$

$$\left[Y_0^0(\theta, \phi) \delta(r - r_s) - \frac{1}{n} Y_0^0(\theta, \phi) \delta(r - r_s) - \left(1 + \frac{1}{n} \right) Y_n^m(\theta, \phi) R e^{i[m\phi]} \delta(r - r_s) \right]$$

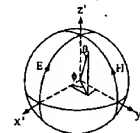
Excited states are radiative since spacetime harmonics of $\frac{\omega}{c} = 1$ or $\frac{\omega}{c} \neq 1$ do exist for which the spacetime Fourier transform of the current density function is nonzero.

Photon Equations

The time-averaged angular-momentum density, m , of the emitted photon is

$$m = \frac{e}{8\pi} R d[r \times (E \times B^*)] = \Lambda$$

The Cartesian coordinate system wherein the first great circle magnetic field line lies in the yz -plane, and the second great circle electric field line lies in the xz -plane is designated the photon orbitsphere reference frame of a photon orbitsphere.



Nested Set of Great Circle Field Lines Generates the Photon Function

H Field:

$$\begin{bmatrix} x_1 \\ y_1 \\ z_1 \end{bmatrix} = \begin{bmatrix} \cos(\Delta\alpha) & -\sin^2(\Delta\alpha) & -\sin(\Delta\alpha)\cos(\Delta\alpha) \\ 0 & \cos(\Delta\alpha) & -\sin(\Delta\alpha) \\ \sin(\Delta\alpha) & \cos(\Delta\alpha)\sin(\Delta\alpha) & \cos^2(\Delta\alpha) \end{bmatrix} \begin{bmatrix} x_1 \\ y_1 \\ z_1 \end{bmatrix}$$

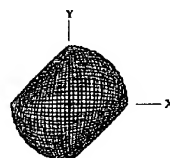
and $\Delta\alpha = -\Delta\alpha$ replaces $\Delta\alpha$ for $\sum_{i=1}^n \Delta\alpha = \sqrt{2}\pi$; $\sum_i |\Delta\alpha| = \sqrt{2}\pi$

E Field:

$$\begin{bmatrix} x_2 \\ y_2 \\ z_2 \end{bmatrix} = \begin{bmatrix} \cos(\Delta\alpha) & -\sin^2(\Delta\alpha) & -\sin(\Delta\alpha)\cos(\Delta\alpha) \\ 0 & \cos(\Delta\alpha) & -\sin(\Delta\alpha) \\ \sin(\Delta\alpha) & \cos(\Delta\alpha)\sin(\Delta\alpha) & \cos^2(\Delta\alpha) \end{bmatrix} \begin{bmatrix} x_2 \\ y_2 \\ z_2 \end{bmatrix}$$

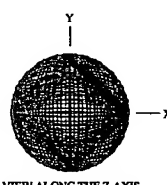
and $\Delta\alpha = -\Delta\alpha$ replaces $\Delta\alpha$ for $\sum_{i=1}^n \Delta\alpha = -\sqrt{2}\pi$; $\sum_i |\Delta\alpha| = \sqrt{2}\pi$

The Field Line Pattern from the Perspective of Looking along the Z-Axis of a Right-Handed Circularly-Polarized Photon



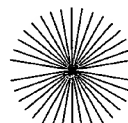
VIEW ALONG THE Z AXIS

The Field Line Pattern from the Perspective of Looking along the Z-Axis of a Linearly-Polarized Photon

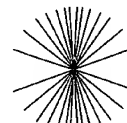


VIEW ALONG THE Z AXIS

Electric Field of a Moving Point Charge $v = 1/3c$



Electric Field of a Moving Point Charge $v = 4/5c$



The Photon Equation in the Lab Frame of a Right-Handed Circularly-Polarized Photon Orbitsphere

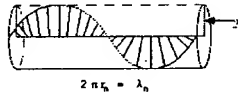
$$\mathbf{E} = \mathbf{E}_0 [x + iy] e^{-\mu z} e^{-j\omega t}$$

$$\mathbf{H} = \left(\frac{\mathbf{E}_0}{\eta} \right) [y - ix] e^{-\mu z} e^{-j\omega t} = \mathbf{E}_0 \sqrt{\frac{\epsilon}{\mu}} [y - ix] e^{-\mu z} e^{-j\omega t}$$

with a wavelength of $\lambda = 2\pi \frac{c}{\omega}$

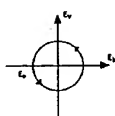
The relationship between the photon orbitsphere radius and wavelength is $2\pi r_0 = \lambda_n$.

The Electric Field Lines of a Right-Handed Circularly-Polarized Photon Orbitsphere



The electric field lines of a right-handed circularly polarized photon orbitsphere as seen along the axis of propagation in the lab inertial reference frame as it passes a fixed point.

The Electric Field Rotation



The electric field rotation of a right-handed circularly polarized photon orbitsphere as seen transverse to the axis of propagation in the lab inertial reference frame as it passes a fixed point.

Elliptically Polarized Photons

Magnitude of the magnetic and electric field lines vary as a function of angular position (ϕ, θ) on the orbitsphere.

$$B_{\phi,\theta} = \frac{e}{4\pi c r_0^2} \left(-1 + \frac{1}{n} [1^2 f(\theta, \phi) + \text{Re}\{Y_l^m(\theta, \phi)[1 + e^{j\Delta\phi}]\}] \right) \delta(r - \frac{\lambda}{2\pi});$$

$$a_s = 0 \quad \text{for } m = n$$

r_0 is the radius of the photon orbitsphere which is equal to $\Delta n a_0$, the change in electron orbitsphere radius.

λ is the photon wavelength which is equal to $\Delta \lambda \frac{c}{\Delta v}$, where $\Delta \lambda$ is the change in orbitsphere de Broglie wavelength and Δv is the change in velocity of the orbitsphere.

$\omega = \frac{2\pi}{\lambda}$ is the photon angular velocity which is equal to $\Delta\omega$, the change in orbitsphere angular velocity.

Spherical Wave

Photons superimpose, and the amplitude due to N photons is

$$E_{\text{sph}} = \sum_{n=1}^N \frac{e^{-j\Delta\phi - j\theta}}{4\pi r} f(\theta, \phi)$$

In the far field, the emitted wave is a spherical wave

$$E_{\text{sph}} = E_0 \frac{e^{-j\omega t}}{r}$$

- The Green Function is given as the solution of the wave equation. Thus, the superposition of photons gives the classical result.
- As r goes to infinity, the spherical wave becomes a plane wave.
- The double slit interference pattern is predicted.
- From the equation of a photon, the wave-particle duality arises naturally.
- The energy is always given by Planck's equation; yet, an interference pattern is observed when photons add over time or space.

Equations of the Free Electron

Mass Density Function of a Free Electron is a two dimensional disk having the mass density distribution in the $xy(\rho)$ -plane

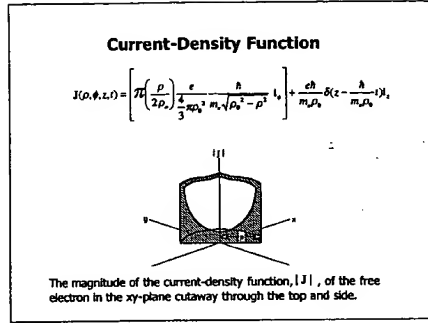
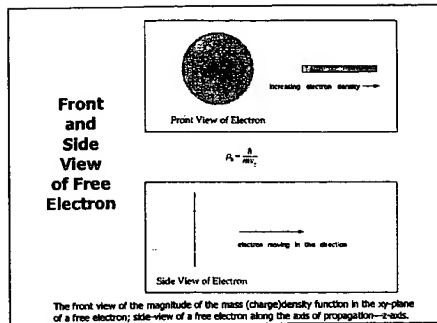
$$\rho_e(\rho, \phi, z) = \frac{m_e}{2} \pi \rho_0^2 \left(\frac{\rho}{2\rho_0} \right) \sqrt{\rho_0^2 - \rho^2} \delta(z)$$

Charge Density Distribution, $\rho_e(\rho, \phi, z)$, in the xy -plane

$$\rho_e(\rho, \phi, z) = \frac{e}{2} \pi \rho_0^3 \left(\frac{\rho}{2\rho_0} \right) \sqrt{\rho_0^2 - \rho^2} \delta(z)$$

The wave-particle duality arises naturally.

Consistent with scattering experiments.



Angular Momentum

$$\mathbf{L}\mathbf{L}_z = \int_0^{2\pi} \int_0^\infty \pi \left(\frac{\rho}{2\rho_0} \right)^2 \frac{m_e}{3\pi\rho_0^3 m_e \sqrt{\rho_0^2 - \rho^2}} \rho^2 \rho d\rho d\phi$$

$$\mathbf{L}\mathbf{L}_z = \hbar$$

Nonradiation Condition

$$\frac{e}{3\pi\rho_0^2 m_e} \frac{\hbar}{2} \sin(2\pi\rho_0 z) + 2\pi \frac{\hbar}{m_e \rho_0} \delta(\omega - \mathbf{k}_z \cdot \mathbf{v}_z)$$

$$I_{1z} = \sin(2\pi\rho_0 z) \frac{\sin 2\pi\rho_0 z}{2\pi\rho_0}$$

$$2\pi\rho_0 = \lambda_0$$

Consider the radial wave vector of the sinc function, when the radial projection of the velocity is c

$$z = v_z t = c t$$

The relativistically corrected wavelength is

$$\tilde{\lambda}_0 = \lambda_0$$

$$\lambda_0 = \frac{\hbar}{m_e V_0} = 2\pi\rho_0$$

Stern-Gerlach Experiment

$$\mathbf{L}_x = \mathbf{L}_z = \hbar \frac{1}{\sqrt{2}} \frac{1}{\sqrt{2}} = \frac{\hbar}{2}$$

$$\langle \mathbf{L}_x \rangle = \frac{\hbar}{2}$$

$$\langle \mathbf{L}_x \rangle_{\text{ave}}^2 + S^2 = \hbar^2$$

$$S = \sqrt{\left(1 - \frac{1}{4}\right)\hbar^2} = \pm \sqrt{\frac{3}{4}}\hbar$$

S rotates about the z -axis; thus, $\langle S_z \rangle$, the time averaged projection of the angular momentum onto the axis of the applied magnetic field is $\pm \frac{\hbar}{2}$.

Two Electron Atoms

Central Force Balance Equation with Nonradiation Condition

$$\frac{m_e v_z^2}{4\mu_2^2 r_2^2} = \frac{e}{4m_e^2} \frac{(Z-1)s}{4\pi\varepsilon_0^2 r_2^2} + \frac{1}{4m_e^2} \frac{\hbar^2}{2m_e r_2^2} \sqrt{s(s+1)}$$

$$r_2 = r_1 = a \left(\frac{1}{Z-1} - \frac{\sqrt{s(s+1)}}{2(Z-1)} \right); s = \frac{1}{2}$$

Two Electron Atoms cont'd

Ionization Energies Calculated Using the Poynting Power Theorem

For helium, which has no electric field beyond r_1 ,

$$\text{Ionization Energy}(He) = -E(\text{electric}) + E(\text{magnetic})$$

$$\text{where } E(\text{electric}) = -\frac{(Z-1)^2}{8\pi r_1^2}$$

$$E(\text{magnetic}) = \frac{2\pi r_1 e^2 h}{m_e^2 r_1^2}$$

Where

For $3 \leq Z$

$$\text{Ionization Energy} = -\text{Electric Energy} - \frac{1}{Z} \text{Magnetic Energy}$$

The Calculated Energies for Some Two-Electron Atoms

Atom	r_1 (\AA)	Electric Energy (eV)	Magnetic Energy (eV)	Calculated Ionization Energy(eV)	Experimental Ionization Energy (eV)
He	0.567	-25.99	0.93	24.06	24.06
Li^+	0.359	-76.41	2.34	73.59	73.64
Be^{2+}	0.261	-186.06	8.42	184.16	185.00
B^{3+}	0.107	-282.84	12.86	280.33	280.37
C^{4+}	0.171	-386.96	22.82	383.16	382.09
N^{5+}	0.146	-554.20	36.74	557.46	552.09
O^{6+}	0.127	-740.89	53.35	739.67	739.32
F^{7+}	0.113	-982.17	78.37	982.33	982.39

The Calculated Energies for Some Two-Electron Atoms cont'd

Atom	r_1 (\AA)	Density Ionization Energy (eV)	Universal Ionization Energy (eV)	Calculated Ionization Energy(eV)	Universal Ionization Energy (eV)
H^{1+}	0.101	-184.0	108.4	112.4	116.00
H^{2+}	0.083	-149.6	108.4	140.2	148.14
H^{3+}	0.060	-117.0	107.7	117.0	178.00
H^{4+}	0.077	-198.2	108.3	207.7	208.00
H^{5+}	0.072	-247.0	90.6	942.0	1497.70
H^{6+}	0.070	-308.0	97.0	300.0	517.00
H^{7+}	0.067	-400.0	98.4	984.0	988.00
C^{4+}	0.100	-546.0	108.3	502.0	508.00
A^{5+}	0.080	-715.0	91.0	600.0	112.00
F^{7+}	0.060	-1072.0	70.7	4772.0	4611.11

* from standard tables for low $\lambda/\lambda_0 < 10^{-4}$

Elastic Electron Scattering from Helium Atoms

Aperture distribution function, $a(\rho, \theta, z)$, for the scattering of an incident electron plane wave $\Pi(z)$

by the He atom

$$\frac{2}{4\pi(0.567a_e)} |\delta(r - 0.567a_e)|$$

is

$$a(\rho, \theta, z) = \Pi(z) \otimes \frac{2}{4\pi(0.567a_e)^2} |\delta(r - 0.567a_e)|$$

$$\frac{2}{4\pi(0.567a_e)^2} \sqrt{(0.567a_e)^2 - z^2} \delta(r - \sqrt{(0.567a_e)^2 - z^2})$$

Far Field Scattering (Circular Symmetry)

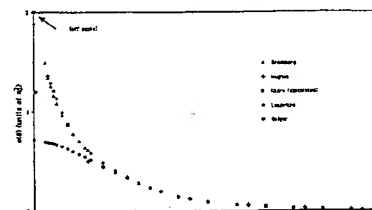
$$F(z) = \frac{2}{4\pi(0.567a_e)^2} z^2 \int_{-\infty}^{\infty} \sqrt{(0.567a_e)^2 - k^2} \delta(k - \sqrt{(0.567a_e)^2 - z^2}) J_0(kz) e^{-k|z|} dk dz$$

$$I_{\rho}^2 = F(z)^2$$

$$= I_{\rho} \left[\left(\frac{2z}{(k_z w)^2 + (k_x w)^2} \right)^{\frac{1}{2}} J_{0,z} \left[(k_z w)^2 + (k_x w)^2 \right] \left(\frac{k_x^2}{(k_z w)^2 + (k_x w)^2} \right)^{\frac{1}{2}} J_{0,x} \left[(k_z w)^2 + (k_x w)^2 \right] \right]$$

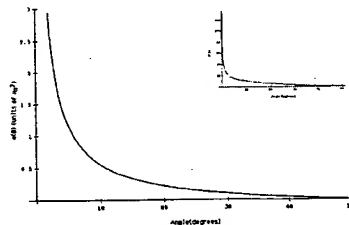
$$z = \frac{4\pi}{\lambda} \sin \frac{\theta}{2}, w = 0 (\text{min of } \text{\AA}^{-1})$$

Experimental Results and Born Approximation



The experimental results of Bresberg, the extrapolated experimental data of Hughes, the small angle data of Cooper, and the extrapolated data of Lamoreaux for the elastic differential cross section for the elastic scattering of an incident electron by a helium atom. The dashed curve is the Born approximation and the dotted curve is the first order exchange approximation. The dash-dot curve is the second order exchange approximation.

The Closed Form Function



The closed form function for the elastic differential cross section for the elastic scattering of electrons by helium atoms. The scattering amplitude function, $F(\theta)$, is shown as an insert.

The Nature of the Chemical Bond of Hydrogen

The Laplacian in ellipsoidal coordinates is solved with the constraint of nonradiation

$$(\eta - \zeta) R_1 \frac{\partial}{\partial \zeta} R_1 \frac{\partial \phi}{\partial \zeta} + (\zeta - \xi) R_2 \frac{\partial}{\partial \xi} R_2 \frac{\partial \phi}{\partial \xi} + (\xi - \eta) R_3 \frac{\partial}{\partial \eta} R_3 \frac{\partial \phi}{\partial \eta} = 0$$

The Force Balance Equation for the Hydrogen Molecule

$$\frac{h^2}{m_e a^2 b^2} 2ab^2 X = \frac{x^2}{4m_e} X + \frac{h^2}{2m_e a^2 b^2} 2ab^2 X \quad \text{where} \quad X = \frac{1}{\sqrt{1+x^2}} \frac{1}{\xi+b^2} \sqrt{\frac{\xi-1}{\xi+1}}$$

has the parametric solution $r(t) = a \cos t + b \sin t$

When the Semimajor Axis, a , is $a = a_r$

The Nature of the Chemical Bond of Hydrogen cont'd

The Internuclear Distance, $2c'$, which is the distance between the foci is

$$2c' = \sqrt{2}a_r$$

The experimental Internuclear distance is $\sqrt{2}a_r$.

The Semiminor Axis is $b = \frac{1}{\sqrt{2}}a_r$.

The Eccentricity, e , is $e = \frac{1}{\sqrt{2}}$

The Energies of the Hydrogen Molecule

The Potential Energy of the Two Electrons in the Central Field of the Protons at the Foci

$$V_e = \frac{-e^2}{mc_e/c^2 - 1} \ln \frac{a + \sqrt{a^2 - b^2}}{a - \sqrt{a^2 - b^2}} = -57.813 \text{ eV}$$

The Potential Energy of the Two Protons

$$V_p = \frac{e^2}{mc_p/c^2 - 1} = 19.23 \text{ eV}$$

The Kinetic Energy of the Electrons

$$T_e = \frac{h^2}{2m_e a^2 b^2} \ln \frac{a + \sqrt{a^2 - b^2}}{a - \sqrt{a^2 - b^2}} = 33.905 \text{ eV}$$

The Energy, V_m , of the Magnetic Force Between the Electrons

$$V_m = \frac{-e^2}{4m_e a^2 b^2} \ln \frac{a + \sqrt{a^2 - b^2}}{a - \sqrt{a^2 - b^2}} = -16.953 \text{ eV}$$

The Energies of the Hydrogen Molecule cont'd

The Total Energy

$$E_t = V_e + T_e + V_p + V_m$$

$$E_t = -13.6 \text{ eV} \left[\left(2\sqrt{2} - \sqrt{2} + \frac{\sqrt{2}}{2} \right) \ln \frac{\sqrt{2} + 1}{\sqrt{2} - 1} - \sqrt{2} \right] = -31.63 \text{ eV}$$

The Energy of Two Hydrogen Atoms

$$E(2H[a_r]) = -27.21 \text{ eV}$$

The Bond Dissociation Energy, E_D , is the difference between the total energy of the corresponding hydrogen atoms and E_t .

$$E_b = E(2H[a_r]) - E_t = 4.43 \text{ eV}$$

The experimental energy

$$E_b = 4.45 \text{ eV}$$

Proton and Neutron

The proton and neutron each comprise three charged fundamental particles called quarks and three massive photons called gluons.

Proton Parameters

$$\lambda_{C_P} = \lambda_{c,q} = \frac{2m_q c \alpha}{\alpha' m_p} = 1.3 \times 10^{-12} \text{ m} = r_p = r_q \quad m_p \text{ proton rest mass}$$

$$m_p = m_q + m_{\bar{q}} = m_q \quad \lambda_{c,p} \text{ is the Compton wavelength bar of the proton}$$

$$m_q = \frac{m_p}{2x} \quad r_p \text{ is the radius of the proton}$$

$$m_{\bar{q}} = 2m_{\bar{q}} = 2\pi X \frac{m_p}{2x} = m_p \quad r_q \text{ is the radius of the quarks}$$

$$m_{\bar{q}} = m_p - m_q = m_q \left[1 - \frac{1}{2x} \right] \quad m_q \text{ is the rest mass of the quarks}$$

$$E = m_p c^2 + m_{\bar{q}} c^2 = \frac{m_p c^2}{2x} + m_q \left[1 - \frac{1}{2x} \right]^2 c^2 = m_p c^2 \quad m_{\bar{q}} \text{ is the relativistic mass of the gluons}$$

$$m_q \text{ is the relativistic mass of the quarks}$$

Proton and Neutron cont'd

Neutron Parameters

$$\begin{aligned}\lambda_{C_n} &= \lambda_{sq} = \frac{2m_n m_q}{e^2 m_p} = 1.3214 \times 10^{-13} \text{ m} = r_c = r_q \\ m_n &= m_q + m_g = m_q' \\ m_q &= \frac{m_q}{2\pi} \\ m_q + 2m_g &= 2\pi X \frac{m_q}{2\pi} = m_N \\ m_q' &= m_q - m_g = m_q \left[1 - \frac{1}{2\pi} \right] \\ E &= m_q c^2 + m_g c^2 + m_q \left[1 - \frac{1}{2\pi} \right]^2 = m_N c^2\end{aligned}$$

m_N neutron rest mass
 λ_{C_n} is the Compton wavelength of the neutron
 r_c is the radius of the neutron
 r_q is the radius of the quarks
 m_q' is the rest mass of the quarks
 m_g is the relative mass of the gluons
 m_q is the relative mass of the quarks

Quark and Gluon Functions of the Proton

The proton functions can be viewed as a linear combination of three fundamental particles, three quarks, of charge $+\frac{2}{3}e$, $-\frac{1}{3}e$, and $-\frac{1}{3}e$. Each quark is associated with its gluon where the quark mass/charge function has the same angular dependence as the gluon mass/charge function.

The quark mass function of a proton is

$$\frac{m_q}{2\pi} \left[\frac{1}{3}(1 + \sin \theta \sin \phi) + \frac{1}{3}(1 + \sin \theta \cos \phi) + \frac{1}{3}(1 + \cos \theta) \right]$$

The charge function of the quarks of a proton is

$$\left[\frac{2}{3}(1 + \sin \theta \sin \phi) + \frac{2}{3}(1 + \sin \theta \cos \phi) - \frac{1}{3}(1 + \cos \theta) \right]$$

The radial electric field of a proton is

$$E_r = \frac{-e^2 e}{4\pi r^2} \frac{2m_q}{m_q' m_g} \left[\frac{3}{2}(1 + \sin \theta \sin \phi) + \frac{3}{2}(1 + \sin \theta \cos \phi) - 3(1 + \cos \theta) \right]$$

Quark and Gluon Functions of the Neutron

The neutron functions can be viewed as a linear combination of three fundamental particles, three quarks, of charge $+\frac{1}{3}e$, $-\frac{1}{3}e$, and $-\frac{1}{3}e$. Each quark is associated with its gluon where the quark mass/charge function has the same angular dependence as the gluon mass/charge function.

The quark mass function of a neutron is

$$\frac{m_q}{2\pi} \left[\frac{1}{3}(1 + \sin \theta \sin \phi) - \frac{1}{3}(1 + \sin \theta \cos \phi) + \frac{1}{3}(1 + \cos \theta) \right]$$

The charge function of the quarks of a neutron is

$$\left[\frac{2}{3}(1 + \sin \theta \sin \phi) - \frac{1}{3}(1 + \sin \theta \cos \phi) - \frac{1}{3}(1 + \cos \theta) \right]$$

The radial electric field of a neutron is

$$E_r = \frac{-e^2 e}{4\pi r^2} \frac{2m_q}{m_q' m_g} \left[\frac{3}{2}(1 + \sin \theta \sin \phi) - 3(1 + \sin \theta \cos \phi) - 3(1 + \cos \theta) \right]$$

Magnetic Moments

Proton Magnetic Moment

$$\mu = \frac{\text{charge} \times \text{angular momentum}}{2 \times \text{mass}}$$

$$\mu_{p\text{mom}} = \frac{2}{3} \frac{\pi^2 h}{m_p} \frac{4}{9} 2\pi \frac{e\hbar}{2m_p} = 2.79255 \mu_N$$

where μ_N is the nuclear magneton $\frac{e\hbar}{2m_p}$
 The experimental magnetic moment of the proton is $2.79268 \mu_N$

Neutron Magnetic Moment

The magnetic moment of the neutron, μ_n , is

$$\mu_n = \left[1 - \frac{4}{9} 2\pi - \frac{3}{23} \right] \mu_N = -1.91253 \mu_N$$

The experimental magnetic moment of the neutron is $-1.91315 \mu_N$

Beta Decay Energy

The nuclear reaction for the beta decay of a neutron is



where $\bar{\nu}$ is the electron antineutrino. The energy terms of the beta decay are

$$E_{\text{mom}} = \mu_p \frac{c}{2\pi} = 1.09 \times 10^4 \text{ eV}$$

$$E_{\text{kin}} = \frac{e^2}{8\pi r_0} = 5.46 \times 10^4 \text{ eV}$$

$$T = \frac{1}{2}mv^2 = \frac{1}{2} \left[\frac{mc^2}{r_0} \right] r_0^2 = 2.553 \times 10^4 \text{ eV} \quad E_{\text{mom}}(\text{gluon}) = \left[\frac{3}{25} \right] E_{\text{mom}} = 15.7 \times 10^4 \text{ eV}$$

The beta decay energy is

$$E_\beta = E_{\text{mom}} - E_{\text{mom}}(\text{gluon}) - E_{\text{kin}} + T$$

$$E_\beta = 1.09 \times 10^4 - 15.7 \times 10^4 - 5.46 \times 10^4 + 2.553 \times 10^4$$

$$E_\beta = 0.7836 \text{ MeV}$$

Maxwell's Equations and Special Relativity

Maxwell's equations and special relativity are based on the law of propagation of an electromagnetic wave front in the form

$$\frac{1}{c^2} \left(\frac{\partial \omega}{\partial t} \right)^2 - \left[\left(\frac{\partial \omega}{\partial x} \right)^2 + \left(\frac{\partial \omega}{\partial y} \right)^2 + \left(\frac{\partial \omega}{\partial z} \right)^2 \right] = 0$$

For any kind of wave advancing with limiting velocity and capable of transmitting signals, the equation of front propagation is the same as the equation for the front of a light wave.

Thus, the equation

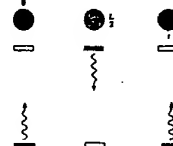
$$\frac{1}{c^2} \left(\frac{\partial \omega}{\partial t} \right)^2 - (r \omega \text{rad})^2 = 0$$

acquires a general character; it is more general than Maxwell's equations from which Maxwell originally derived it.

The Classical Wave Equation Governs:

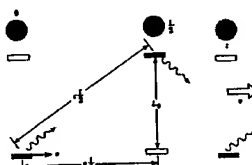
- The motion of bound electrons
- The propagation of any form of energy
- Measurements between inertial frames of reference such as time, mass, momentum, and length (Minkowski tensor)
- A relativistic correction of spacetime due to particle production or annihilation (Schwarzschild metric)
- Fundamental particle production and the conversion of matter to energy
- The basis of the relationship between Maxwell's equations, Planck's equation, the de Broglie equation, Newton's laws, and special, and general relativity

A Light-Pulse Clock at Rest on the Ground As Seen by an Observer on the Ground



The dial represents a conventional clock on the ground.

A Light-Pulse Clock in a Spacecraft As Seen by an Observer on the Ground



The mirrors are parallel to the direction of the motion of the spacecraft.
The dial represents a conventional clock on the ground.

Time Interval Relation Between Ticks t of the Moving Clock and t_0 , the Vertical Distance Between the Mirrors

$$\left(c \frac{t}{2}\right)^2 = t_0^2 + \left(\frac{v t}{2}\right)^2 \quad t = \frac{2t_0}{\sqrt{1 - \frac{v^2}{c^2}}}$$

But $\frac{2t_0}{c}$ is the time t_0 interval between ticks on the clock on the ground, and so the

time dilation relationship based on the constant maximum speed of light in any inertial frame is $t = \frac{t_0}{\sqrt{1 - \frac{v^2}{c^2}}}$

where the parameters are:
 t = time interval on clock at rest relative to an observer
 t_0 = time interval on clock in motion relative to an observer
 v = speed of relative motion
 c = speed of light

Minkowski Tensor $\eta_{\mu\nu}$

The Metric $g_{\mu\nu}$ for Euclidean Space Called the Minkowski Tensor $\eta_{\mu\nu}$ Is

$$\eta_{\mu\nu} = \begin{pmatrix} -1 & 0 & 0 & 0 \\ 0 & \frac{1}{c^2} & 0 & 0 \\ 0 & 0 & \frac{1}{c^2} & 0 \\ 0 & 0 & 0 & \frac{1}{c^2} \end{pmatrix}$$

In this case, the separation of proper time between two events x^μ and $x^\mu + dx^\mu$

$$dt^2 = -\eta_{\mu\nu} dx^\mu dx^\nu$$

The Equivalence of the Gravitational Mass and the Inertial Mass

Experimentally $\frac{m}{m_0} = \text{universal constant}$
which is predicted by Newton's Law of mechanics and gravitation.

The energy equation of Newtonian gravitation

$$E = \frac{1}{2}mv^2 - \frac{GMm}{r} = \frac{1}{2}mv^2 - \frac{GMm}{r_0} = \text{constant}$$

Since h , the angular momentum per unit mass, is

$$h = L/m = |r \times v| = r_0 v_0 \sin \phi$$

Eccentricity e may be written as

$$e = [1 + \left(\frac{v_0^2 - 2GM}{G^2 M^2} \right) \frac{r_0^2 v_0^2 \sin^2 \phi}{h^2}]^{1/2}$$

m is the inertial mass of a particle

v_0 is the speed of the particle

r_0 is the distance of the particle from a massive object

ϕ is the angle between the direction of motion of the particle and the radius vector from the object

M is the total (including a particle) of mass of the object

Classification of the Orbits

The eccentricity e given by Newton's differential equations of motion in the case of the central field permits the classification of the orbits.

According to the total energy E :

$E < 0, e < 1$	ellipse
$E < 0, e = 0$	circle (special case of ellipse)
$E = 0, e = 1$	parabolic orbit
$E > 0, e > 1$	hyperbolic orbit

Classification of the Orbits cont'd

According to the orbital velocity relative to the gravitational velocity squared $\frac{2GM}{r}$:

$v_0^2 < \frac{2GM}{r_0}$	$e < 1$	ellipse
$v_0^2 = \frac{2GM}{r_0}$	$e = 1$	circle (special case of ellipse)
$v_0^2 > \frac{2GM}{r_0}$	$e > 1$	parabolic orbit
$v_0^2 > \frac{2GM}{r_0}$	$e > 1$	hyperbolic orbit

Continuity Conditions for the Production of a Particle From a Photon Traveling at Light Speed

- A photon traveling at the speed of light gives rise to a particle with an initial radius equal to its Compton wavelength bar

$$r = \lambda_C = \frac{\hbar}{mc}$$

- The particle must have an orbital velocity equal to Newtonian gravitational escape velocity v_g of the antiparticle

$$v_g = \sqrt{\frac{2Gm}{r}} = \sqrt{\frac{2Gm_b}{\lambda_C}}$$

- The eccentricity is one
- The orbital energy is zero
- The particle production trajectory is a parabola relative to the center of mass of the antiparticle

A Gravitational Field As a Front Equivalent to a Light Wave Front

The particle with a finite gravitational mass gives rise to a gravitational field that travels out as a front equivalent to a light wave front

The form of the outgoing gravitational field front traveling at the speed of light is

$$\sqrt{1 - \frac{r}{c}}$$

and dr^2 is given by

$$dr^2 = f(r)dt^2 - \frac{1}{c^2} [f(r)^{-1}dr^2 + r^2 d\theta^2 + r^2 \sin^2 \theta d\phi^2]$$

The Speed of Light

The speed of light as a constant maximum as well as phase matching and continuity conditions of the electromagnetic and gravitational waves require the following form of the squared displacements:

$$(ct')^2 + (r')^2 = (ct)^2$$

$$r' = r\left(1 - \frac{v_L}{c}\right)$$

$$\text{Thus, } f(r) = \left(1 - \frac{v_L}{c}\right)^2$$

In order that the wave front velocity does not exceed c in any frame, spacetime must undergo time dilation and length contraction due to the particle production event.

The derivation and result of spacetime time dilation is analogous to the derivation and result of special relativistic time dilation wherein the relative velocity of two inertial frames replaces the gravitational velocity.

Quadratic Form Of The Infinitesimal Squared Temporal Displacement

General form of the metric due to the relativistic effect on spacetime due to mass m ,

$$dt^2 = \left[1 - \left(\frac{r_s}{c}\right)^2\right]dt^2 - \frac{1}{c^2} \left[\left(1 - \left(\frac{r_s}{c}\right)^2\right)^{-1} dr^2 + r^2 d\theta^2 + r^2 \sin^2 \theta d\phi^2 \right]$$

Gravitational radius, r_s , of each orbit sphere of the particle production event, each of mass m

$$r_s = \frac{2Gm}{c^2}$$

$$dr^2 = \left(1 - \frac{r_s}{r}\right)dt^2 - \frac{1}{c^2} \left[\left(1 - \frac{r_s}{r}\right)^{-1} dr^2 + r^2 d\theta^2 + r^2 \sin^2 \theta d\phi^2 \right]$$

Masses and their effects on spacetime superimpose. The separation of proper time between two events and x' is $x^2 + dx'^2$

$$dx^2 = \left(1 - \frac{2Gm}{c^2 r}\right)dt^2 - \frac{1}{c^2} \left[\left(1 - \frac{2Gm}{c^2 r}\right)^{-1} dr^2 + r^2 d\theta^2 + r^2 \sin^2 \theta d\phi^2 \right]$$

The Origin of Gravity

The Schwarzschild metric gives the relationship whereby matter causes relativistic corrections to spacetime that determines the curvature of spacetime and is the origin of gravity.

The metric $g_{\mu\nu}$ for non-euclidean space due to the relativistic effect on spacetime due to mass m_* is

$$g_{\mu\nu} = \begin{pmatrix} -\left(1 - \frac{2Gm_*}{c^2 r}\right) & 0 & 0 & 0 \\ 0 & \frac{1}{c^2} \left(1 - \frac{2Gm_*}{c^2 r}\right)^{-1} & 0 & 0 \\ 0 & 0 & \frac{1}{c^2 r^2} & 0 \\ 0 & 0 & 0 & \frac{1}{c^2 r^2 \sin^2 \theta} \end{pmatrix}$$

Particle Production Continuity Conditions

- The photon to particle event requires a transition state that is continuous.

- The velocity of a transition state orbitsphere is the speed of light.

- The radius, r_* , is the Compton wavelength bar, λ_c

$$\lambda_c = \frac{\hbar}{m_* c} = r_*$$

- The Planck equation energy, the electric potential energy, and the magnetic energy are equal to $m_* c^2$.

The Masses of Fundamental Particles

The Schwarzschild metric gives the relationship whereby matter causes relativistic corrections to spacetime that determines the masses of fundamental particles.

Substitution of $r = \lambda_c$; $dr = 0$; $d\theta = 0$; $\sin^2 \theta = 1$ into the Schwarzschild metric gives

$$d\tau = dr \left(1 - \frac{2Gm_*}{c^2 r_*} - \frac{v^2}{c^2}\right)^{\frac{1}{2}}$$

with, $v^2 = c^2$

$$\tau = \delta \sqrt{\frac{2GM}{c^2 r_*}} = \delta \sqrt{\frac{2GM}{c^2 \lambda_c}} = \delta \frac{v}{c}$$

Relationship of the Equivalent Particle Production Energies

When the orbitsphere velocity is the speed of light:

Continuity conditions based on the constant maximum speed of light given by Maxwell's equations:

(Mass energy = Planck equation energy = electric potential energy = magnetic energy = mass/spacetime metric energy)

$$m_* c^3 = \hbar \omega^2 = V = E_{\text{particle}} = E_{\text{spacetime}}$$

$$m_* c^2 = \hbar \omega^2 = \frac{\hbar^2}{m_* \lambda_c^2} = \alpha^{-1} \frac{c^2}{4\pi \epsilon_0 \lambda_c} = \alpha^{-1} \frac{mc_e^2 \hbar^2}{(2\pi m_e)^2 \lambda_c^2} = \frac{\hbar}{1 \text{ sec}} \sqrt{\frac{\lambda_c^3}{2 G m}}$$

Continuity Conditions Based on the Constant Maximum Speed of Light Given by the Schwarzschild Metric

$$\frac{\text{proper time}}{\text{coordinate time}} = \frac{\text{gravitational wave condition}}{\text{electromagnetic wave condition}} = \frac{\text{gravitational mass phase matching}}{\text{charge/mass phase matching}}$$

$$\frac{\text{proper time}}{\text{coordinate time}} = \frac{\sqrt{\frac{2GM}{c^2 \lambda_c}}}{\alpha} = i \frac{v}{c \omega}$$

Masses of Fundamental Particles

- Each of the Planck equation energy, electric energy, and magnetic energy corresponds to a particle given by the relationship between the proper time and the coordinate time.

- The electron and antielectron correspond to the Planck equation energy.

- The muon and antimuon correspond to the electric energy.

- The tau and antitau correspond to the magnetic energy.

- The particle must possess the escape velocity v_s relative to the antiparticle where $v_s < c$.

- According to Newton's law of gravitation, the eccentricity is one and the particle production trajectory is a parabola relative to the center of mass of the antiparticle.

The Electron-Antielectron Lepton Pair

A clock is defined in terms of a self-consistent system of units used to measure the particle mass.

$$2\pi \frac{\hbar}{mc^2} = \sec \sqrt{\frac{2Gm^2}{c\alpha^2\hbar}}$$

$$m_e = \left(\frac{\hbar\alpha}{mc^2} \right)^{\frac{1}{2}} \left(\frac{e\hbar}{2G} \right)^{\frac{1}{2}} = 9.1097 \times 10^{-31} \text{ kg}$$

$$m_e = 9.1097 \times 10^{-31} \text{ kg} - 18 \text{ eV} (v_e) = 9.1094 \times 10^{-31} \text{ kg}$$

$$m_{e \text{ experimental}} = 9.1095 \times 10^{-31} \text{ kg}$$

The Muon-Antimuon Lepton Pair

$$2\pi \frac{\hbar}{mc^2} = 2\pi \sec \sqrt{\frac{2Gm_e \alpha^2 m}{e\hbar}}$$

The mass of the muon/antimuon is

$$m_\mu = \frac{\hbar}{c} \left(\frac{1}{2Gm_e (\sec)} \right)^{\frac{1}{2}} = 1.8902 \times 10^{-31} \text{ kg}$$

The muon/antimuon mass is corrected for the experimental mass/energy deficit of the 0.25 MeV neutrino.

$$m_\mu = 1.890563 \times 10^{-31} \text{ kg} - 0.25 \text{ MeV} (v_\mu) = 1.8857 \times 10^{-31} \text{ kg}$$

$$m_{\mu \text{ experimental}} = 1.8836 \times 10^{-31} \text{ kg}$$

The Tau-Antitau Lepton Pair

$$2\pi \frac{\hbar}{mc^2} = 2\sec \sqrt{\frac{2Gm_\tau (2\pi)^2 \alpha^2 m}{e\hbar}}$$

The mass of the tau/antitau is

$$m_\tau = \frac{\hbar}{c} \left(\frac{1}{2Gm_e} \right)^{\frac{1}{2}} \left(\frac{1}{2\sec \alpha^2} \right)^{\frac{1}{2}} = 3.17 \times 10^{-31} \text{ kg}$$

The tau/antitau mass is corrected for the experimental mass/energy deficit of the 17 keV neutrino.

$$m_\tau = 3.17 \times 10^{-31} \text{ kg} - 17 \text{ keV} (v_\tau) = 3.17 \times 10^{-31} \text{ kg}$$

$$m_{\tau \text{ experimental}} = 3.17 \times 10^{-31} \text{ kg}$$

Down-Down-Up Neutron (DDU)

$$2\pi \frac{\hbar}{m_n \left[\frac{1}{2\pi} - \frac{\alpha}{2\pi} \right]^{\frac{1}{2}}} = \sec \sqrt{\frac{2G \left[\frac{m_n}{3} \left[\frac{1}{2\pi} - \frac{\alpha}{2\pi} \right] \right]}{3c(2\pi)^2 \hbar}}$$

The neutron mass is

$$m_{n \text{ theoretical}} = (3)(2\pi) \left(\frac{1}{1-\alpha} \right) \left(\frac{2\hbar}{mc^2} \right)^{\frac{1}{2}} \left(\frac{2\pi(2\pi)\hbar}{2G} \right)^{\frac{1}{2}}$$

$$= 1.6744 \times 10^{-27} \text{ kg}$$

$$m_{n \text{ experimental}} = 1.6749 \times 10^{-27} \text{ kg}$$

Strange-Strange-Charmed Neutron (SSC)

$$2\pi \frac{\hbar}{m_n \left[\frac{1}{2\pi} - \frac{\alpha}{2\pi} \right]^{\frac{1}{2}}} = 2\pi \sec \sqrt{\frac{2Gc^2 m_n \left[\frac{m_s}{3} \left[\frac{1}{2\pi} - \frac{\alpha}{2\pi} \right] \right]}{3c(2\pi)^2 \hbar}}$$

The strange-strange-charmed neutron mass is

$$m_{n \text{ theoretical}} = (3)(2\pi) \left(\frac{1}{1-\alpha} \right) \left(\frac{\hbar}{mc^2} \right)^{\frac{1}{2}} \left(\frac{2\pi(2\pi)\hbar}{2m_s(\beta\alpha^2)} \right)^{\frac{1}{2}}$$

$$m_{n \text{ theoretical}} = 4.90 \times 10^{-37} \text{ kg} = 2.75 \text{ GeV}/c^2$$

The observed mass of the Ω^- hyperon that contains three strange quarks (sss) is

$$m_{\Omega^-} = 1673 \text{ MeV}/c^2$$

Strange-Strange-Charmed Neutron (SSC) cont'd

Thus, an estimate for the dynamical mass of the strange quark, m_s , is

$$m_s = \frac{m_{n \text{ s}}}{3} = \frac{1673 \text{ MeV}/c^2}{3} = 558 \text{ MeV}/c^2$$

The dynamical mass of the charmed quark, m_c , has been determined by fitting quarkonia spectra; and from the observed masses of the charmed pseudoscalar mesons $D^+(1600)$ and $D^-(1600)$.

$$m_c = 1.580 \text{ GeV}/c^2$$

Thus,

$$m_{n \text{ experimental}} = 2m_s + m_c = 2(558 \text{ MeV}/c^2) + 1673 \text{ MeV}/c^2$$

$$m_{n \text{ experimental}} = 2.79 \text{ GeV}/c^2$$

Bottom-Bottom-Top Neutron (BBT)

$$2 \frac{m_b}{3} \left[\frac{2m_b}{2\pi - \alpha} \right] = 2 \alpha \sqrt{\frac{2G_F m_b \left[\frac{m_b}{3} \left(\frac{1 - \alpha}{2\pi} \right) \right]}{3(2\pi)^2 \hbar}}$$

The bottom-bottom-top neutron mass is

$$m_{bbt \text{ calculated}} = 3(2\pi) \left(\frac{1}{1-\alpha} \right) \left(\frac{2m_b}{2\pi c^2} \right)^{\frac{1}{2}} \left(\frac{2m_b G \hbar}{m_{bb} G_F c^2} \right)^{\frac{1}{2}}$$

$$m_{bbt \text{ calculated}} = 3.48 \times 10^{-32} \text{ kg} = 195 \text{ GeV/c}^2$$

The dynamical mass of the bottom quark, m_b , has been determined by fitting quarkonia spectra; and from the observed masses of the bottom pseudoscalar mesons $\eta'(3770)$ and $\eta'(3771)$.

$$m_b = 4.580 \text{ GeV/c}^2$$

Bottom-Bottom-Top Neutron (BBT) cont'd

Thus, the predicted dynamical mass of the top quark based on the dynamical mass of the bottom quark is

$$m_t \text{ calculated} = m_{bbt \text{ calculated}} - 2m_b = 195 \text{ GeV/c}^2 - 2(4.580 \text{ GeV/c}^2)$$

$$m_t \text{ calculated} = 186 \text{ GeV/c}^2$$

From about 21 top quark events, the CDF collaboration calculates the mass of the top quark as

$$176 \pm 13 \text{ GeV/c}^2$$

From about 17 top quark events, the D_s collaboration calculates the mass of the top quark as

$$199 \pm 30 \text{ GeV/c}^2$$

Gravitational Potential Energy

The gravitational radius, α_G or r_G , of an orbitsphere of mass m_0 is defined as

$$\alpha_G = r_G = \frac{Gm_0}{c^2}$$

When the $r_G = r_c = \lambda_c$, the gravitational potential energy equals $m_0 c^2$

$$\frac{Gm_0}{c^2} = \lambda_c = \frac{\hbar}{m_0 c}$$

$$\frac{Gm_0^2}{\lambda_c} = \frac{Gm_0^2}{r_c} = \hbar \omega^2 = m_0 c^2$$

Gravitational Potential Energy cont'd

The mass m_0 is the Planck mass, m_P ,

$$m_P c^2 = \hbar \omega^2 = V = E_{\text{max}} = \frac{Gm_0^2}{\lambda_c}$$

$$m_P = m_0 = \sqrt{\frac{\hbar c}{G}}$$

The corresponding gravitational velocity, v_G , is defined as

$$v_G = \sqrt{\frac{Gm_0}{\lambda_c}} = \sqrt{\frac{Gm_0}{\lambda_c}}$$

Relationship of the Equivalent Planck Mass Particle Production Energies

(Mass energy = Planck equation energy = electric potential energy = magnetic energy = gravitational potential energy = mass/spacetime metric energy)

$$m_p c^2 = \hbar \omega^2 = \frac{\lambda^2}{\lambda_c \lambda_c} = \alpha^{-1} \frac{c^4}{4\pi \epsilon_0 \lambda_c} = \alpha^{-1} \frac{m_p c^2 \lambda^2}{(2m_0) \lambda_c} = \alpha^{-1} \frac{m_p c^2 \lambda^2}{2\hbar} \sqrt{\frac{Gm_0}{\lambda_c}} \sqrt{\frac{\hbar c}{G}} = \frac{\alpha^{-1} \hbar c^2}{2\lambda_c} \sqrt{\frac{\lambda c^2}{2Gm_0}}$$

Equivalent energies give the particle masses in terms of the gravitational velocity, v_G , and the Planck mass, m_P ,

$$m_p = \alpha^{-1} \frac{\hbar c^2}{2\lambda_c} v_G = \alpha^{-1} \frac{\hbar c^2}{2\lambda_c} \sqrt{\frac{Gm_0}{\lambda_c}} v_G = \alpha^{-1} \frac{\hbar c^2}{2\lambda_c} \frac{\lambda}{c} v_G = \frac{\lambda}{c} m_p$$

Planck Mass Particles

- A pair of particles each of the Planck mass corresponding to the gravitational potential energy is not observed since the velocity of each transition state orbitsphere is the gravitational velocity v_G that in this case is the speed of light; whereas, the Newtonian gravitational escape velocity v_e is twice the speed of light.

- In this case, an electromagnetic wave of mass energy equivalent to the Planck mass travels in a circular orbit about the center of mass of another electromagnetic wave of mass energy equivalent to the Planck mass wherein the eccentricity is equal to zero and the escape velocity can never be reached.

Planck Mass Particles cont'd

- The Planck mass is a "measuring stick." The extraordinarily high Planck mass ($\sqrt{\frac{hc}{G}} = 2.18 \times 10^{-18} \text{ kg}$) is the unattainable mass bound imposed by the angular momentum and speed of the photon relative to the gravitational constant.
- It is analogous to the unattainable bound of the speed of light for a particle possessing finite rest mass imposed by the Minkowski tensor.

Astrophysical Implications of Planck Mass Particles

- The limiting speed of light eliminates the singularity problem of Einstein's equation that arises as the radius of a black hole equals the Schwarzschild radius.
- When the gravitational potential energy density of a massive body such as a blackhole equals that of a particle having the Planck mass, the matter may transition to photons of the Planck mass.
- Even light from a black hole will escape when the decay rate of the trapped matter with the concomitant spacetime expansion is greater than the effects of gravity which oppose this expansion.

Astrophysical Implications of Planck Mass Particles cont'd

- Gamma-ray bursts are the most energetic phenomenon known that can release an explosion of gamma-rays packing 100 times more energy than a Supernova explosion.
- The annihilation of a black hole may be the source of γ -ray bursts.
- The source may be due to conversion of matter to photons of the Planck mass/energy, which may also give rise to cosmic rays.
- According to the GZK cutoff, the cosmic spectrum cannot extend beyond $5 \times 10^{19} \text{ eV}$, but AGASA, the world's largest air shower array, has shown that the spectrum is extending beyond 10^{20} eV without any clear sign of cutoff. Photons each of the Planck mass may be the source of these inexplicably energetic cosmic rays.

The Schwarzschild Metric Gives the Relationship Whereby Matter Causes Relativistic Corrections to Spacetime

- The limiting velocity c results in the contraction of spacetime due to particle production. The contraction is given by $\frac{r}{r_s}$, where r_s is the gravitational radius of the particle. This has implications for the expansion of spacetime when matter converts to energy.
- The mass/energy to expansion/contraction quotient of spacetime is given by the ratio of the mass of a particle at production divided by T the period of production.
$$Q = \frac{m}{T} = \frac{m}{\frac{2\pi r_s}{c}} = \frac{m}{2\pi \frac{2GM}{c^2}} = \frac{c^2}{4\pi G} = 3.22 \times 10^{44} \frac{\text{Hz}}{\text{mc}}$$
- The gravitational equations with the equivalence of the particle production energies permit the conservation of mass/energy ($E = mc^2$) and spacetime ($\frac{c^2}{4\pi G} = 3.22 \times 10^{44} \frac{\text{Hz}}{\text{mc}}$).

Cosmological Consequences

- The Universe is closed (it is finite but with no boundary).
- The Universe is a 3-sphere Universe-Riemannian three dimensional hyperspace plus time of constant positive curvature at each r-sphere.
- The Universe is oscillatory in matter/energy and spacetime with a finite minimum radius, the gravitational radius.
- Spacetime expands as mass is released as energy which provides the basis of the atomic, thermodynamic, and cosmological arrows of time.
- Different regions of space are isothermal even though they are separated by greater distances than that over which light could travel during the time of the expansion of the Universe.

Cosmological Consequences cont'd

- Presently, stars exist which are older than the elapsed time of the present expansion as stellar evolution also occurred during the contraction phase.
- The maximum power radiated by the Universe which occurs at the beginning of the expansion phase is
$$P_0 = \frac{c^2}{4\pi G} = 2.89 \times 10^{51} \text{ W}$$
- Observations beyond the beginning of the expansion phase are not possible since the Universe is entirely matter filled.

The Period of Oscillation Based on Closed Propagation of Light

- Conservation of mass/energy during harmonic expansion and contraction
 - The gravitational potential energy E_{pot}
- $$E_{pot} = \frac{Gm_U}{r}$$
- is equal to $m_U c^2$ when the radius of the Universe r is the gravitational radius r_G .
- The gravitational velocity v_g is the speed of light in a circular orbit wherein the eccentricity is equal to zero and the escape velocity from the Universe can never be reached.
 - The period of the oscillation of the Universe and the period for light to transverse the Universe corresponding to the gravitational radius r_G must be equal.

The Period of Oscillation Based on Closed Propagation of Light cont'd

- The harmonic oscillation period, T , is
- $$T = \frac{2\pi r_G}{c} = \frac{2\pi G m_U}{c^2} \times \frac{2G(2 \times 10^{44} \text{ kg})}{c} = 3.10 \times 10^{11} \text{ sec} = 9.83 \times 10^{11} \text{ years}$$
- where the mass of the Universe, m_U , is approximately $2 \times 10^{44} \text{ kg}$ (The initial mass of the Universe of $2 \times 10^{44} \text{ kg}$ is based on internal consistency with the size, age, Hubble constant, temperature, density of matter, and power spectrum of the Universe.)
- Thus, the observed Universe will expand as mass is released as photons for 4.92×10^{11} years. At this point in its world line, the Universe will obtain its maximum size and begin to contract.

The Differential Equation of the Radius of the Universe

- Simple harmonic oscillator having a restoring force, F , which is proportional to the radius.
 - The proportionality constant, k , is given in terms of the potential energy, E , gained as the radius decreases from the maximum expansion to the minimum contraction.
- $$\frac{E}{k^2} = 1$$
- The gravitational potential energy E_{pot}
- $$E_{pot} = \frac{Gm_U}{r}$$
- Is equal to $m_U c^2$ when the radius of the Universe r is the gravitational radius r_G
- $$F = -kR = -\frac{m_U c^2}{r_G^2} R = -\frac{m_U c^2}{\left(\frac{Gm_U}{c^2}\right)^2} R$$

The Differential Equation of the Radius of the Universe R , Is

$$m_U \ddot{R} + \frac{m_U c^2}{r_G^2} R = 0$$

$$m_U \ddot{R} + \frac{m_U c^2}{\left(\frac{Gm_U}{c^2}\right)^2} R = 0$$

The Maximum Radius of the Universe

The Maximum Radius of the Universe, the amplitude, r_0 , of the time harmonic variation in the radius of the Universe, is given by the quotient of the total mass of the Universe Q and the mass/energy to expansion/contraction quotient.

$$r_0 = \frac{m_U}{Q} = \frac{m_U}{\frac{c^2}{4\pi G}}$$

$$r_0 = \frac{2 \times 10^{44} \text{ kg}}{\frac{c^2}{4\pi G}} = 1.97 \times 10^{12} \text{ light years}$$

The Minimum Radius

The Minimum Radius corresponds to the gravitational radius

$$r_i = \frac{2Gm_U}{c^3}$$

$$r_i = \frac{2G(2 \times 10^{44} \text{ kg})}{c^3} = 3.12 \times 10^{11} \text{ light years}$$

When the gravitational radius r_i is the radius of the Universe, the proper time is equal to the coordinate time by

$$t = d\sqrt{\frac{2GM}{c^3 r_i}} = d\sqrt{\frac{2GM}{c^3 r_i}} = d\sqrt{\frac{c^3}{c}}$$

And the gravitational escape velocity v_g of the Universe is the speed of light.

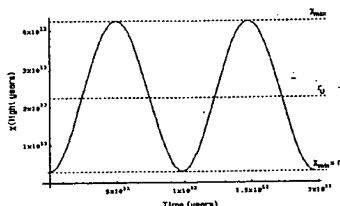
The Radius of the Universe As a Function of Time

$$R = \left(r_0 + \frac{cm_0}{Q} \right) - \frac{cm_0}{Q} \cos \left(\frac{2\pi}{2\pi G m_0/c} t \right)$$

$$R = \left(\frac{2Gm_0}{c^2} + \frac{cm_0}{c^2} \right) - \frac{cm_0}{4\pi G} \cos \left(\frac{2\pi}{2\pi G m_0/c} t \right)$$

$$R = 2.28 \times 10^{12} - 1.97 \times 10^{12} \cos \left(\frac{2\pi}{9.83 \times 10^{11} \text{ yrs}} t \right) \text{ light years}$$

The Radius of the Universe as a Function of Time

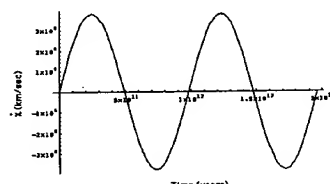


The Expansion/Contraction Rate, \dot{R}

$$\dot{R} = 4\pi c \times 10^{-3} \sin \left(\frac{2\pi}{2\pi G m_0/c} t \right) \frac{\text{km}}{\text{sec}}$$

$$\dot{R} = 3.77 \times 10^6 \sin \left(\frac{2\pi}{9.83 \times 10^{11} \text{ yrs}} t \right) \frac{\text{km}}{\text{sec}}$$

The Expansion/Contraction Rate of the Universe As a Function of Time



The Hubble Constant

The **Hubble Constant** is given by the ratio of the expansion rate given in units of $\frac{\text{km}}{\text{sec}}$ divided by the radius of the expansion in Mpc . The radius of expansion is equivalent to the radius of the light sphere with an origin at the time point when the Universe stopped contracting and started to expand. The radius is the time of expansion t/Mpc .

$$H = \frac{\dot{R}}{t/\text{Mpc}} = \frac{4\pi c \times 10^{-3} \sin \left(\frac{2\pi}{2\pi G m_0/c} t \right) \frac{\text{km}}{\text{sec}}}{t/\text{Mpc}}$$

$$H = \frac{\dot{R}}{t} = \frac{3.77 \times 10^6 \sin \left(\frac{2\pi}{9.83 \times 10^{11} \text{ Mpc}} t \right) \frac{\text{km}}{\text{sec}}}{t}$$

The Hubble Constant cont'd

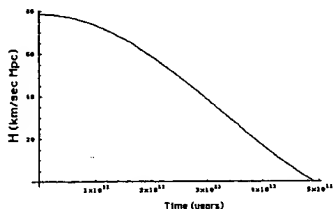
For $t = 10^{11} \text{ light years} = 3.009 \times 10^9 \text{ Mpc}$ the Hubble, H_0 , constant is

$$H_0 = 78.6 \frac{\text{km}}{\text{sec} \cdot \text{Mpc}}$$

The experimental value is

$$H_0 = 80 \pm 17 \frac{\text{km}}{\text{sec} \cdot \text{Mpc}}$$

The Hubble Constant of the Universe As a Function of Time



The Density of the Universe As a Function of Time

The density of the Universe as a function of time $\rho_0(t)$ is given by the ratio of the mass as a function of time and the volume as a function of time.

$$\rho_0(t) = \frac{m_0(t)}{V(t)} = \frac{m_0(t)}{\frac{4}{3}\pi R(t)^3} = \frac{\frac{m_0(t)}{2} \left[1 + \cos\left(\frac{2\pi t}{2\pi G m_0}\right) \right]}{\frac{4}{3}\pi \left[\left(\frac{2Gm_0 + cm_0}{c^3} \right) - \frac{cm_0}{c^3} \cos\left(\frac{2\pi t}{2\pi G m_0}\right) \right]^{\frac{3}{2}}} \\ \rho_0(t) = \frac{1 \times 10^{31}}{\frac{4}{3}\pi \left[2.16 \times 10^{30} - 1.86 \times 10^{30} \cos\left(\frac{2\pi t}{9.83 \times 10^{11} \text{ yrs}}\right) \right]^{\frac{3}{2}}} \text{ g/cm}^3$$

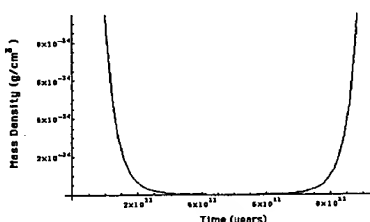
For $t = 10^{10}$ light years $= 3.099 \times 10^{11}$ Mpc

$$\rho_0 = 1.7 \times 10^{-31} \text{ g/cm}^3$$

The density of luminous matter of stars and gas of galaxies is about

$$\rho_0 = 2 \times 10^{-31} \text{ g/cm}^3$$

The Density of the Universe As a Function of Time



The Power of the Universe As a Function of Time, $P_U(t)$

$$P_U(t) = \frac{c^5}{8\pi G} \left[1 + \cos\left(\frac{2\pi t}{2\pi G}\right) \right]$$

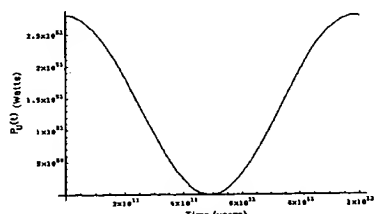
$$P_U(t) = 1.45 \times 10^{51} \left[1 + \cos\left(\frac{2\pi t}{9.83 \times 10^{11} \text{ yrs}}\right) \right] \text{ W}$$

For $t = 10^{10}$ light years

$$P_U(t) = 2.88 \times 10^{51} \text{ W}$$

The observed power is consistent with that predicted.

The Power of the Universe As a Function of Time



The Temperature of the Universe as a Function of Time Follows from the Stefan-Boltzman Law

$$T_U(t) = \left[\frac{1}{\left(1 + \frac{cm_0}{c^2 R(t)} \right)^{\frac{1}{4}}} \right]^{\frac{1}{4}} \left[\frac{A_0(t)^{\frac{1}{4}}}{\left(1 + \frac{cm_0(t)}{c^2 R(t)} \right)^{\frac{1}{4}}} \right]^{\frac{1}{4}} \left[\frac{P_U(t)^{\frac{1}{4}}}{4\pi k_B(t)^{\frac{1}{4}}} \right]^{\frac{1}{4}} \left[\frac{c^{\frac{5}{4}}}{8\pi G} \left(1 + \cos\left(\frac{2\pi t}{2\pi G}\right) \right)^{\frac{1}{4}} \right]^{\frac{1}{4}}$$

$$T_U(t) = \left[\frac{c^{\frac{5}{4}}}{8\pi G} \left(1 + \cos\left(\frac{2\pi t}{2\pi G}\right) \right)^{\frac{1}{4}} \right]^{\frac{1}{4}} \left[\frac{1}{\left(1 + \frac{cm_0}{c^2 R(t)} \right)^{\frac{1}{4}}} \right]^{\frac{1}{4}} \left[\frac{A_0(t)^{\frac{1}{4}}}{\left(1 + \frac{cm_0(t)}{c^2 R(t)} \right)^{\frac{1}{4}}} \right]^{\frac{1}{4}} \left[\frac{P_U(t)^{\frac{1}{4}}}{4\pi k_B(t)^{\frac{1}{4}}} \right]^{\frac{1}{4}}$$

The Temperature of the Universe As a Function of Time – cont'd

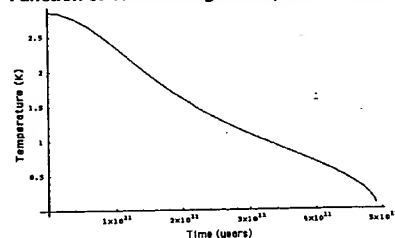
$$T_0(t) = \frac{1}{1 + \cos\left(\frac{2\pi t}{9.83 \times 10^{11} \text{ yrs}}\right)} \cdot \frac{1}{m}$$

$$= \frac{1}{1 + \cos\left(\frac{2\pi t}{9.83 \times 10^{11} \text{ yrs}}\right)} \cdot \frac{1}{2.16 \times 10^9 - 1.86 \times 10^9 \cos\left(\frac{2\pi t}{9.83 \times 10^{11} \text{ yrs}}\right) m}$$

$$= \frac{1}{1 + \cos\left(\frac{2\pi t}{9.83 \times 10^{11} \text{ yrs}}\right)} \cdot \frac{1}{4.45 \times 10^9 + 1.86 \times 10^9 \cos\left(\frac{2\pi t}{9.83 \times 10^{11} \text{ yrs}}\right) m}$$

$$= \frac{1}{1 + \cos\left(\frac{2\pi t}{9.83 \times 10^{11} \text{ yrs}}\right)} \cdot \frac{1}{5.67 \times 10^{-9} \text{ W m}^{-2} \text{ K}^{-1}}$$

The Temperature of the Universe As a Function of Time During the Expansion Phase



Power Spectrum of the Cosmos

- The power spectrum of the cosmos, as measured by the LAS CAMPANAS SURVEY, generally follows the prediction of cold dark matter on the scales of 200 million to 600 million light-years.
- However, the power increases dramatically on scales of 600 million to 900 million light-years.

The infinitesimal temporal displacement, $d\tau^2$, is

$$d\tau^2 = \left(1 - \frac{2Gm_u}{c^2 r}\right) dt^2 - \frac{1}{c^2} \left[\left(1 - \frac{dr^2}{1 - \frac{2Gm_u}{c^2 r}}\right) + r^2 d\theta^2 + r^2 \sin^2 \theta d\phi^2 \right] dr^2$$

The relationship between the proper time and the coordinate time is

$$\tau = t \sqrt{1 - \frac{2Gm_u}{c^2 r}} \quad t = \tau \sqrt{1 - \frac{2}{r}}$$

Power Spectrum of the Cosmos cont'd

- The power maximum in the proper frame occurs at
 $\tau = 5 \times 10^9 \text{ light years}, \quad \begin{cases} 3.12 \times 10^{10} \text{ light years} \\ 3.22 \times 10^{10} \text{ light years} \end{cases}$
 $t = 880 \times 10^9 \text{ light years}$
- The power maximum of the current observable Universe is predicted to occur on the scale of $880 \times 10^9 \text{ light years}$.
- There is excellent agreement between the predicted value and the experimental value $600-900 \times 10^9 \text{ light years}$.

The Expansion/ Contraction Acceleration, \ddot{R}

$$\ddot{R} = 2\pi \frac{c^4}{Gm_u} \cos\left(\frac{2\pi}{\frac{2\pi Gm_u}{c^2} \text{ sec}}\right)$$

$$\ddot{R} = H_0^2 = 78.7 \cos\left(\frac{2\pi}{3.01 \times 10^9 \text{ Mpc}} \frac{\text{km}}{\text{sec Mpc}}\right)$$

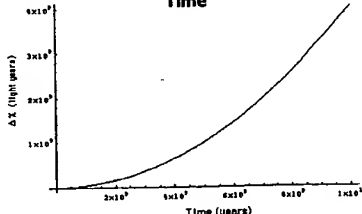
- The differential in the radius of the Universe ΔR due to its acceleration is given by

$$\Delta R = 1/2 \dot{R} t^2$$

- The differential in expanded radius for the elapsed time of expansion, $t = 10^9 \text{ light years} = 3.009 \times 10^{19} \text{ sec}$, corresponds to a decrease in brightness of a supernovae standard candle of about an order of magnitude if the distance is taken as ΔR . This result based on the predicted rate of acceleration of the expansion is consistent with the experimental observation.

- The microwave background radiation images obtained by the BOOMERANG telescope was consistent with a Universe of nearly flat geometry since the commencement of its expansion. The data is consistent with a large offset radius of the Universe with a fractional increase in size since the commencement of expansion about 10 billion years ago.

The Differential Expansion of the Light Sphere Due to the Acceleration of the Expansion of the Cosmos As a Function of Time



The Periods of Spacetime Expansion/Contraction and Particle Decay/Production for the Universe Are Equal

- The period of the expansion/contraction cycle of the radius of the Universe, T , is

$$T = \frac{2\pi G m_U}{c^3} \text{ sec}$$

It follows from the Poynting power theorem with spherical radiation that the transition lifetimes are given by the ratio of energy and the power of the transition.

$$\tau = \frac{\text{energy}}{\text{power}} = \frac{(4\pi r^2) \left(\frac{1}{2} \right) \left(\frac{1}{r} \right)^2 \left(\frac{2l+1}{2} \right) \left(\frac{l+2}{l+1} \right)^2}{\frac{2\pi c}{[(2l+1)\Gamma(l+1)]} \left(\frac{1}{r} \right)^2} = \frac{1}{2\pi} \left(\frac{1}{r^2} \right) \sqrt{\frac{15}{4} \left(\frac{2l+1}{2} \right) \left(\frac{l+2}{l+1} \right)^2} \frac{1}{(2l+1)^2}$$

- Exponential decay applies to electromagnetic energy decay.

$$h(t) = e^{-\frac{t}{T}} u(t)$$

The Coordinate Time Is Imaginary Because Energy Transitions Are Spacelike Due Spacetime Expansion From Matter to Energy Conversion

- For example, the mass of the electron (a fundamental particle) is given by

$$\frac{2m_e}{\sqrt{\frac{GM_e}{c^3}}} = \frac{2\pi c}{v_s} = 10^{-1} \text{ sec}$$

where v_s is Newtonian velocity.

- When the gravitational radius r_s is the radius of the Universe, the proper time is equal to the coordinate time by

$$t = \pi \sqrt{\frac{GM}{c^3 r_s}} = \pi \sqrt{\frac{GM}{c^3 R_s}} = \pi \frac{c}{v_s}$$

and the gravitational escape velocity v_s of the Universe is the speed of light.

- Replacement of the coordinate time, t , by the spacelike time, $i\tau$, gives

$$h(i) = e^{-\frac{i\tau}{T}} = \cos \frac{2\pi i}{T}$$

where the period is T .

Period Equivalents

The periods of spacetime expansion/contraction and particle decay/production for the Universe are equal because only the particles which satisfy Maxwell's equations and the relationship between proper time and coordinate time imposed by the Schwarzschild metric may exist.

Continuity conditions based on the constant maximum speed of light (Maxwell's equations)

$$m_U c^2 = Aa^2 = \frac{A^2}{m_U \lambda_s^2} = C^2 - \frac{c^2}{4\pi G \lambda_s^2} = C^2 - \frac{mc^2 v_s^2}{(2\pi c)^2 \lambda_s^2} = \frac{c^2}{1 + \frac{2\pi c^2}{GM}}$$

Continuity conditions based on the constant maximum speed of light (Schwarzschild metric)

$$\frac{\text{proper time}}{\text{coordinate time}} = \frac{\text{gravitational wave condition}}{\text{electromagnetic wave condition}} = \frac{\text{gravitational mass phase matching}}{\text{charge/gravitational mass phase matching}}$$

$$\frac{\text{proper time}}{\text{coordinate time}} = \sqrt{\frac{GM}{c^3 r}} = \frac{v_s}{c}$$

Wave Equation

$$\frac{1}{c^2} \left(\frac{\partial \omega}{\partial t} \right)^2 - (grad\omega)^2 = 0$$

The equation of the radius of the Universe, R , may be written as

$$R = \left(\frac{2Gm_U}{c^2} + \frac{cm_U}{c^2} \right) - \frac{cm_U}{c^2} \cos \left(\frac{2\pi}{2\pi Gm_U} \left(t - \frac{R}{c} \right) \right) m$$

which is a solution to the wave equation.

Conclusion

Maxwell's equations, Planck's equation, the de Broglie equation, Newton's laws, and Special, and General Relativity are Unified.

The Grand Unified Theory of Classical Quantum Mechanics

POSTED AT
www.blacklightpower.com

THE GRAND UNIFIED THEORY OF CLASSICAL QUANTUM MECHANICS

Randell L. Mills
BlackLight Power, Inc.
493 Old Trenton Road
Cranbury, NJ 08512
(609)490-1090
rmills@blacklightpower.com
www.blacklightpower.com

A theory of classical quantum mechanics (CQM) is derived from first principles that successfully applies physical laws on all scales. Using Maxwell's equations, the classical wave equation is solved with the constraint that a bound electron cannot radiate energy. By further application of Maxwell's equations to electromagnetic and gravitational fields at particle production, the Schwarzschild metric (SM) is derived from the classical wave equation which modifies general relativity to include conservation of spacetime in addition to momentum and matter/energy. The result gives a natural relationship between Maxwell's equations, special relativity, and general relativity. It gives gravitation from the atom to the cosmos.

INTRODUCTION

A theory of classical quantum mechanics (CQM), derived from first principles, successfully applies physical laws on all scales [1]. The classical wave equation is solved with the constraint that a bound electron cannot radiate energy. The mathematical formulation for zero radiation based on Maxwell's equations follows from a derivation by Haus [2]. The function that describes the motion of the electron must not possess spacetime Fourier components that are synchronous with waves traveling at the speed of light. CQM gives closed form solutions for the atom including the stability of the $n=1$ state and the instability of the excited states, the equation of the photon and electron in excited states, the equation of the free electron, and photon which predict the wave particle duality behavior of particles and light. The current and charge density functions of the electron may be directly physically interpreted. For example, spin angular momentum results from the motion of negatively charged mass moving systematically, and the equation for angular momentum, $\mathbf{r} \times \mathbf{p}$, can be applied directly to the wave function (a current density function) that describes the electron. The magnetic moment of a Bohr magneton, Stern Gerlach experiment, g factor, Lamb shift, resonant line width and shape, selection rules, correspondence principle, wave particle duality, excited states, reduced mass, rotational energies, and momenta, orbital and spin splitting, spin-orbital coupling, Knight shift, and spin-nuclear coupling, ionization of two electron atoms, inelastic electron scattering from helium atoms, and the nature of the chemical bond are derived in closed form equations based on Maxwell's equations. The calculations agree with experimental observations.

For or any kind of wave advancing with limiting velocity and capable of transmitting signals, the equation of front propagation is the same as the equation for the front of a light wave. By applying this condition to electromagnetic and gravitational fields at particle production, the Schwarzschild metric (SM) is derived from the classical wave equation which modifies general relativity to include conservation of spacetime in addition to momentum and matter/energy. The result gives a natural relationship between Maxwell's equations, special relativity, and general relativity. It gives gravitation from the atom to the cosmos. The universe is time harmonically oscillatory in matter energy and spacetime expansion and contraction with a minimum radius that is the gravitational radius. In closed form equations with fundamental constants only, CQM gives the deflection of light by stars, the precession of the perihelion of Mercury, the particle masses, the Hubble constant, the age of the universe, the observed acceleration of the expansion, the power of the universe, the power spectrum of the universe, the microwave background temperature, the uniformity of the microwave background radiation, the microkelvin spatial variation of the microwave background radiation, the observed violation of the GZK cutoff, the mass density, the large scale structure of the universe, and the identity of dark matter which matches the criteria for the structure of galaxies. In a special case wherein the gravitational

potential energy density of a blackhole equals that of the Plank mass, matter converts to energy and spacetime expands with the release of a gamma ray burst. The singularity in the SM is eliminated.

CLASSICAL QUANTUM THEORY OF THE ATOM BASED ON MAXWELL S EQUATIONS

One-electron atoms include the hydrogen atom, He^+ , Li^{2+} , Be^{3+} , and so on. The mass-energy and angular momentum of the electron are constant; this requires that the equation of motion of the electron be temporally and spatially harmonic. Thus, the classical wave equation applies and

$$\left[\nabla^2 - \frac{1}{v^2} \frac{\delta^2}{\delta t^2} \right] \rho(r, \theta, \phi, t) = 0 \quad (1)$$

where $\rho(r, \theta, \phi, t)$ is the charge density function of the electron in time and space. In general, the wave equation has an infinite number of solutions. To arrive at the solution which represents the electron, a suitable boundary condition must be imposed. It is well known from experiments that each single atomic electron of a given isotope radiates to the same stable state. Thus, the physical boundary condition of nonradiation of the bound electron was imposed on the solution of the wave equation for the charge density function of the electron [1]. The condition for radiation by a moving point charge given by Haus [2] is that its spacetime Fourier transform does possess components that are synchronous with waves traveling at the speed of light. Conversely, it is proposed that the condition for nonradiation by an ensemble of moving point charges that comprises a current density function is

For non-radiative states, the current-density function must NOT possess spacetime Fourier components that are synchronous with waves traveling at the speed of light.

The time, radial, and angular solutions of the wave equation are separable. The motion is time harmonic with frequency ω_n . A constant angular function is a solution to the wave equation. The solution for the radial function which satisfies the boundary condition is a delta function

$$f(r) = \frac{1}{r^2} \delta(r - r_n) \quad (2)$$

which defines a constant charge function on a spherical shell where $r_n = n\ell$. Given time harmonic motion and a radial delta function, the relationship between an allowed radius and the electron wavelength is given by

$$2\pi r_n = \lambda_n \quad (3)$$

Using the de Broglie relationship for the electron mass where the coordinates are spherical,

$$\lambda_n = \frac{h}{p_n} = \frac{h}{m_e v_n} \quad (4)$$

and the magnitude of the velocity for *every* point on the orbitsphere is

$$v_n = \frac{\hbar}{m_e r_n} \quad (5)$$

The sum of the \mathbf{L}_i , the magnitude of the angular momentum of each infinitesimal point of the orbitsphere of mass m_i , must be constant. The constant is \hbar .

$$\sum |\mathbf{L}_i| = \sum |\mathbf{r} \times m_i \mathbf{v}| = m_e r_n \frac{\hbar}{m_e r_n} = \hbar \quad (6)$$

Thus, an electron is a spinning, two-dimensional spherical surface, called an *electron orbitsphere*, that can exist in a bound state at only specified distances from the nucleus as shown in Figure 1. The corresponding current function shown in Figure 2 which gives rise to the phenomenon of *spin* is derived in the "Spin Function" section.

Nonconstant functions are also solutions for the angular functions. To be a harmonic solution of the wave equation in spherical coordinates, these angular functions must be spherical harmonic functions. A zero of the spacetime Fourier transform of the product function of two spherical harmonic angular functions, a time harmonic function, and an unknown radial function is sought. The solution for the radial function which satisfies the boundary condition is also a delta function given by Eq. (2). Thus, bound electrons are described by a charge-density (mass-density) function which is the product of a radial delta function, two angular functions (spherical harmonic functions), and a time harmonic function.

$$\rho(r, \theta, \phi, t) = f(r)A(\theta, \phi, t) = \frac{1}{r^2} \delta(r - r_n)A(\theta, \phi, t); \quad A(\theta, \phi, t) = Y(\theta, \phi)k(t) \quad (7)$$

In these cases, the spherical harmonic functions correspond to a traveling charge density wave confined to the spherical shell which gives rise to the phenomenon of orbital angular momentum. The orbital functions which modulate the constant "spin" function shown graphically in Figure 3 are given in the "Angular Functions" section.

SPIN FUNCTION

The orbitsphere spin function comprises a constant charge density function with moving charge confined to a two-dimensional spherical shell. The current pattern of the orbitsphere spin function comprises an infinite series of correlated orthogonal great circle current loops wherein each point moves time harmonically with angular velocity

$$\omega_n = \frac{\hbar}{m_e r_n^2} \quad (8)$$

The current pattern is generated over the surface by a series of nested rotations of two orthogonal great circle current loops where the coordinate axes rotate with the two orthogonal

great circles. Half of the pattern is generated as the z-axis rotates to the negative z-axis during a 1st set of nested rotations. The mirror image, second half of the pattern is generated as the z-axis rotates back to its original direction during a 2nd set of nested rotations.

Points on Great Circle Current Loop One:

$$\begin{bmatrix} x_1 \\ y_1 \\ z_1 \end{bmatrix} = \begin{bmatrix} \cos(\Delta\alpha) & -\sin^2(\Delta\alpha) & -\sin(\Delta\alpha)\cos(\Delta\alpha) \\ 0 & \cos(\Delta\alpha) & -\sin(\Delta\alpha) \\ \sin(\Delta\alpha) & \cos(\Delta\alpha)\sin(\Delta\alpha) & \cos^2(\Delta\alpha) \end{bmatrix} \begin{bmatrix} x_1' \\ y_1' \\ z_1' \end{bmatrix} \quad (9)$$

and $\Delta\alpha' = -\Delta\alpha$ replaces $\Delta\alpha$ for $\sum_{n=1}^{\frac{\sqrt{2}\pi}{\Delta\alpha}} \Delta\alpha = \sqrt{2}\pi$; $\sum_{n=1}^{\frac{\sqrt{2}\pi}{|\Delta\alpha'|}} |\Delta\alpha'| = \sqrt{2}\pi$

Points on Great Circle Current Loop Two:

$$\begin{bmatrix} x_2 \\ y_2 \\ z_2 \end{bmatrix} = \begin{bmatrix} \cos(\Delta\alpha) & -\sin^2(\Delta\alpha) & -\sin(\Delta\alpha)\cos(\Delta\alpha) \\ 0 & \cos(\Delta\alpha) & -\sin(\Delta\alpha) \\ \sin(\Delta\alpha) & \cos(\Delta\alpha)\sin(\Delta\alpha) & \cos^2(\Delta\alpha) \end{bmatrix} \begin{bmatrix} x_2' \\ y_2' \\ z_2' \end{bmatrix} \quad (10)$$

and $\Delta\alpha' = -\Delta\alpha$ replaces $\Delta\alpha$ for $\sum_{n=1}^{\frac{\sqrt{2}\pi}{\Delta\alpha}} \Delta\alpha = \sqrt{2}\pi$; $\sum_{n=1}^{\frac{\sqrt{2}\pi}{|\Delta\alpha'|}} |\Delta\alpha'| = \sqrt{2}\pi$

The orbitsphere is given by reiterations of Eqs. (9) and (10). The output given by the non primed coordinates is the input of the next iteration corresponding to each successive nested rotation by the infinitesimal angle where the summation of the rotation about each of the x-axis

and the y-axis is $\sum_{n=1}^{\frac{\sqrt{2}\pi}{\Delta\alpha}} \Delta\alpha = \sqrt{2}\pi$ (1st set) and $\sum_{n=1}^{\frac{\sqrt{2}\pi}{|\Delta\alpha'|}} |\Delta\alpha'| = \sqrt{2}\pi$ (2nd set). The current pattern

corresponding to great circle current loop one and two shown with 8.49 degree increments of the infinitesimal angular variable $\Delta\alpha(\Delta\alpha')$ of Eqs. (9) and (10) is shown from the perspective of looking along the z-axis in Figure 2. The true orbitsphere current pattern is given as $\Delta\alpha(\Delta\alpha')$ approaches zero. This current pattern gives rise to the phenomenon corresponding to the spin quantum number of the electron.

STERN-GERLACH EXPERIMENT

The Stern-Gerlach experiment implies a magnetic moment of one Bohr magneton and an associated angular momentum quantum number of 1/2. Historically, this quantum number is called the spin quantum number, s ($s = \frac{1}{2}$; $m_s = \pm \frac{1}{2}$). The superposition of the vector projection of the orbitsphere angular momentum on to an axis S that precesses about the z -axis called the spin axis at an angle of $\theta = \frac{\pi}{3}$ and an angle of $\phi = \pi$ with respect to $\langle L_y \rangle_{\Sigma \Delta a}$ is

$$S = \pm \sqrt{\frac{3}{4}} \hbar \quad (11)$$

S rotates about the z -axis at the Larmor frequency. $\langle S_z \rangle$, the time averaged projection of the orbitsphere angular momentum onto the axis of the applied magnetic field is

$$\langle L_z \rangle_{\Sigma \Delta a} \pm \frac{\hbar}{2}. \quad (12)$$

ELECTRON g FACTOR

Conservation of angular momentum of the orbitsphere permits a discrete change of its kinetic angular momentum ($r \times mv$) by the applied magnetic field of $\frac{\hbar}{2}$, and concomitantly the potential angular momentum ($r \times eA$) must change by $-\frac{\hbar}{2}$.

$$\Delta L = \frac{\hbar}{2} - r \times eA \quad (13)$$

$$= \frac{\hbar}{2} - \frac{e\phi}{2\pi} \quad (14)$$

In order that the change of angular momentum, ΔL , equals zero, ϕ must be $\Phi_0 = \frac{\hbar}{2e}$, the magnetic flux quantum. The magnetic moment of the electron is parallel or antiparallel to the applied field only. The total energy of the flip transition is the sum of the energy of a fluxon treading the orbitsphere and the energy of reorientation of the magnetic moment.

$$\Delta E_{mag}^{spin} = 2 \left(\mu_B B + \frac{\alpha}{2\pi} \mu_B B \right) \quad (15)$$

$$\Delta E_{mag}^{spin} = 2(1 + \frac{\alpha}{2\pi}) \mu_B B \quad (16)$$

$$\Delta E_{mag}^{spin} = 2g\mu_B B \quad (17)$$

The spin-flip transition can be considered as involving a magnetic moment of g times that of a Bohr magneton. The predicted value of the g factor is 1.00116. The experimental value is 1.00116.

Magnetic Field Equations of the Electron

The orbitsphere is a shell of negative charge current comprising correlated charge motion along great circles. For $\lambda = 0$, the orbitsphere gives rise to a magnetic moment of 1 Bohr magneton [3].

$$\mu_B = \frac{e\hbar}{2m_e} = 9.274 \times 10^{-24} JT^{-1}, \quad (18)$$

The magnetic field of the electron shown in Figure 4 is given by

$$\mathbf{H} = \frac{e\hbar}{m_e r_n^3} (\mathbf{i}_r \cos \theta - \mathbf{i}_\theta \sin \theta) \quad \text{for } r < r_n \quad (19)$$

$$\mathbf{H} = \frac{e\hbar}{2m_e r^3} (\mathbf{i}_r 2 \cos \theta - \mathbf{i}_\theta \sin \theta) \quad \text{for } r > r_n \quad (20)$$

The energy stored in the magnetic field of the electron is

$$E_{mag} = \frac{1}{2} \mu_0 \int_0^{2\pi} \int_0^\pi \int_0^r H^2 r^2 \sin \theta dr d\theta d\Phi \quad (21)$$

$$E_{mag \text{ total}} = \frac{\pi \mu_0 e^2 \hbar^2}{m_e^2 r_1^3} \quad (22)$$

ANGULAR FUNCTIONS

The time, radial, and angular solutions of the wave equation are separable. Also based on the radial solution, the angular charge and current-density functions of the electron, $A(\theta, \phi, t)$, must be a solution of the wave equation in two dimensions (plus time),

$$\left[\nabla^2 - \frac{1}{v^2} \frac{\delta^2}{\delta t^2} \right] A(\theta, \phi, t) = 0 \quad (23)$$

where $\rho(r, \theta, \phi, t) = f(r)A(\theta, \phi, t) = \frac{1}{r^2} \delta(r - r_n)A(\theta, \phi, t)$ and $A(\theta, \phi, t) = Y(\theta, \phi)k(t)$

$$\left[\frac{1}{r^2 \sin \theta} \frac{\delta}{\delta \theta} \left(\sin \theta \frac{\delta}{\delta \theta} \right)_{r, \phi} + \frac{1}{r^2 \sin^2 \theta} \left(\frac{\delta^2}{\delta \phi^2} \right)_{r, \theta} - \frac{1}{v^2} \frac{\delta^2}{\delta t^2} \right] A(\theta, \phi, t) = 0 \quad (24)$$

where v is the linear velocity of the electron. The charge-density functions including the time-function factor are

$$\lambda = 0$$

$$\rho(r, \theta, \phi, t) = \frac{e}{8\pi r^2} [\delta(r - r_n)] [Y_\ell^m(\theta, \phi) + Y_0^0(\theta, \phi)] \quad (25)$$

$$\lambda > 0$$

$$\rho(r, \theta, \phi, t) = \frac{e}{4\pi r^2} [\delta(r - r_n)] [Y_0^0(\theta, \phi) + \text{Re}\{Y_\ell^m(\theta, \phi)[1 + e^{i\omega_n t}]\}] \quad (26)$$

$\text{Re}\{Y_\ell^m(\theta, \phi)[1 + e^{i\omega_n t}]\} = \text{Re}[Y_\ell^m(\theta, \phi) + Y_\ell^m(\theta, \phi)e^{i\omega_n t}] = P_\ell^m(\cos\theta)\cos m\phi + P_\ell^m(\cos\theta)\cos(m\phi + \omega_n t)$
and $\omega_n = 0$ for $m = 0$.

SPIN AND ORBITAL PARAMETERS

The total function that describes the spinning motion of each electron orbitsphere is composed of two functions. One function, the spin function, is spatially uniform over the orbitsphere, spins with a quantized angular velocity, and gives rise to spin angular momentum. The other function, the modulation function, can be spatially uniform in which case there is no orbital angular momentum and the magnetic moment of the electron orbitsphere is one Bohr magneton or not spatially uniform in which case there is orbital angular momentum. The modulation function also rotates with a quantized angular velocity.

The spin function of the electron corresponds to the nonradiative $n=1$, $\ell = 0$ state of atomic hydrogen which is well known as an s state or orbital. (See Figure 1 for the charge function and Figure 2 for the current function.) For orbitals with the ℓ quantum number not equal to zero, the constant spin function is modulated by a time and spherical harmonic function as given by Eq. (26) and shown in Figure 3. The modulation or traveling charge density wave corresponds to an orbital angular momentum in addition to a spin angular momentum. These states are typically referred to as p, d, f, etc. orbitals. Application of Haus's [2] condition also predicts nonradiation for a constant spin function modulated by a time and spherically harmonic orbital function. There is acceleration without radiation. (Also see Abbott and Griffiths and Goedecke [4-5]). However, in the case that such a state arises as an excited state by photon absorption, it is radiative due to a radial dipole term in its current density function since it possess spacetime Fourier Transform components synchronous with waves traveling at the speed of light [2]. (See "Instability of Excited States" section.)

Moment of Inertia and Spin and Rotational Energies

$$\mathbf{\hat{l}} = \mathbf{0}$$

$$I_z = I_{\text{spin}} = \frac{m_e r_n^2}{2} \quad (27)$$

$$L_z = I\omega_i z = \pm \frac{\hbar}{2} \quad (28)$$

$$E_{rotational} = E_{rotational, spin} = \frac{1}{2} \left[I_{spin} \left(\frac{\hbar}{m_e r_n^2} \right)^2 \right] = \frac{1}{2} \left[\frac{m_e r_n^2}{2} \left(\frac{\hbar}{m_e r_n^2} \right)^2 \right] = \frac{1}{4} \left[\frac{\hbar^2}{2 I_{spin}} \right] \quad (29)$$

$\lambda \rightarrow 0$

$$I_{orbital} = m_e r_n^2 \left[\frac{\ell(\ell+1)}{\ell^2 + \ell + 1} \right]^{\frac{1}{2}} \quad (30)$$

$$L_z = m\hbar \quad (31)$$

$$L_{z total} = L_{z spin} + L_{z orbital} \quad (32)$$

$$E_{rotational, orbital} = \frac{\hbar^2}{2I} \left[\frac{\ell(\ell+1)}{\ell^2 + 2\ell + 1} \right] \quad (33)$$

$$T = \frac{\hbar^2}{2m_e r_n^2} \quad (34)$$

$$\langle E_{rotational, orbital} \rangle = 0 \quad (35)$$

From Eq. (35), the time average rotational energy is zero; thus, the principal levels are degenerate except when a magnetic field is applied.

NONRADIATION CONDITION (Acceleration Without Radiation)

The Fourier transform of the electron charge density function is a solution of the four-dimensional wave equation in frequency space (\mathbf{k}, ω space). Then the corresponding Fourier transform of the current density function $K(s, \Theta, \Phi, \omega)$ is given by multiplying by the constant angular frequency.

$$K(s, \Theta, \Phi, \omega) = 4\pi\omega_n \frac{\sin(2s_n r_n)}{2s_n r_n} \otimes 2\pi \sum_{v=1}^{\infty} \frac{(-1)^{v-1} (\pi \sin \Theta)^{2(v-1)}}{(v-1)!(v-1)!} \frac{\Gamma\left(\frac{1}{2}\right)\Gamma\left(v+\frac{1}{2}\right)}{(\pi \cos \Theta)^{2v+1} 2^{v+1}} \frac{2v!}{(v-1)!} s^{-2v} \quad (36)$$

$$\otimes 2\pi \sum_{v=1}^{\infty} \frac{(-1)^{v-1} (\pi \sin \Phi)^{2(v-1)}}{(v-1)!(v-1)!} \frac{\Gamma\left(\frac{1}{2}\right)\Gamma\left(v+\frac{1}{2}\right)}{(\pi \cos \Phi)^{2v+1} 2^{v+1}} \frac{2v!}{(v-1)!} \frac{1}{4\pi} [\delta(\omega - \omega_n) + \delta(\omega + \omega_n)]$$

$$s_n \bullet v_n = s_n \bullet \mathbf{c} = \omega_n \text{ implies } r_n = \lambda_n \text{ Spacetime harmonics of } \frac{\omega_n}{c} = k \text{ or } \frac{\omega_n}{c} \sqrt{\frac{\epsilon}{\epsilon_0}} = k \text{ for which}$$

the Fourier transform of the current-density function is nonzero do not exist. Radiation due to charge motion does not occur in any medium when this boundary condition is met.

FORCE BALANCE EQUATION

The radius of the nonradiative ($n=1$) state is solved using the electromagnetic force equations of Maxwell relating the charge and mass density functions wherein the angular

momentum of the electron is given by Planck's constant bar. The reduced mass arises naturally from an electrodynamic interaction between the electron and the proton.

$$\frac{m_e}{4\pi r_1^2} \frac{v_1^2}{r_1} = \frac{e}{4\pi r_1^2} \frac{Ze}{4\pi\epsilon_0 r_1^2} - \frac{1}{4\pi r_1^2} \frac{\hbar^2}{mr_n^3} \quad (37)$$

$$r_1 = \frac{a_H}{Z} \quad (38)$$

ENERGY CALCULATIONS

From Maxwell's equations, the potential energy V , kinetic energy T , electric energy or binding energy E_{ele} are

$$V = \frac{-Ze^2}{4\pi\epsilon_0 r_1} = \frac{-Z^2 e^2}{4\pi\epsilon_0 a_H} = -Z^2 \times 4.3675 \times 10^{-18} J = -Z^2 \times 27.2 eV \quad (39)$$

$$T = \frac{Z^2 e^2}{8\pi\epsilon_0 a_H} = Z^2 \times 13.59 eV \quad (40)$$

$$T = E_{ele} = -\frac{1}{2} \int_{\infty}^{r_1} \mathbf{E}^2 dv \text{ where } \mathbf{E} = -\frac{Ze}{4\pi\epsilon_0 r^2}. \quad (41)$$

$$E_{ele} = -\frac{Z^2 e^2}{8\pi\epsilon_0 a_H} = -Z^2 \times 2.1786 \times 10^{-18} J = -Z^2 \times 13.598 eV \quad (42)$$

The calculated Rydberg constant is $109,677.58 \text{ cm}^{-1}$; the experimental Rydberg constant is $109,677.58 \text{ cm}^{-1}$.

EXCITED STATES

CQM gives closed form solutions for the resonant photons and excited state electron functions. The angular momentum of the photon given by

$$\mathbf{m} = \frac{1}{8\pi} \operatorname{Re}[\mathbf{r} \times (\mathbf{E} \times \mathbf{B}^*)] = \hbar \quad (43)$$

is conserved [6]. The change in angular velocity of the electron is equal to the angular frequency of the resonant photon. The energy is given by Planck's equation. The predicted energies, Lamb shift, hyperfine structure, resonant line shape, line width, selection rules, etc. are in agreement with observation.

The orbitsphere is a dynamic spherical resonator cavity which traps photons of discrete frequencies. The relationship between an allowed radius and the photon standing wave wavelength is

$$2\pi r = n\lambda \quad (44)$$

where n is an integer. The relationship between an allowed radius and the electron wavelength is

$$2\pi(nr_1) = 2\pi r_n = n\lambda_1 = \lambda_n \quad (45)$$

where $n = 1, 2, 3, 4, \dots$. The radius of an orbitsphere increases with the absorption of electromagnetic energy. The radii of excited states are solved using the electromagnetic force

equations of Maxwell relating the field from the charge of the proton, the electric field the photon, and charge and mass density functions of the electron wherein the angular momentum of the electron is given by Planck's constant bar (Eq. (37)). The solutions to Maxwell's equations for modes that can be excited in the orbitsphere resonator cavity give rise to four quantum numbers, and the energies of the modes are the experimentally known hydrogen spectrum. The relationship between the electric field equation and the trapped photon source charge-density function is given by Maxwell's equation in two dimensions.

$$\mathbf{n} \cdot (\mathbf{E}_1 - \mathbf{E}_2) = \frac{\sigma}{\epsilon_0} \quad (46)$$

The photon standing electromagnetic wave is phase matched with the electron

$$\mathbf{E}_{r_{photon}, n, l, m} = \frac{e(na_H)^l}{4\pi\epsilon_0} \frac{1}{r^{(l+2)}} \left[-Y_0^0(\theta, \phi) + \frac{1}{n} \left[Y_0^m(\theta, \phi) + \text{Re}\{Y_l^m(\theta, \phi)[1 + e^{i\omega_n t}]\} \right] \right] \quad (47)$$

$$\omega_n = 0 \text{ for } m = 0$$

$$l = 1, 2, \dots, n-1$$

$$m = -l, -l+1, \dots, 0, \dots, +l$$

$$\mathbf{E}_{r_{total}} = \frac{e}{4\pi\epsilon_0 r^2} + \frac{e(na_H)^l}{4\pi\epsilon_0 r^{l+2}} \left[-Y_0^0(\theta, \phi) + \frac{1}{n} \left[Y_0^0(\theta, \phi) + \text{Re}\{Y_l^m(\theta, \phi)[1 + e^{i\omega_n t}]\} \right] \right] \quad (48)$$

$$\omega_n = 0 \text{ for } m = 0$$

For $r = na_H$ and $m = 0$, the total radial electric field is

$$\mathbf{E}_{r_{total}} = \frac{1}{n} \frac{e}{4\pi\epsilon_0 (na_H)^2} \quad (49)$$

The energy of the photon which excites a mode in the electron spherical resonator cavity from radius a_H to radius na_H is

$$E_{photon} = \frac{e^2}{8\pi\epsilon_0 a_H} \left[1 - \frac{1}{n^2} \right] = \hbar\nu = \hbar\omega \quad (50)$$

The change in angular velocity of the orbitsphere for an excitation from $n = 1$ to $n = n$ is

$$\Delta\omega = \frac{\hbar}{m_e(a_H)^2} - \frac{\hbar}{m_e(na_H)^2} = \frac{\hbar}{m_e(a_H)^2} \left[1 - \frac{1}{n^2} \right] \quad (51)$$

The kinetic energy change of the transition is

$$\frac{1}{2} m_e (\Delta\nu)^2 = \frac{e^2}{8\pi\epsilon_0 a_H} \left[1 - \frac{1}{n^2} \right] = \hbar\omega \quad (52)$$

The change in angular velocity of the electron orbitsphere is identical to the angular velocity of the photon necessary for the excitation, ω_{photon} . The *correspondence principle holds*. It can be demonstrated that the resonance condition between these frequencies is to be satisfied in order to have a net change of the energy field [7].

ORBITAL AND SPIN SPLITTING

The ratio of the square of the angular momentum, M^2 , to the square of the energy, U^2 , for a pure (ℓ, m) multipole is [8]

$$\frac{M^2}{U^2} = \frac{m^2}{\omega^2} \quad (53)$$

The magnetic moment is defined as

$$\mu = \frac{\text{charge} \times \text{angular momentum}}{2 \times \text{mass}} \quad (54)$$

The radiation of a multipole of order (ℓ, m) carries $m\hbar$ units of the z component of angular momentum per photon of energy $\hbar\omega$. Thus, the z component of the angular momentum of the corresponding excited state electron orbitsphere is

$$L_z = m\hbar \quad (55)$$

Therefore,

$$\mu_z = \frac{em\hbar}{2m_e} = m\mu_B \quad (56)$$

where μ_B is the Bohr magneton. The orbital splitting energy is

$$E_{mag}^{orb} = m\mu_B B \quad (57)$$

The spin and orbital splitting energies superimpose; thus, the principal excited state energy levels of the hydrogen atom are split by the energy $E_{mag}^{spin/orb}$.

$$E_{mag}^{spin/orb} = m \frac{e\hbar}{2m_e} B + m_s g \frac{e\hbar}{m_e} B \text{ where} \quad (58)$$

$$n = 2, 3, 4, \dots$$

$$\ell = 1, 2, \dots, n - 1$$

$$m = -\ell, -\ell + 1, \dots, 0, \dots, +\ell$$

$$m_s = \pm \frac{1}{2}$$

For the electric dipole transition, the selection rules are

$$\Delta n = 0, \pm 1 \quad (59)$$

$$\Delta m_s = 0$$

RESONANT LINE SHAPE AND LAMB SHIFT

The spectroscopic linewidth shown in Figure 5 arises from the classical rise-time band-width relationship, and the Lamb Shift is due to conservation of energy and linear momentum and arises from the radiation reaction force between the electron and the photon. It follows from the Poynting power theorem with spherical radiation that the transition probabilities are given by the ratio of power and the energy of the transition [9]. The transition probability in the case of the electric multipole moment is

$$\frac{1}{\tau} = \frac{\text{power}}{\text{energy}} \quad (60)$$

$$\tau = \left[\frac{[\hbar\omega]}{\frac{2\pi c}{[(2l+1)!!]^2} \left(\frac{l+1}{l} \right) k^{2l+1} |Q_{lm} + Q_{lm}^*|^2} \right] = \frac{1}{2\pi} \left(\frac{\hbar}{e^2} \right) \sqrt{\frac{\mu_0}{\epsilon_0}} \frac{[(2l+1)!!]^2}{2\pi} \left(\frac{l}{l+1} \right) \left(\frac{l+3}{3} \right)^2 \frac{1}{(kr_n)^2 \omega} \quad (61)$$

$$E(\omega) \propto \int_0^\infty e^{-\alpha t} e^{-i\omega t} dt = \frac{1}{\alpha - i\omega} \quad (62)$$

The relationship between the rise-time and the band-width for exponential decay is

$$\tau\Gamma = \frac{1}{\pi} \quad (63)$$

The energy radiated per unit frequency interval is

$$\frac{dI(\omega)}{d\omega} = I_0 \frac{\Gamma}{2\pi} \frac{1}{(\omega - \omega_0 - \Delta\omega)^2 + (\Gamma/2)^2} \quad (64)$$

LAMB SHIFT

The Lamb Shift of the ${}^2P_{1/2}$ state of the hydrogen atom is due to conservation of linear momentum of the electron, atom, and photon. The electron component is

$$\Delta f = \frac{\Delta\omega}{2\pi} = \frac{E_{hv}}{h} = 3 \frac{(E_{hv})^2}{h2m_e c^2} = 1052 \text{ MHz} \quad (65)$$

where E_{hv} is

$$E_{hv} = 13.6 \left(1 - \frac{1}{n^2} \right) \frac{1}{|X_{lm}|_{l=1}^2} - h\Delta f \quad (66)$$

$$E_{hv} = 13.6 \left(1 - \frac{1}{n^2} \right) \frac{3}{8\pi} - h\Delta f \quad (67)$$

$$h\Delta f \ll 1 \quad (68)$$

Therefore,

$$E_{hv} = 13.6 \left(1 - \frac{1}{n^2} \right) \frac{3}{8\pi} \quad (69)$$

The atom component is

$$\Delta f = \frac{\Delta\omega}{2\pi} = \frac{E_{hv}}{h} = \frac{1}{2} \frac{(E_{hv})^2}{2m_H c^2} = 6.5 \text{ MHz} \quad (70)$$

The sum of the components is

$$\Delta f = 1052 \text{ MHz} + 6.5 \text{ MHz} = 1058.5 \text{ MHz} \quad (71)$$

The experimental Lamb Shift is 1058 MHz.

INSTABILITY OF EXCITED STATES

For the excited energy states of the hydrogen atom, σ_{photon} , the two dimensional surface charge due to the trapped photons at the electron orbitsphere, given by Eq. (46) and Eq. (47) is

$$\sigma_{photon} = \frac{e}{4\pi(r_n)^2} \left[Y_0^0(\theta, \phi) - \frac{1}{n} \left[Y_0^0(\theta, \phi) + \text{Re}\{Y_\ell^m(\theta, \phi)[1 + e^{i\omega_n t}]\} \right] \right] \delta(r - r_n) \quad (72)$$

where $n = 2, 3, 4, \dots$. Whereas, $\sigma_{electron}$, the two dimensional surface charge of the electron orbitsphere given by Eq. (26) is

$$\sigma_{electron} = \frac{-e}{4\pi(r_n)^2} \left[Y_0^0(\theta, \phi) + \text{Re}\{Y_\ell^m(\theta, \phi)[1 + e^{i\omega_n t}]\} \right] \delta(r - r_n) \quad (73)$$

The superposition of σ_{photon} (Eq. (72)) and $\sigma_{electron}$ is equivalent to the sum of a radial electric dipole represented by a doublet function and a radial electric monopole represented by a delta function.

$$\sigma_{photon} + \sigma_{electron} =$$

$$\frac{e}{4\pi(r_n)^2} \left[Y_0^0(\theta, \phi) \delta(r - r_n) - \frac{1}{n} Y_0^0(\theta, \phi) \delta(r - r_n) - \left(1 + \frac{1}{n} \right) \text{Re}\{Y_\ell^m(\theta, \phi)[1 + e^{i\omega_n t}]\} \right] \delta(r - r_n) \quad (74)$$

where $n = 2, 3, 4, \dots$. Due to the radial doublet, excited states are radiative since spacetime harmonics of $\frac{\omega_n}{c} = k$ or $\frac{\omega_n}{c} \sqrt{\frac{\epsilon}{\epsilon_0}} = k$ do exist for which the spacetime Fourier transform of the current density function is nonzero.

PHOTON EQUATIONS

The time-averaged angular-momentum density, \mathbf{m} , of an emitted photon is

$$\mathbf{m} = \frac{1}{8\pi} \text{Re}[\mathbf{r} \times (\mathbf{E} \times \mathbf{B}^*)] = \hbar \quad (75)$$

A linearly polarized photon orbitsphere is generated from two orthogonal great circle field lines shown in Figure 6 rather than two great circle current loops as in the case of the electron spin function. The right-handed circularly polarized photon orbitsphere shown in Figure 7 corresponds to the case wherein the summation of the rotation about each of the x-axis and the y-

axis is $\sum_{n=1}^{\frac{\sqrt{2}\pi}{\Delta\alpha}} \Delta\alpha = \sqrt{2}\pi$, and the mirror image left-handed circularly polarized photon orbitsphere

corresponds to the case wherein the summation of the rotation about each of the x-axis and the y-

axis is $\sum_{n=1}^{\frac{\sqrt{2}\pi}{|\Delta\alpha'|}} |\Delta\alpha'| = \sqrt{2}\pi$.

Nested Set of Great Circle Field Lines Generates the Photon Function

H Field:

$$\begin{bmatrix} x_1 \\ y_1 \\ z_1 \end{bmatrix} = \begin{bmatrix} \cos(\Delta\alpha) & -\sin^2(\Delta\alpha) & -\sin(\Delta\alpha)\cos(\Delta\alpha) \\ 0 & \cos(\Delta\alpha) & -\sin(\Delta\alpha) \\ \sin(\Delta\alpha) & \cos(\Delta\alpha)\sin(\Delta\alpha) & \cos^2(\Delta\alpha) \end{bmatrix} \begin{bmatrix} x_1' \\ y_1' \\ z_1' \end{bmatrix} \quad (76)$$

and $\Delta\alpha' = -\Delta\alpha$ replaces $\Delta\alpha$ for $\sum_{n=1}^{\frac{\sqrt{2}\pi}{\Delta\alpha}} \Delta\alpha = \sqrt{2}\pi$; $\sum_{n=1}^{\frac{\sqrt{2}\pi}{|\Delta\alpha'|}} |\Delta\alpha'| = \sqrt{2}\pi$

E Field:

$$\begin{bmatrix} x_2 \\ y_2 \\ z_2 \end{bmatrix} = \begin{bmatrix} \cos(\Delta\alpha) & -\sin^2(\Delta\alpha) & -\sin(\Delta\alpha)\cos(\Delta\alpha) \\ 0 & \cos(\Delta\alpha) & -\sin(\Delta\alpha) \\ \sin(\Delta\alpha) & \cos(\Delta\alpha)\sin(\Delta\alpha) & \cos^2(\Delta\alpha) \end{bmatrix} \begin{bmatrix} x_2' \\ y_2' \\ z_2' \end{bmatrix} \quad (77)$$

and $\Delta\alpha' = -\Delta\alpha$ replaces $\Delta\alpha$ for $\sum_{n=1}^{\frac{\sqrt{2}\pi}{\Delta\alpha}} \Delta\alpha = \sqrt{2}\pi$; $\sum_{n=1}^{\frac{\sqrt{2}\pi}{|\Delta\alpha'|}} |\Delta\alpha'| = \sqrt{2}\pi$

The field lines in the lab frame follow from the relativistic invariance of charge as given by Purcell [10]. The relationship between the relativistic velocity and the electric field of a moving charge shown schematically in Figure 8. From Eqs. (76-77) with $\sum_{n=1}^{\frac{\sqrt{2}\pi}{\Delta\alpha}} \Delta\alpha = \sqrt{2}\pi$, the photon equation in the lab frame of a right-handed circularly polarized photon orbitsphere is

$$\mathbf{E} = \mathbf{E}_0[\mathbf{x} + i\mathbf{y}]e^{-jk_z z} e^{-j\omega t} \quad (78)$$

$$\mathbf{H} = \left(\frac{\mathbf{E}_0}{\eta} \right) [\mathbf{y} - i\mathbf{x}]e^{-jk_z z} e^{-j\omega t} = \mathbf{E}_0 \sqrt{\frac{\epsilon}{\mu}} [\mathbf{y} - i\mathbf{x}]e^{-jk_z z} e^{-j\omega t} \quad (79)$$

with a wavelength of

$$\lambda = 2\pi \frac{c}{\omega} \quad (80)$$

The relationship between the photon orbitsphere radius and wavelength is

$$2\pi r_o = \lambda_o \quad (81)$$

The electric field lines of a right-handed circularly polarized photon orbitsphere as seen along the axis of propagation in the lab inertial reference frame as it passes a fixed point is shown in Figure 9.

Spherical Wave

Photons superimpose, and the amplitude due to N photons is

$$\mathbf{E}_{total} = \sum_{n=1}^N \frac{e^{-ik|\mathbf{r}-\mathbf{r}'|}}{4\pi|\mathbf{r}-\mathbf{r}'|} f(\phi, \theta) \quad (82)$$

In the far field, the emitted wave is a spherical wave

$$\mathbf{E}_{total} = E_o \frac{e^{-ikr}}{r} \quad (83)$$

The Green Function is given as the solution of the wave equation. Thus, the superposition of photons gives the classical result. As r goes to infinity, the spherical wave becomes a plane wave. The double slit interference pattern is predicted. From the equation of a photon, the wave-particle duality arises naturally. The energy is always given by Planck's equation; yet, an interference pattern is observed when photons add over time or space.

EQUATIONS OF THE FREE ELECTRON

Charge Density Function

The radius of an electron orbitsphere increases with the absorption of electromagnetic energy [11]. With the absorption of a photon of energy exactly equal to the ionization energy, the electron becomes ionized and is a plane wave (spherical wave in the limit) with the de Broglie wavelength. The ionized electron traveling at constant velocity is nonradiative and is a two dimensional surface having a total charge of e and a total mass of m_e . The solution of the boundary value problem of the free electron is given by the projection of the orbitsphere into a plane that linearly propagates along an axis perpendicular to the plane where the velocity of the plane and the orbitsphere is given by

$$v = \frac{\hbar}{m_e \rho_0} \quad (84)$$

and the radius of the orbitsphere in spherical coordinates is equal to the radius of the free electron in cylindrical coordinates ($\rho_0 = r_0$). The mass density function of a free electron shown in Figure 10 is a two dimensional disk having the mass density distribution in the $xy(\rho)$ -plane

$$\rho_m(\rho, \phi, z) = \frac{m_e}{\frac{3}{2}\pi\rho_0^3} \mathcal{P}\left(\frac{\rho}{2\rho_0}\right) \sqrt{\rho_0^2 - \rho^2} \delta(z) \quad (85)$$

and charge-density distribution, $\rho_e(\rho, \phi, z)$, in the xy -plane given by replacing m_e with e . The charge density distribution of the free electron has recently been confirmed experimentally [12-]

13]. Researchers working at the Japanese National Laboratory for High Energy Physics (KEK) demonstrated that the charge of the free electron increases toward the particle's core and is symmetrical as a function of ϕ . In addition, the wave-particle duality arises naturally, and the result is consistent with scattering experiments from helium and the double split experiment [1].

Current Density Function

Consider an electron initially bound as an orbitsphere of radius $r = r_n = r_o$ ionized from a hydrogen atom with the magnitude of the angular velocity of the orbitsphere is given by

$$\omega = \frac{\hbar}{m_e r^2} \quad (86)$$

The current-density function of the free electron propagating with velocity v_z along the z-axis in the inertial frame of the proton is given by the vector projection of the current into xy-plane as the radius increases from $r = r_o$ to $r = \infty$. The current-density function of the free electron, is

$$\mathbf{J}(\rho, \phi, z, t) = \left[\pi \left(\frac{\rho}{2\rho_o} \right) \frac{e}{\frac{4}{3}\pi\rho_o^3 m_e \sqrt{\rho_o^2 - \rho^2}} \mathbf{i}_\phi \right] \quad (87)$$

where $\rho_o = r_o$. The angular momentum, \mathbf{L} , is given by

$$\mathbf{L}_{i_z} = m_e r^2 \omega \quad (88)$$

Substitution of m_e for e in Eq. (87) followed by substitution into Eq. (88) gives the angular momentum density function, \mathbf{L}

$$\mathbf{L}_{i_z} = \pi \left(\frac{\rho}{2\rho_o} \right) \frac{m_e}{\frac{4}{3}\pi\rho_o^3 m_e \sqrt{\rho_o^2 - \rho^2}} \rho^2 \quad (89)$$

The total angular momentum of the free electron is given by integration over the two dimensional disk having the angular momentum density given by Eq. (89).

$$\mathbf{L}_{i_z} = \int_0^{2\pi} \int_0^{\rho_o} \pi \left(\frac{\rho}{2\rho_o} \right) \frac{m_e}{\frac{4}{3}\pi\rho_o^3 m_e \sqrt{\rho_o^2 - \rho^2}} \rho^2 \rho d\rho d\phi = \hbar \quad (90)$$

The four dimensional spacetime current-density function of the free electron that propagates along the z-axis with velocity given by Eq. (84) corresponding to $r = r_o = \rho_o$ is given by substitution of Eq. (84) into Eq. (88).

$$\mathbf{J}(\rho, \phi, z, t) = \left[\pi \left(\frac{\rho}{2\rho_o} \right) \frac{e}{\frac{4}{3}\pi\rho_o^3 m_e \sqrt{\rho_o^2 - \rho^2}} \mathbf{i}_\phi \right] + \frac{e\hbar}{m_e \rho_o} \delta(z - \frac{\hbar}{m_e \rho_o} t) \mathbf{i}_z \quad (91)$$

The spacetime Fourier Transform of is

$$\frac{e}{4} \frac{\hbar}{\pi \rho_0^3 m_e} \text{sinc}(2\pi s\rho_o) + 2\pi e \frac{\hbar}{m_e \rho_0} \delta(\omega - \mathbf{k}_z \cdot \mathbf{v}_z) \quad (92)$$

Spacetime harmonics of $\frac{\omega_n}{c} = k$ or $\frac{\omega_n}{c} \sqrt{\frac{\epsilon}{\epsilon_o}} = k$ do not exist. Radiation due to charge motion does not occur in any medium when this boundary condition is met. Thus, no Fourier components that are synchronous with light velocity with the propagation constant $|\mathbf{k}_z| = \frac{\omega}{c}$ exist. Radiation due to charge motion does not occur when this boundary condition is met. It follows from Eq. (84) and the relationship $2\pi\rho_o = \lambda_o$ that the wavelength of the free electron is the de Broglie wavelength.

$$\lambda_o = \frac{\hbar}{m_e v_z} = 2\pi\rho_o \quad (93)$$

In the presence of a z-axis applied magnetic field, the free electron precesses. The time average vector projection of the total angular momentum of the free electron onto an axis S that rotates about the z-axis is $\pm \sqrt{\frac{3}{4}}\hbar$, and the time averaged projection of the angular momentum onto the axis of the applied magnetic field is $\pm \frac{\hbar}{2}$. Magnetic flux is linked by the electron in units of the magnetic flux quantum with conservation of angular momentum as in the case of the orbitsphere as the projection of the angular momentum along the magnetic field axis of $\frac{\hbar}{2}$ reverses direction. The energy, ΔE_{mag}^{spin} , of the spin flip transition corresponding to the $m_s = \frac{1}{2}$ quantum number is given by Eq. (17).

$$\Delta E_{mag}^{spin} = 2g\mu_B B \quad (94)$$

The Stern-Gerlach experiment implies a magnetic moment of one Bohr magneton and an associated angular momentum quantum number of 1/2. Historically, this quantum number is called the spin quantum number, m_s , and that designation is maintained.

TWO ELECTRON ATOMS

Two electron atoms may be solved from a central force balance equation with the nonradiation condition. The force balance equation is

$$\frac{m_e v_2^2}{4\pi r_2^2 r_2} = \frac{e}{4\pi r_2^2} \frac{(Z-1)e}{4\pi \epsilon_o r_2^2} + \frac{1}{4\pi r_2^2} \frac{\hbar^2}{Z m_e r_2^3} \sqrt{s(s+1)} \quad (95)$$

which gives the radius of both electrons as

$$r_2 = r_1 = a_0 \left(\frac{1}{Z-1} - \frac{\sqrt{s(s+1)}}{Z(Z-1)} \right); s = \frac{1}{2} \quad (96)$$

Ionization Energies Calculated using the Poynting Power Theorem

For helium, which has no electric field beyond r_1

$$\text{Ionization Energy}(He) = -E(\text{electric}) + E(\text{magnetic}) \quad (97)$$

where,

$$E(\text{electric}) = -\frac{(Z-1)e^2}{8\pi\epsilon_0 r_1} \quad (98)$$

$$E(\text{magnetic}) = \frac{2\pi\mu_0 e^2 \hbar^2}{m_e^2 r_1^3} \quad (99)$$

For $3 \leq Z$

$$\text{Ionization Energy} = -\text{Electric Energy} - \frac{1}{Z} \text{Magnetic Energy} \quad (100)$$

The energies of several two-electron atoms are given in Table 1.

ELASTIC ELECTRON SCATTERING FROM HELIUM ATOMS

The aperture distribution function, $a(\rho, \phi, z)$, for the elastic scattering of an incident electron plane wave represented by $\pi(z)$ by a helium atom represented by

$$\frac{2}{4\pi(0.567a_o)^2} [\delta(r - 0.567a_o)] \quad (101)$$

is given by the convolution of the plane wave with the helium atom function:

$$a(\rho, \phi, z) = \pi(z) \otimes \frac{2}{4\pi(0.567a_o)^2} [\delta(r - 0.567a_o)] \quad (102)$$

The aperture function is

$$a(\rho, \phi, z) = \frac{2}{4\pi(0.567a_o)^2} \sqrt{(0.567a_o)^2 - z^2} \delta(r - \sqrt{(0.567a_o)^2 - z^2}) \quad (103)$$

Far Field Scattering (circular symmetry)

Applying Huygens principle to a disturbance caused by the plane wave electron over the helium atom as an aperture gives the amplitude of the far field or Fraunhofer diffraction pattern $F(s)$ as the Fourier Transform of the aperture distribution. The intensity I_i^{sd} is the square of the amplitude.

$$F(s) = \frac{2}{4\pi(0.567a_o)^2} 2\pi \int_0^\infty \int_0^\infty \sqrt{(0.567a_o)^2 - z^2} \delta(r - \sqrt{(0.567a_o)^2 - z^2}) J_o(s\rho) e^{-iws} \rho d\rho dz \quad (104)$$

$$I_1^{ed} = F(s)^2$$

$$= I_e \left\{ \left[\frac{2\pi}{(z_o w)^2 + (z_o s)^2} \right]^{\frac{1}{2}} \right. \\ \left. \left\{ 2 \left[\frac{z_o s}{(z_o w)^2 + (z_o s)^2} \right] J_{3/2} \left[((z_o w)^2 + (z_o s)^2)^{1/2} \right] - \left[\frac{z_o s}{(z_o w)^2 + (z_o s)^2} \right]^2 J_{5/2} \left[((z_o w)^2 + (z_o s)^2)^{1/2} \right] \right\} \right\}^2 \quad (105)$$

$$s = \frac{4\pi}{\lambda} \sin \frac{\theta}{2}; w = 0 \text{ (units of } \text{\AA}^{-1}) \quad (106)$$

The experimental results of Bromberg [16], the extrapolated experimental data of Hughes [16], the small angle data of Geiger [17] and the semiexperimental results of Lassetre [16] for the elastic differential cross section for the elastic scattering of electrons by helium atoms is shown graphically in Figure 11. The elastic differential cross section as a function of angle numerically calculated by Khare [16] using the first Born approximation and first-order exchange approximation also appear in Figure 11. These results which are based on a quantum mechanical model are compared with experimentation [16-17]. The closed form function (Eqs. (105) and (106)) for the elastic differential cross section for the elastic scattering of electrons by helium atoms is shown graphically in Figure 12. The scattering amplitude function, $F(s)$ (Eq. (104)), is shown as an insert. It is apparent from Figure 11 that the quantum mechanical calculations fail completely at predicting the experimental results at small scattering angles; whereas, there is good agreement between Eq. (105) and the experimental results.

THE NATURE OF THE CHEMICAL BOND OF HYDROGEN

The hydrogen molecule charge and current density functions, bond distance and energies are solved from the Laplacian in ellipsoidal coordinates with the constraint of nonradiation.

$$(\eta - \zeta) R_\xi \frac{\delta}{\delta \xi} (R_\xi \frac{\delta \phi}{\delta \xi}) + (\zeta - \xi) R_\eta \frac{\delta}{\delta \eta} (R_\eta \frac{\delta \phi}{\delta \eta}) + (\xi - \eta) R_\zeta \frac{\delta}{\delta \zeta} (R_\zeta \frac{\delta \phi}{\delta \zeta}) = 0 \quad (107)$$

The force balance equation for the hydrogen molecule is

$$\frac{\hbar^2}{m_e a^2 b^2} 2ab^2 X = \frac{e^2}{4\pi\epsilon_0} X + \frac{\hbar^2}{2m_e a^2 b^2} 2ab^2 X \quad (108)$$

where

$$X = \frac{1}{\sqrt{\xi + a^2}} \frac{1}{\xi + b^2} \frac{1}{c} \sqrt{\frac{\xi^2 - 1}{\xi^2 - \eta}} \quad (109)$$

Eq. (108) has the parametric solution

$$r(t) = ia \cos \omega t + jb \sin \omega t \quad (110)$$

when the semimajor axis, a , is

$$a = a_o \quad (111)$$

The internuclear distance, $2c'$, which is the distance between the foci is

$$2c' = \sqrt{2}a_o \quad (112)$$

The experimental internuclear distance is $\sqrt{2}a_o$. The semiminor axis is

$$b = \frac{1}{\sqrt{2}}a_o \quad (113)$$

The eccentricity, e , is

$$e = \frac{1}{\sqrt{2}} \quad (114)$$

The Energies of the Hydrogen Molecule

The potential energy of the two electrons in the central field of the protons at the foci is

$$V_e = \frac{-2e^2}{8\pi\varepsilon_o\sqrt{a^2 - b^2}} \ln \frac{a + \sqrt{a^2 - b^2}}{a - \sqrt{a^2 - b^2}} = -67.813 \text{ eV} \quad (115)$$

The potential energy of the two protons is

$$V_p = \frac{e^2}{8\pi\varepsilon_o\sqrt{a^2 - b^2}} = 19.23 \text{ eV} \quad (116)$$

The kinetic energy of the electrons is

$$T = \frac{\hbar^2}{2m_e a \sqrt{a^2 - b^2}} \ln \frac{a + \sqrt{a^2 - b^2}}{a - \sqrt{a^2 - b^2}} = 33.906 \text{ eV} \quad (117)$$

The energy, V_m , of the magnetic force between the electrons is

$$V_m = \frac{-\hbar^2}{4m_e a \sqrt{a^2 - b^2}} \ln \frac{a + \sqrt{a^2 - b^2}}{a - \sqrt{a^2 - b^2}} = -16.9533 \text{ eV} \quad (118)$$

The total energy is

$$E_T = V_e + T + V_m + V_p \quad (119)$$

$$E_T = -13.6 \text{ eV} \left[\left(2\sqrt{2} - \sqrt{2} + \frac{\sqrt{2}}{2} \right) \ln \frac{\sqrt{2} + 1}{\sqrt{2} - 1} - \sqrt{2} \right] = -31.63 \text{ eV} \quad (120)$$

The energy of two hydrogen atoms is

$$E(2H[a_H]) = -27.21 \text{ eV} \quad (121)$$

The bond dissociation energy, E_D , is the difference between the total energy of the corresponding hydrogen atoms (Eq. (121)) and E_T (Eq. (120)).

$$E_D = E(2H[a_H]) - E_T = 4.43 \text{ eV} \quad (122)$$

The experimental energy determined by calorimetry is

$$E_D = 4.45 \text{ eV} \quad (123)$$

COSMOLOGICAL THEORY BASED ON MAXWELL S EQUATIONS

Maxwell s equations and special relativity are based on the law of propagation of a electromagnetic wave front in the form

$$\frac{1}{c^2} \left(\frac{\delta \omega}{\delta t} \right)^2 - \left[\left(\frac{\delta \omega}{\delta x} \right)^2 + \left(\frac{\delta \omega}{\delta y} \right)^2 + \left(\frac{\delta \omega}{\delta z} \right)^2 \right] = 0 \quad (124)$$

For any kind of wave advancing with limiting velocity and capable of transmitting signals, the equation of front propagation is the same as the equation for the front of a light wave. Thus, the equation

$$\frac{1}{c^2} \left(\frac{\delta \omega}{\delta t} \right)^2 - (grad \omega)^2 = 0 \quad (125)$$

acquires a general character; it is more general than Maxwell s equations from which Maxwell originally derived it.

A discovery of the present work is that the classical wave equation governs: (1) the motion of bound electrons, (2) the propagation of any form of energy, (3) measurements between inertial frames of reference such as time, mass, momentum, and length (Minkowski tensor), (4) fundamental particle production and the conversion of matter to energy, (5) a relativistic correction of spacetime due to particle production or annihilation (Schwarzschild metric), (6) the expansion and contraction of the Universe, (7) the basis of the relationship between Maxwell s equations, Planck s equation, the de Broglie equation, Newton s laws, and special, and general relativity.

The relationship between the time interval between ticks t of a clock in motion with velocity v relative to an observer and the time interval t_0 between ticks on a clock at rest relative to an observer is [18]

$$(ct)^2 = (ct_0)^2 + (vt)^2 \quad (126)$$

Thus, the time dilation relationship based on the constant maximum speed of light c in any inertial frame is

$$t = \frac{t_0}{\sqrt{1 - \frac{v^2}{c^2}}} \quad (127)$$

The metric $g_{\mu\nu}$ for Euclidean space is the Minkowski tensor $\eta_{\mu\nu}$. In this case, the separation of proper time between two events x^μ and $x^\mu + dx^\mu$ is $d\tau^2 = -\eta_{\mu\nu}dx^\mu dx^\nu$.

THE EQUIVALENCE OF THE GRAVITATIONAL MASS AND THE INERTIAL MASS

The equivalence of the gravitational mass and the inertial mass, $m_g/m_i =$ universal constant, which is predicted by Newton s law of mechanics and gravitation is experimentally confirmed to less 1×10^{-11} [19]. In physics, the discovery of a universal constant often leads to the

development of an entirely new theory. From the universal constancy of the velocity of light, c the special theory of relativity was derived; and from Planck's constant h , the quantum theory was deduced. Therefore, the universal constant m_g/m_i should be the key to the gravitational problem. The energy equation of Newtonian gravitation is

$$E = \frac{1}{2}mv^2 - \frac{GMm}{r} = \frac{1}{2}mv_0^2 - \frac{GMm}{r_0} = \text{constant} \quad (128)$$

Since h , the angular momentum per unit mass, is

$$h = L/m = |\mathbf{r} \times \mathbf{v}| = r_0 v_0 \sin \phi$$

the eccentricity e may be written as

$$e = [1 + \left(v_0^2 - \frac{2GM}{r_0} \right) \frac{r_0^2 v_0^2 \sin^2 \phi}{G^2 M^2}]^{1/2} \quad (129)$$

where m is the inertial mass of a particle, v_0 is the speed of the particle, r_0 is the distance of the particle from a massive object, ϕ is the angle between the direction of motion of the particle and the radius vector from the object, and M is the total mass of the object (including a particle). The eccentricity e given by Newton's differential equations of motion in the case of the central field permits the classification of the orbits according to the total energy E [20] (column 1) and the orbital velocity squared, v_0^2 , relative to the gravitational velocity squared, $\frac{2GM}{r_0}$ [20] (column 2):

$E < 0$	$v_0^2 < \frac{2GM}{r_0}$	$e < 1$	ellipse
$E < 0$	$v_0^2 = \frac{2GM}{r_0}$	$e = 0$	circle (special case of ellipse)
$E = 0$	$v_0^2 > \frac{2GM}{r_0}$	$e = 1$	parabolic orbit
$E > 0$	$v_0^2 > \frac{2GM}{r_0}$	$e > 1$	hyperbolic orbit

(130)

CONTINUITY CONDITIONS FOR THE PRODUCTION OF A PARTICLE FROM A PHOTON TRAVELING AT LIGHT SPEED

A photon traveling at the speed of light gives rise to a particle with an initial radius equal to its Compton wavelength bar.

$$r = \lambda_C = \frac{\hbar}{mc} = r_a \quad (131)$$

The particle must have an orbital velocity equal to Newtonian gravitational escape velocity v_g of the antiparticle.

$$v_g = \sqrt{\frac{2Gm}{r}} = \sqrt{\frac{2Gm_0}{\lambda_c}} \quad (132)$$

The eccentricity is one. The orbital energy is zero. The particle production trajectory is a parabola relative to the center of mass of the antiparticle.

A Gravitational Field as a Front Equivalent to Light Wave Front

The particle with a finite gravitational mass gives rise to a gravitational field that travels out as a front equivalent to a light wave front. The form of the outgoing gravitational field front traveling at the speed of light is $f\left(t - \frac{r}{c}\right)$, and $d\tau^2$ is given by

$$d\tau^2 = f(r)dt^2 - \frac{1}{c^2}[f(r)^{-1}dr^2 + r^2d\theta^2 + r^2\sin^2\theta d\phi^2] \quad (133)$$

The speed of light as a constant maximum as well as phase matching and continuity conditions of the electromagnetic and gravitational waves require the following form of the squared displacements:

$$(ct)^2 + (v_g t)^2 = (ct)^2 \quad (134)$$

$$f(r) = \left(1 - \left(\frac{v_g}{c}\right)^2\right) \quad (135)$$

In order that the wave front velocity does not exceed c in any frame, spacetime must undergo time dilation and length contraction due to the particle production event. *The derivation and result of spacetime time dilation is analogous to the derivation and result of special relativistic time dilation* wherein the relative velocity of two inertial frames replaces the gravitational velocity.

The general form of the metric due to the relativistic effect on spacetime due to mass m_0 with v_g given by Eq. (132) is

$$d\tau^2 = \left(1 - \left(\frac{v_g}{c}\right)^2\right)dt^2 - \frac{1}{c^2}\left[\left(1 - \left(\frac{v_g}{c}\right)^2\right)^{-1}dr^2 + r^2d\theta^2 + r^2\sin^2\theta d\phi^2\right] \quad (136)$$

The gravitational radius, r_g , of each orbitsphere of the particle production event, each of mass m_0 , and the corresponding general form of the metric are respectively

$$r_g = \frac{2Gm}{c^2}, \quad (137)$$

$$d\tau^2 = \left(1 - \frac{r_g}{r}\right)dt^2 - \frac{1}{c^2}\left[\left(1 - \frac{r_g}{r}\right)^{-1}dr^2 + r^2d\theta^2 + r^2\sin^2\theta d\phi^2\right] \quad (138)$$

The metric $g_{\mu\nu}$ for non-Euclidean space due to the relativistic effect on spacetime due to mass m_0 is

$$g_{\mu\nu} = \begin{pmatrix} -\left(1 - \frac{2Gm_0}{c^2 r}\right) & 0 & 0 & 0 \\ 0 & \frac{1}{c^2} \left(1 - \frac{2Gm_0}{c^2 r}\right)^{-1} & 0 & 0 \\ 0 & 0 & \frac{1}{c^2} r^2 & 0 \\ 0 & 0 & 0 & \frac{1}{c^2} r^2 \sin^2 \theta \end{pmatrix} \quad (139)$$

Masses and their effects on spacetime *superimpose*. The separation of proper time between two events x^μ and $x^\mu + dx^\mu$ is

$$d\tau^2 = \left(1 - \frac{2GM}{c^2 r}\right) dt^2 - \frac{1}{c^2} \left[\left(1 - \frac{2GM}{c^2 r}\right)^{-1} dr^2 + r^2 d\theta^2 + r^2 \sin^2 \theta d\phi^2 \right] \quad (140)$$

The Schwarzschild metric (Eq. (140)) gives the relationship whereby matter causes relativistic corrections to spacetime that determines the curvature of spacetime and is the origin of gravity.

Particle Production Continuity Conditions from Maxwell's Equations, and the Schwarzschild Metric

The photon to particle event requires a transition state that is continuous wherein the velocity of a transition state orbitsphere is the speed of light. The radius, r , is the Compton wavelength bar, λ_c , given by Eq. (131). At production, the Planck equation energy, the electric potential energy, and the magnetic energy are equal to $m_0 c^2$.

The Schwarzschild metric gives the relationship whereby matter causes relativistic corrections to spacetime that determines the masses of fundamental particles. Substitution of $r = \lambda_c$; $dr = 0$; $d\theta = 0$; $\sin^2 \theta = 1$ into the Schwarzschild metric gives

$$d\tau = dt \sqrt{1 - \frac{2Gm_0}{c^2 r_a} - \frac{v^2}{c^2}}^{\frac{1}{2}} \quad (141)$$

with $v^2 = c^2$, the relationship between the proper time and the coordinate time is

$$\tau = ti \sqrt{\frac{2GM}{c^2 r_a}} = ti \sqrt{\frac{2GM}{c^2 \lambda_c}} = ti \frac{v}{c} \quad (142)$$

When the orbitsphere velocity is the speed of light, continuity conditions based on the constant maximum speed of light given by Maxwell's equations are mass energy = Planck equation energy = electric potential energy = magnetic energy = mass/spacetime metric energy. Therefore,

$$m_0 c^2 = \hbar \omega^* = V = E_{mag} = E_{spacetime} \quad (143)$$

$$m_0 c^2 = \hbar \omega^* = \frac{\hbar^2}{m_0 \lambda_c^2} = \alpha^{-1} \frac{e^2}{4\pi \epsilon_0 \lambda_c} = \alpha^{-1} \frac{\pi \mu_0 e^2 \hbar^2}{(2\pi n_0)^2 \lambda_c^3} = \frac{\alpha h}{1 \text{ sec}} \sqrt{\frac{\lambda_c c^2}{2Gm}} \quad (144)$$

The continuity conditions based on the constant maximum speed of light given by the Schwarzschild metric are:

$$\frac{\text{proper time}}{\text{coordinate time}} = \frac{\text{gravitational wave condition}}{\text{electromagnetic wave condition}} = \frac{\text{gravitational mass phase matching}}{\text{charge/inertial mass phase matching}}$$

$$\frac{\text{proper time}}{\text{coordinate time}} = i \sqrt{\frac{2Gm}{c^2 \lambda_c}} = i \frac{v_g}{\alpha c}$$
(145)

MASSES OF FUNDAMENTAL PARTICLES

Each of the Planck equation energy, electric energy, and magnetic energy corresponds to a particle given by the relationship between the proper time and the coordinate time. The electron and down-down-up neutron correspond to the Planck equation energy. The muon and strange-strange-charmed neutron correspond to the electric energy. The tau and bottom-bottom-top neutron correspond to the magnetic energy. The particle must possess the escape velocity v_g relative to the antiparticle where $v_g < c$. According to Newton's law of gravitation, the eccentricity is one and the particle production trajectory is a parabola relative to the center of mass of the antiparticle.

The Electron-Antielectron Lepton Pair

A clock is defined in terms of a self consistent system of units used to measure the particle mass. The proper time of the particle is equated with the coordinate time according to the Schwarzschild metric corresponding to light speed. The special relativistic condition corresponding to the Planck energy gives the mass of the electron.

$$2\pi \frac{\hbar}{mc^2} = \sec \sqrt{\frac{2Gm^2}{c\alpha^2\hbar}} \quad (146)$$

$$m_e = \left(\frac{h\alpha}{\sec c^2} \right)^{\frac{1}{2}} \left(\frac{c\hbar}{2G} \right)^{\frac{1}{4}} = 9.1097 \times 10^{-31} \text{ kg} \quad (147)$$

$$m_e = 9.1097 \times 10^{-31} \text{ kg} - 18 \text{ eV}(v_e) = 9.1094 \times 10^{-31} \text{ kg} \quad (148)$$

$$m_{e \text{ experimental}} = 9.1095 \times 10^{-31} \text{ kg} \quad (149)$$

Down-Down-Up Neutron (DDU)

The corresponding equation for production of the neutron is

$$2\pi \frac{2\pi\hbar}{\frac{m_N}{3} \left[\frac{1}{2\pi} - \frac{\alpha}{2\pi} \right] c^2} = \sec \sqrt{\frac{2G \left[\frac{m_N}{3} \left[\frac{1}{2\pi} - \frac{\alpha}{2\pi} \right] \right]^2}{3c(2\pi)^2 \hbar}} \quad (150)$$

$$m_{N_calculated} = (3)(2\pi) \left(\frac{1}{1-\alpha} \right) \left(\frac{2\pi\hbar}{\sec c^2} \right)^{\frac{1}{2}} \left(\frac{2\pi(3)c\hbar}{2G} \right)^{\frac{1}{4}} = 1.6744 \times 10^{-27} \text{ kg} \quad (151)$$

$$m_{N_experimental} = 1.6749 \times 10^{-27} \text{ kg} \quad (152)$$

GRAVITATIONAL POTENTIAL ENERGY

The gravitational radius, α_G or r_G , of an orbitsphere of mass m_0 is defined as

$$\alpha_G = r_G = \frac{Gm_0}{c^2} \quad (153)$$

When $r_G = r_\alpha^* = \lambda_c$, the gravitational potential energy equals $m_0 c^2$

$$r_G = \frac{Gm_0}{c^2} = \lambda_c = \frac{\hbar}{m_0 c}, \quad (154)$$

$$E_{grav} = \frac{Gm_0^2}{r} = \frac{Gm_0^2}{\lambda_c} = \frac{Gm_0^2}{r_\alpha^*} = \hbar\omega^* = m_0 c^2 \quad (155)$$

The mass m_0 is the Planck mass, m_u ,

$$m_u = m_0 = \sqrt{\frac{\hbar c}{G}} \quad (156)$$

The corresponding gravitational velocity, v_G , is defined as

$$v_G = \sqrt{\frac{Gm_0}{r}} = \sqrt{\frac{Gm_0}{\lambda_c}} = \sqrt{\frac{Gm_u}{\lambda_c}} \quad (157)$$

Relationship of the Equivalent Planck Mass Particle Production Energies

For the Plank mass particle, the relationships corresponding to Eq. (144) are: (mass energy = Planck equation energy = electric potential energy = magnetic energy = gravitational potential energy = mass/spacetime metric energy)

$$m_o c^2 = \hbar\omega^* = V = E_{mag} = E_{grav} = E_{spacetime} \quad (158)$$

$$m_0 c^2 = \hbar\omega^* = \frac{\hbar^2}{m_0 \lambda_c^2} = \alpha^{-1} \frac{e^2}{4\pi\epsilon_0 \lambda_c} = \alpha^{-1} \frac{\pi\mu_0 e^2 \hbar^2}{(2\pi m_0)^2 \lambda_c^3} = \alpha^{-1} \frac{\mu_0 e^2 c^2}{2h} \sqrt{\frac{Gm_0}{\lambda_c}} \sqrt{\frac{\hbar c}{G}} = \frac{\alpha h}{1 \text{ sec}} \sqrt{\frac{\lambda_c c^2}{2Gm}} \quad (159)$$

These equivalent energies give the particle masses in terms of the gravitational velocity, v_G and the Planck mass, m_u

$$m_0 = \alpha^{-1} \frac{\mu_0 e^2 c}{2h} \sqrt{\frac{G m_0}{\lambda_c}} m_u = \alpha^{-1} \frac{\mu_0 e^2 c}{2h} \sqrt{\frac{G m_0}{c^2 \lambda_c}} m_u = \alpha^{-1} \frac{\mu_0 e^2 c}{2h} \frac{v_G}{c} m_u = \frac{v_G}{c} m_u \quad (160)$$

Planck Mass Particles

A pair of particles each of the Planck mass corresponding to the gravitational potential energy is not observed since the velocity of each transition state orbitsphere is the gravitational velocity v_G that in this case is the speed of light; whereas, the Newtonian gravitational escape velocity v_e is twice the speed of light. In this case, an electromagnetic wave of mass energy equivalent to the Planck mass travels in a circular orbit about the center of mass of another electromagnetic wave of mass energy equivalent to the Planck mass wherein the eccentricity is equal to zero and the escape velocity can never be reached. The Planck mass is a measuring stick. The extraordinarily high Planck mass ($\sqrt{\frac{\hbar c}{G}} = 2.18 \times 10^{-8} \text{ kg}$) is the unobtainable mass bound imposed by the angular momentum and speed of the photon relative to the gravitational constant. It is analogous to the unattainable bound of the speed of light for a particle possessing finite rest mass imposed by the Minkowski tensor.

Astrophysical Implications of Planck Mass Particles

The limiting speed of light eliminates the singularity problem of Einstein's equation that arises as the radius of a blackhole equals the Schwarzschild radius. General relativity with the singularity eliminated resolves the paradox of the infinite propagation velocity required for the gravitational force in order to explain why the angular momentum of objects orbiting a gravitating body does not increase due to the finite propagation delay of the gravitational force according to special relativity [21]. When the gravitational potential energy density of a massive body such as a blackhole equals that of a particle having the Planck mass, the matter may transition to photons of the Planck mass. Even light from a blackhole will escape when the decay rate of the trapped matter with the concomitant spacetime expansion is greater than the effects of gravity which oppose this expansion. Gamma-ray bursts are the most energetic phenomenon known that can release an explosion of gamma rays packing 100 times more energy than a supernova explosion [22]. The annihilation of a blackhole may be the source of γ -ray bursts. The source may be due to conversion of matter to photons of the Planck mass/energy which may also give rise to cosmic rays which are the most energetic particles known, and their origin is also a mystery [23]. According to the GZK cutoff, the cosmic spectrum cannot extend beyond $5 \times 10^{19} \text{ eV}$, but AGASA, the world's largest air shower array, has shown that the spectrum is extending beyond

10^{20} eV without any clear sign of cutoff [24]. Photons each of the Planck mass may be the source of these inexplicably energetic cosmic rays.

RELATIONSHIP OF MATTER TO ENERGY AND SPACETIME EXPANSION

The Schwarzschild metric gives the relationship whereby matter causes relativistic corrections to spacetime. The limiting velocity c results in the contraction of spacetime due to particle production, which is given by $2\pi r_g$ where r_g is the gravitational radius of the particle. This has implications for the expansion of spacetime when matter converts to energy. Q the mass/energy to expansion/contraction quotient of spacetime is given by the ratio of the mass of a particle at production divided by T , the period of production.

$$Q = \frac{m_0}{T} = \frac{m_0}{2\pi r_g} = \frac{m_0}{2\pi \frac{2Gm_0}{c^2}} = \frac{c^3}{4\pi G} = 3.22 \times 10^{34} \frac{\text{kg}}{\text{sec}}$$
(161)

The gravitational equations with the equivalence of the particle production energies (Eq. (144)) permit the conservation of mass/energy ($E = mc^2$) and spacetime ($\frac{c^3}{4\pi G} = 3.22 \times 10^{34} \frac{\text{kg}}{\text{sec}}$). With the conversion of 3.22×10^{34} kg of matter to energy, spacetime expands by 1 sec. The photon has inertial mass and angular momentum, but due to Maxwell's equations and the implicit special relativity it does not have a gravitational mass.

Cosmological Consequences

The Universe is closed (it is *finite but with no boundary*). It is a 3-sphere Universe-Riemannian three dimensional hyperspace plus time of constant positive curvature at each r-sphere. The *Universe is oscillatory in matter/energy and spacetime* with a finite minimum radius, the gravitational radius. Spacetime expands as mass is released as energy which provides the basis of the atomic, thermodynamic, and cosmological arrows of time. Different regions of space are isothermal even though they are separated by greater distances than that over which light could travel during the time of the expansion of the Universe [25]. Presently, stars and large scale structures exist which are older than the elapsed time of the present expansion as stellar, galaxy, and supercluster evolution occurred during the contraction phase [26—32]. The maximum power radiated by the Universe which occurs at the beginning of the expansion phase is $P_U = \frac{c^5}{4\pi G} = 2.89 \times 10^{51} W$. Observations beyond the beginning of the expansion phase are not possible since the Universe was entirely matter filled.

The Period of Oscillation of the Universe Based on Closed Propagation of Light

Mass/energy is conserved during harmonic expansion and contraction. The gravitational potential energy E_{grav} given by Eq. (155) with $m_0 = m_U$ is equal to $m_U c^2$ when the radius of the Universe r is the gravitational radius r_G . The gravitational velocity v_G (Eq. (157) with $r = r_G$ and $m_0 = m_U$) is the speed of light in a circular orbit wherein the eccentricity is equal to zero and the escape velocity from the Universe can never be reached. The period of the oscillation of the Universe and the period for light to transverse the Universe corresponding to the gravitational radius r_G must be equal. The harmonic oscillation period, T , is

$$T = \frac{2\pi r_G}{c} = \frac{2\pi Gm_U}{c^3} = \frac{2\pi G(2 \times 10^{54} \text{ kg})}{c^3} = 3.10 \times 10^{19} \text{ sec} = 9.83 \times 10^{11} \text{ years} \quad (162)$$

where the mass of the Universe, m_U , is approximately $2 \times 10^{54} \text{ kg}$. (The initial mass of the Universe of $2 \times 10^{54} \text{ kg}$ is based on internal consistency with the size, age, Hubble constant, temperature, density of matter, and power spectrum.) Thus, the observed Universe will expand as mass is released as photons for $4.92 \times 10^{11} \text{ years}$. At this point in its world line, the Universe will obtain its maximum size and begin to contract.

THE DIFFERENTIAL EQUATION OF THE RADIUS OF THE UNIVERSE

Based on conservation of mass/energy ($E = mc^2$) and spacetime ($\frac{c^3}{4\pi G} = 3.22 \times 10^{34} \frac{\text{kg}}{\text{sec}}$).

The Universe behaves as a simple harmonic oscillator having a restoring force, F , which is proportional to the radius. The proportionality constant, k , is given in terms of the potential energy, E , gained as the radius decreases from the maximum expansion to the minimum contraction.

$$\frac{E}{R^2} = k \quad (163)$$

Since the gravitational potential energy E_{grav} is equal to $m_U c^2$ when the radius of the Universe r is the gravitational radius r_G

$$F = -kR = -\frac{m_U c^2}{r_G^2} R = -\frac{m_U c^2}{\left(\frac{Gm_U}{c^2}\right)^2} R \quad (164)$$

And, the differential equation of the radius of the Universe, R is

$$m_U \ddot{R} + \frac{m_U c^2}{r_G^2} R = m_U \ddot{R} + \frac{m_U c^2}{\left(\frac{Gm_U}{c^2}\right)^2} R = 0 \quad (165)$$

The *maximum radius of the Universe*, the amplitude, r_o , of the time harmonic variation in the radius of the Universe, is given by the quotient of the total mass of the Universe and Q ((Eq. (161)), the mass/energy to expansion/contraction quotient.

$$r_0 = \frac{m_U}{Q} = \frac{m_U}{\frac{c^3}{4\pi G}} = \frac{2 \times 10^{54} \text{ kg}}{\frac{c^3}{4\pi G}} = 1.97 \times 10^{12} \text{ light years} \quad (166)$$

The *minimum radius* which corresponds to the gravitational radius, r_g , given by Eq. (137) with $m_0 = m_U$ is

$$r_g = \frac{2Gm_U}{c^2} = 2.96 \times 10^{27} \text{ m} = 3.12 \times 10^{11} \text{ light years} \quad (167)$$

When the radius of the Universe is the gravitational radius, r_g , the proper time is equal to the coordinate time by Eq. (142), and the gravitational escape velocity v_g of the Universe is the speed of light. The radius of the Universe as a function of time as shown in Figure 13 is

$$R = \left(r_g + \frac{cm_U}{Q} \right) - \frac{cm_U}{Q} \cos \left(\frac{2\pi t}{\frac{2\pi G}{c}} \right) = \left(\frac{2Gm_U}{c^2} + \frac{cm_U}{\frac{c^3}{4\pi G}} \right) - \frac{cm_U}{\frac{c^3}{4\pi G}} \cos \left(\frac{2\pi t}{\frac{2\pi Gm_U}{c^3}} \right) \quad (168)$$

The expansion/contraction rate, \dot{R} , as shown in Figure 14 is given by time derivative of Eq. (168)

$$\dot{R} = 4\pi c \times 10^{-3} \sin \left(\frac{2\pi t}{\frac{2\pi Gm_U}{c^3}} \right) \frac{\text{km}}{\text{sec}} \quad (169)$$

THE HUBBLE CONSTANT

The *Hubble constant* is given by the ratio of the expansion rate given in units of $\frac{\text{km}}{\text{sec}}$ divided by the radius of the expansion in *Mpc*. The radius of expansion is equivalent to the radius of the light sphere with an origin at the time point when the Universe stopped contracting and started to expand.

$$H = \frac{\dot{R}}{t \text{ Mpc}} = \frac{4\pi c \times 10^{-3} \sin \left(\frac{2\pi t}{\frac{2\pi Gm_U}{c^3}} \right) \frac{\text{km}}{\text{sec}}}{t \text{ Mpc}} \quad (170)$$

For $t = 10^{10} \text{ light years} = 3.069 \times 10^3 \text{ Mpc}$, the Hubble constant, H_0 , is

$$H_0 = 78.6 \frac{\text{km}}{\text{sec} \cdot \text{Mpc}} \quad (171)$$

The experimental value [33] as shown in Figure 15 is

$$H_0 = 80 \pm 17 \frac{\text{km}}{\text{sec} \cdot \text{Mpc}} \quad (172)$$

THE DENSITY OF THE UNIVERSE AS A FUNCTION OF TIME

The density of the Universe as a function of time $\rho_u(t)$ given by the ratio of the mass as a function of time and the volume as a function of time as shown in Figure 16 is

$$\rho_u(t) = \frac{m_u(t)}{V(t)} = \frac{m_u(t)}{\frac{4}{3}\pi R(t)^3} = \frac{\frac{m_u}{2} \left(1 + \cos \left(\frac{2\pi t}{2\pi G m_u} \right) \right)}{\frac{4}{3}\pi \left(\left(\frac{2Gm_u}{c^2} + \frac{cm_u}{c^3} \right) - \frac{cm_u}{c^3} \cos \left(\frac{2\pi t}{2\pi G m_u} \right) \right)^3}, \quad (173)$$

For $t = 10^{10}$ light years, $\rho_u = 1.7 \times 10^{-32}$ g/cm³. The density of luminous matter of stars and gas of galaxies is about $\rho_u = 2 \times 10^{-31}$ g/cm³ [34—35].

THE POWER OF THE UNIVERSE AS A FUNCTION OF TIME, $P_u(t)$

From $E = mc^2$ and Eq. (161),

$$P_u(t) = \frac{c^5}{8\pi G} \left(1 + \cos \left(\frac{2\pi t}{2\pi R_G} \right) \right) \quad (174)$$

For $t = 10^{10}$ light years, $P_u(t) = 2.88 \times 10^{51}$ W. The observed power is consistent with that predicted. The power of the Universe as a function of time is shown in Figure 17.

THE TEMPERATURE OF THE UNIVERSE AS A FUNCTION OF TIME

The temperature of the Universe as a function of time, $T_u(t)$, as shown in Figure 18, follows from the Stefan-Boltzmann law.

$$T_u(t) = \left(\frac{1}{1 + \frac{Gm_u(t)}{c^2 R(t)}} \right) \left[\frac{R_u(t)}{e\sigma} \right]^{\frac{1}{4}} = \left(\frac{1}{1 + \frac{Gm_u(t)}{c^2 R(t)}} \right) \left[\frac{\frac{P_u(t)}{4\pi R(t)^2}}{e\sigma} \right]^{\frac{1}{4}} \quad (175)$$

The calculated uniform temperature is about 2.7 K which is in agreement with the observed microwave background temperature [33].

POWER SPECTRUM OF THE COSMOS

The power spectrum of the cosmos, as measured by the Las Campanas survey, generally follows the prediction of cold dark matter on the scales of 200 million to 600 million light-years.

However, the power increases dramatically on scales of 600 million to 900 million light-years [32]. This discrepancy means that the universe is much more structured on those scales than current theories can explain.

The universe is oscillatory in matter/energy and spacetime with a finite minimum radius. The *minimum radius* which corresponds to the gravitational radius, r_g , given by Eq. (167) is 3.12×10^{11} light years. The minimum radius is larger than that provided by the current expansion, approximately 10 billion light years [33]. The universe is a four dimensional hyperspace of constant positive curvature at each r-sphere. The coordinates are spherical, and the space can be described as a series of spheres each of constant radius r whose centers coincide at the origin. The existence of the mass m_u causes the area of the spheres to be less than $4\pi r^2$ and causes the clock of each r-sphere to run so that it is no longer observed from other r-spheres to be at the same rate. The Schwarzschild metric given by Eq. (140) is the general form of the metric which allows for these effects. Consider the present observable universe that has undergone expansion for 10 billion years. The radius of the universe as a function of time from the coordinate r-sphere is of the same form as Eq. (168). The average size of the universe, r_u , is given as the sum of the gravitational radius, r_g , and the observed radius, 10 billion light years.

$$r_u = r_g + 10^{10} \text{ light yrs} = 3.12 \times 10^{11} \text{ light yrs} + 10^{10} \text{ light years} = 3.22 \times 10^{11} \text{ light yrs} \quad (176)$$

The frequency of Eq. (168) is one half the amplitude of spacetime expansion from the conversion of the mass of universe into energy according to Eq. (161). Thus, keeping the same relationships, the frequency of the current expansion function is the reciprocal of one half the current age. Substitution of the average size of the universe, the frequency of expansion, and the amplitude of expansion, 10 billion light years, into Eq. (168) gives *the radius of the universe as a function of time for the coordinate r-sphere*.

$$x = 3.22 \times 10^{11} - 1 \times 10^{10} \cos\left(\frac{2\pi}{5 \times 10^9 \text{ light years}} t\right) \text{ light years} \quad (177)$$

The Schwarzschild metric gives the relationship between the proper time and the coordinate time. The infinitesimal temporal displacement, $d\tau^2$, is given by Eq. (140). In the case that $dr^2 = d\theta^2 = d\phi^2 = 0$, the relationship between the proper time and the coordinate time is

$$d\tau^2 = \left(1 - \frac{2Gm_u}{c^2 r}\right) dt^2 \quad (178)$$

$$\tau = t \sqrt{1 - \frac{r_g}{r}} \quad (179)$$

The maximum power radiated by the universe is given by Eqs. (174) which occurs when the proper radius, the coordinate radius, and the gravitational radius r_g are equal. For the present universe, the coordinate radius is given by Eq. (176). The gravitational radius is given by Eq.

(167). The maximum of the power spectrum of a trigonometric function occurs at its frequency [36]. Thus, the coordinate maximum power according to Eq. (177) occurs at 5×10^9 light years. The maximum power corresponding to the proper time is given by the substitution of the coordinate radius, the gravitational radius r_g , and the coordinate power maximum into Eq. (179).

The power maximum in the proper frame occurs at

$$\tau = 5 \times 10^9 \text{ light years} \sqrt{1 - \frac{3.12 \times 10^{11} \text{ light years}}{3.22 \times 10^{11} \text{ light years}}} \quad (180)$$

$$\tau = 880 \times 10^6 \text{ light years}$$

The power maximum of the current observable universe is predicted to occur on the scale of 880×10^6 light years. There is excellent agreement between the predicted value and the experimental value of $600 - 900 \times 10^6$ light years [32].

THE EXPANSION/CONTRACTION ACCELERATION, $\ddot{\aleph}$

The expansion/contraction acceleration rate, $\ddot{\aleph}$, as shown in Figure 19, is given by the time derivative of Eq. (169).

$$\ddot{\aleph} = 2\pi \frac{c^4}{Gm_u} \cos\left(\frac{2\pi t}{\frac{2\pi Gm_u}{c^3} \text{ sec}}\right) \ddot{\aleph} = H_o = 78.7 \cos\left(\frac{2\pi t}{3.01 \times 10^5 \text{ Mpc}}\right) \frac{\text{km}}{\text{sec Mpc}} \quad (181)$$

The differential in the radius of the Universe, $\Delta \aleph$, due to its acceleration is given by $\Delta \aleph = 1/2 \ddot{\aleph} t^2$. The differential in expanded radius for the elapsed time of expansion, $t = 10^{10}$ light years corresponds to a decease in brightness of a supernovae standard candle of about an order of magnitude of that expected where the distance is taken as $\Delta \aleph$. This result based on the predicted rate of acceleration of the expansion is consistent with the experimental observation [37—39].

Furthermore, the microwave background radiation image obtained by the Boomerang telescope [40] is consistent with a Universe of nearly flat geometry since the commencement of its expansion. The data is consistent with a large offset radius of the Universe with a fractional increase in size since the commencement of expansion about 10 billion years ago.

THE PERIODS OF SPACETIME EXPANSION/CONTRACTION AND PARTICLE DECAY/PRODUCTION FOR THE UNIVERSE ARE EQUAL

The period of the expansion/contraction cycle of the radius of the Universe, T , is given by Eq. (162). It follows from the Poynting power theorem with spherical radiation that the transition lifetimes are given by the ratio of energy and the power of the transition (Eqs. (60-61)). Exponential decay applies to electromagnetic energy decay

$$h(t) = e^{-\frac{1}{T}t} u(t) \quad (182)$$

The coordinate time is imaginary because energy transitions are spacelike due spacetime expansion from matter to energy conversion. For example, the mass of the electron (a fundamental particle) is given by

$$\frac{2\pi\lambda_c}{\sqrt{\frac{2Gm_e}{\lambda_c}}} = \frac{2\pi\lambda_c}{v_g} = i\alpha^{-1} \text{ sec} \quad (183)$$

where v_g is Newtonian gravitational velocity (Eq. (132)). When the gravitational radius r_g is the radius of the Universe, the proper time is equal to the coordinate time by Eq. (142), and the gravitational escape velocity v_g of the Universe is the speed of light. Replacement of the coordinate time, t , by the spacelike time, it , gives

$$h(t) = \text{Re} \left[e^{-\frac{i}{T}t} \right] = \cos \frac{2\pi}{T} t \quad (184)$$

where the period is T (Eq. (162)). The continuity conditions based on the constant maximum speed of light (Maxwell's equations) are given by Eqs. (143-144). The continuity conditions based on the constant maximum speed of light (Schwarzschild metric) are given by Eq. (145). The periods of spacetime expansion/contraction and particle decay/production for the Universe are equal because only the particles which satisfy Maxwell's equations and the relationship between proper time and coordinate time imposed by the Schwarzschild metric may exist.

WAVE EQUATION

The general form of the light front wave equation is given by Eq. (124). The equation of the radius of the Universe, \aleph , may be written as

$$\aleph = \left(\frac{2Gm_u}{c^2} + \frac{cm_u}{c^3} \right) - \frac{cm_u}{4\pi G} \cos \left(\frac{2\pi}{\frac{2\pi Gm_u}{c^3}} \sec \left(t - \frac{\aleph}{c} \right) \right) m, \quad (185)$$

which is a solution of the wave equation for a light wave front.

CONCLUSION

Maxwell's equations, Planck's equation, the de Broglie equation, Newton's laws, and special, and general relativity are unified.

REFERENCES

1. R. Mills, *The Grand Unified Theory of Classical Quantum Mechanics*, January 2000 Edition, BlackLight Power, Inc., Cranbury, New Jersey, Distributed by Amazon.com.

2. H. A. Haus, On the radiation from point charges, *American Journal of Physics*, **54**, 1126—1129 (1986).
3. D. A. McQuarrie, *Quantum Chemistry*, University Science Books, Mill Valley, CA, (1983), pp. 238-241.
4. T. A. Abbott and D. J. Griffiths, Am. J. Phys., Vol. 153, No. 12, (1985), pp. 1203-1211.
5. G. Goedecke, Phys. Rev 135B, (1964), p. 281.
6. J. D. Jackson, *Classical Electrodynamics*, Second Edition, John Wiley & Sons, New York, (1962), pp. 739-779.
7. Mizushima, M., *Quantum Mechanics of Atomic Spectra and Atomic Structure*, W.A. Benjamin, Inc., New York, (1970), p.17.
8. Jackson, J. D., *Classical Electrodynamics*, Second Edition, John Wiley & Sons, New York, (1962), pp. 739-752.
9. J. D. Jackson, *Classical Electrodynamics*, Second Edition, John Wiley & Sons, New York, (1962), pp. 758-763.
10. E. Purcell, *Electricity and Magnetism*, McGraw-Hill, New York, (1965), pp. 156-167.
11. D. Clark, Very large hydrogen atoms in interstellar space , Journal of Chemical Education, 68, No. 6, (1991), pp. 454-455.
12. J. Gribbin, New Scientist, January, 25, (1997), p. 15.
13. Levine, I., et al., Physical Review Letters, Vol. 78., No. 3, (1997), pp. 424-427.
14. C. E. Moore, Ionization Potentials and Ionization Limits Derived from the Analyses of Optical Spectra, Nat. Stand. Ref. Data Ser.-Nat. Bur. Stand. (U.S.), No. 34, 1970.
15. R. C. Weast, *CRC Handbook of Chemistry and Physics*, 58 Edition, CRC Press, West Palm Beach, Florida, (1977), p. E-68.
16. P. J. Bromberg, Absolute differential cross sections of elastically scattered electrons. I. He, N₂, and CO at 500 eV, *The Journal of Chemical Physics*, **50**(9), (3906-3921 1969).
17. J. Geiger, Elastische und unelastische streuung von elektronen an gasen, *Zeitschrift fur Physik*, **175**,530-542 (1963).
18. A. Beiser., *Concepts of Modern Physics*, 4th Edition, McGraw-Hill Book Company, New York, (1978), 2—10.
19. E. G. Adelberger, C. W. Stubbs, B. R. Heckel, Y. Su, H. E. Swanson, G. Smith, J. H. Gundlach, *Phys. Rev. D*, **42**(10), 3267-3292 (1990).
20. G. R. Fowles, *Analytical Mechanics*, Third Edition, Holt, Rinehart, and Winston, New York, (1977), pp. 154—155.
21. T. Van Flandern, The Speed of Gravity What the Experiments Say, *Physics Letters A*, **250**, 1—11 (1998).
22. R Cowen, Gamma-ray burst makes quite a bang, *Science News*,**153**(19), 292(1998).

23. M. Chown, The ultimate free lunch, *New Scientist*, 154(2081), 50—51 (1997)/
24. B. Schwarzschild, Giant air shower array shows cosmic-ray spectrum violating greisen cutoff, *Physics Today*, 51(10), 19—21 (1998).
25. J. C. Mather, E. S. Cheng, A preliminary measurement of the cosmic microwave background spectrum by the Cosmic Background Explorer (COBE) satellite, *Astrophysical Journal Letters*, 354, L37—L40 (May 10, 1990).
26. W. Saunders, C. Frenk; et al; The density field of the local universe; *Nature*, 349(6304), 32—38 (1991):
27. R. P. Kirshner, A. Oemler, Jr., P.L. Schechter, S. A. Shectman, A deep survey of galaxies, *Astronomical Journal*, 88, 1285—1300 (September 1983).
28. V. de Lapparent, M.J. Geller, J.P. Huchra, The mean density and two-point correlation function for the CfA redshift survey slices, *Astrophysical Journal*, 332(9) 44—56 (September 1, 1988).
29. A. Dressler, D. Lynden-Bell, D. Burstein, et. al., Spectroscopy and photometry of elliptical galaxies. I—A new distance estimator, *Astrophysical Journal*, 313(2), 42—58 (1987).
30. S. Flamsteed, Crisis in the Cosmos, *Discover*, 16(3), 66(1995).
31. J. Glanz, CO in the early universe clouds cosmologists views, *Science*, 273(5275), 581 (1996)
32. S. D. Landy, Mapping the Universe, *Scientific American*, 280(6), 38—45 (1999).
33. W.L. Freeman, et al., Distance to the Virgo cluster galaxy M100 from Hubble Space, *Nature*, 371(6500), 757—762 (1994).
34. R. M. Wald, *General Relativity*, University of Chicago Press, Chicago, (1984), pp. 114-116.
35. P. J. E. Peebles, J. Silk, Joseph, A cosmic book of phenomena, *Nature*, 346(6281), 233 (1990).
36. Siebert, W. McC., *Circuits, Signals, and Systems*, The MIT Press, Cambridge, Massachusetts, (1986), pp. 597-603.
37. J. Glanz; Astronomers see a cosmic antigravity force at work, *Science*, 279(5355), 1298—1299 (1998).
38. R. Cowen, Living with lambda, *Science News*, 153(22), 344 (1998).
39. R. Cowen, Studies support an accelerating Universe, *Science News*, 154(18), 277 (1998).
40. P. de Bernardis et al., A flat Universe from high-resolution maps of the cosmic microwave background radiation, *Nature*, Vol. 404, (2000), p. 955; <http://www.physics.ucsb.edu/~boomerang>.

Table 1. The calculated electric (per electron), magnetic (per electron), and ionization energies for some two-electron atoms.

Atom	r_1 (a_o) ^a	Electric Energy ^b (eV)	Magnetic Energy ^c (eV)	Calculated Ionization Energy ^d (eV)	Experimental ^e Ionization Energy (eV)
<i>He</i>	0.567	-23.96	0.63	24.59	24.59
<i>Li</i> ⁺	0.356	-76.41	2.54	75.56	75.64
<i>Be</i> ²⁺	0.261	-156.08	6.42	154.48	153.89
<i>B</i> ³⁺	0.207	-262.94	12.96	260.35	259.37
<i>C</i> ⁴⁺	0.171	-396.98	22.83	393.18	392.08
<i>N</i> ⁵⁺	0.146	-558.20	36.74	552.95	552.06
<i>O</i> ⁶⁺	0.127	-746.59	55.35	739.67	739.32
<i>F</i> ⁷⁺	0.113	-962.17	79.37	953.35	953.89

^a from Equation (96)
^b from Equation (98)
^c from Equation (99)
^d from Equations (97) and (100)

Figure Captions

Figure 1. The orbitsphere is a two dimensional spherical shell with the Bohr radius of the hydrogen atom.

Figure 2. The current pattern of the orbitsphere from the perspective of looking along the z-axis. The current and charge density are confined to two dimensions at $r_n = nr_1$. The corresponding charge density function is uniform.

Figure 3. The orbital function modulates the constant (spin) function (shown for $t = 0$; cross-sectional view).

Figure 4. The magnetic field of an electron orbitsphere.

Figure 5. Broadening of the spectral line due to the rise-time and shifting of the spectral line due to the radiative reaction. The resonant line shape has width Γ . The level shift is $\Delta\omega$.

Figure 6. The Cartesian coordinate system wherein the first great circle magnetic field line lies in the yz-plane, and the second great circle electric field line lies in the xz-plane is designated the photon orbitsphere reference frame of a photon orbitsphere.

Figure 7. The field line pattern from the perspective of looking along the z-axis of a right-handed circularly polarized photon.

Figure 8. The electric field of a moving point charge ($v = \frac{4}{5}c$).

Figure 9. The electric field lines of a right-handed circularly polarized photon orbitsphere as seen along the axis of propagation in the lab inertial reference frame as it passes a fixed point.

Figure 10. The front view of the magnitude of the mass (charge) density function in the xy-plane of a free electron; side view of a free electron along the axis of propagation--z-axis.

Figure 11. The experimental results for the elastic differential cross section for the elastic scattering of electrons by helium atoms and a Born approximation prediction.

Figure 12. The closed form function (Eqs. (8.55) and (8.56)) for the elastic differential cross section for the elastic scattering of electrons by helium atoms. The scattering amplitude function, $F(s)$ (Eq. (8.50)), is shown as an insert.

Figure 13. The radius of the universe as a function of time.

Figure 14. The expansion/contraction rate of the universe as a function of time.

Figure 15. The Hubble constant of the universe as a function of time.

Figure 16. The density of the universe as a function of time.

Figure 17. The power of the universe as a function of time.

Figure 18. The temperature of the universe as a function of time during the expansion phase.

Figure 19. The differential expansion of the light sphere due to the acceleration of the expansion of the cosmos as a function of time.

Fig. 1

The orbitsphere has zero thickness.
It is a two-dimensional surface.

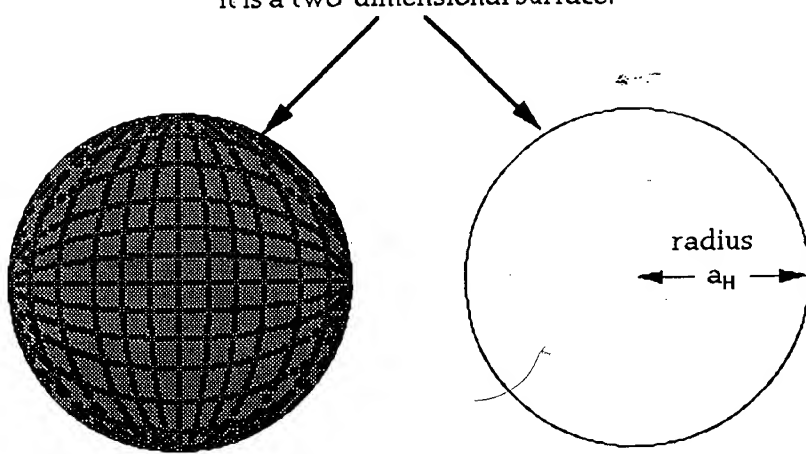


Fig. 2

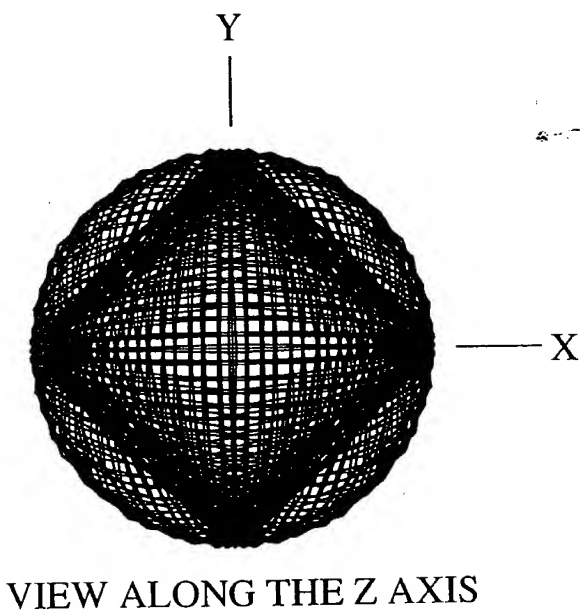


Fig. 3

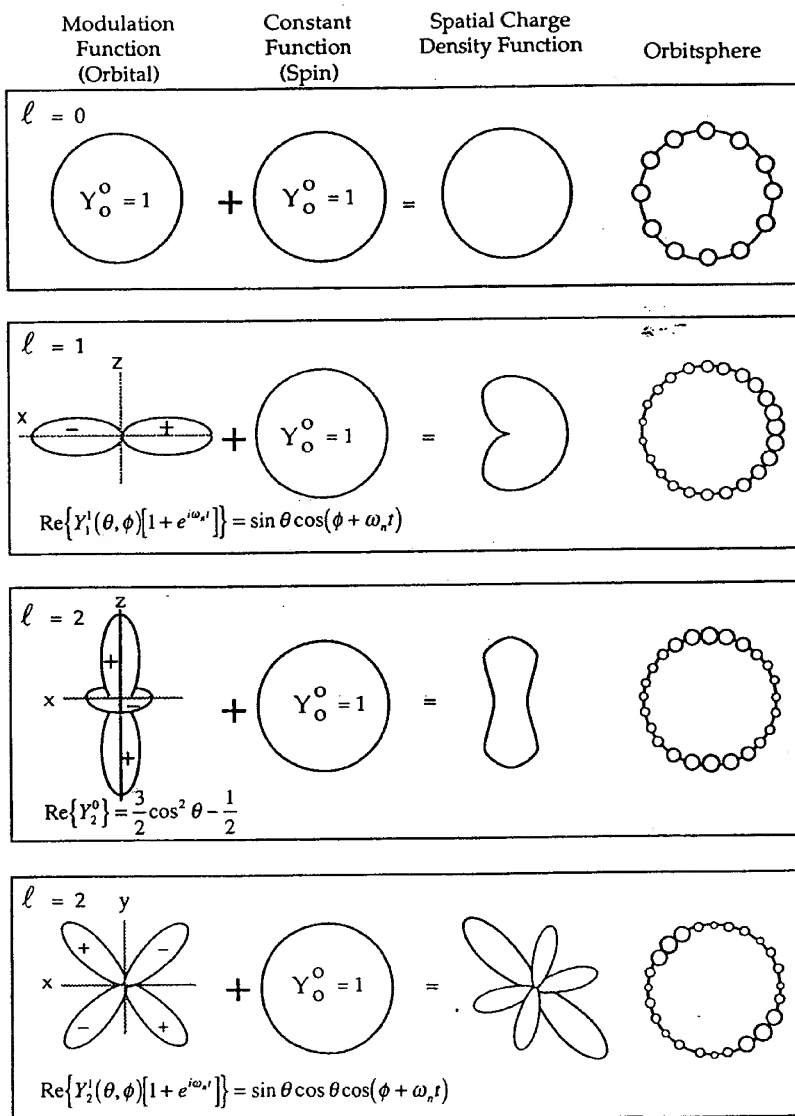


Fig. 4

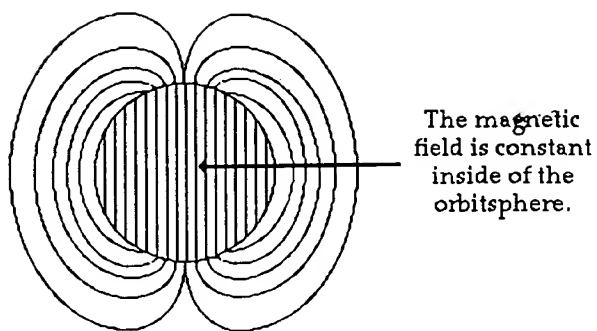


Fig. 5

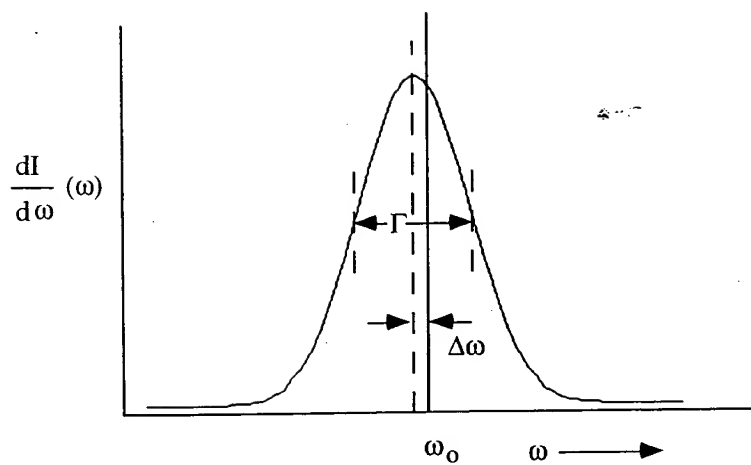


Fig. 6

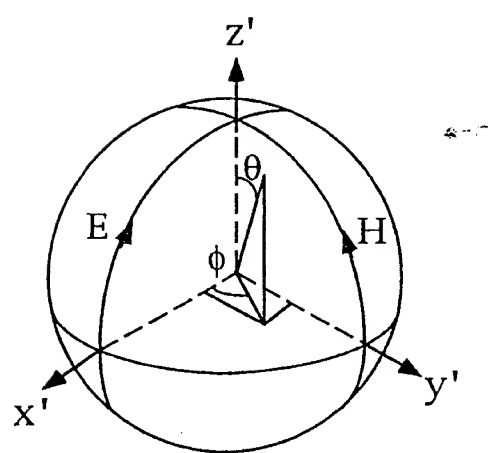
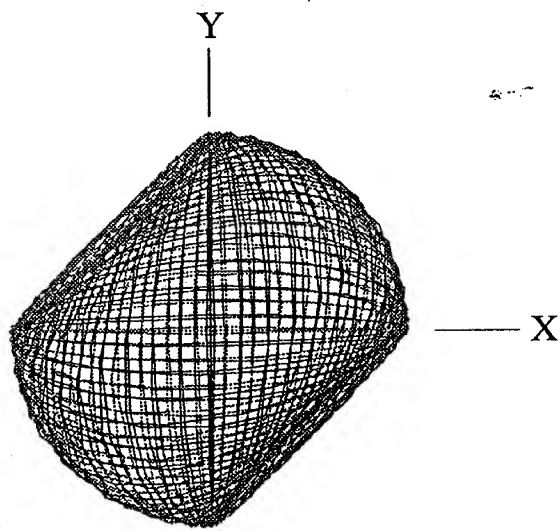


Fig. 7



VIEW ALONG THE Z AXIS

Fig. 8

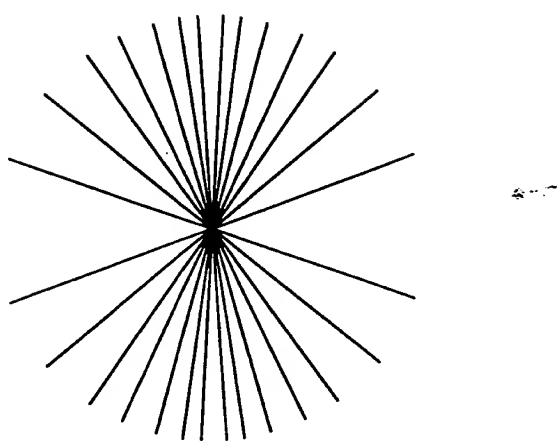
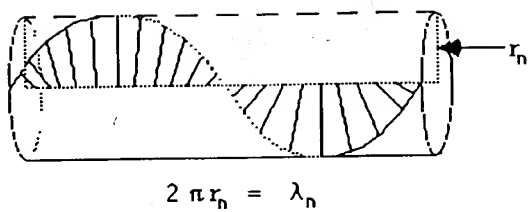
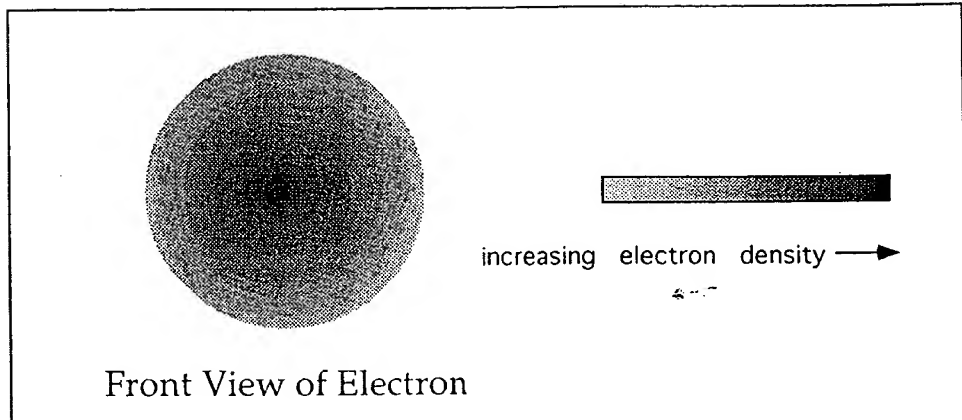


Fig. 9



$$2 \pi r_n = \lambda_n$$

Fig. 10



$$\rho_0 = \frac{\hbar}{mv_z}$$

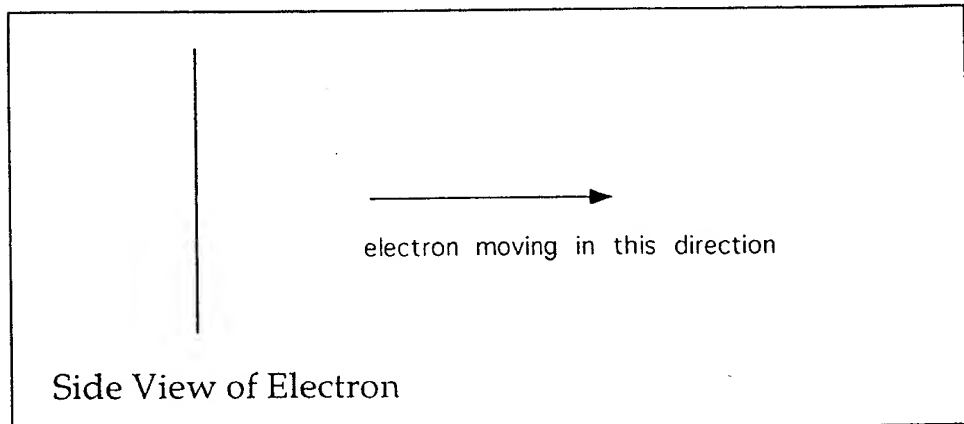


Fig. 11

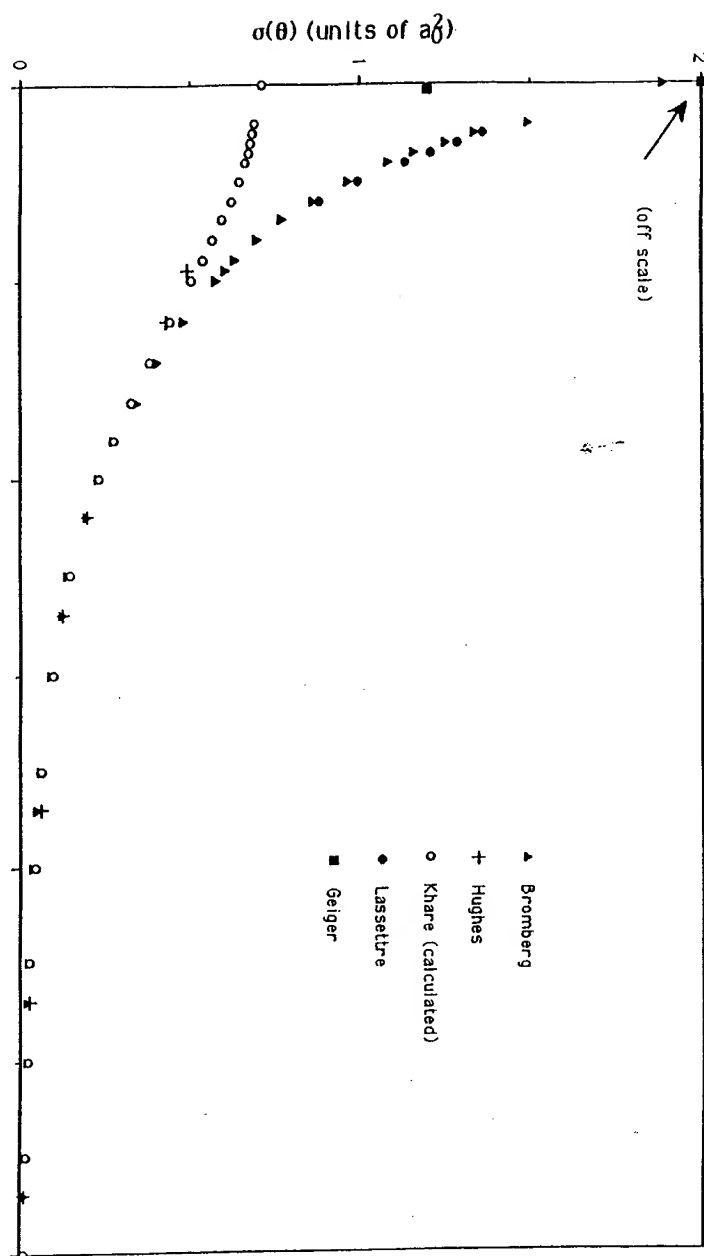


Fig. 12

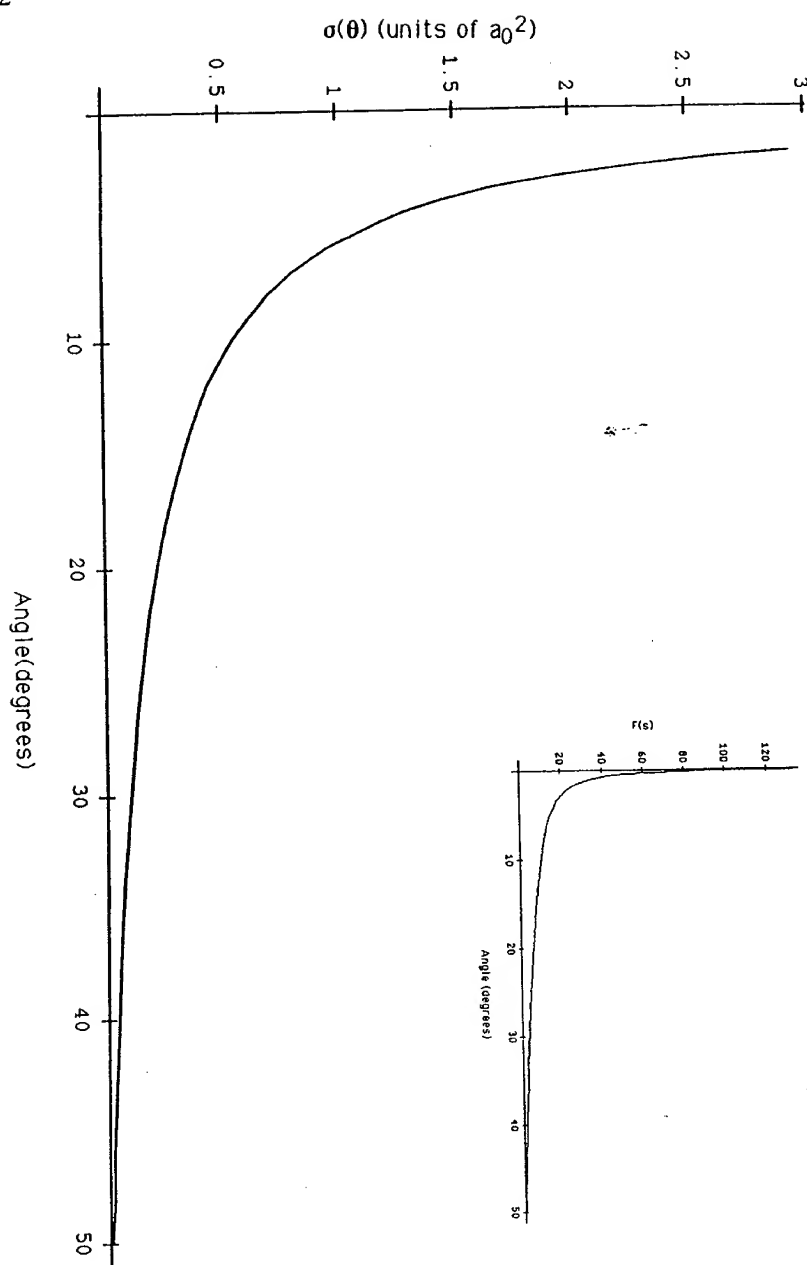


Fig. 13

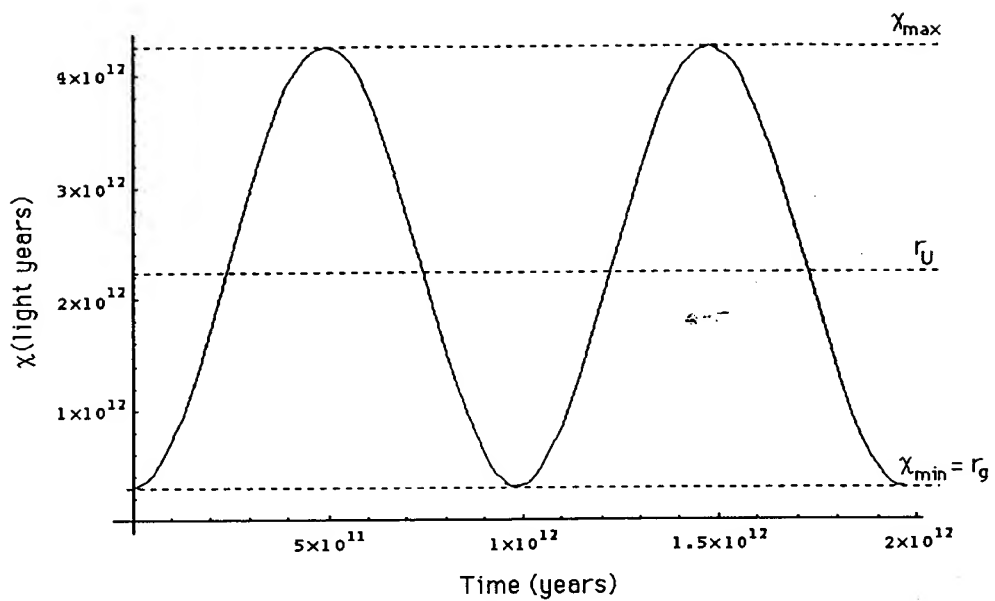


Fig. 14

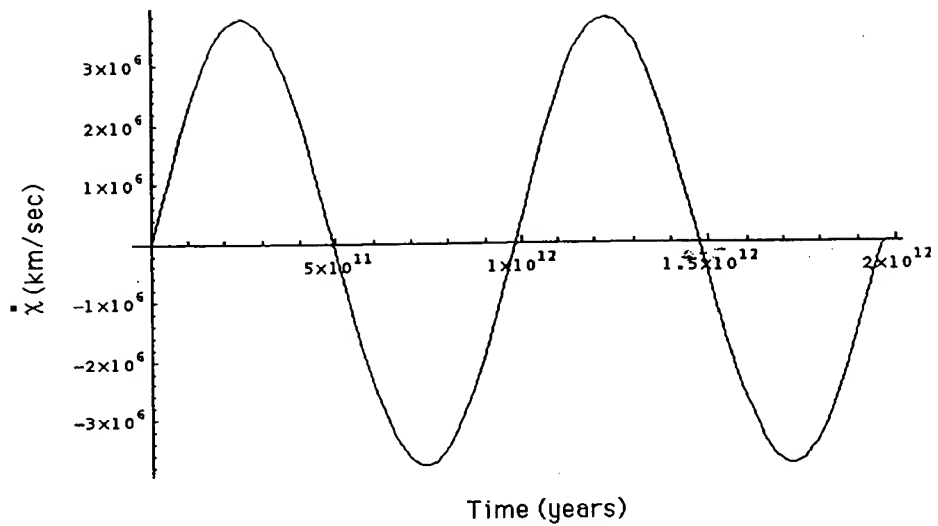


Fig. 15

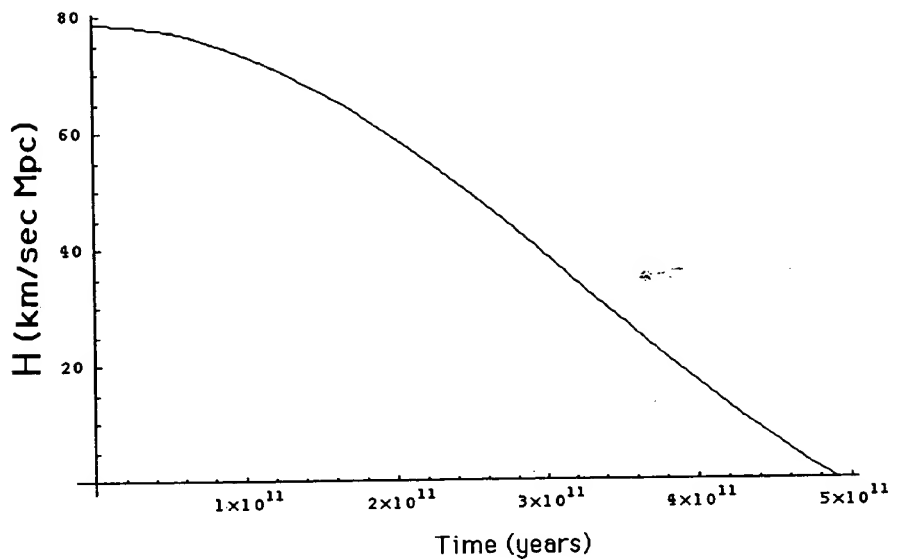


Fig. 16

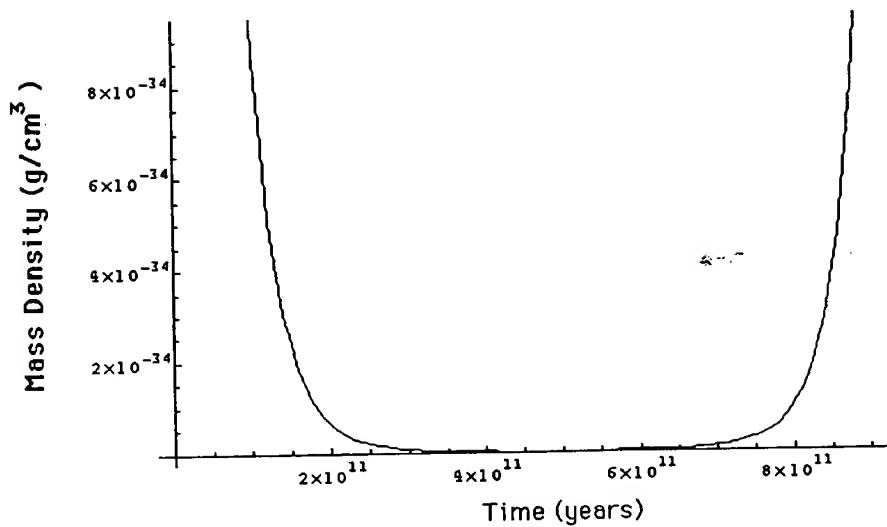


Fig. 17

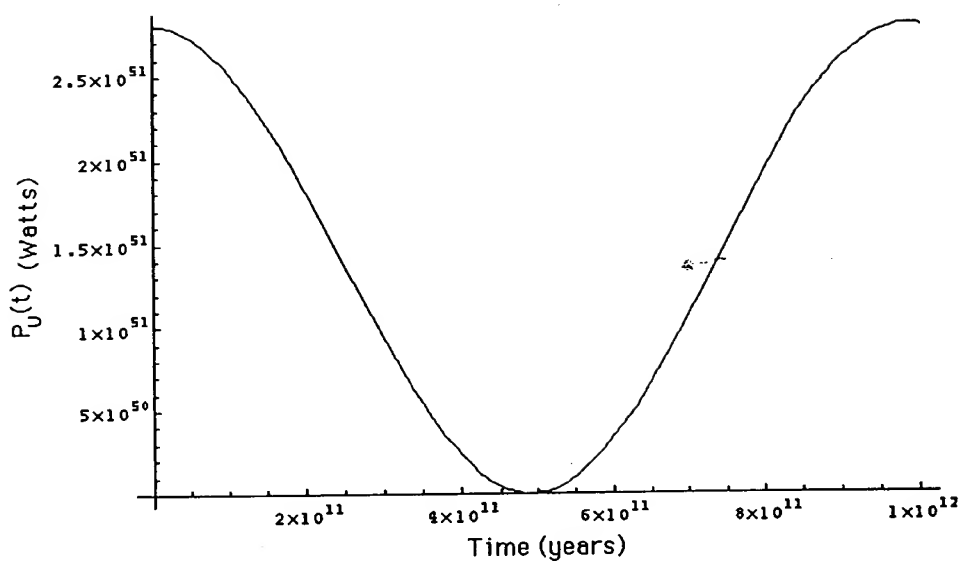


Fig. 18

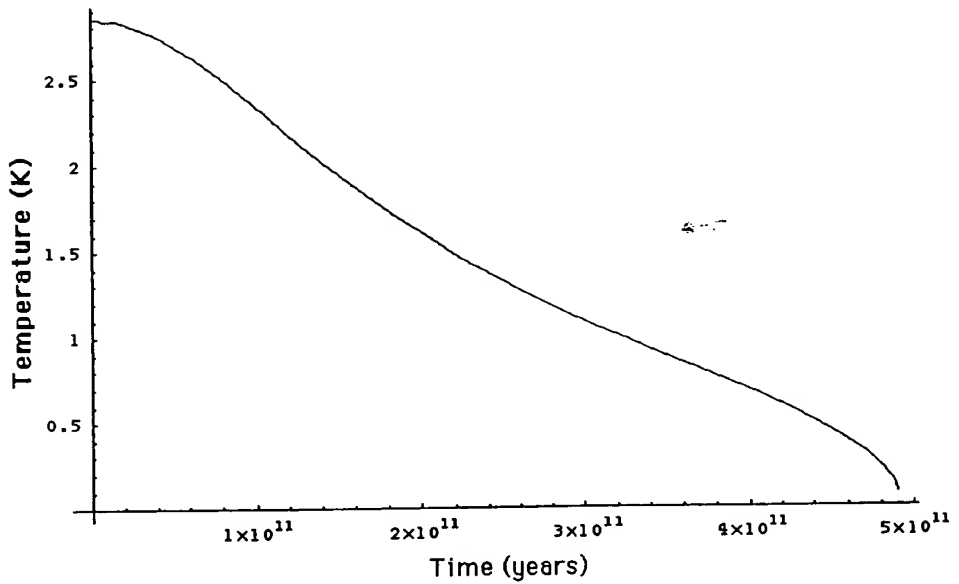
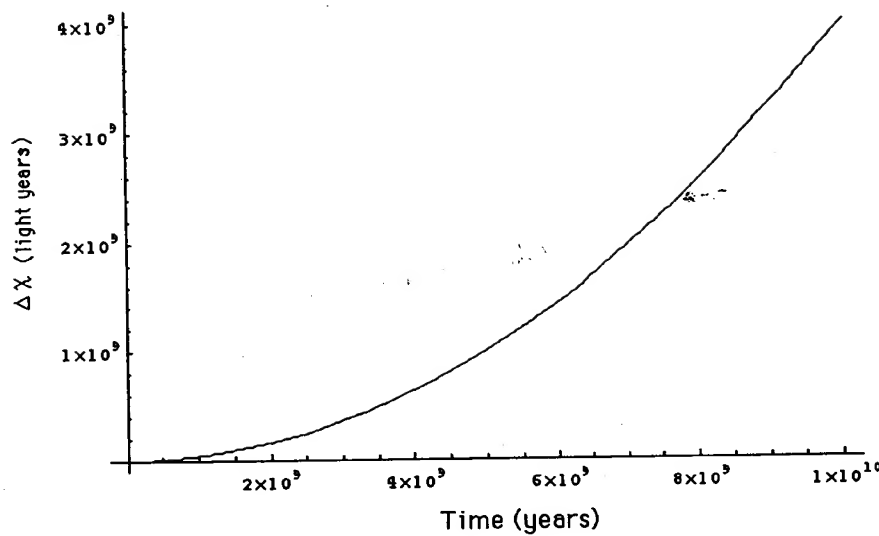


Fig. 19



THIS PAGE BLANK (USPTO)

Anomalous Argon-Hydrogen-Strontium Discharge

Randell L. Mills

Mark Nansteel

BlackLight Power, Inc.

493 Old Trenton Road

Cranbury, NJ 08512

We report the observation of intense extreme ultraviolet (EUV) emission from incandescently heated atomic hydrogen and atomized strontium that increased with argon. Typically the emission of extreme ultraviolet light from hydrogen gas is achieved via a discharge at high voltage, a high power inductively coupled plasma, or a plasma created and heated to extreme temperatures by RF coupling (e.g. $> 10^6 K$) with confinement provided by a toroidal magnetic field. The observed plasma formed at low temperatures (e.g. $\approx 10^3 K$) from atomic hydrogen generated at a tungsten filament that heated a titanium dissociator and atomic strontium which was vaporized from the metal by heating. The emission intensity of the plasma generated by atomic strontium increased significantly with the introduction of argon gas only when Ar^+ emission was observed. No emission was observed with hydrogen when sodium, magnesium, or barium replaced strontium or with hydrogen, hydrogen-argon mixtures, or strontium alone. The power balance of a gas cell having vaporized strontium and atomized hydrogen from pure hydrogen or argon-hydrogen mixture (77/23%) was measured by integrating the total light output corrected for spectrometer system response and energy over the visible range. Hydrogen control cell experiments were identical except that sodium, magnesium, or barium replaced strontium. In the case of hydrogen-sodium, hydrogen-magnesium, and hydrogen-barium mixtures, 4000, 7000, and 6500 times the power of the hydrogen-strontium mixture was required, respectively, in order to achieve that same optically measured light output power. With the addition of argon to the hydrogen-strontium plasma, the power required to achieve that same optically measured light output power was reduced by a factor of about two. The power required to maintain a plasma of equivalent optical brightness with strontium atoms present was 8600 and 6300 times less than that required for argon-hydrogen and argon control, respectively. A plasma formed at a cell voltage of about 250 V for hydrogen alone and sodium-hydrogen mixtures, 140-150 V for hydrogen-magnesium and hydrogen-barium mixtures, 224 V for an argon-hydrogen mixture, and 190 V for argon alone; whereas, a plasma formed for hydrogen-strontium mixtures and argon-hydrogen-strontium mixtures at extremely low voltages of about 2 V and 6.6 V, respectively.

I. INTRODUCTION

A historical motivation to cause EUV emission from a hydrogen gas was that the spectrum of hydrogen was first recorded from the only known source, the Sun [1]. Developed sources that provide a suitable intensity are high voltage discharge, synchrotron, and inductively coupled plasma generators [2]. An important variant of the later type of source is a tokomak [3] wherein a plasma is created and heated to extreme temperatures by RF coupling (e.g. $>10^6 K$) with confinement provided by a toroidal magnetic field. In contrast, it has been reported that intense EUV emission was observed at low temperatures (e.g. $\approx 10^3 K$) from atomic hydrogen and certain atomized elements or certain gaseous ions which singly or multiply ionize at integer multiples of the potential energy of atomic hydrogen, 27.2 eV [4-18]. The ionization energy of Ar^+ to Ar^{2+} is 27.6 eV [19], and an electric field may adjust the energy of ionizing Ar^+ to Ar^{2+} to match the energy of 27.2 eV. Thus, a discharge of argon is anticipated to cause an anomalous discharge when hydrogen is present.

Kuraica and Konjevic [20] observed intense wing developments of hydrogen Balmer lines with argon present in the negative glow of a glow discharge of an argon-hydrogen mixture irrespective of cathode material (carbon, copper, and silver). An anomalous discharge was not observed in neon-hydrogen and pure hydrogen mixtures. The authors offer a tentative explanation for hydrogen line shapes in the presence of argon which is based on a quasiresonance charge transfer between metastable argon ions and hydrogen molecules and the formation of a hydrogen molecular ion. According to the authors,

"... it is essential that the H_2^+ or H_3^+ ion must gain energy in the electric field before dissociation. Otherwise, the large energy of excited hydrogen atoms (on the average 50 eV per atom) cannot be explained".

The source of 50 eV anomalous thermal broadening of the Balmer lines observed by Kuraica and Konjevic [20] may be dependent on the presence of an atom or ion which ionizes at about an integer multiple of

27.2 eV since Ar^+ ionizes at 27.6 eV.

Strontium ionizes at integer multiples of the potential energy of atomic hydrogen; thus, a hydrogen-strontium mixture was tested for anomalous EUV emission and plasma formation relative to mixtures of hydrogen and chemically similar controls that do not have electron ionization energies which are a multiple of 27.2 eV.

We report that a hydrogen plasma is formed at low temperatures (e.g. $\approx 10^3$ K) by reaction of atomic hydrogen with strontium atoms, but not with magnesium, barium, or sodium atoms. In the case of EUV measurements, atomic hydrogen was generated by dissociation at a tungsten filament and at a transition metal dissociator that was incandescently heated by the filament. Strontium atoms were vaporized by heating to form a low vapor pressure (e.g. 1 torr). The kinetic energy of the thermal electrons at the experimental temperature of $\approx 10^3$ K were about 0.1 eV, and the average collisional energies of electrons accelerated by the field of the filament were less than 1 eV. (No blackbody emission was recorded for wavelengths shorter than 400 nm.). Strontium atoms caused hydrogen EUV emission; whereas, the chemically similar atoms, sodium, magnesium, and barium, caused no emission. The emission intensity of the plasma generated by atomic strontium increased significantly with the introduction of argon gas only when Ar^+ emission was observed. No emission was observed with argon or argon-hydrogen mixtures without strontium.

Furthermore, an anomalous hydrogen-strontium discharge was observed by visible emission. A cylindrical nickel mesh hydrogen dissociator of a gas cell also served as an electrode to produce an essentially uniform radial electric field between the dissociator and the wall of the cylindrical stainless steel gas cell. Power was applied to the electrode to achieve a bright plasma which was recorded over the wavelength range $350 \leq \lambda \leq 750$ nm. The power balance of a gas cell having atomized hydrogen and strontium was measured by integrating the total light output corrected for spectrometer system response and energy over the visible range. Control experiments were identical except that sodium, magnesium, or barium replaced strontium. In the case of hydrogen-sodium, hydrogen-magnesium, and hydrogen-barium mixtures, 4000, 7000, and 6500 times the power of the hydrogen-strontium mixture was

required, respectively, in order to achieve that same optically measured light output power. With the addition of argon to the hydrogen-strontium plasma, the power required to achieve that same optically measured light output power was reduced by a factor of about two. In the case of an argon-hydrogen mixture and argon alone, the power requirement was 8600 and 6300 times the power input of the argon-hydrogen-strontium mixture, respectively.

II. EXPERIMENTAL

A. EUV spectroscopy

Due to the extremely short wavelength of this radiation, "transparent" optics do not exist for EUV spectroscopy. Therefore, a windowless arrangement was used wherein the source was connected to the same vacuum vessel as the grating and detectors of the EUV spectrometer. Windowless EUV spectroscopy was performed with an extreme ultraviolet spectrometer that was mated with the cell. Differential pumping permitted a high pressure in the cell as compared to that in the spectrometer. This was achieved by pumping on the cell outlet and pumping on the grating side of the collimator that served as a pin-hole inlet to the optics. The cell was operated under gas flow conditions while maintaining a constant gas pressure in the cell. The gas pressure inside the cell was maintained at about 300 mtorr with a hydrogen flow rate of 5.5 sccm controlled by a 20 sccm range mass flow controller (MKS 1179A21CS1BB) with a readout (MKS type 246). The argon-hydrogen gas mixture which produced the maximum EUV emission was determined by adjusting the flow rate of hydrogen and argon with two mass flow controllers.

The experimental set up shown in Figure 1 comprised a quartz cell which was 500 mm in length and 50 mm in diameter. Three ports for gas inlet, outlet, and photon detection were on a Pyrex cap of the cell that sealed to the quartz cell with a Viton O ring and a C-clamp. A tungsten filament (0.508 mm in diameter and 800 cm in length, total resistance ~2.5 ohm) heater and hydrogen dissociator and in the case of the hydrogen gas experiments, a titanium cylindrical screen (300 mm long

and 40 mm in diameter) that performed as a second hydrogen dissociator were inside the quartz cell. A new dissociator was used for each hydrogen gas experiment. The filament was coiled on a grooved ceramic tube support to maintain its shape when heated. The return lead passed through the inside of the ceramic tube. The titanium screen was electrically floated. The power was applied to the filament by a Sorensen 80-13 power supply which was controlled by a constant power controller. The temperature of the tungsten filament was estimated to be in the range of 1100 to 1500 °C. The external cell wall temperature was about 700 °C. The entire quartz cell was enclosed inside an insulation package comprised of Zircar AL-30 insulation. Several K type thermocouples were placed in the insulation to measure key temperatures of the cell and insulation. The thermocouples were read with a multichannel computer data acquisition system.

In the present study, the light emission phenomena was studied for 1.) hydrogen, argon, neon, and helium alone; 2.) sodium, magnesium, barium, and strontium metals alone; 3.) sodium, magnesium, barium, and strontium with hydrogen; and 4.) sodium, magnesium, barium, and strontium with an argon-hydrogen mixture (97/3%). The pure elements of magnesium, barium, and strontium were placed in the bottom of the cell and vaporized by the filament heater. The power applied to the filament was 300 W in the case of strontium and up to 600 watts in the case of magnesium, barium, and sodium metals. The voltage across the filament was about 55 V and the current was about 5.5 ampere at 300 watts. For the controls, magnesium, barium, and sodium metals, the cell was increased in temperature to the maximum permissible with the power supply.

The light emission was introduced to an EUV spectrometer for spectral measurement. The spectrometer was a McPherson 0.2 meter monochromator (Model 302, Seya-Namioka type) equipped with a 1200 lines/mm holographic grating with a platinum coating. The wavelength region covered by the monochromator was 30–560 nm. A channel electron multiplier (CEM) was used to detect the EUV light. The wavelength resolution was about 1 nm (FWHM) with an entrance and exit slit width of 300 μm. The vacuum inside the monochromator was maintained below 5×10^{-4} torr by a turbo pump. The EUV spectrum

(40–160 nm) of the cell emission with strontium present was recorded at about the point of the maximum Lyman α emission.

The UV/VIS spectrum (40–560 nm) of the cell emission with hydrogen alone was recorded with a photomultiplier tube (PMT) and a sodium salicylate scintillator. The PMT (Model R1527P, Hamamatsu) used has a spectral response in the range of 185–680 nm with a peak efficiency at about 400 nm. The scan interval was 0.4 nm. The inlet and outlet slit were 500 μm with a corresponding wavelength resolution of 2 nm.

B. Power cell apparatus and procedure

Plasma studies with 1.) hydrogen, argon, or argon-hydrogen mixture alone, 2.) hydrogen with strontium, sodium, magnesium, or barium, and 3.) argon-hydrogen mixture (77/23%) with strontium were carried out in the cylindrical stainless steel gas cell shown in Figure 2. The experimental setup for generating a glow discharge hydrogen plasma and for optically measuring the power balance is shown in Figure 3. The cell was heated in a 10 kW refractory brick kiln (L & L Kiln Model JD230) as shown in Figure 3. The cell was evacuated and pressurized with hydrogen, argon, or argon and hydrogen through a single 0.95 cm feed through. The discharge was started and maintained by an alternating current electric field in the 1.75 cm annular gap between an axial electrode and the cell wall. The cylindrical cell was 9.21 cm in diameter and 14.5 cm in height. The axial electrode was a 5.08 cm OD by 7.2 cm long stainless steel tube wound with several layers of nickel screen. The overall diameter of the axial electrode was 5.72 cm. A 1.6 mm thick UV-grade sapphire window with 1.5 cm view diameter provided a visible light path from inside the cell. The viewing direction was normal to the cell axis. A 1.27 cm diameter stainless steel tube passed through the furnace wall and connected to a view port welded to the cell wall at mid-height to provide an optical light path from the sapphire window to the furnace exterior. An 8 mm quartz rod channeled the light from the view port through the stainless tube to a collimating lens which was focused on a 100 μm optical fiber located outside the furnace. Spectral data was recorded with a visible spectrometer (Ocean Optics S2000) and stored by

a personal computer.

The field voltage was controlled by a variable voltage transformer operating from 115 VAC, 60 Hz. A step-up transformer was used when necessary. True rms voltage at the axial electrode was monitored by a digital multimeter (Fluke 8010 A or Tenma 726202). A second multimeter (Extech 380763) in series with the discharge gap was used to indicate the current. The cell temperature was measured by a thermocouple probe located in the cell interior approximately 2 cm from the discharge gap. The pressure in the hydrogen and argon supply tube outside the furnace was monitored by 10 torr and 1000 torr MKS Baratron absolute pressure gauges. In the absence of gas flow, the gas supply tube pressure was essentially the cell pressure. The pressure of each gas in an argon-hydrogen mixture was determined by adding one pure gas to a given pressure and increasing the pressure with a second gas to a final pressure. The partial pressure of the second gas was given by the incremental increase in total gas pressure.

Strontium (Aldrich Chemical Company 99.9 %), sodium (Aldrich Chemical Company 99.95 %), magnesium (Alfa Aesar 99.98 %), or barium (Aldrich Chemical Company 99.99 %) metal was loaded into the cell under a dry argon atmosphere. The cell was evacuated with a turbo vacuum pump to a pressure of 4 mtorr during most of the heating process. During the heat-up the cell was periodically pressurized with hydrogen (99.999% purity) to approximately 100 torr and subsequently evacuated to purge gaseous contaminants from the system. When the cell temperature stabilized hydrogen was added until the steady pressure was approximately 1 torr. The field voltage was increased until breakdown occurred. This was confirmed by the spectrometer response to visible light emitted from the cell. The hydrogen or hydrogen-argon pressure was adjusted, as much as possible, to maximize the light emission from the cell. The voltage was maintained at the minimum level which resulted in a stable discharge during data acquisition.

The spectrometer system comprised a 100 μm optical fiber and visible spectrometer (Ocean Optics S2000). To correct for the nonuniform response of the spectrometer system as a function of wavelength and the dependence of energy on wavelength, the system was calibrated against a reference light source (Ocean Optics LS-1-CAL). A spectral calibration

factor was applied to the count rate data at each wavelength to yield the irradiation of the detector in units of energy/time/area/wavelength. The total visible radiant flux incident on the detector was calculated by integrating the spectral irradiation between 400 and 700 nm.

III. RESULTS

A. EUV spectroscopy

The cell without any test material present was run to establish the baseline of the spectrometer. The intensity of the Lyman α emission as a function of time from the gas cell at a cell temperature of 700 °C comprising a tungsten filament, a titanium dissociator, and 300 mtorr hydrogen with a flow rate of 5.5 sccm is shown in Figure 4. The corresponding UV/VIS spectrum (40–560 nm) is shown in Figure 5. The spectrum was recorded with a photomultiplier tube (PMT) and a sodium salicylate scintillator. No emission was observed except for the blackbody filament radiation at the longer wavelengths. No emission was also observed from the pure elements alone or when argon, neon, or helium replaced hydrogen.

The intensity of the Lyman α emission as a function of time from the gas cell at a cell temperature of 700 °C comprising a tungsten filament, a titanium dissociator, vaporized sodium, magnesium, or barium metal, and 300 mtorr hydrogen with a flow rate of 5.5 sccm are shown in Figures 6, 7, and 8, respectively. Sodium, magnesium, or barium metal was vaporized by filament heating. No emission was observed in any case. The maximum filament power was greater than 500 watts. At 500 watts, the temperature of the magnesium was 1000 °C which would correspond to a vapor pressure of about 100 mtorr. A metal coating formed in the cap of the cell over the course of the experiment in each case.

The intensity of the Lyman α emission as a function of time from the gas cell at a cell temperature of 700 °C comprising a tungsten filament, a titanium dissociator, a vaporized strontium metal, and 300 mtorr hydrogen with a flow rate of 5.5 sccm is shown in Figure 9. Strong emission was observed from vaporized strontium and hydrogen. The

EUV spectrum (40–160 nm) of the cell emission recorded at about the point of the maximum Lyman α emission is shown in Figure 10. No emission was observed in the absence of hydrogen flow. A metal coating formed in the cap of the cell over the course of the experiment.

Hydrogen was replaced by a 97% argon and 3% hydrogen mixture. The intensity of the Lyman α emission as a function of time from each gas cell was recorded. The intensity of the Lyman α emission as a function of time from the gas cell at a cell temperature of 700 °C comprising a tungsten filament, and 300 mtorr argon-hydrogen mixture (97/3%) that was recorded with a CEM is shown in Figure 11. No emission was observed with argon-hydrogen mixtures alone. The EUV spectrum (40–160 nm) of the sodium, magnesium, and barium gas cell emission that was recorded with a PMT and a sodium salicylate scintillator two hours after the cell reached 700 °C are shown in Figures 12, 13, and 14, respectively. Each cell comprised a tungsten filament, vaporized metal, and 300 mtorr argon-hydrogen mixture (97/3%). No emission was observed in any case.

The EUV spectrum (40–160 nm) of the cell emission recorded at about the point of the maximum Lyman α emission from the gas cell at a cell temperature of 700 °C comprising a tungsten filament, vaporized strontium metal, and 300 mtorr argon-hydrogen mixture (97/3%) that was recorded with a PMT and a sodium salicylate scintillator is shown in Figure 15. Strong EUV emission was observed that was more intense than with hydrogen and strontium. The Lyman series corresponded to atomic hydrogen emission and strong Ar^+ ion emission was observed at 92.0 nm and 93.2 nm.

The anomalous plasma required the presence of hydrogen. It was found that increasing the hydrogen pressure initially increased the atomic hydrogen emission lines, but with increasing hydrogen partial pressure at a constant total pressure, the Ar^+ emission in the EUV at 92.0 nm and 93.2 nm decreased which resulted in a decrease of the plasma intensity including the hydrogen emission. The zero order emission in the EUV was observed with titration of increasing partial pressure of hydrogen added to argon gas. The optimum argon-hydrogen gas mixture which produced the greatest emission was determined to be 95% argon and 5% hydrogen which is similar to the 97% argon and 3% hydrogen

mixture of Kuraica and Konjevic [20]. The optimum ratio was consistent with an anomalous discharge mechanism which required maximum concentrations of both atomic hydrogen and Ar^+ .

B. Optically measured power balance

Count rate and spectrometer system irradiation of the background spectrum of hydrogen and strontium vapor over the wavelength range $350 \leq \lambda \leq 750 nm$ in the absence of power applied to the electrode and in the absence of a discharge is shown in Figure 16. This data was collected during cell evacuation following the test with strontium and hydrogen at a cell temperature of 664 °C. The maximum visible irradiation of $0.004 \mu W/cm^2 nm$ occurred at the red end of the visible spectrum. The results are summarized in Table I where T is the temperature, P_{hyd} and P_{Ar} are the hydrogen and argon partial pressures, and P_e is the equilibrium metal vapor pressure calculated from standard curves of the vapor pressure as a function of temperature [21].

Power was applied to the electrode to achieve a bright plasma in the strontium-hydrogen mixture and the controls of hydrogen alone, and sodium-hydrogen, magnesium-hydrogen, and barium-hydrogen mixtures for cell temperatures in the range 335-666 °C. In each case, the spectral radiant flux at the spectrometer system was recorded. If possible, the power driving the controls was adjusted such that the peak spectrometer system spectral irradiation was about $0.1 \mu W/cm^2 nm$ in each case. The integrated visible irradiation levels were of the order of $1 \mu W/cm^2$. One exception was the case of hydrogen-barium. In this case, the maximum spectral irradiation levels and integrated visible irradiation levels were only of the order of $0.01 \mu W/cm^2 nm$ and $0.03 \mu W/cm^2$, respectively.

The power required to maintain a plasma of equivalent optical brightness with strontium atoms present was 4000, 7000, and 6500 times less than that required for the sodium, magnesium, and barium control, respectively. A driving power of 33.7 W and 58 W was necessary to achieve a total visible radiant flux of about $1 \mu W/cm^2$ from a sodium-hydrogen mixture and a magnesium-hydrogen mixture, respectively. For a hydrogen-barium mixture, a power input of about 55 W was required to achieve a total visible irradiation of about $0.03 \mu W/cm^2$.

Whereas, in the case of a strontium-hydrogen mixture, a power input of 8.5 mW resulted in a plasma with a total visible radiant flux of about the same optical brightness as sodium and magnesium. A plasma formed at a cell voltage of about 250 V for hydrogen alone and sodium-hydrogen mixtures, and 140-150 V for hydrogen-magnesium and hydrogen-barium mixtures; whereas, a plasma formed for hydrogen-strontium mixtures at the extremely low voltage of about 2 V. The results are summarized in Table I.

Power was applied to the electrode to achieve a bright plasma in the strontium-argon-hydrogen mixture and the controls of argon alone and argon-hydrogen alone for cell temperatures in the range 514-520 °C. In each case, the spectral radiant flux at the spectrometer system was recorded. If possible, the power driving the controls was adjusted such that the peak spectrometer system spectral irradiation was about $0.1 \mu\text{W}/\text{cm}^2\text{nm}$ in each case. The integrated visible irradiation levels were of the order of $1 \mu\text{W}/\text{cm}^2$.

The power required to maintain a plasma of equivalent optical brightness with strontium atoms present was 8600 and 6300 times less than that required for argon-hydrogen and argon control, respectively. A driving power of 33.5 W and 24.7 W was necessary to achieve a total visible radiant flux of about $1 \mu\text{W}/\text{cm}^2$ from an argon-hydrogen mixture and argon, respectively. Whereas, in the case of a strontium-argon-hydrogen mixture, a power input of 4 mW resulted in a plasma with a total visible radiant flux of about the same optical brightness as the argon-hydrogen mixture and argon. A plasma formed at a cell voltage of 224 V for an argon-hydrogen mixture alone, and 190 V for argon alone; whereas, a plasma formed for argon-hydrogen-strontium mixtures at an extremely low voltage of about 6.6 V. The results are summarized in Table I.

The count rate and the spectrometer system irradiation for a mixture of hydrogen and strontium vapor at 664 °C is shown in Figure 17. Optimal light emission was observed after several hours of cell evacuation. The hydrogen partial pressure was unknown under these conditions. The calculated equilibrium vapor pressure of strontium at 664 °C is approximately 270 mtorr. The measured breakdown voltage was approximately 2 V. The maintenance voltage for a stable discharge

was 2.2 V and input power was 8.5 mW. Spectral characteristics are noted in Table II. The hydrogen Balmer α and β peaks were obscured by strong strontium emission near 654.7 and 487.2 nm, respectively.

The spectrometer system irradiation for a hydrogen discharge at a cell temperature of 664 °C and 1 torr is shown in Figure 18. The breakdown voltage was approximately 220 V. The field voltage required to form a stable discharge was 224 V. The input power was 24.6 W. Spectral features are tabulated in Table III. The peak at 589.1 nm may be due to sodium contamination from a previous experimental run. The minor peaks at 518.2 and 558.7 nm have not been identified.

The spectrometer system irradiation for mixtures of hydrogen and sodium vapor are shown in Figures 19-21 for temperatures of 335, 516, and 664 °C, respectively. Corresponding hydrogen pressures are 1, 1.5, and 1.5 torr, respectively. The calculated sodium vapor pressure was 51 mtorr, 5.3 torr, and 63 torr at 335, 516, and 664 °C, respectively. At least 200 V was required to maintain a discharge. The input power for a stable discharge ranged from approximately 10 W at 664 °C to 34 W at 335 °C. Spectral features corresponding to 335 °C are summarized in Table IV. Strong emission observed near 656-657 nm was probably due, in-part, to hydrogen. The relative contribution to the intensity was masked by strong sodium emission at a slightly shorter wavelength. The peak at 486.2 nm could only be due to hydrogen emission. Sodium does not have emission lines in the neighborhood of this wavelength. The intensity of this peak diminishes relative to the more prominent sodium peaks with increasing temperature as shown in Figures 19-21. This may have been due to a decreasing hydrogen concentration as the sodium vapor pressure increased.

The spectral response for mixtures of magnesium vapor and hydrogen are shown in Figures 22-24 for temperatures of 449, 582, and 654 °C, respectively. The corresponding hydrogen pressures are 4, 4.2, and 3 torr, respectively. A minimum of 150 V was required to maintain a discharge. The minimum input power required to maintain a stable discharge was 58 W at 449 °C. Spectral features corresponding to 449 °C are summarized in Table V. Both hydrogen and magnesium spectral features are observed. The modest sodium emission at 588 nm may be due to sodium contamination from previous control experiments.

The spectral response for a mixture of barium vapor and hydrogen at 666°C is shown in Figure 25. The hydrogen partial pressure and barium vapor pressure are 2 torr and 25 mtorr, respectively. It was not possible to achieve a total visible irradiation level of $1\mu\text{W}/\text{cm}^2$ even with voltages approaching 150 V. The voltage and power input corresponding to Figure 25 are 138 V and 55 W, respectively. Spectral features are summarized in Table VI. Both barium and hydrogen spectral features are observed as well as sodium features which are presumably due to contamination. The peak at 493 nm has not been identified.

The spectral response for a mixture of hydrogen, argon, and strontium vapor at 514°C is shown in Figure 26. The hydrogen and argon partial pressures were 0.3 and 1 Torr, respectively. The strontium vapor pressure was approximately 6 mtorr at this temperature. The voltage required for a stable discharge was 6.6 V. The corresponding power input to the cell was approximately 4 mW. The spectral characteristics are tabulated in Table VII. The two major features were due to strontium emission. The very minor spectral features at 639 and 654 nm were due to argon. The total visible irradiation of the spectrometer detector was $1.3\mu\text{W}/\text{cm}^2$. The spectral responses for a mixture of argon and hydrogen and for pure argon are shown in Figures 27 and 28, respectively. For irradiation levels in the range $1\text{-}2\mu\text{W}/\text{cm}^2$, voltages of 224 and 190 V and power inputs of 33.5 and 24.7 W were required for discharges in argon and hydrogen, and pure argon, respectively. The spectral characteristics are tabulated in Tables VIII and IX for these gas discharges. In the case of pure argon, the emission at 656 nm was most likely hydrogen Balmer alpha emission due to some hydrogen contamination.

IV. DISCUSSION

Intense EUV emission was observed at low temperatures (e.g. $\approx 10^3 K$) from atomic hydrogen and strontium which ionizes at integer multiple of the potential energy of atomic hydrogen. The emission intensity of the plasma generated by atomic strontium increased significantly with the introduction of argon gas only when Ar^+ emission was observed. The ionization energy of Ar^+ to Ar^{2+} is 27.6 eV. In the

cases where Lyman α emission was observed, no possible chemical reactions of the tungsten filament, the dissociator, the vaporized strontium, and 300 mtorr hydrogen or argon-hydrogen mixture at a cell temperature of 700 °C could be found which accounted for the hydrogen α line emission. In fact, no known chemical reaction releases enough energy to excite Lyman α emission from hydrogen. The emission was not observed with hydrogen or an argon-hydrogen mixture alone or with helium, neon, or argon gas. Intense emission was observed for strontium with hydrogen gas, but no emission was observed with hydrogen or strontium alone. This result indicates that the emission may be due to a reaction of hydrogen. The increase in intensity with the formation of Ar^+ and the equal dependency of the emission on the presence of both Ar^+ and atomic hydrogen indicates a reaction between these species.

Other studies support the possibility of a novel reaction of atomic hydrogen which produces an anomalous discharge. It has been previously reported that intense extreme ultraviolet (EUV) emission was observed at low temperatures (e.g. $\approx 10^3 K$) from atomic hydrogen and certain atomized elements or certain gaseous ions [4-18]. The only pure elements that were observed to emit EUV were those wherein the ionization of t electrons from an atom to a continuum energy level is such that the sum of the ionization energies of the t electrons is approximately $m \cdot 27.2\text{ eV}$ where t and m are each an integer. Strontium atoms ionize at integer multiples of the potential energy of atomic hydrogen and caused emission. Whereas, the chemically similar atoms, sodium, magnesium and barium, do not ionize at integer multiples of the potential energy of atomic hydrogen and caused no emission. The ionization of Sr to Sr^{5+} has a net enthalpy of reaction of 188.2 eV [19], which is equivalent to $m=7$. Argon ions can also provide a net enthalpy of a multiple of that of the potential energy of the hydrogen atom. The second ionization energy of argon is 27.63 eV . The reaction Ar^+ to Ar^{2+} has a net enthalpy of reaction of 27.63 eV , which is equivalent to $m=1$.

The power balance of the gas cell having atomized hydrogen and strontium was measured by integrating the total light output corrected for spectrometer system response and energy over the visible range. A control cell was identical except that sodium, magnesium, or barium replaced strontium. In the hydrogen controls, 4000-7000 times the

power of the strontium cell was required in order to achieve the same optically measured light output power. With the addition of argon to the hydrogen-strontium plasma, the light output for power input increased by a factor of about two. In the argon-hydrogen controls up to 8600 times the power input was required to match the light output of the argon-hydrogen-strontium plasma. A plasma formed at a cell voltage of about 250 V for hydrogen alone and sodium-hydrogen mixtures, 140-150 V for hydrogen-magnesium and hydrogen-barium mixtures, 224 V for an argon-hydrogen mixture alone, and 190 V for argon alone; whereas, a plasma formed for hydrogen-strontium mixtures and argon-hydrogen-strontium mixtures at extremely low voltages of about 2 V and 6.6 V, respectively. This is two orders of magnitude lower than the starting voltages measured for gas glow discharges, cf. Table X.

An anomalous plasma with hydrogen-potassium mixtures has been reported in an experiment identical to the present EUV experiments [9-10, 12]. In experiments performed at the Institut Fur Niedertemperatur-Plasmaphysik e.V., an anomalous plasma formed with hydrogen/potassium mixtures wherein the plasma decayed with a two second half-life which was the thermal decay time of the filament which dissociated molecular hydrogen to atomic hydrogen when the electric field was set to zero [9, 12]. This experiment showed that hydrogen line emission was occurring even though the voltage between the heater wires was set to and measured to be zero and indicated that the emission was due to a reaction of potassium atoms with atomic hydrogen. Potassium atoms ionize at an integer multiple of the potential energy of atomic hydrogen, $m \cdot 27.2 \text{ eV}$. The enthalpy of ionization of K to K^{3+} has a net enthalpy of reaction of 81.7426 eV , which is equivalent to $m=3$.

An anomalous plasma of hydrogen and certain alkali ions formed at low temperatures (e.g. $\approx 10^3 \text{ K}$) as recorded via EUV spectroscopy and the hydrogen Balmer and alkali line emissions in the visible range [10]. The observed plasma formed at low temperatures (e.g. $\approx 10^3 \text{ K}$) from atomic hydrogen generated at a tungsten filament that heated a titanium dissociator and one of potassium, rubidium, cesium, and their carbonates and nitrates. These atoms and ions ionize to provide a net enthalpy of reaction of an integer multiple of the potential energy of atomic hydrogen ($m \cdot 27.2 \text{ eV}$, $m = \text{integer}$) to within 0.17 eV and comprise only a single

ionization in the case of a potassium or rubidium ion. Whereas, the chemically similar atoms of sodium and sodium and lithium carbonates and nitrates which do not ionize with these constraints caused no emission. To test the electric dependence of the emission, the weak electric field of about 1 V/cm was set and measured to be zero in $< 0.5 \times 10^{-6}$ sec. An anomalous afterglow duration of about one to two seconds was recorded in the case of potassium, rubidium, cesium, K_2CO_3 , $RbNO_3$, and $CsNO_3$. Hydrogen line or alkali line emission was occurring even though the voltage between the heater wires was set to and measured to be zero. These atoms and ions ionize to provide a net enthalpy of reaction of an integer multiple of the potential energy of atomic hydrogen to within less than the thermal energies at $\approx 10^3 K$ and comprise only a single ionization in the case of a potassium or rubidium ion. Since the thermal decay time of the filament for dissociation of molecular hydrogen to atomic hydrogen was similar to the anomalous plasma afterglow duration, the emission was determined to be due to a reaction of atomic hydrogen with each of the atoms or ions that did not require the presence of an electric field to be functional.

In the present experiments, it was determined that the presence of a weak electric field was necessary in order for strontium to produce an anomalous discharge of hydrogen. In the case that electrons are ionized to a continuum energy level, the presence of a low strength electric field alters the continuum energy levels. For strontium, the minimum electric field in this experiment was about 2 V over the annular gap of about 2 cm. The ionization energy of 188.2 eV is 1% less than $m \cdot 27.2$ eV where $m = 7$. In the anomalous discharge of hydrogen due to the presence of strontium, the weak field may adjust the energy of ionizing strontium to match the energy of $m \cdot 27.2$ eV to permit a novel reaction of atomic hydrogen. For Ar^+ , the minimum electric field in this experiment was about 6.6 V. The ionization energy of Ar^+ to Ar^{2+} is 27.6 eV, and an electric field may adjust the energy of ionizing Ar^+ to Ar^{2+} to match the energy of 27.2 eV.

Reports of the formation of novel compounds provide substantial evidence supporting a novel reaction of hydrogen as the mechanism of the observed EUV emission and anomalous discharge. Novel hydrogen compounds have been isolated as products of the reaction of atomic

hydrogen with atoms and ions which formed an anomalous plasma as reported in the EUV studies [4-18, 25-39]. Novel inorganic alkali and alkaline earth hydrides of the formula MH^* and MH^*X wherein M is the metal, X , is a singly negatively charged anion, and H^* comprises a novel high binding energy hydride ion were synthesized in a high temperature gas cell by reaction of atomic hydrogen with a catalyst such as potassium metal and MH , MX or MX_2 corresponding to an alkali metal or alkaline earth metal compound, respectively [25-26, 29]. Novel hydride compounds were identified by 1.) time of flight secondary ion mass spectroscopy which showed a dominant hydride ion in the negative ion spectrum, 2.) X-ray photoelectron spectroscopy which showed novel hydride peaks and significant shifts of the core levels of the primary elements bound to the novel hydride ions, 3.) 1H nuclear magnetic resonance spectroscopy (NMR) which showed extraordinary upfield chemical shifts compared to the NMR of the corresponding ordinary hydrides, and 4.) thermal decomposition with analysis by gas chromatography, and mass spectroscopy which identified the compounds as hydrides [26, 29]. The implications are that a new field of novel hydrogen chemistry has been discovered. The catalytic reaction of hydrogen may give rise to an energetic anomalous discharge such as an anomalous strontium-argon-hydrogen discharge.

ACKNOWLEDGMENT

Special thanks to Takeyoshi Onuma and Ying Lu for recording EUV spectra and to Bala Dhandapani and Jiliang He for reviewing this manuscript.

REFERENCES

1. Phillips, J. H., *Guide to the Sun*, Cambridge University Press, Cambridge, Great Britain, (1992), pp. 16-20.
2. J. A. R. Sampson, *Techniques of Vacuum Ultraviolet Spectroscopy*, Pied Publications, (1980), pp. 94-179.
3. Science News, 12/6/97, p. 366.
4. R. Mills, M. Nansteel, and Y. Lu, "Anomalous Hydrogen-Strontium Discharge", European Journal of Physics D, submitted.
5. R. Mills, "Spectroscopic Identification of a Novel Catalytic Reaction of Atomic Hydrogen and the Hydride Ion Product", Int. J. Hydrogen Energy, submitted.
6. R. Mills, N. Greenig, S. Hicks, "Optically Measured Power Balances of Anomalous Discharges of Mixtures of Argon, Hydrogen, and Potassium, Rubidium, Cesium, or Strontium Vapor", Int. J. Hydrogen Energy, submitted.
7. R. Mills, J. Dong, Y. Lu, "Observation of Extreme Ultraviolet Hydrogen Emission from Incandescently Heated Hydrogen Gas with Certain Catalysts", Int. J. Hydrogen Energy, Vol. 25, (2000), pp. 919-943.
8. R. Mills, "Observation of Extreme Ultraviolet Emission from Hydrogen-KI Plasmas Produced by a Hollow Cathode Discharge", Int. J. Hydrogen Energy, in press.
9. R. Mills, "Temporal Behavior of Light-Emission in the Visible Spectral Range from a Ti-K₂CO₃-H-Cell", Int. J. Hydrogen Energy, in press.
10. R. Mills, Y. Lu, and T. Onuma, "Formation of a Hydrogen Plasma from an Incandescently Heated Hydrogen-Catalyst Gas Mixture with an Anomalous Afterglow Duration", Int. J. Hydrogen Energy, in press.
11. R. Mills, M. Nansteel, and Y. Lu, "Observation of Extreme Ultraviolet Hydrogen Emission from Incandescently Heated Hydrogen Gas with Strontium that Produced an Anomalous Optically Measured Power Balance", Int. J. Hydrogen Energy, in press.
12. R. Mills, J. Dong, Y. Lu, J. Conrads, "Observation of Extreme Ultraviolet Hydrogen Emission from Incandescently Heated Hydrogen Gas with Certain Catalysts", 1999 Pacific Conference on Chemistry and Spectroscopy and the 35th ACS Western Regional Meeting, Ontario Convention Center, California, (October 6-8, 1999).
13. R. Mills, J. Dong, N. Greenig, and Y. Lu, "Observation of Extreme

Ultraviolet Hydrogen Emission from Incandescently Heated Hydrogen Gas with Certain Catalysts", National Hydrogen Association, 11 th Annual U.S. Hydrogen Meeting, Vienna, VA, (February 29-March 2, 2000).

14. R. Mills, B. Dhandapani, N. Greenig, J. He, J. Dong, Y. Lu, and H. Conrads, "Formation of an Energetic Plasma and Novel Hydrides from Incandescently Heated Hydrogen Gas with Certain Catalysts", National Hydrogen Association, 11 th Annual U.S. Hydrogen Meeting, Vienna, VA, (February 29-March 2, 2000).
15. Mills, J. Dong, N. Greenig, and Y. Lu, "Observation of Extreme Ultraviolet Hydrogen Emission from Incandescently Heated Hydrogen Gas with Certain Catalysts", 219 th National ACS Meeting, San Francisco, California, (March 26-30, 2000).
16. R. Mills, B. Dhandapani, N. Greenig, J. He, J. Dong, Y. Lu, and H. Conrads, "Formation of an Energetic Plasma and Novel Hydrides from Incandescently Heated Hydrogen Gas with Certain Catalysts", 219 th National ACS Meeting, San Francisco, California, (March 26-30, 2000).
17. R. Mills, B. Dhandapani, N. Greenig, J. He, J. Dong, Y. Lu, and H. Conrads, "Formation of an Energetic Plasma and Novel Hydrides from Incandescently Heated Hydrogen Gas with Certain Catalysts", June ACS Meeting (29th Northeast Regional Meeting, University of Connecticut, Storrs, CT, (June 18-21, 2000)).
18. R. Mills, B. Dhandapani, N. Greenig, J. He, J. Dong, Y. Lu, and H. Conrads, "Formation of an Energetic Plasma and Novel Hydrides from Incandescently Heated Hydrogen Gas with Certain Catalysts", August National ACS Meeting (220th ACS National Meeting, Washington, DC, (August 20-24, 2000)).
19. David R. Linde, *CRC Handbook of Chemistry and Physics*, 79 th Edition, CRC Press, Boca Raton, Florida, (1998-9), p. 10-175 to p. 10-177.
20. Kuraica, M., Konjevic, N., Physical Review A, Volume 46, No. 7, October (1992), pp. 4429-4432.
21. C. L. Yaws, *Chemical Properties Handbook*, McGraw-Hill, (1999).
22. David R. Linde, *CRC Handbook of Chemistry and Physics*, 79 th Edition, CRC Press, Boca Raton, Florida, (1998-9), pp. 10-1 to p. 10-87.
23. A. von Engel, *Ionized Gases*, American Institute of Physics, (1965).
24. M. S. Naidu and V. Kamaraju, *High Voltage Engineering*, McGraw-Hill,

(1996).

25. R. Mills, B. Dhandapani, M. Nansteel, J. He, A. Voigt, Identification of Compounds Containing Novel Hydride Ions by Nuclear Magnetic Resonance Spectroscopy, *Int. J. Hydrogen Energy*, submitted.
26. R. Mills, B. Dhandapani, N. Greenig, J. He, "Synthesis and Characterization of Potassium Iodo Hydride", *Int. J. of Hydrogen Energy*, Vol. 25, Issue 12, December, (2000), pp. 1185-1203.
27. R. Mills, "Novel Inorganic Hydride", *Int. J. of Hydrogen Energy*, Vol. 25, (2000), pp. 669-683.
28. R. Mills, "Novel Hydrogen Compounds from a Potassium Carbonate Electrolytic Cell", *Fusion Technology*, Vol. 37, No. 2, March, (2000), pp. 157-182.
29. R. Mills, B. Dhandapani, M. Nansteel, J. He, T. Shannon, A. Echezuria, "Synthesis and Characterization of Novel Hydride Compounds", *Int. J. of Hydrogen Energy*, in press.
30. R. Mills, "Highly Stable Novel Inorganic Hydrides", *Journal of Materials Research*, submitted.
31. R. Mills, "Novel Hydride Compound", 1999 Pacific Conference on Chemistry and Spectroscopy and the 35th ACS Western Regional Meeting, Ontario Convention Center, California, (October 6-8, 1999).
32. R. Mills, B. Dhandapani, N. Greenig, J. He, "Synthesis and Characterization of Potassium Iodo Hydride", 1999 Pacific Conference on Chemistry and Spectroscopy and the 35th ACS Western Regional Meeting, Ontario Convention Center, California, (October 6-8, 1999).
33. R. Mills, J. He, and B. Dhandapani, "Novel Hydrogen Compounds", 1999 Pacific Conference on Chemistry and Spectroscopy and the 35th ACS Western Regional Meeting, Ontario Convention Center, California, (October 6-8, 1999).
34. R. Mills, "Novel Hydride Compound", National Hydrogen Association, 11 th Annual U.S. Hydrogen Meeting, Vienna, VA, (February 29-March 2, 2000).
35. R. Mills, J. He, and B. Dhandapani, "Novel Alkali and Alkaline Earth Hydrides", National Hydrogen Association, 11 th Annual U.S. Hydrogen Meeting, Vienna, VA, (February 29-March 2, 2000).
36. R. Mills, "Novel Hydride Compound", 219 th National ACS Meeting, San Francisco, California, (March 26-30, 2000).

37. R. Mills, J. He, and B. Dhandapani, "Novel Alkali and Alkaline Earth Hydrides", 219 th National ACS Meeting, San Francisco, California, (March 26-30, 2000).
38. R. Mills, J. He, and B. Dhandapani, "Novel Alkali and Alkaline Earth Hydrides", August National ACS Meeting (220 th ACS National Meeting, Washington, DC, (August 20-24, 2000)).
39. R. Mills, W. Good, A. Voigt, Jinquan Dong, "Minimum Heat of Formation of Potassium Iodo Hydride", Int. J. Hydrogen Energy, submitted.

Table I. Discharge conditions and comparison of the driving power to achieve a total visible radiant flux of about $1 \mu\text{W}/\text{cm}^2$.

	T (°C)	P _{hyd.} (torr)	P _{Ar} (torr)	P _v (torr) ^a	Voltage (V)	Current (mA)	Integ. time (ms)	Detector irradiation ($\mu\text{W}/\text{cm}^2$)	Power (W)
Ar+H ₂ +Sr	514	0.3	1.0	0.006	6.56	0.6	204	1.3	0.0039
Ar+H ₂	519	0.295	0.5	----	224	184	409	1.9	33.5 ^b
Ar	520	----	1.0	----	190	170	307	1.1	24.7 ^b
H ₂ +Sr	664	----		0.270	2.20	3.86	768	1.17	0.0085
H ₂	664	1.0		----	224	110	1130	2.08	24.6
H ₂ +Na	335	1.0		0.051	272	124	122	1.85	33.7
H ₂ +Na	516	1.5		5.3	220	68	768	0.40	15.0
H ₂ +Na	664	1.5		63	240	41	768	0.41	9.84
H ₂ +Mg	449	4.0		0.016	153	380	500	1.7	58
H ₂ +Mg	582	4.2		0.6	233	290	500	0.16	68
H ₂ +Mg	654	3.0		2.8	250	400	1000	0.18	100.0
H ₂ +Ba	666	2.0		0.025	138	730	716	0.03	55 ^b
Bkgnd.	664	----		0.270	0	0	768	0.20	0

^a Calculated [21]

^b Power input differs from volt-amperes due to non-unity power factor.

TABLE II. Spectral features of hydrogen and strontium at 664 °C.

Measured Wavelength (nm)	Spectrometer System Irradiation ($\mu\text{W}/\text{cm}^2\text{nm}$)	Published Data [22] (nm)	Emission
460.6	0.156	460.73 (Sr)	
487.2	0.00290	487.25 (Sr), 486.13 (H ₂)	
639.8	0.00813	638.82 (Sr)	
654.7	0.0139	654.68 (Sr), 656.29 (H ₂)	
689.4	0.0386	689.26 (Sr)	

TABLE III. Spectral features of hydrogen at 664 °C.

Measured Wavelength (nm)	Spectrometer System	Published Emission Data [22]
	Irradiation ($\mu W/cm^2 nm$)	
485.8	0.0165	486.13 (H_2)
518.2	0.00894	
558.7	0.00694	
589.1	0.0174	589.00 (Na), 589.59 (Na)
656.7	0.0752	656.29 (H_2)

TABLE IV. Spectral features of hydrogen and sodium at 335 °C.

Measured wavelength (nm)	Spectrometer System	Published emission data [22]
	Irradiation ($\mu W/cm^2 nm$)	
467.2	0.00400	466.86 (Na)
486.2	0.0055	486.13 (H_2)
498.4	0.0176	498.28 (Na)
516.1	0.00380	515.34 (Na)
569.0	0.114	568.82 (Na)
589.3	0.302	589.00 (Na), 589.59 (Na)
615.9	0.0310	616.07 (Na)
656.0	0.0422	656.29 (H_2), 655.24 (Na)
657.0	0.0421	656.29 (H_2)

TABLE V. Spectral features of hydrogen and magnesium at 449 °C.

Measured wavelength (nm)	Spectrometer system irradiation ($\mu\text{W}/\text{cm}^2\text{nm}$)	Published emission data [22] (nm)
382.6	0.0843	382.93 (Mg), 383.23 (Mg)
384.0	0.0643	383.83 (Mg)
485.2	0.0122	486.13 (H_2)
517.3	0.0353	517.27 (Mg), 518.36 (Mg)
588.1	0.0167	589.00 (Na), 589.59 (Na)
655.8	0.109	656.29 (H_2)

Table VI. Spectral features of hydrogen and barium at 666°C.

Measured wavelength (nm)	Spectrometer system irradiation ($\mu\text{W}/\text{cm}^2\text{nm}$)	Published emission data [22] (nm)
456.2	0.0021	455.40 (Ba)
492.6	0.002	
552.7	8.4×10^{-4}	553.55 (Ba)
568.4	0.003	568.26 (Na)
588.8	0.006	589.00 (Na)
614.7	9.0×10^{-4}	614.17 (Ba)
655.9	0.002	656.29 (H_2)

Table VII. Spectral features of argon, hydrogen, and strontium at 514 °C.

Measured wavelength (nm)	Spectrometer system irradiation ($\mu\text{W}/\text{cm}^2\text{nm}$)	Published emission data [22] (nm)
459.9	0.176	460.73 (Sr)
639.4	0.004	638.47 (Ar)
653.9	0.007	653.81 (Ar)
688.8	0.116	687.84 (Sr)

Table VIII. Spectral features of argon and hydrogen at 519 °C.

Measured wavelength (nm)	Spectrometer system irradiation ($\mu W/cm^2 nm$)	Published emission data [22] (nm)
486.0	0.032	486.13 (H ₂)
588.5	0.020	588.86 (Ar)
656.2	0.176	656.29 (H ₂)
738.5	0.034	738.40 (Ar)

Table IX. Spectral features of argon at 520 °C.

Measured wavelength (nm)	Spectrometer system irradiation ($\mu W/cm^2 nm$)	Published emission data [22] (nm)
588.8	0.039	588.86 (Ar)
655.9	0.046	656.29 (H ₂)
696.4	0.028	696.54 (Ar)
706.5	0.028	706.72 (Ar)
738.5	0.058	738.40 (Ar)

TABLE X. Glow discharge parameters from von Engel [23] and Naidu Kamaraju [24].

Gas	Minimum starting voltage (V)	Pressure-discharge gap product at minimum starting voltage (cm-torr)
N ₂	251	0.67
H ₂	273	1.15
Air	327	0.567
CO ₂	420	0.51
Ar	137	0.9
He	156	4.0
Hg	520	2
Na	335	0.04

Figure Captions

Figure 1. The experimental set up comprising a gas cell light source and an EUV spectrometer which was differentially pumped.

Figure 2. Cylindrical stainless steel gas cell for plasma studies with 1.) hydrogen, argon, or argon-hydrogen mixture alone, 2.) hydrogen with strontium, sodium, magnesium, or barium, and 3.) argon-hydrogen mixture (97/5%) with strontium.

Figure 3. The experimental setup for generating a glow discharge hydrogen plasma and for optically measuring the power balance.

Figure 4. The intensity of the Lyman α emission as a function of time from the gas cell at a cell temperature of 700 °C comprising a tungsten filament, a titanium dissociator, and 300 mtorr hydrogen that was recorded with a CEM.

Figure 5. The UV/VIS spectrum (40–560 nm) of the cell emission from the gas cell at a cell temperature of 700 °C comprising a tungsten filament, a titanium dissociator, and 300 mtorr hydrogen that was recorded with a photomultiplier tube (PMT) and a sodium salicylate scintillator.

Figure 6. The intensity of the Lyman α emission as a function of time from the gas cell at a cell temperature of 700 °C comprising a tungsten filament, a titanium dissociator, vaporized sodium metal, and 300 mtorr hydrogen that was recorded with a CEM.

Figure 7. The intensity of the Lyman α emission as a function of time from the gas cell at a cell temperature of 700 °C comprising a tungsten filament, a titanium dissociator, vaporized magnesium, and 300 mtorr hydrogen that was recorded with a CEM.

Figure 8. The intensity of the Lyman α emission as a function of time from the gas cell at a cell temperature of 700 °C comprising a tungsten filament, a titanium dissociator, vaporized barium metal, and 300 mtorr hydrogen that was recorded with a CEM.

Figure 9. The intensity of the Lyman α emission as a function of time from the gas cell at a cell temperature of 700 °C comprising a tungsten filament, a titanium dissociator, vaporized strontium metal, and 300 mtorr hydrogen that was recorded with a CEM.

Figure 10. The EUV spectrum (40–160 nm) of the cell emission

recorded at about the point of the maximum Lyman α emission from the gas cell at a cell temperature of 700 °C comprising a tungsten filament, a titanium dissociator, vaporized strontium metal, and 300 mtorr hydrogen that was recorded with a CEM.

Figure 11. The intensity of the Lyman α emission as a function of time from the gas cell at a cell temperature of 700 °C comprising a tungsten filament, and 300 mtorr argon-hydrogen mixture (97/3%) that was recorded with a CEM.

Figure 12. The EUV emission spectrum (40–160 nm) from a gas cell comprising a tungsten filament, vaporized sodium metal, and 300 mtorr argon-hydrogen mixture (97/3%) that was recorded with a PMT and a sodium salicylate scintillator two hours after the cell reached 700 °C.

Figure 13. The EUV emission spectrum (40–160 nm) from a gas cell comprising a tungsten filament, vaporized magnesium metal, and 300 mtorr argon-hydrogen mixture (97/3%) that was recorded with a PMT and a sodium salicylate scintillator two hours after the cell reached 700 °C.

Figure 14. The EUV emission spectrum (40–160 nm) from a gas cell comprising a tungsten filament, vaporized barium metal, and 300 mtorr argon-hydrogen mixture (97/3%) that was recorded with a PMT and a sodium salicylate scintillator two hours after the cell reached 700 °C.

Figure 15. The EUV spectrum (40–160 nm) of the cell emission recorded at about the point of the maximum Lyman α emission from the gas cell at a cell temperature of 700 °C comprising a tungsten filament, vaporized strontium metal, and 300 mtorr argon-hydrogen mixture (97/3%) that was recorded with a PMT and a sodium salicylate scintillator.

Figure 16. Count rate and spectrometer system irradiation of the background spectrum of hydrogen and strontium vapor over the wavelength range $350 \leq \lambda \leq 750$ nm in the absence of power applied to the electrode and in the absence of a discharge.

Figure 17. The count rate and the spectrometer system irradiation for a mixture of hydrogen and strontium vapor at 664 °C.

Figure 18. The spectrometer system irradiation for a hydrogen discharge at a cell temperature of 664 °C and a hydrogen pressure of 1 torr.

Figure 19. The spectrometer system irradiation for a mixture of hydrogen and sodium vapor at 335 °C.

Figure 20. The spectrometer system irradiation for a mixture of hydrogen and sodium vapor at 516 °C.

Figure 21. The spectrometer system irradiation for a mixture of hydrogen and sodium vapor at 664 °C.

Figure 22. The spectrometer system irradiation for a mixture of hydrogen and magnesium vapor at 449 °C.

Figure 23. The spectrometer system irradiation for a mixture of hydrogen and magnesium vapor at 582 °C.

Figure 24. The spectrometer system irradiation for a mixture of hydrogen and magnesium vapor at 654 °C.

Figure 25. The spectrometer system irradiation for a mixture of hydrogen and barium vapor at 666 °C.

Figure 26. The spectrometer system irradiation for a mixture of argon-hydrogen and strontium vapor at 514 °C.

Figure 27. The spectrometer system irradiation for a mixture of argon and hydrogen at 519 °C.

Figure 28. The spectrometer system irradiation for an argon discharge at a cell temperature of 520 °C and argon pressure of 1 torr.

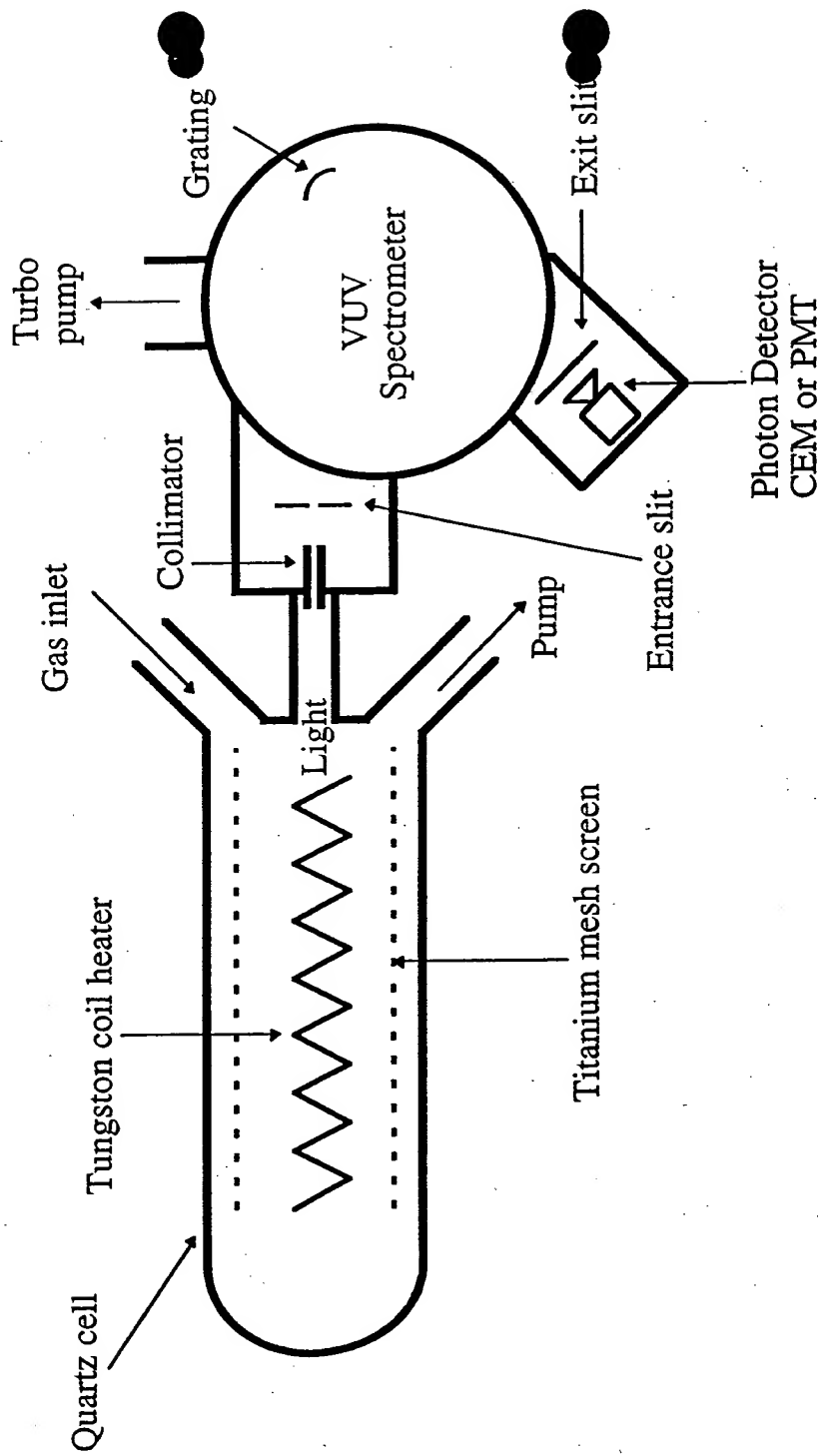


Figure 1

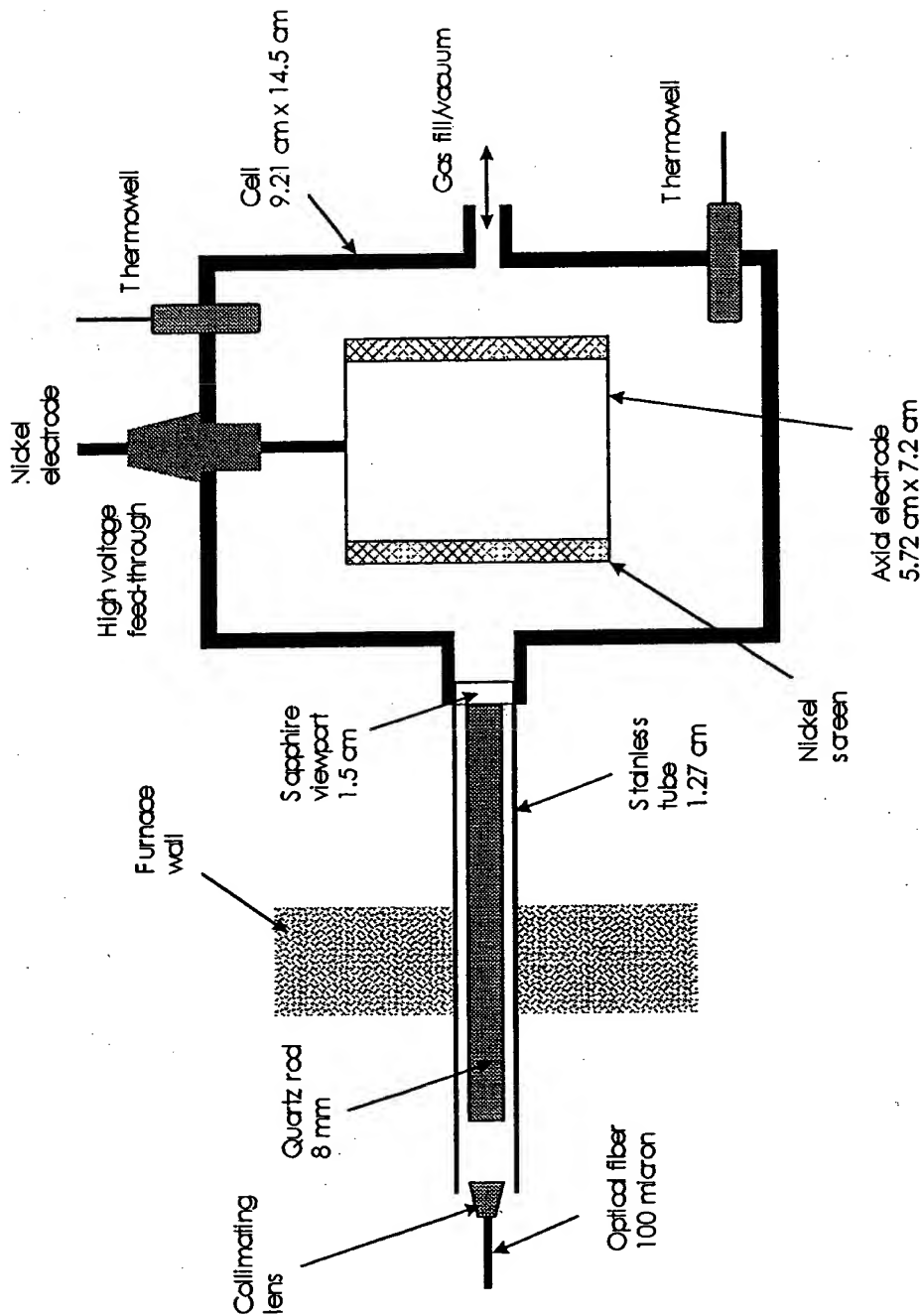
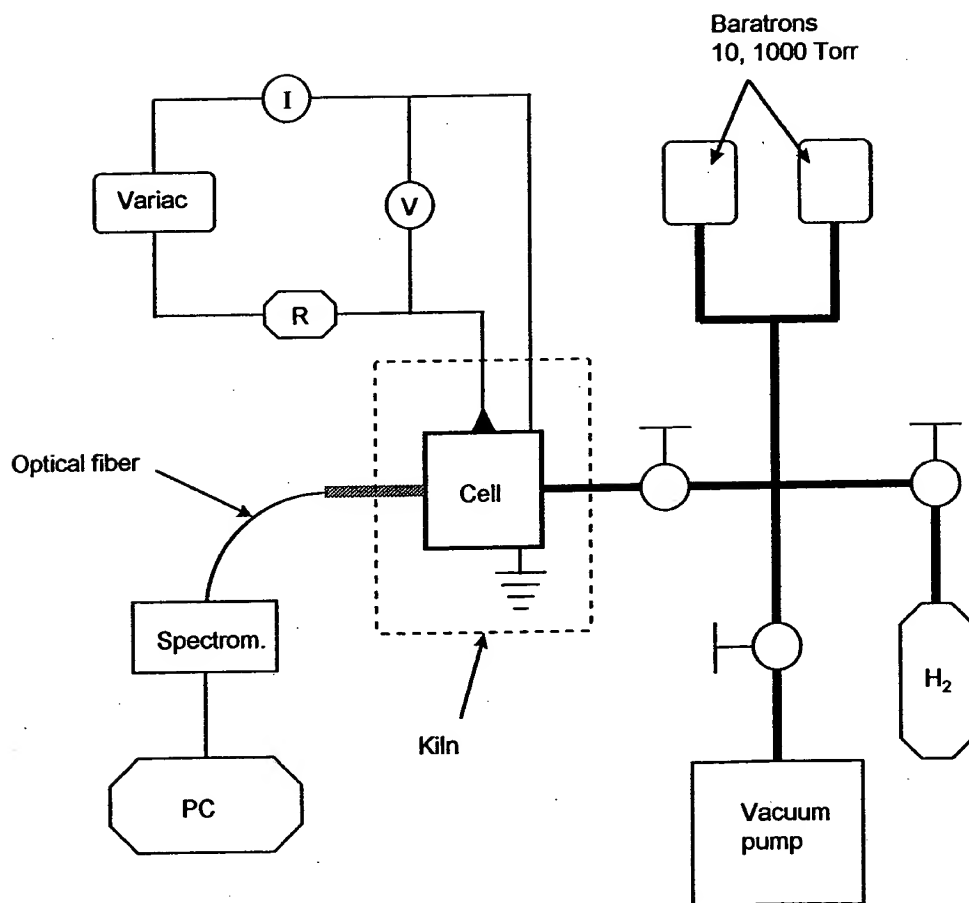


Figure 2

Figure 3



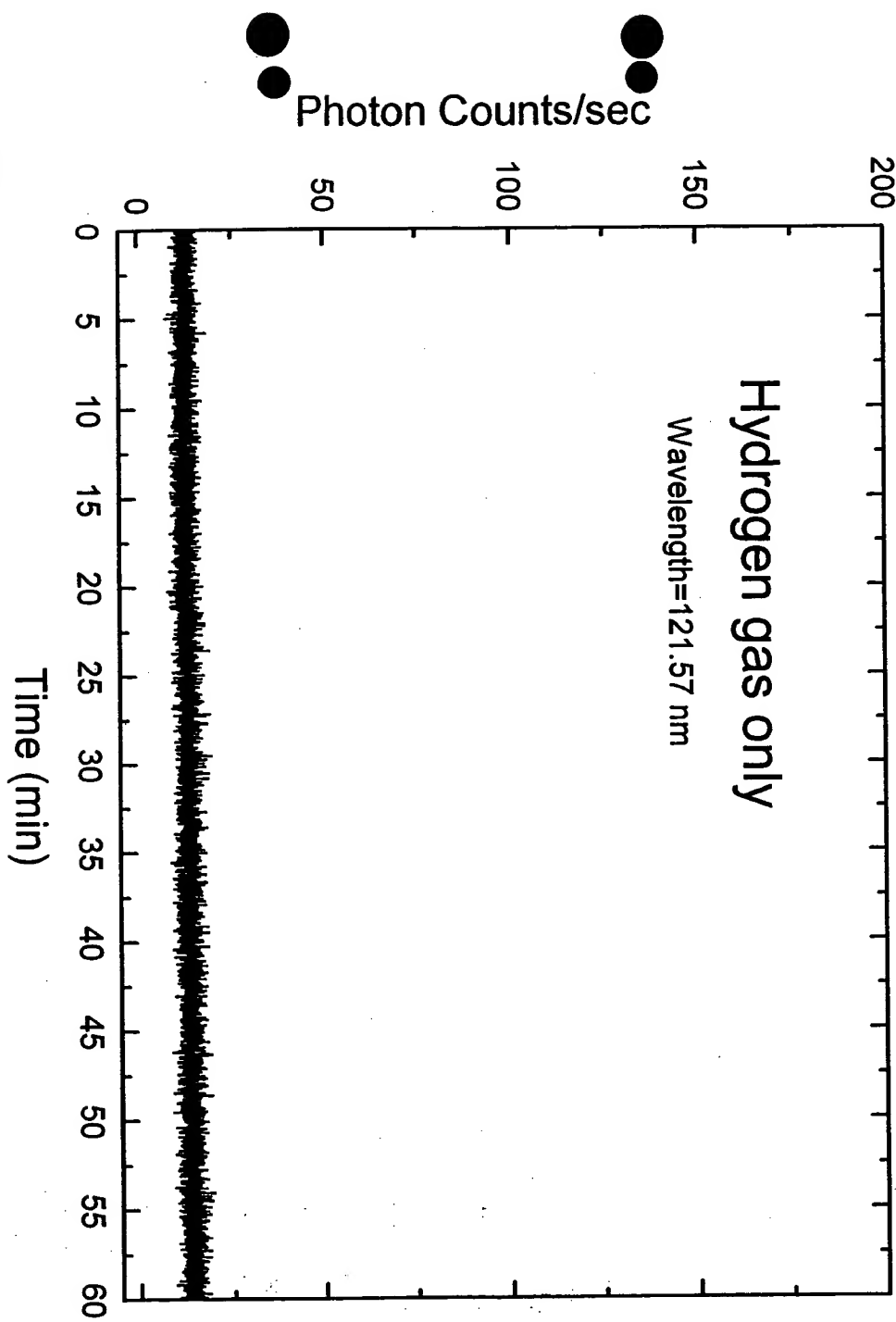


Figure 4

Figure 5

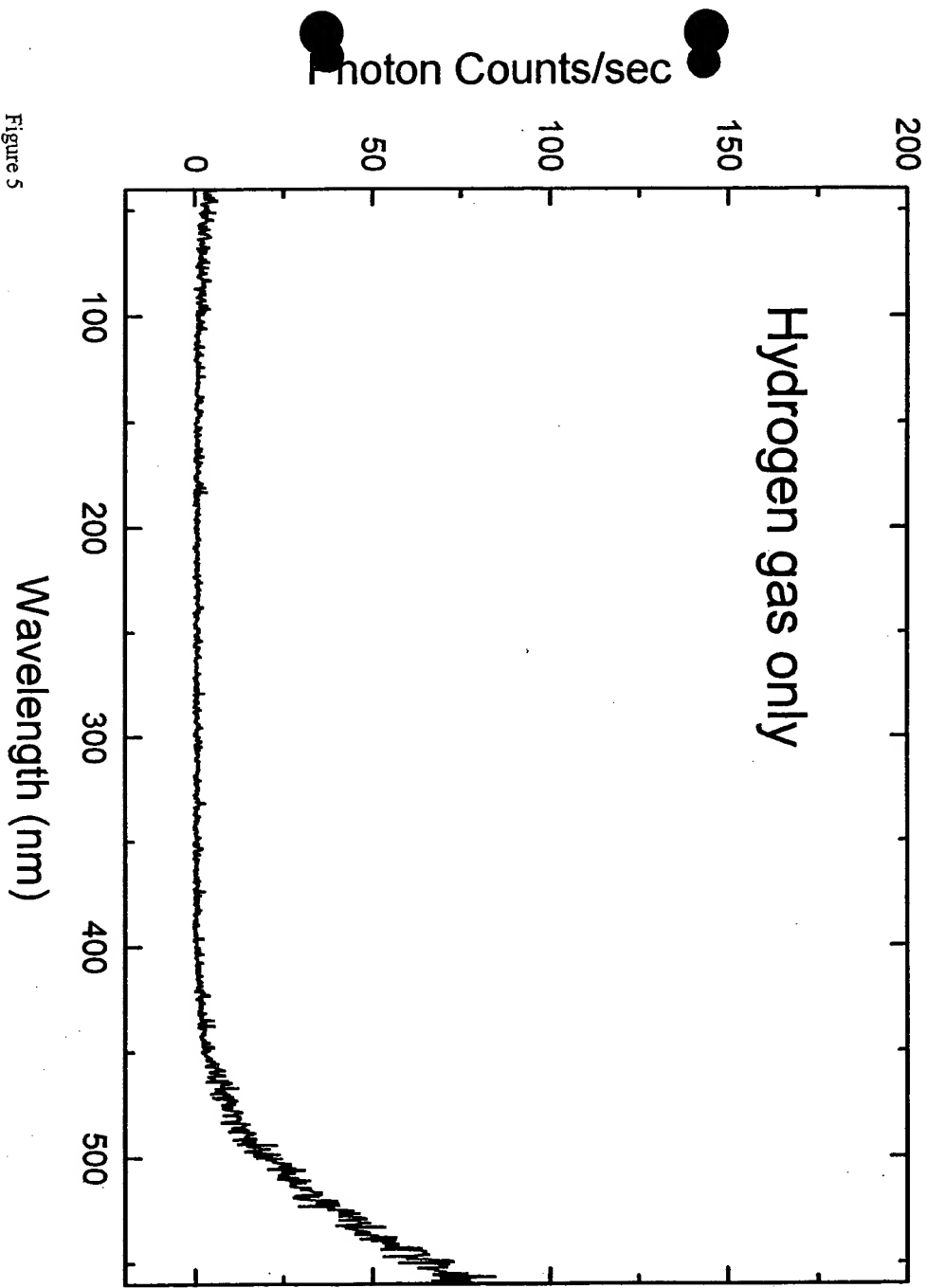


Figure 6

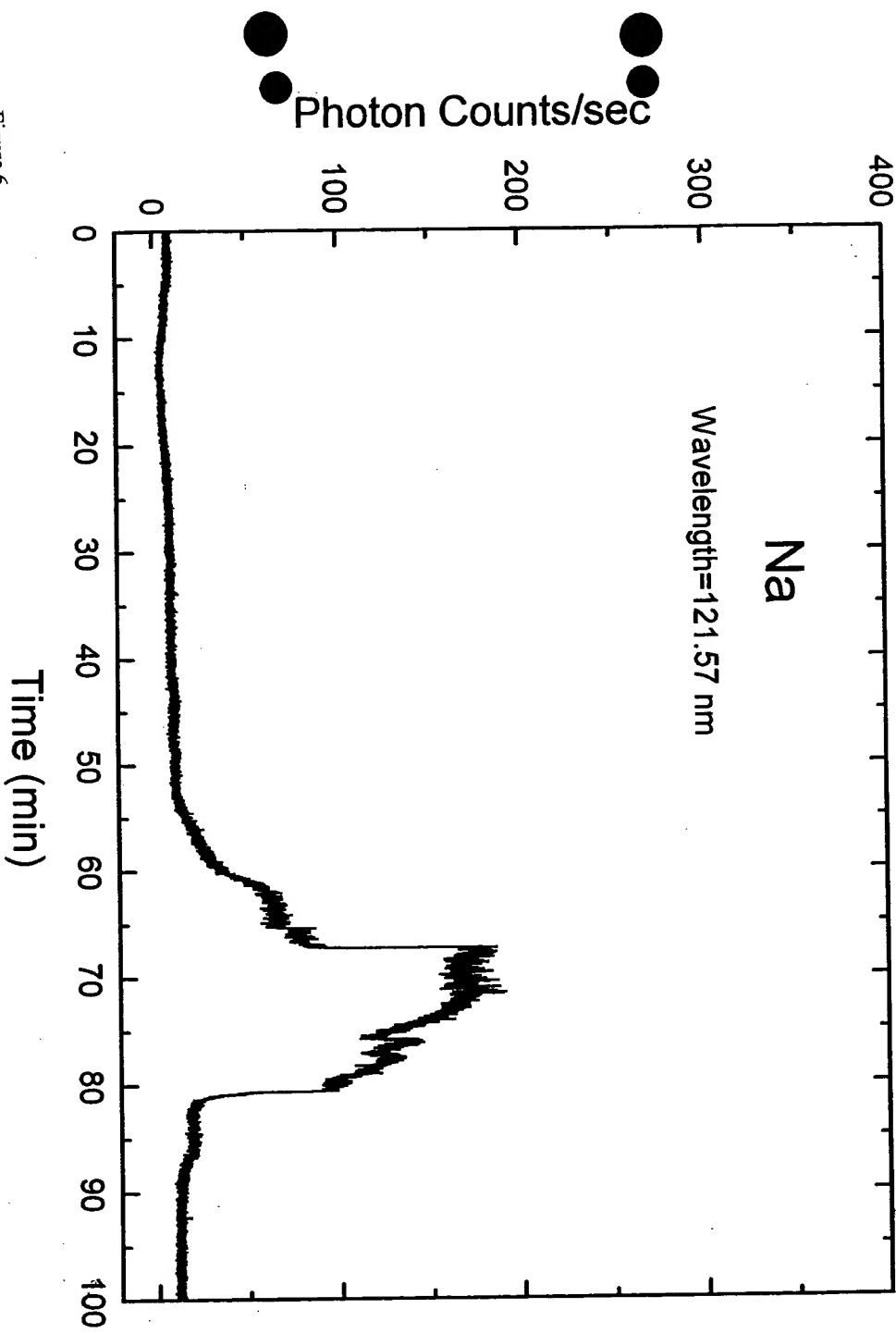


Figure 7

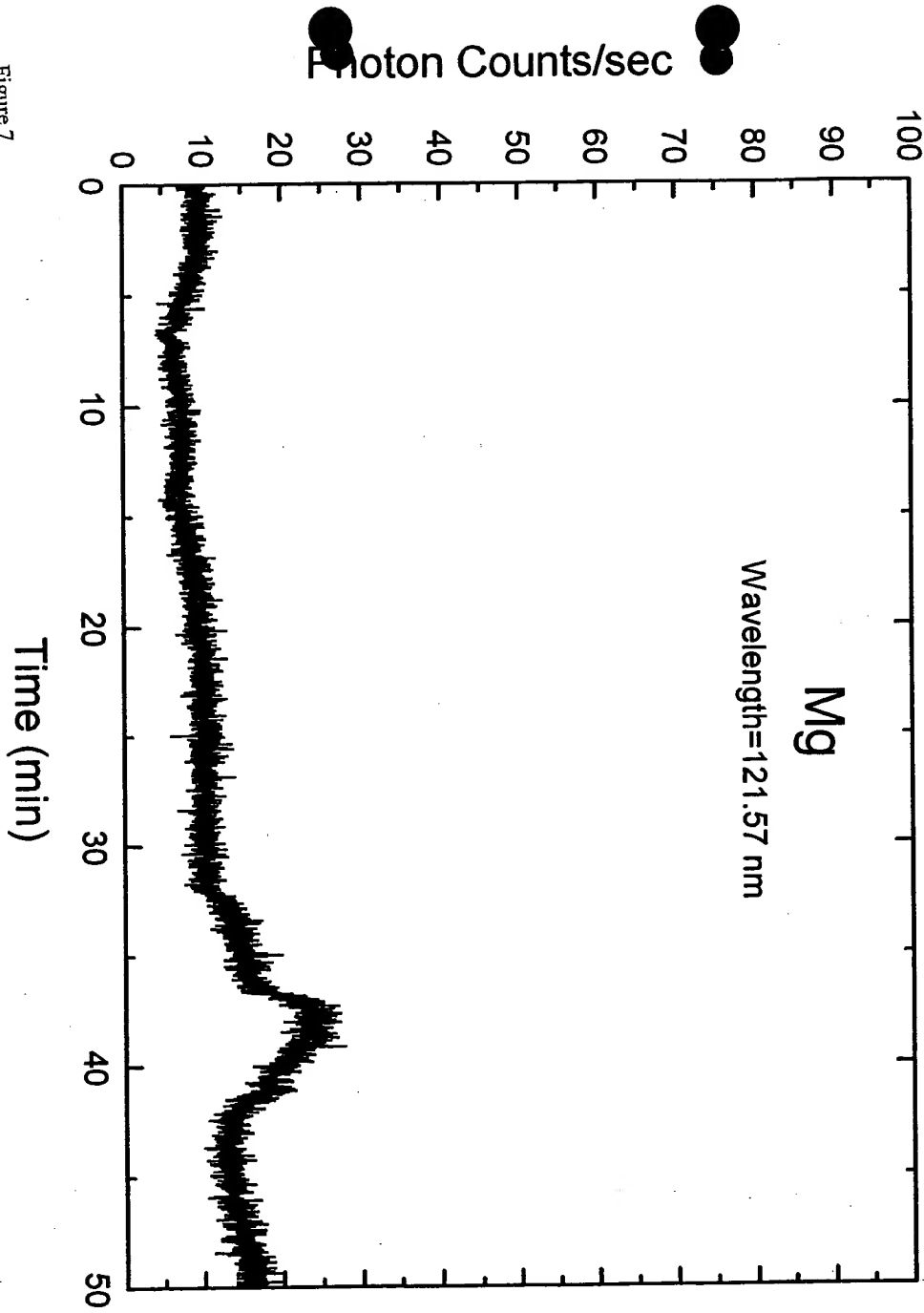


Figure 8

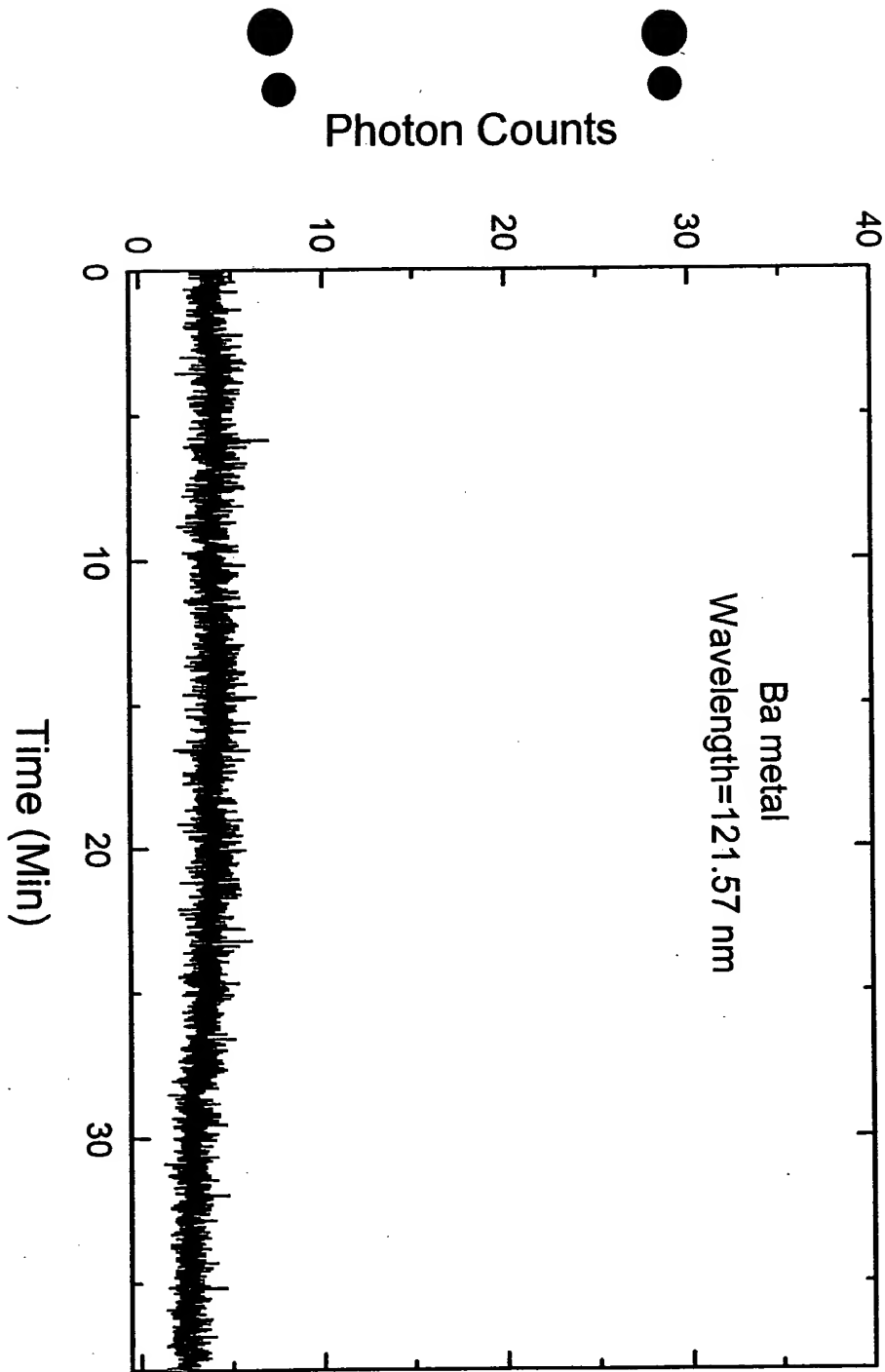


Figure 9

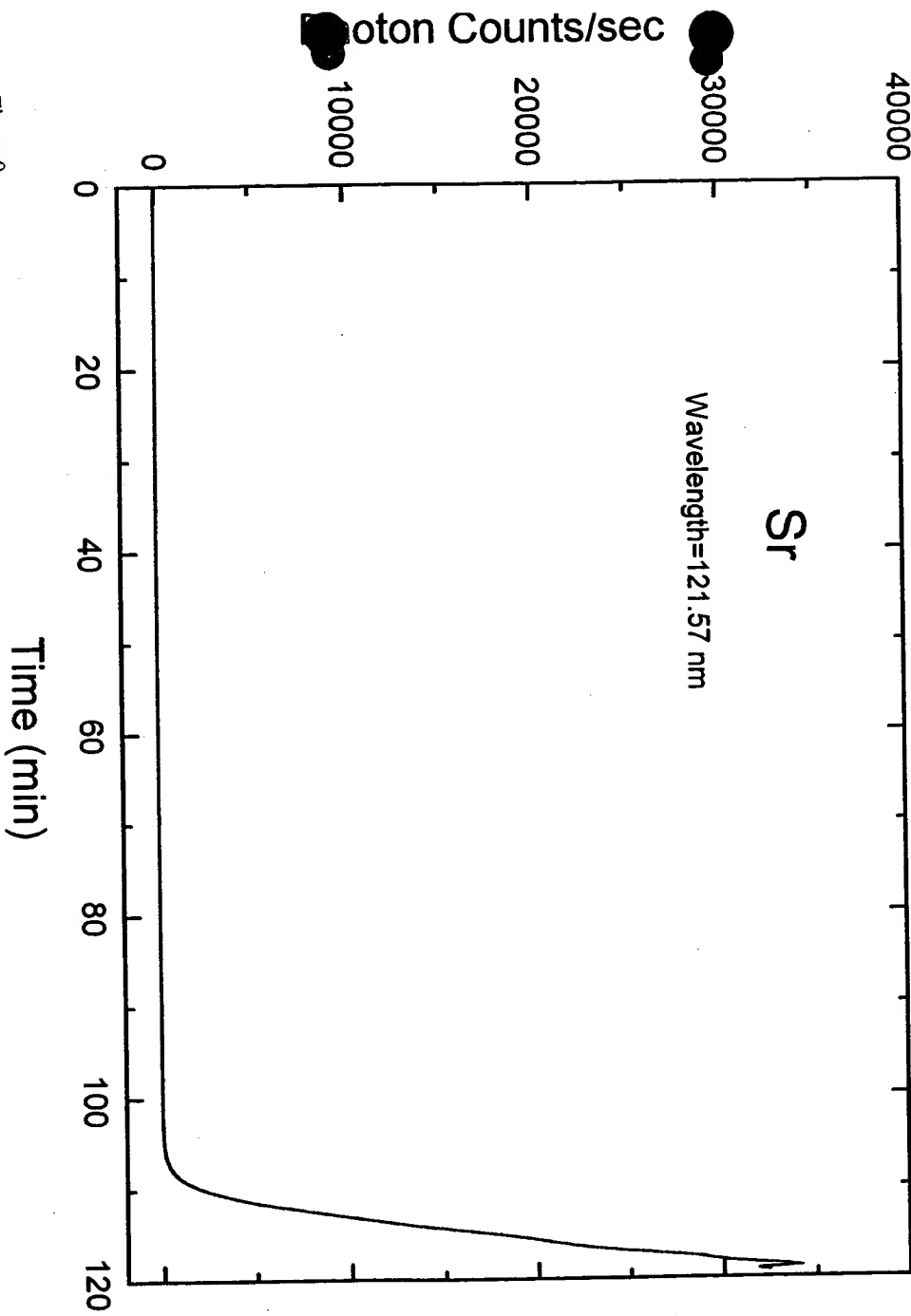
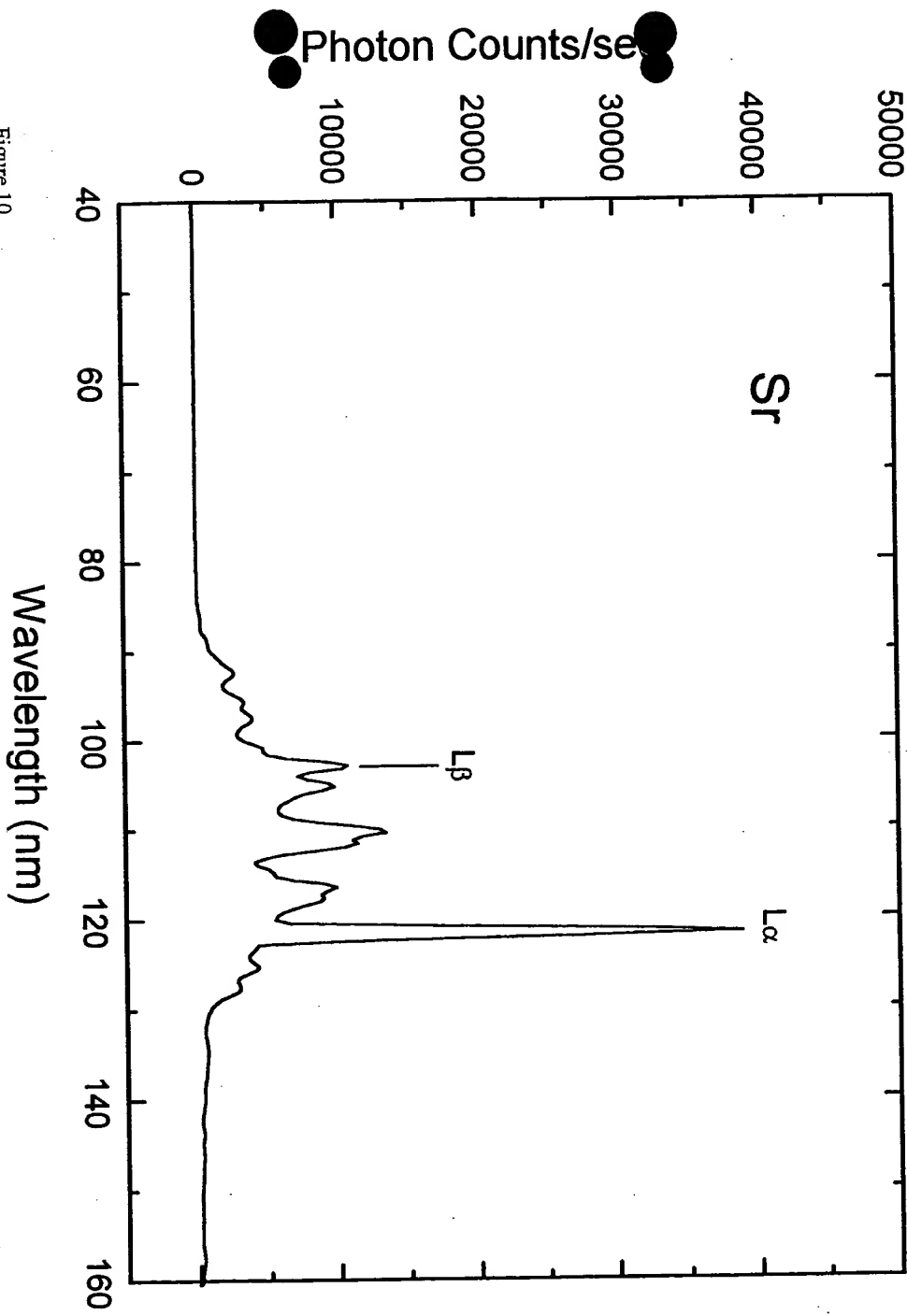


Figure 10



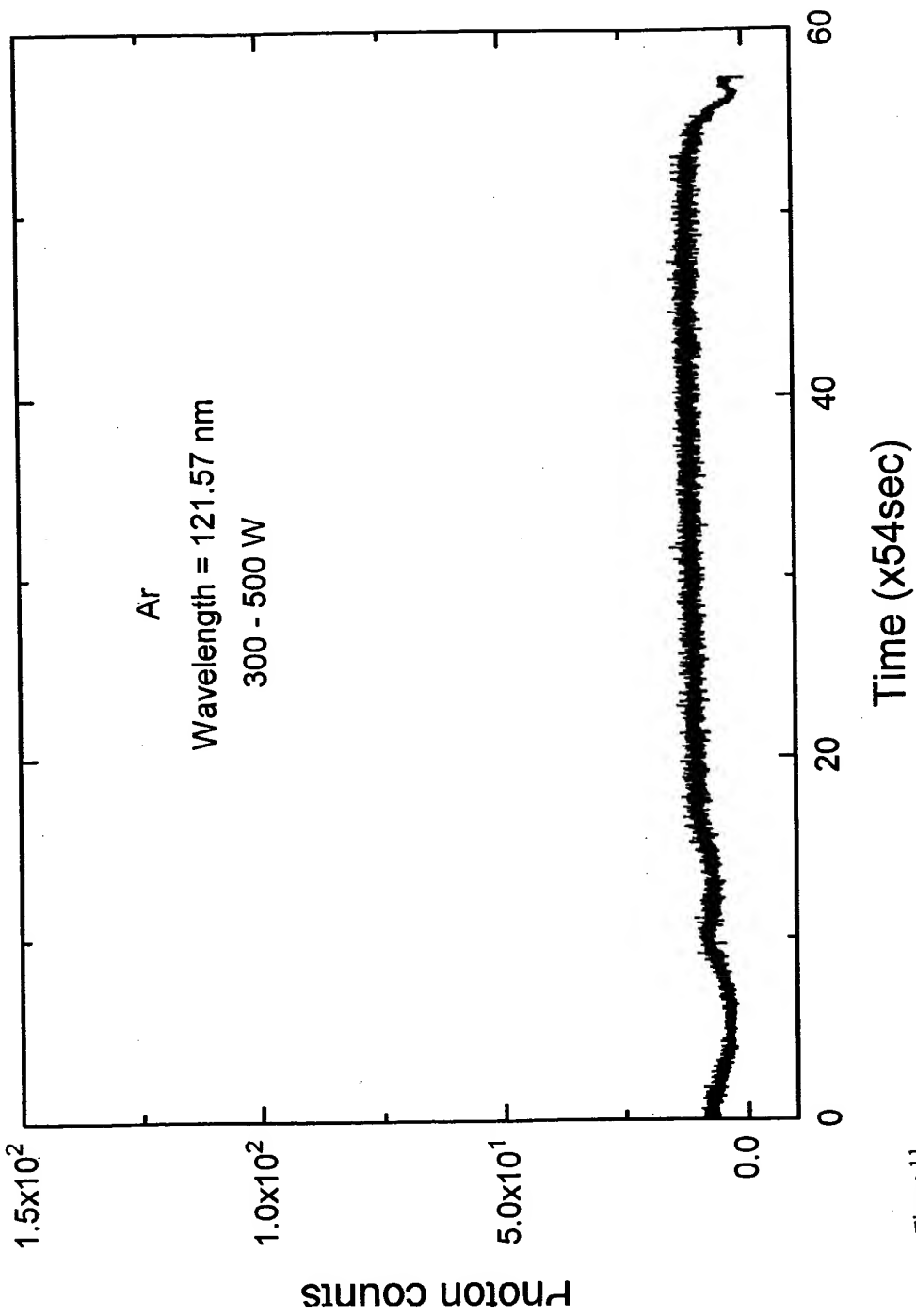


Figure 11

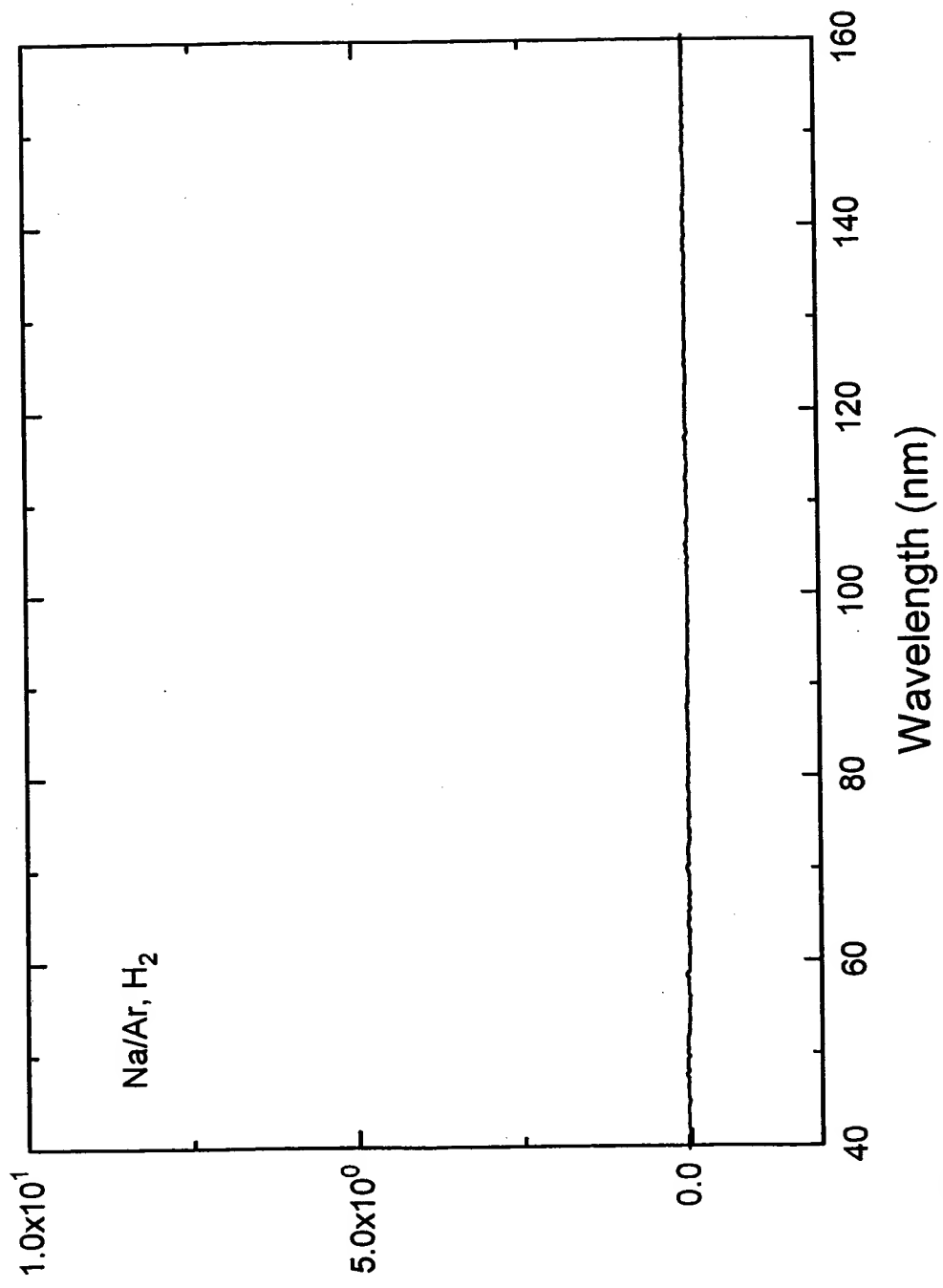


Figure 12

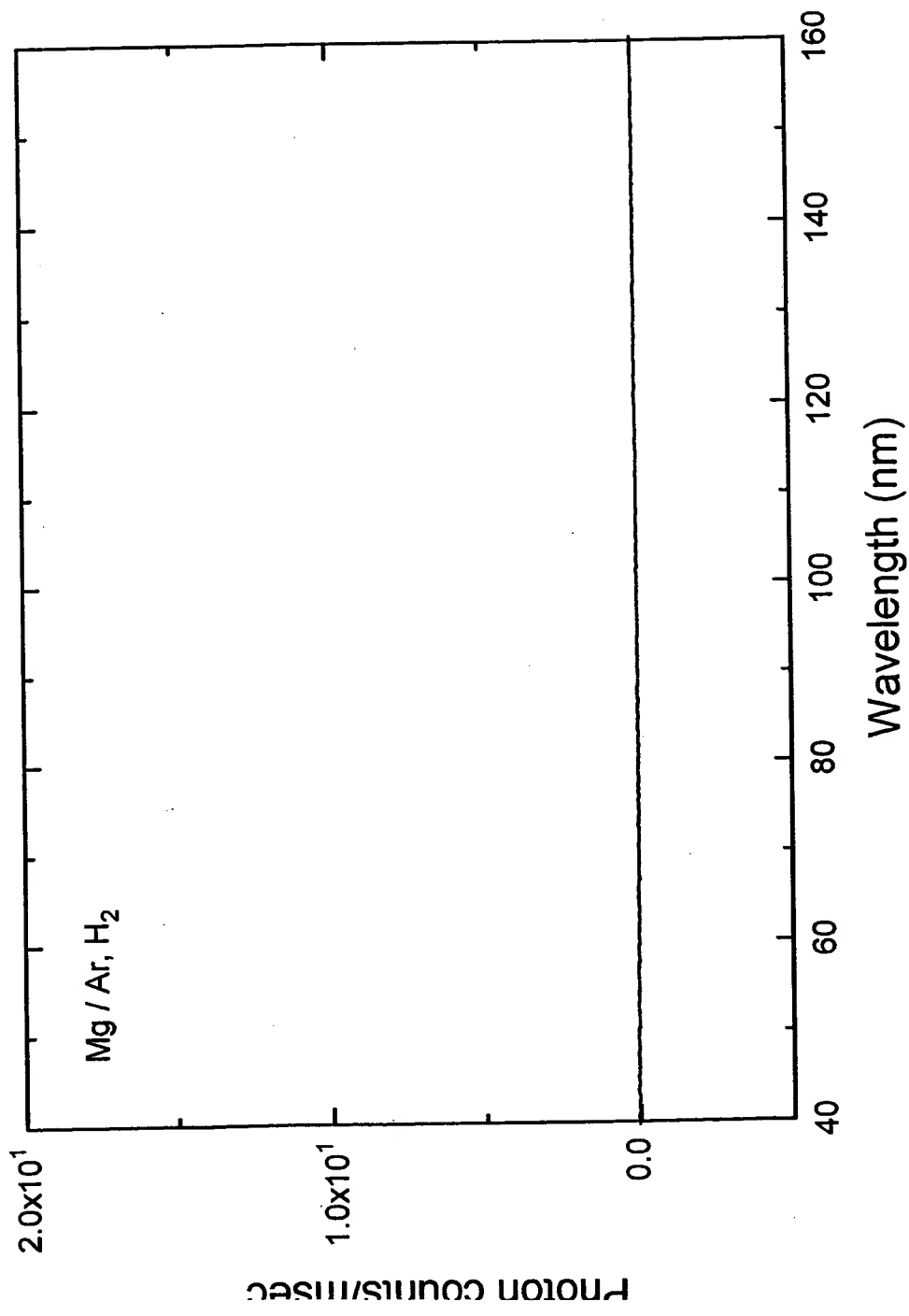


Figure 13

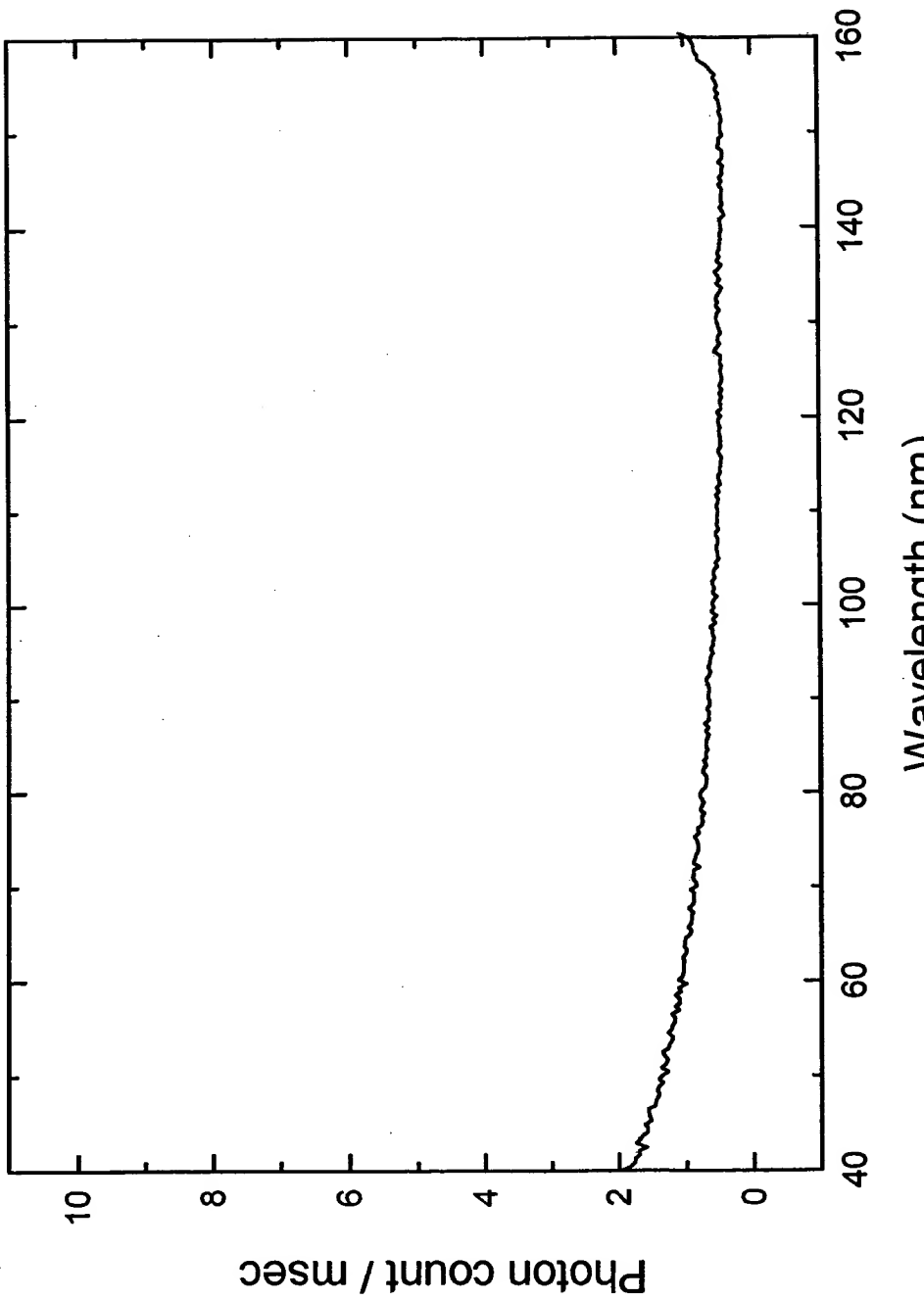


Figure 14

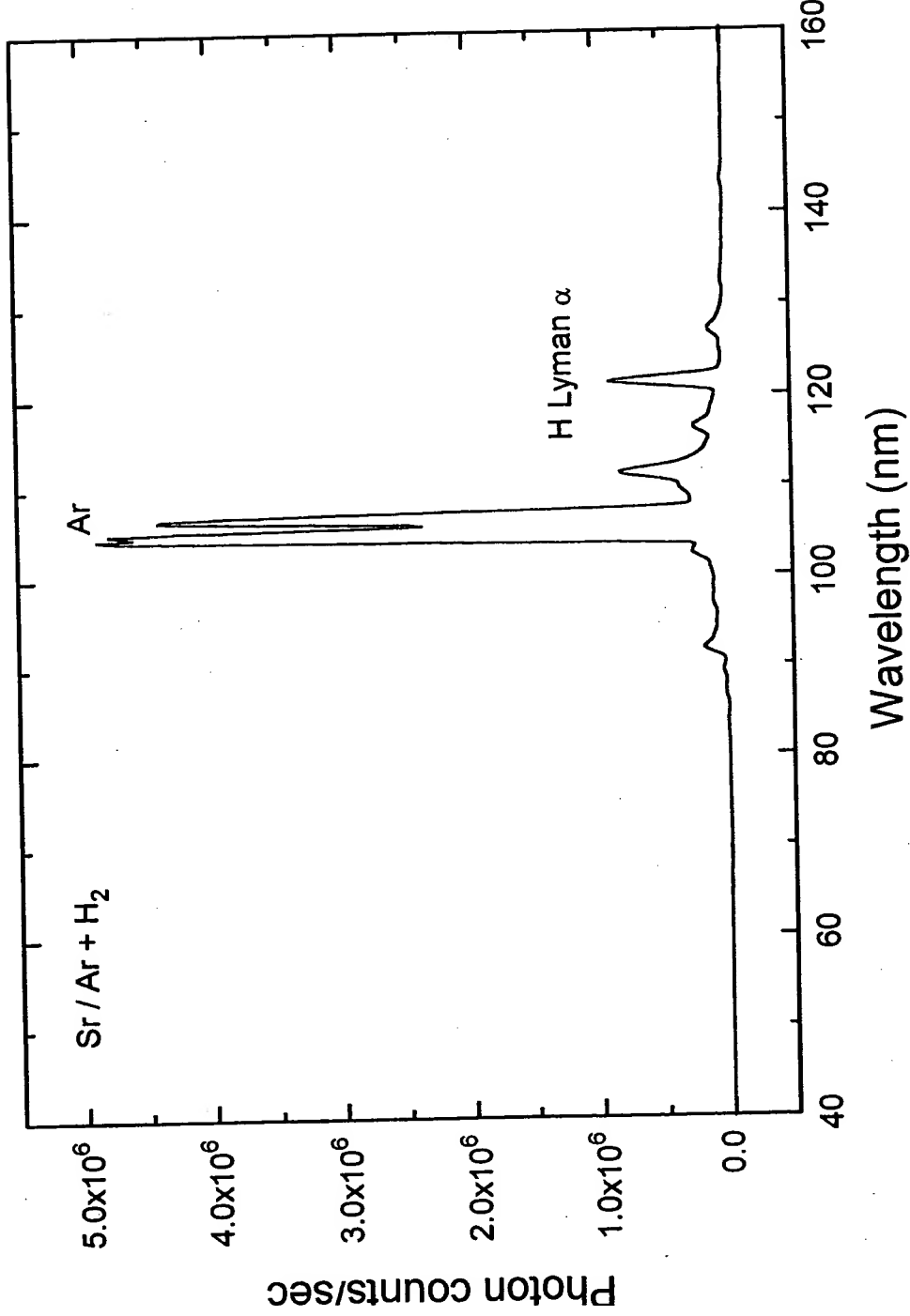


Figure 15

Figure 16

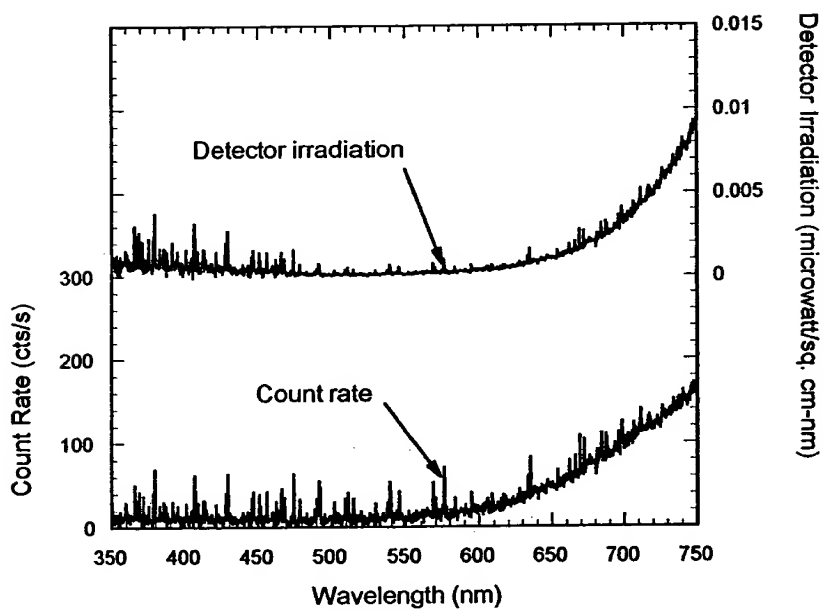


Figure 17

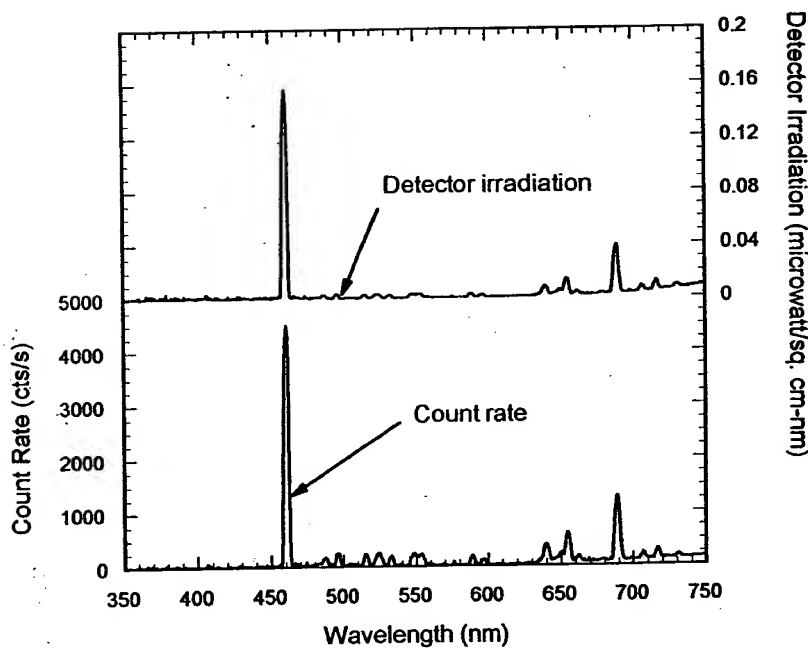


Figure 18

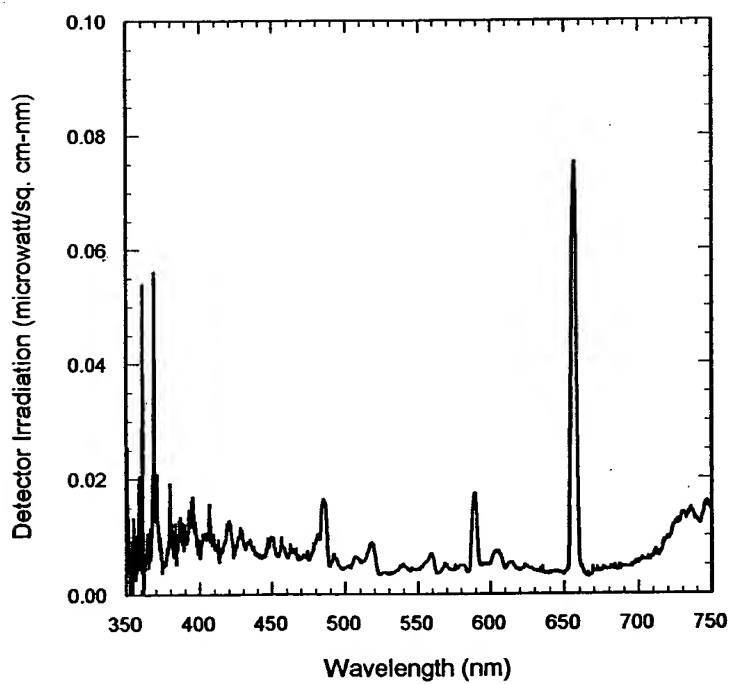


Figure 19

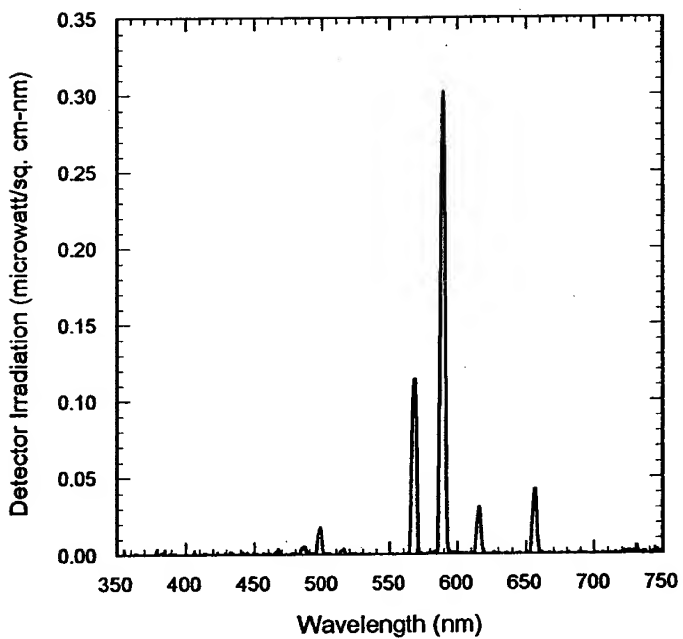


Figure 20

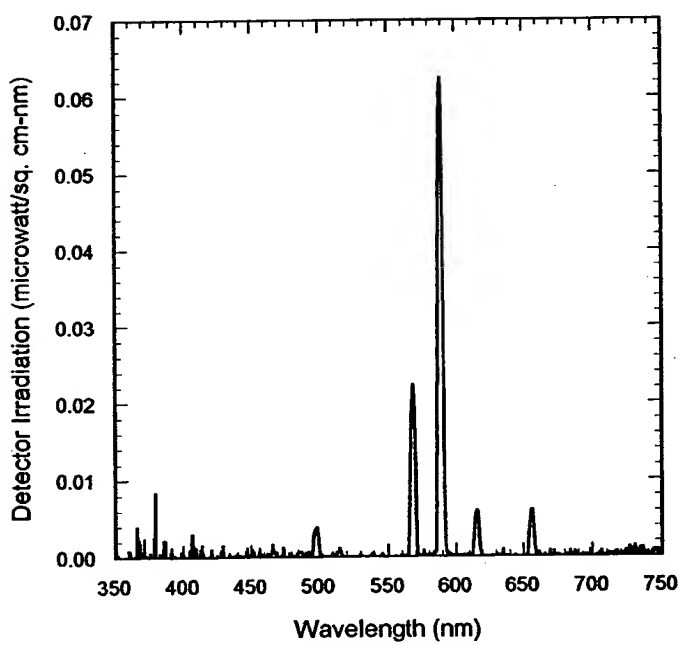


Figure 21

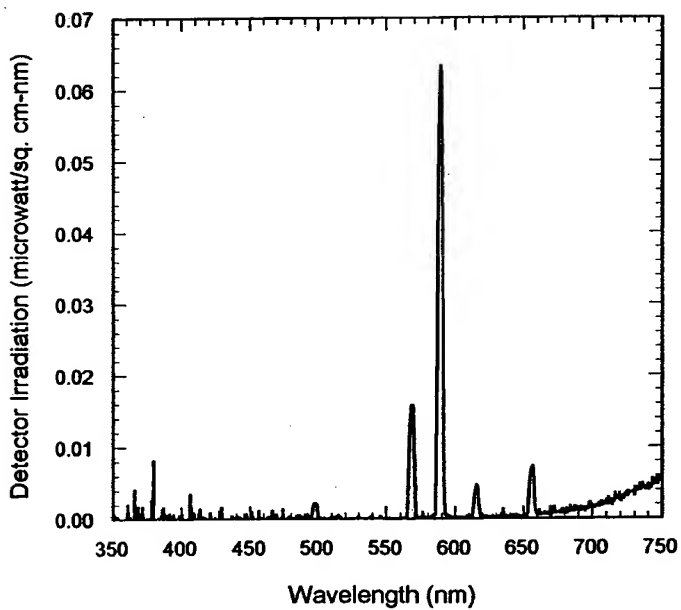


Figure 22

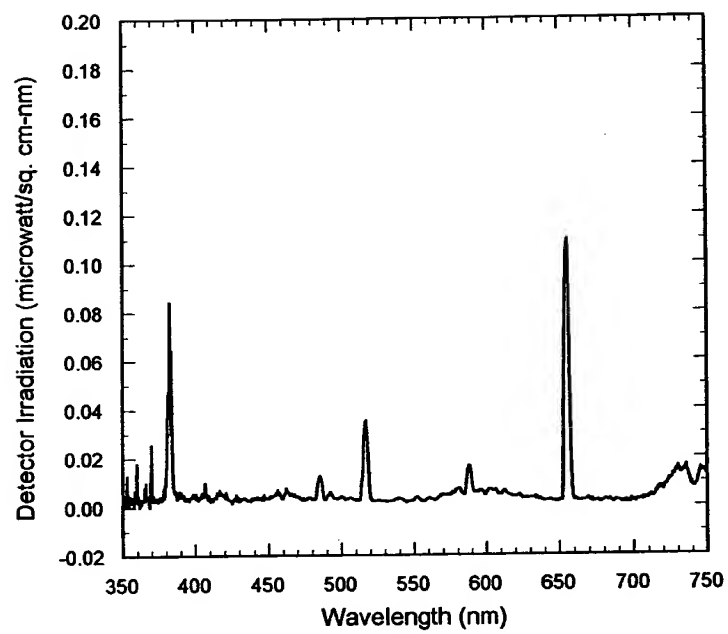


Figure 23

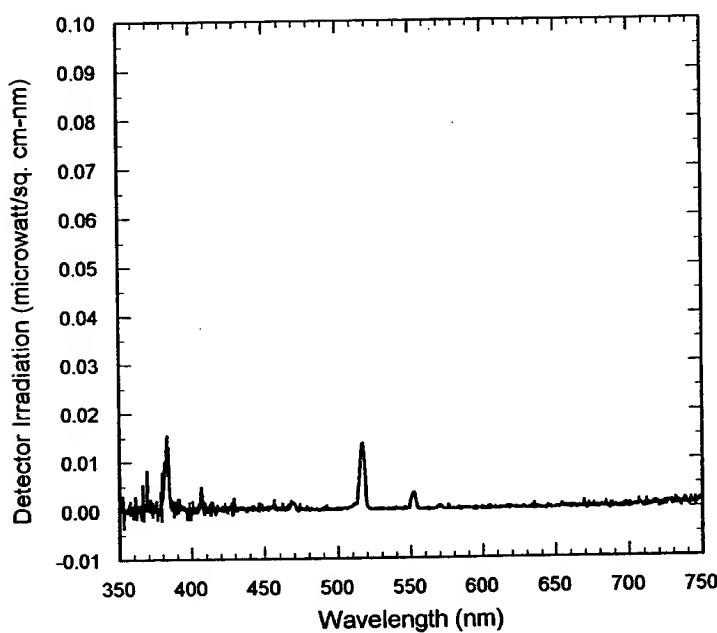


Figure 24

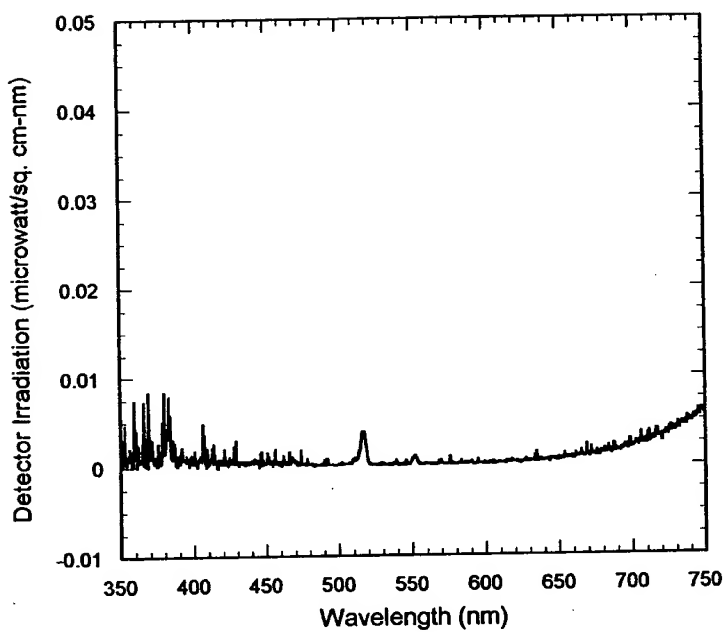


Figure 25

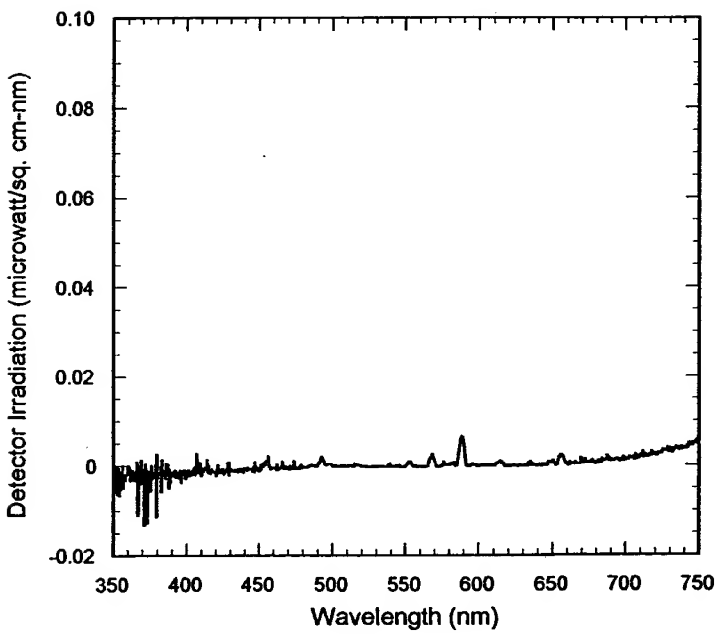


Figure 26

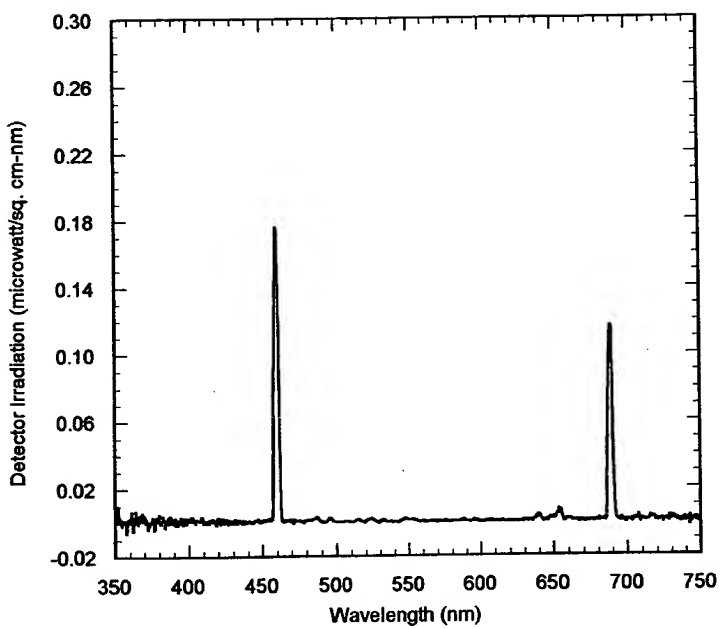


Figure 27

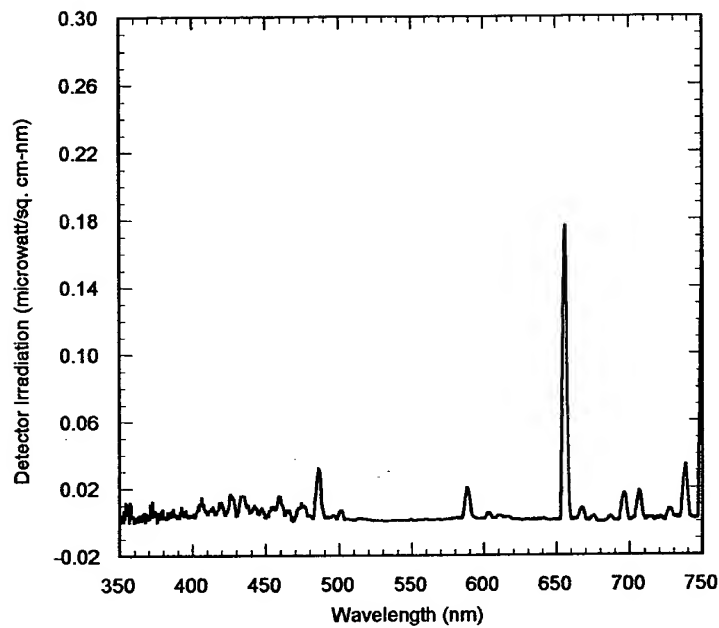
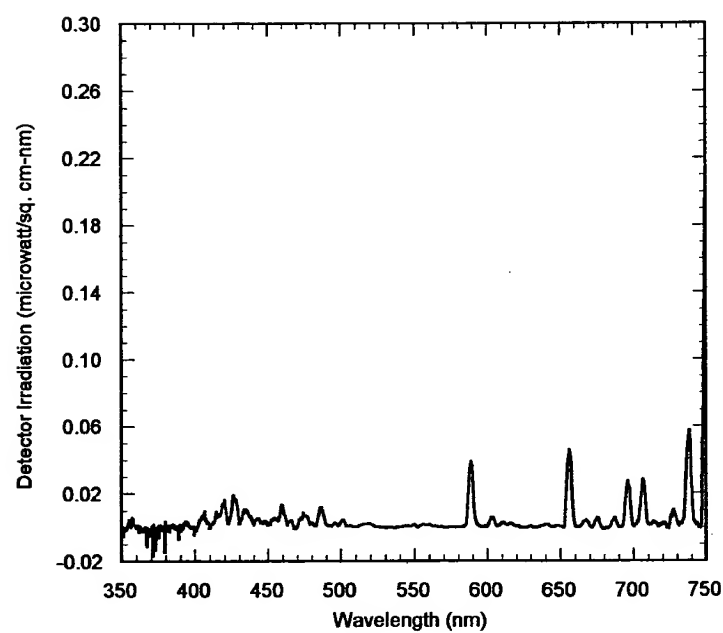


Figure 28



Identification of Compounds Containing Novel Hydride Ions by Nuclear Magnetic Resonance Spectroscopy

Randell L. Mills

Bala Dhandapani

Mark Nansteel

Jiliang He

Andreas Voigt

BlackLight Power, Inc.

493 Old Trenton Road

Cranbury, NJ 08512

Novel inorganic alkali and alkaline earth hydrides of the formula MH^* , MH_2^* , and MH^*X wherein M is the metal, X , is a halide, and H^* comprises a novel high binding energy hydride ion were synthesized in a high temperature gas cell by reaction of atomic hydrogen with a catalyst and MH , MH_2 , or MX corresponding to an alkali metal or alkaline earth metal compound, respectively. Novel hydride ions of the corresponding novel hydride compounds were characterized by an extraordinary upfield shifted peak observed by 1H nuclear magnetic resonance spectroscopy.

INTRODUCTION

Based on the solution of a Schrödinger-type wave equation with a nonradiative boundary condition based on Maxwell's equations, Mills [1-31] predicts that atomic hydrogen may undergo a catalytic reaction with certain atomized elements or certain gaseous ions which singly or multiply ionize at integer multiples of the potential energy of atomic hydrogen, 27.2 eV. For example, potassium atoms ionize at an integer multiple of the potential energy of atomic hydrogen, $m \cdot 27.2$ eV. The enthalpy of ionization of K to K^{3+} has a net enthalpy of reaction of 81.7426 eV, which is equivalent to $m=3$ [32]. The reaction involves a nonradiative energy transfer to form a hydrogen atom that is lower in energy than unreacted atomic hydrogen. The product hydrogen atom has an energy state that corresponds to a fractional principal quantum number. Recent analysis of mobility and spectroscopy data of individual electrons in liquid helium show direct experimental confirmation that electrons may have fractional principal quantum energy levels [33]. The lower-energy hydrogen atom is a highly reactive intermediate which further reacts to form a novel hydride ion. Emission was observed previously from a continuum state of Cs^{2+} and Ar^{2+} at 53.3 nm and 45.6 nm, respectively [4]. The single emission feature with the absence of the other corresponding Rydberg series of lines from these species confirmed the resonate nonradiative energy transfer of 27.2 eV from atomic hydrogen to atomic cesium or Ar^+ . The catalysis product, a lower-energy hydrogen atom, was predicted to be a highly reactive intermediate which further reacts to form a novel hydride ion. The predicted hydride ion of hydrogen catalysis by either cesium atom or Ar^+ catalyst is the hydride ion $H^- (1/2)$. This ion was observed spectroscopically at 407 nm corresponding to its predicted binding energy of 3.05 eV. The catalytic reaction with the formation the hydride ions are given in the Appendix.

Prior studies support the possibility of a novel reaction of atomic hydrogen which produces an anomalous discharge and produces novel hydride compounds. Experiments that confirm the novel hydrogen chemistry include extreme ultraviolet (EUV) spectroscopy [2-4, 6-7, 9-17], plasma formation [2-17], power generation [2-3, 5, 10, 31], and analysis of chemical compounds [13, 15-31]. For examples: 1.) Lines

observed by EUV spectroscopy could be assigned to transitions of atomic hydrogen to lower energy levels corresponding to lower energy hydrogen atoms and the emission from the excitation of the corresponding hydride ions [7, 11, 13, 15-17]. 2.) The chemical interaction of catalysts with atomic hydrogen at temperatures below 1000 K has shown surprising results in terms of the emission of the Lyman and Balmer lines [2-17] and the formation of novel chemical compounds [13, 15-31]. 3.) An energetic plasma in hydrogen was generated by a catalysis reaction at 1% of the theoretical or prior known voltage requirement and with 1000's of times less power input in a system wherein the plasma reaction was controlled with a weak electric field [2-3, 10]. 4.) The optically measured output power of gas cells for power supplied to the glow discharge increased by over two orders of magnitude depending on the presence of less than 1% partial pressure of certain of catalysts in hydrogen gas or argon-hydrogen gas mixtures [5]. 5.) A hydrogen plasma formed by reacting a catalyst with hydrogen was recorded when there was no electric energy input to the reaction which confirms a new chemical source of power [8-9].

Typically the emission of extreme ultraviolet light from hydrogen gas is achieved via a discharge at high voltage, a high power inductively coupled plasma, or a plasma created and heated to extreme temperatures by RF coupling (e.g. $>10^6$ K) with confinement provided by a toroidal magnetic field. Observation of intense extreme ultraviolet (EUV) emission has been reported at low temperatures (e.g. $\approx 10^3$ K) from atomic hydrogen and certain atomized elements or certain gaseous ions [2-17]. The only pure elements that were observed to emit EUV were those wherein the ionization of t electrons from an atom to a continuum energy level is such that the sum of the ionization energies of the t electrons is approximately $m \cdot 27.2$ eV where t and m are each an integer. Potassium, cesium, and strontium atoms and Rb^+ ion ionize at integer multiples of the potential energy of atomic hydrogen and caused emission. Whereas, the chemically similar atoms, sodium, magnesium and barium, do not ionize at integer multiples of the potential energy of atomic hydrogen and caused no emission. An anomalous plasma with hydrogen/potassium mixtures has been reported wherein the plasma decayed with a two second half-life which was the thermal decay time of the filament which

dissociated molecular hydrogen to atomic hydrogen when the electric field was set to zero [8-9]. This experiment showed that hydrogen line emission was occurring even though the voltage between the heater wires was set to and measured to be zero and indicated that the emission was due to a reaction of potassium atoms with atomic hydrogen.

Reports of the formation of novel compounds provide substantial evidence supporting a novel reaction of hydrogen as the mechanism of the observed EUV emission and anomalous discharge. Novel hydrogen compounds have been isolated as products of the reaction of atomic hydrogen with atoms and ions identified as catalysts in the reported EUV studies [2-31]. Novel inorganic alkali and alkaline earth hydrides of the formula MH^* and MH^*X wherein M is the metal, X , is a singly negatively charged anion, and H^* comprises a novel high binding energy hydride ion were synthesized in a high temperature gas cell by reaction of atomic hydrogen with a catalyst such as potassium metal and MH , MX or MX_2 corresponding to an alkali metal or alkaline earth metal compound, respectively [18, 21]. Novel hydride compounds were identified by 1.) time of flight secondary ion mass spectroscopy which showed a dominant hydride ion in the negative ion spectrum, 2.) X-ray photoelectron spectroscopy which showed novel hydride peaks and significant shifts of the core levels of the primary elements bound to the novel hydride ions, 3.) 1H nuclear magnetic resonance spectroscopy (NMR) which showed extraordinary upfield chemical shifts compared to the NMR of the corresponding ordinary hydrides, and 4.) thermal decomposition with analysis by gas chromatography, and mass spectroscopy which identified the compounds as hydrides [18, 21].

An upfield shifted NMR peak is consistent with a hydride ion with a smaller radius as compared with ordinary hydride since a smaller radius increases the shielding or diamagnetism. Thus, the NMR shows that the hydride formed in the catalytic reaction has been reduced in distance to the nucleus indicating that the electrons are in a lower-energy state. Compared to the shift of known corresponding hydrides the NMR provides direct evidence of reduced energy state hydride ions. We report that novel hydride ions of the corresponding novel hydride compounds of the formula MH^* , MH_2^* , and MH^*X were synthesized by a reaction of potassium or rubidium catalyst and atomic hydrogen. The

compounds showed extraordinary upfield shifted NMR peaks. The synthesis and analysis was shown to be reproducible. Several NMR instruments at independent centers were used to demonstrate the reproducibility of the unique upfield NMR peaks which corresponded to and identified novel hydride ions.

EXPERIMENTAL

Synthesis

A series of novel alkali and alkaline earth hydrides and alkali halido hydrides were synthesized by reaction of atomic hydrogen with a catalyst. The series KH^*Cl , KH^*Br , and KH^*I was synthesized from the corresponding alkali halide KCl (Alfa Aesar ACS grade 99+%), KBr (Alfa Aesar 99.9%), KI (Aldrich Chemical Company 99.9 %) using potassium metal (Aldrich Chemical Company 99%) as the catalyst. KH^* was synthesized from KH (Aldrich Chemical Company 99%) using potassium metal as the catalyst. RbH^*F was synthesized from RbF (Alfa Aesar 99.9%) using potassium metal as the catalyst. RbH^*I was synthesized from RbI (Alfa Aesar 99.9%) using rubidium metal (Aldrich Chemical Company 99%) which is a catalyst as a hydride having Rb^+ . CaH_2^* was synthesized using CaH_2 (Alfa Aesar 99.9%) and potassium metal as the catalyst. In the analytical analyses, each starting compound was also used as a control.

Each compound was prepared in a stainless steel gas cell shown in Figure 1 comprising a Ni screen hydrogen dissociator (Belleville Wire Cloth Co., Inc.), catalyst, and alkali halide or alkaline earth hydride. The 316-stainless steel cell was in the form of a tube having an internal cavity of 375 millimeters in length and 140 millimeters in diameter. The wall thickness was 6.35 mm. The bottom of the cell was closed by a 6.35 mm thick circular plate of 316 stainless steel that was welded to the cylinder. The top end of the cell was welded to a bored-through 304 stainless steel conflat-type flange with 8 in. nominal diameter. A mating blank flange was bolted to the bored-through flange with 20 silver-plated bolts. A flange gasket was silver-plated copper. A 1.27 cm OD tube was welded into a hole at the center of the blank flange. This tube was closed at one end and extended 20 cm into the reactor, serving as a thermowell. A 9.5 mm OD stainless steel tube was welded to the flange

approximately 4 cm from the flange center. This tube served as the vacuum line from the cell as well as a hydrogen or helium supply line to the cell.

The reactor was heated in a 10 kW refractory brick kiln (L & L Kiln Model JD230). The kiln had three heating zones and a heated floor that were each heated by separate radiant elements. The zone temperatures were independently controlled by a Dynatrol controller. The reactor was instrumented with 5 type-K thermocouples. Two thermocouples were located in the central thermowell at approximately reactor mid-height and at flange-level. Three thermocouples were fixed to the external surface of the reactor and were located near the base, at mid-height, and near flange-level. The reactor was connected through bellows-type valves to a turbo vacuum pump. The vacuum level was measured by a 0 - 100 torr Baratron vacuum gauge. Pressures above 100 torr were measured by standard dial-type pressure gauges. Temperature and pressure data was logged to a data acquisition system at 5 minute intervals.

Approximately 290 g of nickel screen (0.5 mm wire, 2 mm mesh) was placed circumferentially around the reactor inner wall of the cell. In an environmental chamber under argon gas, about 50 mmoles of dry alkali halide or alkaline earth hydride were placed in a stainless steel crucible on the reactor base. 1 mmole of metallic catalyst was placed in a smaller stainless steel crucible and this crucible was placed in the larger one with the alkali halide or alkaline earth hydride. The reactor was sealed and placed in the kiln. The system was evacuated for 2.5 hours. The reactor was pressurized with hydrogen gas to a pressure of 10 torr and sealed. The kiln was heated to 650 °C at the rate of 300 °C/h. The reactor was held at 650 °C for 72 hours. Hydrogen was added to the system periodically to maintain a pressure level of 10 torr. The reactor was then evacuated for 1 hour while at 650 °C. The kiln and reactor were cooled to room temperature by forced convection in about 2 hours while pumping continued. At room temperature the system was filled with helium gas to a pressure of 1.3 bar. The sealed reactor was then opened in the environmental chamber. NMR samples were placed in glass ampules, sealed with a rubber septa, and transferred out of the chamber to be flame sealed in atmosphere.

NMR Spectroscopy

1H MAS NMR was performed on solid samples of KH^*Cl , KH^*Br , KH^*I , KH^* , RbH^*F , RbH^*I , and CaH_2^* at Spectral Data Services, Inc., Champaign, Illinois. The data was obtained on a custom built spectrometer operating with a Nicolet 1280 computer. Final pulse generation was from a tuned Henry radio amplifier. The 1H NMR frequency was 270.6196 MHz. A 5 μ sec pulse corresponding to a 41° pulse length and a 3 second recycle delay were used. The window was ± 20 kHz. The spin speed was 4.0 kHz. (The spin speed was varied to confirm real peaks versus side bands. The latter changed position with spin speed, the former were independent of spin speed.) The number of scans was 600. The offset was 1541.6 Hz, and the magnetic flux was 6.357 T.

The samples were handled under a inert atmosphere. Chemical shifts were referenced to external tetramethylsilane (TMS). To eliminate the possibility that the alkali halide MX influenced the local environment of the ordinary alkali hydride MH to produce an NMR resonance that was shifted upfield relative to MH alone, controls comprising MH and an equimolar MH/MX mixture were run. The reference of each novel hydride comprised the corresponding ordinary hydride MH or MH_2 (Aldrich Chemical Company 99%) and equivalent molar mixtures of MH and MX prepared in a glove box under argon. In the case of the references of $RbHF$ and RbH^*I , RbH was synthesized by reaction of rubidium metal (Aldrich Chemical Company 99%) with 2 atmospheres of hydrogen in the gas cell at 300 °C for 8 hours.

To confirm that the upfield shifted peak of the KH^*Cl samples was reproducible when recorded on different instruments, 1H MAS NMR was performed on solid samples of KH^*Cl and KH^*I at four additional independent laboratories. The data were recorded on a Bruker DSX-400 spectrometer at 400.13 MHz at the National Research Council of Canada, a Bruker DSX-300 spectrometer at 300.132 MHz at the University of Massachusetts, a Bruker MSL-300 spectrometer at 300.13 MHz at the University of Delaware, and Chemagnetics CMX Infinity 400 spectrometer at 359.7539 MHz at Grace Davison.

¹H MAS NMR was performed on KH*I (blue crystals) at the National Research Council of Canada. The data were recorded on a Bruker DSX-400 spectrometer at 400.13 MHz. Samples were packed in zirconia rotors and sealed with airtight O-ring caps under an inert atmosphere. The MAS frequency was 4.5 kHz. During data acquisition, the sweep width was 60.06 kHz; the dwell time was 8.325 μ sec, and the acquisition time was 0.03415 sec/scan. The number of scans was typically 32 or 64. Chemical shifts were referenced to external tetramethylsilane (TMS). The reference comprised KH (Aldrich Chemical Company 99%).

¹H MAS NMR was performed on solid samples of KH*Cl at the University of Massachusetts. The data were recorded on a Bruker DSX-300 spectrometer at 300.132 MHz. Samples were packed and sealed in 5 mm diameter NMR tubes under an inert atmosphere. The samples were spun at a MAS frequency of 4.1 kHz. During data acquisition, the 90 degree pulse length for a single pulse ¹H excitation was 3.4 μ sec; the sweep width was 147.058 kHz; the dwell time was 5.5 μ sec, and the acquisition time was 0.0139764 sec/scan. The number of scans was typically 32.

¹H MAS NMR was performed on solid samples of KH*Cl and KH*I (green crystals) at the University of Delaware. The data were recorded on a Bruker MSL-300 spectrometer at 300.13 MHz. Samples were packed and sealed in 5 mm diameter NMR tubes under an inert atmosphere. The samples were spun at a MAS frequency of 3 kHz. During data acquisition, the 90 degree pulse length for a single pulse ¹H excitation was 4 μ sec; the dwell time was 5 μ sec, and the acquisition time was 5120 μ sec/scan. The number of scans was typically 540.

¹H MAS NMR was performed on solid samples of KH*Cl and KH*I (blue crystals) at Grace Davison. The data were recorded on a Chemagnetics CMX Infinity 400 spectrometer at 359.7539 MHz. Each sample was packed and sealed in a 4 mm diameter Chemagnetics probe under an inert atmosphere. The samples were spun at a MAS frequency of 12 kHz. During data acquisition, the 90 degree pulse length for a single pulse ¹H excitation was 4.0 μ sec; the spectrum window was ± 20 kHz; the dwell time was 50 μ sec, the recovery delay was 15 μ sec, and the acquisition time was 2930 μ sec/scan. The number of scans was typically 1024.

RESULTS AND DISCUSSION

A. NMR of Potassium Chloro Hydride Sample

The 1H MAS NMR spectra of six KH^*Cl samples from independent syntheses, the control comprising an equal molar mixture of KH and KCl , and the control KH relative to external tetramethylsilane (TMS) are shown in Figures 2A-H, respectively. Ordinary hydride ion has a resonance at 1.1 ppm and 0.8 ppm in the KH/KCl mixture and in KH alone as shown in Figures 2G and 2H, respectively. The sharp peak at 4.3 ppm and the broad peak at 6 ppm shown in Figure 2G are assigned to water in the KCl crystal and to $KHCO_3$ formed from air exposure of K during sample handling, respectively. The broad peak at 4.6 ppm shown in Figure 2H is assigned KOH formed from air exposure of KH during sample handling.

The presence of KCl does not shift the resonance of ordinary hydride as shown in Figure 2G. The resonance at 1.1 ppm which is assigned to ordinary hydride ion was observed in the spectrum of each KH^*Cl sample as shown in Figures 2A-F. The distinct 0.8 and 1.1 ppm resonances could not be resolved if they were present. A large distinct upfield resonance was observed in each case at -4.4 to -4.6 ppm which was not observed in either control. The upfield peak in each sample is assigned to a novel hydride ion of KH^*Cl .

B. NMR of Potassium Bromo Hydride Sample

The 1H MAS NMR spectra of the KH^*Br sample, the control comprising an equal molar mixture of KH and KBr , and the control KH relative to external tetramethylsilane (TMS) are shown in Figures 3A-C, respectively. Ordinary hydride ion has a resonance at 1.1 ppm and 0.8 ppm in the KH/KBr mixture and in KH alone as shown in Figures 3B and 3C, respectively. The additional sharp peaks at 4.3 ppm and 5.9 ppm shown in Figure 3A are assigned to water and $KHCO_3$ formed from air exposure of K during sample handling. The additional sharp peak at 4.2

ppm shown in Figure 3B is assigned to water in the *KBr* crystals. The additional broad peak at 4.6 ppm shown in Figure 3C is assigned *KOH* formed from air exposure of *KH* during sample handling.

The presence of *KBr* does not shift the resonance of ordinary hydride. The resonance at 1.2 ppm which is assigned to ordinary hydride ion was observed in the spectrum of the *KH*Br* sample as shown in Figure 3A. The distinct 0.8 and 1.1 ppm resonances could not be resolved if they were present. A large distinct upfield resonance was observed at -4.1 ppm which was not observed in either control. This upfield shifted peak is assigned to a novel hydride ion of *KH*Br*.

C. NMR of Potassium Iodo Hydride Sample

With an increase of the time of synthesis Mills et al. [18] report that a first blue crystalline compound is formed from the reaction of potassium catalyst with *KI*. With an increase in reaction time the product becomes increasingly green colored. NMR resonances at -1.209 ppm and possibly at -2.5 ppm (See Figure 15) are observed in the case of the blue crystals, and the resonance shifts further upfield to -2.5 ppm as the compound becomes more green colored as shown in Figure 4. These NMR results as well as the previously reported [18] liquid chromatography and X-ray photoelectron spectroscopy data support the production of two distinct hydride ions with different binding energies. This may be due to the ability of two potassium ions as well as a potassium atom to catalyze atomic hydrogen to different energy states as shown in the Appendix. In the present study, the NMR was obtained on blue crystal, light green crystals, and dark green crystals which formed with a reaction time of progressively longer duration.

The ^1H MAS NMR spectra of *KH*I* samples from separate syntheses of longer duration relative to external tetramethylsilane (TMS) is shown in Figure 4A-C. Distinguishable upfield resonances were observed at -3.2, -2.5, and -1.8 ppm for the dark green crystals, the green crystals, and the blue crystals as shown in Figure 4A-C, respectively. The upfield peak in each sample is assigned to a novel hydride ion of *KH*I*. The down field shifted peaks may be ordinary hydride in a different chemical environment.

The presence of *KI* does not shift the resonance of ordinary hydride. Ordinary hydride ion has a resonance at 1.1 ppm and 0.8 ppm in the *KH/KI* mixture and in *KH* alone as shown in Figures 4D and 4E, respectively. The additional peaks at 4.5 to 4.6 ppm are assigned to *KOH* formed from air exposure of *KH* during sample handling.

D. Comparison of NMR of Potassium Iodo Hydride and Potassium Chloro Hydride Samples at Independent Laboratories

To confirm that the upfield shifted peaks of the *KH*Cl* and *KH*I* samples were reproducible when recorded on different instruments, ^1H MAS NMR was performed on solid samples of *KH*Cl* and *KH*I* at four additional independent laboratories. The spectra are shown in Figures 9-17 and the results are summarized in Table 1. The ^1H MAS NMR spectra of six *KH*Cl* samples from independent syntheses shown in Figures 2A-F are in agreement with the independently obtained results run on *KH*Cl* samples as given in Table 1. Two different novel hydride ions were reported by Mills et al. [18] in the case of the *KH*I* samples. The ^1H MAS NMR spectra of the *KH*I* blue crystal sample shown in Figure 4C and the light green sample shown in Figure 4B are in agreement with the independently obtained results run on corresponding samples as given in Table 1. These results demonstrate that the upfield shifted peaks are reproducible and that they can not be attributed to instrument artifact.

E. NMR of Potassium Hydride Sample

The ^1H MAS NMR spectra of the *KH** sample and control *KH* relative to external tetramethylsilane (TMS) are shown in Figures 5A and 5B, respectively. Ordinary hydride ion has a resonance at 1.1 ppm and 0.8 ppm in *KH* as shown in Figure 5B. The peak at 4.1 ppm shown in Figure 5A is assigned to water. The additional broad peak at 4.6 ppm shown in Figure 5B is assigned *KOH* formed from air exposure of *KH* during sample handling. The spin speed was varied to confirm real peaks versus side bands. The latter changed position with spin speed, the former were independent of spin speed. The peaks labeled SB shown in Figure 5A were found to be sidebands.

The resonance at 1.1 ppm which is assigned to ordinary hydride ion was observed in the spectrum of the KH^* sample as shown in Figure 5A. The distinct 0.8 and 1.1 ppm resonances could not be resolved if they were present. A large distinct upfield resonance was observed at -2.8 ppm which was not observed in the control. This upfield shifted peak is assigned to a novel hydride ion of KH^* .

F. NMR of Rubidium Fluoro Hydride Sample

The 1H MAS NMR spectra of three RbH^*F samples from separate syntheses, the control comprising an equal molar mixture of RbH and RbF , and the control RbH relative to external tetramethylsilane (TMS) are shown in Figures 6A-E, respectively. Ordinary hydride ion has a resonance at about 1 ppm in the RbH/RbF mixture and in RbH alone as shown in Figures 6D and 6E, respectively. The broad peaks at 4 ppm and 4.6 ppm shown in Figures 6D and 6E, respectively, are assigned to $RbOH$ formed from air exposure of RbH during sample handling. The spin speed was varied to confirm real peaks versus side bands. The latter changed position with spin speed, the former were independent of spin speed. The SB labeled peaks shown in Figure 6D were found to be sidebands.

The presence of RbF does not shift the resonance of ordinary hydride. The resonance at 1.2 ppm which is assigned to ordinary hydride ion was observed in the spectrum of each RbH^*F sample as shown in Figures 6A-C. A large distinct upfield resonance was observed in each case at -4.1 and -4.4 ppm which was not observed in either control. The upfield peak in each sample is assigned to a novel hydride ion of RbH^*F .

G. NMR of Rubidium Iodo Hydride Sample

The 1H MAS NMR spectra of two RbH^*I samples from separate syntheses and the control comprising RbH relative to external tetramethylsilane (TMS) are shown in Figures 7A-C, respectively. Ordinary hydride ion has a resonance at about 1 ppm in RbH alone as shown in Figure 7C. The broad peaks at 4 ppm shown in Figures 7A-C are assigned to $RbOH$ formed from air exposure of RbH during sample

handling. The peak at 6 ppm shown in Figures 7A-B are assigned to $RbHCO_3$ formed from air exposure of RbH during sample handling.

The resonance at 1.2 ppm which is assigned to ordinary hydride ion was observed in the spectrum of each RbH^*I sample as shown in Figures 7A-B. A large distinct upfield resonance was observed in each case at -3.7 ppm which was not observed in either control. The upfield peak in each sample is assigned to a novel hydride ion of RbH^*I .

H. NMR of Calcium Hydride Sample

The 1H MAS NMR spectra of the CaH_2^* sample and control CaH_2 relative to external tetramethylsilane (TMS) are shown in Figures 8A and 8B, respectively. The spin speed was varied to confirm real peaks versus side bands. The latter changed position with spin speed, the former were independent of spin speed. The peaks labeled SB shown in Figures 8A and 8B were found to be sidebands. Resonances at 1.2 ppm and 4.4 ppm were observed in ordinary CaH_2 as shown in Figure 8B.

Three distinct resonances were observed in the case of the CaH_2^* sample at 5.4 ppm, 1.2 ppm, and -1.2 ppm as shown in Figure 8A. The large distinct upfield resonance observed at -1.2 ppm which was not observed in the control is assigned to a novel hydride ion of CaH_2^* .

CONCLUSIONS

The NMR results confirm the identification of novel hydride compounds MH^*X wherein M is the metal, X , is a halide, and H^* comprises a novel high binding energy hydride ion. Large distinct upfield resonances were observed at -4.5 ppm (KH^*Cl), -4.1 ppm (KH^*Br), -3.2 ppm (KH^*I), -4.4 ppm (RbH^*F), and -3.7 ppm (RbH^*I). The presence of a halide in each compound MH^*X does not explain the upfield shifted NMR peak since the same NMR spectrum was observed for an equimolar mixture of the pure hydride and the corresponding alkali halide (MH/MX) as was observed for the pure hydride, MH .

The NMR results further confirm the identification of novel hydride compounds MH^* and MH_2^* wherein M is the metal and H^* comprises a

novel high binding energy hydride ion. Large distinct upfield resonances were observed at -2.8 ppm and -1.2 ppm in the case of KH^* and CaH_2^* , respectively. Whereas, the resonances for the ordinary hydride ion of KH were observed at 0.7 and 1.1 ppm, and the resonances for the ordinary hydride ion of CaH_2 were observed at 1.2 ppm and 4.4 ppm. The synthesis of alkaline and alkaline earth hydrides, KH^* and CaH_2^* , respectively, with upfield shifted peaks prove that the hydride ion is different from the hydride ion of the corresponding known compound of the same composition.

The upfield shifted peak observed in each novel hydride sample identifies a hydride ion with a smaller radius as compared with ordinary hydride since a smaller radius increases the shielding or diamagnetism. The peaks are assigned to novel hydride ions that have substantially smaller radii than that of ordinary hydride ion since the shift was extraordinarily far upfield. The reproducibility of the syntheses and the results from independent laboratories confirm the formation of novel hydride ions.

The identification of compounds containing novel hydride ions is indicative of a new field of hydrogen chemistry. Novel hydride ions may combine with other cations such as other alkali cations and alkaline earth, rare earth, and transition element cations. Numerous novel compounds may be synthesized with extraordinary properties relative to the corresponding compounds having ordinary hydride ions. These novel compounds may have a breath of applications. For example, a high voltage battery according to the hydride binding energies previously observed by XPS [18-19, 21] may be possible having projected specifications that are comparable to those of the internal combustion engine [19]. An exemplary redox reaction is given in the Appendix.

APPENDIX

Mills [1] predicts that certain atoms or ions serve as catalysts to release energy from hydrogen to produce an increased binding energy hydrogen atom called a *hydrino atom* having a binding energy of

$$\text{Binding Energy} = \frac{13.6 \text{ eV}}{n^2} \quad (1)$$

where

$$n = \frac{1}{2}, \frac{1}{3}, \frac{1}{4}, \dots, \frac{1}{p} \quad (2)$$

and p is an integer greater than 1, designated as $H\left[\frac{a_H}{p}\right]$ where a_H is the radius of the hydrogen atom. Hydrinos are predicted to form by reacting an ordinary hydrogen atom with a catalyst having a net enthalpy of reaction of about

$$m \cdot 27.2 \text{ eV} \quad (3)$$

where m is an integer. This catalysis releases energy from the hydrogen atom with a commensurate decrease in size of the hydrogen atom, $r_n = n a_H$. For example, the catalysis of $H(n=1)$ to $H(n=1/2)$ releases 40.8 eV, and the hydrogen radius decreases from a_H to $\frac{1}{2}a_H$.

The excited energy states of atomic hydrogen are also given by Eq. (1) except that

$$n = 1, 2, 3, \dots \quad (4)$$

The $n=1$ state is the "ground" state for "pure" photon transitions (the $n=1$ state can absorb a photon and go to an excited electronic state, but it cannot release a photon and go to a lower-energy electronic state).

However, an electron transition from the ground state to a lower-energy state is possible by a nonradiative energy transfer such as multipole coupling or a resonant collision mechanism. These lower-energy states have fractional quantum numbers, $n = \frac{1}{\text{integer}}$. Processes that occur

without photons and that require collisions are common. For example, the exothermic chemical reaction of $H+H$ to form H_2 does not occur with the emission of a photon. Rather, the reaction requires a collision with a third body, M , to remove the bond energy- $H+H+M \rightarrow H_2 + M^*$ [34]. The third body distributes the energy from the exothermic reaction, and the end result is the H_2 molecule and an increase in the temperature of the system. Some commercial phosphors are based on nonradiative energy transfer involving multipole coupling. For example, the strong absorption strength of Sb^{3+} ions along with the efficient nonradiative transfer of excitation from Sb^{3+} to Mn^{2+} , are responsible for the strong manganese luminescence from phosphors containing these ions [35]. Similarly, the

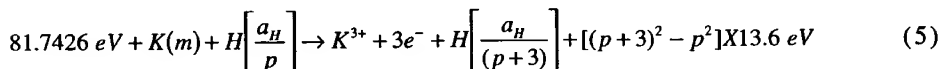
$n=1$ state of hydrogen and the $n=\frac{1}{\text{integer}}$ states of hydrogen are

nonradiative, but a transition between two nonradiative states is possible via a nonradiative energy transfer, say $n=1$ to $n=1/2$. In these cases, during the transition the electron couples to another electron transition, electron transfer reaction, or inelastic scattering reaction which can absorb the exact amount of energy that must be removed from the hydrogen atom. Thus, a catalyst provides a net positive enthalpy of reaction of $m \cdot 27.2 \text{ eV}$ (i.e. it absorbs $m \cdot 27.2 \text{ eV}$ where m is an integer). Certain atoms or ions serve as catalysts which resonantly accept energy from hydrogen atoms and release the energy to the surroundings to effect electronic transitions to fractional quantum energy levels.

Inorganic Catalysts

Potassium

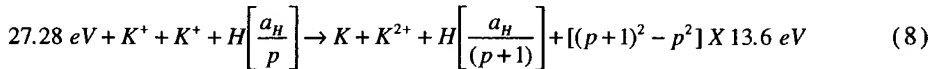
A catalytic system is provided by the ionization of t electrons from an atom to a continuum energy level such that the sum of the ionization energies of the t electrons is approximately $m \cdot 27.2 \text{ eV}$ where m is an integer. One such catalytic system involves potassium. A catalytic system is provided by the ionization of 3 electrons from a potassium atom each to a continuum energy level such that the sum of the ionization energies of the 3 electrons is approximately $3 \cdot 27.2 \text{ eV}$. The first, second, and third ionization energies of potassium are 4.34066 eV , 31.63 eV , 45.806 eV , respectively [32]. The triple ionization ($t=3$) reaction of K to K^{3+} , then, has a net enthalpy of reaction of 81.7426 eV , which is equivalent to $m=3$ in Eq. (3).



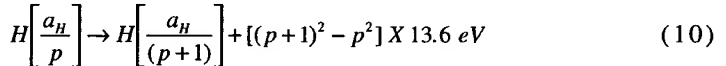
And, the overall reaction is

$$H\left[\frac{a_H}{p}\right] \rightarrow H\left[\frac{a_H}{(p+3)}\right] + [(p+3)^2 - p^2] \times 13.6 \text{ eV} \quad (7)$$

Potassium ions can also provide a net enthalpy of a multiple of that of the potential energy of the hydrogen atom. The second ionization energy of potassium is 31.63 eV; and K^+ releases 4.34 eV when it is reduced to K [32]. The combination of reactions K^+ to K^{2+} and K^+ to K , then, has a net enthalpy of reaction of 27.28 eV, which is equivalent to $m=1$ in Eq. (3).

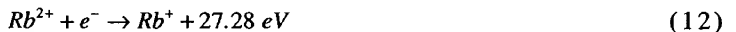
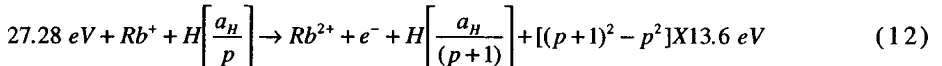


The overall reaction is

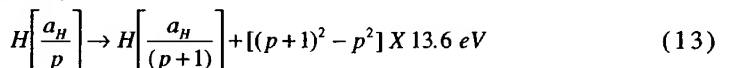


Rubidium

Rubidium ions can also provide a net enthalpy of a multiple of that of the potential energy of the hydrogen atom. A catalytic system is provided by the ionization of an electron from a Rb^+ ion to a continuum energy level since the second ionization energy of rubidium is 27.28 eV [32]. The reaction Rb^+ to Rb^{2+} has a net enthalpy of reaction of 27.28 eV, which is equivalent to $m=1$ in Eq. (3).



The overall reaction is



Hydride Ion

A novel hydride ion having extraordinary chemical properties given by Mills [1] is predicted to form by the reaction of an electron with a hydrino (Eq. (14)). The resulting hydride ion is referred to as a hydrino hydride ion, designated as $H^-(1/p)$.



The hydrino hydride ion is distinguished from an ordinary hydride ion having a binding energy of 0.8 eV. The hydrino hydride ion is predicted [1] to comprise a hydrogen nucleus and two indistinguishable electrons at a binding energy according to the following formula:

$$\text{Binding Energy} = \frac{\hbar^2 \sqrt{s(s+1)}}{8\mu_e a_0^2 \left[\frac{1+\sqrt{s(s+1)}}{p} \right]^2} - \frac{\pi \mu_0 e^2 \hbar^2}{m_e^2 a_0^3} \left(1 + \frac{2^2}{\left[\frac{1+\sqrt{s(s+1)}}{p} \right]^3} \right) \quad (15)$$

where p is an integer greater than one, $s=1/2$, π is pi, \hbar is Planck's constant bar, μ_0 is the permeability of vacuum, m_e is the mass of the electron, μ_e is the reduced electron mass, a_0 is the Bohr radius, and e is the elementary charge. The ionic radius is

$$r_i = \frac{a_0}{p} \left(1 + \sqrt{s(s+1)} \right); s = \frac{1}{2} \quad (16)$$

From Eq. (16), the radius of the hydrino hydride ion $H^-(1/p)$; p = integer is $\frac{1}{p}$ that of ordinary hydride ion, $H^-(1/1)$. Compounds containing hydrino hydride ions have been isolated as products of the reaction of atomic hydrogen with atoms and ions identified as catalysts by EUV emission [2-31].

Hydride ions having extraordinary binding energies may stabilize a cation M^{x+} in an extraordinarily high oxidation state such as +2 in the case of lithium. Thus, these hydride ions may be used as the basis of a

high voltage battery of a rocking chair design wherein the hydride ion moves back and forth between the cathode and anode half cells during discharge and charge cycles. Exemplary reactions for a cation M^{x+} are:

Cathode reaction:



Anode reaction:



Overall reaction:



REFERENCES

1. R. Mills, *The Grand Unified Theory of Classical Quantum Mechanics*, January 2000 Edition, BlackLight Power, Inc., Cranbury, New Jersey, Distributed by Amazon.com.
2. R. Mills and M. Nansteel, "Anomalous Argon-Hydrogen-Strontium Discharge", *IEEE Transactions of Plasma Science*, submitted.
3. R. Mills, M. Nansteel, and Y. Lu, "Anomalous Hydrogen-Strontium Discharge", *European Journal of Physics D*, submitted.
4. R. Mills, "Spectroscopic Identification of a Novel Catalytic Reaction of Atomic Hydrogen and the Hydride Ion Product", *Int. J. Hydrogen Energy*, submitted.
5. R. Mills, N. Greenig, S. Hicks, "Optically Measured Power Balances of Anomalous Discharges of Mixtures of Argon, Hydrogen, and Potassium, Rubidium, Cesium, or Strontium Vapor", *Int. J. Hydrogen Energy*, submitted.
6. R. Mills, J. Dong, Y. Lu, "Observation of Extreme Ultraviolet Hydrogen Emission from Incandescently Heated Hydrogen Gas with Certain Catalysts", *Int. J. Hydrogen Energy*, Vol. 25, (2000), pp. 919-943.
7. R. Mills, "Observation of Extreme Ultraviolet Emission from Hydrogen-KI Plasmas Produced by a Hollow Cathode Discharge", *Int. J. Hydrogen Energy*, in press.
8. R. Mills, "Temporal Behavior of Light-Emission in the Visible Spectral Range from a Ti-K₂CO₃-H-Cell", *Int. J. Hydrogen Energy*, in press.
9. R. Mills, Y. Lu, and T. Onuma, "Formation of a Hydrogen Plasma from an Incandescently Heated Hydrogen-Catalyst Gas Mixture with an Anomalous Afterglow Duration", *Int. J. Hydrogen Energy*, in press.
10. R. Mills, M. Nansteel, and Y. Lu, "Observation of Extreme Ultraviolet Hydrogen Emission from Incandescently Heated Hydrogen Gas with Strontium that Produced an Anomalous Optically Measured Power Balance", *Int. J. Hydrogen Energy*, in press.
11. R. Mills, J. Dong, Y. Lu, J. Conrads, "Observation of Extreme Ultraviolet Hydrogen Emission from Incandescently Heated Hydrogen Gas with Certain Catalysts", 1999 Pacific Conference on Chemistry and Spectroscopy and the 35th ACS Western Regional Meeting, Ontario Convention Center, California, (October 6-8, 1999).

12. R. Mills, J. Dong, N. Greenig, and Y. Lu, "Observation of Extreme Ultraviolet Hydrogen Emission from Incandescently Heated Hydrogen Gas with Certain Catalysts", National Hydrogen Association, 11 th Annual U.S. Hydrogen Meeting, Vienna, VA, (February 29-March 2, 2000).
13. R. Mills, B. Dhandapani, N. Greenig, J. He, J. Dong, Y. Lu, and H. Conrads, "Formation of an Energetic Plasma and Novel Hydrides from Incandescently Heated Hydrogen Gas with Certain Catalysts", National Hydrogen Association, 11 th Annual U.S. Hydrogen Meeting, Vienna, VA, (February 29-March 2, 2000).
14. Mills, J. Dong, N. Greenig, and Y. Lu, "Observation of Extreme Ultraviolet Hydrogen Emission from Incandescently Heated Hydrogen Gas with Certain Catalysts", 219 th National ACS Meeting, San Francisco, California, (March 26-30, 2000).
15. R. Mills, B. Dhandapani, N. Greenig, J. He, J. Dong, Y. Lu, and H. Conrads, "Formation of an Energetic Plasma and Novel Hydrides from Incandescently Heated Hydrogen Gas with Certain Catalysts", 219 th National ACS Meeting, San Francisco, California, (March 26-30, 2000).
16. R. Mills, B. Dhandapani, N. Greenig, J. He, J. Dong, Y. Lu, and H. Conrads, "Formation of an Energetic Plasma and Novel Hydrides from Incandescently Heated Hydrogen Gas with Certain Catalysts", June ACS Meeting (29th Northeast Regional Meeting, University of Connecticut, Storrs, CT, (June 18-21, 2000)).
17. R. Mills, B. Dhandapani, N. Greenig, J. He, J. Dong, Y. Lu, and H. Conrads, "Formation of an Energetic Plasma and Novel Hydrides from Incandescently Heated Hydrogen Gas with Certain Catalysts", August National ACS Meeting (220th ACS National Meeting, Washington, DC, (August 20-24, 2000)).
18. R. Mills, B. Dhandapani, N. Greenig, J. He, "Synthesis and Characterization of Potassium Iodo Hydride", Int. J. of Hydrogen Energy, Vol. 25, Issue 12, December, (2000), pp. 1185-1203.
19. R. Mills, "Novel Inorganic Hydride", Int. J. of Hydrogen Energy, Vol. 25, (2000), pp. 669-683.
20. R. Mills, "Novel Hydrogen Compounds from a Potassium Carbonate Electrolytic Cell", Fusion Technology, Vol. 37, No. 2, March, (2000), pp. 157-182.

21. R. Mills, B. Dhandapani, M. Nansteel, J. He, T. Shannon, A. Echezuria, "Synthesis and Characterization of Novel Hydride Compounds", Int. J. of Hydrogen Energy, in press.
22. R. Mills, "Highly Stable Novel Inorganic Hydrides", Journal of Materials Research, submitted.
23. R. Mills, "Novel Hydride Compound", 1999 Pacific Conference on Chemistry and Spectroscopy and the 35th ACS Western Regional Meeting, Ontario Convention Center, California, (October 6-8, 1999).
24. R. Mills, B. Dhandapani, N. Greenig, J. He, "Synthesis and Characterization of Potassium Iodo Hydride", 1999 Pacific Conference on Chemistry and Spectroscopy and the 35th ACS Western Regional Meeting, Ontario Convention Center, California, (October 6-8, 1999).
25. R. Mills, J. He, and B. Dhandapani, "Novel Hydrogen Compounds", 1999 Pacific Conference on Chemistry and Spectroscopy and the 35th ACS Western Regional Meeting, Ontario Convention Center, California, (October 6-8, 1999).
26. R. Mills, "Novel Hydride Compound", National Hydrogen Association, 11 th Annual U.S. Hydrogen Meeting, Vienna, VA, (February 29-March 2, 2000).
27. R. Mills, J. He, and B. Dhandapani, "Novel Alkali and Alkaline Earth Hydrides", National Hydrogen Association, 11 th Annual U.S. Hydrogen Meeting, Vienna, VA, (February 29-March 2, 2000).
28. R. Mills, "Novel Hydride Compound", 219 th National ACS Meeting, San Francisco, California, (March 26-30, 2000).
29. R. Mills, J. He, and B. Dhandapani, "Novel Alkali and Alkaline Earth Hydrides", 219 th National ACS Meeting, San Francisco, California, (March 26-30, 2000).
30. R. Mills, J. He, and B. Dhandapani, "Novel Alkali and Alkaline Earth Hydrides", August National ACS Meeting (220 th ACS National Meeting, Washington, DC, (August 20-24, 2000)).
31. R. Mills, W. Good, A. Voigt, Jinquan Dong, "Minimum Heat of Formation of Potassium Iodo Hydride", Int. J. Hydrogen Energy, submitted.
32. David R. Linde, *CRC Handbook of Chemistry and Physics*, 79 th Edition, CRC Press, Boca Raton, Florida, (1998-9), p. 10-175 to p. 10-177.

33. R. Mills, The Nature of Free Electrons in Superfluid Helium--a Test of Quantum Mechanics and a Basis to Review its Foundations and Make a Comparison to Classical Theory, *Int. J. Hydrogen Energy*, in press.
34. N. V. Sidgwick, *The Chemical Elements and Their Compounds*, Volume I, Oxford, Clarendon Press, (1950), p.17.
35. M. D. Lamb, *Luminescence Spectroscopy*, Academic Press, London, (1978), p. 68.

Table 1. Comparison of solid-state 1H MAS NMR spectral data of KH^*Cl and KH^*I from various analytical laboratories.

Sample	Laboratory	Novel features
KH^*Cl	Spectral Data Services	-4.6 ppm
KH^*Cl	University of Massachusetts	-4.4 ppm
KH^*Cl	University of Delaware	-4.9 ppm
KH^*Cl	Grace Davison	-4.5 ppm
KH^*I (blue crystals)	Spectral Data Services	-1.8 ppm
KH^*I (green crystals)	Spectral Data Services	-2.6 ppm
KH^*I (blue crystals)	National Research Council of Canada	-1.2 ppm -2.5 ppm ^a
KH^*I (blue crystals)	Grace Davison	-1.5 ppm -2.3 ppm ^a
KH^*I (green crystals)	University of Delaware	-2.8 ppm

^a (smaller peak)

Figure Captions

Figure 1. Stainless steel gas cell comprising a screen dissociator, metal catalyst, and alkali halide or alkali or alkaline earth hydride as the reactant. The components were: 101-stainless steel cell; 117- internal cavity of cell; 118-high vacuum conflat flange; 119-mating blank conflat flange; 102-stainless steel tube vacuum line and gas supply line; 103-lid to the kiln or top insulation, 104 heater; 108-screen dissociator; 109-alkali halide or alkali or alkaline earth hydride reactant; 110-high vacuum turbo pump; 112- pressure gauge; 111-vacuum pump valve; 113-valve; 114-valve; 115-regulator; 116-hydrogen tank.

Figure 2A-F. The 1H MAS NMR spectra of six KH^*Cl samples from independent syntheses relative to external tetramethylsilane (TMS).

Figure 2G. The 1H MAS NMR spectrum of the control comprising an equal molar mixture of KH and KCl relative to external tetramethylsilane (TMS).

Figure 2H. The 1H MAS NMR spectrum of the control KH relative to external tetramethylsilane (TMS).

Figure 3A. The 1H MAS NMR spectrum of KH^*Br relative to external tetramethylsilane (TMS).

Figure 3B. The 1H MAS NMR spectrum of the control comprising an equal molar mixture of KH and KBr relative to external tetramethylsilane (TMS).

Figure 3C. The 1H MAS NMR spectrum of the control KH relative to external tetramethylsilane (TMS).

Figure 4A. The 1H MAS NMR spectrum of KH^*I (dark green crystals) relative to external tetramethylsilane (TMS).

Figure 4B. The 1H MAS NMR spectrum of KH^*I (green crystals) relative to external tetramethylsilane (TMS).

Figure 4C. The 1H MAS NMR spectrum of KH^*I (blue crystals) relative to external tetramethylsilane (TMS).

Figure 4D. The 1H MAS NMR spectrum of the control comprising an equal molar mixture of KH and KI relative to external tetramethylsilane (TMS).

Figure 4E. The 1H MAS NMR spectrum of the control KH relative to external tetramethylsilane (TMS).

Figure 5A. The 1H MAS NMR spectra of KH^* relative to external tetramethylsilane (TMS).

Figure 5B. The 1H MAS NMR spectrum of the control KH relative to external tetramethylsilane (TMS).

Figure 6A-C. The 1H MAS NMR spectra of three RbH^*F samples from separate syntheses relative to external tetramethylsilane (TMS).

Figure 6D. The 1H MAS NMR spectrum of the control comprising an equal molar mixture of RbH and RbF relative to external tetramethylsilane (TMS).

Figure 6E. The 1H MAS NMR spectrum of the control RbH relative to external tetramethylsilane (TMS).

Figure 7A-B. The 1H MAS NMR spectra of two RbH^*I samples from separate syntheses relative to external tetramethylsilane (TMS).

Figure 7C. The 1H MAS NMR spectrum of the control RbH relative to external tetramethylsilane (TMS).

Figure 8A. The 1H MAS NMR spectra of the CaH_2^* relative to external tetramethylsilane (TMS).

Figure 8B. The 1H MAS NMR spectrum of the control CaH_2 relative to external tetramethylsilane (TMS).

Figure 9. The 1H MAS NMR spectrum of KH^*Cl performed at Spectral Data Services relative to external tetramethylsilane (TMS).

Figure 10. The 1H MAS NMR spectrum of KH^*Cl performed at University of Massachusetts relative to external tetramethylsilane (TMS).

Figure 11. The 1H MAS NMR spectrum of KH^*Cl performed at University of Delaware relative to external tetramethylsilane (TMS).

Figure 12. The 1H MAS NMR spectrum of KH^*Cl performed at Grace Davison relative to external tetramethylsilane (TMS).

Figure 13. The 1H MAS NMR spectrum of KH^*I (blue crystals) performed at Spectral Data Services relative to external tetramethylsilane (TMS).

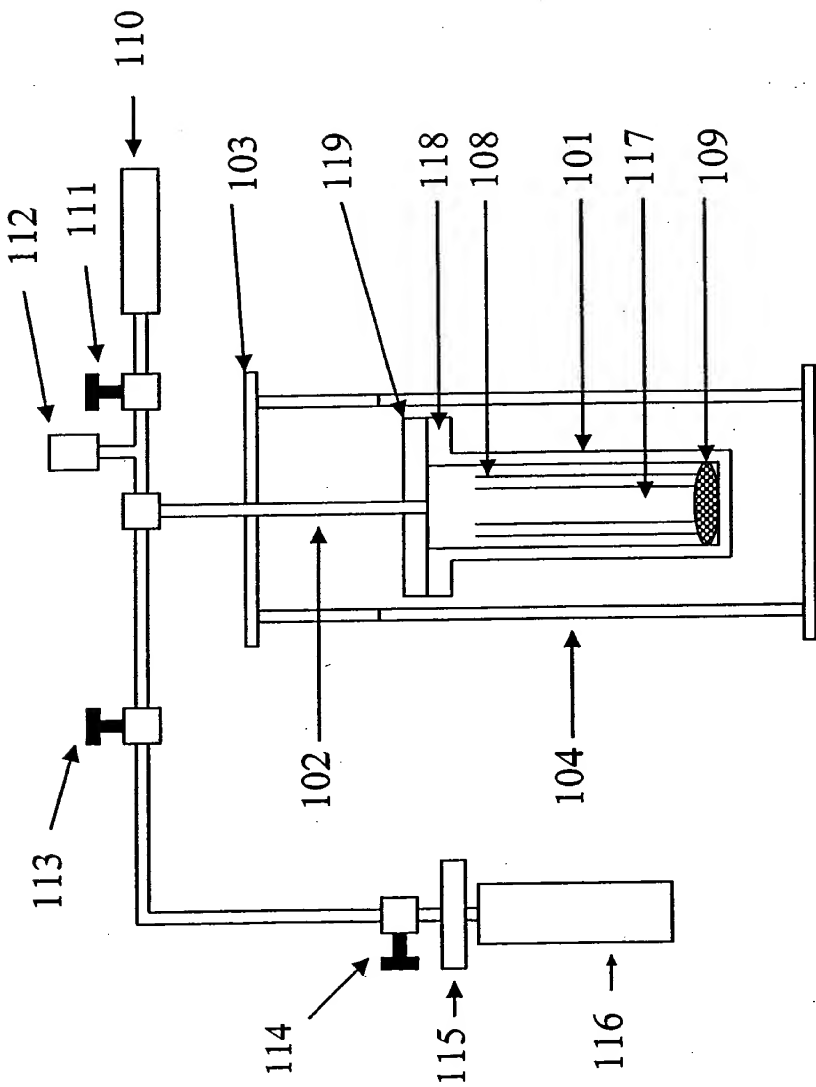
Figure 14. The 1H MAS NMR spectrum of KH^*I (green crystals) performed at Spectral Data Services relative to external tetramethylsilane (TMS).

Figure 15. The 1H MAS NMR spectrum of KH^*I (blue crystals) performed at National Research Council of Canada relative to external tetramethylsilane (TMS).

Figure 16. The 1H MAS NMR spectrum of KH^+I^- (blue crystals) performed at Grace Davison relative to external tetramethylsilane (TMS).

Figure 17. The 1H MAS NMR spectrum of KH^+I^- (blue crystals) performed at National University of Delaware relative to external tetramethylsilane (TMS).

Fig. 1



Intensity/AU

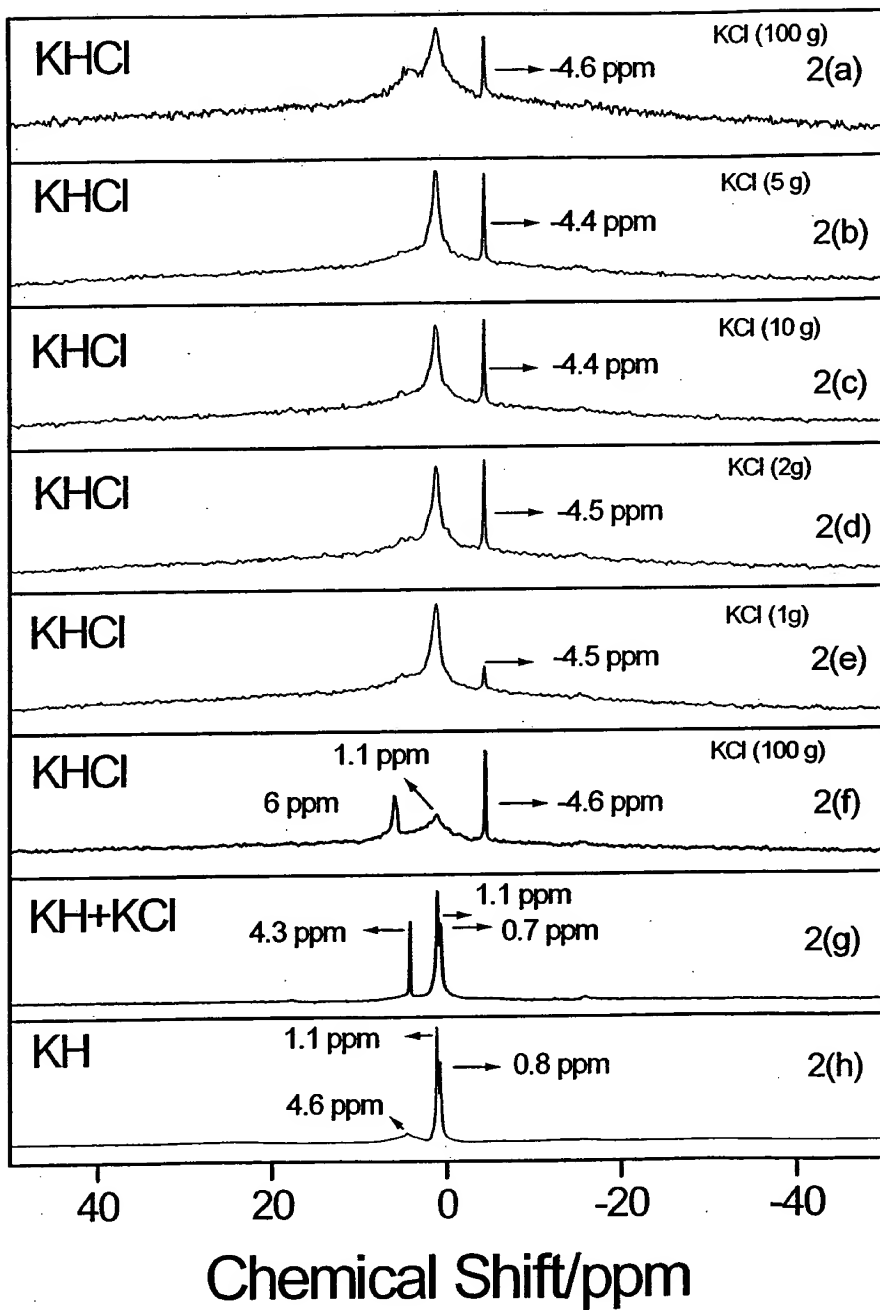


Fig. 2

Fig. 3

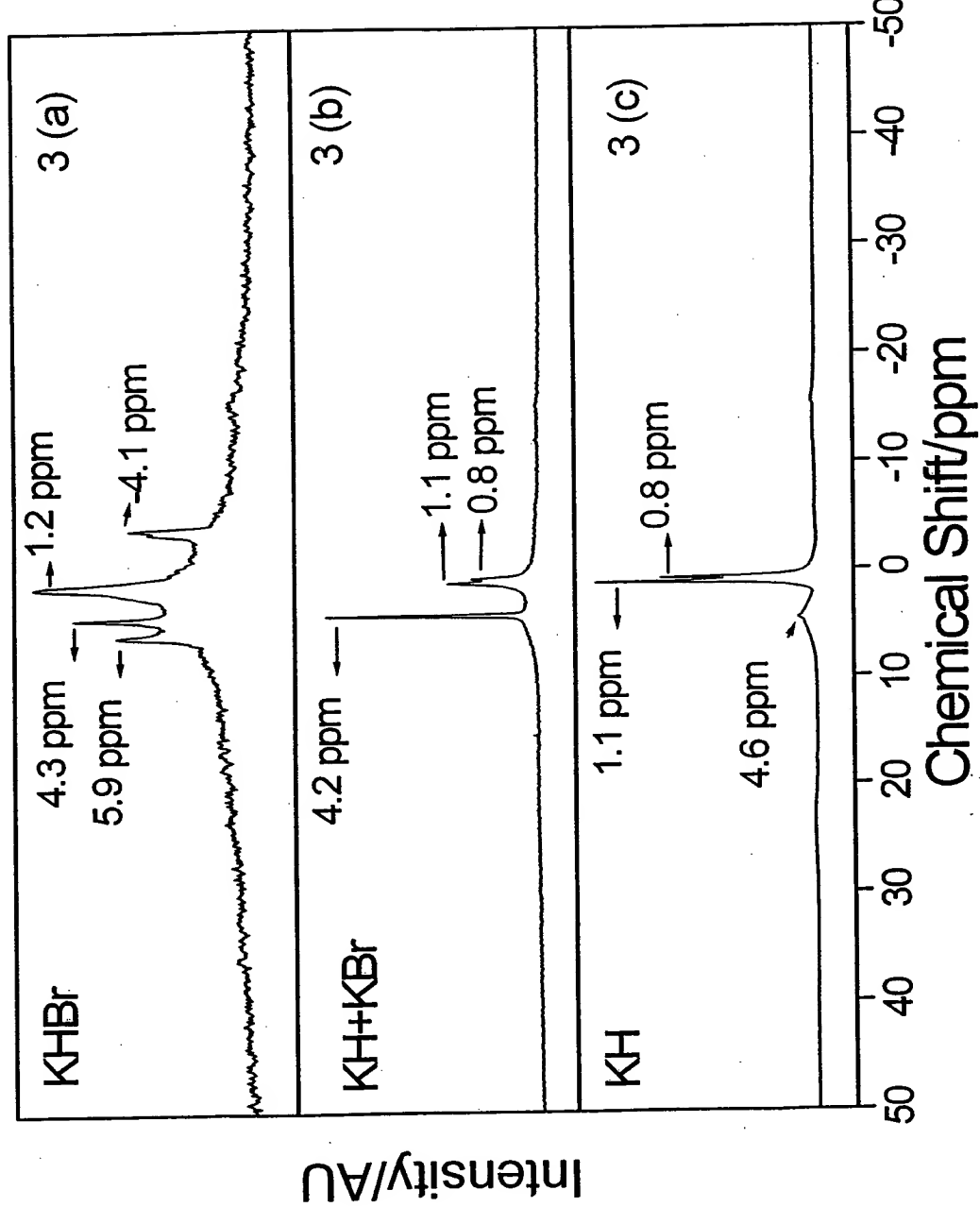


Fig. 4

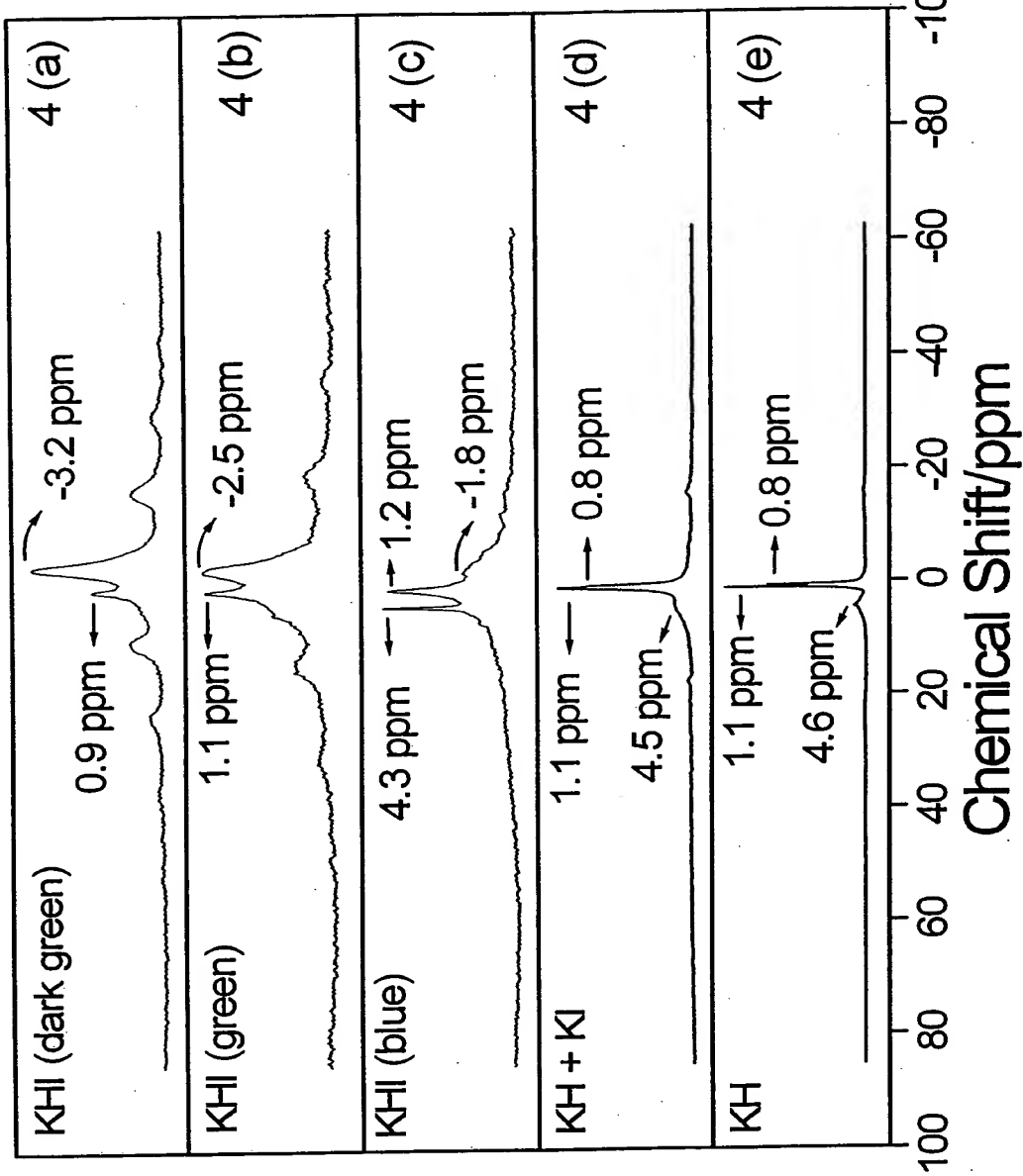


Fig. 5

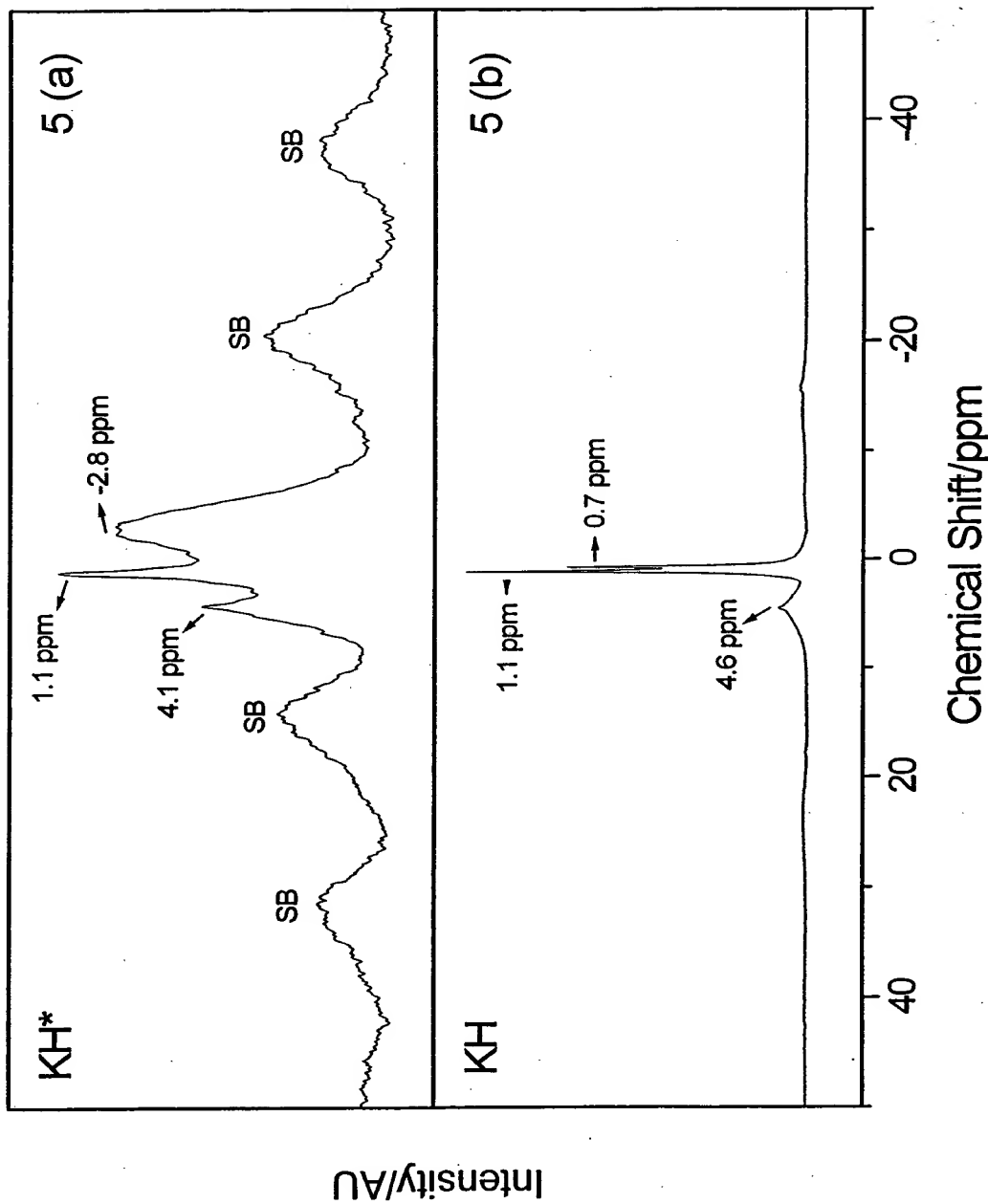
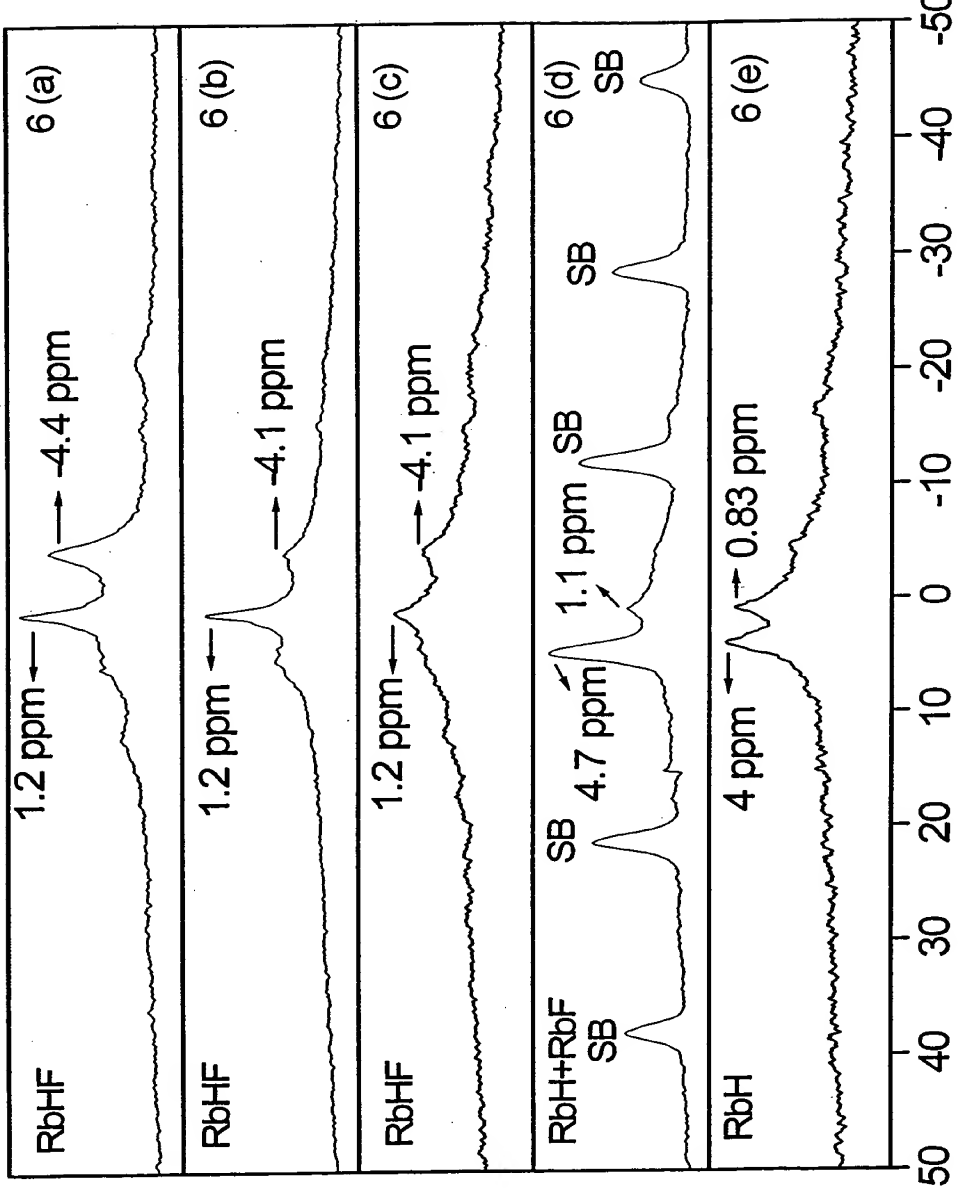


Fig. 6

Chemical Shift/ppm



Intensity/AU

Fig. 7

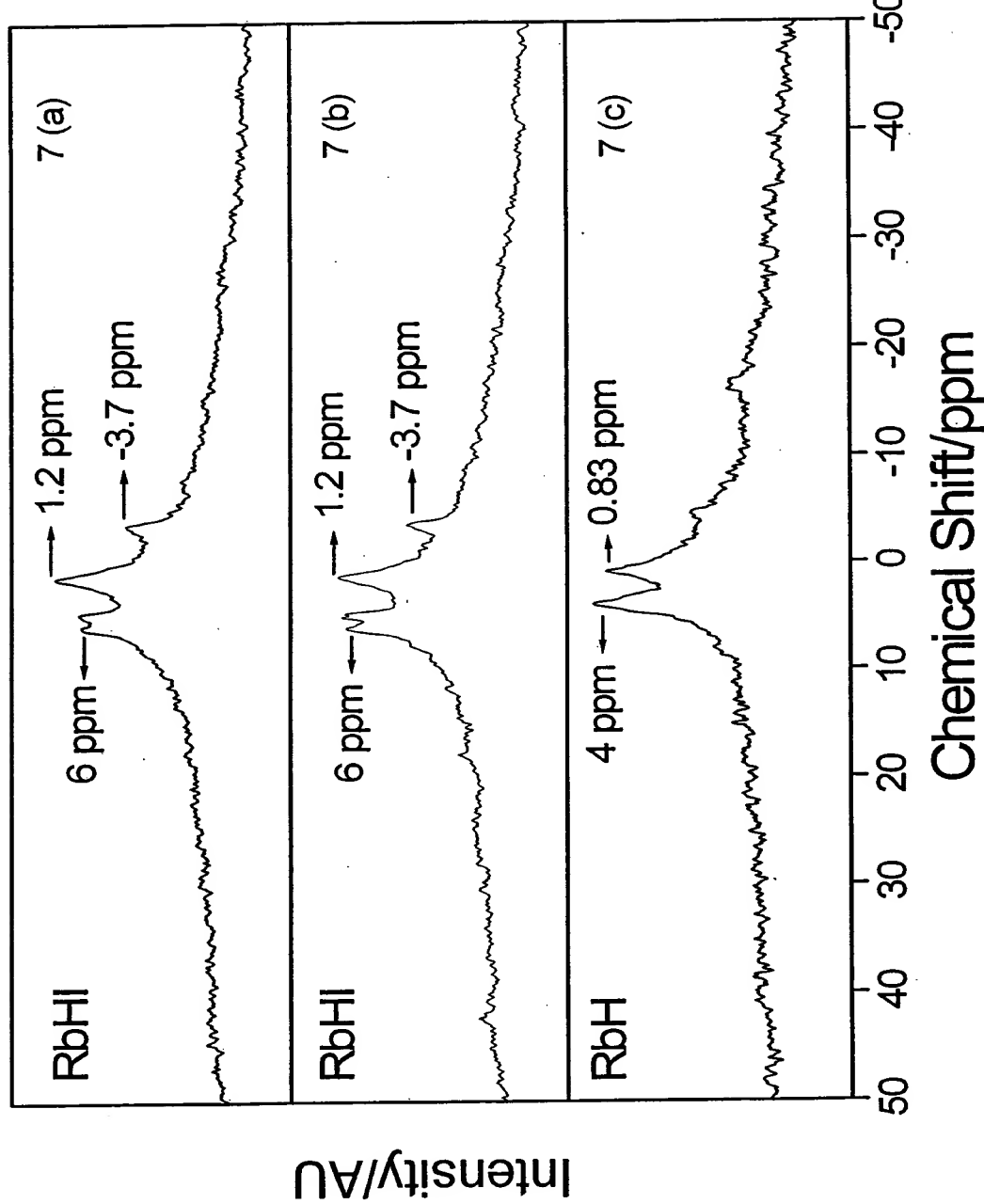
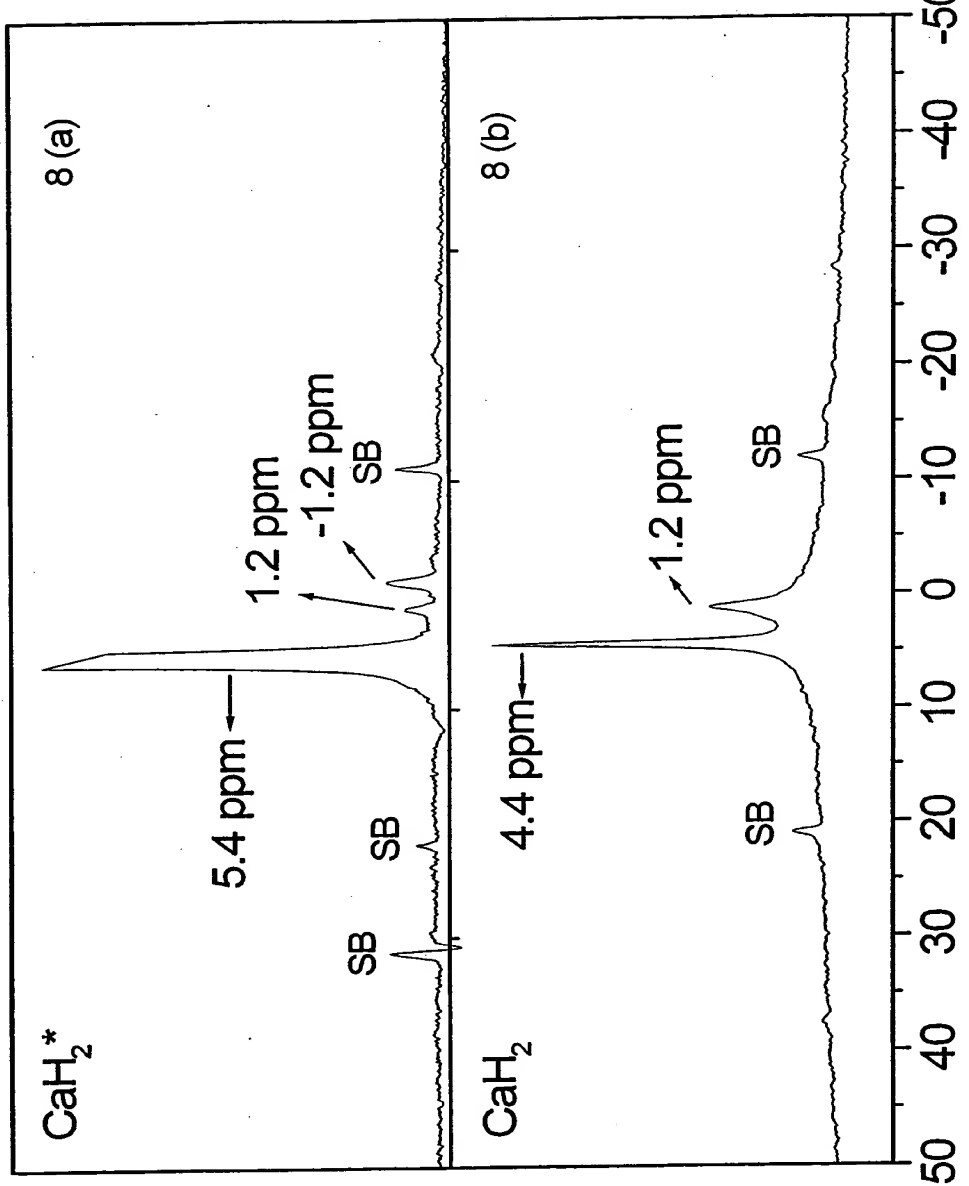


Fig. 8

Chemical Shift/ppm



Intensity/AU

Fig. 9

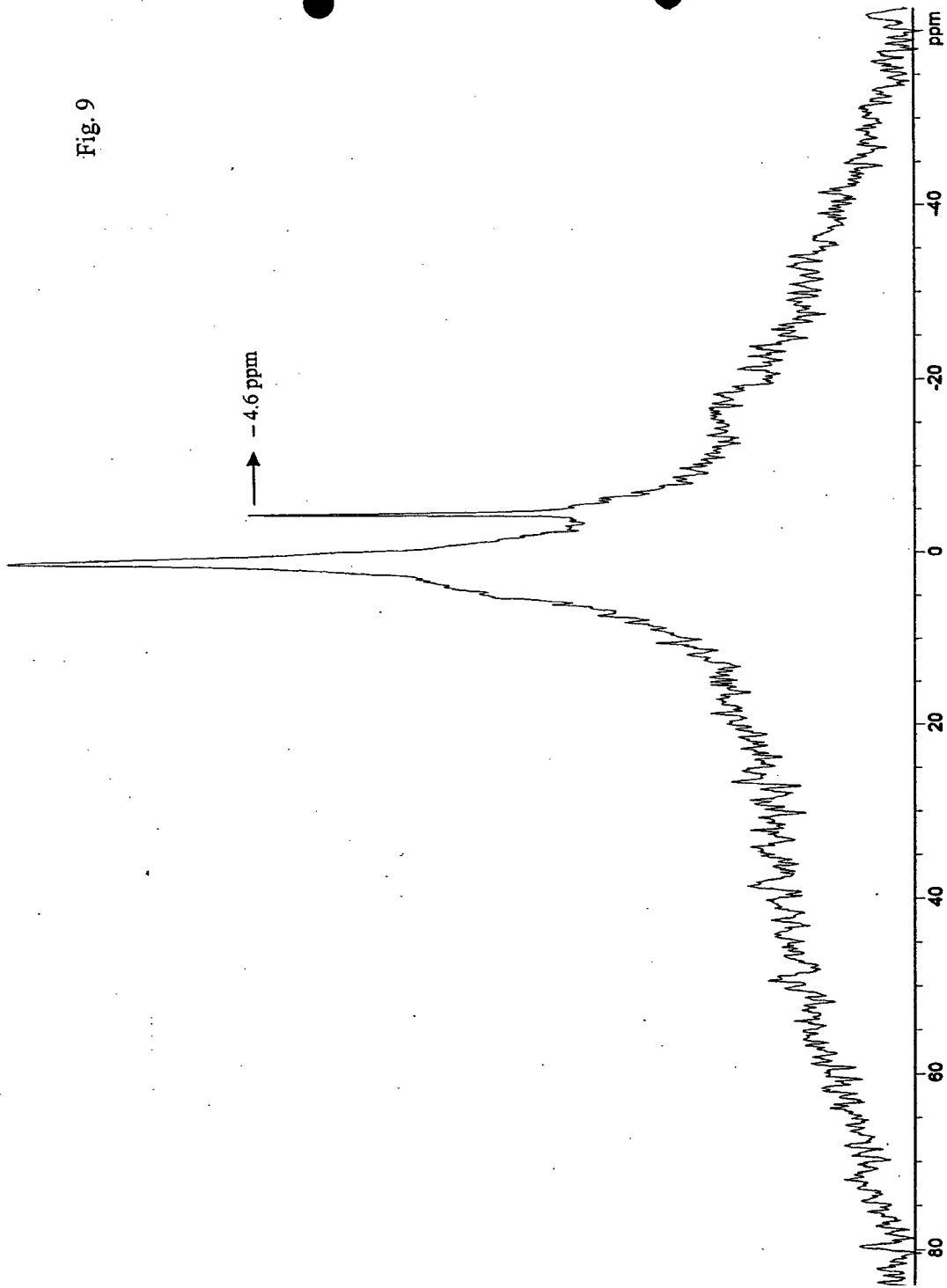


Fig. 10

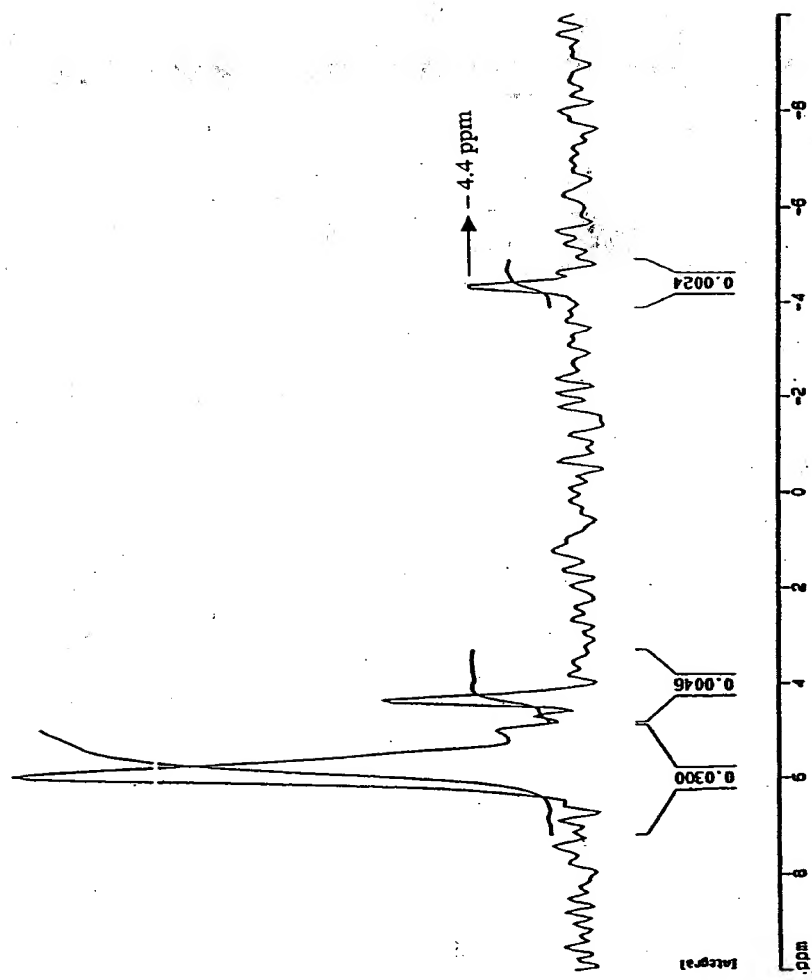


Fig. 11

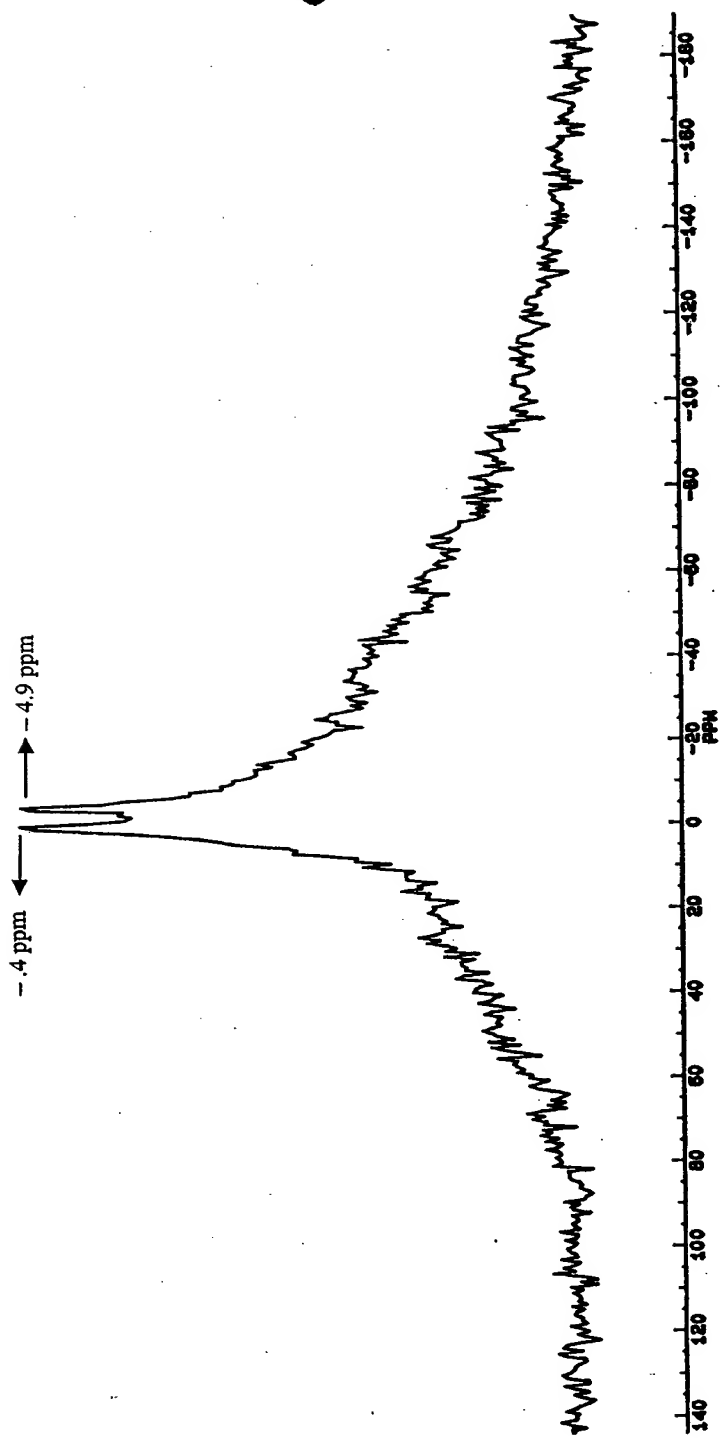


Fig. 12

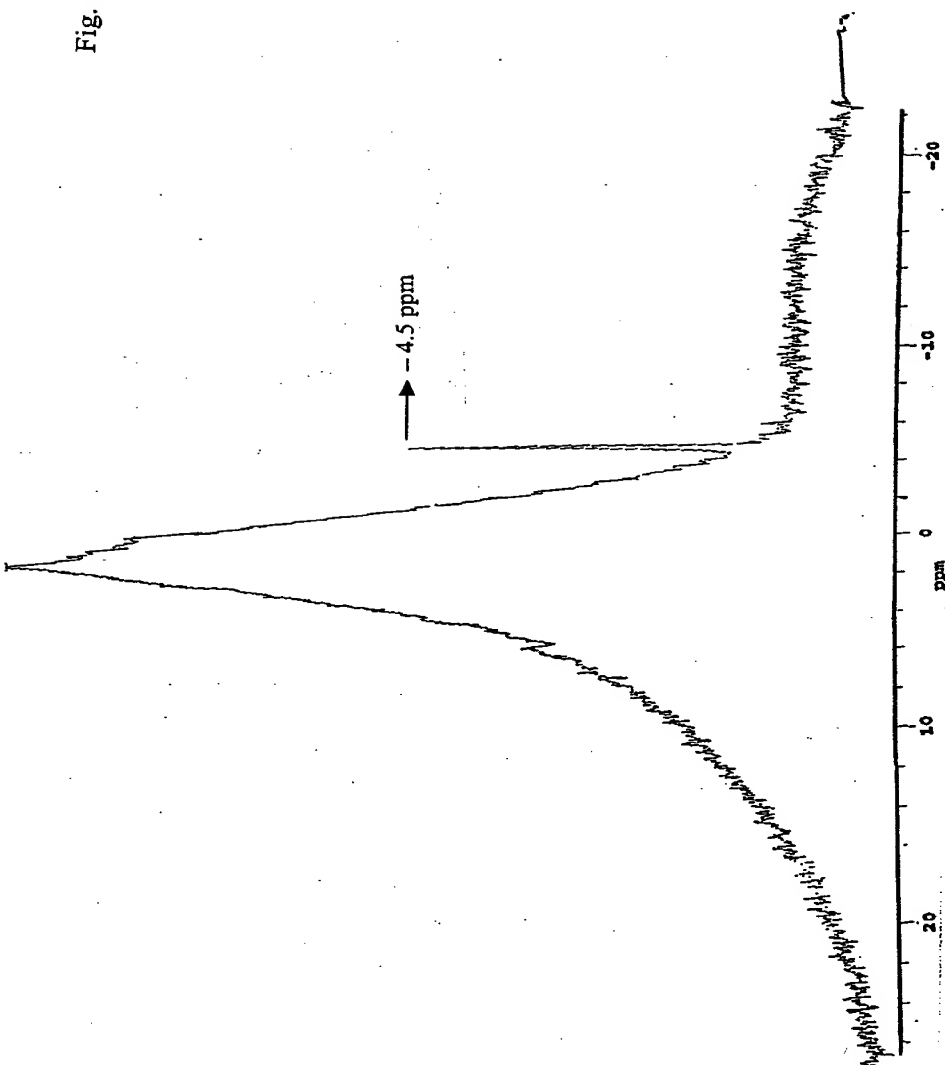


Fig. 13

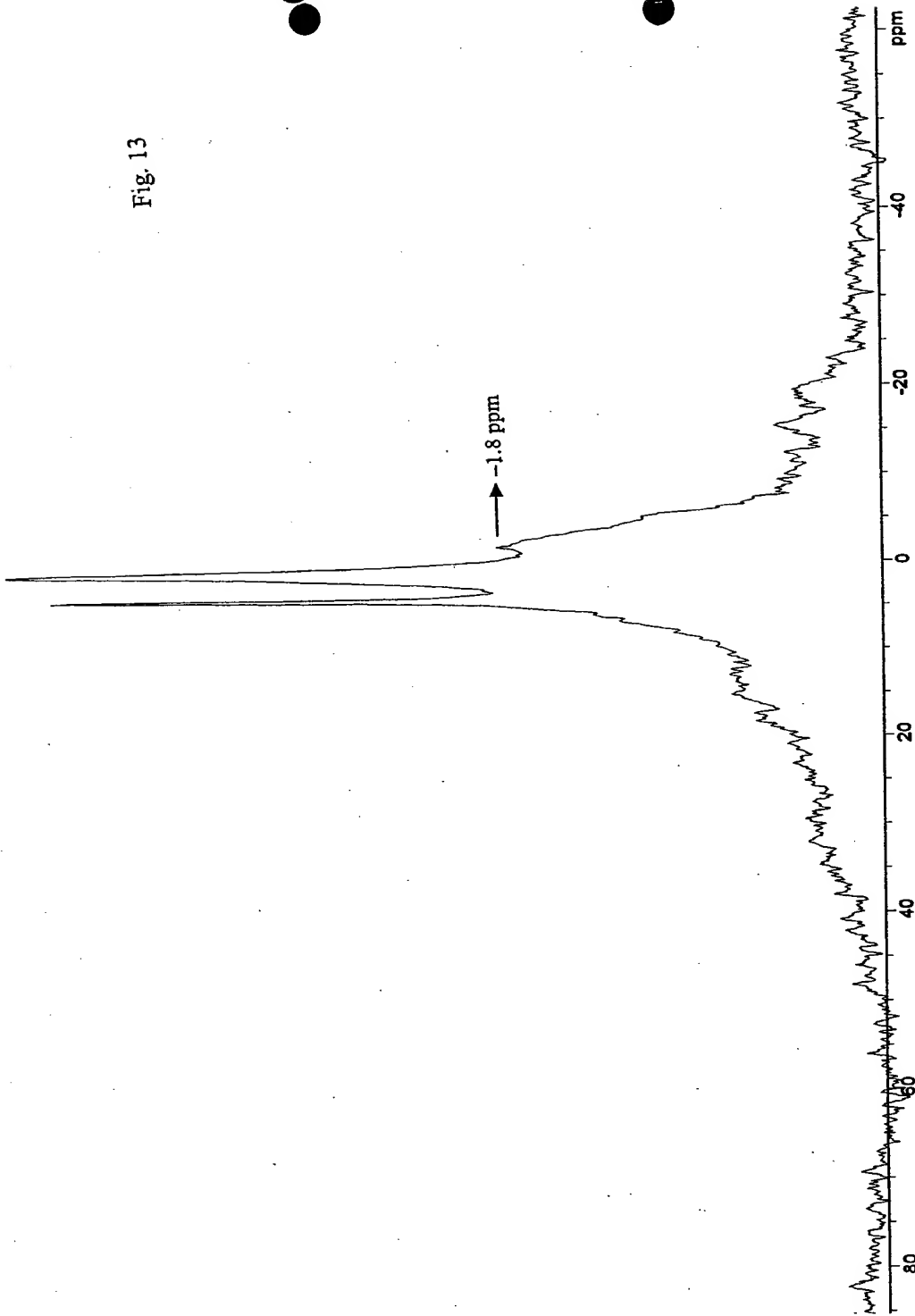


Fig. 14

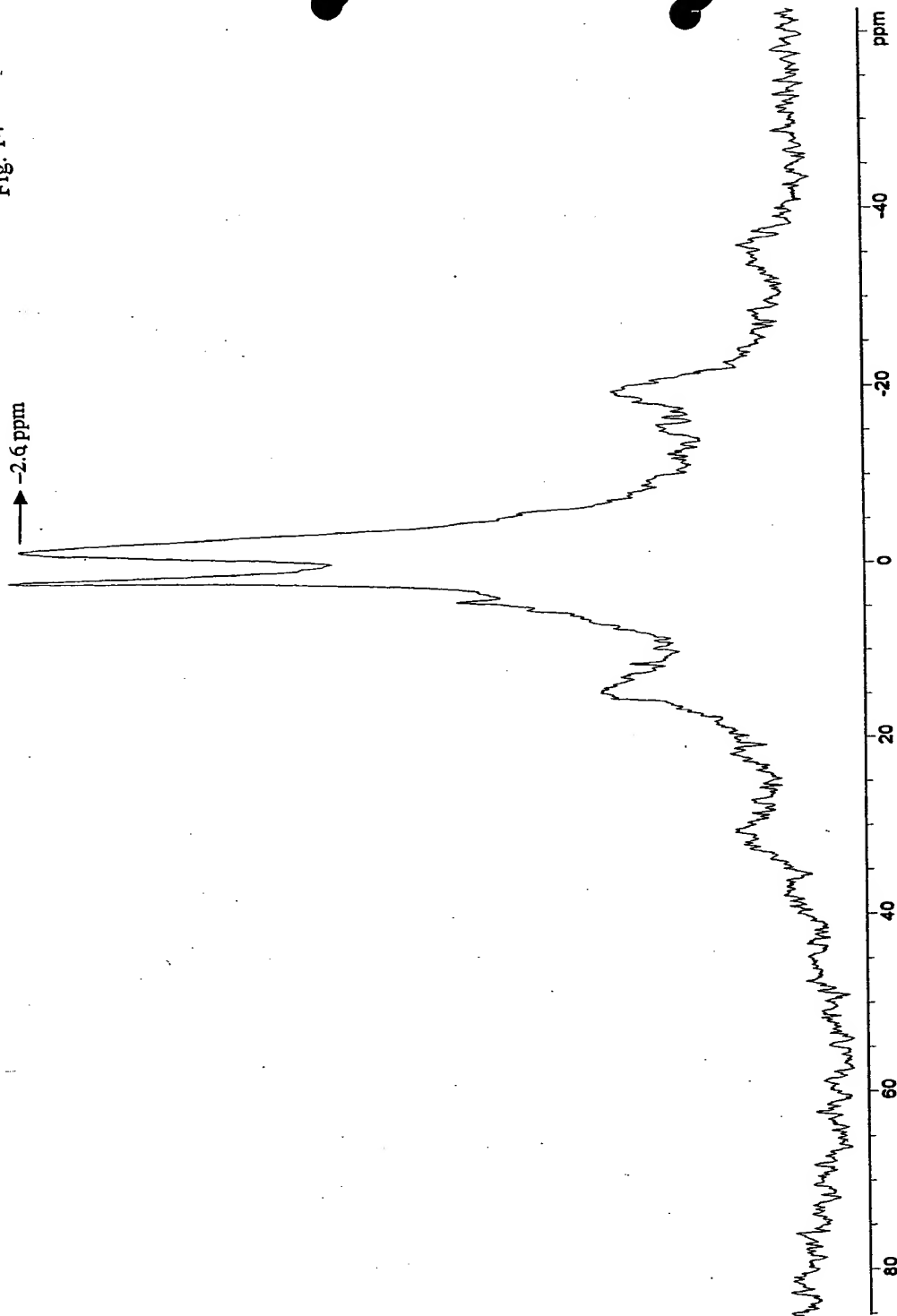


Fig. 15

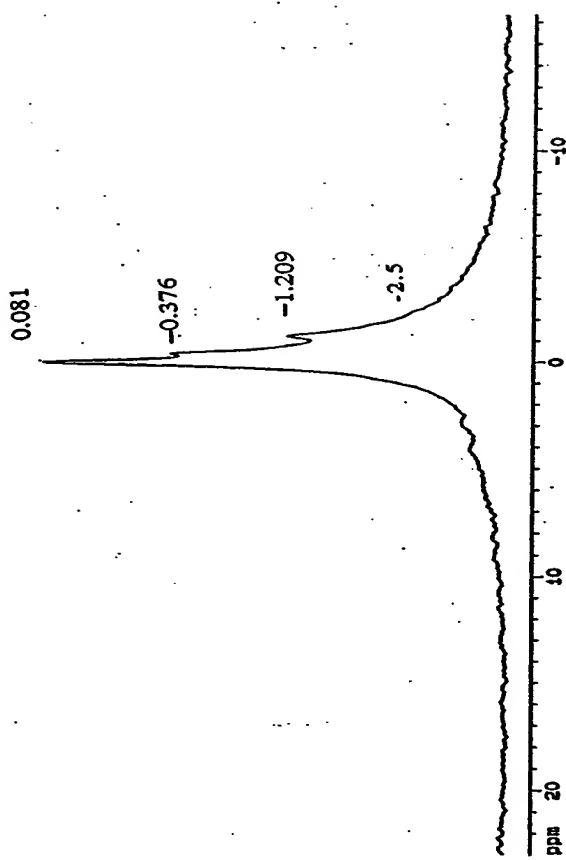


Fig. 16

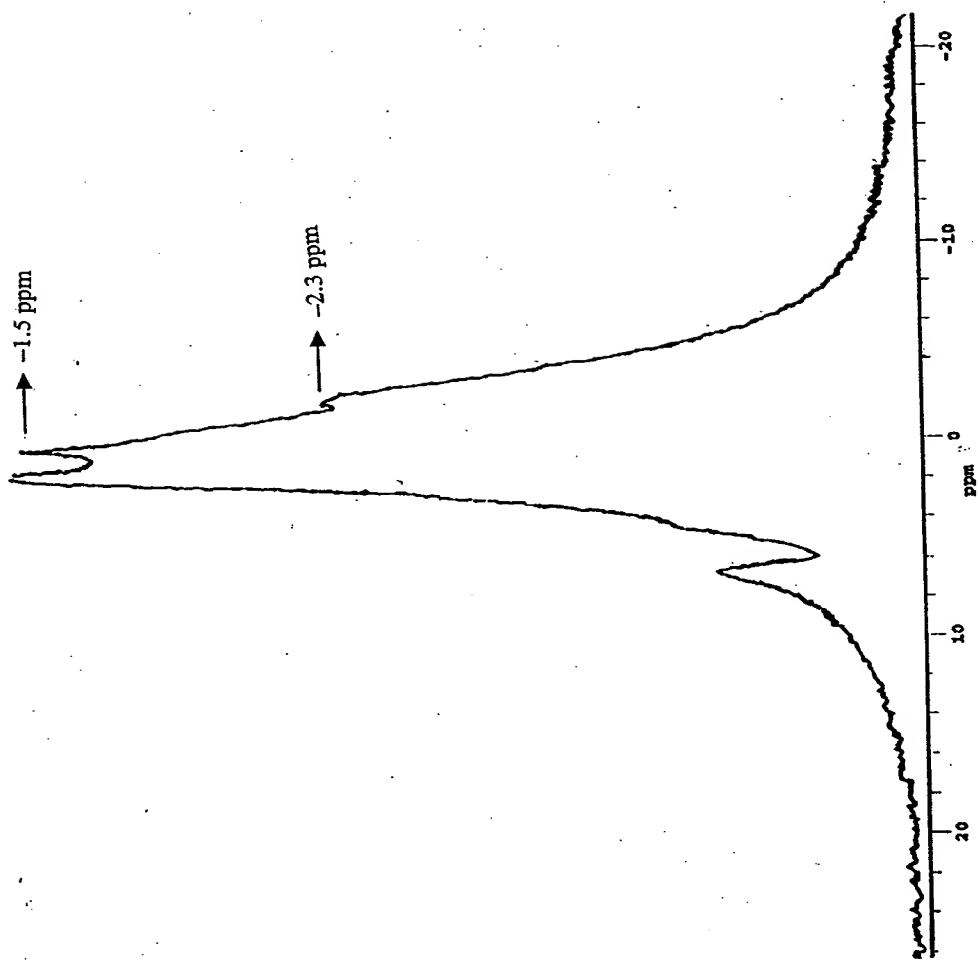
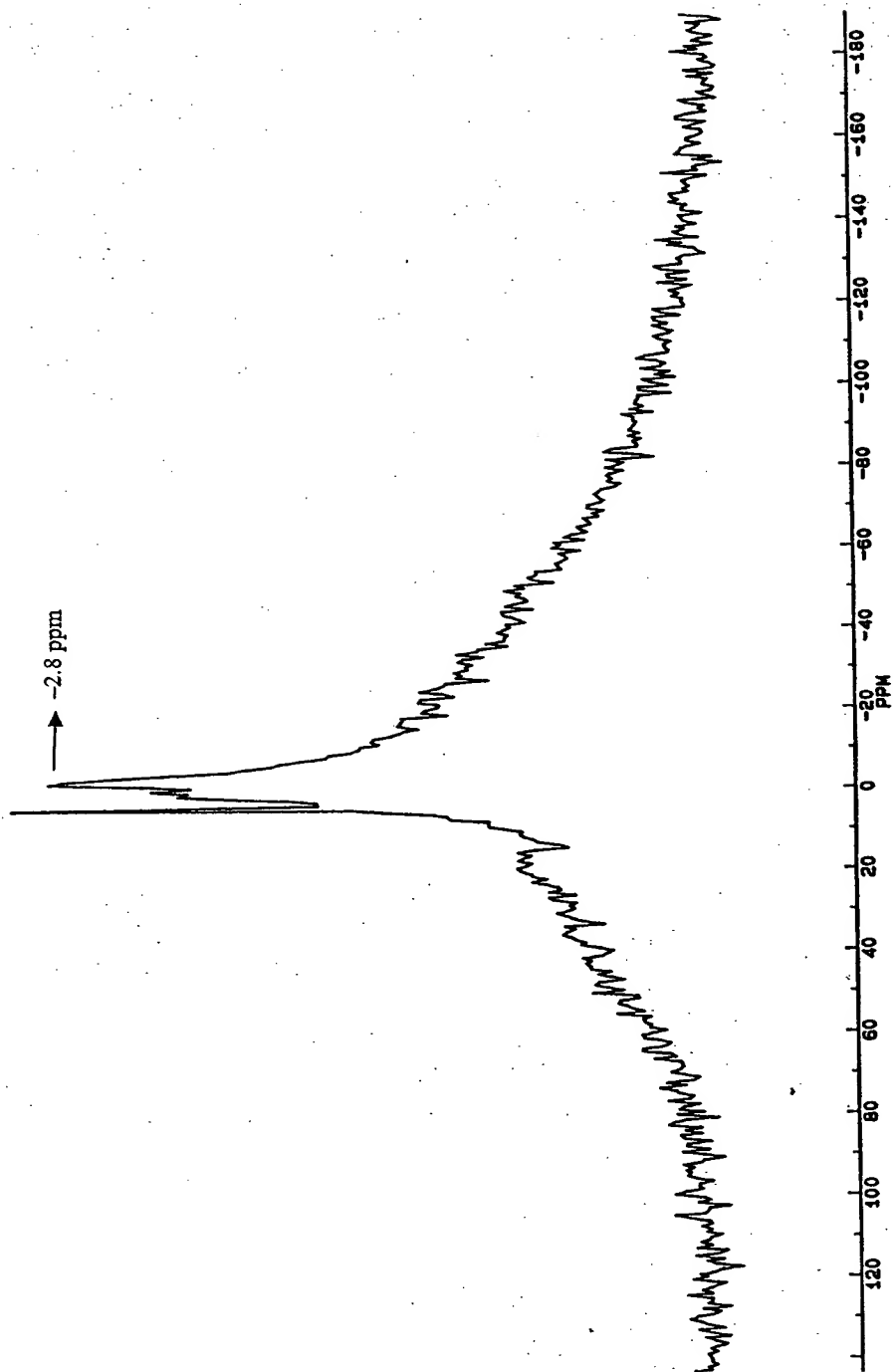


Fig. 17



Presented at International Conference on
Global Warming and Energy Policy
Ft. Lauderdale, FL
November 26-28, 2000
Sponsored by Global Foundation, Inc.
Dr. Behram N. Kursunoglu, Chairman

BLACKLIGHT POWER TECHNOLOGY

A New Clean Energy Source with the Potential for Direct Conversion to Electricity

Randell L. Mills*

1. INTRODUCTION

BlackLight Power, Inc. (the Company), a Delaware corporation based in its 53,000 sq. ft. headquarters in Cranbury, New Jersey, believes it has developed a new hydrogen chemical process that generates power, plasma (a hot ionized glowing gas), and a vast class of new compositions of matter. Specifically, the Company has designed and tested a new proprietary energy-producing chemical process. The Company has developed high-power density, high-temperature, hydrogen gas cells that produce intense light, power of orders of magnitude greater than that of the combustion of hydrogen at high temperatures, and power densities equal to those of many electric power plants. The Company is focusing on cells for generating light and plasma for lighting applications and direct conversion to electricity, respectively.

The cells generate energy through a chemical process (BlackLight Process) which the Company believes causes the electrons of hydrogen atoms to drop to lower orbits thus releasing energy in excess of the energy required to start the process. The lower-energy atomic hydrogen product of the BlackLight Process reacts with an electron to form a hydride ion which further reacts with elements other than hydrogen to form novel compounds called hydrino hydride compounds (HHCs) which are proprietary to the Company. The Company is developing the vast class of proprietary chemical compounds formed via the BlackLight Process. Its technology has far-reaching applications in many industries.

The power may be in the form of a plasma, a hot ionized glowing gas. The plasma may be converted directly to electricity with high efficiency using a known microwave device called a gyrotron, thus, avoiding a heat engine such as a turbine. The Company is

* Randell L Mills, President, BlackLight Power, Inc., 493 Old Trenton Road, Cranbury, NJ 08512, Phone: 609-490-1090, e-mail: rmls@blacklightpower.com; www.blacklightpower.com

working on direct plasma to electricity conversion. The device is linearly scaleable from the size of hand held units to large units which could replace large turbines.

There are many advantages of the technology. The energy balance permits the use of electrolysis of water to split water into its elemental constituents of hydrogen and oxygen as the source of hydrogen fuel using a small fraction of the output electricity. Additionally, pollution produced by fossil and nuclear fuels should be eliminated since no green house gases, air pollutants, or hazardous wastes are produced. As no fossil fuels are required, the projected commercial operating costs are much less than that of any known competing energy source.

The Company's process may start with water as the hydrogen source and convert it to HHCs; whereas, fuel cells typically require a hydrocarbon fuel and an expensive reformer to convert hydrocarbons to hydrogen and carbon dioxide. The Company's plasma to electric conversion technology with no reformer, no fuel cost, creation of a valuable chemical by-product rather than pollutants such as carbon dioxide, and significantly lower capital costs and operating and maintenance (O&M) costs are anticipated to result in household units that are competitive with central power and significantly superior to competing microdistributed power technologies such as fuel cells.

2. THE BLACKLIGHT PROCESS

Based on physical laws of nature, Dr. Mills theory predicts that additional lower energy states are possible for the hydrogen atom, but are not normally achieved because transitions to these states are not directly associated with the emission of radiation. Thus, the ordinary hydrogen atom as well as lower-energy hydrogen atoms (termed hydrinos by Dr. Mills) are stable in isolation. Mills theory further predicts that hydrogen atoms can achieve these states by a radiationless energy transfer with a nearby atom, ion, or combination of ions (a catalyst) having the capability to absorb the energy required to effect the transition. Radiationless energy transfer is common. For example, it is the basis of the performance of the most common phosphor used in fluorescent lighting. Thus, the Company believes hydrogen atoms can be induced to collapse to a lower-energy state, with release of the net energy difference between states. Successive stages of collapse of the hydrogen atom are predicted, resulting in the release of energy in amounts many times greater than the energy released by the combustion of hydrogen. Since the combustion energy is equivalent to the energy required to liberate hydrogen from water, a process which takes water as a feed material and produces net energy is possible. The equivalent energy content of water would thus be several hundred to several thousand times that of crude oil, depending on the average number of stages of collapse.

The Company is the pioneer of technology based on the chemical process of releasing further chemical energy from hydrogen called the "BlackLight Process." More specifically, energy is released as the electrons of hydrogen atoms are induced by a catalyst to transition to lower-energy levels (i.e. drop to lower base orbits around each atom's nucleus) corresponding to fractional quantum numbers. The lower energy atomic hydrogen product is called "hydrino," and the hydrogen catalyst to form hydrino is called a "transition catalyst." As hydrogen atoms are normally found bound together as molecules, a hot dissociator is used to break hydrogen molecules into individual hydrogen atoms. A vaporized catalyst then causes the normal hydrogen atoms to transition to lower-energy states by allowing their electrons to fall to smaller radii around the nucleus with a

release of energy that is intermediate between chemical and nuclear energies. The products are power, plasma, light, and novel HHCs.

The catalysts used and the BlackLight Process are the proprietary intellectual property of the Company. The theory, data, and analysis supporting the existence of this new form of energy have been made publicly available.¹⁻¹⁵ Also see the BlackLight Power web page: www.blacklightpower.com. Laboratory scale devices demonstrating means of extracting the energy have been operated at the Company and at independent laboratories. Results to date indicate that the process can eventually provide economically competitive products in a wide range of applications including lighting, thermal, and electric power generation. The Company's gas energy cells, even in prototype stage, are frequently operating at power densities and temperatures equivalent to those of many coal fired electric power plants and produce about 100 times the energy of the combustion of the hydrogen fuel. The plasma is permissive of a direct plasma to electricity conversion technology as well as the production of electricity by conventional heat engines. The Company currently believes that the scale-up of energy cells to commercial power generation level will require mainly the application of existing industry knowledge in catalysis and power engineering.

The lower-energy atomic hydrogen product of the BlackLight Process reacts with an electron to form a hydride ion which further reacts with elements other than hydrogen to form novel compounds which are proprietary to the Company. The Company is developing the vast class of proprietary chemical compounds formed via the BlackLight Process. Test results indicate that the properties of HHCs are rich in diversity due to their extraordinary binding energy (i.e. the energy required to remove an electron which determines the chemical reactivity and properties). This new class of matter may be comparable to carbon in terms of the possibilities of new compositions of matter. Carbon is a base element for many useful compounds ranging from diamonds, to synthetic fibers, to liquid gasoline, to pharmaceuticals. The Company believes hydrino hydride ions have the potential to be as useful as carbon as a base "element." The novel compositions of matter and associated technologies have far-reaching applications in many industries including the chemical, lighting, computer, defense, energy, battery, propellant, munitions, surface coatings, electronics, telecommunications, aerospace, and automotive industries. The Company is focusing on developing a high voltage battery and silane materials based on the novel hydride chemical products. Many additional applications of the chemical compounds are possible.

2.1 Validation

Based on the solution of a Schrödinger-type wave equation with a nonradiative boundary condition based on Maxwell's equations, Mills¹⁻¹⁵ predicts that atomic hydrogen may undergo a catalytic reaction with certain atomized elements or certain gaseous ions which singly or multiply ionize at integer multiples of the potential energy of atomic hydrogen, 27.2 eV.

For example, potassium ions can provide a net enthalpy of a multiple of that of the potential energy of the hydrogen atom. The second ionization energy of potassium is 31.63 eV, and K^+ releases 4.34 eV when it is reduced to K.¹⁶ The combination of reactions $K^+ \rightarrow K^{2+}$ and $K^+ \rightarrow K$, then, has a net enthalpy of reaction of 27.28 eV.

The reaction involves a nonradiative energy transfer to form a hydrogen atom that is lower in energy than unreacted atomic hydrogen. The product hydrogen atom has an

energy state that corresponds to a fractional principal quantum number. Recent analysis of mobility and spectroscopy data of individual electrons in liquid helium show direct experimental confirmation that electrons may have fractional principal quantum energy levels.¹⁴ The lower-energy hydrogen atom is a highly reactive intermediate which further reacts to form a novel hydride ion. Single line emission from the excited catalyst ion having accepted the energy from atomic hydrogen has been observed with the emission from the predicted hydride ion product.¹⁵ Thus, the catalytic reaction with the formation of the novel hydride ions is confirmed spectroscopically.

Typically, the emission of extreme ultraviolet (EUV) light from hydrogen gas is achieved by a discharge at high voltage, a high power inductively coupled plasma, or in hot fusion research, a plasma is created and heated by radio waves to 10s of millions of degrees with confinement of the hot plasma by a toroidal (donut shaped) magnetic field. The Company has observed intense EUV emission at low temperatures from atomic hydrogen and certain atomized pure elements or certain gaseous ions which ionize at integer multiples of the potential energy of atomic hydrogen. The Company has tested over 130 elements and compounds which covers essentially all of the elements of the periodic chart. The chemical interaction of catalysts with atomic hydrogen at temperatures below 1000 K has shown surprising results in terms of the emission of the Lyman and Balmer lines²⁻⁷ (atomic hydrogen emission ten times more energetic than the combustion of hydrogen), emission of lines corresponding to lower-energy hydrogen states and the corresponding hydride ions, and the formation of novel chemical compounds.⁸⁻¹³

Over 20 independent labs have performed 25 types of analytical experiments that confirm the Company's novel catalytic reaction of atomic hydrogen which produces an anomalous discharge or plasma and produces novel hydride compounds.²⁻¹³

Experiments that confirm the novel hydrogen chemistry include extreme ultraviolet (EUV) spectroscopy, plasma formation, power generation, and analysis of chemical compounds. For example:

1. Pennsylvania State University Chemical Engineering Department has determined heat production associated with hydrido formation with a Calvet calorimeter that showed the generation of 10^7 J/mole of hydrogen, as compared to $2.5 \times 10^5 \text{ J/mole}$ of hydrogen anticipated for standard hydrogen combustion.¹⁷ Thus, the total heats generated appear to be 100 times too large to be explained by conventional chemistry, but the results are completely consistent with Mills model.

2. Lines observed by EUV spectroscopy could be assigned to transitions of atomic hydrogen to lower-energy levels corresponding to lower-energy hydrogen atoms and to the emission from the excitation of the corresponding hydride ions.⁴

For example, the product of the catalysis of atomic hydrogen with potassium metal, $\text{H}[a_{\text{H}}/4]$ may serve as both a catalyst and a reactant to form $\text{H}[a_{\text{H}}/3]$ and $\text{H}[a_{\text{H}}/6]$. The transition of $\text{H}[a_{\text{H}}/4]$ to $\text{H}[a_{\text{H}}/6]$ induced by a multipole resonance transfer of 54.4 eV ($2.27.2 \text{ eV}$) and a transfer of 40.8 eV with a resonance state of $\text{H}[a_{\text{H}}/3]$ excited in $\text{H}[a_{\text{H}}/4]$ is represented by $\text{H}[a_{\text{H}}/4] + \text{H}[a_{\text{H}}/4] \rightarrow \text{H}[a_{\text{H}}/6] + \text{H}[a_{\text{H}}/3] + 176.8 \text{ eV}$.

The predicted 176.8 eV (70.2 \AA) photon is a close match with the 73.0 \AA line observed by a team headed by Dr. Johannes P. F. Conrads, then Director and Chairman of the Board, of Institut Fur NiederTemperatur-Plasmaphysik e.V. and the Ernst-Moritz Arndt-Universität Greifswald ("INP"), a top plasma physics laboratory in Greifswald, Germany. The energy of this line emission corresponds to an equivalent temperature of $1,000,000^\circ\text{C}$ and an energy over 100 times the energy of combustion of hydrogen.

3. Observation of intense extreme ultraviolet (EUV) emission has been reported at low temperatures ($\text{e.g.} \approx 10^3 \text{ K}$) from atomic hydrogen and certain atomized elements or certain gaseous ions.^{2,7} The only pure elements that were observed to emit EUV were those wherein the ionization of t electrons from an atom to a continuum energy level is such that the sum of the ionization energies of the t electrons is approximately $m 27.2 \text{ eV}$ where t and m are each an integer. Potassium, cesium, and strontium atoms and Rb^+ ion ionize at integer multiples of the potential energy of atomic hydrogen and caused emission. Whereas, the chemically similar atoms, sodium, magnesium, and barium do not ionize at integer multiples of the potential energy of atomic hydrogen and caused no emission.

4. An energetic plasma in hydrogen was generated using strontium atoms as the catalyst. The plasma formed at 1% of the theoretical or prior known voltage requirement with 4,000–7,000 times less power input power compared to noncatalyst controls, sodium, magnesium, or barium atoms, wherein the plasma reaction was controlled with a weak electric field.^{2,7}

5. An anomalous plasma with hydrogen/potassium mixtures has been reported wherein the plasma decayed with a two second half-life which was the thermal decay time of the filament which dissociated molecular hydrogen to atomic hydrogen when the electric field was set to zero.⁵⁻⁶ This experiment showed that hydrogen line emission was occurring even though the voltage between the heater wires was set to and measured to be zero and indicated that the emission was due to a reaction of potassium atoms with atomic hydrogen which confirms a new chemical source of power.

Reports of the formation of novel compounds provide substantial evidence supporting a novel reaction of hydrogen as the mechanism of the observed EUV emission and anomalous discharge. Novel hydrogen compounds have been isolated as products of the reaction of atomic hydrogen with atoms and ions identified as catalysts in the reported EUV studies.²⁻¹³ Novel inorganic alkali and alkaline earth hydrides of the formula MH^* and $MH^* X$ wherein M is the metal, X , is a singly negatively charged anion, and H^* comprises a novel high binding energy hydride ion were synthesized in a high temperature gas cell by reaction of atomic hydrogen with a catalyst such as potassium metal and MH , MX or MX_2 , corresponding to an alkali metal or alkaline earth metal compound, respectively.^{8,11} Novel hydride compounds were identified by (1) time of flight secondary ion mass spectroscopy which showed a dominate hydride ion in the negative ion spectrum, (2) X-ray photoelectron spectroscopy which showed novel hydride peaks and significant shifts of the core levels of the primary elements bound to the novel hydride ions, (3) proton nuclear magnetic resonance spectroscopy (NMR) which showed extraordinary upfield chemical shifts compared to the NMR of the corresponding ordinary hydrides, and (4) thermal decomposition with analysis by gas chromatography, and mass spectroscopy which identified the compounds as hydrides.^{8,11}

An upfield shifted NMR peak is consistent with a hydride ion with a smaller radius as compared with ordinary hydride since a smaller radius increases the shielding or diamagnetism. Thus, the NMR shows that the hydride formed in the catalytic reaction has been reduced in distance to the nucleus indicating that the electrons are in a lower-energy state. Compared to the shift of known corresponding hydrides the NMR provides direct evidence of reduced energy state hydride ions.

The NMR results confirm the identification of novel hydride compounds MH^* , MH_2^* , and MH_2^{*+} wherein M is the metal, H , is a halide, and H^* comprises a novel high binding energy hydride ion. For example, large distinct upfield resonances were observed at -4.6 ppm and -2.8 ppm in the case of KH^*Cl and KH^* , respectively. Whereas, the

resonances for the ordinary hydride ion of KH were observed at 0.8 and 1.1 ppm. The presence of a halide in each compound MH^*X does not explain the upfield shifted NMR peak since the same NMR spectrum was observed for an equimolar mixture of the pure hydride and the corresponding alkali halide (MH/MX) as was observed for the pure hydride, MH . The synthesis of novel hydrides such as KH^* with upfield shifted peaks prove that the hydride ion is different from the hydride ion of the corresponding known compound of the same composition. The reproducibility of the syntheses and the results from independent laboratories confirm the formation of novel hydride ions.

3. BUSINESS UNITS

The Company believes that it has created a commercially competitive new source of energy, a new source of plasma which releases rather than consumes energy, a new source of light, and a revolutionary new field of hydrogen chemistry. With its achievements of a sustained 100,000+ °C plasma of hydrogen with essentially no power input to its power cell and synthesis of over 40 novel compounds in bulk with extraordinary properties the Company is focusing on product development. Initial target products are a direct plasma to electric power cell targeted at the residential and commercial microdistributed markets and the premium power market. Additional market objectives for the plasma and chemistry technologies are lighting sources, a high voltage battery to power portable electronics and electric vehicles, and chemical products and processes based on silicon and hydrido chemistry.

The Company has two basic business units—power and chemical. The plasma-electric technology may represent a near-term huge energy market. But, in the case of a large central power plant, the Company estimates that the potential revenues from the chemicals produced with power generation may eclipse the electricity sales. However, both offer extraordinary potential revenue and profit. Since enormous power (easily convertible to electricity) is a product of the BlackLight Process, the two units can operate in tandem seamlessly.

The priorities of the Company's power business is the residential and commercial microdistributed markets and the premium power market based on its plasma-electric power cell technology. The time to market should be near term for these relatively small-scale, simple devices that are projected to be inexpensive to manufacture, service, and use, and vastly superior to competing technologies such as internal combustion engine gensets, fuel cells, and microturbines. Selected statistics on electric generation are given in Table 1.

Early adopters of BlackLight power systems are expected to be those that require premium power generated on-site. The premium power market* includes businesses where brief electrical outages can cause severe monetary loss: telecommunications sites, computer centers, server hotels, e-commerce centers, semiconductor fabrication facilities, and others. The market size was estimated to be 30,000 MW in 1999 and growth to be multiples of the entire energy market rate.¹⁸⁻¹⁹ The Glider Group and Stephens Inc.

*The premium power market is also known as the 9's market and the powercosm market. Utility grids provide 99.9% reliability, or 8 hours of disruption per year. For the Internet economy even small fractions of a second can cost millions of dollars. In high technology manufacturing industries even hours of disruption can shut down operations for days, again costing millions. More reliability is measured in %, the more 9's required (99.999...%), the smaller the fractions of a second power is disrupted, and the more valuable the power.

Table 1. Statistics on electric generation.

US Electric Market	
• \$217 billion in annual US sales (1998).	
• 43% Residential	
• 32% Commercial	
• 22% Industrial	
• 5% Other	
Capital Expenditures Required to Meet New Generation Demand	
• Estimated at \$90 Billion Globally with 10% in US in 1999	
• \$21 Billion will be spent on Premium Power in 2000	
• \$30 Billion in 2002	
• \$50 Billion in 2005	
Premium Power Consumption/Demand	
• Estimated to be 30,000 MW in 1999	
• Estimated to be 500,000 MW in 2000	
• Double digit growth expected over next five years	
Cost Per KWH of Alternative Energy Sources	
Coal	4-5 ¢
Natural Gas	4-5 ¢
Oil	4-5 ¢
Nuclear Power	5-6 ¢
Hydroelectric	4-7 ¢
Geothermal	5-8 ¢
Wind	5-9 ¢
Solar	10-12 ¢
Photovoltaic	30-40 ¢
BlackLight *	<1 ¢

Table 2. Competitive Advantages of The BlackLight Power Process.

Cost Per KWH of Alternative Energy Sources	
Coal	4-5 ¢
Natural Gas	4-5 ¢
Oil	4-5 ¢
Nuclear Power	5-6 ¢
Hydroelectric	4-7 ¢
Geothermal	5-8 ¢
Wind	5-9 ¢
Solar	10-12 ¢
Photovoltaic	30-40 ¢
BlackLight *	<1 ¢

*Cost figures include operating, maintenance, capital generating expense of plasma-electric system (Source: EPRI, BLP)

estimates²⁰⁻²¹ that this market is 15% of the current US energy market; and will be 30-50% within 3-5 years as the internet economy build-out continues. This market is characterized by early adoption of emerging technologies and an insensitivity to cost. For example, a typical rate is over \$1,000 per kWh rate and the rate for the upper-end of the reliability scale, six 9's reliable power, is about \$1 million per kWh compared to 5 ¢ per kWh for three 9's power supplied by the grid. The premium power market is a multi-billion dollar market. The current equipment market is \$21 billion in hardware alone and is projected to ellipse the profitability of the entire utility market in the near term.²²

BlackLight's Energy Systems design advantages are: virtually instantaneous turn on/off, simplicity, easy logistics, low capital cost, low operational and maintenance cost, easy redundancy (for reliability), and no pollution. With our current design, BlackLight projects capital costs around \$25-100 per kW, and very low generation cost (<\$0.01 per kWh). This is lower than competitive solutions, but in this market segment cost is not a driver. Our chief competitors are reciprocating engine-based gensets built by Catapillar, Cummins, and others. Additional competition might be from newer entrants: microturbines and fuel cells. The former competitors, fossil-fueled engines, have an advantage because they are an incumbent technology, but they will not be able to significantly improve their reliability, have a short lifetime, do not meet pollution requirements, and can not reduce their O&M costs to be competitive with our solution. The latter competitors have a slight advantage in name recognition relative to BlackLight, but microturbines and fuel cells are not suited for the premium power market. Fuel cells and turbine systems take too long to start up, and are difficult to harmonize with grid-supplied power. Thus they are ineffective at improving power reliability.

Due to superior performance of its technology, the Company expects early adoption by the premium power market with expansion into the broader microdistributed market. The broader market which includes hundreds of millions of homes and businesses in the US and Europe will be drawn by significant cost savings and increasing unreliability of the grid with a lack of viable microdistributed alternatives. The populace of the third world, particularly Asia, represents a further enormous market opportunity for which

BlackLight technology is particularly suited, since in addition to very low capital and O&M costs, no fuel or electrical grid infrastructure is required.

In terms of its development strategy for large scale systems, the Company has decided to focus on developing the chemical business unit as a first priority over large power plants. In addition to the possibility of larger revenue, the chemical business offers several other initial advantages. A power generation plant based on thermal energy would have to be scaled-up while maintaining current or higher levels of power density before it could be commercialized. Scaling up to a power plant of very large proportions has engineering risks. While there are engineering risks associated with the scale-up for chemical production, they are not as daunting. Some potential product areas such as electronics are projected to have very high value in small quantity. Moreover, in terms of gaining widespread scientific and commercial acceptance for the BlackLight Process, it is relatively easy to validate the properties of a chemical compound. A solid chemical compound is a product that can be examined directly and its existence proven unequivocally—it either exists or it doesn't. This also means that its patents are well defined and easy to defend. The products are much more diverse, so broad industry adoption is anticipated.

In addition to direct cell power to electric power conversion, thermal power from the plasma produced by the BlackLight Process may be converted to electricity by powering a turbine. Contemporary central station thermal generation systems have been optimized to match their respective thermal sources. Since BlackLight-technology is not combustion or nuclear, an opportunity exists to dramatically reduce the complexity of the generation station. The BlackLight Process may be used as a thermal source for central or distributed power through use of a modified steam or gas turbine. The BlackLight adaptation of the steam-based system replaces the heat source of the boiler with the gas cell. The BlackLight adaptation of the gas turbine replaces the combustor of a conventional machine with a gas cell and a heat exchanger incorporating the BlackLight Process. High pressure air from the compressor is heated by the BlackLight energy cell heat exchanger before expanding through the power turbine. The exhaust would contain no combustion products. With energy production from hydrogen at a hundred times combustion energy, fuel cost would become an inconsequential consideration, and refueling intervals would be consistent with other maintenance. Alternatively, an on-site electrolysis system producing hydrogen from water could provide unlimited fuel with periodic additions of small quantities of water.

A typical chemical plant is projected to produce 100 MW electric power as a side product. Power and chemical cells may be fabricated using readily available materials, and systems such as steam or gas turbine systems are scalable over a large range [e.g. distributed units (1 MW) to central power plants (1 GW)]. The projected cost for a combined chemical and energy plant is about \$250/kW. The two functions could work seamlessly together and generate a dual income stream with a reduction of business risk. Rather than producing nuclear or fossil fuel waste which requires disposal, the BlackLight chemical plant will produce HHCs which have potential for far-reaching applications in many industries such as batteries for electric vehicles at significant earnings. For example, a 100 MW chemical plant is projected to produce \$300 M in electric vehicle battery revenue from 200,000 batteries with \$23 M from electricity sales at 3 ¢ kWh.

4. SOLUTION TO THE ENERGY PROBLEM?

The world's current energy system is unsustainable. Furthermore, the world's current energy system is not sufficiently reliable or affordable to support widespread economic growth. The productivity of one-third of the world's peoples is compromised by lack of access to commercial energy, and perhaps another third suffer economic hardships and insecurity due to unreliable energy supplies.²³

Solar and wind power are prohibitively expensive. Billions of dollars have been spent to harness the energy of hydrogen through hot fusion using extremely hot plasmas created with enormous energy input using complex, expensive systems. By contrast, the Company's reactions indicate that over 100 times the energy of its combustion is released from hydrogen with the formation of a plasma as a by-product at relatively low temperatures with simple, inexpensive systems. And, in the Company's reactors, the plasma may be converted directly to electricity with high efficiency avoiding a heat engine such as a turbine. In addition, rather than producing radioactive waste, the BlackLight Process produces compounds having extraordinary properties. The implications are that a vast new energy source and a new field of hydrogen chemistry have been discovered.

The advantages of the BlackLight process over existing energy forms, such as fossil fuels and nuclear power, include: (1) the water, which is the fuel for the process, is safe and inexpensive to contain; (2) the reaction is prospectively easily controlled; and (3) the byproduct, HHCs, have great potential commercial value. The projection of the capital cost per kilowatt capacity of a gyrotron system may be an order of magnitude less than that of the typical capital cost for a fossil fuel system and two orders of magnitude less than that of the typical capital cost for a nuclear system. The power cell may also be interfaced with conventional steam-cycle or gas turbine equipment used in fossil fuel power plants. In either case, fuel costs are eliminated since the fuel, hydrogen, can be generated by a fraction of the electrical output power. The cost factors per kilowatt/hour are the capital, maintenance and operation costs of the gas cell and plant. These costs are further reduced by elimination of the costs of handling fossil fuels and managing the pollution of the air, water, and ground caused by the ash generated by fossil fuels.

4.1. BlackLight Distributed Generation

Central station generation and distribution, the mainstay of electrical power production for the last 100 years worldwide, is now being supplemented in an increasing number of areas by smaller power units closer to the end-user group. Most distributed-generation units are in the capacity range of 100 kW-3 MW (electric), but some could be as large as 250 MW (electric). Distributed generation solves some of centralized power's inherent problems of transmission and distribution line losses, electromagnetic pollution fears from high-tension lines, cost and difficulty of transmission-line maintenance, and inefficiencies in load factor design of power plants (wherein the use of a 20% capacity safety factor is still a common industry practice when estimating peak loading). The Company's technology may be ideal for distributed generation with significant reductions in grid complexity and generation capital equipment requirements.

The Company projects that the residential market may be broadly served by a 25 kW unit, and the commercial market may be broadly served by modular 1 MW units. This approach may replace the grid since in addition to avoidance of line losses, a major economic advantage of distributed power is the avoidance of transmission tariffs which

could amount to 50% of the cost of electricity to a customer. Using BlackLight's distributed power generation technology, considerable savings can be realized by eliminating the transmission and distribution capital equipment, operations, and maintenance costs. Also, energy can be saved, given that electricity "demand" also includes substantial transmission and distribution losses from the traditional central-station type power generation systems. These considerations are important considerations for developing nations.

As the world's population grows from about 6 billion (in 1999) to an estimated 7 billion by 2010, most of the new energy demand will come from less-developed countries (LDCs), as these countries' living standards increase. LDC energy demand has long been answered by economic development programs generally aimed at the development of large, central-station power plants. These do not adequately address the thermal and lighting needs of the half the world's population which is poor, many of whom still use carbon fuels for these purposes. The solution for LDC's may be distributed power facilitated by BlackLight Power technology since no fuel, power plant, or transmission grid infrastructure is required.

5. BLACKLIGHT POWER TECHNOLOGY—A NEW PARADIGM IN ENERGY AND ELECTRICITY GENERATION

The products of the BlackLight Process are power, plasma, light, and novel HHCs. Using advanced catalysts in its gas power cell, the Company has sustained an energetic plasma in hydrogen at 1% of the theoretical or prior-known voltage requirement and with 1000's of times less power input in a system wherein the plasma reaction is controlled with a weak electric field. A plasma is a very hot, glowing, ionized gas. The plasma is produced from reactions which release energies over 100 times the energy of the combustion of hydrogen and correspond to an equivalent electron temperature of over 1,000,000 °C. The plasma produced in the Company's cells cannot be produced by any chemical reaction other than the Company's process.

Typically, a heat engine such as a turbine is used for converting heat into electricity. However, plasma power may be directly converted into electrical power. The technology is not based on heat. Thus, heat sinks such as a river or cooling towers as well as thermal pollution are largely eliminated. Based on research and development in this area of converters, the Company expects that routine engineering will result in devices that have

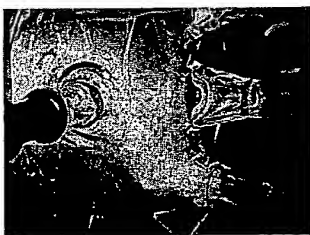


Figure 1. Plasma Generated by the BlackLight Process.

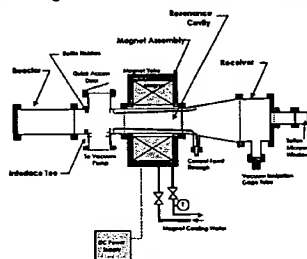


Figure 2. Gyrotron Schematic.

higher conversion efficiencies than turbines. The device is linearly scaleable from the size of hand held units to large units which could replace large turbines. And, unlike turbine technology wherein the cost per unit capacity soars with miniaturization, the Company anticipates that the unit cost per capacity will be insensitive to scale. The Company anticipates applications for its technology in broad markets such as premium power, microdistributed power, motive power, consumer electronics, portable electronics, telecommunications, aerospace, and uninterrupted, remote, and satellite power supplies.

Plasma may be directly converted into electricity using a device called a gyrotron which is established technology for converting energetic electrons into microwaves. Conventionally the source of energetic electrons comprises an electron beam or a plasma formed by electrical input such as a high voltage discharge. Prior to the development of the Company's technology, it was not possible to generate a plasma in hydrogen chemically. The BlackLight Process generates an energetic plasma in hydrogen which is a new source of energy.

The energy released by the catalysis of hydrogen to form HHCs produces a plasma in the cell. The energetic electrons of the plasma produced by the BlackLight Process are introduced into an axial magnetic field where they undergo cyclotron motion. The force on a charged ion in a magnetic field is perpendicular to both its velocity and the direction of the applied magnetic field. The electrons of the plasma orbit in a circular path in a plane transverse to the applied magnetic field for sufficient field strength at an ion cyclotron frequency ω_c that is independent of the electron velocity. Thus, a typical case which involves a large number of electrons with a distribution of velocities will be characterized by a unique cyclotron frequency that is only dependent on the electron charge to mass ratio and the strength of the applied magnetic field. There is no dependence on their velocities. The velocity distribution will, however, be reflected by a distribution of orbital radii. The electrons emit electromagnetic radiation with a maximum intensity at the cyclotron frequency. The velocity and radius of each electron may decrease due to loss of energy and a decrease of the temperature.

The gyrotron comprises a resonator cavity which has a dominate resonator mode at the cyclotron frequency. The plasma contains electrons with a range of energies and trajectories (momenta) and randomly distributed phases initially. Electromagnetic oscillations are generated from the electrons to produce induced radiation due to the grouping of electrons under the action of the self-consistent field produced by the electrons themselves with coherent radiation of the resulting packets. In this case, the device is a feedback oscillator. The theory of induced radiation of excited classical oscillators such as electrons under the action of an external field and its use in high-frequency electronics is described by A. Gaponov et al.²⁴ The electromagnetic radiation emitted from the electrons excites the mode of the cavity and is received by a resonant receiving antenna.

The radiated power and the power produced by the BlackLight Process may be matched such that a steady state of power production and power flow from the cell may be achieved. The rate of the hydrogen catalysis reaction may be controlled by controlling the total pressure, the atomic hydrogen pressure, the catalyst pressure, the particular catalyst, and the cell temperature. Very fast response times may be achieved by controlling the rate of reaction and plasma formation with an applied electric or magnetic field which influences the catalysis rate. Plasma and a gyrotron can respond essentially instantaneously. Thus, unpreceded load following capability is possible.

The gyrotron relies on established microwave technology which may achieve very high efficiencies (e.g. 80%) conversion of energetic electrons into microwaves.²⁵ A 0.1

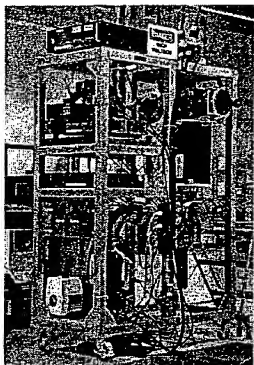


Figure 2. Gyrotron Prototype.

Table 3. Economics of International Fuel Cells Corp.

Basis: Installed Cost < \$1,000/kW DOE Credit—\$3,000/kW	
Capital Recovery Factor—12%	
Annual Load Factor—95% (8,322 hrs of operation)	
Electric Efficiency (higher heating value)—36%	
Heat Rate—9,480 Btu / kWh	
Waste Heat Recovery as Hot Water	
(Equivalent to 875,000 Btu/hr of fuel input at 80% efficiency)	
Implicit Overall Thermal Efficiency—82%	
Natural Gas Cost—\$3.50 / million Btu	
<i>Cents/kWh</i>	
Capital Charges	4.3
Fuel	3.3
O&M	2.0*
Subtotal	9.6
Hot Water Credit	-1.5
Net Power Cost	8.1

* Includes \$600/kW overhaul costs every six years

Tesla magnetic field will produce about 2.5 GHz microwaves. The microwaves are then rectified into DC electricity. Rectification efficiency at 2.5 GHz is about 95%.²⁶⁻²⁹ The DC electricity may be inverted and transformed into any desired voltage and frequency with conventional power conditioning equipment.

The plasma formed by the BlackLight Process and the gyrotron have been tested independently. Current work is in progress on testing gyrotron powered by the BlackLight Process generated plasma.

5.1. Power Balance Analysis

The commercial unit would comprises a 3-stage power generator. Stage 1 would be electrolysis to provide hydrogen fuel; stage 2—production of plasma in a gas cell; and stage 3—conversion of plasma to microwaves to electricity.

Using even relatively conservative assumptions for reaction yield and power density, a competitive power generation unit appears easily possible: (1) Production of about 100 times electrical power as electrolysis power; (2) Production of *green* emission (oxygen only) zero CO_2 emission; (3) No fossil-fuel combustion by-products; (4) Essentially no waste heat since the gyrotron is not a heat engine; (5) Tremendously more efficient at energy conversion to electricity; and (5) Projected to dominate the home and microdistributed markets.

5.2. Comparison with Competing Microdistributed Technologies

The Company's process may start with water as the hydrogen source and convert it to HHCs; whereas, fuel cells typically require a hydrocarbon fuel and an expensive reformer to convert hydrocarbons to hydrogen and carbon dioxide. The Company's plasma to electric conversion technology with no reformer, no fuel cost, creation of a valuable chemical by-product, and significantly lower capital costs and O&M costs are anticipated to result in household units that are competitive with central power and significantly

superior to competing microdistributed power technology such as fuel cells and micro combustion turbines. With a focus on large scale production of microdistributed devices, the Company anticipates rapid penetration of the electricity energy market. In this case, the Company plans to form strategic alliances with component manufacturers, systems assemblers, and service companies to provide power for consumers with units under lease or by sale. The service companies may be utilities. Other services or utility companies such as water, gas, telephone, cable, plumbing, and HVAC companies are also potential partners. The Company may have its plasma-electric power cell manufactured under contract or license. Alternatively, the Company may manufacture the units itself.

Some of the competitive advantages of BlackLight Power generation over the competing microdistributed technologies fuel cells and micro combustion turbines are no fuel costs, no fuel handling issues nor pollution, not a heat engine and not electrochemical, no reformer, solid state device, chemically-generated plasma with proven microwave technology, linearly scalable, cost competitive (lower capital and O&M costs), long product lifetime, appliance-like, load following, no grid connection (gas or electric for fuel or load leveling), high 9's power capability, closed system, and valuable solid chemical by-product.

With strategic alliances, the Company plans to develop, manufacture, and market a unit of approximately 25 kWe which is a desirable size for a modular uninterruptable power supply for the premium power market. 25 kWe is also capable of providing for the total power requirements of a single family residence or a light commercial load. The potential advantages of the Company's power system compared to fuel cells are (1) zero fuel costs, (2) capital and O&M costs that are 10% that of fuel cells, and (3) valuable chemicals are produced rather than pollutants such as carbon dioxide. Thereby, the cost per kilowatt of electric generated by the Company's plasma-electric power cell is projected to be about 10% of that of a fuel cell. In addition, an energy consumer may also derive revenue by selling power back onto the distribution system when the full capacity of the system is not required by such consumer.

The only mass manufacturable components required to produce a gyrotron system are a magnet, a resonator cavity or waveguide, and a antenna-rectifier. For implementation in the third world and acquisition of market share in the first world, the plasma-electric cell requires essentially no fuel and fuel distribution infrastructure, no regional or on-site pipelines, no utility connection (gas or electrical), no electric lines, and no specialized or centralized manufacturing expertise. In each category, competing technologies are at a competitive disadvantage which could prevent broad adoption even if they were viable based on logistics and costs.

Fuel cells are not cost competitive with BlackLight technology. The cost of electricity with a molten carbonate fuel cell which has a much lower capital cost compared to a proton exchange membrane fuel (PEM). The projected capital cost for a BlackLight 5-25 kW plasma-electric system is as follows: rectifier—\$200; inverter—\$200, permanent magnet—\$150, and cell—\$100, totaling \$650.

Also with strategic alliances, the Company further plans to develop, manufacture, and market a unit of approximately 1 MWe. One to ten of these units should provide the total power load requirements of a central power grid substation. The potential advantages of the Company's power system compared to central power are the same as with plasma-electric power cell. The cost per kilowatt of electric generated by the Company's plasma-electric power cell is projected to be about 20% of that of central power (see Table 2). With the installation of substation units, light commercial, and residential units, all

components of the present central power generation infrastructure upstream from the substation may be eliminated. Some infrastructure components that may be eliminated by the Company's technology with associated cost savings are: (1) high voltage transformers, (2) high voltage transmission lines, and (3) central power plants, including their associated turbines, fuel and pollution handling systems, ash, pollution, coal trains, coal mines, gas pipelines, gas fields, super tankers, oil fields, nuclear power plants, uranium processing plants, and uranium mines.

5.3. Motive Power—Plasma-Electric and Battery

The capital cost for BlackLight power for motive power are comparable to the cost of an automotive internal combustion engine. Whereas, fuel cells are two orders of magnitude too expensive and require trillions of dollars to be invested in a hydrocarbon to hydrogen refueling system. In contrast, a motive power plant based on BlackLight technology uses water as the fuel and requires no infrastructure. The Company is considering several promising options to commercialize its process in the motive power market. In addition to stationary power, the plasma-electric system may be used for motive power. The Company is also developing a high voltage battery which may power an electric vehicle.

5.4. Conclusion

The BlackLight Process has potentially very broad applications including: electrical power generation, space and process heating, motive power, and production of HHCs.

The technology generates plasma and heat from hydrogen, which may be obtained from ordinary water. The implications of this development could be significant. If the technology becomes proven, then the energy from this process could possibly be used to cleanly and cheaply meet the world's demand for thermal, chemical, and mechanical energy as well as electricity. Over time, it may be possible to replace or retrofit coal-fired, gas-fired, and oil-fired electric power plants. This would help to abate global warming and air and water pollution. Moreover, it may be possible to replace or retrofit some of the world's nuclear power plants. With BlackLight technology, an opportunity exists to dramatically reduce the complexity and the cost of the generation station, which includes fuel handling, thermal generation, thermal to electrical conversion, pollution abatement and spent fuel disposal or storage systems.

The Company is focusing on possible electrical and heating applications for its technology including a fit with a converter to make electricity. Electrical power generation with the Company's plasma-electric power technology may represent a major opportunity to use a microdistributed system to replace existing infrastructure at considerable savings in capital and generation costs. Residential/light commercial units, substation units, and a low voltage local distribution system could replace the central power based current system. Adaptation of the Company's technology is facilitated by the deregulation of the utility industry.

6. REFERENCES

1. R. Mills, *The Grand Unified Theory of Classical Quantum Mechanics*, January 2000 Edition, BlackLight Power, Inc., Cranbury, New Jersey, Distributed by Amazon.com.

2. R. Mills, M. Nansteel, and Y. Lu, Anomalous hydrogen/strontium discharge, *European Journal of Physics D*, submitted.
3. R. Mills, J. Dong, Y. Lu, Observation of extreme ultraviolet hydrogen emission from incandescently heated hydrogen gas with certain catalysts, *Int. J. Hydrogen Energy*, 25, 919-943 (2000).
4. R. Mills, Observation of extreme ultraviolet emission from hydrogen-KI plasmas produced by a hollow cathode discharge, *Int. J. Hydrogen Energy*, in press.
5. R. Mills, Temporal behavior of light-emission in the visible spectral range from a Ti-K₂CO₃-H-cell, *Int. J. Hydrogen Energy*, in press.
6. R. Mills, Y. Lu, and T. Onuma, Formation of a hydrogen plasma from an incandescently heated hydrogen-catalyst gas mixture with an anomalous afterglow duration, *Int. J. Hydrogen Energy*, in press.
7. R. Mills, M. Nansteel, and Y. Lu, Observation of extreme ultraviolet hydrogen emission from incandescently heated hydrogen gas with strontium that produced an anomalous optically measured power balance, *Int. J. Hydrogen Energy*, in press.
8. R. Mills, B. Dhandapani, N. Greenig, J. He, Synthesis and characterization of potassium iodo hydride, *Int. J. of Hydrogen Energy*, 25, 1185-1203 (2000).
9. R. Mills, Novel Inorganic Hydride, *Int. J. of Hydrogen Energy*, 25, 669-683 (2000).
10. R. Mills, Novel hydrogen compounds from a potassium carbonate electrolytic cell, *Fusion Technology*, 37(2) 157-182 (2000).
11. R. Mills, B. Dhandapani, M. Nansteel, J. He, T. Shannon, A. Echezuria, Synthesis and characterization of novel hydride compounds, *Int. J. of Hydrogen Energy*, in press.
12. R. Mills, Highly stable novel inorganic hydrides, *Journal of Materials Research*, submitted.
13. R. Mills, B. Dhandapani, M. Nansteel, J. He, A. Voigt, Identification of compounds containing novel hydride ions by nuclear magnetic resonance spectroscopy, *Int. J. Hydrogen Energy*, submitted.
14. R. Mills, The nature of free electrons in superfluid helium—a test of quantum mechanics and a basis to review its foundations and make a comparison to classical theory, *Int. J. Hydrogen Energy*, submitted.
15. R. Mills, N. Greenig, S. Hicks, Y. Lu, T. Onuma, Spectroscopic identification of a novel catalytic reaction of atomic hydrogen and the hydride ion product, in progress.
16. David R. Linde, *CRC Handbook of Chemistry and Physics*, 79 th Edition, CRC Press, Boca Raton, Florida, (1998-9), p. 10-175 to p. 10-177.
17. J. Phillips, J. Smith, S. Kurtz, Report On Calorimetric Investigations Of Gas-Phase Catalyzed Hydride Formation, Final Report for Period October-December 1996, January 1, 1997, A Confidential Report submitted to BlackLight Power, Inc. provided by BlackLight Power, Inc., 493 Old Trenton Road, Cranbury, NJ, 08512.
18. USDOE 1999 Report
19. Merrill Lynch Report on Plug Power and Fuel Cell Market Size. December 6, 1999
20. S. Sanders, J. Chumler, M. P. Zhang, Powering the Digital Economy/Digital Power Demand Meets Industrial Power Supply/Emerging Power Technologies for the Next 100 Years, Published by Stephens Inc. Investment Bankers, 111 Center Street, Little Rock, Arkansas, 72201, August, (2000).
21. T. Cooper, H. Harvey, Power Electronics, "Power Semiconductors and Power Supplies-The Building Blocks of the Digital Power Revolution, Published by Stephens Inc. Investment Bankers, 111 Center Street, Little Rock, Arkansas, 72201, (2000).
22. P. Huber, M. Mills, The Huber Mills Digital Power Report, *Powering the Telecosm*, Gilder Publishing, June 2000, Issue 3.
23. World Energy Assessment, <http://services.sciencewise.com/content/index.cfm?objectid=309>.
24. A. Gaponov, M. I. Petelin, V. K. Yulpatov, Izvestiya VUZ. Radiofizika, 10(9-10) 1414-1453 (1965).
25. V. A. Flyagin, A. V. Gaponov, M. I. Petelin, and V. K. Yulpatov, IEEE Transactions on Microwave Theory and Techniques, Vol. MTT-25, No. 6, June (1977), pp. 514-521.
26. R. M. Dickinson, Performance of a high-power, 2.388 GHz receiving array in wireless power transmission over 1.5 km, in 1976 IEEE MTT-S International Microwave Symposium, (1976), pp. 139-141.
27. R. M. Dickinson, Bill Brown's Distinguished Career, <http://www.mit.org/awards/WCB's%20distinguished%20career.htm>.
28. J. O. McSpadden, Wireless power transmission demonstration, Texas A&M University, <http://www.tsgc.utexas.edu/power/general/wpt.html>; *History of microwave power transmission before 1980*, <http://rasc5.kurasc.kyoto-u.ac.jp/docs/plasma-group/sps/history2-e.html>.
29. J. O. McSpadden, R. M. Dickson, L. Fan, K. Chang, A novel oscillating rectenna for wireless microwave power transmission, Texas A&M University, Jet Propulsion Laboratory, Pasadena, CA, <http://www.tamu.edu>, Microwave Engineering Department.

THIS PAGE BLANK (USPTO)

The Nature of Free Electrons in Superfluid Helium--a Test of Quantum Mechanics and a Basis to Review its Foundations and Make a Comparison to Classical Theory

Randell L. Mills

BlackLight Power, Inc.
493 Old Trenton Road
Cranbury, NJ 08512

The Schrödinger equation was originally postulated in 1926 as having a solution of the one electron atom. It gives the principal energy levels of the hydrogen atom as eigenvalues of eigenfunction solutions of the Laguerre differential equation. But, as the principal quantum number $n \gg 1$, the eigenfunctions become nonsensical. Despite its wide acceptance, on deeper inspection, the Schrödinger solution is plagued with many failings as well as difficulties in terms of a physical interpretation that have caused it to remain controversial since its inception. Only the one electron atom may be solved without approximations, but it fails to predict electron spin and leads to models with nonsensical consequences such as negative energy states of the vacuum, infinities, and negative kinetic energy. In addition to many predictions which simply do not agree with observations, the Schrödinger equation predicts noncausality, nonlocality, spook actions at a distance or quantum telepathy, perpetual motion, and many internal inconsistencies where contradicting statements have to be taken true simultaneously. Recently, the behavior of free electrons in superfluid helium has again forced the issue of the meaning of the wavefunction. Electrons form bubbles in superfluid helium which reveal that the electron is real and that a physical interpretation of the wavefunction is necessary. Furthermore, when irradiated with light of energy of about a 0.5 to several electron volts [1], the electrons carry current at different rates as if they exist with different sizes. It has been proposed that the behavior of free electrons in superfluid helium can be explained in terms of the electron breaking into pieces at superfluid helium temperatures [1]. Yet, the electron has proven to be indivisible even under particle accelerator collisions at 90 GeV (LEPII). The nature of the wavefunction must now be addressed. It is time for the physical rather than the mathematical nature of the wavefunction to be determined. A theory of classical quantum mechanics (CQM) was derived from first principles by Mills [2] that successfully applies physical laws on all scales. Using the classical wave equation with the constraint of nonradiation based on Maxwell's equations, CQM gives closed form physical solutions for the electron in atoms, the free electron, and the free electron in superfluid helium. The prediction of fractional principal quantum energy states of the electron in liquid helium match the photoconductivity and mobility observations without requiring that the electron is divisible.

DIVISIBLE ELECTRON?--IS QUANTUM MECHANICS FUNDAMENTALLY FLAWED?

In the 103 years since its discovery, there has been no evidence whatsoever that the electron is divisible. But, in order to explain, the rise in current of free electrons in superfluid helium when irradiated with low energy light and the observation of an unexpected plethora of exotic negative charge carriers in superfluid helium with mobilities greater than that of the normal electron, Maris [1] has proposed that the electron breaks into fractional pieces. One piece acquires all of the charge and the other is neutral. Maris shows that the Schrödinger equation solution of the wavefunction of the $1p$ state, an excited state, will break into two following the $1s$ to $1p$ transition of an electron in superfluid helium. This result is a consequence of the localization of the maximum electron density in the extremes of the dumb-bell shaped $1p$ orbital with the existence of a node at the center of the orbital. The large differences in time scales of the motion of the electron and the motion of the bubble wall means that the Franck-Condon principle should apply and that the wave function of the electron will deform adiabatically (Born-Oppenheimer principle) at this node to result in electron fission. Following the break, one half of the electron's wave function is trapped in each of the two daughter bubbles. As the wave function is the essence of an electron, the electron splits into two.

Electrons may be trapped in superfluid helium as autonomous electron bubbles interloped between helium atoms that have been excluded from the space occupied by the bubble. The surrounding helium atoms maintain the spherical bubble through van der Waals forces. Superfluid helium is an ideal medium to study individual trapped electrons in much the same way that individual ions may be studied in Penning traps. Both represent an ideal system to test quantum mechanics. Maris and other experimental physicists believe that the data on electrons in liquid helium reveals a fundamental flaw in quantum theory which has caused a furor [3-5]. Electrons bubbles in superfluid helium reveal that the electron is real and that a physical interpretation of the wavefunction is necessary. Physicists have always been content to think of the wave function, the unmeasurable entity which describes quantum systems, as a mathematical device with observable

consequences. The time has come for the idea to be grounded in reality. For the electron bubbles in helium, Maris's position is that the size of the bubble is determined by how much of the wave function is trapped inside the bubble. If there is no part of the wave function inside the bubble, the bubble will collapse. This makes the wave function seem to be a tangible object. Theoreticians are going to have to address the question: what is a wave function? Is it a real thing, or just a mathematical convenience?" [5].

From the time of its inception, quantum mechanic (QM) has been controversial because its foundations are in conflict with physical laws and are internally inconsistent. Interpretations of quantum mechanics such as hidden variables, multiple worlds, consistency rules, and spontaneous collapse have been put forward in an attempt to base the theory in reality. Unfortunately many theoreticians ignore the requirement that the wave function must be real and physical in order for it to be considered a valid description of reality. For example, regarding this issue Fuchs and Peres believe [6] "Contrary to those desires, quantum theory does *not* describe physical reality. What it does is provide an algorithm for computing *probabilities* for macroscopic events ("detector ticks") that are the consequences of our experimental interventions. This strict definition of the scope of quantum theory is the only interpretation ever needed, whether by experimenters or theorists".

With Penning traps, it is possible to measure transitions including those with hyperfine levels of electrons of single ions. This case can be experimentally distinguished from statistics over equivalent transitions in many ions. Whether many or one, the transition energies are always identical within the resonant line width. So, *probabilities* have no place in describing atomic energy levels. Moreover, quantum theory is incompatible with probability theory as shown in the Appendix.

The Copenhagen interpretation provides another meaning of quantum mechanics. It asserts that what we observe is all we can know; any speculation about what an electron, photon, atom, or other atomic-sized entity is really is or what it is doing when we are not looking is just that--speculation. The postulate of quantum measurement asserts that the process of measuring an observable forces it into a state of reality. In other words, reality is irrelevant until a measurement is made. In the

case of electrons in helium, the fallacy with this position is that the "ticks" (migration times of electron bubbles) reveal that the electron is real before a measurement is made. Furthermore, experiments on Ba^+ in a Penning trap discussed in the Appendix demonstrate that the postulate of quantum measurement of quantum mechanics is experimentally disproved. These issues and other such flawed philosophies and interpretations of experiments that arise from quantum mechanics are discussed in the Appendix.

QM gives correlations with experimental data. It does not explain the mechanism for the observed data. But, it should not be surprising that it gives good correlations given that the constraints of internal consistency and conformance to physical laws are removed for a wave equation with an infinite number of solutions wherein the solutions may be formulated as an infinite series of eigenfunctions with variable parameters. There are no physical constraints on the parameters. They may even correspond to unobservables such as virtual particles, hyperdimensions, effective nuclear charge, polarization of the vacuum, worm holes, spooky action at a distance, infinities, parallel universes, faster than light travel, etc. If you invoke the constraints of internal consistency and conformance to physical laws, quantum mechanics has never successfully solved a physical problem.

Throughout the history of quantum theory; wherever there was an advance to a new application, it was necessary to repeat a trial-and-error experimentation to find which method of calculation gave the right answers. Often the textbooks present only the successful procedure as if it followed from first principles; and do not mention the actual method by which it was found. In electromagnetic theory based on Maxwell's equations, one deduces the computational algorithm from the general principles. In quantum theory, the logic is just the opposite. One chooses the principle to fit the empirically successful algorithm. For example, we know that it required a great deal of art and tact over decades of effort to get correct predictions out of Quantum Electrodynamics (QED). For the right experimental numbers to emerge, one must do the calculation (i.e. subtract off the infinities) in one particular way and not in some other way that appears in principle equally valid. There is a corollary , noted by Kallen: from an inconsistent theory, any result may be derived.

Reanalysis of old experiments and many new experiments including electrons in superfluid helium challenge the Schrödinger equation predictions. These issues are discussed in context of a theory of classical quantum mechanics (CQM) derived from first principles by Mills [2]. Using the classical wave equation with the constraint of nonradiation based on Maxwell's equations, CQM gives closed form physical solutions for the electron in atoms, the free electron, and the free electron in superfluid helium which match the observations without requiring that the electron is divisible.

Schrödinger Theory of the Hydrogen Atom

In 1911, Rutherford proposed a planetary model for the atom where the electrons revolved about the nucleus (which contained the protons) in various orbits to explain the spectral lines of atomic hydrogen. There was, however, a fundamental conflict with this model and the prevailing classical physics. According to classical electromagnetic theory, an accelerated particle radiates energy (as electromagnetic waves). Thus, an electron in a Rutherford orbit, circulating at constant speed but with a continually changing direction of its velocity vector is being accelerated; thus, the electron should constantly lose energy by radiating and spiral into the nucleus.

An explanation was provided by Bohr in 1913, when he assumed that the energy levels were quantized and the electron was constrained to move in only one of a number of allowed states. Niels Bohr's theory for atomic hydrogen was based on an unprecedented postulate of stable circular orbits that do not radiate. Although no explanation was offered for the existence of stability for these orbits, the results gave energy levels in agreement with Rydberg's equation. Bohr's solution is trivial in that he specified a circular bound orbit which determined that the eccentricity was zero, and he specified the angular momentum as a integer multiple of Planck's constant bar. The solution given by Mills [7] in CGS units is

$$E = -\frac{1}{2} \frac{me^4}{n^2 \hbar^2} = -\frac{e^2}{2n^2 a_0} \quad (1)$$

In 1923, de Broglie suggested that the motion of an electron has a

wave aspect— $\lambda = \frac{h}{p}$. This was confirmed by Davisson and Germer in

1927 by observing diffraction effects when electrons were reflected from metals. Schrödinger reasoned that if electrons have wave properties, there must be a wave equation that governs their motion. And, in 1926, he proposed the time independent Schrödinger equation

$$H\Psi = E\Psi \quad (2)$$

where Ψ is the wave function, H is the wave operator, and E is the energy of the wave. To give the sought three quantum numbers, the Schrödinger equation solutions are three dimensional in space and four dimensional in spacetime

$$\left[\nabla^2 - \frac{1}{r^2} \frac{\delta^2}{\delta t^2} \right] \Psi(r, \theta, \phi, t) = 0 \quad (3)$$

where $\Psi(r, \theta, \phi, t)$ according to quantum theory is the probability density function of the electron as described below and the Appendix under Wave Function Solutions of Quantum Mechanics as Probability Waves are Inconsistent with Probability Theory. When the time harmonic function is eliminated [8],

$$-\frac{\hbar^2}{2\mu} \left[\frac{1}{r^2} \frac{\delta}{\delta r} \left(r^2 \frac{\delta\Psi}{\delta r} \right) + \frac{1}{r^2 \sin\theta} \frac{\delta}{\delta\theta} \left(\sin\theta \frac{\delta\Psi}{\delta\theta} \right)_{r,\phi} + \frac{1}{r^2 \sin^2\theta} \left(\frac{\delta^2\Psi}{\delta\phi^2} \right)_{r,\theta} \right] + V(r)\Psi(r, \theta, \phi) = E\Psi(r, \theta, \phi) \quad (4)$$

where the potential energy $V(r)$ in CGS units is

$$V(r) = -\frac{e^2}{r} \quad (5)$$

The Schrödinger equation (Eq. (4)) can be transformed into a sum comprising a part that depends only on the radius and a part that is a function of angle only obtained by separation of variables and linear superposition in spherical coordinates. The general form of the solutions for $\psi(r, \theta, \phi)$ are

$$\psi(r, \theta, \phi) = \sum_{l,m} R_{nlm}(r) Y_{lm}(\theta, \phi) \quad (6)$$

where l and m are separation constants. The azimuthal (θ) part of Eq. (4) is the generalized Legendre equation which is derived from the Laplace equation by Jackson (Eq. (3.9) of Jackson [9]). The solutions for the full angular part of Eq. (4), $Y_{lm}(\theta, \phi)$, are the spherical harmonics

$$Y_{lm}(\theta, \phi) = \sqrt{\frac{(2l+1)(l-m)!}{4\pi(l+m)!}} P_l^m(\cos \theta) e^{im\phi} \quad (7)$$

By substitution of the eigenvalues corresponding to the angular part [10], the Schrödinger equation becomes the radial equation, $R(r)$, given by

$$-\frac{\hbar^2}{2mr^2} \frac{d}{dr} \left(r^2 \frac{dR}{dr} \right) + \left[\frac{\hbar^2 l(l+1)}{2mr^2} + V(r) \right] R(r) = ER(r) \quad (8)$$

The time independent Schrödinger equation is similar to Eq. (20) of Mills [7] except that the solution is for the distribution of a spatial wavefunction in three dimensions rather than the dynamical motion of a point particle of mass m along a one dimensional trajectory. Electron motion is implicit in the Schrödinger equation. For wave propagation in three dimensions, the full time dependent Schrödinger equation is required; whereas, the classical case contains time derivatives. The kinetic energy of rotation K_{rot} is given classically by

$$K_{rot} = \frac{1}{2} mr^2 \omega^2 \quad (9)$$

where m is the mass of the electron. In the time independent Schrödinger equation, the kinetic energy of rotation K_{rot} is given by

$$K_{rot} = \frac{\ell(\ell+1)\hbar^2}{2mr^2} \quad (10)$$

where

$$L = \sqrt{\ell(\ell+1)\hbar^2} \quad (11)$$

is the value of the electron angular momentum L for the state $Y_{lm}(\theta, \phi)$.

In the case of the ground state of hydrogen, the Schrödinger equation solution is trivial for an implicit circular bound orbit which determines that the eccentricity is zero, and with the specification that the electron angular momentum is Planck's constant bar. With $k = e^2$, Eq. (25) of Mills [7] in CGS units becomes

$$E = -\frac{1}{2} \frac{me^4}{\hbar^2} = -\frac{e^2}{2a_0} \quad (12)$$

which corresponds to $n=1$ in Eq. (1). Many problems in classical physics give three quantum numbers when three spatial dimensions are considered. In order to obtain three quantum numbers, the Schrödinger equation requires that the solution is for the distribution of a spatial wavefunction in three dimensions with implicit motion rather than a one dimensional trajectory of a point particle as shown below. However, this

approach gives rise to predictions about the angular momentum and angular energy which are not consistent with experimental observations as well as a host of other problems which are summarized below.

The radial equation may be written as [11]

$$\frac{d}{dr} \left(r^2 \frac{dR}{dr} \right) + \frac{2mr^2}{\hbar^2} \left[E - V(r) - \frac{l(l+1)\hbar^2}{2mr^2} \right] R(r) = 0 \quad (13)$$

Let $U(r) = rR(r)$, then the radial equation reduces to

$$U'' + \frac{2m}{\hbar^2} \left[E - V(r) - \frac{l(l+1)\hbar^2}{2mr^2} \right] U = 0 \quad (14)$$

where

$$\psi = \frac{1}{r} U_{lm}(r) Y_{lm}(\theta, \phi) \quad (15)$$

Substitution of the potential energy given by Eq. (5) into Eq. (14) gives for sufficiently large r

$$U'' - \left(\frac{\alpha}{2} \right)^2 U = 0 \quad (16)$$

provided we define

$$\left(\frac{\alpha}{2} \right)^2 = \frac{-2mE}{\hbar^2} \quad (17)$$

where α is the eigenvalue of the eigenfunction solution of the Schrödinger equation given *infra* having units of reciprocal length and E is the energy levels of the hydrogen atom. To arrive at the solution which represents the electron, a suitable boundary condition must be imposed. Schrödinger postulated a boundary condition: $\Psi \rightarrow 0$ as $r \rightarrow \infty$, which leads to a purely mathematical model of the electron. This equation is *not* based on first principles, has no validity as such, and should not be represented as so. The right hand side of Eq. (17) must be *postulated* in order that the Rydberg equation is obtained as shown below. The postulate is implicit since Eq. (17) arises from the Schrödinger which is postulated. It could be defined *arbitrarily*, but is justified because it gives the Rydberg formula. That Schrödinger guessed the accepted approach is not surprising since many approaches were contemplated at this time [12], and since none of these approaches were superior, Schrödinger's approach prevailed.

The solution of Eq. (16) that is consistent with the boundary condition is

$$U_{\infty} = c_1 e^{(\alpha/2)r} + c_2 e^{-(\alpha/2)r} \quad (18)$$

In the case that α is real, the energy of the particle is negative. In this case U_∞ will not have an integrable square if c_1 fails to vanish wherein the radial integral has the form

$$\int_0^\infty R^2 r^2 dr = \int U_\infty^2 dr \quad (19)$$

It is shown below that the solution of the Schrödinger equation corresponds to the case wherein c_1 fails to vanish. Thus, the solutions with sufficiently large r are infinite. The same problem arises in the case of a free electron that is ionized from hydrogen. If α is imaginary, which means that E is positive, Eq. (16) is the equation of a linear harmonic oscillator [13]. U_∞ shows sinusoidal behavior; thus, the wavefunction for the free electron can not be normalized and is infinite. In addition, the angular momentum of the free electron is infinite since it is given by $\ell(\ell+1)\hbar^2$ (Eq. (11)) where $\ell \rightarrow \infty$.

In order to solve the bound electron states, let

$$E = -W \quad (20)$$

so that W is positive. In Eq. (13), let $r = x/\alpha$ where α is given by Eq. (17).

$$x \frac{d^2R}{dx^2} + 2 \frac{dR}{dx} + \left[\frac{2me^2}{\hbar^2\alpha} - \frac{x}{4} - \frac{\ell(\ell+1)}{x} \right] R = 0 \quad (21)$$

Eq. (21) is the differential equation for associated Laguerre functions given in general form by

$$y'' + 2y' + \left[n^* - \frac{k-1}{2} - \frac{x}{4} - \frac{k^2-1}{4x} \right] y = 0 \quad (22)$$

which has a solution possessing an integrable square of the form

$$y = e^{-x/2} x^{(k-1)/2} L_{n^*}^k(x) \quad (23)$$

provided that n^* and k are positive integers. However, n^* does not have to be an integer, it may be any arbitrary constant β . Then the corresponding solution is [14]

$$y = e^{-x/2} x^{(k-1)/2} \frac{d^k}{dx^k} L_\beta(x) \quad (24)$$

In the case that n^* is chosen to be an integer in order to obtain the Rydberg formula, $n^* - k \geq 0$ since otherwise $L_{n^*}^k(x)$ of Eq. (23) would vanish.

By comparing Eq. (21) and Eq. (22),

$$\frac{k^2-1}{4} = \ell(\ell+1) \quad (25)$$

Thus,

$$k = 2\ell + 1 \quad (26)$$

and

$$n^* - \frac{k-1}{2} = n^* - \ell = \frac{me^2}{\hbar} \left(\frac{\alpha}{2} \right)^{-1} \quad (27)$$

Substitution of the value of α and solving for W gives

$$W = \frac{1}{2} \frac{me^4}{(n^* - \ell)^2 \hbar^2} \quad (28)$$

Because of the conditions on n^* and k , the quantity $n^* - \ell$ can not be zero. It is usually denoted by n and called the principal quantum number. The energy states of the hydrogen atom are

$$W_n = -E_n = \frac{1}{2} \frac{me^4}{n^2 \hbar^2} \quad (29)$$

and the corresponding eigenfunctions from Eq. (23) are

$$R_{n,\ell} = c_{n,\ell} e^{-x^{1/2}} x^\ell L_{n+\ell}^{2\ell+1}(x) \quad (30)$$

where the variable x is defined by

$$x = \alpha r = \frac{\sqrt{8mW}}{\hbar} r = \frac{2me^2}{n\hbar^2} r \quad (31)$$

In the Bohr theory of the hydrogen atom, the first orbital has a radius in CGS units given by

$$a_0 = \frac{\hbar^2}{me^2} = 0.53 \times 10^{-8} \text{ cm} \quad (32)$$

Thus, $\alpha = 2/n a_0$ and

$$x = \frac{2}{n} \frac{r}{a_0} \quad (33)$$

The energy states of the hydrogen atom in CGS units in terms of the Bohr radius are given by Eq. (1). From Eq. (30), $R_{n,\ell}$ for the hydrogen atom ground state is

$$R_{1,0} = c_{1,0} e^{-r/a_0} L_1^1 = 2a_0^{-3/2} e^{-r/a_0} \quad (34)$$

For this state

$$Y_{00} = \text{constant} = (4\pi)^{-1/2} \quad (35)$$

when the function is normalized. Thus, the "ground state function" defined by the arbitrary selection of n^* at Eq. (22) is

$$\psi_0 = (\pi a_0^3)^{-1/2} e^{-r/a_0} \quad (36)$$

In fact, the Schrödinger can only yield integer eigenvalue solutions by selection from an infinite number of possibilities since the solution is over all space with no boundary (i.e. 0 to ∞). In contrast, wave equation solutions with integers are common for boundary constrained systems

such as waveguides and resonators.

The POSTULATED Schrödinger Equation Fails to Solve the Hydrogen Atom Correctly.

The paper by Mills [7] rigorously analyzes the Schrödinger equation. One of many possible solutions of the postulated Schrödinger equation gives the Rydberg levels as does the theory of Bohr. On this basis alone, it is justified despite its inconsistency with physical laws and numerous experimental observations such as

- The appropriate eigenvalue must be postulated and the variables of the Laguerre differential equation must be defined as integers in order to obtain the Rydberg formula.
- The Schrödinger equation is not Lorentzian invariant.
- The Schrödinger equation violates first principles including special relativity and Maxwell's equations.
- The Schrödinger equation gives no basis why excited states are radiative and the 13.6 eV state is stable. Mathematics does not determine physics. It only models physics.
- In the time independent Schrödinger equation, the kinetic energy of rotation K_m is given by Eq. (10) where the value of the electron angular momentum L for the state $\psi_{lm}(\theta, \phi)$ is given by Eq. (11). The Schrödinger equation solutions, Eq. (10) and Eq. (11), predict that the ground state electron has zero angular energy and zero angular momentum, respectively.
- The Schrödinger equation solution, Eq. (11), predicts that the ionized electron may have infinite angular momentum.
- The Schrödinger equation solutions, Eq. (10) and Eq. (11), predict that the excited state rotational energy levels are nondegenerate as a

function of the ℓ quantum number even in the absence of an applied magnetic field, and the predicted energy is over six orders of magnitude of the observed nondegenerate energy in the presence of a magnetic field. In the absence of a magnetic field, no preferred direction exists. In this case, the ℓ quantum number is a function of the orientation of the atom with respect to an arbitrary coordinate system. Therefore, the nondegeneracy is nonsensical and violates conservation of angular momentum of the photon.

- The Schrödinger equation predicts that each of the functions that corresponds to a highly excited state electron is not integrable and can not be normalized; thus, each is infinite.
- The Schrödinger equation predicts that the ionized electron is sinusoidal over all space and can not be normalized; thus, it is infinite.
- The Heisenberg uncertainty principle arises as the standard deviation in the electron probability wave, but experimentally it is not the basis of wave particle duality as shown in the Appendix.
- Quantum mechanical textbooks express the movement of the electron, and the Heisenberg uncertainty principle is an expression of the statistical aspects of this movement. McQuarrie [15], gives the electron speed in the $n=1$ state of hydrogen as 2.18764×10^6 m/sec. Remarkably, the uncertainty in the electron speed according to the uncertainty principle is 1.4×10^7 m/sec [16] which is an order of magnitude larger than the speed.
- Experimentally the electron has precise velocity, kinetic energy, and angular momentum. Acquiring these exact properties instantaneously defies all known physical principles.
- The correspondence principle does not hold experimentally.
- The Schrödinger equation does not predict the electron magnetic moment and misses the spin quantum number all together.

- The Schrödinger equation is not a wave equation since it gives the velocity squared proportional to the frequency.
- The Schrödinger equation is not consistent with conservation of energy in an inverse potential field wherein the binding energy is equal to the kinetic energy and the sum of the binding energy and the kinetic energy is equal to the potential energy.
- The Schrödinger equation permits the electron to exist in the nucleus which is a state that is physically nonsensical with infinite potential energy and infinite negative kinetic energy.
- The Schrödinger equation interpreted as a probability wave of a point particle can not explain neutral scattering of electrons from hydrogen.
- The Schrödinger equation interpreted as a probability wave of a point particle gives rise to infinite magnetic and electric energy in the corresponding fields of the electron.
- A modification of the Schrödinger equation was developed by Dirac to explain spin which relies on the unfounded notions of negative energy states of the vacuum, virtual particles, and gamma factors.

The success of quantum mechanics can be attributed to 1.) the lack of rigor and unlimited tolerance to ad hoc assumptions in violation of physical laws, 2.) fantastical experimentally immeasurable corrections such as virtual particles, vacuum polarizations, effective nuclear charge, shielding, ionic character, compactified dimensions, and renormalization, and 3.) curve fitting parameters that are justified solely on the basis that they force the theory to match the data. Quantum mechanics is now in a state of crisis with constantly modified versions of matter represented as undetectable minuscule vibrating strings that exist in many unobservable hyperdimensions, that can travel back and forth between undetectable interconnected parallel universes. (An analysis of the many failings of

quantum mechanics are given in the Appendix.) And, recent data shows that the expansion of the universe is accelerating. This observation has shattered the long held unquestionable doctrine of the origin of the universe as a big bang [17]. It may be time to reconsider the roots of quantum theory, namely the theory of the hydrogen atom. Especially in light of the observation of real electron bubbles in helium which require that the electron is divisible in order for the Schrödinger equation to explain the increase in conductivity upon irradiation with low energy light. This argument is reinforced by the demonstration that the electron in atoms, the free electron, and the free electron in superfluid helium can be solved physically rather than mathematically in closed form equations from first principles. The predictions match the observations without requiring that the electron is a probability wave or is divisible.

A CLASSICAL APPROACH TO QUANTUM MECHANICS

Introduction

A theory of classical quantum mechanics (CQM) was derived from first principles by Mills [2] that successfully applies physical laws on all scales. The classical wave equation is solved with the constraint that a bound electron cannot radiate energy. The mathematical formulation for zero radiation based on Maxwell's equation's follows from a derivation by Haus [18]. The function that describes the motion of the electron must not possess spacetime Fourier components that are synchronous with waves traveling at the speed of light. CQM gives closed form solutions for the atom including the stability of the $n=1$ state and the instability of the excited states, the equation of the photon and electron in excited states, the equation of the free electron, and photon which predict the wave particle duality behavior of particles and light. The current and charge density functions of the electron may be directly physically interpreted. For example, spin angular momentum results from the motion of negatively charged mass moving systematically, and the equation for angular momentum, $\mathbf{r} \times \mathbf{p}$, can be applied directly to the wave function (a current density function) that describes the electron. The magnetic moment of a Bohr magneton, Stern Gerlach experiment, g factor, Lamb shift, resonant line width and shape, selection rules, correspondence

principle, wave particle duality, excited states, reduced mass, rotational energies, and momenta, orbital and spin splitting, spin-orbital coupling, Knight shift, and spin-nuclear coupling are derived in closed form equations based on Maxwell's equations. The calculations agree with experimental observations.

Many great physicists rejected quantum mechanics. Feynman also attempted to use first principles including Maxwell's Equations to discover new physics to replace quantum mechanics [19]. Other great physicists of the 20th century searched. "Einstein [...] insisted [...] that a more detailed, wholly deterministic theory must underlie the vagaries of quantum mechanics" [20]. He felt that scientists were misinterpreting the data.

The results of Mills theory demonstrate that classical physical laws describe reality on all scales. Unlike quantum mechanics which postulates that different laws apply on the atomic level, the premise of Mills theory is that a valid theory must comply with ALL of the following:

- theory must be internally consistent even between widely different phenomena
- Maxwell's equations
- conservation of matter/energy
- conservation of linear and angular momentum
- charge conservation
- first and second law of thermodynamics
- Newton's law in the low speed limit; special relativity otherwise
- general relativity (e.g. Schwarzschild metric)--no cosmological constant; and Newtonian gravitation in the weak field limit (which demands no cosmological constant)
- a vacuum is a vacuum
- constant maximum of the speed of light in a vacuum
- 4 dimensional spacetime
- the only allowed parameters are the measured fundamental constants

Quantum mechanics is based on engendering the electron with a wave nature as suggested by the Davisson-Germer experiment and fabricating a set of associated postulates and mathematical rules for wave

operators. Quantum mechanics is in violation of Maxwell's equations as shown through application of Haus's condition to the Schrödinger wave functions [18]. Nonradiation based on Maxwell's equations is a necessary boundary constraint since nonradiation is observed experimentally. The short coming of QM regarding violation of Maxwell's equations and other first principles are further discussed in the Appendix.

Mills Approach to the Solution of the Electron:

Mills solves the electron by a different approach than that used to solve the Schrödinger wave equation. Rather than using a postulated wave equation with time eliminated in terms of the energy of the electron in a Coulomb field and solving the charge wave (Schrödinger interpretation) or the probability wave (Born interpretation), the solution for the scalar (charge) and vector potential (current) functions of the electron are sought based on first principles. Mills first assumes that the functions that physically describe the mass and charge of the electron in space and time obeys the wave equation since it conserves energy and angular momentum. The solution is generalized to be three dimensional plus time. Rather than use the postulated Schrödinger boundary condition: $\Psi \rightarrow 0$ as $r \rightarrow \infty$, which leads to a purely mathematical model of the electron, the constraint is based on experimental observation that the moving charge must not radiate. Application of the Haus condition based on Maxwell's equations to a generalized three dimension plus time wave equation requires that the functions must be solutions of Eq. (45), a two dimensional wave equation plus time. This is consistent with first principle laws and ultimately matches experimentation. However, it is unconventional.

The two dimensional wave equation plus time is given by McQuarrie [21]. The electron is confined to two dimensions (θ and ϕ) plus time. Spherical harmonic functions and time harmonic functions are well known solutions of the angular and time components of the two dimensional wave equation plus time, respectively. The solutions appear in McQuarrie [22]. A constant current function is also a solution of the wave equation. A constant function corresponding to the electron spin function is added to each of the spherical harmonic functions to give the charge (mass) density functions of the electron as a function of time. The

integral of a spherical harmonic function over the orbitsphere is zero. The integral of the constant function over the orbitsphere is the total charge (mass) of the electron. These functions comprise the well known s, p, d, f, etc. electrons or orbitals. In the case that such an electron state arises as an excited state by photon absorption, it is radiative due to a radial dipole term in its current density function since it possesses spacetime Fourier components synchronous with waves traveling at the speed of light.

The excited states are solved including the radii of the orbitspheres using Maxwell's equations with the traditional source current boundary constraints at the electron. Quantization arises from the equation of the photon and the electron--not from the solution of the electron alone. After all, each solution is for an excited state created by the absorption of a photon. The solutions are analogous to those of excited resonator modes except that the cavity is dynamic. The field lines from the proton end on the current density function of the electron, and the electric field is zero for $r > r_n$. The trapped photons are a solution of the three dimensional wave equation plus time given by Maxwell's equations. The electrodynamic field of the photon's is a constant function plus a time and spherical harmonic function that is in phase with source currents at the electron which is given by a constant plus a time and spherical harmonic function. Only particular solutions are possible as resonant photons of the electron which is a dynamic resonator cavity. The results are in agreement with first principle physics and experimental observations of the hydrogen atom, excited states, free electron, and free space photon including the wave particle duality aspects.

Spin and Orbital Parameters Arise from First Principles:

An electron is a spinning, two-dimensional spherical surface, called an *electron orbitsphere*, that can exist in a bound state only at specific radii r_n from the nucleus. (See Figure 1 for a pictorial representation of an orbitsphere.) The result for the $n=1$ state of hydrogen is that the charge density function remains constant with each point on the surface moving at the same angular and linear velocity. The constant function solution of the two dimensional wave equation corresponds to the spin function which has a corresponding spin angular momentum that may be

calculated from $\mathbf{r} \times \mathbf{p}$ applied directly to the current density function that describes the electron. The radius of the nonradiative ($n=1$) state is solved using the electromagnetic force equations of Maxwell relating the charge and mass density functions wherein the angular momentum of the electron is given by Planck's constant bar (Eq. (1.165) of [2]). The reduced mass arises naturally from an electrodynamic interaction between the electron and the proton rather than from a point mass revolving around a point nucleus in the case of Schrödinger wave equation solutions which presents an internal inconsistency since the wave functions are spherically symmetrical.

CQM gives closed form solutions for the resonant photons and excited state electron functions. Angular momentum of the photon given by $m = \frac{1}{8\pi} \text{Re}[\mathbf{r} \times (\mathbf{E} \times \mathbf{B}^*)]$ is conserved. The change in angular velocity of the electron is equal to the angular frequency of the resonant photon. The energy is given by Planck's equation. The predicted energies, Lamb shift, hyperfine structure, resonant line shape, line width, selection rules, etc. are in agreement with observation.

The radii of excited states are solved using the electromagnetic force equations of Maxwell relating the field from the charge of the proton, the electric field the photon, and charge and mass density functions of the electron wherein the angular momentum of the electron is given by Planck's constant bar (Eq. (1.165) of [2]).

For excited states of the hydrogen atom, the constant function solution of the two dimensional wave equation corresponds to the spin function. Each spherical harmonic function modulates the constant spin function and corresponds to an orbital function of a specific excited state with a corresponding phased matched trapped photon and orbital angular momentum. Thus, the spherical harmonic function behaves as a charge density wave which travels time harmonically on the surface of the orbitsphere about a specific axis. (See Figure 2 for a pictorial representation.) An amplitude of the corresponding orbital energy may be calculated from Maxwell's equations. Since the constant function is modulated harmonically, the time average of the orbital energy is zero except in the presence of a magnetic field. Nondegeneracy of energy levels arises from spin, orbital, and spin-orbital coupling interactions

with the applied field. The electrodynamics interaction with the magnetic field gives rise to the observed hyperfine splitting of the hydrogen spectrum.

Many inconsistencies arise in the case of the corresponding solutions of the Schrödinger wave equation. For example, where is the photon in excited states given by the Schrödinger equation? And a paradox arises for the change in angular momentum due to photon absorption. The Schrödinger equation solutions for the kinetic energy of rotation K_{ro} is given by Eq. (10) and the value of the electron angular momentum L for the state $Y_{lm}(\theta, \phi)$ given by Eq. (11) predict that the excited state rotational energy levels are nondegenerate as a function of the ℓ quantum number even in the absence of an applied magnetic field, and the predicted energy is over six orders of magnitude of the observed nondegenerate energy in the presence of a magnetic field. In the absence of a magnetic field, no preferred direction exists. In this case, the ℓ quantum number is a function of the orientation of the atom with respect to an arbitrary coordinate system. Therefore, the nondegeneracy is nonsensical and violates conservation of angular momentum of the photon.

In quantum mechanics, the spin angular momentum of the electron is called the "intrinsic angular momentum" since no physical interpretation exists. The Schrödinger equation is not Lorentzian invariant in violation of special relativity. It failed to predict the results of the Stern-Gerlach experiment which indicated the need for an additional quantum number. Quantum electrodynamics was proposed by Dirac in 1926 to provide a generalization of quantum mechanics for high energies in conformity with the theory of special relativity and to provide a consistent treatment of the interaction of matter with radiation. It is fatally flawed. From Weisskopf [23], "Dirac's quantum electrodynamics gave a more consistent derivation of the results of the correspondence principle, but it also brought about a number of new and serious difficulties." Quantum electrodynamics; 1.) DOES NOT EXPLAIN NONRADIATION OF BOUND ELECTRONS; 2.) contains an internal inconsistency with special relativity regarding the classical electron radius - the electron mass corresponding to its electric energy is infinite (The Schrödinger equation fails to predict the classical electron radius);

3.) it admits solutions of negative rest mass and negative kinetic energy; 4.) the interaction of the electron with the predicted zero-point field fluctuations leads to infinite kinetic energy and infinite electron mass; 5.) Dirac used the unacceptable states of negative mass for the description of the vacuum; yet, infinities still arise. Dirac's equation which was postulated to explain spin relies on the unfounded notions of negative energy states of the vacuum, virtual particles, and gamma factors. All of these features are untenable or are inconsistent with observation. These problems regarding spin and orbital angular momentum and energies and the classical electron radius are nonexistence with CQM solutions [2].

Furthermore, Mills [24] shows that the Schrödinger equation may be transformed into a form consistent with first principles. In the case that the potential energy of the Hamiltonian, H , is a constant times the wavenumber, the Schrödinger equation is the well known Bessel equation. Then with one of the solutions for the wavefunction Ψ (a current density function rather than a probability wave) is equivalent to an inverse Fourier transform. According to the duality and scale change properties of Fourier transforms, the energy equation of Mills theory and that of quantum mechanics are identical, the energy of a radial Dirac delta function of radius equal to an integer multiple of the radius of the hydrogen atom.

Mills Theory-a classical quantum theory

One-electron atoms include the hydrogen atom, He^+ , Li^{2+} , Be^{3+} , and so on. The mass-energy and angular momentum of the electron are constant; this requires that the equation of motion of the electron be temporally and spatially harmonic. Thus, the classical wave equation applies and

$$\left[\nabla^2 - \frac{1}{v^2} \frac{\delta^2}{\delta t^2} \right] \rho(r, \theta, \phi, t) = 0 \quad (37)$$

where $\rho(r, \theta, \phi, t)$ is the charge density function of the electron in time and space. In general, the wave equation has an infinite number of solutions. To arrive at the solution which represents the electron, a suitable boundary condition must be imposed. It is well known from experiments that each single atomic electron of a given isotope radiates to the same stable state. Thus, Mills chose the physical boundary condition of

nonradiation of the bound electron to be imposed on the solution of the wave equation for the charge density function of the electron. The condition for radiation by a moving point charge given by Haus [18] is that its spacetime Fourier transform does possess components that are synchronous with waves traveling at the speed of light. Conversely, it is proposed that the condition for nonradiation by an ensemble of moving point charges that comprises a charge density function is

For non-radiative states, the current-density function must NOT possess spacetime Fourier components that are synchronous with waves traveling at the speed of light.

The Haus derivation applies to a moving charge-density function as well because charge obeys superposition. The Haus derivation is summarized below.

The Fourier components of the current produced by the moving charge are derived. The electric field is found from the vector equation in Fourier space (\mathbf{k} , w-space). The inverse Fourier transform is carried over the magnitude of \mathbf{k} . The resulting expression demonstrates that the radiation field is proportional to $\mathbf{J}_\perp\left(\frac{\omega}{c}\mathbf{n}, \omega\right)$, where $\mathbf{J}_\perp(\mathbf{k}, \omega)$ is the spacetime Fourier transform of the current perpendicular to \mathbf{k} and $\mathbf{n} = \frac{\mathbf{k}}{|\mathbf{k}|}$. Specifically,

$$\mathbf{E}_\perp(\mathbf{r}, \omega) \frac{d\omega}{2\pi} = \frac{c}{2\pi} \int \rho(\omega, \Omega) d\omega d\Omega \sqrt{\frac{\mu_0}{\epsilon_0}} \mathbf{n} X \left(\mathbf{n} X \mathbf{J}_\perp\left(\frac{\omega}{c}\mathbf{n}, \omega\right) e^{i\left(\frac{\omega}{c}\right)\mathbf{n}\cdot\mathbf{r}} \right) \quad (38)$$

The field $\mathbf{E}_\perp(\mathbf{r}, \omega) \frac{d\omega}{2\pi}$ is proportional to $\mathbf{J}_\perp\left(\frac{\omega}{c}\mathbf{n}, \omega\right)$, namely, the Fourier component for which $\mathbf{k} = \frac{\omega}{c}$. Factors of ω that multiply the Fourier component of the current are due to the density of modes per unit volume and unit solid angle. An unaccelerated charge does not radiate in free space, not because it experiences no acceleration, but because it has no Fourier component $\mathbf{J}_\perp\left(\frac{\omega}{c}\mathbf{n}, \omega\right)$.

The time, radial, and angular solutions of the wave equation are

separable. The motion is time harmonic with frequency ω_n . To be a harmonic solution of the wave equation in spherical coordinates, the angular functions must be spherical harmonic functions. A zero of the spacetime Fourier transform of the product function of two spherical harmonic angular functions, a time harmonic function, and an unknown radial function is sought. The solution for the radial function which satisfies the boundary condition is a delta function

$$f(r) = \frac{1}{r^2} \delta(r - r_n) \quad (39)$$

where $r_n = nr_1$ is an allowed radius. Thus, bound electrons are described by a charge-density (mass-density) function which is the product of a radial delta function ($f(r) = \frac{1}{r^2} \delta(r - r_n)$), two angular functions (spherical harmonic functions), and a time harmonic function. Thus, an electron is a spinning, two-dimensional spherical surface, called an *electron orbitsphere*, that can exist in a bound state at only specified distances from the nucleus as shown in Figure 1. More explicitly, the orbitsphere comprises a two-dimensional spherical shell of moving charge.

The total function that describes the spinning motion of each electron orbitsphere is composed of two functions. One function, the spin function, is spatially uniform over the orbitsphere, spins with a quantized angular velocity, and gives rise to spin angular momentum. The other function, the modulation function, can be spatially uniform—in which case there is no orbital angular momentum and the magnetic moment of the electron orbitsphere is one Bohr magneton—or not spatially uniform—in which case there is orbital angular momentum. The modulation function also rotates with a quantized angular velocity.

The corresponding current pattern of the constant charge function of the orbitsphere corresponding to the spin function comprises an infinite series of correlated orthogonal great circle current loops. The current pattern is generated over the surface by two orthogonal sets of an infinite series of nested rotations of two orthogonal great circle current loops where the coordinate axes rotate with the two orthogonal great circles. Each infinitesimal rotation of the infinite series is about the new x-axis and new y-axis which results from the preceding such rotation. For each of the two sets of nested rotations, the angular sum of

the rotations about each rotating x-axis and y-axis totals $\sqrt{2}\pi$ radians.

Consider the electron to be evenly distributed within two orthogonal great circle current loops. Then consider two infinitesimal point masses (charges), one and two, of two orthogonal great circle current loops. The Cartesian coordinate system wherein the first current loop lies in the yz-plane, and the second current loop lies in the xz-plane is designated the orbitsphere reference frame. Consider the two point masses, one and two, in the reference frame of the orbitsphere at time zero. Point one is at $x' = 0$, $y' = 0$, and $z' = r_n$ and point two is at $x' = r_n$, $y' = 0$, and $z' = 0$. Let point one move on a great circle toward the negative y' -axis, as shown in Figure 3, and let point two move on a great circle toward the positive z' -axis, as shown in Figure 3. The equations of motion, in the reference frame of the orbitsphere are given by

point one:

$$\dot{x}_1 = 0 \quad \dot{y}_1 = -r_n \sin(\omega_n t) \quad \dot{z}_1 = r_n \cos(\omega_n t) \quad (40)$$

point two:

$$\dot{x}_2 = r_n \cos(\omega_n t) \quad \dot{y}_2 = 0 \quad \dot{z}_2 = r_n \sin(\omega_n t) \quad (41)$$

The great circles are rotated by an infinitesimal angle $\Delta\alpha$ (a rotation around the x-axis) and then by $\Delta\alpha$ (a rotation around the new y-axis). The coordinates of each point on the rotated great circle is expressed in terms of the first (x,y,z) coordinates by the following transforms:

point one:

$$\begin{bmatrix} x_1 \\ y_1 \\ z_1 \end{bmatrix} = \begin{bmatrix} \cos(\Delta\alpha) & -\sin^2(\Delta\alpha) & -\sin(\Delta\alpha)\cos(\Delta\alpha) \\ 0 & \cos(\Delta\alpha) & -\sin(\Delta\alpha) \\ \sin(\Delta\alpha) & \cos(\Delta\alpha)\sin(\Delta\alpha) & \cos^2(\Delta\alpha) \end{bmatrix} \begin{bmatrix} x'_1 \\ y'_1 \\ z'_1 \end{bmatrix} \quad (42)$$

and $\Delta\alpha' = -\Delta\alpha$ replaces $\Delta\alpha$ for $\sum_{n=1}^{\frac{\sqrt{2}\pi}{\Delta\alpha}} \Delta\alpha = \sqrt{2}\pi$; $\sum_{n=1}^{\frac{\sqrt{2}\pi}{|\Delta\alpha'|}} |\Delta\alpha'| = \sqrt{2}\pi$

point two:

$$\begin{bmatrix} x_2 \\ y_2 \\ z_2 \end{bmatrix} = \begin{bmatrix} \cos(\Delta\alpha) & -\sin^2(\Delta\alpha) & -\sin(\Delta\alpha)\cos(\Delta\alpha) \\ 0 & \cos(\Delta\alpha) & -\sin(\Delta\alpha) \\ \sin(\Delta\alpha) & \cos(\Delta\alpha)\sin(\Delta\alpha) & \cos^2(\Delta\alpha) \end{bmatrix} \begin{bmatrix} x'_2 \\ y'_2 \\ z'_2 \end{bmatrix} \quad (43)$$

and $\Delta\alpha' = -\Delta\alpha$ replaces $\Delta\alpha$ for $\sum_{n=1}^{\frac{\sqrt{2}\pi}{\Delta\alpha}} \Delta\alpha = \sqrt{2}\pi$; $\sum_{n=1}^{\frac{\sqrt{2}\pi}{|\Delta\alpha'|}} |\Delta\alpha'| = \sqrt{2}\pi$

The total orbitsphere is given by reiterations of Eqs. (42) and (43). The output given by the non primed coordinates is the input of the next iteration corresponding to each successive nested rotation by the infinitesimal angle where the summation of the rotation about each of the

x-axis and the y-axis is $\sum_{n=1}^{\frac{\sqrt{2}\pi}{\Delta\alpha}} \Delta\alpha = \sqrt{2}\pi$ and $\sum_{n=1}^{\frac{\sqrt{2}\pi}{|\Delta\alpha'|}} |\Delta\alpha'| = \sqrt{2}\pi$. The current pattern

corresponding to point one and point two shown with 8.49 degree increments of the infinitesimal angular variable $\Delta\alpha(\Delta\alpha')$ of Eqs. (42) and (43) is shown from the perspective of looking along the z-axis in Figure 4. The complete orbitsphere current pattern corresponds to all such correlated points, point one and point two, of the orthogonal great circles shown in Figure 3 which are rotated according to Eqs. (42) and (43) where $\Delta\alpha(\Delta\alpha')$ approaches zero and the summation of the infinitesimal angular rotations of $\Delta\alpha(\Delta\alpha')$ about the successive x-axes and y-axes is

$\sqrt{2}\pi$. The current pattern gives rise to the phenomenon corresponding to the spin quantum number.

The fourth quantum number arises naturally in the Mills theory as derived in the Electron g Factor Section [2]. The Stern-Gerlach experiment implies a magnetic moment of one Bohr magneton and an associated angular momentum quantum number of 1/2. Historically, this quantum number is called the spin quantum number, s ($s = \frac{1}{2}$; $m_s = \pm \frac{1}{2}$).

Conservation of angular momentum of the orbitsphere permits a discrete change of its "kinetic angular momentum" ($\mathbf{r} \times m\mathbf{v}$) by the field of $\frac{\hbar}{2}$, and concomitantly the "potential angular momentum" ($\mathbf{r} \times e\mathbf{A}$) must change by $-\frac{\hbar}{2}$. The flux change, ϕ , of the orbitsphere for $r < r_n$ is determined as follows:

$$\Delta \mathbf{L} = \frac{\hbar}{2} - \mathbf{r} \times e\mathbf{A} \quad (44)$$

$$= \frac{\hbar}{2} - \frac{e2\pi r A}{2\pi} \quad (45)$$

$$= \frac{\hbar}{2} - \frac{e\phi}{2\pi} \quad (46)$$

In order that the change of angular momentum, $\Delta \mathbf{L}$, equals zero, ϕ must be $\Phi_0 = \frac{\hbar}{2e}$, the magnetic flux quantum. Thus, to conserve angular momentum in the presence of an applied magnetic field, the orbitsphere magnetic moment can be parallel or antiparallel to an applied field as observed with the Stern-Gerlach experiment, and the flip between orientations (a rotation of $\frac{\pi}{2}$) is accompanied by the "capture" of the magnetic flux quantum by the orbitsphere. And, the total energy of the flip transition is the sum of the energy of a fluxon treading the orbitsphere and the energy of reorientation of the magnetic moment (Eq. (1.148) and Eq. (1.136) of [2], respectively).

$$\Delta E_{mag}^{spin} = 2 \left(\mu_B \mathbf{B} + \frac{\alpha}{2\pi} \mu_B \mathbf{B} \right) \quad (47)$$

$$\Delta E_{mag}^{spin} = 2(1 + \frac{\alpha}{2\pi}) \mu_B \mathbf{B} \quad (48)$$

$$\Delta E_{mag}^{spin} = 2g\mu_B \mathbf{B} \quad (49)$$

The spin-flip transition can be considered as involving a magnetic

moment of g times that of a Bohr magneton. The factor g is redesignated the fluxon g factor as opposed to the anomalous g factor and its value is 1.00116. The experimental value is 1.00116.

The Mills theory solves the wave equation for the charge density function of the electron. The time, radial, and angular solutions of the wave equation are separable. Also, the radial function for the electron indicates that the electron is two-dimensional. Therefore, the angular mass-density function of the electron, $A(\theta, \phi, t)$, must be a solution of the wave equation in two dimensions (plus time),

$$\left[\nabla^2 - \frac{1}{v^2} \frac{\delta^2}{\delta t^2} \right] A(\theta, \phi, t) = 0 \quad (50)$$

where $\rho(r, \theta, \phi, t) = f(r)A(\theta, \phi, t) = \frac{1}{r^2} \delta(r - r_n)A(\theta, \phi, t)$ and $A(\theta, \phi, t) = Y(\theta, \phi)k(t)$

$$\left[\frac{1}{r^2 \sin \theta} \frac{\delta}{\delta \theta} \left(\sin \theta \frac{\delta}{\delta \theta} \right)_{r, \phi} + \frac{1}{r^2 \sin^2 \theta} \left(\frac{\delta^2}{\delta \phi^2} \right)_{r, \theta} - \frac{1}{v^2} \frac{\delta^2}{\delta t^2} \right] A(\theta, \phi, t) = 0 \quad (51)$$

where v is the linear velocity of the electron. The charge-density functions including the time-function factor are

$$\ell = 0$$

$$\rho(r, \theta, \phi, t) = \frac{e}{8\pi r^2} [\delta(r - r_n)] [Y_\ell^m(\theta, \phi) + Y_0^0(\theta, \phi)] \quad (52)$$

$$\ell \neq 0$$

$$\rho(r, \theta, \phi, t) = \frac{e}{4\pi r^2} [\delta(r - r_n)] [Y_0^0(\theta, \phi) + \operatorname{Re} \{ Y_\ell^m(\theta, \phi) [1 + e^{i\omega_n t}] \}] \quad (53)$$

where

$$\operatorname{Re} \{ Y_\ell^m(\theta, \phi) [1 + e^{i\omega_n t}] \} = \operatorname{Re} \{ Y_\ell^m(\theta, \phi) + Y_\ell^m(\theta, \phi) e^{i\omega_n t} \} = P_\ell^m(\cos \theta) \cos m\phi + P_\ell^m(\cos \theta) \cos(m\phi + \omega_n t)$$

and $\omega_n = 0$ for $m = 0$.

The spin function of the electron (see Figure 1 for the charge function and Figure 4 for the current function) corresponds to the nonradiative $n=1, \ell = 0$ state of atomic hydrogen which is well known as an s state or orbital. The constant spin function is modulated by a time and spherical harmonic function as given by Eq. (53) and shown in Figure 2. The modulation or traveling charge density wave corresponds to an orbital angular momentum in addition to a spin angular momentum. These states are typically referred to as p, d, f, etc. orbitals and

correspond to an ℓ quantum number not equal to zero. Application of Haus's [18] condition (Eqs. (54-56)) also predicts nonradiation for a constant spin function modulated by a time and spherically harmonic orbital function. There is acceleration without radiation. (Also see Abbott and Griffiths and Goedecke [25-26]). However, in the case that such a state arises as an excited state by photon absorption, it is radiative due to a radial dipole term in its current density function since it possesses spacetime Fourier Transform components synchronous with waves traveling at the speed of light [2].

The Fourier transform of the electron charge density function is a solution of the four-dimensional wave equation in frequency space (\mathbf{k} , w-space). Then the corresponding Fourier transform of the current density function $K(s, \Theta, \Phi, \omega)$ is given by multiplying by the constant angular frequency.

$$K(s, \Theta, \Phi, \omega) = 4\pi\omega_n \frac{\sin(2s_n r_n)}{2s_n r_n} \otimes 2\pi \sum_{v=1}^{\infty} \frac{(-1)^{v-1} (\pi \sin \Theta)^{2(v-1)}}{(v-1)! (v-1)!} \frac{\Gamma\left(\frac{1}{2}\right) \Gamma\left(v + \frac{1}{2}\right)}{(\pi \cos \Theta)^{2v+1} 2^{v+1}} \frac{2v!}{(v-1)!} s^{-2v}$$

$$\otimes 2\pi \sum_{v=1}^{\infty} \frac{(-1)^{v-1} (\pi \sin \Phi)^{2(v-1)}}{(v-1)! (v-1)!} \frac{\Gamma\left(\frac{1}{2}\right) \Gamma\left(v + \frac{1}{2}\right)}{(\pi \cos \Phi)^{2v+1} 2^{v+1}} \frac{2v!}{(v-1)!} s^{-2v} \frac{1}{4\pi} [\delta(\omega - \omega_n) + \delta(\omega + \omega_n)]$$
(54)

The motion on the orbitsphere is angular; however, a radial component exists due to special relativistic effects. Consider the radial wave vector of the sinc function. When the radial projection of the velocity is c

$$\mathbf{s}_n \bullet \mathbf{v}_n = \mathbf{s}_n \bullet \mathbf{c} = \omega_n$$
(55)

the relativistically corrected wavelength is

$$r_n = \lambda_n$$
(56)

(i.e. the lab frame motion in the angular direction goes to zero as the velocity approaches the speed of light). Substitution of Eq. (56) into the sinc function results in the vanishing of the entire Fourier transform of the current-density function. Thus, spacetime harmonics of $\frac{\omega_n}{c} = k$ or

$$\frac{\omega_n}{c} \sqrt{\frac{\epsilon}{\epsilon_0}} = k \text{ for which the Fourier transform of the current-density function}$$

is nonzero do not exist. Radiation due to charge motion does not occur in any medium when this boundary condition is met.

The orbitsphere is a resonator cavity which traps photons of

discrete frequencies. The radius of an orbitsphere increases with the absorption of electromagnetic energy. The solutions to Maxwell's equations for modes that can be excited in the orbitsphere resonator cavity give rise to four quantum numbers, and the energies of the modes are the experimentally known hydrogen spectrum.

The subscript n is used in Eq. (39) and Eq. (74), the quantization condition, appears in the Excited States of the One Electron Atom (Quantization) Section of Mills [2]. Quantization arises as "allowed" solutions of the wave equation corresponding to a resonance between the electron and a photon.

More explicitly, it is well known that resonator cavities can trap electromagnetic radiation of discrete resonant frequencies. The orbitsphere is a resonator cavity which traps photons of discrete frequencies. Thus, photon absorption occurs as an excitation of a resonator mode. The "trapped photon" is a "standing electromagnetic wave" which actually is a circulating wave that propagates along with each great circle current loop of the orbitsphere. The time-function factor, $k(t)$, for the "standing wave" is identical to the time-function factor of the orbitsphere in order to satisfy the boundary (phase) condition at the orbitsphere surface. Thus, the angular frequency of the "trapped photon" has to be identical to the angular frequency of the electron orbitsphere, ω_n . Furthermore, the phase condition requires that the angular functions of the "trapped photon" have to be identical to the spherical harmonic angular functions of the electron orbitsphere. Combining $k(t)$ with the ϕ -function factor of the spherical harmonic gives $e^{i(m\phi - \omega_n t)}$ for both the electron and the "trapped photon" function. The photon is "glued" to the inner orbitsphere surface and the outer nuclear surface as photon source charge-density with a radial electric field.

From the application of the nonradiative boundary condition, the instability of excited states as well as the stability of the "ground" state arise naturally in the Mills theory as derived in Stability of Atoms and Hydrinos Section [2]. In addition to the above known states of hydrogen (Eq. (1), the theory predicts the existence of a previously unknown form of matter: hydrogen atoms and molecules having electrons of lower

energy than the conventional "ground" state, called *hydrinos* and *dihydrinos*, respectively, where each energy level corresponds to a fractional quantum number.

The central field of the proton corresponds to integer one charge. Excited states comprise an electron with a trapped photon. In all energy states of hydrogen, the photon has an electric field which superposes with the field of the proton. In the $n=1$ state, the sum is one, and the sum is zero in the ionized state. In an excited state, the sum is a fraction of one (i.e. between zero and one). Derivations from first principles given by Mills demonstrate that each "allowed" fraction corresponding to an excited state is $\frac{1}{\text{integer}}$. The relationship between the electric field equation and the "trapped photon" source charge-density function is given by Maxwell's equation in two dimensions.

$$\mathbf{n} \cdot (\mathbf{E}_1 - \mathbf{E}_2) = \frac{\sigma}{\epsilon_0} \quad (57)$$

where \mathbf{n} is the radial normal unit vector, $\mathbf{E}_1 = 0$ (\mathbf{E}_1 is the electric field outside of the orbitsphere), \mathbf{E}_2 is given by the total electric field at $r_n = n a_H$, and σ is the surface charge-density. The electric field of an excited state is fractional; therefore, the source charge function is fractional. It is well known that fractional charge is not "allowed". The reason is that fractional charge typically corresponds to a radiative current density function. The excited states of the hydrogen atom are examples. They are radiative; consequently, they are not stable. Thus, an excited electron decays to the first nonradiative state corresponding to an integer field, $n=1$ (i.e. a field of integer one times the central field of the proton).

Equally valid from first principles are electronic states where the magnitude of the sum of the electric field of the photon and the proton central field are an integer greater than one times the central field of the proton. These states are nonradiative. A catalyst can effect a transition between these states via a nonradiative energy transfer. Substantial experimental evidence exists that supports the existence of this novel hydrogen chemistry and its applications [27-62] which was missed entirely due to the erroneous concept of the hydrogen atom "ground state" based on the Schrödinger equation. An analysis of the

shortcomings of the Schrödinger equation are given in the Appendix and in a paper by Mills [7]. The success of the classical theory of Mills is demonstrated in a recent presentation and recent publications [59-62].

Furthermore, it is a mistake to take the position that solutions of the POSTULATED Schrödinger equation which correspond to $n = \text{integer}$ prohibit the existence of hydrogen atoms having a binding energy corresponding to $n = \frac{1}{\text{integer}}$. Specifically, it is wrong to take the position that $n = \frac{1}{\text{integer}}$ values cannot exist according to conventional scientific theories since the Schrödinger equation may be solved for either case with equal validity. However, in neither case does the Schrödinger equation provide a physical basis for their existence or behavior with regard to radiation. For example, the Schrödinger equation does not explain the observation that spontaneous emission of radiation does not occur for the state having a binding energy of 13.6 eV. See the Appendix and Mills [7].

Schrödinger States Below $n=1$

In Eq. (22), n^* does not have to be an integer, it may be any arbitrary constant β . Then the corresponding solution is [14]

$$y = e^{-x^{1/2}} x^{(k-1)/2} \frac{d^k}{dx^k} L_\beta(x) \quad (58)$$

where k is a positive integer. By comparing Eq. (21) and Eq. (22),

$$\frac{k^2 - 1}{4} = \ell(\ell + 1) \quad (59)$$

Thus,

$$k = 2\ell + 1 \quad (60)$$

and

$$n^* - \frac{k-1}{2} = n^* - \ell = \frac{me^2}{\hbar} \left(\frac{\alpha}{2} \right)^{-1} \quad (61)$$

Substitution of the value of α and solving for W gives

$$W = \frac{1}{2} \frac{me^4}{(n^* - \ell)^2 \hbar^2} \quad (62)$$

Because of the conditions on n^* and k , the quantity $n^* - \ell$ can not be zero. In the case that n^* is given as $n^* = \frac{1}{p} + \ell$ where p is a positive integer, the

condition is satisfied. In this case, the principal quantum number is given as $\frac{1}{p}$ where p is a positive integer. The energy states of the hydrogen atom are

$$W_n = -E_n = \frac{1}{2} \frac{me^4}{\left(\frac{1}{p}\right)^2 \hbar^2} \quad (63)$$

and the corresponding eigenfunctions from Eq. (58) are

$$R_{p,\ell} = c_{p,\ell} e^{-x^{1/2}} x^\ell \frac{d^{2\ell+1}}{dx^{2\ell+1}} L_{\frac{1}{p}+\ell}(x) \quad (64)$$

where the variable x is defined by

$$x = \alpha r = \frac{\sqrt{8mW}}{\hbar} r = \frac{2me^2}{\frac{1}{p} \hbar^2} r \quad (65)$$

In the Bohr theory of the hydrogen atom, the first orbital has a radius in CGS units given by

$$a_0 = \frac{\hbar^2}{me^2} = 0.53 \times 10^{-8} \text{ cm} \quad (66)$$

Thus, $\alpha = 2p/a_0$ and

$$x = \frac{2pr}{a_0} \quad (67)$$

The energy states of the hydrogen atom in CGS units in terms of the Bohr radius are given by

$$E = -\frac{1}{2} \frac{me^4}{\left(\frac{1}{p}\right)^2 \hbar^2} = -\frac{e^2}{2\left(\frac{1}{p}\right)a_0} \quad (68)$$

Eq. (68) corresponds to hydrogen atoms having a binding energy corresponding to $n = \frac{1}{p}$. It is an equally valid solution of the Schrödinger equation for the energy of the hydrogen atom as Eq. (29) corresponding to hydrogen atoms having a binding energy corresponding to $n = \text{integer}$.

Schrödinger equation for the energy of the hydrogen atom as Eq. (29) corresponding to hydrogen atoms having a binding energy corresponding to $n = \text{integer}$.

The Electron of Atomic Hydrogen Does Not Spontaneously Emit Radiation at the $n=1$ State, but that Does Not Preclude Radiationless Processes Including Formation of Molecular Hydrogen.

The nonradiative state of atomic hydrogen which is historically called the "ground state" forms the basis of the boundary condition of Mills theory [63] to solve the wave equation. Mills further predicts [64] that certain atoms or ions serve as catalysts to release energy from hydrogen to produce an increased binding energy hydrogen atom called a *hydrino atom* having a binding energy of

$$\text{Binding Energy} = \frac{13.6 \text{ eV}}{n^2} \quad (69)$$

where

$$n = \frac{1}{2}, \frac{1}{3}, \frac{1}{4}, \dots, \frac{1}{p} \quad (70)$$

and p is an integer greater than 1, designated as $H\left[\frac{a_H}{p}\right]$ where a_H is the radius of the hydrogen atom. Hydrinos are predicted to form by reacting an ordinary hydrogen atom with a catalyst having a net enthalpy of reaction of about

$$m \cdot 27.2 \text{ eV} \quad (71)$$

where m is an integer. This catalysis releases energy from the hydrogen atom with a commensurate decrease in size of the hydrogen atom, $r_n = n a_H$. For example, the catalysis of $H(n=1)$ to $H(n=1/2)$ releases 40.8 eV, and the hydrogen radius decreases from a_H to $\frac{1}{2}a_H$.

It is taught in textbooks that atomic hydrogen cannot go below the ground state. Atomic hydrogen having an experimental ground state of 13.6 eV can only exist in a vacuum or in isolation, and atomic hydrogen cannot go below this ground state in isolation. However, there is no known composition of matter containing hydrogen in the ground state of 13.6 eV. Atomic hydrogen is radical and is very reactive. It may react to form a hydride ion or compositions of matter. It is a chemical intermediate which may be trapped as many chemical intermediates may be by methods such as isolation or cryogenically. A hydrino atom may be considered a chemical intermediate that may be trapped in vacuum or isolation. A hydrino atom may be very reactive to form a hydride ion or a novel composition of matter. Hydrogen at predicted lower energy levels, hydrino atoms, has been identified in the extreme ultraviolet emission spectrum from interstellar medium [7]. In addition, new compositions of matter containing hydrogen at predicted lower energy

levels have recently been observed in the laboratory [38, 40-58], -which energy levels are achieved using the novel catalysts. Spectroscopic experiments confirm the catalysis of hydrogen [27-44].

The excited energy states of atomic hydrogen are also given by Eq. (69) except that

$$n = 1, 2, 3, \dots \quad (72)$$

The $n=1$ state is the "ground" state for "pure" photon transitions (the $n=1$ state can absorb a photon and go to an excited electronic state, but it cannot release a photon and go to a lower-energy electronic state).

However, an electron transition from the ground state to a lower-energy state is possible by a nonradiative energy transfer such as multipole coupling or a resonant collision mechanism. These lower-energy states have fractional quantum numbers, $n = \frac{1}{\text{integer}}$. Processes that occur

without photons and that require collisions are common. For example, the exothermic chemical reaction of $H + H$ to form H_2 does not occur with the emission of a photon. Rather, the reaction requires a collision with a third body, M , to remove the bond energy- $H + H + M \rightarrow H_2 + M^*$ [65]. The third body distributes the energy from the exothermic reaction, and the end result is the H_2 molecule and an increase in the temperature of the system. Some commercial phosphors are based on nonradiative energy transfer involving multipole coupling [66]. For example, the strong absorption strength of Sb^{3+} ions along with the efficient nonradiative transfer of excitation from Sb^{3+} to Mn^{2+} , are responsible for the strong manganese luminescence from phosphors containing these ions.

Similarly, the $n=1$ state of hydrogen and the $n = \frac{1}{\text{integer}}$ states of hydrogen are nonradiative, but a transition between two nonradiative states is possible via a nonradiative energy transfer, say $n=1$ to $n=1/2$. In these cases, during the transition the electron couples to another electron transition, electron transfer reaction, or inelastic scattering reaction which can absorb the exact amount of energy that must be removed from the hydrogen atom. Thus, a catalyst provides a net positive enthalpy of reaction of $m \cdot 27.2 \text{ eV}$ (i.e. it absorbs $m \cdot 27.2 \text{ eV}$ where m is an integer). Certain atoms or ions serve as catalysts which resonantly accept energy from hydrogen atoms and release the energy to the surroundings to

effect electronic transitions to fractional quantum energy levels. -

Once formed hydrinos have a binding energy given by Eqs. (71-72); thus, they may serve as catalysts which provide a net enthalpy of reaction given by Eq. (71). Also, the simultaneous ionization of two hydrogen atoms may provide a net enthalpy given by Eq. (71). Since the surfaces of stars comprise significant amounts of atomic hydrogen, hydrinos may be formed as a source to interstellar space where further transitions may occur.

A number of experimental observations lead to the conclusion that atomic hydrogen can exist in fractional quantum states that are at lower energies than the traditional "ground" ($n=1$) state. For example, the existence of fractional quantum states of hydrogen atoms explains the spectral observations of the extreme ultraviolet background emission from interstellar space [67], which may characterize dark matter as demonstrated in Table 2 of Mills [7].

Laboratory experiments that confirm the novel hydrogen chemistry include extreme ultraviolet (EUV) spectroscopy [27, 29-32, 35-39, 42-44], plasma formation [27-39, 42-44], power generation [28-30, 35, 62], and analysis of chemical compounds [38, 42-58, 62]. For example, lines observed by EUV spectroscopy could be assigned to transitions of atomic hydrogen to lower energy levels corresponding to lower energy hydrogen atoms called hydrino atoms and the emission from the excitation of the corresponding hydride ions formed from the hydrino atoms [29]. The chemical interaction of catalysts with hydrogen at temperatures below 1000 K has shown surprising results in terms of the emission of the Lyman and Balmer lines [27-44] and the formation of novel chemical compounds [38, 40-58]. An energetic plasma in hydrogen was generated by a catalysis reaction at 1% of the theoretical or prior known voltage requirement and with 1000's of times less power input in a system wherein the plasma reaction is controlled with a weak electric field [29-30, 35]. The optically measured output power of gas cells for power supplied to the glow discharge increased by over two orders of magnitude depending on the presence of less than 1% partial pressure of certain of catalysts in hydrogen gas or argon-hydrogen gas mixtures [28]. A hydrogen plasma formed by reacting a catalyst with hydrogen was recorded when there was no electric energy input to the reaction [33-34].

The optically measured output power of gas cells for power supplied to the glow discharge increased by over two orders of magnitude depending on the presence of less than 1% partial pressure of certain of catalysts in hydrogen gas or argon-hydrogen gas mixtures [28]. Continuum state emission of Cs^{2+} and Ar^{2+} at 53.3 nm and 45.6 nm, respectively, with the absence of the other corresponding Rydberg series of lines from these species confirmed the resonant nonradiative energy transfer of 27.2 eV from atomic hydrogen to atomic cesium or Ar^+ . The predicted hydride ion of hydrogen catalysis by either cesium atom or Ar^+ catalyst is the hydride ion $H^- (1/2)$. This ion was observed spectroscopically at 407 nm corresponding to its predicted binding energy of 3.05 eV [27].

Theory of One Electron States (Hydrogen Atom and Electron Bubble in Superfluid Helium)

Recently a new challenge to the fundamental foundations of quantum mechanics has arisen based on experiments of free electrons injected into superfluid helium. In order to explain the increase in conductivity observed when electrons in superfluid helium are irradiated with light, British physicist Humphrey Maris has proposed that the electron breaks into equal sized fragments which he calls "electrinos". According to Maris, this process of division of the electron may continue to such that the electron breaks into two and then the 1/2 electrons may divide into two forming 1/4 electrons, and the process may repeat indefinitely.

Electrons do not break into pieces. It is shown *infra* that the free electron in superfluid helium is an orbitsphere which can act as a resonator cavity and absorb resonant radiation to form stable nonradiative states of radii $n = \frac{1}{p}$ times that of the radius of the electron without an absorbed photon. The solutions are analogous to the solutions of lower-energy states of hydrogen called hydrinos with principal energy levels given by Eqs. (71-72) and radii given by $\frac{a_H}{p}$ where a_H is the radius of the hydrogen atoms and p is an integer.

For the electron of the hydrogen atom which comprises a dynamic spherical resonator cavity, the relationship between an allowed radius

and the "photon standing wave" wavelength is

$$2\pi r = n\lambda \quad (73)$$

where n is an integer. Now, the question arises: given that this is a resonator cavity, which nonradiative states are possible where the transition is effected by a "trapped photon"? For the electron orbitsphere, a spherical resonator cavity, the relationship between an allowed radius and the electron wavelength is

$$2\pi(nr_1) = 2\pi r_n = n\lambda_1 = \lambda_n \quad (74)$$

where

$$n = 1, 2, 3, 4, \dots$$

$$n = \frac{1}{2}, \frac{1}{3}, \frac{1}{4}, \dots, \frac{1}{p} \text{ where } p \text{ is an integer}$$

λ_1 is the allowed wavelength for $n=1$

r_1 is the allowed radius for $n=1$

The nonradiative boundary condition from Haus [18] and the relationship between the electron and the photon give the "allowed" hydrogen energy states which are quantized as a function of the parameter n . That is the nonradiative boundary condition and the relationship between an allowed radius and the photon standing wave wavelength Eq. (73) gives rise to Eq. (74), the boundary condition for allowed radii and allowed electron wavelengths as a function of the parameter n . Each value of n corresponds to an allowed transition effected by a resonant photon which excites the transition in the orbitsphere resonator cavity. In addition to the traditional integer values (1, 2, 3,...) of n , values of fractions are allowed according to Eq. (74) which correspond to transitions with an increase in the central field (charge) and decrease in the radius of the orbitsphere. This occurs, for example, when the orbitsphere transfers energy nonradiatively to a catalyst which resonantly accepts the energy. The electron undergoes a transition to a lower energy nonradiative state. The "Excited States of the One Electron Atom (Quantization)" section of Mills [2] gives the solutions of the excited states of atomic hydrogen and the "BlackLight Process" section gives the solutions of lower-energy states.

The photon equation must be a solution of Laplace's equation in spherical coordinates. The "trapped photon" field comprises an electric field which provides force balance and a nonradiative orbitsphere. The

solution to this boundary value problem of the radial photon electric field of hydrogen states is given by

$$\mathbf{E}_{r_{\text{photon}}, n, l, m} = \frac{e(na_H)^l}{4\pi\epsilon_0} \frac{1}{r^{(l+2)}} \left[-Y_0^0(\theta, \phi) + \frac{1}{n} \left[Y_0^0(\theta, \phi) + \operatorname{Re} \left\{ Y_l^m(\theta, \phi) [1 + e^{i\omega_n t}] \right\} \right] \right]$$

$$\omega_n = 0 \text{ for } m = 0 \quad (75)$$

$$l = 1, 2, \dots, n-1$$

$$m_l = -l, -l+1, \dots, 0, \dots, +l$$

And, the quantum numbers of the electron are n , l , m_l , and $m_s = \pm 1/2$ are the same as the corresponding quantum numbers for excited states. $\mathbf{E}_{r_{\text{total}}}$ is the sum of the "trapped photon" and proton electric fields,

$$\mathbf{E}_{r_{\text{total}}} = \frac{e}{4\pi\epsilon_0 r^2} + \frac{e(na_H)^l}{4\pi\epsilon_0} \frac{1}{r^{(l+2)}} \left[-Y_0^0(\theta, \phi) + \frac{1}{n} \left[Y_0^0(\theta, \phi) + \operatorname{Re} \left\{ Y_l^m(\theta, \phi) [1 + e^{i\omega_n t}] \right\} \right] \right]$$

$$\omega_n = 0 \text{ for } m = 0 \quad (76)$$

For $r = na_H$ and $m = 0$, the total radial electric field is

$$\mathbf{E}_{r_{\text{total}}} = \frac{1}{n} \frac{e}{4\pi\epsilon_0 (na_H)^2} \quad (77)$$

In Eqs. (75-77), the excited states of hydrogen correspond to $n = 1, 2, 3, 4, \dots$, and the hydrino states correspond to $n = \frac{1}{2}, \frac{1}{3}, \frac{1}{4}, \dots, \frac{1}{p}$ where p is an integer.

The "trapped photon" is a "standing electromagnetic wave" which actually is a circulating wave that propagates along with each great circle current loop of the electron orbitsphere. The time-function factor, $k(t)$, for the "standing wave" is identical to the time-function factor of the orbitsphere in order to satisfy the boundary (phase) condition at the orbitsphere surface. Thus, the angular frequency of the "trapped photon" has to be identical to the angular frequency of the electron orbitsphere, ω_n . Furthermore, the phase condition requires that the angular functions of the "trapped photon" have to be identical to the spherical harmonic angular functions of the electron orbitsphere. Combining $k(t)$ with the ϕ -function factor of the spherical harmonic gives $e^{i(m\phi - \omega_n t)}$ for both the electron and the "trapped photon" function. The photon is "glued" to the inner orbitsphere surface and the outer nuclear surface as photon source charge-density with a radial electric field. The angular functions in phase with the corresponding photon functions are given by Eqs. (52-53).

The solution of the "trapped photon" field of electrons in helium is

analogous to those for hydrinos except that the $-Y_0^0(\theta, \phi)$ term is not present since the central field of the proton is absent and the nature of the field at the origin is equivalent to the solution of the Poisson equation with a delta function inhomogeneity at the origin [68].

$$\begin{aligned} E_{r_{\text{photon}}, n, l, m} &= C \frac{e(na)^l}{4\pi\epsilon_0} \frac{1}{r^{(l+2)}} \left[\frac{1}{n} \left[Y_0^0(\theta, \phi) + \operatorname{Re} \{ Y_l^m(\theta, \phi) [1 + e^{i\omega_n t}] \} \right] \right] \\ \omega_n &= 0 \quad \text{for } m = 0 \\ n &= 1, \frac{1}{2}, \frac{1}{3}, \frac{1}{4}, \dots, \frac{1}{p} \\ l &= 1, 2, \dots, n-1 \\ m &= -l, -l+1, \dots, 0, \dots, +l \end{aligned} \quad (78)$$

In Eq. (78), a is the radius of the electron in helium without an absorbed photon. C is a constant expressed in terms of an equivalent central charge. It is determined by the force balance between the centrifugal force of the electron orbitsphere and the radial force provided by the pressure from the van der Waals force of attraction between helium atoms given *infra*.

Stability of "Ground", Hydrino, and Helium States

For the below "ground" (fractional quantum) energy states of the hydrogen atom, σ_{photon} , the two dimensional surface charge due to the "trapped photon" at the electron orbitsphere, is given by Eqs. (5.13) and (2.11) of Mills [2].

$$\sigma_{\text{photon}} = \frac{e}{4\pi(r_n)^2} \left[Y_0^0(\theta, \phi) - \frac{1}{n} \left[Y_0^0(\theta, \phi) + \operatorname{Re} \{ Y_l^m(\theta, \phi) [1 + e^{i\omega_n t}] \} \right] \right] \delta(r - r_n) \quad n = 1, \frac{1}{2}, \frac{1}{3}, \frac{1}{4}, \dots, \quad (79)$$

And, σ_{electron} , the two dimensional surface charge of the electron orbitsphere is

$$\sigma_{\text{electron}} = \frac{-e}{4\pi(r_n)^2} \left[Y_0^0(\theta, \phi) + \operatorname{Re} \{ Y_l^m(\theta, \phi) [1 + e^{i\omega_n t}] \} \right] \delta(r - r_n) \quad (80)$$

The superposition of σ_{photon} (Eq. (79)) and σ_{electron} , (Eq. (80)) where the spherical harmonic functions satisfy the conditions given in the "Angular Function" section of Mills [2] is a radial electric monopole represented by a delta function.

$$\sigma_{\text{photon}} + \sigma_{\text{electron}} = \frac{-e}{4\pi(r_n)^2} \left[\frac{1}{n} Y_0^0(\theta, \phi) + \left(1 + \frac{1}{n} \right) \operatorname{Re} Y_l^m(\theta, \phi) [1 + e^{i\omega_n t}] \right] \delta(r - r_n) \quad n = 1, \frac{1}{2}, \frac{1}{3}, \frac{1}{4}, \dots, \quad (81)$$

As given in the "Spacetime Fourier Transform of the Electron Function" section of Mills [2], the radial delta function does not possess spacetime Fourier components synchronous with waves traveling at the speed of light (Eqs. (54-56)). Thus, the below "ground" (fractional quantum) energy states of the hydrogen atom are stable. The "ground" ($n=1$ quantum) energy state is just the first of the nonradiative states of the hydrogen atom; thus, it is the state to which excited states decay.

The speed of light in vacuum c is given by

$$c = \frac{1}{\sqrt{\mu_0 \epsilon_0}} \quad (82)$$

where μ_0 is the permeability of free-space and ϵ_0 is the permittivity of free-space. The wavenumber is given by

$$k_{vacuum} = \frac{2\pi}{\lambda} = \omega \sqrt{\mu_0 \epsilon_0} \quad (83)$$

The speed of light in a medium such as superfluid helium v is given by

$$v = \frac{1}{\sqrt{\mu_0 \epsilon}} \quad (84)$$

where μ_0 is the permeability of free-space and ϵ is the permittivity of the medium. The wavenumber is given by

$$k_{medium} = \frac{2\pi}{\lambda} = \omega \sqrt{\mu_0 \epsilon} \quad (85)$$

The ratio of the wavenumber in vacuum and the wavenumber in superfluid helium is given by

$$\frac{k_{helium}}{k_{vacuum}} = \frac{\frac{2\pi}{\lambda_{helium}}}{\frac{2\pi}{\lambda_{vacuum}}} = \frac{\omega \sqrt{\mu_0 \epsilon}}{\omega \sqrt{\mu_0 \epsilon_0}} \quad (86)$$

The frequency of the photon in free space and in helium at the electron must be the same. Thus,

$$k_{helium} = k_{vacuum} \frac{\epsilon}{\epsilon_0} \quad (87)$$

Since $\epsilon > \epsilon_0$, the wavenumber in helium is greater than the wavenumber in vacuum. Thus, a photon traveling in liquid helium may excite a mode in an electron bubble which is nonradiative. In this case, spacetime

harmonics of $\frac{\omega_n}{c} = k$ or $\frac{\omega_n}{c} \sqrt{\frac{\epsilon}{\epsilon_0}} = k$ for which the Fourier transform of the

current-density function is nonzero do not exist. Radiation due to charge motion does not occur in any medium when this boundary condition is

met.

The viscosity of superfluid helium is a function of temperature. The observation of the temperature dependence of photon absorption by electrons in superfluid helium to give rise to an increase in conductivity may be explained on this basis. That is, at 1.7 K, the viscosity is sufficiently close to zero such that the angular current of the electron may propagate without energy loss. Roton scattering dominates over phonon scattering at this temperature and below [69]. In this case, resonant absorption may occur between stable nonradiative states; wherein the forces are central. The two dimensional surface charge due to the "trapped photon" at the electron orbitsphere of an electron in helium has the same form as that given by Eq. (81). Thus, the states of photons absorbed by electrons in helium are stable under these conditions.

Conservation of Angular Momentum

The field is time harmonic which is satisfied by the fields spinning around the z-axis at frequency ω_n in phase with the electron. The relationship between the electric field equation and the "trapped photon" source charge-density function is given by Maxwell's equation in two dimensions.

$$\mathbf{n} \cdot (\mathbf{E}_1 - \mathbf{E}_2) = \frac{\sigma}{\epsilon_0} \quad (88)$$

where \mathbf{n} is the radial normal unit vector, $\mathbf{E}_1 = 0$ (\mathbf{E}_1 is the electric field outside of the orbitsphere), \mathbf{E}_2 is given by the total electric field at $r_n = n a_H$, and σ is the surface charge-density. In order that the radial electric field is always positive and the surface charge density is always negative, a constant function adds to a spherical harmonic function; thus, the spherical harmonic function modulates the constant function. The surface charge density has a phase matched pattern. This provides a central force to balance the centrifugal force of the electron. The magnitude of the radial electric field is that which satisfies the boundary condition of force balance at the allowed radii of electron states.

The time harmonic condition is satisfied by the rotation of the fields in phase with the source currents. The spinning field and the corresponding source current at the electron orbitsphere conserves the

angular momentum of the photon. The time-averaged angular-momentum density, \mathbf{m} , of the emitted photon is given by Eq. (16.61) of Jackson [70]

$$\mathbf{m} = \frac{1}{8\pi} \operatorname{Re}[\mathbf{r} \times (\mathbf{E} \times \mathbf{B}^*)] \quad (89)$$

The ratio of the square of the angular momentum, M^2 , to the square of the energy, U^2 , for a pure (l,m) multipole [70] is

$$\frac{M^2}{U^2} = \frac{m^2}{\omega^2} \quad (90)$$

Experimentally, the photon can carry $\pm \hbar$ units of angular momentum. Thus, during excitation the spin, orbital, or total angular momentum of the orbitsphere can change by zero or $\pm \hbar$. The electron transition rules arise from conservation of angular momentum. The selection rules for multipole transitions between quantum states arise from conservation of total angular momentum and component angular momentum where the photon carries \hbar of angular momentum. The radiation of a multipole of order (l, m) carries $m\hbar$ units of the z component of angular momentum per photon of energy $\hbar\omega$.

Consider the angular frequency of the electron orbitsphere. Given time harmonic motion and a radial delta function, the relationship between an allowed radius and the electron wavelength is given by Eq. (74). Using the de Broglie relationship for the electron momentum where the coordinates are spherical,

$$\lambda_n = \frac{\hbar}{p_n} = \frac{\hbar}{m_e v_n} \quad (91)$$

and the magnitude of the velocity for every point on the orbitsphere is

$$v_n = \frac{\hbar}{m_e r_n} \quad (92)$$

The corresponding angular frequencies are related to r_n by

$$\nu_n = r_n \omega_n \quad (93)$$

Thus,

$$\omega_n = \frac{\hbar}{m_e r_n^2} \quad (94)$$

The sum of the \mathbf{L}_i , the magnitude of the angular momentum of each infinitesimal point of the orbitsphere of mass m_i , must be constant. The constant is \hbar .

$$\sum |L_i| = \sum |\mathbf{r} \times m_i \mathbf{v}| = m_e r_n \frac{\hbar}{m_e r_n} = \hbar \quad (95)$$

where the velocity is given by Eq. (92). The vector projections of the orbitsphere spin angular momentum relative to the Cartesian coordinates are given in the "Spin Angular Momentum of the Orbitssphere with $\lambda = 0$ " section of Mills [2]. The result is that the electron possesses a projection of the angular momentum onto an axis S of $\pm \sqrt{\frac{3}{4}}\hbar$ which precesses about the axis of an applied magnetic field at the Larmor frequency.

Photon Absorption

In order that the excitation can occur, the correspondence principle holds such that the frequency of the photon that is absorbed is equal to the change in angular frequency of the electron. The energy of the photon which excites a mode in a stationary spherical resonator cavity from radius a_H to radius na_H is

$$E_{photon} = \frac{e^2}{4\pi\epsilon_0 a_H} \left[1 - \frac{1}{n^2} \right] = \hbar v = \hbar\omega \quad (96)$$

where $n = \text{integer}$. After multiplying Eq. (96) by $\frac{a_H}{a_H} = \frac{4\pi\epsilon_0\hbar^2}{e^2\mu_e a_H}$, where a_H is the radius of the hydrogen atom, ω_{photon} is

$$\omega_{photon} = \frac{\hbar}{m_e a_H^2} \left[1 - \frac{1}{n^2} \right] \quad (97)$$

In the case of an electron orbitssphere, the resonator possesses kinetic energy before and after the excitation. The kinetic energy is always one-half of the potential energy because the centripetal force is an inverse squared central force. As a result, the energy and angular frequency to excite an electron orbitssphere is only one-half of the values above, Eqs. (96) and (97). From Eq. (94), the angular velocity of an electron orbitssphere of radius na_H is

$$\omega_n = \frac{\hbar}{m_e (na_H)^2} \quad (98)$$

The change in angular velocity of the orbitssphere for an excitation from $n=1$ to $n=n$ is

$$\Delta\omega = \frac{\hbar}{m_e (a_H)^2} - \frac{\hbar}{m_e (na_H)^2} = \frac{\hbar}{m_e (a_H)^2} \left[1 - \frac{1}{n^2} \right] \quad (99)$$

The kinetic energy change of the transition is

$$\frac{1}{2} m_e (\Delta v)^2 = \frac{1}{2} \frac{e^2}{4\pi\epsilon_0 a_H} \left[1 - \frac{1}{n^2} \right] = \frac{1}{2} \hbar \omega \quad (100)$$

The change in angular velocity of the electron orbitsphere, Eq. (99), is identical to the angular velocity of the photon necessary for the excitation, ω_{photon} (Eq. (97)). The energy of the photon necessary to excite the equivalent transition in an atomic hydrogen electron orbitsphere is one-half of the excitation energy of the stationary cavity because the change in kinetic energy of the electron orbitsphere supplies one-half of the necessary energy. The change in the angular frequency of the orbitsphere during a transition and the angular frequency of the photon corresponding to the superposition of the free space photon and the photon corresponding to the kinetic energy change of the orbitsphere during a transition are equivalent. The correspondence principle holds. It can be demonstrated that the resonance condition between these frequencies is to be satisfied in order to have a net change of the energy field [71].

SUPERFLUID HELIUM ION MOBILITY RESULTS AND DISCUSSION

Experiments to study the effect of light on ion mobility have been conducted by Northby and Sanders [72-73], Zipfel and Sanders [74-75], and Grimes and Adams [76-77]. For example, in the Northby and Sanders experiments [72-73], ions were introduced into the liquid from a radioactive source, and had to pass through two grids in order to reach the detector. The voltages on the grids were varied in time in a way such that normal negative ions could not reach the detector. It was found that when the liquid was illuminated, a small ion current reached the detector. Thus, they observed an increase in ion mobility under illumination, but recognized that the origin of the effect was unclear. It appears that the absorption of a photon by an electron bubble or orbitsphere in superfluid helium provides a natural explanation for the majority of the photo-conductivity results.

The photon absorption is determined by the correspondence principle. Thus, the radius of the electron following the absorption of a resonant photon is given by $n = \frac{1}{\text{integer}}$ times that of the original radius.

$$r = nr_i \quad - \quad (101)$$

where $n = \frac{1}{\text{integer}}$ and r_i is the radius of the electron in superfluid helium

which has not absorbed a photon. This radius is determined by a force balance between the van der Waals pressure (force per unit area) of superfluid helium and the centrifugal force of the electron. The latter is given by

$$\mathbf{F}_{\text{centrifugal}} = \frac{m_e}{4\pi r_i^2} \frac{\mathbf{v}_i^2}{r_i} \quad (102)$$

where $\frac{m_e}{4\pi r_i^2}$ is the mass density of the orbitsphere and \mathbf{v}_i is given by Eq. (92).

The radius r_i can be determined from the photo-conductivity experiments of Zipfel and Sanders [75]. At zero pressure a photo-conductivity peak was observed at approximately 0.5 eV. From Eq. (97), the change in the frequency of the electron which matches frequency of the exciting photon is given by

$$\omega_{\text{photon}} = \frac{\hbar}{m_e r_i^2} \left[\frac{1}{n^2} - 1 \right] \quad (103)$$

where $n = \frac{1}{\text{integer}}$. The radius r_i is given by

$$r_i = \sqrt{\frac{\hbar}{m_e \omega_{\text{photon}}} \left(\frac{1}{n^2} - 1 \right)} \quad (104)$$

The relationship between energy and angular frequency of a photon is given by Planck's equation.

$$E = \hbar \omega_{\text{photon}} \quad (105)$$

The angular frequency corresponding to a photon of 0.5 eV is

$$\omega_{\text{photon}} = \frac{8.0 \times 10^{-20} \text{ J}}{\hbar} = 7.6 \times 10^{14} \text{ rad/sec} \quad (106)$$

In the case that 0.5 eV is the lowest energy transition for an electron in superfluid helium, the $n=1 \rightarrow n=\frac{1}{2}$ transition corresponds to $n=\frac{1}{2}$ in Eq. (103). From Eq. (103) and Eq. (106), the radius r_i is

$$r_i = \sqrt{\frac{\hbar}{m_e (7.6 \times 10^{14} \text{ rad/sec})} \left(\frac{1}{\left(\frac{1}{2}\right)^2} - 1 \right)} = 6.7 \times 10^{-10} \text{ m} = 6.7 \text{ \AA} \quad (107)$$

where $n=\frac{1}{2}$. Comparing the case of the electron of a hydrogen atom to

the case of an electron in helium, no initial central Coulomb field due to a proton is present, and the electron increases in kinetic energy upon photon absorption. Thus, the energy required to cause a transition in the latter case is twice that of the former. The photon stores energy in the electric field of the resonator mode and increases the potential energy of the electron. The potential is the sum of the binding energy and the kinetic energy. The corresponding photon wavelength that will be absorbed by the electron is $2.5 \mu m$.

The radius calculated in Eq. (107), is an approximation since the energy due to the pressure volume work and the surface energy change of the bubble were neglected. The former is given by

$$P \int dV = \frac{4}{3} \pi (r_i^3 - r_n^3) P \quad (108)$$

where P is the applied pressure, the integral is over the volume of the bubble, and r_i and r_n are the initial and final radii of the electron bubble. The latter is given by

$$\alpha \int dA = 4\pi (r_i^2 - r_n^2) \alpha \quad (109)$$

where α is the surface energy of helium per unit area, the integral is over the surface of the bubble, and r_i and r_n are the initial and final radii of the electron bubble.

The contribution of these terms can be estimated by comparing the next experimental photo-conductivity peak at higher energy compared to the prediction given by Eqs. (103) and (105). Northby and Sanders [72-73] found that in the range of $0.7 eV$ to $3 eV$ the photo-induced current had a peak when the photon energy was $1.21 eV$ at zero pressure. Zipfel and Sanders [74-75] confirmed the peak at $1.21 eV$. In experiments similar to those of Northby and Sanders [72-73], Zipfel and Sanders [74-75] made measurements of the photo-conductivity as a function of pressure up to 16 bars. The photo-conductivity peak detected by Northby and Sanders [72-73] was found to shift to higher photon energies as the pressure increased. This is expected since the radius of the normal electron decreases and the corresponding initial angular frequency increases with increasing pressure. Thus, the transition angular frequencies and energies increase (Eq. (103)).

The next higher energy transition for an electron in superfluid

helium is $n=1 \rightarrow n=\frac{1}{2}$. The transition energy corresponds to $n=\frac{1}{3}$ in Eqs. (103) and (105).

The calculated energy neglecting the energy due to the pressure volume work and the surface energy change of the bubble is

$$E = \hbar\omega_{\text{photon}} = \frac{\hbar^2}{m_e r_i^2} \left[\frac{1}{\left(\frac{1}{3}\right)^2} - 1 \right] = \frac{\hbar^2}{m_e (6.7 \times 10^{-10} \text{ m})^2} \left[\frac{1}{\left(\frac{1}{3}\right)^2} - 1 \right] = 1.3 \text{ eV} \quad (110)$$

where r_i is given by Eq. (107). Given the experimental uncertainty of the energy of the lowest energy transition, 1.21 eV, this result confirms that the contributions due to pressure volume work and the surface energy change of the bubble may be neglected.

In the experiments of Northby and Sanders [72-73], Zipfel and Sanders [74-75], and Grimes and Adams [76-77], it was noted that the photo-conductivity effect was absent above a critical temperature. This temperature was approximately 1.7 K at zero pressure, and decreased to 1.2 K at 20 bars. Roton scattering dominates over phonon scattering at 1.7 K and below [69]. The photo-conductivity signal disappears because of phonon excitation of the bubble motion which causes the excited electron state to decay. As the pressure is increased, the roton energy gap goes down, and so the phonon scattering increases. Thus, it is to be expected that the critical temperature decreases with increasing pressure.

Each stable excited state electron bubble which has a radius of $\frac{r_i}{\text{integer}}$ may migrate in an applied electric field. The bubble may be scattered by rotons, phonons, and He^3 impurities. At temperatures less than 1.7 K, roton scattering dominates [69]. An equation for the electron bubble mobility is derived by Baym, Barrera, and Pethick [78] in terms of the roton-bubble momentum transfer cross section by calculating the rate of roton-bubble momentum transfer using a statistical mechanical approach. In the case of an elementary excitation \vec{k} scattered by the bubble with a differential cross section $\sigma(k, \theta)$ and obeying $|\vec{k}'| \equiv |\vec{k}|$, their result may be written

$$\frac{e}{\mu} = -\frac{\hbar^2}{6\pi^2} \int_0^\infty k^4 \frac{\delta n}{\delta \epsilon} v_s(k) \sigma_T(k) dk \quad (111)$$

where μ is the bubble mobility, n is the distribution function of the excitation, $v_g(k)$ is the group velocity of the excitation, and $\sigma_r(k)$ is the momentum-transfer cross section defined by

$$\sigma_r(k) = \int (1 - \cos \theta) \sigma(k, \theta) d\Omega \quad (112)$$

Schwarz and Stark [69] made the reasonable assumption that $\sigma_r(k)$ is a weak function of $k - k_0$. Because of the strong minimum at $k_0 = 1.91 \text{ \AA}^{-1}$ in the roton energy spectrum, Eq. (111) then gives to a good approximation

$$\mu = \frac{3\pi^2 e}{\hbar k_0^3 \sigma_r(k_0)} \exp(\Delta/k_B T) = \frac{3.38 \times 10^{-25} m^4 V^{-1} \text{ sec}^{-1}}{\sigma_r(k_0)} \exp(8.65 K/T) \quad (113)$$

where $\Delta/k_B = 8.65 \pm 0.04 \text{ K}$ is the roton energy gap derived from neutron scattering [79]. Schwarz and Stark [69] propose that the roton de Broglie wavelength corresponding to $k_0 = 1.91 \text{ \AA}^{-1}$ is $\lambda_0 = 3.3$ which is small

compared with $\sqrt{\frac{\sigma_r(k_0)}{\pi}}$; thus, the collision cross section may be nearly geometrical. Although the roton carries a great deal of energy and momentum, its effective mass is much less than that of the ion. Assume that the scattering is elastic, then $|\vec{k}'| \equiv |\vec{k}|$ is satisfied. They conclude a hard-sphere cross section given by

$$\sigma_r(k_0) \equiv \pi(a_+ + a_r)^2 \quad (114)$$

where a_+ is the radius of the ion and a_r is the effective collision radius of the roton. Using experimental values for a_+ and $\sigma_r(k)$, they find that

$$a_r = 3.7 \pm 0.2 \text{ \AA} \quad (115)$$

They surmise from this that the roton is localized within a region of radius $\approx 3.7 - 4.0 \text{ \AA}$, and that it interacts strongly with any disturbance which penetrates this region. They point out that $\approx 3.7 - 4.0 \text{ \AA}$ is only slightly larger than the nearest neighbor distance in liquid helium [80] and that a roton may thus be pictured as a highly correlated motion of an energetic He^4 atom and its nearest neighbors only.

The geometric cross-section of the normal electron bubble σ_e is given as

$$\sigma_e = \pi r_i^2 \quad (116)$$

where r_i is the radius of the unexcited electron bubble given by Eq. (107). From Eq. (107) and Eqs. (113-116), the mobility of the normal electron bubble is given by

$$\mu = \frac{3\pi^2 e}{\hbar k_0^3 \pi (a_r + r_i)^2} \exp(\Delta/k_B T) = \frac{3.38 \times 10^{-25} m^4 V^{-1} \text{sec}^{-1}}{\pi (3.7 \times 10^{-10} m + 6.7 \times 10^{-10} m)^2} \exp(8.65 K/T) \quad (117)$$

At 1 K, Eq. (117) gives $\mu = 5.7 \text{ cm}^2 \text{V}^{-1} \text{sec}^{-1}$ for the mobility of the normal electron bubble ($n=1$) which is in reasonable agreement with the experimental value of $5 \text{ cm}^2 \text{V}^{-1} \text{sec}^{-1}$ from Figure 6.

The normal electron bubble has a uniform constant spherical charge density. This charge density may be modulated by a time and spherically harmonic function as given by Eq. (53). (See [81] for a discussion of the spherical harmonic solutions of the rigid roton version of the Schrödinger equation). In the case of excited state electron bubbles, the contribution to the roton scattering cross section given by Eq. (112) is larger than the geometric cross section given in Eq. (116) where the radius is given by Eq. (101). In this case, $\sigma_T(k)$ given by Eq. (112) follows the derivation of Baym, Barrera, and Pethick [82] where the spherical harmonic angular function causes a gain in the scattering cross section that may be modeled after that of a Hertzian dipole antenna. The radiation power pattern of a Hertzian dipole is given by Kong [83]. The radiation power pattern is

$$\langle S \rangle = \frac{1}{2} \operatorname{Re}[\mathbf{E} \times \mathbf{H}] = \hat{\mathbf{r}} \frac{\eta}{2} \left(\frac{k|I|\Delta z}{4\pi r} \right) \sin^2 \theta \quad (118)$$

where I is the current, Δz is the length of the dipole, and η is the impedance of free space. The antenna directive gain $D(\theta, \phi)$ is defined as the radiation of the Poynting power density $\langle S \rangle$ over the power P , divided by the area of the sphere:

$$D(\theta, \phi) = \frac{\langle S \rangle}{P/4\pi r^2} = \frac{3}{2} \sin^2 \theta \quad (119)$$

The plot of $D(\theta, \phi)$ given by Eq. (119) is known as the gain pattern. The directivity of an antenna is defined as the value of the gain in the direction of its maximum value. For the Hertzian dipole the maximum of 1.5 occurs at $\theta = \frac{\pi}{2}$. Thus, the directivity of a Hertzian dipole is 1.5.

The spherical harmonic angular functions are

$$Y_{lm}(\theta, \phi) = \sqrt{\frac{(2l+1)(l-m)!}{4\pi(l+m)!}} P_l^m(\cos \theta) e^{im\phi} = N_{l,m} P_l^m(\cos \theta) e^{im\phi} \quad (120)$$

where $N_{l,m}$ is the normalization constant given by

$$N_{\ell,m_\ell} = \sqrt{\frac{(2l+1)(l-m)!}{4\pi(l+m)!}} \quad (121)$$

In the case of excited states, $\sigma(k,\theta)$ of Eq. (112) is

$$\sigma(k,\theta) = k^{-2} \left| \frac{\int P_0^0(\cos\theta)e^{i0\phi} d\Omega}{\int P_l^m(\cos\theta)e^{im\phi} d\Omega} \right|^2 = k^{-2} \left(\frac{N_{\ell,m_\ell}}{N_{0,0}} \right)^2 \quad (122)$$

For excited states, the geometric cross-section of the electron bubble σ_e is then given as

$$\sigma_e = \pi n r_{n,\ell,m_\ell}^2 \quad (123)$$

where

$$r_{n,\ell,m_\ell} = \frac{N_{\ell,m_\ell}}{N_{0,0}} r_i \quad (124)$$

r_i is the radius of the unexcited electron bubble given by Eq. (107) and

$n = \frac{1}{\text{integer}}$. The angular parameters $\frac{N_{\ell,m_\ell}}{N_{0,0}}$ are given with the first few

spherical harmonics in Table 1. In this case, $\sigma_T(k)$ is given by Eq. (112) where r_i is replaced by r_{n,ℓ,m_ℓ} (Eq. (124)). The roton scattering cross section given by the hard-sphere cross section is then

$$\sigma_T(k_0) \approx \pi (r_{n,\ell,m_\ell} + a_r)^2 \quad (125)$$

where a_r is the effective collision radius of the roton given by Eq. (115).

From Eq. (117) and Eqs. (124-125), the mobilities of electron bubbles are given by

$$\mu = \frac{3\pi^2 e}{\hbar k_0^4 \pi (a_r + r_{n,\ell,m_\ell})^2} \exp(\Delta/k_B T) = \frac{3.38 \times 10^{-25} m^4 V^{-1} \text{sec}^{-1}}{\pi \left(3.7 \times 10^{-10} m + n \frac{N_{\ell,m_\ell}}{N_{0,0}} 6.7 \times 10^{-10} m \right)^2} \exp(8.65 K/T) \quad (126)$$

where $n = \frac{1}{\text{integer}}$. The mobility of an excited state electron bubble having a fractional principal quantum number ($n = \frac{1}{\text{integer}}$) relative to the normal electron bubble as a function of quantum numbers n , ℓ , and m_ℓ is given in Table 2. A plot of Eq. (126) normalized to the mobility of the normal bubble as a function of p corresponding to fractional principal quantum number $n = \frac{1}{\text{integer}} = 1/p$ for given ℓ , and m_ℓ quantum numbers appears in

Figure 5.

Using time-of-flight, Doake and Gribbon [84] detected negatively-charged ions that had a mobility substantially higher than the normal electron bubble negative ion. This ion, which has become known as the "fast ion", was next seen in another time-of-flight experiment by Ihas and Sanders in 1971 [85]. They showed that the fast ion could be produced by an α or β source, or by an electrical discharge in the helium vapor above the liquid. In addition, they reported the existence of two additional negative carriers, referred to as "exotic ions", that had mobilities larger than the mobility of the normal negative ion, but less than the mobility of the fast ion. These exotic ions were detected only when there was an electrical discharge above the liquid surface. In a paper the following year [86], Ihias and Sanders (IS) reported on further experiments in which at least 13 carriers with different mobilities were detected. The experimental details are described in the thesis of Ihias [87]. Eden and McClintock (EM) [88-89] also detected as many as 13 ions with different mobilities. Both IS and EM put forward a number of proposals to explain the exotic ions, but all of these proposals were shown to be unsatisfactory by Maris [1]. It is significant that the exotic ions appear only when an electrical discharge takes place close to the free surface of the liquid. Under these conditions, the electrons that enter the liquid and form bubbles may absorb light emitted from the discharge. Thus, it is natural to consider the possibility that the exotic ions are electron bubbles in fractional energy states.

The mobility of several electron bubbles in superfluid helium plotted versus the inverse of the temperature is shown in Figure 6. The temperature dependence of the mobility predicted by Eq. (126) is in good agreement with the data of Ihias [87] and the plots of Maris [1]. The ion assignments given in Figure 6 are based on their mobilities relative to the normal ion as given in Table 3.

Following a pulse discharge with an electric field applied to superfluid helium, Ihias [87] recorded ion peaks using time of flight. Fifteen ion peaks recorded by Ihias and Sanders are identified in Figure 7. The mobilities relative to the normal electron bubble ($n=1$) are given in Table 3. The assignments of the mobilities of excited state electron bubbles having fraction principal quantum number ($n=\frac{1}{\text{integer}}$) relative to

the normal electron bubble as a function of quantum numbers n , ℓ , and m_l is also given in Table 3 based on the theoretical values given in Table 2. The agreement between theory and experiment is excellent.

Peaks 14-15 of Figure 7 and Table 3 represent a band with a cutoff at a migration velocity of about 7.5 times the velocity of the normal ion as $n = \frac{1}{\text{integer}}$ approaches zero ($n = \frac{1}{100}$ was used to calculate this limiting case).

The electron radius is predicted to decrease such that the effective collision radius of the roton determines the maximum mobility as given by Eq. (126). The theoretically predicted maximum of electron bubble mobility of about seven times that of the normal ion is confirmed by the Ihara data [87] where the band comprising peaks 14-15 correspond to $n \leq \frac{1}{7}$. Furthermore, Eden and McClintock [88] and Doake and Gribbon [84] measured the drift velocity as a function of applied electric field. The fast ion showed a slope of the drift velocity versus applied electric field of about seven times that of the normal ion. Thus, these results agree with the data of Ihara and with theoretical predictions.

The small deviation of the data from the theoretical in Table 3 may be due to differences in ion production rates and mechanisms based on the spectrum of the arc. Transitions between states may also be a peak broadened factor wherein a peak undergoes a transition to a faster or slower state during migration. This may provide an explanation for the large peak width of peak # 4 of Figure 7 as well as the broad continuum background in this region. Scattering other than roton scattering may also be involved, and these mechanisms such as phonon scattering and inter-bubble "impurity" scattering would effect larger ions more than smaller ions due to their larger geometric cross section. A preferred method to determine the migration times of each electron bubble ($n = \frac{1}{\text{integer}}$) is to cause the formation of each specific state with resonant radiation (Eq. (103) and Eq (105)) and to measure the migration time of each ion separately relative to the $n=1$ bubble.

Using a time-of-flight method, Doake and Gribbon [84] discovered that a fast ion can exist in superfluid helium which unlike the normal ion may be accelerated to the Landau critical velocity v_L for roton creation without undergoing metamorphosis to a charged vortex ring, even under

the saturated vapor pressure. As a consequence, Eden and McClintock [88] studied the behavior of the exotic ions in strong electric field and reported evidence suggesting that intermediate mobility negative ions can nucleate quantized vortex rings in superfluid helium when subject to strong electric fields. Eden and McClintock observed that the drift velocity of intermediate ions may not be linear with electric field and that this effect varies with the particular intermediate ion. Eden and McClintock [88] further observed a decrease in drift velocities of intermediate ions with inter-ion variation for increasing sufficiently strong electric fields. They attributed this to the formation of negatively charged vortex rings. However, for an appropriate electric field, the drift velocity approaches a maximum independent of the field, and formation of charged vortex rings does not explain the field independence [88]. The limiting velocities shown in the data traces of Figure 8 may be a function of the size of the ion for all intermediate ions. In this case, the limiting velocity data of Eden and McClintock [88] are plotted in Figure 9 with the mobility of the normal ion as a function of p corresponding to principal quantum number $n = \frac{1}{\text{integer}} = 1/p$. The agreement between the experimental data and theoretical mobilities is excellent. The existence of multiple peaks under the fast peak such as peak #14 and #15 of Figure 7 is also supported by the data of Eden and McClintock [88] because the peak of highest mobility split into the two peaks shown in Figure 8 at higher fields.

CONCLUSION

Recently, the behavior of free electrons in superfluid helium has again forced the issue of the meaning of the wavefunction. Electrons form bubbles in superfluid helium which reveal that the electron is real and that a physical interpretation of the wavefunction is necessary. Furthermore, when irradiated with low energy light, the electrons carry increased current at different rates as if they exist with at least 15 different sizes. Peaks are observed in the photo-conductivity absorption spectrum at 0.5 and 1.21 eV. A theory of classical quantum mechanics derived from first principles by Mills [2] gives closed form physical solutions for the electron in atoms, the free electron, and the free electron

in superfluid helium. The predicted photo-conductivity absorption spectrum and the mobilities of the 15 identified ions match the experimental results. The data support the existence of fractional principal quantum energy states of free electrons in superfluid helium predicted by Mills classical theory. The results have implications that the concept of probability waves of quantum mechanics must be abandoned and atomic theory must be based in reality.

APPENDIX

Quantum Electrodynamics is Purely Mathematical and Has No Basis in Reality

Quantum mechanics failed to predict the results of the Stern-Gerlach experiment which indicated the need for an additional quantum number. Quantum electrodynamics was proposed by Dirac in 1926 to provide a generalization of quantum mechanics for high energies in conformity with the theory of special relativity and to provide a consistent treatment of the interaction of matter with radiation. From Weisskopf [90], "Dirac's quantum electrodynamics gave a more consistent derivation of the results of the correspondence principle, but it also brought about a number of new and serious difficulties." Quantum electrodynamics; 1.) does not explain nonradiation of bound electrons; 2.) contains an internal inconsistency with special relativity regarding the classical electron radius - the electron mass corresponding to its electric energy is infinite; 3.) it admits solutions of negative rest mass and negative kinetic energy; 4.) the interaction of the electron with the predicted zero-point field fluctuations leads to infinite kinetic energy and infinite electron mass; 5.) Dirac used the unacceptable states of negative mass for the description of the vacuum; yet, infinities still arise. In 1947, Lamb discovered a 1000 MHz shift between the $^2S_{1/2}$ state and the $^2P_{1/2}$ state of the hydrogen atom. This so called Lamb Shift marked the beginning of modern quantum electrodynamics. In the words of Dirac [91], "No progress was made for 20 years. Then a development came initiated by Lamb's discovery and explanation of the Lamb Shift, which fundamentally changed the character of theoretical physics. It involved setting up rules for discarding ...infinities..." Renormalization is presently believed to be required of any fundamental theory of physics [92]. However, dissatisfaction with renormalization has been expressed at various times by many physicists including Dirac [93] who felt that, "This is just not sensible mathematics. Sensible mathematics involves neglecting a quantity when it turns out to be small - not neglecting it just because it is infinitely great and you do not want it!"

Furthermore, Oskar Klein pointed out a glaring paradox implied by the Dirac equation which was never resolved [94]. "Electrons may

penetrate an electrostatic barrier even when their kinetic energy, $-E - mc^2$ is lower than the barrier. Since in Klein's example the barrier was infinitely broad this could not be associated with wave mechanical tunnel effect. It is truly a paradox: Electrons too slow to surpass the potential, may still only be partially reflected. ...Even for an infinitely high barrier, i.e. $r_2 = 1$ and energies $\approx 1 \text{ MeV}$, (the reflection coefficient) R is less than 75%! From (2) and (3) it appears that as soon as the barrier is sufficiently high: $V > 2mc^2$, electrons may transgress the repulsive wall--seemingly defying conservation of energy. ...Nor is it possible by way of the positive energy spectrum of the free electron to achieve complete Einstein causality."

The Rutherford experiment demonstrated that even atoms are comprised of essentially empty space [95]. Zero-point field fluctuations, virtual particles, and states of negative energy and mass invoked to describe the vacuum are nonsensical and have no basis in reality since they have never been observed experimentally and would correspond to an essentially infinite cosmological constant throughout the entire universe including regions of no mass. As given by Waldrop [96], "What makes this problem into something more than metaphysics is that the cosmological constant is observationally zero to a very high degree of accuracy. And yet, ordinary quantum field theory predicts that it ought to be enormous, about 120 orders of magnitude larger than the best observational limit. Moreover, this prediction is almost inescapable because it is a straightforward application of the uncertainty principle, which in this case states that every quantum field contains a certain, irreducible amount of energy even in empty space. Electrons, photons, quarks--the quantum field of every particle contributes. And that energy is exactly equivalent to the kind of pressure described by the cosmological constant. The cosmological constant has accordingly been an embarrassment and a frustration to every physicist who has ever grappled with it."

The spin of the electron and the Lamb shift are calculated from first principles in closed form by Mills [2]. The spin angular momentum results from the motion of negatively charged mass moving systematically, and the equation for angular momentum, $\mathbf{r} \times \mathbf{p}$, can be applied directly to the wave function (a current density function) that

describes the electron. The Lamb shift results from conservation of linear momentum of the photon.

The Postulate of Quantum Measurement is Experimentally Disproved.

Modern quantum mechanics has encountered several obstacles that have proved insurmountable as pointed out previously in the "General Considerations" section and the "Classical Electron Radius" section of Mills [2]. And, quantum mechanics leads to certain philosophical interpretations [97] which are not sensible. Some conjure up multitudes of universes including "mind" universes; others require belief in a logic that allows two contradictory statements to be true. The question addressed is whether the universe is determined or influenced by the possibility of our being conscious of it.

The meaning of quantum mechanics is debated, but the Copenhagen interpretation is predominant. Its asserts that "what we observe is all we can know; any speculation about what a photon, an atom or even a SQUID (Superconducting Quantum Interference Device) really is or what it is doing when we are not looking is just that speculation" [97]. According to this interpretation every observable exists in a state of superposition of possible states, and observation or the potential for knowledge causes the wavefunction corresponding to the possibilities to collapse into a definite. As shown by Platt [98] in the case of the Stern-Gerlach experiment, "the postulate of quantum measurement [which] asserts that the process of measuring an observable forces the state vector of the system into an eigenvector of that observable, and the value measured will be the eigenvalue of that eigenvector".

According to the Zeno no-go theorem which is a consequence of the postulate of quantum measurement, observation of an atom collapses its state into a definite; thus, transitions cannot occur under continuous observation. Recently, it has become possible to test this postulate via an experiment involving transitions of a single atom, and the results are inconsistent with the predictions. Quoting from the caption of Figure 10 of the article, by Dehmelt [99],

"Shelving" the Ba^+ optical electron in the metastable D level.

Illuminating the ion with a laser tuned close to its resonance line produces strong resonance fluorescence and an easily detectable photon count of 1600 photons/sec. When later an auxiliary, weak Ba^+ spectral lamp is turned on, the ion is randomly transported into the metastable $D_{5/2}$ level for 30-s lifetime and becomes invisible. After dwelling in this shelving level for 30 s on average, it drops down to the S ground state spontaneously and becomes visible again. This cycle repeats randomly. According to the Zeno no-go theorem, no quantum jumps should occur under continuous observation.

In Scientific American [97] at "Superimposed Philosophers"--- Pritchard says that physicists may one day be able to pass biologically significant molecules such as proteins or nucleic acids through an interferometer. In principle, one could even observe wave like behavior in a whole organism, such as an amoeba. There are some obstacles, though: the amoeba would have to travel very slowly, so slowly, in fact that it would take some three years to get through the interferometer, according to Pritchard. The experiment would also have to be conducted in an environment completely free of gravitation or other influences-- that is, in outer space.

Getting a slightly larger or more intelligent organism, for instance, a philosopher, to take two paths through a two-slit apparatus would be even trickier. "It would take longer than the age of the universe," Pritchard says."

This article is a good example of how far fetched QM has become (e.g. PARALLEL MIND UNIVERSES).

In addition to the interpretation that photons, electrons, neutrons, and even human beings [97] have no definite form until they are measured, a more disturbing interpretation of quantum mechanics is that a measurement of a quantum entity can instantaneously influence another light years away. Einstein argued that a probabilistic versus deterministic nature of atomic particles leads to disagreement with special relativity. In fact, the nonlocality result of the Copenhagen interpretation violates causality. As a consequence of the indefinite nature of the universe according to quantum mechanics and the implied uncertainty principle, Einstein, Podolsky, and Rosen (EPR) in a classic

paper [100] presented a paradox which led them to infer that quantum mechanics is not a complete theory. See the section entitled, "Heisenberg Uncertainty Principle Predicts Nonlocality, Noncausality, Spooky Actions at a Distance, and Perpetual Motion which can be Shown to be Experimentally Incorrect".

Louis de Broglie, one of the founders of quantum mechanics, also condemned the probability wave approach. "But the causal link between two phenomenon implies the existence of a trajectory, and to deny this existence is to renounce causality and to deprive oneself of any understanding" [101].

Quantum Mechanics based on the Schrödinger Equation (SE) is an Incomplete Theory Since It Does Not Explain Gravity or Particle Masses.

Quantum mechanics can not explain the existence of particles with precise masses and gives no basis of gravity. If fact, a straight forward application of the uncertainty principle predicts that particles of precise mass/energy can not exist. These shortcomings are compounded by the prediction of zero-point field fluctuations, virtual particles, and states of negative energy and mass invoked to describe the vacuum. These consequences of the uncertainty principle are nonsensical and have no basis in reality since they have never been observed experimentally and would correspond to an essentially infinite cosmological constant throughout the entire universe including regions of no mass [102].

Mills [2] derives a theory from first principles that gives closed form solutions based on general relativity and Maxwell's equations for particle masses. It gives gravitation from the atom to the cosmos.

For any kind of wave advancing with limiting velocity and capable of transmitting signals, the equation of front propagation is the same as the equation for the front of a light wave. By applying this condition to electromagnetic and gravitational fields at particle production, the Schwarzschild metric (SM) is derived from the classical wave equation which modifies general relativity to include conservation of spacetime in addition to momentum and matter/energy. The result gives a natural relationship between Maxwell's equations, special relativity, and general relativity. It gives gravitation from the atom to the cosmos. The

universe is time harmonically oscillatory in matter energy and spacetime expansion and contraction with a minimum radius that is the gravitational radius. In closed form equations with fundamental constants only, CQM gives the deflection of light by stars, the precession of the perihelion of Mercury, the particle masses, the Hubble constant, the age of the universe, the observed acceleration of the expansion, the power of the universe, the power spectrum of the universe, the microwave background temperature, the uniformity of the microwave background radiation, the microkelvin spatial variation of the microwave background radiation, the observed violation of the GZK cutoff, the mass density, the large scale structure of the universe, and the identity of dark matter which matches the criteria for the structure of galaxies. In a special case wherein the gravitational potential energy density of a blackhole equals that of the Plank mass, matter converts to energy and spacetime expands with the release of a gamma ray burst. The singularity in the SM is eliminated.

The Wave Function Solutions of Quantum Mechanics as Probability Waves are Inconsistent with Probability Theory

Wavefunction solutions of the Schrödinger equation are interpreted as probability density functions. This interpretation is fatally flawed since the use of "probability" in this instance does not conform to the mathematical rules and principles of probability theory.

Schrödinger sought a physical interpretation of his equation. He interpreted $e\Psi^*(x)\Psi(x)$ as the charge-density or the amount of charge between x and $x+dx$ (Ψ^* is the complex conjugate of Ψ). Presumably, then, he pictured the electron to be spread over large regions of space. Three years after Schrödinger's interpretation, Max Born, who was working with scattering theory, found that this interpretation led to logical difficulties, and he replaced the Schrödinger interpretation with the probability of finding the electron between r,θ,ϕ and $r+dr,\theta+d\theta,\phi+d\phi$ as

$$\int \Psi(r,\theta,\phi)\Psi^*(r,\theta,\phi)drd\theta d\phi \quad (130)$$

Born's interpretation is generally accepted. The electron IS VIEWED AS A DISCRETE PARTICLE that moves here and there (from $r=0$ to $r=\infty$), and

$\Psi\Psi^*$ gives the time average of this MOTION.

Born's interpretation is generally accepted. Nonetheless, interpretation of the wave function is a never-ending source of confusion and conflict. Many scientists have solved this problem by conveniently adopting the Schrödinger interpretation for some problems and the Born interpretation for others. This duality allows the electron to be everywhere at one time—yet have no volume. Alternatively, the electron can be viewed as a discrete particle that moves here and there (from $r=0$ to $r=\infty$), and $\Psi\Psi^*$ gives the time average of this motion.

There is profound internal inconsistency in using probability theory as the foundation of quantum theory. In the tradition of Einstein, a Gedanken experiment is proposed. At a given time, there exists an exact average of the amount of money in the wallets of the members of a given group such as the visitors to BLP's web site. So, I postulate some statistical test and sample 0 to all of the visitors. If I sample all of the visitors, I would know the average exactly. If I sample less than all, I could apply statistics. Using the sampling data with the assumption of a statistical distribution (e.g. Normal Distribution), I could perform a two-sided null test and determine the average within a confidence limit based on the statistical model. Probability theory permits statistical projections based on incomplete knowledge. But, according to the quantum mechanical definition of "probability", before the sampling, the number is between negative infinity and positive infinity simultaneously, and the act of sampling creates the money in the wallets of the visitors. Another example is that the capture of the numbered balls by a lottery machine creates the numbers on lottery tickets.

The basis of this paradox is that STATISTICAL THEORY IS BASED ON AN EXISTING DETERMINISTIC REALITY WITH INCOMPLETE INFORMATION; WHEREAS, QUANTUM MEASUREMENT ACTS ON A "PROBABILITY DENSITY FUNCTION" TO DETERMINE A REALITY THAT DID NOT EXIST BEFORE THE MEASUREMENT.

Consider the simplest of systems, the "ground state wave function of the hydrogen atom". The wavefunction ascribes the electron an infinite number of positions and energies simultaneously including states with infinite negative kinetic energy and infinite positive potential energy. But, experiments are consistent with 13.6 eV of kinetic energy

and 27.2 eV of potential energy in every case. Atomic hydrogen has been extensively studied. For example, hydrogen has long been the focus of combustion research involving kinetic and spectroscopic studies.

Neutral scattering of hydrogen atoms is always observed. How can the point electron have a statistical distribution of separate positions and energies and still always give rise to neutral scattering? If position follows a probability density function, why do all of the positions give rise to the identical scattering behavior wherein the positions of the point particles (proton and electron of the incoming hydrogen atom and the point scattered electron) are random independent variables? How do all of the electric fields always identically cancel if positions are statistical? Even one neutral scattering event violates Chebyshev's Inequality.

It is also nonsense to interpret the "probability" ascribed by the wavefunction of the electron as equivalent to that of statistical thermodynamics. The latter corresponds to a classical statistical distribution of particles such as photons or molecules over states such as energy states for a macroscopic system. It is nonsensical to assign a single particle (e.g. an electron) to a statistical distribution over many states. It is similarly nonsensical to associate a stable property such as a thermodynamic property to a single particle based on such statistics.

Quantum mechanical textbooks express the movement of the electron, and the Heisenberg uncertainty principle is an expression of the statistical aspects of this movement. McQuarrie [15], gives the electron speed in the $n=1$ state of hydrogen as 2.18764×10^6 m/sec. Remarkably, the uncertainty in the electron speed according to the uncertainty principle is 1.4×10^7 m/sec [16] which is an order of magnitude larger than the speed. With Penning traps, it is possible to measure transitions of electrons of single ions. This case can be experimentally distinguished from statistics over equivalent transitions in many ions. Whether many or one, the transition energies are always identical within the resonant line width. So, probability has no place in describing atomic energy levels on this basis either.

According to quantum mechanics, the existence of the electron in the nucleus is the basis of spin-nuclear coupling called Fermi contact interaction [103] where $4\pi r^2 \Psi^2 dr$ is not zero since the Ψ^2 is not zero and the nucleus is comprised of baryons. According to the Standard Model,

baryons as opposed to leptons have structure, contain more fundamental particles--namely quarks and gluons, and are not point particles. For example, the proton has an experimentally measured radius of $r_p = 1.3 \times 10^{-15} m$. The spin-nuclear coupling energy is of the order of $10^{-24} J$ despite the infinite Coulombic energy of the electron when found in the nucleus (i.e. $r \rightarrow 0$ in the Schrödinger equation). This consequence of quantum mechanics is further flawed since this state is experimentally disproved. The nucleus does not contain electrons [104]. Since the electron has no volume, based on this logic, the probability that an electron can capture a photon to form an excited state is zero. This internal inconsistency based on the description of the electron as a point particle probability wave does not arise in Mills classical theory of quantum mechanics. The spin nuclear energies are calculated by Mills in closed form based on first principles without the requirement that the electron is in the nucleus [105] and are in close agreement with the experimental results.

What does the wave function represent? It certainly does not represent the probability that a point particle will be found in a given region in space at any given instant of time if sampled. And, it has positive as well as negative values of probability which is nonsensical. This is circumvented by squaring it. But, why not take the root mean squared value or the magnitude? In the case of a wave such as an acoustic or electromagnetic wave, the energy or intensity is given as the square of the amplitude. But, when did it become correct that a probability density function (pdf) has an energy or intensity? Quantum theory confuses the concepts of a wave and a pdf that are based on totally different mathematical and physical principles. It is further meaningless to normalize such a function with the interpretation that the expectation value must be one. In addition, the postulates of the "probability" wave are internally inconsistent since negative probability density functions are often invoked to describe "antibonding orbitals" in molecules. It appears that the word "probability" as applied to quantum mechanics has nothing to do with classical probability theory.

The Schrödinger Equation Fails to Explain Scattering Experiments

Scattering experiments are not consistent with an uncertainty in the radial or angular position of the electron. The Schrödinger equation interpreted as a probability wave of a point particle can not explain that the hydrogen atom is neutral. For example, it can not explain neutral scattering of electrons or light from hydrogen. The point particles must align perfectly; otherwise Rutherford scattering would be observed. In this case, the uncertainty principle is violated. The Born interpretation can only be valid if the speed of the electron is equal to infinity. (The electron must be in all positions weighted by the probability density function during the time of the scattering event). The correct aperture function for the Born interpretation is a Dirac delta function having a Fourier transform of a constant divided by s^2 which is equivalent to the case of the point nucleus (Rutherford Equation). The Born interpretation must be rejected because the electron velocity can not exceed the speed of light without violating special relativity.

The elastic scattering of electrons from an atomic beam of helium atoms provides a test of the wavefunction solutions of the Schrödinger equation. Mills [106] gives a closed form solution of the elastic scattering of 500 eV electrons from helium atoms as the Fraunhofer pattern in the far field. Mills gives a closed form equation of the free electron [107] and a closed form equation of the helium atom [108]. This is the case of Z=2, in the closed form equation that Mills has solved for all two electron atoms. The calculation is a Fourier optics type which reduces to a spherical lens calculation. The math is well known. The resultant closed form equation has no adjustable parameters. The predictions identically and continuously match the experimental scattering data [109-111]. In the case of the quantum mechanical calculation, the calculation is on a point-by point basis without regard to internal consistency or physical laws. Furthermore, it is unstable--blows up to positive or negative infinity based on round-off error, contains adjustable parameters, and in the words of the authors, "at smaller scattering angles, however, the Born approximation calculation fails utterly, the experimental curve rising much more steeply than the theoretical" [109].

Furthermore, QM calculations are not even internally consistent. Take the inelastic scattering of electrons from He atoms as an example. Rather than using point particles which is the norm, a single plane wave

is used as the equation of all of the incident electrons [112]. And, the Schrödinger equation predicts that each of the functions that corresponds to a highly excited state electron as well as the ionized electron are sinusoidal over all space which is nonsensical, are not integrable, and can not be normalized. Thus, each is infinite [7]. The SE does not give a point or a plane wave as the function of an ionized electron.

Measurements of the resistivity of hydrogen as a function of pressure provides a test of quantum mechanics which is similar to scattering experiments. The scalar and vector potential functions of the electrons of the hydrogen molecule are given by Mills [113] as a closed form solution of the Laplacian in elliptic coordinates with the nonradiative boundary constraint. The many solutions of the hydrogen molecule based on quantum mechanics have many flaws such as internal inconsistency, violation of fundamental laws, and use of variable parameters such as "effective nuclear charge for the proton". For example, Kolos and Wolniewicz [114] use a 100 terms and an effective nuclear charge of 1.072. Whereas, Kolos and Roothaan [115] use an effective nuclear charge of 1.197, and their predicted bond energy is 30% less than the experimental value. The proton charge in Mills' closed form calculation is identically equal to the experimentally measured charge of the proton, and Mills' bond energy matches the experimental energy. Recent measurements of the resistivity of hydrogen as a function of pressure confirm Mills' solution rather than quantum mechanics. The finite dimensions of the hydrogen molecule are evident in the plateau of the resistivity versus pressure curve of metallic hydrogen [116]. This is in contradiction to the predictions of quantum probability functions such as an exponential distribution in space.

It has Been Shown Experimentally that the Heisenberg Uncertainty Principle Has Nothing to Do with Wave-Particle Duality

Feynman states [117], " It is impossible to design an apparatus to determine which hole the electron passes through, that will not at the same time disturb the electrons enough to destroy the interference pattern." If an apparatus is capable of determining which hole the electron goes through, it *cannot* be so delicate that it does not disturb the

pattern in an essential way. No one has ever found (or even thought of) a way around the uncertainty principle. *So we must assume that it describes a basic characteristic of nature.*"

Feynman's position has recently been over turned by an experiment by Durr et al. [118]. According to Gerhard Rempe [119], who lead the Durr et al. experimental team, "*The Heisenberg uncertainty principle has nothing to do with wave-particle duality.*" Durr et al. report [118], "We show that the back action onto the atomic momentum implied by Heisenberg's position-momentum uncertainty relation cannot explain the loss of interference."

Uncertainty Principle

More than 60 years after the famous debate between Niels Bohr and Albert Einstein on the nature of quantum reality, a question central to their debate --the nature of quantum interference--has resurfaced. The usual textbook explanation of wave-particle duality in terms of unavoidable 'measurement disturbances' is experimentally proven incorrect by an experiment reported by Durr, Nonn, and Rempe [118]. They report on the interference fringes produced when a beam of cold atoms is diffracted by standing waves of light. Their interferometer displayed fringes of high contrast--but when they manipulated the electronic state within the atoms with a microwave field according to which path was taken, the fringes disappeared entirely. The interferometer produced a spatial distribution of electronic populations which were observed via fluorescence. The microwave field canceled the spatial distribution of electronic populations. The key to this new experiment was that although the interferences are destroyed, the initially imposed atomic momentum distribution left an envelope pattern (in which the fringes used to reside) at the detector. A careful analysis of the pattern demonstrated that it had not been measurably distorted by a momentum kick of the type invoked by Bohr, and therefore that any locally realistic momentum kicks imparted by the manipulation of the internal atomic state according to the particular path of the atom are too small to be responsible for destroying interference.

Durr et al. conclude that the "Heisenberg uncertainty relationship has nothing to do with wave-particle duality" and further conclude that

the phenomenon is based on entanglement and correlation. Their interpretation of the principles of the experiment is that directional information is encoded by manipulating the internal state of an atom with a microwave field, which entangles the atom's momentum with its internal electronic state. Like all such entangled states, the constituent parts lose their separate identity. But the attachment of a distinguishable electronic label to each path means that the total electronic-plus-path wavefunction along one path becomes orthogonal to that along the other, and so the paths can't interfere. By encoding information as to which path is taken within the atoms, the fringes disappear entirely. The internal labeling of paths does not even need to be read out to destroy the interferences: all you need is the option of being able to read it out.

According to Durr et al., the mere existence of information about an entity's path causes its wave nature to disappear. But, correlations are observations about relationships between quantities and do not cause physical processes to occur. The existence of information about an entity's path is a consequence of the manipulation of the momentum states of the atoms which resulted in cancellation of the interference pattern. It was not the cause of the cancellation. The cancellation is calculated by Mills [120] as the superposition of two single slit patterns as opposed to a double slit pattern which is based on determinism. In this case, an appropriate replacement terminology for "correlations are responsible for the loss of the interference pattern" is "determinism is responsible for the loss of the interference pattern".

In contrast to QM, in Mills' theory, a particle has one position and one energy in the absence of measurement. It does not have an infinite number of superimposed positions and energies simultaneously with no physical form until measurement is made. The rise-time band width relationship holds during measurement. This is a conservation statement. Mills regards the Heisenberg uncertainty principle which is based on the probability model of fundamental particles to be wrong as well as the implicit spontaneous creation of energy and virtual particles from a perfect vacuum. The Heisenberg uncertainty principle violates first principle laws which are directly proven experimentally, and the predicted virtual particles generated from vacuum are rejected since they are not experimentally observed. Mills' theory predicts wave

particle duality nature of light and particles based on first principles rather than requiring that different physics applies on the atomic scale.

The Heisenberg Uncertainty Principle Predicts Nonlocality, Noncausality, Spooky Actions at a Distance, and Perpetual Motion which can be Shown to be Experimentally Incorrect.

Flawed Interpretation of the Results of the Aspect Experiment -There Is No Spooky Action at a Distance

Bell [121] showed that in a Gedanken experiment of Bohm [122] (a variant of that of EPR) no local hidden-variable theory can reproduce all of the statistical predictions of quantum mechanics. Thus, a paradox arises from Einstein's conviction that quantum-mechanical predictions concerning spatially separated systems are incompatible with his condition for locality unless hidden variables exist. Bell's theorem provides a decisive test of the family of local hidden-variable theories (LHVT). In a classic experiment involving measurement of coincident photons at spatially separated detectors, Aspect [123] showed that local hidden-variable theories are inconsistent with the experimental results. Although Aspect's results are touted as a triumph of the predictions of quantum mechanics, the correct coincidence rate of detection of photons emitted from a doubly excited state of calcium requires that the z component of the angular momentum is conserved on a photon pair basis. As a consequence, a paradox arises between the deterministic conservation of angular momentum and the Heisenberg uncertainty principle. The prediction derived from the quantum nature of the electromagnetic fields for a single photon is inconsistent with Aspect's results, and Bell's theorem also disproves quantum mechanics. Furthermore, the results of Aspect's experiment are predicted by Mills' theory wherein locality and causality hold. Mills derives the predicted coincidence rate based on first principles [124]. The predicted rate identically matches the observed rate.

The Aspect experiment is a test of locality and local hidden variable theories. The Aspect experiment is also a test of quantum mechanics and the HUP. In one design of the experiment, photons are incident to a beam splitter which causes each photon to be split into two that travel along

opposite paths to separate detectors. The separate detectors measure the polarization of the arriving photons. By using synchronous detection, photons of a pair may be later compared. The data indicate a random pattern at each detector individually; however, when photons are matched up as pairs, an essentially perfect correlation exists. The quantum mechanical explanation is that before the photon was split its state of polarization was indeterminate. It possessed an infinite number of states in superposition. Then when one element of the pair was detected information traveled instantaneously (infinitely faster than the speed of light--otherwise known as a spooky action at a distance) to cause the other photon to have a matching polarization. In quantum mechanical terms, the states were entangled, and measurement of one photon caused the other photon's wavefunction to collapse into the matching state.

The correct explanation is that each photon entering the beam splitter originally had a determined state, and angular momentum was conserved on a photon by photon basis at the splitter. Thus, each photon of a pair had a matching polarization before it hit the detector. Locality and cause and effect hold. There is no spooky action at a distance. This experiment actually disproves quantum mechanics. It also disproves local hidden variable theories. The data of the Aspect experiment matches a classical derivation, not a quantum mechanical one.

Everyday observation demonstrates that causality and locality always hold. Bell's theorem postulates that a statistical correlation of A(a) and B(b) is due to information carried by and localized within each photon, and that at some time in the past the photons constituting one pair were in contact and in communication regarding this information. This is the case in many everyday experiences such as transmission, processing, and reception of signals in microelectronics devices. Locality and causality always hold. They hold on the scale of the universe also. But, according to the Big Bang theory of quantum mechanics all photons were at one time in contact; thus, no locality or causality should be observed at all. This is nonsense. The results of the Aspect experiment support the EPR paradox that QM does not describe physical reality. There is a mistake in the derivation of the analysis of the data from Aspect's experiment [125-126].

Bell's theorem is just an inequality relationship between ARBITRARY probability density functions with certain assumptions about independence, expectation value equal to one, etc. wherein an additional probability distribution function is introduced which may represent local hidden variables or something else for that matter. And, the initial functions may correspond to quantum mechanical statistics or something else for that matter. Standard probability rules are accepted such as the probability of two independent events occurring simultaneously is the product of their independent probabilities. What is calculated and plugged into the formula for the functions and whether the substitutions are valid are the issues that determine what Bell's inequality tests when compared with data. Historically, Bell's inequality is a simple proof of statistical inequalities of expectation values of observables given that quantum statistics is correct and that the physical system possesses "hidden variables". However, if deterministic statistics are actually calculated and quantum statistics is equivalent to deterministic statistics (e.g. detection of a wave at an inefficient detector) but possesses further statistics based on the probability nature of the theory (statistical conservation of photon angular momentum), then Bell's inequality is actually testing determinism versus quantum theory when compared to the data.

Rather than demonstrating that QM does not give us all of the information about the physical world, the data is consistent with the result that QM does not describe the physical world, and that deterministic physics does. A deterministic theory is not required to possess local hidden variables. Maxwell's equations is a deterministic theory. It does not have local hidden variables (LHV). There is no corresponding statistical distribution function. Bell's theorem is a simple proof of statistical inequalities of expectation values of observables given that "QUANTUM" statistics is correct and that the physical system possesses "hidden variables" corresponding to an additional statistical distribution function. What was actually derived to explain the results of the Aspect experiment [123] was a classical calculation of the detection of an extended particle, the polarized photon, at an inefficient detector wherein determinism holds with respect to conservation of angular momentum [125-126]. Thus, the statistics defined as "QUANTUM" was

actually deterministic. (The derivation is given by Mills [124]). Furthermore, in actuality, quantum statistics must also possess other statistical distribution functions corresponding to the probability nature of the theory such as a statistical distribution for the z component of angular momentum which is conserved statistically as the number of photons goes to infinity. Thus, the real quantum mechanics statistics corresponds to a local hidden variable theory (LHVT) with respect to the definitions of the arbitrary probability distribution functions in Bell's inequality. Aspect recorded the expectation value of the coincidence rate at separated randomly oriented inefficient polarization analyzers for pairs of photons emitted from a doubly excited state calcium atom. The data showed a violation of Bell's inequality. This proves determinism and the real QM statistics fails the test. Furthermore, the observed coincidence count rate of Aspect [123] is equal to that predicted classically from the statistics of measurement at an inefficient detector only. The additional finite distribution function required in the case of quantum mechanics and QED results in incorrect predictions. There is no spooky action at a distance.

The Aspect experiment shows that momentum is conserved on a photon by photon basis, not statistically as predicted by the HUP. Similar experiments regarding tests of entanglement predicted by the HUP are shown to be consistent with first principle predictions and reveal flaws in the interpretations based on the HUP. The HUP implies nonlocality, noncausality, and spooky actions at a distance which can be shown to be experimentally incorrect.

Flawed Interpretation of the Results on a Single ${}^9Be^+$ Ion in a Trap in a Continuous Stern-Gerlach Experiment--An Ion Can Not Be at Two Places at the Same Time

There is a mistake in the analysis of the data from Monroe et al. [127]. Their interpretation that the same beryllium ion was observed to be at widely separated points at the same time is absolute nonsense. Their experimental results show that locality and causality hold [128].

A report in New York Times [129] entitled "Physicists Put Atom in 2 Places at Once" states, "a team of physicists has proved that an entire atom can simultaneously exist in two widely separated places". The

article further states, "In the quantum "microscale" world, objects can tunnel magically through impenetrable barriers. A single object can exist in a multiplicity of forms and places. In principle, two quantum-mechanically "entangled" objects can respond instantly to each other's experiences, even when the two objects are at the opposite ends of the universe". Experimentally, interference patterns were observed by Monroe et al. [127] for a single ${}^9Be^+$ ion in a trap in a continuous Stern-Gerlach experiment. Monroe's interpretation of the experimental observation was that the ion wave-function interfered with itself wherein the ion was at two separate places at the same time corresponding to a wave function state called a "Schrödinger cat" state [127, 129-130]. According to Monroe et al.,

"A "Schrödinger cat"-like state of matter was generated at the single atom level. A trapped ${}^9Be^+$ ion was laser-cooled to the zero-point energy and then prepared in a superposition of spatially separated coherent oscillator states. This state was created by application of a sequence of laser pulses, which entangles internal (electronic) and external (motional) states of the ion. The "Schrödinger cat" superposition was verified by detection of the quantum mechanical interference between the localized wave packets. This mesoscopic system may provide insight into the fuzzy boundary between the classical and quantum worlds by allowing controlled studies of quantum measurement and quantum decoherence."

The "Schrödinger cat" state analysis relies on the postulate that the Pauli Exclusion Principle applies to Rabi states wherein a rotation of the magnetic moment of the unpaired electron of an RF-trapped ${}^9Be^+$ ion is represented by a linear combination of spin 1/2 ($|\uparrow\rangle_i$) and spin -1/2 ($|\downarrow\rangle_i$) states. Three steps of rotation of the spin magnetic moment by a time harmonic field provided by pairs of copropagating off-resonant laser beams which drove two-photon-stimulated Raman magnetic resonance transitions were each separated by displacement laser pulses which excited a resonant translational harmonic oscillator level of the trapped ion by coupling only with the $|\uparrow\rangle_i$ state. According to Monroe, "this

selectivity of the displacement force provides quantum entanglement of the internal state with the external motional state. Although the motional state can be thought of as nearly classical, its entanglement with the internal atomic quantum levels precludes any type of semiclassical analysis". The interference was detected by exciting a fluorescent transition which only appreciatively coupled to the $|\downarrow\rangle_i$ state. Thus, the fluorescence reading was proportional to the probability P_{\downarrow} the ion was in state $|\downarrow\rangle_i$. The "Schrödinger cat" superposition was supposedly verified by detection of the quantum mechanical interference between the localized wave packets.

However, the interference arises not from the existence of the ion at two places at once. The positively charged ion was excited to a time harmonic translational energy state, and the spin quantization axis was defined by an applied 0.20 mT magnetostatic field at an angle of $\frac{\pi}{4}$ with respect to the x-axis of the RF-trap. The frequency of the energy to "flip" the spin state was equivalent to the projection of that of the translational harmonic oscillator onto the spin axis

$$\frac{\omega_x}{2\pi} \cos^2 \frac{\pi}{4} = (11.2\text{ MHz})(0.5) = 5.605\text{ MHz} = \frac{\Delta E_{mag}^{spin}}{h} \quad (132)$$

given by Eqs. (37.45-37.48) of Mills [128]. Thus, interference occurred between the Stern-Gerlach transition and the synchrotron radiation corresponding to the charged harmonic oscillator. Since the displacement beams affected only motion correlated with the $|\uparrow\rangle_i$ state, a rotation of the magnetic moment such that $\delta \neq 0$ with application of the displacement beams gives rise to a phase shift of the interference pattern. The closed form calculation is given in Mills [128].

Flawed Interpretation of the Results of Experiments on a Small SQUID Coupled to a Biased Large Superconducting Current Loop--A Superconducting Current Can Not Flow in Opposite Directions at the Same Time

There is a mistake in the analysis of the data from Friedman et al. [131]. Their interpretation that a superconducting current loop can exist as a superposition of contradictory states at the same time is absolute nonsense. It is shown by Mills [132] that their experimental results are

consistent with locality and causality.

A recent report in The New York Times [133] entitled "Here, There and Everywhere: A Quantum State of Mind" states, "Physicists at Delft University of Technology have put a 5-micrometer-wide loop of superconducting wire into a "quantum superposition" of two contradictory possibilities: in one, the current flows clockwise; in the other, current flows counterclockwise." The article further states, "In the realm of atoms and smaller particles, objects exist not so much as objects as mists of possibilities being here there and everywhere at the same time-and then someone looks and the possibilities suddenly collapse into definite locations." The experiment was a simplified version of the concept of Schrödinger's cat. In 1935, Schrödinger [134] attempted to demonstrate the limitations of quantum mechanics using a thought experiment in which a cat is put in a quantum superposition of alive and dead states.

Instead of a cat, Friedman et al. [131] used a small square loop of superconducting wire linked to a SQUID (Superconducting Quantum Interference Device). A SQUID comprises a superconducting loop with a Josephson junction, a weak link that causes magnetic flux to be linked in integer units of the magnetic flux quantum. When the loop is placed in an external magnetic field, the loop spontaneously sets up an electrical current to cancel the field or generate an additional magnetic field, adjusting the magnetic field to a unit of the magnetic flux quantum, one of the allowed values. In the experiment of Friedman et al., the loop was placed in a magnetic field equal to one half of the first allowed value, a magnetic flux quantum. Thus, the loop could set up either a current to raise the field strength to the first allowed value, or with equal probability, a current of equal magnitude flowing in the opposite direction to cancel out the external field. A pulse of microwaves was applied at the frequency to cause a transition of the magnetic moment of the current loop as an entirety. The absorption of microwaves caused the magnetic state of the SQUID to change and the current to reverse its direction.

Experimentally, a measurement always gave one of the two possible answers, clockwise or counterclockwise, never a zero cancellation. A difference in energy at which the flip transition occurred

between the two possibilities was detected by a group led by J. Lukens and J. Friedman at the State University of New York (SUNY). A simple explanation was that the microwaves simply flipped the current direction which had an energy bias in one direction versus the opposite based on the corresponding presence or absence of a magnetic flux quantum within the SQUID. Rather, they interpreted the results as experimental evidence that a SQUID can be put into a superposition of two magnetic flux states: one corresponding to a few microamperes of current flowing clockwise and the other corresponding to the same amount of current flowing anticlockwise. "Just as the cat is neither alive nor dead but a ghostly mix of the two possibilities, the current flows neither clockwise or counterclockwise, but is a mix of the two possibilities [133]." According to Friedman, "we can have two of these macroscopically well-defined states at the same time. Which is something of an affront to our classical intuitions about the world [133]."

Current running in both directions simultaneously is nonsensical. Current is a vector and must have only one direction. The energy difference observed by Friedman et al. can be explained CLASSICALLY. The experimental apparatus comprised a small SQUID coupled to a large current loop. A second SQUID magnetometer read the flux state of the first sample SQUID. The energy difference was not due to superposition of flux states. Rather, it was due to the nature of the electron which carries the superconducting current and links flux in units of the magnetic flux quantum. Consequently, the sample SQUID linked zero or one magnetic flux quantum. When excited by electromagnetic radiation of a resonant frequency, individual electrons undergo a spin-flip or Stern Gerlach transition corresponding to a reversal of the electron magnetic moment, angular momentum, and current. The Stern Gerlach transition energies of electrons superimpose. The energy difference observed by Friedman et al. matches the energy corresponding to the flux linkage of the magnetic flux quantum by the ensemble of superconducting electrons in their entirety with a reversal of the corresponding macroscopic current. The linkage was caused by high power microwave excitation of a Stern Gerlach transition of the magnetically biased loop which caused a concomitant change in the flux state of the separately magnetically biased sample SQUID. In this case, the microwave frequency was kept

constant, and the bias flux of the loop was scanned at a fixed magnetic bias of the sample SQUID until the resonance with the superposition of the Stern Gerlach transitions of the superconducting electrons in their entirety was achieved.

Flawed Prediction of Perpetual Motion by the Heisenberg Uncertainty Principle

Another consequence of HUP wherein entanglement of states is implicit is the prediction of perpetual motion. Schewe and Stein report on the work of Allahverdyan and Nieuwenhuizen [135]:

"Armen Allahverdyan of, CEA Saclay (France)/University of Amsterdam (Netherlands)/Yerevan Physics Institute (Armenia), aarmen@sph.t.saclay.cea.fr, and Theo Nieuwenhuizen of the University of Amsterdam (nieuwenh@wins.uva.nl, 011-31-20-525- 6332) [136] suggest that a quantum particle (such as an electron) interacting strongly with a reservoir of particles may violate the Clausius inequality--one formulation of the second law of thermodynamics, which states that it is impossible to do work without losing heat. What the researchers term "appalling behavior" can be traced to the quantum mechanical property of entanglement, in which a quantum particle (such as an electron) is so strongly interlinked with another particle or group of particles that the resulting behavior cannot be treated by standard thermodynamic approaches. In this paper, the Amsterdam scientists study the entanglement of a particle with a "quantum thermal bath," a reservoir of particles with which the first particle can exchange energy and momentum. According to the researchers, entanglement prevents the quantum bath from observing the normal requirements for a heat bath. Therefore, thermodynamics simply cannot say anything useful about the system."

Standard thermodynamics dictates that the bath be in thermal equilibrium and not interact strongly with an external object. To the contrary, the bath strongly interacts with something external to it (the entangled particle) and it cannot reach equilibrium, since it constantly exchanges energy and momentum with the particle. At low temperatures where entanglement could be easily preserved, the

researchers state that this system can apparently violate the Clausius inequality--in which the heat gained by the particle must be less than or equal to the temperature multiplied by the change in its entropy (or disorder). Near absolute zero temperatures, a situation which would ordinarily require the particle to lose heat, the researchers show that the particle could gain heat, by the Clausius relation. According to this scenario, applying a cyclic parameter such a periodically varying external magnetic field can cause the entangled particle to extract work from the bath--something forbidden in a classical system. Further, the researchers say that this phenomenon could be said to constitute a perpetual motion machine of the second kind.

The POSTULATED Schrödinger Equation Does Not Explain the Stability of the Hydrogen Atom.

QM theory does not say why an atom radiates. Quantum states of QM refer to energy levels of probability waves. From these, emission and absorption of radiation is inferred. But QM doesn't explain why it is emitted or absorbed or why certain states are stable. For example, the Schrödinger equation (SE) was POSTULATED in 1926. It does not explain the stability of the hydrogen atom. To say that the atom obeys the SE is nonsensical. Consider the hydrogen atom without regard to the mathematical formula called the SE. Mathematics does not determine physics. It only models physics. The SE is not based on directly testable physical laws such as Maxwell's equations. It only gives correlations, and is in fact inconsistent with physical laws.

As a historical note:

[My father] said, "I understand that they say that light is emitted from an atom when it goes from one state to another, from an excited state to a state of lower energy."

I said, "That's right."

"And light is kind of a particle, a photon, I think they call it."

"Yes."

"So if the photon comes out of the atom when it goes from the excited to the lower state, the photon must have been in the atom

in the excited state."

I said, "Well no."

He said, "Well, how do you look at it so you can think of a particle photon coming out without it having been there in the excited state?"

I thought a few minutes, and I said, "I'm sorry; I don't know. I can't explain it to you."

-Richard P. Feynman, *The Physics Teacher* (September 1969).

As shown in "Schrödinger States Below n=1" section, the definition of the "ground state" is mathematically purely arbitrary. It is always experimentally observed that the hydrogen atom does not spontaneously emit light once it has achieved an energy level of 13.6 eV. Thus, it is taught in textbooks that atomic hydrogen cannot go below the ground state. But, atomic hydrogen having an experimental ground state of 13.6 eV can only exist in a vacuum or in isolation, and atomic hydrogen cannot go below this ground state only when it is in isolation. Atomic hydrogen is extremely reactive, and there is no known composition of matter containing hydrogen in the ground state of 13.6 eV.

Since the Schrödinger equation offers no foundation for the stability of isolated atomic hydrogen, Feynman attempted to find a basis for the definition of the "ground state" in the Heisenberg uncertainty principle [137]. Feynman's based his derivation on the determination of the momentum as $p = h/a$ from the uncertainty principle wherein he argues, "We need not trust our answer to within factors like 2, π , etc. We have not even defined a very precisely." The kinetic energy follows classically from the momentum, and the electrostatic energy is given classically to give the total energy as

$$E = \frac{h^2}{2ma^2} - \frac{e^2}{a} \quad (131)$$

Feynman determined the minimum energy in order to solve for the radius of the hydrogen atom.

$$\frac{dE}{da} = -\frac{h^2}{ma^3} + \frac{e^2}{a^2} = 0 \quad (132)$$

The result is exactly the Bohr radius.

The uncertainty principle [138] is

$$\sigma_x \sigma_p \geq \frac{\hbar}{2} \quad (133)$$

where σ_x and σ_p are given by

$$\sigma_x^2 = \int \psi^* (\hat{X} - \langle x \rangle)^2 \psi dx \quad (134)$$

$$\sigma_p^2 = \int \psi^* (\hat{P} - \langle p \rangle)^2 \psi dx \quad (135)$$

The definition of the momentum operator in a *one dimensional* system is [138]

$$\hat{P}_x = -i\hbar \frac{d}{dx} \quad (136)$$

and the position operator is

$$\hat{X} = x \quad (\text{multiply by } x) \quad (137)$$

Based on the uncertainty principle, Feynman's derivation of the Bohr radius is flawed on the basis of at least five points:

1.) The uncertainty principle gives a lower limit to the product of the UNCERTAINTY in the momentum and the position-NOT the momentum and the position. The momentum or position could be arbitrarily larger or smaller than its uncertainty. For example, quantum mechanical textbooks express the movement of the electron, and the Heisenberg uncertainty principle is an expression of the statistical aspects of this movement. McQuarrie [15], gives the electron speed in the $n=1$ state of hydrogen as $2.18764 \times 10^6 \text{ m/sec}$. Remarkably, the uncertainty in the electron speed according to the uncertainty principle is $1.4 \times 10^7 \text{ m/sec}$ [16] which is an order of magnitude larger than the speed.

2.) Feynman's derivation of the Bohr radius is internally inconsistent since the kinetic and electrostatic energies were derived CLASSICALLY; whereas, quantum mechanics and the uncertainty principle are not consistent with classical mechanics.

3.) Feynman's derivation of the Bohr radius is internally inconsistent since the uncertainty principle requires UNCERTAINTY in the position and momentum. Yet, Eqs. (2.10-2.11) of Feynman (Eqs. (131-132)) can be solved to give an EXACT rather than a most probable electron position, momentum, and energy.

4.) Feynman's derivation of the Bohr radius is flawed since Eq. (2.11) of Feynman (Eq. (132)) is nothing more than the Bohr force balance equation given by McQuarrie [139] and also derived by Mills [7]. Thus, this approach fails at explaining the stability of the 13.6 eV state beyond an arbitrary definition wherein "We need not trust our answer to

within factors like 2, π , etc. [137]."

5.) The faulty logic is compounded by the fact that the uncertainty principle is founded on the definition of the momentum operator given by Eq. (136) and the position operator given by Eq. (137). Thus, the uncertainty principle is based on the postulated Schrödinger equation and its associated postulates and descriptions of particles as probability waves. IT IS NOT BASED ON PHYSICS. In fact, it is nonsensical in many physical tests such as scattering of electrons from neutral atoms, confining electrons to atoms, confining electrons to atoms in excited states wherein a photon causing a transition carries \hbar of angular momentum, and the cosmological consequences of the uncertainty principle as described previously. Also, it is disproved experimentally that it provides a basis for the wave-particle duality nature of light and particles; even though, the opposite is widely touted as discussed in the "It has Been Shown Experimentally that the Heisenberg Uncertainty Principle Has Nothing to Do with Wave-Particle Duality" section.

According to the generally accepted Born interpretation of the meaning of the wavefunction, the probability of finding the electron between r, θ, ϕ and $r+dr, \theta+d\theta, \phi+d\phi$ is given by Eq. (130). The electron IS VIEWED AS A DISCRETE PARTICLE that moves here and there (from $r=0$ to $r=\infty$), and $\Psi\Psi^*$ gives the time average of this MOTION. The Schrödinger equation possesses terms corresponding to the electron radial and angular kinetic energy which sum with the potential energy to give the total energy. These are necessary conditions for an electron bound by a central field [11]. Herman Haus derived a test of radiation based on Maxwell's equations [18]. Applying Haus's theorem to the point particle that must have radial kinetic energy demonstrates that the Schrödinger solution for the $n=1$ state of hydrogen is radiative; thus, it violates Maxwell's equations. Since none is observed for the $n=1$ state, QM is inconsistent with observation. The derivation is shown in the "Schrödinger Wave Functions in Violation of Maxwell's Equations" section of Mills [140].

In contrast, the classical theory of Mills is derived from Maxwell's equation with the constraint that the $n=1$ state is nonradiative. This approach leads to the prediction of stable states below the traditional $n=1$ state. Corresponding states are confirmed by the data on the free

electrons in superfluid helium.

ACKNOWLEDGMENTS

Special thanks to Professor T. N. Veziroglu for bringing Maris's paper to my attention.

REFERENCES

1. H. J. Maris, *Journal of Low Temperature Physics*, Vol. 120, (2000), p. 173.
2. R. Mills, *The Grand Unified Theory of Classical Quantum Mechanics*, January 2000 Edition, BlackLight Power, Inc., Cranbury, New Jersey, Distributed by Amazon.com; posted at www.blacklightpower.com.
3. P. Weiss, *Science News*, Vol. 158, No. 14, September 30, (2000), p. 216.
4. P. Ball, *Nature*, <http://helix.nature.com/nsu/000921/000921-1.html>.
5. I Jackson, *New Scientist*, October 14, (2000),
<http://www.newscientist.com/nl/1014/double.html>.
6. C. A. Fuchs and A. Peres, "Quantum Theory Needs No "Interpretation", *Physics Today*, March (2000), p. 70.
7. R. Mills, "The Hydrogen Atom Revisited", *Int. J. of Hydrogen Energy*, Vol. 25, Issue 12, December, (2000), pp. 1171-1183.
8. McQuarrie, D. A., *Quantum Chemistry*, University Science Books, Mill Valley, CA, (1983), pp. 78-79.
9. Jackson, J. D., *Classical Electrodynamics*, Second Edition, John Wiley & Sons, New York, (1962), pp. 84-108.
10. McQuarrie, D. A., *Quantum Chemistry*, University Science Books, Mill Valley, CA, (1983), pp. 221-224.
11. H. Margenau, G. M. Murphy, *The Mathematics of Chemistry and Physics*, D. Van Nostrand Company, Inc., New York, (1956), Second Edition, pp. 363-367.
12. W. Moore, *Schrödinger life and thought*, Cambridge University Press, (1989), p.198.
13. Fowles, G. R., *Analytical Mechanics*, Third Edition, Holt, Rinehart, and Winston, New York, (1977), pp. 57-60.
14. H. Margenau, G. M. Murphy, *The Mathematics of Chemistry and Physics*, D. Van Nostrand Company, Inc., New York, (1943), pp. 77-78.
15. McQuarrie, D. A., *Quantum Chemistry*, University Science Books, Mill

- Valley, CA, (1983), back cover.
16. McQuarrie, D. A., *Quantum Chemistry*, University Science Books, Mill Valley, CA, (1983), p. 38.
 17. N. A. Bahcall, J. P. Ostriker, S. Perlmutter, P. J. Steinhardt, *Science*, May 28, 1999, Vol. 284, pp. 1481-1488.
 18. Haus, H. A., "On the radiation from point charges", *American Journal of Physics*, 54, (1986), pp. 1126-1129.
 19. Dyson, F., "Feynman's proof of Maxwell equations", *Am. J. Phys.*, Vol. 58, (1990), pp. 209-211.
 20. Horgan, J., "Quantum Philosophy", *Scientific American*, July, (1992), p. 96.
 21. McQuarrie, D. A., *Quantum Chemistry*, University Science Books, Mill Valley, CA, (1983), p. 207.
 22. McQuarrie, D. A., *Quantum Chemistry*, University Science Books, Mill Valley, CA, (1983), pp. 206-225.
 23. Weisskopf, V. F., *Reviews of Modern Physics*, Vol. 21, No. 2, (1949), pp. 305-315.
 24. R. Mills, *The Grand Unified Theory of Classical Quantum Mechanics*, January 2000 Edition, BlackLight Power, Inc., Cranbury, New Jersey, Distributed by Amazon.com, pp. 1-21.
 25. T. A. Abbott and D. J. Griffiths, *Am. J. Phys.*, Vol. 153, No. 12, (1985), pp. 1203-1211.
 26. G. Goedecke, *Phys. Rev* 135B, (1964), p. 281.
 27. R. Mills, "Spectroscopic Identification of a Novel Catalytic Reaction of Atomic Hydrogen and the Hydride Ion Product", *Int. J. Hydrogen Energy*, submitted.
 28. R. Mills, N. Greenig, S. Hicks, "Optically Measured Power Balances of Anomalous Discharges of Mixtures of Argon, Hydrogen, and Potassium, Rubidium, Cesium, or Strontium Vapor", *Int. J. Hydrogen Energy*, submitted.
 29. R. Mills and M. Nansteel, "Anomalous Argon-Hydrogen-Strontium Discharge", *IEEE Transactions of Plasma Science*, submitted.
 30. R. Mills, M. Nansteel, and Y. Lu, "Anomalous Hydrogen-Strontium Discharge", *European Journal of Physics D*, submitted.
 31. R. Mills, J. Dong, Y. Lu, "Observation of Extreme Ultraviolet Hydrogen Emission from Incandescently Heated Hydrogen Gas with Certain

- Catalysts", Int. J. Hydrogen Energy, Vol. 25, (2000), pp. 919-943.
- 32. R. Mills, "Observation of Extreme Ultraviolet Emission from Hydrogen-KI Plasmas Produced by a Hollow Cathode Discharge", Int. J. Hydrogen Energy, in press.
 - 33. R. Mills, "Temporal Behavior of Light-Emission in the Visible Spectral Range from a Ti-K₂CO₃-H-Cell", Int. J. Hydrogen Energy, in press.
 - 34. R. Mills, T. Onuma, and Y. Lu, "Formation of a Hydrogen Plasma from an Incandescently Heated Hydrogen-Catalyst Gas Mixture with an Anomalous Afterglow Duration", Int. J. Hydrogen Energy, in press.
 - 35. R. Mills, M. Nansteel, and Y. Lu, "Observation of Extreme Ultraviolet Hydrogen Emission from Incandescently Heated Hydrogen Gas with Strontium that Produced an Anomalous Optically Measured Power Balance", Int. J. Hydrogen Energy, in press.
 - 36. R. Mills, J. Dong, Y. Lu, J. Conrads, "Observation of Extreme Ultraviolet Hydrogen Emission from Incandescently Heated Hydrogen Gas with Certain Catalysts", 1999 Pacific Conference on Chemistry and Spectroscopy and the 35th ACS Western Regional Meeting, Ontario Convention Center, California, (October 6-8, 1999).
 - 37. R. Mills, J. Dong, N. Greenig, and Y. Lu, "Observation of Extreme Ultraviolet Hydrogen Emission from Incandescently Heated Hydrogen Gas with Certain Catalysts", National Hydrogen Association, 11 th Annual U.S. Hydrogen Meeting, Vienna, VA, (February 29-March 2, 2000).
 - 38. R. Mills, B. Dhandapani, N. Greenig, J. He, J. Dong, Y. Lu, and H. Conrads, "Formation of an Energetic Plasma and Novel Hydrides from Incandescently Heated Hydrogen Gas with Certain Catalysts", National Hydrogen Association, 11 th Annual U.S. Hydrogen Meeting, Vienna, VA, (February 29-March 2, 2000).
 - 39. Mills, J. Dong, N. Greenig, and Y. Lu, "Observation of Extreme Ultraviolet Hydrogen Emission from Incandescently Heated Hydrogen Gas with Certain Catalysts", 219 th National ACS Meeting, San Francisco, California, (March 26-30, 2000).
 - 40. R. Mills, "BlackLight Power Technology-A New Clean Energy Source with the Potential for Direct Conversion to Electricity", Global Foundation, Inc. conference entitled *Global Warming and Energy Policy*, Fort Lauderdale, FL, November 26-28, 2000.

41. R. Mills, "BlackLight Power Technology-A New Clean Energy Source with the Potential for Direct Conversion to Electricity", Global Foundation International Conference on "Global Warming and Energy Policy", Dr. Behram N. Kursunoglu, Chairman, Fort Lauderdale, FL, November 26-28, 2000, in press.
42. R. Mills, B. Dhandapani, N. Greenig, J. He, J. Dong, Y. Lu, and H. Conrads, "Formation of an Energetic Plasma and Novel Hydrides from Incandescently Heated Hydrogen Gas with Certain Catalysts", 219 th National ACS Meeting, San Francisco, California, (March 26-30, 2000).
43. R. Mills, B. Dhandapani, N. Greenig, J. He, J. Dong, Y. Lu, and H. Conrads, "Formation of an Energetic Plasma and Novel Hydrides from Incandescently Heated Hydrogen Gas with Certain Catalysts", June ACS Meeting (29th Northeast Regional Meeting, University of Connecticut, Storrs, CT, (June 18-21, 2000)).
44. R. Mills, B. Dhandapani, N. Greenig, J. He, J. Dong, Y. Lu, and H. Conrads, "Formation of an Energetic Plasma and Novel Hydrides from Incandescently Heated Hydrogen Gas with Certain Catalysts", August National ACS Meeting (220th ACS National Meeting, Washington, DC, (August 20-24, 2000)).
45. R. Mills, B. Dhandapani, M. Nansteel, J. He, A. Voigt, "Identification of Compounds Containing Novel Hydride Ions by Nuclear Magnetic Resonance Spectroscopy", Int. J. Hydrogen Energy, submitted.
46. R. Mills, B. Dhandapani, N. Greenig, J. He, "Synthesis and Characterization of Potassium Iodo Hydride", Int. J. of Hydrogen Energy, Vol. 25, Issue 12, December, (2000), pp. 1185-1203.
47. R. Mills, "Novel Inorganic Hydride", Int. J. of Hydrogen Energy, Vol. 25, (2000), pp. 669-683.
48. R. Mills, "Novel Hydrogen Compounds from a Potassium Carbonate Electrolytic Cell", Fusion Technology, Vol. 37, No. 2, March, (2000), pp. 157-182.
49. R. Mills, B. Dhandapani, M. Nansteel, J. He, "Synthesis and Characterization of Novel Hydride Compounds", Int. J. of Hydrogen Energy, in press.
50. R. Mills, "Highly Stable Novel Inorganic Hydrides", Journal of Materials Research, submitted.
51. R. Mills, "Novel Hydride Compound", 1999 Pacific Conference on

- Chemistry and Spectroscopy and the 35th ACS Western Regional Meeting, Ontario Convention Center, California, (October 6-8, 1999).
52. R. Mills, B. Dhandapani, N. Greenig, J. He, "Synthesis and Characterization of Potassium Iodo Hydride", 1999 Pacific Conference on Chemistry and Spectroscopy and the 35th ACS Western Regional Meeting, Ontario Convention Center, California, (October 6-8, 1999).
53. R. Mills, J. He, and B. Dhandapani, "Novel Hydrogen Compounds", 1999 Pacific Conference on Chemistry and Spectroscopy and the 35th ACS Western Regional Meeting, Ontario Convention Center, California, (October 6-8, 1999).
54. R. Mills, "Novel Hydride Compound", National Hydrogen Association, 11 th Annual U.S. Hydrogen Meeting, Vienna, VA, (February 29-March 2, 2000).
55. R. Mills, J. He, and B. Dhandapani, "Novel Alkali and Alkaline Earth Hydrides", National Hydrogen Association, 11 th Annual U.S. Hydrogen Meeting, Vienna, VA, (February 29-March 2, 2000).
56. R. Mills, "Novel Hydride Compound", 219 th National ACS Meeting, San Francisco, California, (March 26-30, 2000).
57. R. Mills, J. He, and B. Dhandapani, "Novel Alkali and Alkaline Earth Hydrides", 219 th National ACS Meeting, San Francisco, California, (March 26-30, 2000).
58. R. Mills, J. He, and B. Dhandapani, "Novel Alkali and Alkaline Earth Hydrides", August National ACS Meeting (220th ACS National Meeting, Washington, DC, (August 20-24, 2000)).
59. R. Mills, "The Grand Unified Theory of Classical Quantum Mechanics", Global Foundation, Inc. Orbis Scientiae entitled *The Role of Attractive and Repulsive Gravitational Forces in Cosmic Acceleration of Particles The Origin of the Cosmic Gamma Ray Bursts*, (29th Conference on High Energy Physics and Cosmology Since 1964) Dr. Behram N. Kursunoglu, Chairman., December 14-17, 2000, Lago Mar Resort, Fort Lauderdale, FL.
60. R. Mills, "The Grand Unified Theory of Classical Quantum Mechanics", Global Foundation, Inc. Orbis Scientiae entitled *The Role of Attractive and Repulsive Gravitational Forces in Cosmic Acceleration of Particles The Origin of the Cosmic Gamma Ray Bursts*, (29th Conference on High Energy Physics and Cosmology Since 1964) Dr. Behram N. Kursunoglu,

- Chairman., December 14-17, 2000, Lago Mar Resort, Fort Lauderdale, FL, in press.
61. R. Mills, "The Grand Unified Theory of Classical Quantum Mechanics", *Il Nuovo Cimento*, submitted.
 62. R. Mills, W. Good, A. Voigt, Jinquan Dong, "Minimum Heat of Formation of Potassium Iodo Hydride", *Int. J. Hydrogen Energy*, submitted.
 63. R. Mills, *The Grand Unified Theory of Classical Quantum Mechanics*, January 2000 Edition, BlackLight Power, Inc., Cranbury, New Jersey, Distributed by Amazon.com, pp. 33-109.
 64. R. Mills, *The Grand Unified Theory of Classical Quantum Mechanics*, January 2000 Edition, BlackLight Power, Inc., Cranbury, New Jersey, Distributed by Amazon.com, pp. 138-175.
 65. N. V. Sidgwick, *The Chemical Elements and Their Compounds*, Volume I, Oxford, Clarendon Press, (1950), p.17.
 66. M. D. Lamb, *Luminescence Spectroscopy*, Academic Press, London, (1978), p. 68.
 67. Labov, S., Bowyer, S., "Spectral observations of the extreme ultraviolet background", *The Astrophysical Journal*, 371, (1991), pp. 810-819.
 68. Jackson, J. D., *Classical Electrodynamics*, Second Edition, John Wiley & Sons, New York, (1962), pp. 110-113.
 69. K. W. Schwarz and R. W. Stark, *Phys. Rev. Lett.* Vol. 22, No. 24, (1969), pp. 1278-1280.
 70. Jackson, J. D., *Classical Electrodynamics*, Second Edition, John Wiley & Sons, New York, (1962), pp. 739-779.
 71. Mizushima, M., *Quantum Mechanics of Atomic Spectra and Atomic Structure*, W. A. Benjamin, Inc., New York, (1970), p.17
 72. J. A. Northby, Ph.D. thesis, University of Minnesota, 1966, (unpublished).
 73. J. A. Northby and T. M. Sanders, *Phys. Rev. Lett.* 18, (1967), p.1184.
 74. C. L. Zipfel, Ph.D. thesis, University of Michigan, 1969, unpublished.
 75. C. L. Zipfel and T. M. Sanders, in *Proceedings of the 11th International Conference on Low Temperature Physics*, edited by J. F. Allen, D. M. Finlayson, and D. M. McCall (St. Andrews University, St. Andrews, Scotland, 1969), p. 296.
 76. C. C. Grimes and G. Adams, *Phys. Rev.* B41, (1990), p. 6366.
 77. C. C. Grimes and G. Adams, *Phys. Rev.* B45, (1992), p. 2305.

78. G. Baym, R. G. Barrera, and C. J. Pethick, Phys. Rev. Letters, Vol. 22, No. 1, (1969), pp. 20-23.
79. D. G. Henshaw and A. D. B. Woods, Phys. Rev. Letters, Vol. 121, (1961), p. 1266.
80. F. London, *Superfluids* (Dover Publications, New York, 1964), Vol. III.
81. It is interesting to consider that the solutions for the full angular part of the Schrödinger equation (Eq. (4)), $Y_{lm}(\theta, \phi)$, are also the spherical harmonics. McQuarrie [McQuarrie, D. A., *Quantum Chemistry*, University Science Books, Mill Valley, CA, (1983), pp. 206-221] shows that the Schrödinger equation for the rigid rotor is

$$\hat{H}Y_l^m(\theta, \phi) = \frac{\hbar^2 \ell(\ell+1)}{2I} Y_l^m(\theta, \phi) \quad (127)$$

and that \hat{H} and \hat{L}^2 differ only by the factor $2I$ for a rigid rotor. So, Eq. (127) is equivalent to

$$\hat{L}^2 Y_l^m(\theta, \phi) = \hbar^2 \ell(\ell+1) Y_l^m(\theta, \phi) \quad (128)$$

Thus, we see that the spherical harmonics are also eigenfunctions of \hat{L}^2 and that the square of the angular momentum can have values given by

$$L^2 = \hbar^2 \ell(\ell+1) \quad \ell = 0, 1, 2, 3, \dots \quad (129)$$

The flaw with this result with regard to the hydrogen atom is given in the "Schrödinger Theory of the Hydrogen Atom" section. In the case of the electron in helium, the moment of inertia in Eq. (127) decreases with increasing energy states as the corresponding ℓ quantum number increases. The Schrödinger equation is flawed based on the prediction of infinite rotational energy for electron in superfluid helium.

82. G. Baym, R. G. Barrera, C. J. Pethick, Phys. Rev. Lett., Vol. 22, No. 1, (1969), pp. 20-23.
83. L. C. Shi, J. A. Kong, *Applied Electromagnetism*, Brooks/Cole Engineering Division, Monterey, CA, (1983), pp. 210-215.
84. C. S. M. Doake and P. W. F. Gribbon, Phys. Lett. Vol. 30A, No. 4, (1969), pp. 251-253.
85. G. G. Ihas and T. M. Sanders, Phys. Rev. Lett. 27, (1971), p. 383.
86. G. G. Ihas and T. M. Sanders, in Proceedings of the 13 th International Conference on Low Temperature Physics, editors K. D. Timmerhaus, W. J. O'Sullivan and E. F. Hammel, (Plenum, New York, 1972), Vol. 1, p. 477.
87. G. G. Ihas, Ph.D. thesis, University of Michigan, 1971.

88. V. L. Eden and P. V. E. McClintock, Phys. Lett. Vol. 102A, No. 4; (1984), pp. 197-200
89. V. L. Eden, M. Phil. thesis, University of Lancaster, 1986.
90. Weisskopf, V. F., Reviews of Modern Physics, Vol. 21, No. 2, (1949), pp. 305-315.
91. Dirac, P. A. M., *From a Life of Physics*, ed. A. Salam, et al., World Scientific, Singapore, (1989).
92. Milonni, P. W., *The Quantum Vacuum*, Academic Press, Inc., Boston, p. 90.
93. Dirac, P. A. M., *Directions in Physics*, ed. H. Hora and J. R. Shepanski, Wiley, New York, (1978), p. 36.
94. H. Wergeland, "The Klein Paradox Revisited", *Old and New Questions in Physics, Cosmology, Philosophy, and Theoretical Biology*, A. van der Merwe, Editor, Plenum Press, New York, (1983), pp. 503-515.
95. Beiser, A., *Concepts of Modern Physics*, Fourth Edition, McGraw-Hill Book Company, New York, (1978), pp. 119-122.
96. M. M. Waldrop, Science, Vol. 242, December, 2, (1988), pp. 1248-1250.
97. J. Horgan, "Quantum Philosophy", Scientific American, Vol. 276, July, (1992), pp. 94-104.
98. D. E. Platt, Am. J. Phys., 60 (4), April, 1992, pp. 306-308.
99. H. J. Dehmelt, American Journal of Physics, Vol. 58, No. 1, January, (1990). pp. 17-27.
100. A. Einstein, B. Podolsky, N. Rosen, Phys. Rev., Vol. 47, (1935), p. 777.
101. L. de Broglie, *Old and New Questions in Physics, Cosmology, Philosophy, and Theoretical Biology*, A. van der Merwe, Editor, Plenum Press, New York, (1983) pp. 83-86.
102. M. M. Waldrop, Science, Vol. 242, December, 2, (1988), pp. 1248-1250.
103. M. Karplus and R. N. Porter, *Atoms and Molecules an Introduction for Students of Physical Chemistry*, The Benjamin/Cummings Publishing Company, Menlo Park, California, (1970), p. 567.
104. Beiser, A., *Concepts of Modern Physics*, Fourth Edition, McGraw-Hill Book Company, New York, (1978), p. 407.
105. R. Mills, *The Grand Unified Theory of Classical Quantum Mechanics*, January 2000 Edition, BlackLight Power, Inc., Cranbury, New Jersey,

- Distributed by Amazon.com, pp. 98-109.
106. R. Mills, *The Grand Unified Theory of Classical Quantum Mechanics*, January 2000 Edition, BlackLight Power, Inc., Cranbury, New Jersey, Distributed by Amazon.com, pp. 192-213.
107. R. Mills, *The Grand Unified Theory of Classical Quantum Mechanics*, January 2000 Edition, BlackLight Power, Inc., Cranbury, New Jersey, Distributed by Amazon.com, pp. 110-120.
108. R. Mills, *The Grand Unified Theory of Classical Quantum Mechanics*, January 2000 Edition, BlackLight Power, Inc., Cranbury, New Jersey, Distributed by Amazon.com, pp. 176-191.
109. Bromberg, P. J., "Absolute differential cross sections of elastically scattered electrons. I. He, N₂, and CO at 500 eV", *The Journal of Chemical Physics*, Vol. 50, No. 9, (1969), pp. 3906-3921.
110. Geiger, J., "Elastische und unelastische Streuung von Elektronen an Gasen", *Zeitschrift fur Physik*, Vol. 175, (1963), pp. 530-542.
111. Peixoto, E. M., Bunge, C. F., Bonham, R. A., "Elastic and inelastic scattering by He and Ne atoms in their ground states", *Physical Review*, Vol. 181, (1969), pp. 322-328.
112. Bonham, R. A., Fink, M., *High Energy Electron Scattering*, ACS Monograph, Van Nostrand Reinhold Company, New York, (1974).
113. R. Mills, *The Grand Unified Theory of Classical Quantum Mechanics*, January 2000 Edition, BlackLight Power, Inc., Cranbury, New Jersey, Distributed by Amazon.com. pp. 234-259.
114. W. Kolos and L. Wolniewicz, *J. Chem. Phys.*, Vol. 41, (1964), p. 3663; Vol. 49, (1968), p. 404.
115. W. Kolos and C. C. J. Roothaan, *Rev. Mod. Phys.*, Vol. 32,(1960), p. 219.
116. W. J. Nellis, "Making Metallic Hydrogen", *Scientific American*, May, (2000), pp. 84-90.
117. R. P. Feynman, R. B. Leighton, M. Sands, *The Feynman Lectures on Physics Quantum Mechanics*, Addison-Wesley Publishing Company, Reading, Massachusetts, p. 1-9.
118. S. Durr, T. Nonn, G. Rempe, *Nature*, September 3, (1998), Vol. 395, pp. 33-37.
119. Science News, "Wave or particle? Heisenberg, take a hike!" Vol. 154, September 5, 1998.

120. R. Mills, *The Grand Unified Theory of Classical Quantum Mechanics*, January 2000 Edition, BlackLight Power, Inc., Cranbury, New Jersey, Distributed by Amazon.com, pp. 405-413.
121. J. S. Bell, Physics, Vol. 1, (1965), p. 195.
122. D. Bohm, *Quantum Theory*, Prentice-Hall, Inc., Englewood Cliffs, New Jersey, (1951), p. 614.
123. A. Aspect, P. Grangier and R. Gerard, Physical Review Letters, Vol. 47, No. 7, (1981), pp. 460-463.
124. R. Mills, *The Grand Unified Theory of Classical Quantum Mechanics*, January 2000 Edition, BlackLight Power, Inc., Cranbury, New Jersey, Distributed by Amazon.com, pp. 511-521.
125. J. F. Clauser et al., Physical Review Letters, Vol. 23, No. 15, (1969), pp. 880-884.
126. M. A. Horne, "Experimental Consequences of Local Hidden Variable Theories", thesis, Boston University, (1969).
127. C. Monroe, D. M. Meekhof, B. E. King, D. J. Wineland, Science, Vol. 272, (1996), pp. 1131-1135.
128. R. Mills, *The Grand Unified Theory of Classical Quantum Mechanics*, January 2000 Edition, BlackLight Power, Inc., Cranbury, New Jersey, Distributed by Amazon.com, pp. 521-536.
129. M. W. Browne, "Physicist Put Atom in Two Places at Once", New York Times, Tuesday, May 28, 1996, pp. B5-B6.
130. G. Taubes, Science, Vol. 272, (1996), p. 1134.
131. J. R. Friedman, V. Patella, W. Hen, S. K. Tolpygo, J. E. Lukens, "Quantum superposition of distinct macroscopic states", Nature, Vol. 406, July, 6, (2000), pp. 43-45.
132. R. Mills, *The Grand Unified Theory of Classical Quantum Mechanics*, January 2001 Edition, BlackLight Power, Inc., Cranbury, New Jersey, www.blacklightpower.com.
133. K. Chang, The New York Times, Tuesday, July 11, 2000, p. F3.
134. E. Schrödinger, "Die gegenwärtige situation in der quantenmechanik," Naturwissenschaften, Vol. 23, (1935), pp. 807-812, 823-828, 844-849.
135. P. F. Schewe and B. Stein, Physic News Update, The American Institute of Physics Bulletin of Physics News, Number 494, July 17, (2000).
136. A. Allahverdyan and T. Nieuwenhuizen, Phys. Rev. Lett., Vol. 85, No.

9, August 28, (2000), pp. 1799-1802.

137. R. P. Feynman, R. B. Leighton, M. Sands, *The Feynman Lectures on Physics Quantum Mechanics*, Addison-Wesley Publishing Company, Reading, Massachusetts, p. 2-6.
138. McQuarrie, D. A., *Quantum Chemistry*, University Science Books, Mill Valley, CA, (1983), pp. 135-140.
139. McQuarrie, D. A., *Quantum Chemistry*, University Science Books, Mill Valley, CA, (1983), pp. 22-26.
140. R. Mills, *The Grand Unified Theory of Classical Quantum Mechanics*, January 2000 Edition, BlackLight Power, Inc., Cranbury, New Jersey, Distributed by Amazon.com, pp. 487-489.

Table 1. The first few spherical harmonics and $\frac{N_{\ell,m_\ell}}{N_{0,0}}$ of Eq. (121) as a function of ℓ , and m_ℓ .

Spherical Harmonics

$Y_{m_\ell}^\ell$	ℓ	m_ℓ	$\frac{N_{\ell,m_\ell}}{N_{0,0}}$
$Y_0^0 = \frac{1}{(4\pi)^{1/2}}$	0	0	1
$Y_1^0 = \left(\frac{3}{4\pi}\right)^{1/2} \cos\theta$	1	0	$\sqrt{3}$
$Y_1^1 = \left(\frac{3}{8\pi}\right)^{1/2} \sin\theta e^{i\phi}$	1	1	$\sqrt{\frac{3}{2}}$
$Y_1^{-1} = \left(\frac{3}{8\pi}\right)^{1/2} \sin\theta e^{-i\phi}$	1	-1	$\sqrt{\frac{3}{2}}$
$Y_2^0 = \left(\frac{5}{16\pi}\right)^{1/2} (3\cos^2\theta - 1)$	2	0	$\sqrt{\frac{5}{4}}$
$Y_2^1 = \left(\frac{15}{8\pi}\right)^{1/2} (\sin\theta \cos\theta e^{i\phi})$	2	1	$\sqrt{\frac{15}{2}}$
$Y_2^{-1} = \left(\frac{15}{8\pi}\right)^{1/2} (\sin\theta \cos\theta e^{-i\phi})$	2	-1	$\sqrt{\frac{15}{2}}$
$Y_2^2 = \left(\frac{15}{32\pi}\right)^{1/2} \sin^2\theta e^{2i\phi}$	2	2	$\sqrt{\frac{15}{8}}$
$Y_2^{-2} = \left(\frac{15}{32\pi}\right)^{1/2} \sin^2\theta e^{-2i\phi}$	2	-2	$\sqrt{\frac{15}{8}}$

Table 2. The mobility of an excited state electron bubble having a fraction principal quantum number ($n = \frac{1}{\text{integer}}$) relative to the normal electron bubble as a function of quantum numbers n , ℓ , and m_ℓ given by Eq. (126). The peaks that appear in Figure 7 and Table 3 are indicated.

n	$\ell = 0$	$\ell = 1$ $m_\ell = 0$	$\ell = 1$ $m_\ell = \pm 1$	$\ell = 2$ $m_\ell = 0$	$\ell = 2$ $m_\ell = \pm 1$	$\ell = 2$ $m_\ell = \pm 2$
$\frac{1}{2}$	2.21 peak # 8	1.22 peak # 3	1.81 peak # 5			
$\frac{1}{3}$	3.12 peak # 10	1.92 peak # 6	2.66	2.86	1.14 peak # 2	2.41
$\frac{1}{4}$	3.81 peak # 11	2.52 peak # 9	3.33	3.54	1.60 peak # 4	3.06
$\frac{1}{5}$	4.33 peak # 12	3.03	3.86	4.07	2.03 peak # 7	3.59
$\frac{1}{6}$	4.74 peak # 13	3.47	4.28	4.49	2.41	4.02
$\frac{1}{7}$	5.07 peak # 14	3.83	4.63	4.83	2.75	4.38
$\frac{1}{8}$	5.34 peak # 15	4.15	4.93	5.12	3.06	4.68
$\frac{1}{9}$	5.57 peak # 15	4.42	5.17	5.35	3.34	4.94
$\frac{1}{10}$	5.76 peak # 15	4.66	5.38	5.56	3.59	5.16
$\frac{1}{11}$	5.92 peak # 15	4.87	5.56	5.73	3.82	5.35
$\frac{1}{12}$	6.07 peak # 15	5.05	5.72	5.88	4.02	5.52
$\frac{1}{100}$	7.75 peak # 15	7.55	7.69	7.72	7.29	7.65

Table 3. The migration times and experimental mobilities of the 15 ion peaks shown in Figure 7 relative to the normal ion with their assignments to excited state electron bubbles with quantum numbers n , ℓ , and m_ℓ and theoretical mobilities given in Table 2.

Peak #	Migration Time (Arbitrary Units)	Mobility Relative to Peak #1	Theoretical Mobility Relative to Peak #1	Assignment n , ℓ , and m_ℓ .
1	9.8	1.00	1	$n = 1 \ell = 0 m_\ell = 0$
2	8.2	1.20	1.14	$n = \frac{1}{3} \ell = 2 m_\ell = \pm 1$
3	7.6	1.29	1.22	$n = \frac{1}{2} \ell = 1 m_\ell = 0$
4	6.2	1.58	1.6	$n = \frac{1}{4} \ell = 2 m_\ell = \pm 1$
5	5.4	1.81	1.81	$n = \frac{1}{2} \ell = 1 m_\ell = \pm 1$
6	5	1.96	1.92	$n = \frac{1}{3} \ell = 1 m_\ell = 0$
7	4.85	2.02	2.03	$n = \frac{1}{5} \ell = 2 m_\ell = \pm 1$
8	4.35	2.25	2.21	$n = \frac{1}{2} \ell = 0 m_\ell = 0$
9	3.9	2.51	2.52	$n = \frac{1}{4} \ell = 1 m_\ell = 0$
10	3.3	2.97	3.12	$n = \frac{1}{3} \ell = 0 m_\ell = 0$
11	2.8	3.50	3.81	$n = \frac{1}{4} \ell = 0 m_\ell = 0$
12	2.1	4.67	4.33	$n = \frac{1}{5} \ell = 0 m_\ell = 0$
13	2	4.90	4.74	$n = \frac{1}{6} \ell = 0 m_\ell = 0$
14	1.8	5.44	5.07	$n = \frac{1}{7} \ell = 0 m_\ell = 0$
15	1.3	7.54	7.75	$n = \frac{1}{100} \ell = 0 m_\ell = 0$

Figure Captions

- Figure 1. The orbitsphere is a two dimensional spherical shell with the Bohr radius of the hydrogen atom.
- Figure 2. The orbital function modulates the constant (spin) function (shown for $t = 0$; cross-sectional view).
- Figure 3. Two infinitesimal point masses (charges) of two orthogonal great circle current loops in the orbitsphere frame.
- Figure 4. The current pattern of the orbitsphere shown with 8.49 degree increments of the infinitesimal angular variable $\Delta\alpha(\Delta\alpha')$ from the perspective of looking along the z-axis.
- Figure 5. The mobility (Eq. (126)) of an excited state electron bubble having a fraction principal quantum number ($n = \frac{1}{\text{integer}} = 1/p$) relative to the normal electron bubble as a function of p for given ℓ , and m_ℓ quantum numbers.
- Figure 6. The mobility from the data of Ihás [1, 87] of electron bubbles in superfluid helium plotted versus the inverse of the temperature. Solid triangles are for the normal electron bubble, open squares, circles, triangles and solid circles are for the four ions of the same peak assigned in Figure 7 and Table 3.
- Figure 7. Data trace from Ihás [87] showing the detected ion signal as a function of time. N and F denote the normal and fast ion peaks. The peaks labeled 1 to 15 are assigned in Table 3. For a description of experimental condition see Ihás [87].
- Figure 8. Data traces from Eden and McClintock [88] of the current at the collector of the velocity spectrometer (arbitrary units) as a function of the elapsed time t after a pulse was applied to release exotic ions. Signals are shown for a range of strong electric fields as indicated in units of 10^5 V/m by the number above each trace. The steep rise on the right-hand sides of the signals indicates the arrival of the normal ion current. For a description of experimental condition see Eden and McClintock [88].

Figure 9. The limiting electron bubble velocities shown in the data traces of Figure 8 relative to the normal electron bubble as a function of p corresponding to principal quantum number $n = \frac{1}{\text{integer}} = 1/p$ where $\ell = 0$, and $m_\ell = 0$.

The orbitsphere has zero thickness.
It is a two-dimensional surface.

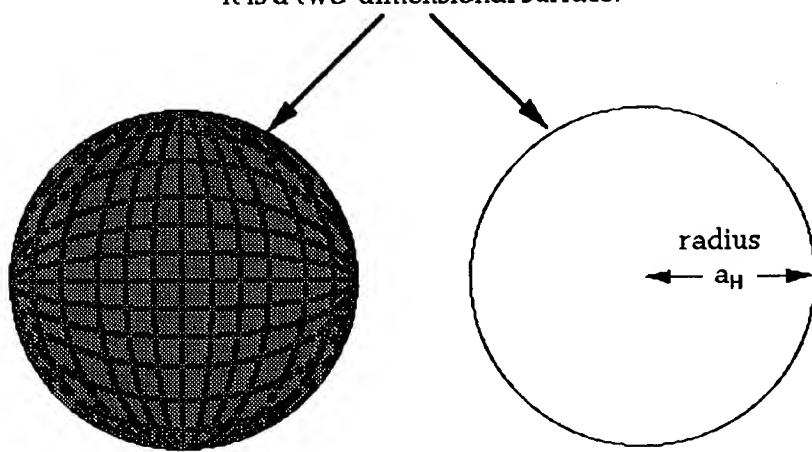


Fig. 1

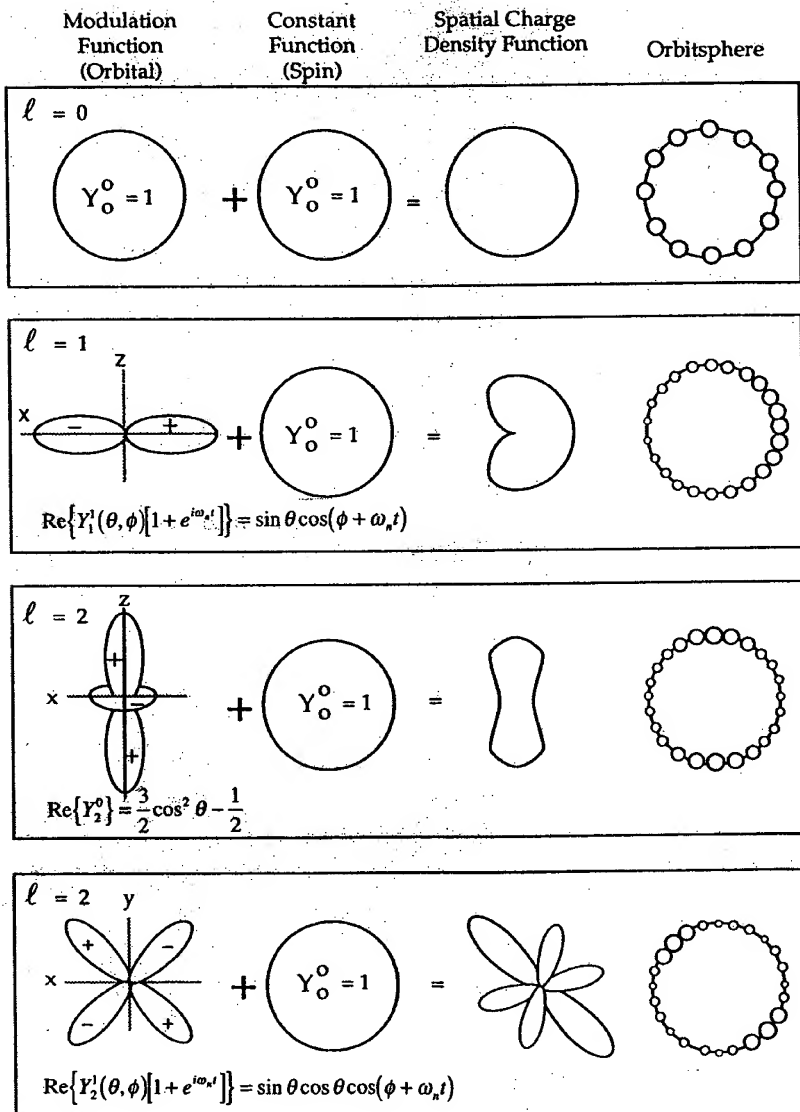


Fig. 2

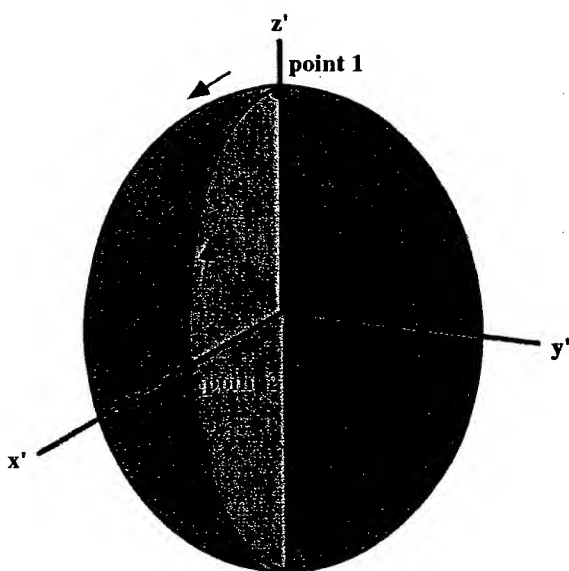
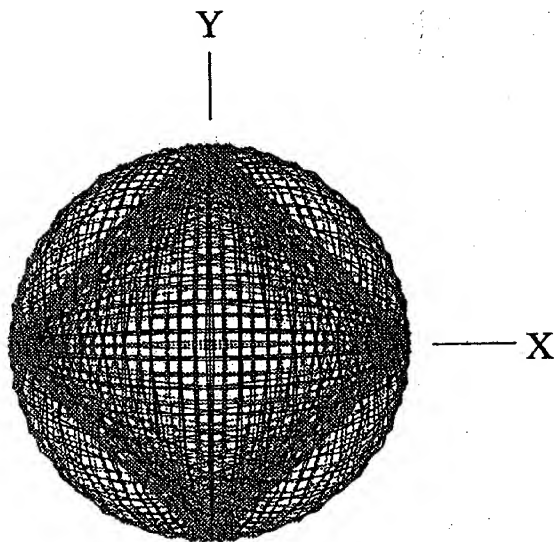


Fig. 3



VIEW ALONG THE Z AXIS

Fig. 4

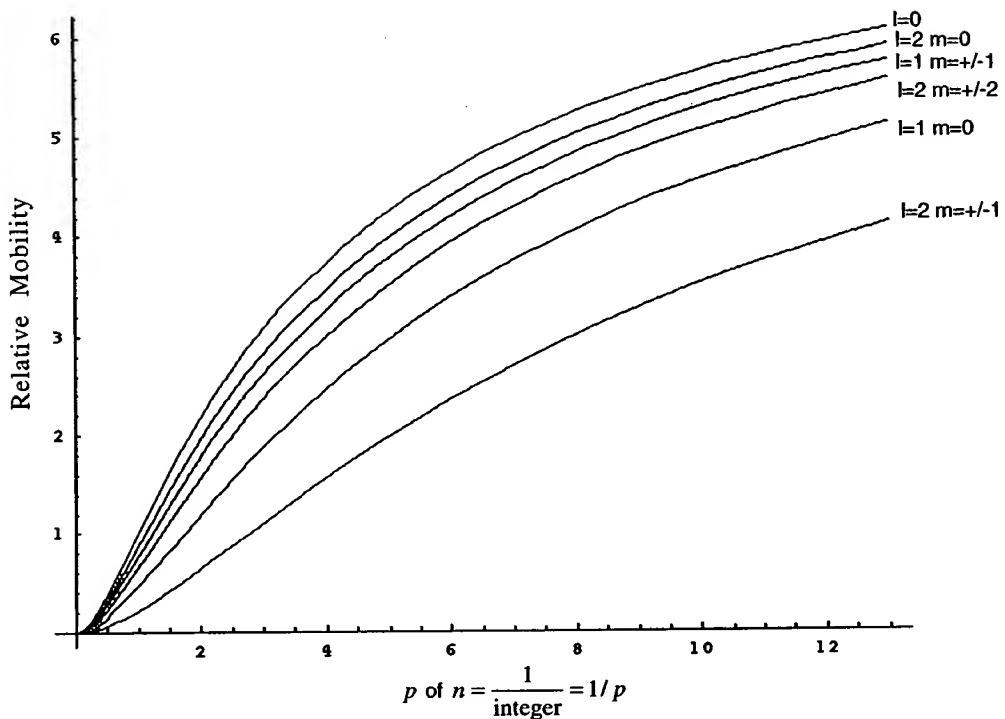


Fig. 5

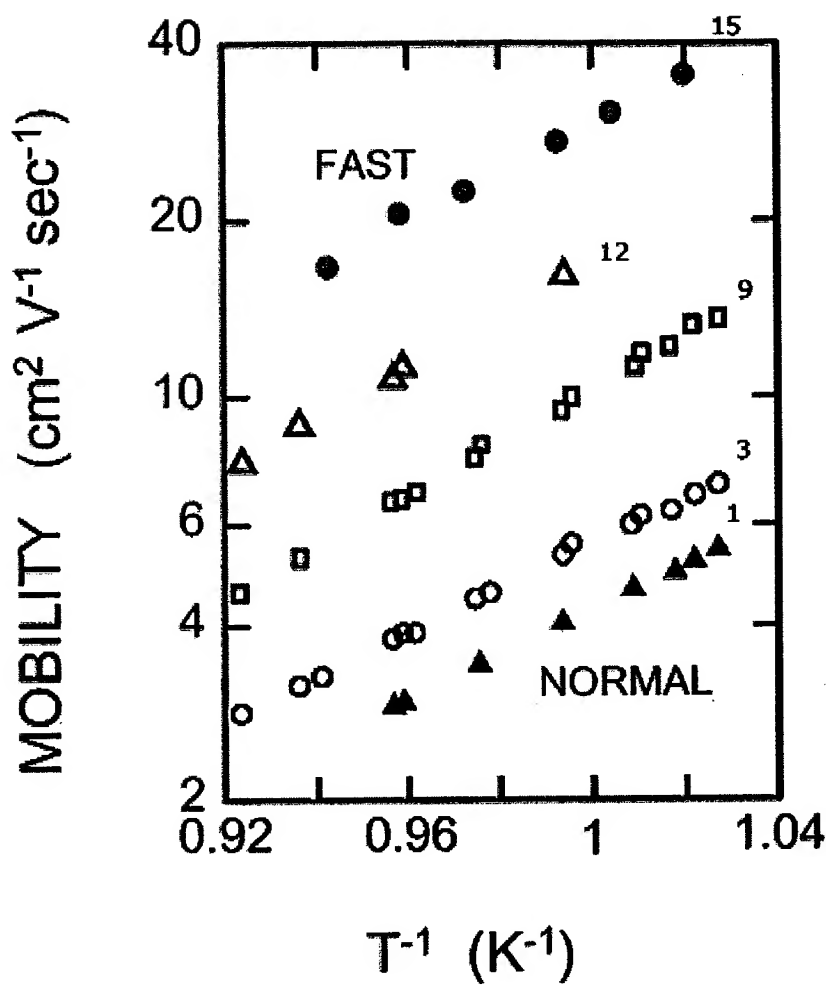


Fig. 6

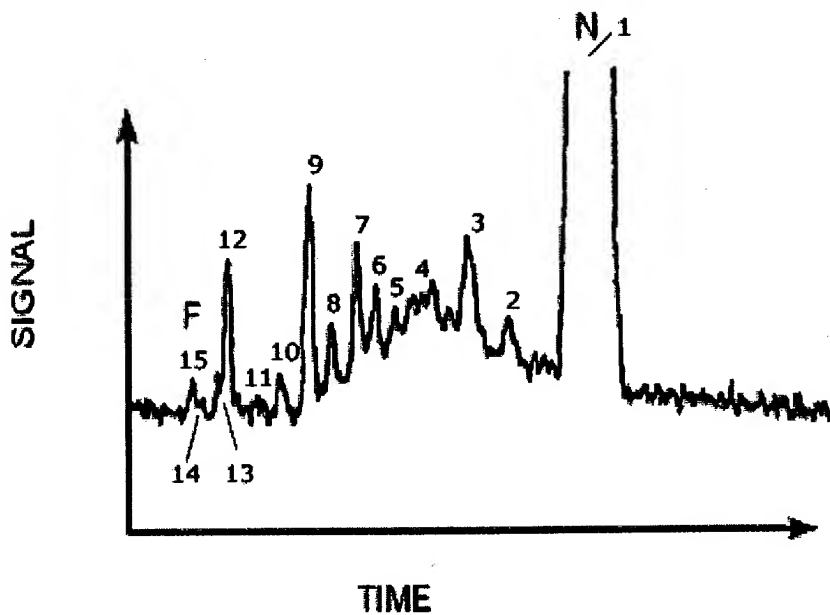


Fig. 7

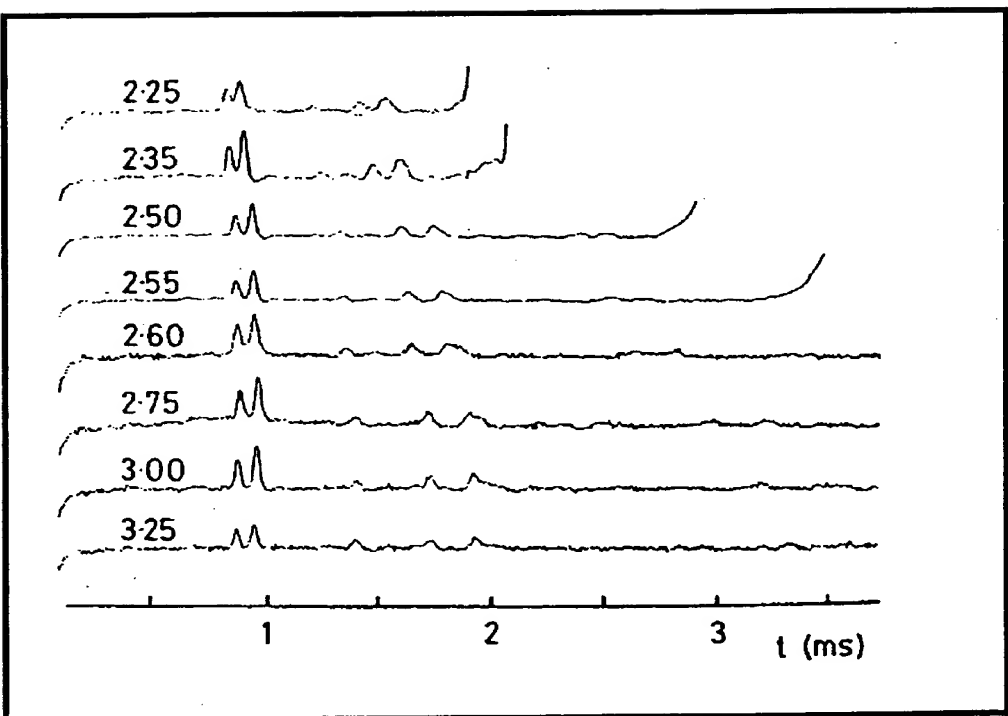
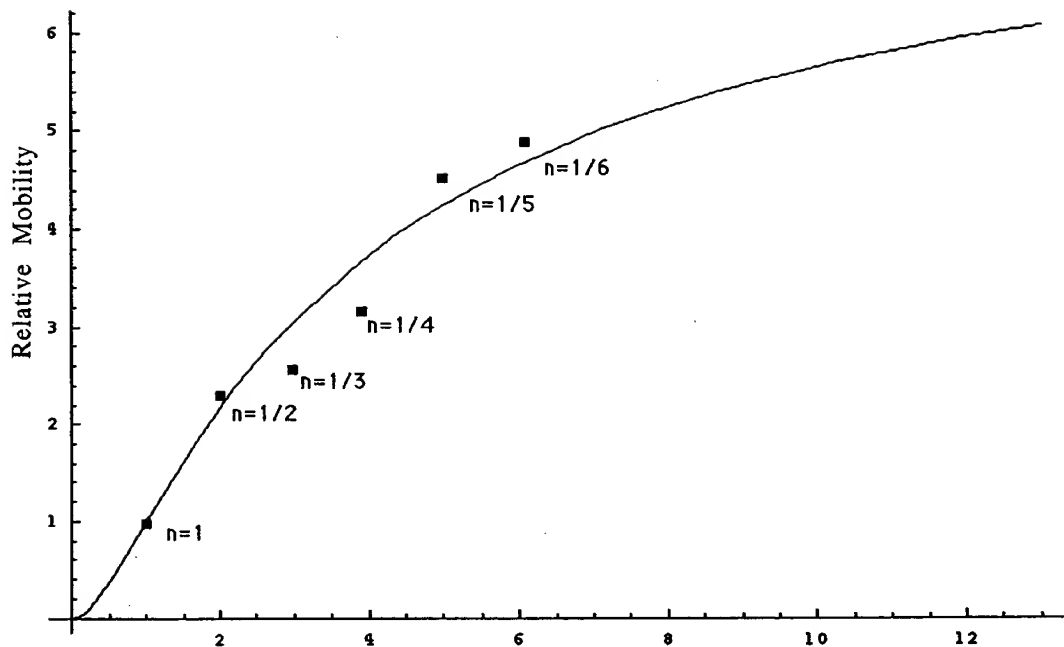


Fig. 8



$$p \text{ of } n = \frac{1}{\text{integer}} = 1/p$$

Fig. 9